Ab-initio Structure Calculation of Few-Body Atomic Systems in Free and Plasma Environment

Dissertation submitted for the degree of
Doctor of Philosophy (Science)
of Jadavpur University

by

Sayantan Dutta
Department of Physics
Jadavpur University
Kolkata–700032

July 2024

Ab-initio Structure Calculation of Few-Body Atomic Systems in Free and Plasma Environment

Dissertation submitted for the degree of
Doctor of Philosophy (Science)
of Jadavpur University

By

Sayantan Dutta
Ph. D. Registration no.: SOPHY1114122 *of* 2022

Under the supervision of

Dr. Sukhamoy Bhattacharyya
Assistant Professor, Department of Physics
Jadavpur University
Kolkata 700032, West Bengal, India

and

Dr. Tapan Kumar Mukhopadhyay
Professor, Department of Physics
Narula Institute of Technology
Kolkata 700109, West Bengal, India

যাদবপুর বিশ্ববিদ্যালয়
কলকাতা-৭০০ ০৩২, ভারত

*JADAVPUR UNIVERSITY
KOLKATA-700 032,INDIA

FACULTY OF SCIENCE : DEPARTMENT OF PHYSICS

CERTIFICATE FROM THE SUPERVISOR(S)

This is to certify that the thesis entitled **"Ab-initio Structure Calculation of Few-Body Atomic Systems in Free and Plasma Environment"** submitted by **Sri Sayantan Dutta** who got his name registered on **09.06.2022** for the award of Ph. D. (Science) Degree of Jadavpur University, is absolutely based upon his own work under the supervision of **Dr. Sukhamoy Bhattacharyya** and **Dr. Tapan Kumar Mukhopadhyay** and that neither this thesis nor any part of it has been submitted for either any degree / diploma or any other academic award anywhere before.

Sukhamoy Bhattacharyya 8/7/24

(Signature of the Supervisor(s), date with official seal)

Dr. Sukhamoy Bhattacharyya
Assistant Professor
Department of Physics
Jadavpur University
Kolkata – 700 032

Narula Institute of Technology
81, Nilgunj Road, Agarpara, Kolkata-700 109
Phone: +91 33 2563 8888 / 7777, Telefax: +91 33 2583 7029
Website : www.nit.ac.in, Email : info@nit.ac.in

CERTIFICATE FROM THE SUPERVISOR(S)

This is to certify that the thesis entitled **"Ab-initio Structure Calculation of Few-Body Atomic Systems in Free and Plasma Environment"** Submitted by **Sri Sayantan Dutta** who got his name registered on **09.06.2022** for the award of Ph. D. (Science) Degree of Jadavpur University, is absolutely based upon his own work under the supervision of **Dr. Sukhamoy Bhattacharyya** and **Dr. Tapan Kumar Mukhopadhyay** and that neither this thesis nor any part of it has been submitted for either any degree / diploma or any other academic award anywhere before.

Tapan Mukherjee 08/07/2024

(Signature of the Supervisor(s), date with official seal)

TAPAN KUMAR MUKHOPADHYAY
Professor
Department of Physics
Narula Institute of Technology
81, Nilgunj Road, Agarpara, Kol-109

CERTIFICATE OF SIMILARITY CHECK

This is to certify that the plagiarism checking for this thesis titled **'Ab-initio Structure Calculation of Few-Body Atomic Systems in Free and Plasma Environment'** authored by **Mr. Sayantan Dutta** has been performed using professional plagiarism prevention software **iThenticate**. According to the report generated after plagiarism checking there is an **8%** similarity in this thesis, which is in the category **'Level 0'** (minor similarities) as per the 'Promotion of Academic Integrity and Prevention of Plagiarism in Higher Education Institutions Regulations, 2018' of the University Grants Commission (UGC) of India. The common knowledge or coincidental terms up to 10 (ten) consecutive words (as prescribed in the above said UGC Regulation up to 14 (fourteen) terms for such common knowledge or coincidental terms can be excluded) and own works of the candidate published in various peer-reviewed journals (those are attached in the thesis) are excluded from the similarity checking. It is certified that the present thesis submitted by Mr. Sayantan Dutta is plagiarism-free and has followed standard norms of academic integrity and scientific ethics.

Sukhamoy Bhattacharyya 8/7/26

Dr. Sukhamoy Bhattacharyya
Assistant Professor
Department of Physics
Jadavpur University
Kolkata – 700 032

Tapan Mukherjee 08/07/2026

TAPAN KUMAR MUKHOPADHYAY
Professor
Department of Physics
Narula Institute of Technology
81, Nilgunj Road, Agarpara, Kol-109

Dedicated to my Mother, Grandparents and Teachers

Contents

Acknowledgements

First and foremost, I would want to convey my heartfelt gratitude to my supervisor, Dr. Sukhamoy Bhattacharyya, for his continuous encouragement, guidance, and mentorship during this research project. I will be eternally thankful to him for introducing me to the domain of theoretical Atomic Physics research. His skill, persistence, and hard efforts have helped shape my thesis significantly. Because of his kind and welcoming nature, he has most likely become my elder brother than a guide.

I am appreciative of my co-supervisor, Prof. Tapan Kumar Mukhopadhyay for his insightful advice, scholarly contributions, and unwavering support. He is the first teacher who taught me 'how–to–learn' any topic in an effective manner, and I am extremely grateful for this. His advice on seeing a new problem and tackling new challenges in this field of research is invaluable to me.

Any appreciation will fall short of acknowledging Dr. Jayanta Kumar Saha, my senior research colleague. He was quite helpful in accompanying me through the algebra, computer codes, and other skills required to conduct research. He always comes with new ideas and discussions with him brings fresh air perhaps in every occasion. His enthusiasm and drive in research have always inspired me.

I am grateful to Prof. Prasanta Kumar Mukherjee for all of his appreciation and good wishes which have boosted my confidence to new heights. Academic discussions with him always enriched me a lot.

I am extremely indebted to Jadavpur University for granting me permission to register for Ph. D. degree. I would like to thank Prof. Partha Pratim Ray, Prof. Debasish Biswas, Prof. Subenoy Chakraborty, Prof. Saikat Kumar Seth, Prof. Kaustuv Das and other faculties and staffs of Jadavpur University for their all out support for seamlessly conducting the research work.

I am also grateful to Narula Institute of Technology, Agarpara, Kolkata for providing computational resources and other necessary facilities to carry out some of the studies covered in this thesis.

It is my utmost happiness to acknowledge the contributions of Dr. Partha Sarathi Majumder, Dr. Ananda Sarkar, Dr. Syed Rafi Ahmed and Dr. Subhro Ghoshal from Acharya Prafulla Chandra College, Kolkata, for their care, affection and encouragement to

pursue research.

I am thankful to Dr. Amar Nath Sil, Mr. Reet Chandra and Dr. Anjan Sadhukhan for sharing the load of my research works during the collaboration phases and also for supporting in all possible ways during my hard times in research. A special thanks is reserved for Mr. Mohan Kundu for his immense cooperation during the entire tenure of Ph. D. programme, particularly during the days of the course work. I feel myself fortunate to have Dr. Santanu Mandal, Dr. Aparajita Das, Dr. Rohit Hazra, Dr. Deepanwita Ghosh, Mr. Tusar Subhra Sarkar, Mr. Saumya Sarkar, Mr. Salil Sikdar, Mr. Sayan Bag, Mr. Surajit Saha, Mr. Gurupada Barik, Mr. Saurav Nandi, Mr. Rejjak Laskar, Mr. Kaustav Chakladar as my research colleagues and friends from the laboratories at Jadavpur University, Narula Institute of Technology and Aliah University.

I want to express my gratitude to Belgharia Texmaco Estate School, Agarpara, Kolkata, for giving permission to enroll into the Ph.D programme at Jadavpur University. I am fortunate enough to have colleagues like Mr. Malay Sanyal, Swapan Kumar Mandal and others who always encourage and help me to continue my research.

No mission is ever successful without the support of family. I am grateful to my mother, Smt. Beauty Dutta, for providing all the comforts in life and being a constant support behind all my personal and professional decisions. I am thankful to my wife, Smt. Swati Mondal who has been encouraging me to pass through the process even if it meant sacrificing her own comfort. I will always remember the presence of my little daughter, Kahini, on my back when I was working on my laptop. Her charm and smile stimulates the secretion of the 'Dopamine' hormone, even at the challenging times in my career.

Finally, I owe very much to my friends Avijit, Barun, Indra, Pranabesh, Prasenjit, Proloy, Subhasis, Subrata and many others who stood by me throughout the progress of this work.

Date: 08.07.2024

SAYANTAN DUTTA
Department of Physics
Jadavpur University
Kolkata–700032
West Bengal, India

Abstract

The study of structural properties of few–body atomic systems (H–like, He–like etc.) provides a key testing ground for many quantum mechanical approximation methods such as perturbation, variation, WKB method etc. These theoretical studies have immense application in the field of confined systems, plasma diagnostics, astrophysical data analysis etc. In this course of studies, we focus on studying the structural properties of few-body atomic systems in free case (only Coulombic attraction and repulsion among the constituent particles) and also in plasma environment.

This dissertation's work has been organized into five chapters. The following paragraphs provide an outline of these chapters:

Chapter 1

At the beginning of the first chapter "Introduction", we have given a detailed account on the rapid growth towards the production of relatively long-lived plasma using tunable ultra-short intense X–ray free-electron laser (FEL) or orion laser etc. and the importance of accurate theoretical estimation of the structural and spectral properties of plasma embedded few–body systems for diagnostic determination of such plasmas. In this context, the progress of atomic structure calculation starting from the hydrogen atom problem to general three–body problem is discussed. The fundamental notions of classifying and defining the quantum states of a three–body or two–electron system have been given. In this chapter we have introduced 'plasma' by defining its salient features, controlling parameters (particle density, temperature etc.) and abundance in both laboratory and astrophysical environments. Classification of plasma has been made on the basis of plasma particle distribution function (*classical plasma* and *quantum plasma*) as well as plasma coupling parameter (*weakly coupled plasma* and *strongly coupled plasma*) defined as the ratio of the average electrostatic energy to the average kinetic energy of the plasma particles. As plasma contains a large number of charged particles, the collective interaction is very difficult to tackle theoretically. Hence, a suitable model potentials are considered which incorporate the collective behaviors of the plasma particles. The analytic expressions of the model potentials in case of classical weakly coupled plasma, classical strongly coupled plasma, quantum plasma and dusty plasma are given at the end of this chapter.

Chapter 2

In recent studies, H–like ions in motion within the plasma environment have become increasingly significant from an experimental standpoint. Depending on plasma parameters and ion velocity, a moving ion produces a 'wake' which alters the potential of the medium. This potential modifies the energy levels and transition properties of the ion. Firstly we give a detailed account of the works on structural properties of H–like ions under classical weakly coupled plasma, quantum plasma and dusty plasma environments. Starting from electrostatic considerations, we have presented the mathematical development of the model potential in plasma environment using Meijer's G function for an ion moving through classical weakly coupled plasma, classical dusty plasma and quantum plasma environments. We have used trial wavefuntion expanded in Slater-type orbitals and subsequently solved the

Schrödinger equation under the framework of Ritz variational principle to estimate the energy eigenvalues of ions moving through plasma. The analytic forms of the matrix elements and relevant basis integrals are given in relevant sections of this chapter. In the subsequent section, the results and discussions are illustrated in detail. It is observed that the plasma potential removes the l–degeneracy of the energy levels and the motion of the ion removes the $|m|$–degeneracy ('Stark-like' splitting). The present work discusses how plasma density, temperature, and ion velocity affect hydrogenic energy levels and the transition wavelengths of π and σ components of Lyman-α lines.

Chapter 3

In this chapter we have discussed the variation of ground state energy of different quantum mechanical three–body systems with arbitrary comparable masses, embedded under classical weakly coupled plasma. We have also estimated the energy and width of resonance S^e state of free hadronic three–body systems. In first section an extensive literature review is given describing the works on both bound and resonance state properties of three–body systems under plasma environments. At the beginning of methodology section, the construction of trial wavefunction and variational equation are given in a most exhaustive way possible. The trial wavefunction is expanded in multi-exponent Hylleraas-type basis set. The analytic form of necessary basis integral is given and demonstrated with some practical examples. In the last part of the methodology section, we have made a detailed discussion on the theory of stabilization method to estimate resonance parameters (energy and width). The results are given separately for bound and resonance states. In case of bound state, we have reported "Borromean binding" for various three–body systems under classical WCP whereas resonance parameters of S^e state of three–body exotic ppY and pYY $[Y : \mu, \pi, K]$ ions in the free environment are given.

Chapter 4

In this chapter we focus on the determination of structural properties of doubly excited F^e state of two–electron systems under both free and plasma (WCP) environment. A detailed account on doubly excited states of two–electron systems under different plasma scenario is given at the starting of this chapter. In the next section we elaborate the present methodology in the following steps: formation of trial wavefunction, construction of variational equation, expansion of trial wavefunction in multi–exponent Hyllerass–type basis set and analytical formulation of the relevant basis integrals. A detailed discussion on different structural properties (energy eigenvalues, one– and two–particle moments, inter–electronic angles etc.) of both meta–stable bound and resonance F^e states of free two–electron systems is given in the next segment. The methodology established for free systems is then extended to estimate different structural properties of two–electron systems embedded in classical WCP environment. The study on the variation of transition energies for the dipole transitions $F^e \rightarrow D^o$ with respect to the plasma screening strength is also included in this section.

Chapter 5

In this chapter we finally conclude all the findings from the present dissertation's works as described in previous chapters. A consolidated account of the present work on the accurate determination of the structural properties of the few–body atomic systems which are necessary for astrophysical data analysis as well as in laboratory plasma diagnostics is presented. We also discuss the potential future scopes of these works involving atomic structure calculation in different external confining environment which may be significant in different fields of research.

List of Publications

Peer reviewed publication included in the thesis:

1) *Exotic systems under screened Coulomb interactions: a study on Borromean windows*
S. Dutta, J. K. Saha, S. Bhattacharyya, P. K. Mukherjee and T. K. Mukherjee
Phys. Scr., **89**, 015401 (2014).

2) *Precise energy eigenvalues of hydrogen-like ion moving in quantum plasmas*
S. Dutta, J. K. Saha and T. K. Mukherjee
Phys. Plasmas, **22**, 062103 (2015).

3) *Binding Energies of Hydrogenlike Carbon under Maxwellian Dusty Plasma Environment*
S. Dutta, J. K. Saha, S. Bhattacharyya and T. K. Mukherjee
Int. Rev. of Atomic and Molecular Physics. **6(2)**, 73 (2015).

4) *Ritz variational method for the high-lying nonautoionizing doubly excited* $^{1,3}F^e$ *states of two-electron atoms*
S. Dutta, A. N. Sil, J. K. Saha and T. K. Mukherjee
Int. J. Quan. Chem., **118**, e25577 (2017).

5) *Extensive investigations for metastable-bound and resonance* $^{3}F^e$ *states of He atom*
S. Dutta, A. N. Sil, J. K. Saha and T. K. Mukherjee
Int. J. Quan. Chem., **119**, 25981 (2019).

6) *Doubly Excited* $^{1,3}F^e$ *States of Two-Electron Atoms under Weakly Coupled Plasma Environment*
S. Dutta, J. K. Saha, S. Bhattacharyya and T. K. Mukherjee
Commun. Theor. Phys., **71**, 853 (2019).

7) *Resonance States of Hadronic Three-Body Ions: Stabilization Method*
S. Dutta, J. K. Saha, S. Bhattacharyya and T. K. Mukherjee
Jour. At. Mol. Cond. Nano Phys., **7**, 51 (2020).

8) *Precise structure calculations of* $^{1,3}F^e$ *states of helium atom under exponentially screened Coulomb potential*

A. N. Sil, S. Dutta, D. Ghosh, J. K. Saha, S. Bhattacharyya and T. K. Mukhopadhyay
Atomic Data and Nuclear Data Tables, **158**, 101649 (2024).

9) *A study of hydrogenic ions moving through plasma environment: formulation of model potential and determination of energy levels*
S. Dutta, J. K. Saha, S. Bhattacharyya and T. K. Mukhopadhyay
Final version submitted for publication as a chapter in the book 'A closer look at the H atom' Ed. A K Roy, Nova Science Publisher.

Peer reviewed publication not included in the thesis:

1) *Structural properties of lithium atom under weakly coupled plasma environment*
S. Dutta, J. K. Saha, R. Chandra and T. K. Mukherjee
Phys. Plasmas, **23**, 042107 (2016).

2) *A survey on modelling and structural modification of atomic systems in plasma environment*
S. Dutta, J. K. Saha, S. Bhattacharyya and T. K. Mukherjee
Asian Journal of Physics, **25**, 1339 (2016).

3) *Critical stability and quantum phase transition of screened two–electron system* A. Sadhukhan, S. Dutta and J. K. Saha
Int. J. Quan. Chem., **119**, 26042 (2019).

4) *Critical stability and structural properties of screened two–electron system in Feshbach resonance state* A. Sadhukhan, S. Dutta and J. K. Saha
Eur. Phys. J. D , **73**, 250 (2019).

List of Conferences Attended

Presentation in Conferences/Seminars:

1) Participated in "*3rd DAE-BRNS Symposium on Atomic, Molecular and Optical Physics*" held at Indian Institute of Science Education and Research (IISER), Kolkata, during December 14–17, 2012.

2) Participated in "*DST-SERC School on Physics of Highly Charged Ions*" held at TIFR, Mumbai, during February 10–March 3, 2013.

3) Participated in "*Topical Conference on Atomic Processes in Plasma ISAMP-TC-2013*" held at Institute for Plasma Research (IPR), Gandhinagar, Gujrat, during November 18–20, 2013.

4) Participated and delivered a talk in "*International Conference on Dynamical Systems and Mathematical Biology(ICDSMB 2014)*" held at Department of Mathematics, Jadavpur University, Kolkata–700026, during November 17–19, 2014.

5) Participated and delivered a talk in "*UGC Sponsored National Seminar on Frontiers in Modern Physics*" held at Department of Physics, Jogamaya Devi College, Kolkata–700026, during November 21–22, 2016.

6) Participated and delivered a talk in "*International Conference on Science, Technology and Communication Skills (TCSCON-2024)*" held at Department of Basic Science and Humanities, Narula Institute of Technology, Kolkata, during February 22–24 , 2024.

Chapter 1

Introduction

Introduction

In the microscopic world, few–body physics includes the studies of light nuclei, light atoms, small molecules etc. Since the very infant age of quantum mechanics, few–body atomic systems are always under the spotlight for being an important candidate for testing the hypotheses and laws of the quantum mechanics. In 1926, Schrödinger computed [1] the energy eigenvalues of hydrogen atom from his revolutionary matter-wave equation and arrived in good agreement with that of obtained by Neils Bohr using quantum theory [2]. While the hydrogen atom or the two–body atomic problem is exactly solved by the wave-mechanics [1], difficulty arises when there are more than two interacting particles, even though all the interacting forces are known. The presence of $\frac{1}{r_{ij}}$ term in the Hamiltonian of the few-body systems makes the Schrödinger equation non-separable, r_{ij} being the distance between the $i-$th and the $j-$th particles. Since the earlier days of quantum mechanics theoreticians assumed [3–8] approximation techniques like perturbation, variation etc., to solve the two–electron problem which is the simplest candidate among the few-electron systems. In case of the few–electron systems, the Born–Oppenheimer approximation [9] is applied where the nucleus is assumed to be infinitely heavy and its motion is negligible with respect to the motion of the electrons. Slater [3] used perturbation technique to find the energy spectra of helium atom without making any attempt to separate the variables at all. Hartree [4, 5] made the central field approximations to solve the wave equation of helium atom problem where the Hamiltonian boils down to effective one-electron Hamiltonians. Slater [3] and Hartree [4, 5] calculated the ground state energy of helium atom as -2.895 a.u. and -2.86168 a.u. respectively. These values are little above the experimental value -2.9035 a.u. known at that time which was obtained by Lyman [10] in 1924. The experimental determination of ground state of helium atom become more precise in later years. For example, Bergeson *et. al.* [11] reported the energy of helium in ground state as $-2.903\ 693\ 775$ a.u. In 1928 and 1929, Hylleraas [6–8] adopted Ritz variational method with 18 to 38 terms in the basis set of trial function which contained the inter-electronic distance r_{12} explicitly. For obvious reason, this type of basis functions are called correlated basis. The best result he got for the ground state energy of helium atom is -2.9037 a.u. [7]. Since this work, till now the researchers are applying quantum-mechanical approximation techniques using various basis sets and optimization programs to determine highly precise energy levels of helium atom. The works of Pekeris [12] and Drake [13] are quite significant in this matter where they estimated the non-relativistic energy eigenvalue of the ground state of helium as $-2.903\ 724\ 376$ a.u. and $-2.903\ 724\ 377\ 03415$ a.u. respectively. Over the years theoreticians enjoyed competing with one another on the determination of more and more precise ground state energy of helium atom [14–22] just like the mathematicians do to add more digits of the number 'π'. Moreover, it can be seen that the variational non-relativistic energy estimates [12–22] are lower than that of the experimental result [11]. This

is because of the fact that the non-relativistic energy values needs corrections regarding the nuclear motion or the QED effects. These corrections were made by the researchers [23–26] considering the nuclear mass of ^{4}He atom as $M(^4\text{He}) = 7294.299508$ a.u. which produces ground state energy of helium atom as $-2.903\ 304\ 557\ 7$ a.u. (upto 10-th decimal place). Before we proceed further, we first describe the spectroscopic notations used here. Here we have used the usual spectroscopic notation $^{2S+1}L^{\pi}$ under the $LS-$coupling scheme, where S, L and π are the total spin, orbital angular momentum and parity quantum numbers respectively. It is to be noted that the parity of the coupled state is determined by the formula $\pi = (-1)^{l_1+l_2}$ where l_1 and l_2 are the individual angular momenta of the particles. If $\pi = +1$, the corresponding coupled state (L) is called as *even parity* ('e') state and for $\pi = -1$, the corresponding coupled state (L) is called as *odd parity* ('o') state. Again, if the factor $(-1)^L$ becomes equal to $(-1)^{l_1+l_2}$, then the coupled state L is called a *natural parity* state. On the other hand, if the factor $(-1)^{L+1}$ becomes equal to $(-1)^{l_1+l_2}$, then the coupled state L is called an *unnatural parity* state. Table (1.0.1) shows some examples of natural and unnatural parity states. Expanding the trial function in Hylleraas basis is the most efficient technique to include correlation effects on the two-electron energy levels. Hylleraas's calculations are applied to the ground state of helium with a spherically symmetric angular part of the wave function. The distance of the electrons (r_1, r_2) from the nucleus at origin and the angle (θ_{12}) between them were employed to express the wave function. The situation is more challenging for the states other than S symmetry. A two–electron system has 9 degrees of freedom. Due to the invariance of the Hamiltonian under translation and rotation, Wigner [27] and Breit [28, 29] demonstrated that the number of independent variables in the Schrödinger equation can be reduced from nine to three. By taking the advantage of translational symmetry of Hamiltonian, the problem of two electrons with a fixed nucleus is represented in six coordinates, three of which are the sides of the triangle formed by the nucleus and two electrons and the remaining three are the Eulerian angles defining the triangle's orientation in space. These angles are needed to be separated out leaving the Schrödinger equation in only three radial coordinates. Since the total angular momentum is a constant of motion, the problem could be reduced to three dimensions regardless of how the Eulerian angles were specified. Breit [28, 29] adopted Hylleraas coordinates using the same Eulerian angles as were introduced by Hylleraas [7], known as 'Hylleraas-Breit angles' which were quite unsymmetrical with respect to two electrons and hence very difficult to separate it out from the Schrödinger equation. As a result, Breit's [29] research was limited to the $(1s2p;\ ^1\text{P}^o)$ state of helium atom. Bhatia and Temkin [30] made the first successful attempt at generalizing the helium atom problem by using symmetric Eulerian angle decomposition technique. Because of their symmetry and exchange properties, the Euler angles utilized by Bhatia and Temkin [30] have an obvious advantage over the Hylleraas-Breit angles, and consequently the Eulerian angles were removed from the Schrödinger equation for any angular momentum state of a two-electron system just like the separation of the

Table 1.0.1: Spectroscopic notation of coupled angular momentum (L) states of two–electron systems along with the electronic configurations (having individual angular momenta l_1 and l_2) for each coupled state. The superscripts e and o in the notation stand for 'even' and 'odd' parities respectively.

Parity of states	Spectroscopic terms	Configurations
Natural	$^{}\mathrm{S}^{e}$ $(L=0)$	ss $(l_1=0, l_2=0)$
		pp $(l_1=1, l_2=1)$
		etc...
	$^{}\mathrm{P}^{o}$ $(L=1)$	sp $(l_1=0, l_2=1)$
		pd $(l_1=1, l_2=2)$
		etc...
	$^{}\mathrm{D}^{e}$ $(L=2)$	sd $(l_1=0, l_2=2)$
		pp $(l_1=1, l_2=1)$
		etc...
Unnatural	$^{}\mathrm{P}^{e}$ $(L=1)$	pp $(l_1=1, l_2=1)$
		dd $(l_1=2, l_2=2)$
		etc...
	$^{}\mathrm{P}^{0}$ $(L=2)$	pd $(l_1=1, l_2=2)$
		df $(l_1=2, l_2=3)$
		etc...
	$^{}\mathrm{P}^{e}$ $(L=3)$	pf $(l_1=1, l_2=3)$
		dd $(l_1=2, l_2=2)$
		etc...

polar and azimuthal angles from the Schrödinger equation of hydrogen atom problem. This symmetric Eulerian angle decomposition technique was employed later in many works to investigate P, D, F states [31–37]. In 1994, Mukherjee and Mukherjee [38] were able to put out the general variational equation for states of arbitrary angular momentum for two–electron systems in radial co–ordinates (r_1, r_2, r_{12}) of the triangle formed by the nucleus and two electrons using the wave function provided by Bhatia and Temkin [30].

Among all these two–electronic states, doubly excited states (DES) lie above the first $(N = 1)$ ionization threshold of the one–electron sub–system. In DES of two–electron systems, $2s^2$ ($^1\mathrm{S}^e$), ($2s2p^{1,3}\mathrm{P}^o$), $2p^2$ ($^1\mathrm{S}^e$,$^3\mathrm{P}^e$,$^1\mathrm{D}^e$) etc. lie below $N = 2$ ionization threshold, $3s^2$ ($^1\mathrm{S}^e$), ($3s2p^{1,3}\mathrm{P}^o$), $3p^2$ ($^1\mathrm{S}^e$,$^3\mathrm{P}^e$,$^1\mathrm{D}^e$) etc. lie below $N = 3$ ionization threshold and so on. DES are embedded in continuum and hence the effect of continuum states are inherent in their description or structure. The DES may be formed experimentally in two different ways which are illustrated below:

1. **Electron scattering experiment:** If a He^+ ion in any arbitrary angular momentum

state nl above $N = 1$ ionization threshold, is bombarded by an electron with right amount of kinetic energy, a DES He** ($nln'l'$) can be formed ($n, n' \geq 2$), where l and l' are the angular momentum quantum numbers of the electrons in He–atom.

$$e^- + \mathrm{He}^+(nl) \rightarrow \mathrm{He}^{**}(nln'l')$$

2. **Photo-absorption experiment:** In this case, He–atom absorbs a photon, *e.g.* when placed in a synchrotron radiation chamber, to get excited to a DES as

$$h\nu + \mathrm{He}(1snl) \rightarrow \mathrm{He}^{**}(nln'l')$$

DESs can go through transitions to lower levels by emitting photons (*radiative* or *fluorescence* decay). On the other hand, since the DES are embedded in the continuum they interact with the continuum states due to the repulsive potential $\frac{1}{r_{12}}$. As a result the two-electron system in DES can undergo a non-radiative transition, called '*auto-ionization*', in which DES decay to a lower state of ionized one–electron sub–system of the two–electron system. For example:

$$\mathrm{He}^{**}(2s2p;^{1,3}P^o) \rightarrow \mathrm{He}^+(1s) + e^-$$
$$\mathrm{He}^{**}(2p^2;^1D^e) \rightarrow \mathrm{He}^+(1s) + e^-$$

As discussed earlier, a projectile needs to have an exact amount of energy to form an autoionizing DES. At this particular energy a sharp peak or 'resonance' can be seen in the continuous absorption spectrum (in photo-absorption experiment) or scattering cross-section (in electron-scattering experiment). For this reason, autoionizing states are also known as *resonance states*. On the basis of angular momentum and parity conservation rule under the LS-coupling scheme, Feldman and Novick [39] showed that autoionization is allowed only for those transitions for which $\triangle L = 0$, $\triangle S = 0$ and $\triangle \pi = 0$. The above examples satisfy these criteria whereas the following examples are forbidden:

$$\mathrm{He}^{**}(2p^2;^3P^e) \nrightarrow \mathrm{He}^+(1s) + e^-$$
$$\mathrm{He}^{**}(2p3d;^{1,3}D^o) \nrightarrow \mathrm{He}^+(1s) + e^-$$

Between $N = 1$ to $N = 2$ ionization threshold the DESs with natural parity shows auto-ionization/resonance character whereas the DESs with unnatural parity is stable against auto-ionization, called *meta-stable bound states* (MBSs) which are prone to decay via fluorescence transitions. Above $N = 2$ ionization threshold, all the DESs are auto-ionizing in nature. This theory is well supported by a number of experiments where the fluorescence

and auto-ionizing lifetimes of various DESs are measured [40–44]. For example, the fluorescence lifetime of $2p^2$ ($^3P^e$) and $2p3d$ ($^{1,3}D^o$) states of He-atom are 80 ± 7 ps [40] and 110 ± 20 ps [41] respectively. On the other hand, the auto-ionization lifetimes of $2s2p$ ($^{1,3}P^o$) and $2p^2$ ($^1D^e$) states of He-atom are found to be 17 ± 2 fs [42] and 9.1 ± 2.3 fs [44] respectively. In the beginning of this century, a new feature of the DESs is discovered due to the experiments [45,46] which found that fluorescence decay is more probable than auto-ionization for some definite resonance states. Saha *et. al.* [47] showed theoretically that the angular part of the wavefunction determines which resonance states will show fluorescence activeness over the auto-ionizing phenomena. This theory was verified in a heavy-ion collision experiment performed by Kasthurirangan *et. al.* [48] where they measured both fluorescence and auto-ionization rates of the $2p3d$ ($^1P^o$) state of highly charged two–electronic systems like Si^{13+}, S^{14+} and Cl^{15+}. For example, the experiment [48] showed that the auto-ionization rate (3.204×10^{12} s^{-1}) is lesser than the fluorescence rate (3.28×10^{12} s^{-1}) of the $2p3d$ ($^1P^o$) state of Si^{13+} ion. DESs have attracted a lot of attention in researches because they are best suited for theoretical studies on resonance phenomena which are important in plasma physics, astrophysics, laser-technology etc [49–51].

In case of general three–body systems with comparable masses Born-Oppenheimer approximation [9] of fixed nucleus is not applicable for constructing the variational equation. The centre of mass coordinates and the symmetric Eulerian angles can be separated out of the equation [52] by exploiting the translational and rotational invariance of Hamiltonian respectively. The effective variational equation of three–body system is then reduced to three dimension which may be taken as the sides (r_1, r_2, r_{12}) of the triangle formed by the three–body system [53]. The classification scheme of various states of a general three-body system is similar to that of the two–electron systems.

Structural calculation of atomic systems under plasma environment is a field of active research due to its application in plasma diagnostics. H–like and He–like spectral transitions in plasma environment play a major role in these aspects. Lyman-α line ($n = 2 \rightarrow 1$ transition) and Balmer-α line ($n = 3 \rightarrow 2$ transition) are of particular importance in case of H–like systems. Lyman lines are used for diagnostics of ions with higher energies. Balmer lines are used to measure many things like magnetic and electric fields through Stark-Zeeman splitting, fluctuations in the electron density *etc.* For He–like systems, He_α ($1s2p \rightarrow 1s^2$), He_β ($1s3p \rightarrow 1s^2$) lines as well as He–like satellite lines ($2p^2 \rightarrow 1s2p$) etc. play significant role in plasma diagnostics. Line shifts, line profile and broadening, line merging phenomenon, relative intensities of spectral lines, continuum lowering and ionization potential depression, disappearance of spectral lines *etc.* are useful tools for plasma diagnostics *i.e.* to measure particle density and equilibrium temperature of the plasma. Hence, precise atomic data are needed for the understanding of them. Depending on plasma conditions *i.e.* equilibrium temperature and densities of plasma species, the atomic energy levels and transitions are

modified. This modification of atomic data is important for determining the plasma conditions. Huge technological advances have occurred in the last couple of decades, as a result of which atomic spectroscopy has taken on an intriguing shape in plasma studies. The use of X-ray free electron lasers (XFELs) in Linac coherent light source (LCLS), Orion lasers and other lasers, is critical in such advancements [54–57].

For a free atom/ion, all the particles within the atom interact with each other via Coulomb potential. But the inter–particle interaction changes its form from Coulombic to non–Coulombic when the atom/ion is placed in plasma, which will alter the structural properties of the atom/ion as compared to the free environment. It is true that most of the structural modifications can be addressed considering the atom/ion to be static. However, the motion of the ions or nucleus of atom with high velocity through the 'sea' of electrons in plasma creates a 'wake'. Depending on the plasma parameters and ion velocity, this 'wake' can sufficiently alter the potential 'seen' by the ion. As a consequence, the energy levels and transition properties are also modified. It is worth noting that the fast ions in plasma are quite difficult to detect, but their 'wakes' can be detected experimentally, *e.g.* by Collective Thomson Scattering (CTS) technique [58]. Tracking the fast ions, *e.g.* hydrogen, deuterium, tritium, α-particles inside plasma has attracted sufficient interest from researchers in recent years because these ions are often major source of energy and momentum of plasma and it carries important information about the plasma. Fast ions are also crucial ingredients of a burning fusion plasma. Many techniques like Fast Ion D-α (FIDA) Spectroscopy [59], $\gamma-$ray spectroscopy (GRS) [60], CTS *etc.* are employed to detect fast ions in plasma in various experimental projects *e.g.* the ITER project [61–63], ASDEX Upgrade [64], Joint European Torus (JET) [65] *etc.* These experiments require precise theoretical atomic data of H-like systems moving in such plasma environments. Within the plasma, some of the injected fast ions undergo nuclear reactions and other fast ions neutralize and emit light. By analyzing the signals coming out of the fast ions, information about the velocity and the distribution of fast ions in plasma can be obtained.

The present study focuses on application of atomic data inside plasma environment. In ion-atom or electron-atom collision experiments, all kind of bound and resonance states are produced simultaneously in the collision chamber. The possibility of the formation of plasma in collision experiment is very high as large number of electrons and different charge states of ions are produced. By using advanced technologies such as ion source technology, storage ring capabilities and trapped ion techniques, a wide spectrum of target atom is attainable to study ionic resonances and even spectral properties of ions embedded within plasma. Hence, atomic structure calculations under plasma confinement is a very significant topic of research for both theoreticians and experimentalists.

Let us now construct a conjunctive idea on plasma. The name "*plasma*" was first introduced by Irving Langmuir in 1928 [66] while studying oscillations in ionized gas. In the Greek dictionary, "plasma" means something "formed" or "moulded". In the following year,

Tonks and Langmuir developed the theory of oscillating ions in the ionized gas which is famously known as "plasma oscillation theory" [67]. A very compact review on the historical developments of plasma can be found in a book written by Paul M. Bellan [68]. Plasma is considered as a medium which contains a large number of charged particles (electrons and ions), charge-neutral particles, macroscopic particles (large molecules or dust particles) etc., all moving due to thermal agitation. At any instant the interior of a plasma net charge within a macroscopic volume remains zero. With the help of terrestrial and astrophysical observations, scientists believe that 99% of the universe is made up of plasma. Very common examples of astrophysical plasma are Solar corona, nebulae, rings of Saturn, tails of comet etc. Plasma is the reason behind their continuous source of energy. In earth's atmosphere, lightening, ionosphere etc. behave like plasma medium. Due to plethora of plasma in natural objects, scientists are always keeping their eyes on the making of such plasma environments in the laboratory scenario so that we can understand our universe better and produce a sustained source of energy [61, 69–71].

If the plasma temperature (T) becomes very high $\left(T \backsim 10^4 - 10^8 K\right)$, the thermal de Broglie wavelength of the particles (λ_B) turns out to be less than the average inter-particle distance (d_m), which causes the plasma particles to become distinguishable and obey the Maxwell-Boltzmann distribution. This type of the plasma is called *classical plasma*. Classical plasma can be found in ionosphere [72], interstellar space [73], solar coronal region [74], typical electric discharge [75], tokamak experiment (magnetic confinement fusion) [71], inertial confinement fusion (ICF) experiments [61, 70] etc. On the other hand, for very low temperature ($T \backsim 0 - 20K$), λ_B becomes greater than d_m. As a result, the plasma particles become indistinguishable and follow the quantum distribution laws. Such type of plasma is called *quantum plasma* (QP) which can be found in astrophysical objects like Jupiter's core, white dwarf star (high temperature quantum plasma) etc. [76] and can be produced in laboratory experiments such as metals and metal clusters, quantum dots and quantum wires [77], intense laser-solid density plasma interaction experiments [78] etc.

A quantity called *Coulomb coupling parameter* or simply *Coupling parameter* (Γ), defined as the ratio of the average electric interaction energy to the average kinetic energy of the plasma particles, plays a pivotal role to classify plasma on the basis of the plasma particle correlations. The plasma for which $\Gamma < 1$ is called *weakly coupled plasma* (WCP) and for $\Gamma \geq 1$, the plasma is called *strongly coupled plasma* (SCP) or non-ideal plasma. WCPs are generally of very high or moderately high temperature and low density (n) plasma which can be found [79, 80] in gaseous nebula ($T \sim 10^4 K$ and $n \sim 10^3/c.c$), solar coronal plasma ($T \sim 10^6 - 10^7 K$ and $n \sim 10^6 - 10^7/c.c$), solar wind ($T \sim 10^5 K$ and $n \sim 10/c.c$), the gaseous discharge plasma ($T \sim 10^4 K$ and $n \sim 10^7 - 10^{12}/c.c$), plasma in controlled thermo-nuclear reaction ($T \sim 10^8 K$ and $n \sim 10^{15}/c.c$), inertial confinement fusion plasma ($T \sim 10^8 K$ and $n \sim 10^{25}/c.c$), Tokamak plasma ($T \sim 10^5 - 10^7 K$ and $n \sim 10^{14}/c.c$). Typical densities of SCPs are $n \geq 10^{23}/c.c.$ and temperatures are low (in few Kelvin). Such plasmas can

be found in laser produced plasmas, highly evolved stars in high density states, interior of Jovian planets, pulsed MHD generators, explosive shock tubes, two-dimensional states of electrons trapped in surface states of liquid helium etc. [81, 82].

The most important part of theoretical investigations is to model the plasma environment by an effective potential $V_{eff}(r)$ felt by a foreign atom/ion placed inside the plasma. There are many types of plasma model potentials $V_{eff}(r)$ available in literature, some of which are listed below.

1. **Classical WCP:** If the atom or ion is embedded in the classical WCP environment, the effective potential at a point around the nucleus having charge Z can be modeled by [83]

$$V_{eff}(r) = -\frac{Z}{r}e^{-\mu_D r} \tag{1.0.1}$$

This potential is known as *Exponentially Screened Coulomb Potential* (ESCP) or *Debye-Hückel Potential*. In this equation (1.0.1) the *screening parameter* is given by

$$\mu_D = \frac{1}{\lambda_D} = \left(\frac{K_B T}{4\pi q^2 n}\right)^{-1/2} \quad \text{(in C.G.S unit)} \tag{1.0.2}$$

where λ_D is called *plasma screening length* or *Debye screening length* which depends on plasma density (n) and temperature (T) of plasma.

2. **Classical SCP:** Over the years, many compact forms of the effective potential $V_{eff}(r)$ are constructed to model the classical SCP or dense plasma environment, such as ion-sphere model [81], Thomas-Fermi model [84, 85], Quasi-molecular model [86, 87], Crowly's fried egg model [88], DFT based ion-correlation models [89], Libernan's inferno model [90,91] etc. Among these models, the ion-sphere model [81] is quite simple yet capable in estimating the plasma parameters with the help of atomic structure calculations under classical SCP environment. In this model the charge neutrality is maintained by both free and bound electrons with the central positive ion inside the ion-sphere (IS) or Wigner-Seitz sphere. The effective potential is given as following

$$V_{eff}(r) \quad = \quad -\frac{Z}{r} - \frac{(Z-N)}{2R}\left[3 - \left(\frac{r}{R}\right)^2\right] \tag{1.0.3}$$

From the charge neutrality condition within the sphere, the IS radius (R) is connected with the plasma electron density (n) by the following relation

$$n = \frac{Z-N}{\frac{4}{3}\pi R^3} \tag{1.0.4}$$

where Z is the nuclear charge of the ion at the centre of IS and N is the number of bound electrons in the ion.

3. **Quantum plasma:** Generally this kind of plasma falls into the SCP category. In 2008, Shukla and Eliasson [92] modeled the potential around a test charge (of charge Z) embedded in a cold and dense quantum plasma under the framework of linearized quantum hydrodynamic theory where it is assumed that the quantum force acting on the electrons are dominant over the quantum statistical pressure. The potential is known as *exponentially cosine screened Coulomb potential* (ECSCP) which assumes the following form

$$V_{eff}(r) = -\frac{Z}{r}\exp\left(-\frac{k_Q r}{\sqrt{2}}\right)\cos\left(\frac{k_Q r}{\sqrt{2}}\right) \tag{1.0.5}$$

where $k_Q = \left(\frac{4m^2\omega_{pe}^2}{\hbar^2}\right)^{1/2}$ is the quantum wavenumber. The plasma electron frequency (ω_{pe}) is given by the relation

$$\omega_{pe} = \left(\frac{4\pi n_e q_e^2}{m_e}\right)^{\frac{1}{2}} \quad \text{(in C.G.S)} \tag{1.0.6}$$

n_e, q_e and m_e being the number density, charge and mass of electron respectively.

In addition to the plasma model potentials described above there are some other model potentials which are also important for the atomic structure calculations under plasma environments *e.g.* potential in classical dusty plasma (DP) [93], potential in non-Maxwellian astrophysical plasma [94–96] etc. A unified model potential in dense plasma is given by Stanton and Murillo [97].
These models, in conjunction with various quantum mechanical approximation techniques, yield valuable outcomes that are significant within the context of plasma diagnostic studies. In the subsequent chapters of this dissertation, different structural properties of two–body and three–body systems have been demonstrated under various plasma scenario. Our study starts with the hydrogen atom (or H–like ion) moving through different types of plasma environments like classical WCP, QP and classical DP. The effective potential of the atom is evaluated by solving Poisson's equation where the plasmas are considered as dielectric media. Variation of energy eigenvalues with respect to plasma parameters (density and temperature) as well as ion velocity is studied using Ritz variation principle. We have further investigated the effect of plasma and ion velocity on different dipole transitions.

In the next phase, we have studied the structural properties of different three–body systems (including exotic ions) embedded in classical WCP where the effective potential is modelled by ESCP (1.0.1). For a wide range of plasma screening parameter (1.0.2), energy

eigenvalues of the ground state $1s^2$ ($^1S^e$) of three–body systems are estimated under the Ritz variational framework using a trial function expanded in multi-exponent Hylleraas-type basis set. Energy and width of resonance $^1S^e$ state below second ionization threshold of different hadronic three–body exotic ions are evaluated using stabilization method.

In the last part of the present study we focus on high-lying doubly excited F^e state of two–electron systems under both free and classical WCP environment. Ritz variational principle has been employed to determine the energy eigenvalues of metastable bound F^e states while stabilization method is used to estimate resonance parameters (energy and width) of resonance F^e states for different plasma screening. In this case, the trial function contains not only the most fundamental pf configuration but also a high–lying dd configuration for the F^e state, where both pf and dd parts are expanded in multi-exponent Hylleraas-type basis set. Other structural properties like one– and two–particle moments, inter–electronic angles etc. of both metastable bound and resonance F^e states of helium atom are also given for different plasma screening parameters.

Chapter 2

Moving H–like atom under plasma environment

Moving H-like atom under plasma environment

The structural properties of hydrogen–like (H–like) ions are quite important in plasma diagnostics because the features of hydrogenic lines (Lyman-α, Lyman-β, Balmer-α, Balmer-β etc.) in plasma environment carry important information about the plasma parameters like density and temperature. Plenty of works have been carried out by researchers in this direction where the ion is considered to be static. However, H–like ions which are in motion inside the plasma environment have become quite important from recent experimental point of view. As the ions move through the 'sea' of electrons, they leave a 'wake', the effect of which depends on the plasma parameters as well as on the ion velocity. The 'wake' alters the potential experienced by the ion and hence, the energy levels and transition properties are modified. In this chapter, we give a detailed account of formation of the model potential felt by the moving ion in both classical and quantum plasma. The dusty plasma environment is also considered. Starting from electrostatic considerations, we have presented the mathematical development of the model potential in plasma environment. This model potential is subsequently used to solve the Schrödinger equation using the variational principle to estimate the energy values and transition energies of ions moving through plasma. The effects of plasma density, temperature and ion velocity on the hydrogenic energy levels as well as on transition wavelengths of π and σ components of Lyman-α lines are discussed. Energy eigenvalues of several states of H-like carbon (C^{5+}) ion moving through electron–hole quantum plasma are provided at the end of this chapter for a range of plasma densities and ion velocities.

2.1 Literature review

In the presence of weakly coupled plasma (WCP), the interaction between the particles of an atom/ion changes from Coulomb to exponentially screened Coulomb potential (ESCP) as given in equation (1.0.1). Analytic solution of Schrödinger equation with ESCP is not possible even for the H-like atoms/ions which is the simplest candidate among the few body atomic systems. After the pioneering work by Ecker and Wiezel [98] using suitable physical approximations (known as 'Ecker-Wiezel approximation'), several other quantum mechanical approximation techniques like perturbation [99–104], variation [105–111], variation–perturbation theory [112], numerical techniques [113–116] etc. were adopted to solve the Schrödinger equation with ESCP for the H–like atomic systems. The removal of $l-$degeneracy and the reduction of the number of bound states of H–atom under WCP were reported in literature with different methodologies [100,101,105,106,113–115]. Using numerical techniques, Roger *et.al.* [115] showed that the number of bound states decrease almost linearly with plasma screening strength. Using variation technique, Lam and Varshni [107]

and Garavelli and Oliveira [109] reported comparable results with Rodger *et.al.* [115] except in the region very close to critical screening where the energy eigenvalues become zero. Alteration of other structural properties like the size of atoms, transition probability for spontaneous emission etc. under WCP can be found in literature [107, 108, 111, 117]. The estimation of structural properties of H–like atomic systems under WCP formed within spherical box grabbed attention of many researchers [103, 104, 111, 112] where modifications of transition energy, oscillator strength, transition probability, hyperpolarizability of photo-excitation etc., due to the alteration of the both plasma screening and the box radius were explored. The simultaneous effect of Plasma screening and external static electric field on the atomic properties was also studied for H–like systems [118, 119].

Theoretical investigations on the spectral properties of few-body systems under strongly coupled plasma (SCP) are limited as compared with those under WCP model. The main effects of SCP on H-like systems are to modify the energy levels, ionization potential of the systems, fine structure splitting, photo-absorption cross-sections etc. [120–123]. Structural properties of H-like systems like the spectral line shift, line broadening, continuum merging of bound states etc. under SCP are used by the theoreticians [124–127] to predict the density of hot-dense plasma produced by laser implosion. In these works, besides the adoption of ion–sphere (IS) model people also used self-consistent method or random phase approximation to the dielectric function of the medium to incorporate the effect of density of the plasma medium. Bhattacharyya *et. al.* [128] predicted line shifts of Lyman lines of H-like C^{5+}, Al^{12+} and Ar^{17+} and compared the IS and truncated Debye models using both non-relativistic and relativistic methods. The modifications of the dynamic polarizabilities, oscillator strengths and transition probabilities of H-like $He^{+}, Li^{2+}, Be^{3+}, B^{4+}$ and C^{5+} ions under SCP are reported by Sil *et. al.* [129] where they have assumed IS potential to model the plasma environment where the time-dependent variation-perturbation theory was employed. They have shown that the dynamic polarizability of the ions remains nearly invariant as IS radius decreases, but below a certain value of radius dynamic polarizability falls off abruptly. Li and Rosmej [130] proposed an analytic method where the energy values of LSJ-levels of H-like Al^{12+} ion are estimated using finite temperature and high density plasma represented by modified IS–model. Relativistic multi-configuration Dirac-Fock method has been employed by Chen *et. al.* [131] to estimate the effect of density of SCP on the energy levels, transition energies and oscillator strengths of transitions of highly charged H-like Ne^{9+}, Al^{12+} and Ca^{19+} ions. While in this work [131] the authors assumed IS-model, in a later investigation Chen *et. al.* [132] assumed a general model potential [97] to mimic the SCP environment which is dependent on both temperature and density. Within the relativistic framework built in Flexible Atomic Codes (FAC), Chen *et. al.* [132] estimated the variations of the ionization potentials, transition energies and photoionization cross-sections of H-like Al^{12+} ion with respect to different plasma temperatures and densities. Mukherjee *et. al.* [133] adopted non-relativistic generalized pseudospectral

method to estimate the multipole oscillator strengths, multipole polarizabilities and Shannon entropy of one-electron systems ($Z = 1 - 4$) under both WCP and SCP environments. Atomic structure calculations under dense quantum plasma grabs attention of a large number of theoreticians due to its huge abundance in semiconductor devices, quantum dots, quantum wires [134], neutron stars, white dwarfs [135], laser produced plasma [136], fusion plasma [137, 138] etc. The most celebrated model potential of the dense quantum plasma medium is exponentially cosine screened Coulomb potential (ECSCP) as given in equation (1.0.5). The effect of ECSCP on the bound states of one–electron systems started by adopting different approximation techniques like Ecker–Weizel approximation [139,140], hypervirial Pade scheme [141], 1/N expansion technique [142,143] etc. In the course of last few years, a large number of works [144–150] has been performed regarding the structure calculations of one–electron systems under dense quantum plasma environment. The variation of energy eigenvalues of nl ($n \leq 10, l = 0-9$) and $n'l'$ ($n' \leq 8, l' = 0-7$) states with respect to the screening parameters of ECSCP and generalized ESCP was extensively studied by Roy [144] where it was reported that the effect of ECSCP is stronger on the energy levels as compared to generalized ESCP. Hu *et.al.* [151] compared five different models used to describe dense quantum plasma, by calculating their effects on $1s$ energy level of H-atom using Ritz variation technique. Using Ritz variation technique with relativistic correction, Hu *et. al.* [146] showed that the probability of the radiative transition $1s \rightarrow np$ ($n = 2, 3$) of C^{5+}, O^{7+}, Al^{12+} and Si^{13+} ions, decreases as plasma density increases. Variation of oscillator strength and transition probability for the Lyman and Balmer series upto $n = 5$ with respect to temperature and density of dense quantum plasma was investigated by Zhou *et. al.* [148] where the authors used the finite temperature unified model potential given by Stanton and Murillo [97] to mimic the dense quantum plasma environment. Nayek *et. al.* [149] revealed the changes in the energy eigenvalues as well as the radial distribution of the wavefunction with respect to the screening of both ESCP and ECSCP for 36 bound states within $n \leq 8$ of one–electron systems having $Z = 1 - 18$. The critical screening parameters for every bound states of each systems are given in their study [149], for both ESCP and ECSCP. Ly *et. al.* [150] solved Schrödinger equation of H–atom under dense quantum plasma and uniform magnetic field by using highly accurate numerical technique to determine different bound state energy eigenvalues for different screening parameters of ECSCP describing the dense quantum plasma. Few studies on the variation of photoionization cross-section of H–atom under dense quantum plasma can be found in literature [145, 147].

From the above discussion on some of the earlier works done in the field of plasma–embedded H–like systems, it is evident that since the early days, the H–like ions play a key role in understanding plasma environment in various aspects. However, all of them were static. The moving H–ion in plasma for various reasons are gaining attention over the past few years. The modification of bound state properties of slowly moving one-electron systems under quantum plasma is studied by very few researchers in the literature [152, 153] where

the authors adopted Ritz variation principle and perturbation method with necessary relativistic corrections. The model potential considered in their works consisted of ESCP part and 'wake' part which is proportional to the velocity of the nucleus and varies as $\sim \frac{\cos\theta}{r^2}$ (θ is the polar angle and r is the radial distance from the nucleus). They have found [152] "Zeeman"–like splitting of the energy levels due to the influence of the wake part and the rates of different dipole transitions between the energy levels vary with the velocity of the nucleus.

In the subsequent sections of this chapter we will present different structural properties of H–like systems under classical weakly coupled plasma, quantum plasma and dusty plasma environments. Beginning with electrostatic considerations, we provided the mathematical development of the model potential for an ion moving through the plasma environments considered here. In the next step, we have employed Ritz variational principle using trial wavefuntion expanded in Slater-type basis set, to estimate the energy eigenvalues of H–like systems moving through plasma. In pertinent sections of this chapter, the analytical forms of the matrix elements and the necessary basis integrals are provided. The results and discussions are detailed in the next section. At the end of this chapter, the effects of temperature, ion velocity, and plasma density on hydrogenic energy levels as well as the transition wavelengths of π and σ components of Lyman-α lines are discussed.

2.2 Formulation of model potential: *the present method*

To obtain atomic data in plasma environment, we need to solve the Schrödinger equation for which the potential term is needed. As the number of the particles in the plasma medium is very large, it is difficult to obtain any ab-initio solution of the Schrödinger equation by incorporating all the interactions in the Hamiltonian under plasma environment. This difficulty may be overcome by considering a suitable model which may mimic all the collective interactions within the plasma.

2.2.1 Moving ion in classical weakly coupled plasma

Let us consider a test charge q moving with velocity $\vec{v}$ within a plasma medium which is considered as a linear dielectric medium. In figure (2.2.1) O is the origin where the charge q was initially ($t = 0$) situated and O$'$ is the present position of q at the instant 't' *i.e.* $\vec{OO'} = \vec{v}t$. We are interested to find the electric potential (V) at P due to the moving test charge q surrounded by the plasma particles and $\vec{OP} = \vec{R}$. Hence, $\vec{O'P} = \vec{r} = \vec{R} - \vec{v}t$ is the position vector of the field point with respect to the present position O$'$ of the test charge q. We begin from the Gauss's law in the medium as [154] (in S.I.),

$$\vec{\nabla}.\vec{D} = \frac{q}{\epsilon_0}\delta(\vec{R} - \vec{v}t) \qquad [\epsilon_0 = \text{Permittivity of free space}] \tag{2.2.1}$$

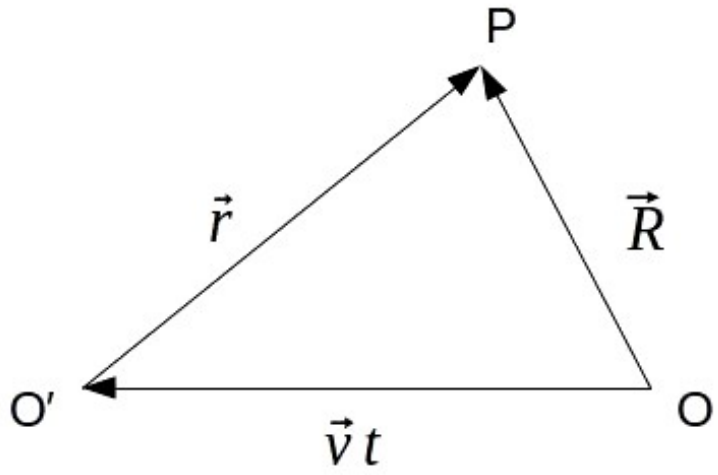

Figure 2.2.1: Relative position of the point of investigation P with respect to the initial position (O) and the later position (O′) of the moving charge q.

For a linear dielectric medium having dielectric function ϵ, the displacement vector is $\vec{D} = \epsilon_0\epsilon\vec{E}$; $\vec{E}$ being the electric field and is derived from the scalar potential V as $\vec{E} = -\vec{\nabla}V$. Equation (2.2.1) will become,

$$-\vec{\nabla}\epsilon.\vec{\nabla}V - \epsilon\nabla^2 V = \frac{q}{\epsilon_0}\delta(\vec{R} - \vec{v}t) \tag{2.2.2}$$

Taking Fourier transform on both sides of equation (2.2.2) into the momentum space ($\vec{k}$) of the moving plasma particles, we can get

$$\begin{aligned}
& -F.T.\left[\vec{\nabla}\epsilon.\vec{\nabla}V\right] - F.T.\left[\epsilon\nabla^2 V\right] = \frac{q}{\epsilon_0}F.T.\left[\delta(\vec{R} - \vec{v}t)\right] \\
\Rightarrow\quad & -\frac{1}{(2\pi)^{3/2}}\int\left(\vec{\nabla}\epsilon.\vec{\nabla}V\right)e^{-i\vec{k}.\vec{R}}d^3\vec{R} - \frac{1}{(2\pi)^{3/2}}\int\left(\epsilon\nabla^2 V\right)e^{-i\vec{k}.\vec{R}}d^3\vec{R} \\
& \qquad = \frac{q}{\epsilon_0}\frac{1}{(2\pi)^{3/2}}\int\delta(\vec{R} - \vec{v}t)e^{-i\vec{k}.\vec{R}}d^3\vec{R} \\
\Rightarrow\quad & +\frac{1}{(2\pi)^{3/2}}\int\left(\vec{\nabla}\epsilon.\vec{\nabla}V\right)e^{-i\vec{k}.\vec{R}}d^3\vec{R} + \frac{1}{(2\pi)^{3/2}}\left[|\vec{\nabla}V|\epsilon e^{-i\vec{k}.\vec{R}}\right]_{\text{at}\infty} \\
& -\frac{1}{(2\pi)^{3/2}}\int\left[\vec{\nabla}\epsilon - i\epsilon\vec{k}\right].\vec{\nabla}Ve^{-i\vec{k}.\vec{R}}d^3\vec{R} = -\frac{q}{\epsilon_0}\frac{1}{(2\pi)^{3/2}}e^{-i\vec{k}.\vec{v}t} \\
\Rightarrow\quad & i\frac{1}{(2\pi)^{3/2}}\int\left(\epsilon\vec{k}.\vec{\nabla}V\right)e^{-i\vec{k}.\vec{R}}d^3\vec{R} = -\frac{q}{\epsilon_0}\frac{1}{(2\pi)^{3/2}}e^{-i\vec{k}.\vec{v}t} \\
\Rightarrow\quad & ik\frac{1}{(2\pi)^{3/2}}\int\epsilon|\vec{\nabla}V|e^{-i\vec{k}.\vec{R}}d^3\vec{R} = -\frac{q}{\epsilon_0}\frac{1}{(2\pi)^{3/2}}e^{-i\vec{k}.\vec{v}t}
\end{aligned}$$

$$\Rightarrow \quad ikF.T.\left[\epsilon|\vec{\nabla}V|\right] = -\frac{q}{\epsilon_0}\frac{1}{(2\pi)^{3/2}}e^{-i\vec{k}.\vec{v}t}$$

$$\Rightarrow \quad ikF.T.\left[\epsilon\right] \times F.T.\left[|\vec{\nabla}V|\right] = -\frac{q}{\epsilon_0}\frac{1}{(2\pi)^{3/2}}e^{-i\vec{k}.\vec{v}t}$$

$$\Rightarrow \quad ik\epsilon(\vec{k}) \times ikV(\vec{k}) = -\frac{q}{\epsilon_0}\frac{1}{(2\pi)^{3/2}}e^{-i\vec{k}.\vec{v}t}$$

$$\Rightarrow \quad V(\vec{k}) = \frac{q}{\epsilon_0}\frac{1}{(2\pi)^{3/2}}\frac{e^{-i\vec{k}.\vec{v}t}}{k^2\epsilon(\vec{k})} \tag{2.2.3}$$

Here we have assumed that $\vec{\nabla}V$ or $(-\vec{E})$ is parallel to $\vec{k}$ *i.e.* the flow of plasma particles is longitudinal. $V(\vec{k})$ and $\epsilon(\vec{k})$ are the Fourier transform of the potential V and the dielectric function ϵ.
From the inverse Fourier transform of equation (2.2.3) into the $\vec{R}$-space and putting $\vec{r} = \vec{R} - \vec{v}t$, we obtain the potential $V(\vec{r})$ at field point P with respect to the instantaneous position of the test charge q as

$$V(\vec{r}) = \frac{q}{8\pi^3\epsilon_0}\int \frac{e^{i\vec{k}.\vec{r}}}{k^2\epsilon(\vec{k})}d^3\vec{k} \tag{2.2.4}$$

The dielectric function $\epsilon(\vec{k})$ carries all the information about the interactions including all types of collisions among the plasma particles and the charge velocity $\vec{v}$. The dielectric function for the classical electron-ion plasma [155] is given by

$$\epsilon(\vec{k}) = 1 + \sum_s \frac{1}{\lambda_s^2 k^2}\left(1 - i\sqrt{\frac{\pi}{2}}\frac{\vec{k}.\vec{v}}{kv_s}\right) = \frac{1+k^2\lambda_D^2}{k^2\lambda_D^2} - i\sqrt{\frac{\pi}{2}}\sum_s \frac{1}{v_s\lambda_s^2}\frac{\vec{k}.\vec{v}}{k^3} \tag{2.2.5}$$

where the *Debye Length* (λ_D) or often called the *screening length* is given by,

$$\lambda_D = \left(\sum_s \frac{1}{\lambda_s^2}\right)^{-\frac{1}{2}} \tag{2.2.6}$$

with

$$\lambda_s = \left(K_B T_s \epsilon_0 / q_s^2 n_s\right)^{1/2} \tag{2.2.7}$$

Here s signifies type of plasma species *i.e.* $s = e$ for plasma electrons, $s = i$ for plasma ions, $s = n$ for neutral atoms present in the plasma etc. λ_s is called the *screening length* or *Debye length* corresponding to the plasma species s. In equation (2.2.7) K_B is the Boltzmann constant and T_s, n_s and q_s are the plasma temperature, plasma number density

and charge state of the species s respectively. Thermal velocity of the species 's' is given by

$$v_s = \left(\frac{K_B T_s}{m_s}\right)^{1/2} \tag{2.2.8}$$

If the velocity of the test charge is assumed to be lower than the thermal velocities of the plasma particles *i.e.* $v < v_s$, then the inverse of the dielectric function may be approximated as

$$\frac{1}{\epsilon(\vec{k})} \approx \frac{k^2\lambda_D^2}{1+k^2\lambda_D^2} + i\sqrt{\frac{\pi}{2}}\frac{k\lambda_D^4}{(1+k^2\lambda_D^2)^2}\vec{k}.\vec{v} \times \sum_s \frac{1}{v_{ts}\lambda_s^2} \tag{2.2.9}$$

Substituting (2.2.9) into (2.2.4) we obtain $V(\vec{r}) = V_1 + V_2$, where

$$V_1 = \frac{q}{8\pi^3\epsilon_0}\int \frac{\lambda_D^2}{1+k^2\lambda_D^2} e^{i\vec{k}.\vec{r}} d^3\vec{k} \tag{2.2.10}$$

and

$$V_2 = i\sqrt{\frac{\pi}{2}}\frac{q}{8\pi^3\epsilon_0}\int \frac{\lambda_D^4}{k(1+k^2\lambda_D^2)^2}\vec{k}.\vec{v}\sum_s \frac{1}{v_s\lambda_s^2} \times e^{i\vec{k}.\vec{r}} d^3\vec{k} \tag{2.2.11}$$

Let us take a spherical polar coordinate (k, α, β) system such that the polar angle α is the angle between $\vec{r}$ and $\vec{k}$ and β is the azimuthal angle which lies in a plane perpendicular to $\vec{r}$. The volume element becomes $d^3\vec{k} = k^2 \sin\alpha d\alpha d\beta dk$ where $0 \le \alpha \le \pi$ and $0 \le \beta \le 2\pi$. Integrating over α and β, V_1 reduces to

$$V_1 = \frac{q\lambda_D^2}{2\epsilon_0\pi^2 r}\int_o^\infty \frac{k}{1+k^2\lambda_D^2}\sin krdk \tag{2.2.12}$$

We will solve the integral in equation (2.2.12) using Meijer's G function (MGF) technique, which will be further useful to evaluate other integrals appearing in V_2. The MGF is defined as [156]

$$G_{p\ q}^{m\ n}\left(\left.\begin{matrix}a_1,...,a_p\\ b_1,...,b_q\end{matrix}\right|z\right) = \frac{1}{2\pi i}\int_L \frac{\prod_{j=1}^m \Gamma(b_j - t)\prod_{j=1}^n \Gamma(1-a_j+t)}{\prod_{j=m+1}^q \Gamma(1-b_j+t)\prod_{j=n+1}^p \Gamma(a_j-t)} \times z^t dt \tag{2.2.13}$$

with the following conditions :

1. $0 \le m \le q$ and $0 \le n \le p$.
2. Poles of $\Gamma(b_j - t)$ must not coincide with the poles of $\Gamma(1 - a_j + t)$ for any j and l (where $j = 1, ..., m; l = 1, ..., n$), Γ being the Euler Gamma function.

3. Residue of $\Gamma(-p)$, p being a positive integer, is $Res\{\Gamma(-p)\} = \frac{(-1)^p}{p!}$

4. The integration path L (equation 2.2.12) are of three types :

   (a) where L runs from $-\infty$ to $+\infty$: the poles of $\Gamma(1-a_l+t)$ lie to the left and the poles of $\Gamma(b_j-t)$ lie to the right of L (where $j=1,...,m; l=1,...,n$). The conditions of convergence of the integration (2.2.13) are $p+q<2(m+n)$ and $|arg\ z|<\left(m+n-\frac{p}{2}-\frac{q}{2}\right)\pi$.

   (b) where L is a loop, begining and ending at $+\infty$: It encircles the poles of $\Gamma(b_j-t)$ $(j=1,...,m)$ once in the negative direction and all poles of $\Gamma(1-a_l+t)$ $(l=1,...,n)$ must remain outside the loop. The conditions of convergence of the integration (2.2.13) are, $q\geq 1$ and either $p<q$ or $p=q$ and $|z|<1$.

   (c) where L is a loop, begining and ending at $-\infty$: It encircles the poles of $\Gamma(1-a_l+t)$ $(l=1,...,n)$ once in the negative direction and all poles of $\Gamma(b_j-t)$ $(j=1,...,m)$ must remain outside the loop. The conditions of convergence of the integration (2.2.13) are, $p\geq 1$ and either $p>q$ or $p=q$ and $|z|>1$.

5. $G^{m\ n}_{p\ q}\left(\begin{matrix}a_1,...,a_p\\ b_1,...,b_q\end{matrix}\middle|z\right)$ is symmetric with respect to the set of parameters $(a_1,...,a_n)$, $(a_{n+1},...,a_p)$, $(b_1,...,b_m)$ and $(b_{m+1},...,b_q)$ *e.g.*

$$G^{2\ 3}_{5\ 4}\left(\begin{matrix}a_1,a_2,a_3,a_4,a_5\\ b_1,b_2,b_3,b_4\end{matrix}\middle|z\right) = G^{2\ 3}_{5\ 4}\left(\begin{matrix}a_2,a_1,a_3,a_5,a_4\\ b_1,b_2,b_4,b_3\end{matrix}\middle|z\right)$$
$$= G^{2\ 3}_{5\ 4}\left(\begin{matrix}a_1,a_2,a_4,a_3,a_5\\ b_2,b_1,b_4,b_3\end{matrix}\middle|z\right) = ... \tag{2.2.14}$$

We can associate several elementary and special functions with MGF. Let us take the following example:

$$G^{2\ 0}_{0\ 2}\left(\begin{matrix}-\\ b,b+\frac{1}{2}\end{matrix}\middle|z\right) = \frac{1}{2\pi i}\int_L \prod_{j=1}^{2}\Gamma(b_j-t)\times z^t dt$$
$$= \frac{1}{2\pi i}\int_L \Gamma(b-t)\Gamma(b+\frac{1}{2}-t)\times z^t dt \tag{2.2.15}$$

The poles of $\Gamma(b-t)$ are at $t=b+n; n=0,1,2,...$ and that of for $\Gamma(b+\frac{1}{2}-t)$ are at $t=b+\frac{1}{2}+n; n=0,1,2,....$ Thus the residues of the integral in (2.2.15), due to the poles of $\Gamma(b-t)$ are:

$$R_n = 2\pi i\left\{\frac{(-1)^n}{n!}\Gamma\left(\frac{1}{2}-n\right)z^{b+n}\right\} \qquad [n=0,1,2,...]$$
$$= 2\pi i\left\{\frac{4^n}{(2n)!}\sqrt{\pi}z^{b+n}\right\} \qquad \left[\text{as, } \Gamma\left(\frac{1}{2}-n\right)=\frac{(-4)^n n!}{(2n)!}\sqrt{\pi}\right] \tag{2.2.16}$$

and the residues due to the poles of $\Gamma(b+\frac{1}{2}-t)$ are:

$$\begin{aligned} R'_n &= 2\pi i\left\{\frac{(-1)^n}{n!}\Gamma\left(-\frac{1}{2}-n\right)z^{b+\frac{1}{2}+n}\right\} \qquad [n=0,1,2,...] \\ &= -2\pi i\left\{\frac{2^{n+1}}{n!}\sqrt{\pi}z^{b+n+\frac{1}{2}}\right\} \end{aligned} \tag{2.2.17}$$

According to the residue theorem the equation (2.2.15) becomes,

$$\begin{aligned} G^{2\ 0}_{0\ 2}\left(\begin{matrix}-\\ b, b+\frac{1}{2}\end{matrix}\middle| z\right) &= \frac{1}{2\pi i}\sum_{n=0}^{\infty}\left[R_n + R'_n\right] \\ &= \sqrt{\pi}z^b\left(1-2z^{\frac{1}{2}}+2z-\frac{8z^{\frac{3}{2}}}{3!}+\frac{16z^2}{4!}-.....\right) \\ &= \sqrt{\pi}z^b e^{-2\sqrt{z}} \end{aligned} \tag{2.2.18}$$

The relevant terms in equation (2.2.12) can be evaluated using MGF as [156, 157]

$$\sin kr = \sqrt{\pi}G^{1\ 0}_{0\ 2}\left(\begin{matrix}-\\ \frac{1}{2}, 0\end{matrix}\middle|\frac{k^2r^2}{4}\right) \tag{2.2.19}$$

$$\frac{z^\beta}{(1+az^b)^\alpha} = \frac{a^{-\frac{\beta}{b}}}{\Gamma(\alpha)}G^{1\ 1}_{1\ 1}\left(\begin{matrix}1-\alpha+\frac{\beta}{b}\\ \frac{\beta}{b}\end{matrix}\middle| az^b\right) \tag{2.2.20}$$

Hence, equation (2.2.12) becomes

$$\begin{aligned} V_1 &= \frac{q\lambda_D^2}{4\epsilon_0\pi^2 r}\int_o^\infty \frac{1}{1+k^2\lambda_D^2}\sin krd(k^2) \\ &= \frac{q\lambda_D^2}{4\epsilon_0\pi^2 r}\sqrt{\pi}\int_o^\infty G^{1\ 1}_{1\ 1}\left(\begin{matrix}0\\ 0\end{matrix}\middle|\lambda_D^2k^2\right)G^{1\ 0}_{0\ 2}\left(\begin{matrix}-\\ \frac{1}{2}, 0\end{matrix}\middle|\frac{k^2r^2}{4}\right)d(k^2) \end{aligned} \tag{2.2.21}$$

where we have used the identities (2.2.19) and (2.2.20). Now, applying the following property of MGF

$$\begin{aligned} &\int_0^\infty G^{s\ t}_{u\ v}\left(\begin{matrix}c_1,...,c_u\\ d_1,...,d_v\end{matrix}\middle|\xi z\right)G^{m\ n}_{p\ q}\left(\begin{matrix}a_1,...,a_p\\ b_1,...,b_q\end{matrix}\middle|\eta z\right)dx \\ &= \frac{1}{\xi}G^{t+m\ s+n}_{p+v\ q+u}\left(\begin{matrix}a_1,...,a_n,-d_1,...,-d_v,a_{n+1},...,a_p\\ b_1,...,b_m,-c_1,...,-c_u,b_{m+1},...,b_q\end{matrix}\middle|\frac{\eta}{\xi}\right) \end{aligned} \tag{2.2.22}$$

equation (2.2.21) becomes

$$V_1 = \frac{q\lambda_D^2}{4\epsilon_0\pi^2 r}\sqrt{\pi}\frac{1}{\lambda_D^2}G_{1\ 3}^{2\ 1}\left(\begin{matrix}-,0,-\\ \frac{1}{2},0,0\end{matrix}\middle|\frac{r^2}{4\lambda_D^2}\right) \tag{2.2.23}$$

With the help of reduction property of MGF [156] given by

$$G_{p\ q}^{m\ n}\left(\begin{matrix}a_1,...,a_p\\ b_1,...,b_{q-1},a_1\end{matrix}\middle|z\right) = G_{p-1\ q-1}^{m\ n-1}\left(\begin{matrix}a_2,...,a_p\\ b_1,...,b_q-1\end{matrix}|z\right) \tag{2.2.24}$$

and the symmetry property (2.2.14), we can write,

$$\begin{aligned} V_1 &= \frac{q\sqrt{\pi}}{4\epsilon_0\pi^2 r}G_{0\ 2}^{2\ 0}\left(\begin{matrix}-\\ 0,\frac{1}{2}\end{matrix}\middle|\frac{r^2}{4\lambda_D^2}\right) \\ &= \frac{q\sqrt{\pi}}{4\epsilon_0\pi^2 r}\sqrt{\pi}e^{-\frac{r}{\lambda_D}} \qquad \text{[using (2.2.18)]} \\ &= \frac{q}{4\pi\epsilon_0 r}e^{-\frac{r}{\lambda_D}} \end{aligned} \tag{2.2.25}$$

We will call this potential V_1 as *exponentially screened Coulomb potential* (ESCP). The potential (2.2.25) is of the form of Debye–Hückel screening potential [83].
We now proceed to evaluate V_2. Performing integration over the azimuthal angle (τ) in equation (2.2.11), we write

$$V_2 = \frac{qv\lambda_D^4}{8\pi\epsilon_0}\sqrt{\frac{2}{\pi}}\sum_s\frac{1}{v_{ts}\lambda_s^2}\int_o^\infty\frac{k^2}{(1+k^2\lambda_D^2)^2}\int_0^\pi\cos(\sigma+\theta)e^{ikr\cos\sigma}\sin\sigma d\sigma \tag{2.2.26}$$

where, θ is the angle between $\vec{r}$ and $\vec{v}$ and hence, $(\theta+\sigma)$ will be the angle between $\vec{k}$ and $\vec{v}$. The polar angle part of the integral can be written as

$$\int_0^\pi\cos(\sigma+\theta)e^{ikr\cos\sigma}\sin\sigma d\sigma = I_1 - I_2 \tag{2.2.27}$$

$$\begin{aligned} \text{where}\quad I_1 &= \cos\theta\int_0^\pi\cos\sigma e^{ikr\cos\sigma}\sin\sigma d\sigma \\ &= \frac{2\cos\theta}{i}\left[\frac{\cos(kr)}{kr}-\frac{\sin(kr)}{k^2r^2}\right] = -\frac{2}{i}j_1(kr)\cos\theta \end{aligned} \tag{2.2.28}$$

$j_l(x)$ is the spherical Bessel function of first kind [158] and

$$I_2 = \sin\theta\int_0^\pi\sin\sigma e^{ikr\cos\sigma}\sin\sigma d\sigma = \sin\theta I_2' + i\sin\theta I_2'' \tag{2.2.29}$$

$$\text{with} \quad I_2' = \int_0^{\pi} \sin^2\sigma \cos(kr\cos\sigma)d\sigma \tag{2.2.30}$$

$$\text{and} \quad I_2'' = \int_0^{\pi} \sin^2\sigma \sin(kr\cos\sigma)d\sigma \tag{2.2.31}$$

Now, using the following properties [158]

$$\begin{aligned} \cos(x\cos\theta) &= j_0(x) - 2j_2(x)\cos 2\theta + 2j_4(x)4\cos\theta - ..... \\ \text{and} \quad \sin(x\cos\theta) &= 2j_1(x)\cos\theta - 2j_3(x)\cos 3\theta + 2j_5(x)\cos 5\theta - ..... \end{aligned}$$

equations (2.2.30) and (2.2.31) give

$$\begin{aligned} I_2' &= \int_0^{\pi} \sin^2\sigma \cos(kr\cos\sigma)d\sigma \\ &= \frac{1}{2}\int_0^{\pi} (1-\cos 2\sigma)\left[j_0(kr) - 2j_2(kr)\cos 2\sigma + 2j_4(kr)4\cos\sigma - ...\right]d\sigma \\ &= \frac{\pi}{2}\left[j_0(kr) + j_2(kr)\right] \\ \text{and } I_2'' &= \int_0^{\pi} \sin^2\sigma \sin(kr\cos\sigma)d\sigma \\ &= \frac{1}{2}\int_0^{\pi} (1-\cos 2\sigma)\left[2j_1(kr)\cos\sigma - 2j_3(kr)\cos 3\sigma + 2j_5(kr)\cos 5\sigma - ...\right]d\sigma = 0 \end{aligned}$$

Thus, equation (2.2.29) becomes

$$I_2 = \frac{\pi}{2}\sin\theta\left[j_0(kr) + j_2(kr)\right] \tag{2.2.32}$$

Putting the values of I_1 and I_2 from equations (2.2.28) and (2.2.32) respectively, we can write the angular integral (2.2.27) as

$$\int_0^{\pi} \cos(\sigma+\theta)e^{ikr\cos\sigma}\sin\sigma d\sigma = -\frac{2}{i}j_1(kr)\cos\theta + \frac{\pi}{2}\sin\theta\left[j_0(kr) + j_2(kr)\right] \tag{2.2.33}$$

Using equations (2.2.27) to (2.2.29) and considering the real parts, equation (2.2.26) turns to

$$V_2 = -\frac{qv\lambda_D^4}{4\pi\epsilon_0}\sqrt{\frac{2}{\pi}}\sum_s \frac{1}{v_s\lambda_s^2}\cos\theta\int_0^{\infty}\frac{k^2 j_1(kr)}{(1+k^2\lambda_D^2)^2}dk \tag{2.2.34}$$

We have employed MGF to find a closed analytic form of the potential V_2. Using the following identities:

- $\dfrac{z^{\beta}}{(1+az^b)^{\alpha}} = \dfrac{a^{-\frac{\beta}{b}}}{\Gamma(\alpha)}G_{1\ 1}^{1\ 1}\left(\begin{matrix}1-\alpha+\frac{\beta}{b}\\ \frac{\beta}{b}\end{matrix}\middle| az^b\right), \quad j_\nu(z) = G_{0\ 2}^{1\ 0}\left(\begin{matrix}-\\ \frac{\nu}{2},\frac{\nu}{2}\end{matrix}\middle|\frac{z^2}{4}\right)$

- $j_\nu(z) = G^{1\ 0}_{0\ 2}\left(\begin{matrix} - \\ \frac{\nu}{2}, \frac{\nu}{2} \end{matrix}\middle| \frac{z^2}{4}\right)$
- $\int_0^\infty G^{s\ t}_{u\ v}\left(\begin{matrix} c_1,...,c_u \\ d_1,...,d_v \end{matrix}\middle| \xi z\right) G^{m\ n}_{p\ q}\left(\begin{matrix} a_1,...,a_p \\ b_1,...,b_q \end{matrix}\middle| \eta z\right) dx$
  $= \frac{1}{\xi} G^{t+m\ s+n}_{p+v\ q+u}\left(\begin{matrix} a_1,...,a_n,-d_1,...,-d_v,a_{n+1},...,a_p \\ b_1,...,b_m,-c_1,...,-c_u,b_{m+1},...,b_q \end{matrix}\middle| \frac{\eta}{\xi}\right)$

we can write

$$V_2 = -\frac{qv\lambda_D}{8\pi\epsilon_0}\sqrt{\frac{2}{\pi}}\sum_s \frac{1}{v_s\lambda_s^2}\cos\theta G^{2\ 1}_{1\ 3}\left(\begin{matrix} -\frac{1}{2} \\ \frac{1}{2}, \frac{1}{2}, -\frac{1}{2} \end{matrix}\middle| \frac{r^2}{4\lambda_D^2}\right) \tag{2.2.35}$$

Further simplification can be done by using the following properties:

- $z^k G^{m\ n}_{p\ q}\left(\begin{matrix} a_1,...,a_p \\ b_1,...,b_q \end{matrix}\middle| z\right) = G^{m\ n}_{p\ q}\left(\begin{matrix} a_1+k,...,a_p+k \\ b_1+k,...,b_q+k \end{matrix}\middle| z\right)$
- $G^{m\ n}_{p\ q}\left(\begin{matrix} a_1,...,a_p \\ b_1,...,b_{q-1},a_1 \end{matrix}\middle| z\right) = G^{m\ n-1}_{p-1\ q-1}\left(\begin{matrix} a_2,...,a_p \\ b_1,...,b_q-1 \end{matrix}\middle| z\right)$
- $2^{\mu-1} G^{2\ 0}_{0\ 2}\left(\begin{matrix} - \\ \frac{\mu}{2}+\frac{\nu}{2}, \frac{\mu}{2}-\frac{\nu}{2} \end{matrix}\middle| z\right) = z^\mu K_\nu(z)$

where $K_\nu(z)$ is called the Macdonald function or modified Bessel function of second kind. The final form of V_2 becomes

$$V_2 \quad = -\frac{qv}{8\pi\epsilon_0}\sqrt{\frac{2}{\pi}}\textstyle\sum_s \frac{1}{v_s\lambda_s^2} r K_0\left(\frac{r}{\lambda_D}\right)\cos\theta \tag{2.2.36}$$

This potential is called the *near field wake potential* (NFWP). From the convergence condition [156] of $G^{2\ 0}_{0\ 2}\left(\begin{matrix} - \\ \frac{\mu}{2}+\frac{\nu}{2}, \frac{\mu}{2}-\frac{\nu}{2} \end{matrix}\middle| z\right)$ it can be seen that the NFWP is effective for $r < 2\lambda_D$.

2.2.2 Moving ion in classical dusty plasma

The effect of dust charge fluctuation on the potential around a slowly moving test charge in un-magnetized classical dusty plasma was studied by Shukla [93] where the plasma was considered to be consisted of electrons (e), positive ions (i) and negatively charged dust grains (d). The plasma dielectric function is given as,

$$\epsilon(\vec{k}) = 1 + \sum_{s=e,i,d}\frac{1}{k^2\lambda_s^2}\left(1 - i\sqrt{\frac{\pi}{2}}\frac{\vec{k}.\vec{v}}{kv_{ts}}\right) + \frac{1}{k^2\lambda_i^2}\frac{\nu_e}{\nu_c + i\vec{k}.\vec{v}} \tag{2.2.37}$$

The Debye screening length of the species s are given by

$$\lambda_s(s=e,i) = \left(\epsilon_0 m_s T_s/n_s e^2\right)^{1/2} \quad and \quad \lambda_d = \left(\epsilon_0 m_d T_d/n_d Z_d^2 e^2\right)^{1/2}$$

where n_s is the equilibrium number density and $T_s(s=e,i,d)$ is the temperature of the species 's' $(s=e,i,d)$. In this plasma the quasi charge neutrality condition becomes $n_e + Z_d n_d = n_i$, Z_d being the number of electrons accumulated on the dust grain of radius r_d. Following the work of Varma *et.al* [159], the dust charging frequency corresponding to dust charge fluctuations can be written as,

$$\nu_c = 1/4\pi^{3/2}\,(r_d/\lambda_i)\left[1+(m_i T_i/m_e T_e)^{1/2}\,n_e/n_i\right]\omega_{pi} \tag{2.2.38}$$

and the electron-dust collision frequency as,

$$\nu_e = \sqrt{8\pi} n_d r_d^2 \lambda_i \omega_{pi}\,(1+T_i/T_e)\,(1-e\psi_0/T_i) \tag{2.2.39}$$

where $\psi_0 = -Z_d e/4\pi\epsilon_0 r_d$ is the floating potential of the dust grain and $\omega_{pi} = \sqrt{\dfrac{n_s e^2}{\epsilon_0 m_i}}$ is the plasma oscillation frequency of the ions. When the dust charging effect is very high, we can assume $\nu_c \gg |\vec{k}.\vec{v}|$ and equation (2.2.37) can be re-written as,

$$\begin{aligned}
\epsilon(\vec{k}) &= 1+\sum_{s=e,i,d}\frac{1}{k^2\lambda_s^2}\left(1-i\sqrt{\frac{\pi}{2}}\frac{\vec{k}.\vec{v}}{kv_{ts}}\right)+\frac{\nu_e}{k^2\lambda_i^2\nu_c}-i\frac{\nu_e(\vec{k}.\vec{v})}{k^2\lambda_i^2\nu_c^2}\\
&= 1+\frac{1}{k^2}\left(\sum_{s=e,i,d}\frac{1}{\lambda_s^2}+\frac{\nu_e}{\nu_c\lambda_i^2}\right)-i\sqrt{\frac{\pi}{2}}\frac{\vec{k}.\vec{v}}{k^3}\sum_{s=e,i,d}\frac{1}{v_{ts}\lambda_s^2}-i\frac{1}{k^2\lambda_i^2}\frac{\nu_e(\vec{k}.\vec{v})}{\nu_c^2}\\
&= \frac{1+k^2\lambda_t^2}{k^2\lambda_t^2}\left[1-i\frac{k^2\lambda_t^2}{1+k^2\lambda_t^2}\left\{\sqrt{\frac{\pi}{2}}\frac{\vec{k}.\vec{v}}{k^3}\sum_{s=e,i,d}\frac{1}{v_{ts}\lambda_s^2}+\frac{1}{k^2\lambda_i^2}\frac{\nu_e(\vec{k}.\vec{v})}{\nu_c^2}\right\}\right]
\end{aligned} \tag{2.2.40}$$

where,

$$\frac{1}{\lambda_t^2} = \sum_{s=e,i,d}\frac{1}{\lambda_s^2}+\frac{\nu_e}{\nu_c\lambda_i^2} \tag{2.2.41}$$

λ_t is called the effective screening length of the plasma. Now on imposing the slowly moving charge condition *i.e* for $|\vec{k}.\vec{v}| \ll kv_{ts}$ the inverse of dielectric function gives

$$\frac{1}{\epsilon(\vec{k})} \simeq \frac{k^2\lambda_t^2}{1+k^2\lambda_t^2}+i\sqrt{\frac{\pi}{2}}\frac{k^4\lambda_t^4}{(1+k^2\lambda_t^2)^2}\frac{\vec{k}.\vec{v}}{k^3}\sum_{s=e,i,d}\frac{1}{v_{ts}\lambda_s^2}+i\frac{k^4\lambda_t^4}{(1+k^2\lambda_t^2)^2}\frac{1}{k^2\lambda_i^2}\frac{\nu_e(\vec{k}.\vec{v})}{\nu_c^2} \tag{2.2.42}$$

Using this relation, the potential $V(\vec{r})$ in (2.2.4) may be written as

$$\begin{aligned} V(\vec{r}) &= V_1 + V_2 + V_3 \\ \text{where, } V_1 &= \frac{q}{8\pi^2\epsilon_0}\int \frac{\lambda_t^2}{1+k^2\lambda_t^2} e^{i\vec{k}.\vec{r}} d^3\vec{k} \\ V_2 &= i\sqrt{\frac{\pi}{2}}\frac{q}{8\pi^2\epsilon_0}\int \frac{\lambda_t^4}{k(1+k^2\lambda_t^2)^2}\vec{k}.\vec{v}\sum_{s=e,i,d}\frac{1}{v_{ts}\lambda_s^2} \times e^{i\vec{k}.\vec{r}} d^3\vec{k} \\ V_3 &= i\frac{\nu_e}{\lambda_i^2\nu_c^2}\frac{q}{8\pi^2\epsilon_0}\int \frac{\lambda_t^4}{(1+k^2\lambda_t^2)^2}\vec{k}.\vec{v} \times e^{i\vec{k}.\vec{r}} d^3\vec{k} \end{aligned}$$

The solutions for V_1 and V_2 are same as given in the equations (2.2.10) and (2.2.11) respectively, where λ_D is to be replaced by λ_t.
After performing the angular integral over α and β as described in the previous subsection, the third part of the potential becomes

$$V_3 = \frac{qv\nu_e\lambda_t^4}{2\pi^2\epsilon_0\lambda_i^2\nu_c^2} \times \frac{\cos\theta}{r^2} \times \int_0^\infty \frac{\left(k^2 r\cos kr - k\sin kr\right)}{(1+k^2\lambda_t^2)^2} dk \tag{2.2.43}$$

Now consider a standard integral [156],

$$\int_0^\infty \frac{k\sin kr}{(1+k^2\lambda_t^2)^2} dk = \frac{\pi r}{4\lambda_t^3} e^{-\frac{r}{\lambda_t}} \tag{2.2.44}$$

The cosine part of the integral (2.2.43) will be,

$$\int_0^\infty \frac{k^2 r\cos kr}{(1+k^2\lambda_t^2)^2} dk = r\frac{\partial}{\partial r}\int_0^\infty \frac{k\sin kr}{(1+k^2\lambda_t^2)^2} dk = \frac{\pi}{4\lambda_t^3}\left(r - \frac{r^2}{\lambda_t}\right) e^{-\frac{r}{\lambda_t}} \tag{2.2.45}$$

Using equations (2.2.44) and (2.2.45), equation (2.2.43) becomes

$$V_3 = -\frac{q}{4\pi\epsilon_0}\frac{v\nu_e}{2\nu_c^2\lambda_i^2} e^{-\frac{r}{\lambda_t}}\cos\theta \tag{2.2.46}$$

This part of the potential is called 'dusty potential' (DP).

2.2.3 Moving ion in quantum qlasma

In the present section we will concentrate on the models for the collision-less quantum plasma. The modeling of the potential in the quantum plasma scenario was first given by Shukla *et.al.* [160] around a moving test charge within a semiconductor substance having

electrons (e) and holes (h) as the plasma species (s). The dielectric function for the electron-hole plasma was first given by Pine [155] as

$$\epsilon(\vec{k}) = 1 + \sum_s \frac{1}{\lambda_s^2 k^2}\left(1 - i\frac{\pi}{2}\frac{\vec{k}.\vec{v}}{kv_s}\right) = \frac{1+k^2\lambda_Q^2}{k^2\lambda_Q^2} - i\frac{\pi}{2}\sum_s \frac{1}{v_s\lambda_s^2}\frac{\vec{k}.\vec{v}}{k^3} \tag{2.2.47}$$

where,

1. $v_s = \frac{\hbar}{m_s}(3\pi^2 n_s)^{\frac{1}{3}}$ is the Fermi velocity of the species s with n_s and m_s being the number density and mass respectively.

2. λ_s is the screening length corresponding to the plasma species 's'. Using the Thomas-Fermi model we may write $\lambda_s = \dfrac{v_s}{\sqrt{3}\omega_s}$, where $\omega_s = \left(\dfrac{n_s q_s}{\epsilon_0 m_s}\right)^{1/2}$ is the plasma oscillation angular frequency (in S.I.) of species 's'.

3. The overall screening length λ_Q of the quantum plasma is given by

$$\lambda_Q = \left(\sum_s \frac{1}{\lambda_s^2}\right)^{-\frac{1}{2}} \tag{2.2.48}$$

Let us consider a slowly moving test charge through the medium *i.e.* $v \ll v_s$, for which inverse of the dielectric function becomes

$$\begin{aligned}\frac{1}{\epsilon(\vec{k})} &= \frac{k^2\lambda_Q^2}{1+k^2\lambda_Q^2}\left[1 - i\frac{\pi}{2}\sum_s \frac{1}{v_s\lambda_s^2}\frac{\vec{k}.\vec{v}}{k^3}\frac{k^2\lambda_Q^2}{1+k^2\lambda_Q^2}\right]^{-1} \\ &\approx \frac{k^2\lambda_Q^2}{1+k^2\lambda_Q^2} + i\frac{\pi}{2}\frac{k\lambda_Q^4}{(1+k^2\lambda_Q^2)^2}\vec{k}.\vec{v} \times \sum_{s=e,h}\frac{1}{v_{ts}\lambda_s^2}\end{aligned} \tag{2.2.49}$$

Substituting (2.2.49) into (2.2.4) we can write, $V(\vec{r}) = V_1 + V_2$, where

$$V_1 = \frac{q}{8\pi^3\epsilon_0}\int \frac{\lambda_Q^2}{1+k^2\lambda_Q^2}e^{i\vec{k}.\vec{r}}d^3\vec{k} \tag{2.2.50}$$

$$\text{and } V_2 = i\frac{\pi}{2}\frac{q}{8\pi^3\epsilon_0}\int \frac{\lambda_Q^4}{k(1+k^2\lambda_Q^2)^2}\vec{k}.\vec{v}\sum_s \frac{1}{v_s\lambda_s^2} \times e^{i\vec{k}.\vec{r}}d^3\vec{k} \tag{2.2.51}$$

Since these two integrals are similar as the integrals in equations (2.2.10) and (2.2.11), we can directly write the solutions as

$$V_1 = \frac{q}{4\pi\epsilon_0 r}e^{-\frac{r}{\lambda_Q}} \tag{2.2.52}$$

$$\text{and } V_2 = -\frac{qv}{8\pi\epsilon_0}\sum_s \frac{1}{v_s\lambda_s^2} r K_0\left(\frac{r}{\lambda_Q}\right)\cos\theta \tag{2.2.53}$$

It is ,therefore, clear that in case of quantum plasma the velocity independent or static potential V_1 has the same form as Debye–Hückel potential [83] appeared in case of classical WCP with only difference being the plasma screening length λ_Q replacing the classical screening length λ_D. Similarly, V_2 is called the near field wake potential (NFWP) which is effective upto $r < 2\lambda_Q$ and can be considered to be zero for $r > 2\lambda_Q$.

2.3 Determination of energy levels: *the present method*

To estimate energy eigenvalues of H–like systems moving through different plasma environments Ritz variation technique has been employed. In the first step, a suitable trial wavefunction is considered where the radial part is expanded in Slater–type basis set. Subsequently, the variational equations for the plasma environments are given. In the last part of this section, the relevant matrix elements of hydrogenic states upto $n = 4$ level are given in closed analytic forms. and the analytic form of the necessary basis–integrals are provided in detail. For the calculation of matrix elements, it is required to solve few particular types of integrals. These integrals are known as 'basis integrals'. The analytic expressions of the basis integrals are also provided.

2.3.1 Wavefunction

The trial wavefunction is taken as

$$\Psi(r, \theta, \phi) = \psi(r) Y_{lm}(\theta, \phi)(a + b\cos\theta) \tag{2.3.1}$$

where, $\psi(r)$ is the radial part and $Y_{lm}(\theta, \phi)$ is the the spherical harmonics with l and m being the orbital and azimuthal quantum numbers, respectively. $(a + b\cos\theta)$ is the orbital distortion term that arises due to the wake part of the potential (a and b are the distortion parameters). The radial wavefunction $\psi(r)$ is expanded in terms of Slater–type orbitals as

$$\psi(r) = \sum_{i=1}^{N} C_i r^{n_i} e^{-\rho_i r} \tag{2.3.2}$$

ρ_i is the non-linear parameter which is generated in geometrical progression as $\rho_i = \rho_{i-1}\gamma$, γ being the geometrical progression ratio. The starting value of ρ_i is taken by employing Nelder–Mead optimization algorithm [161] using single term in equation (2.3.2), whereas the ending value of ρ_i is taken as $\sim \frac{1}{100}$–th of the starting value of ρ_i. In equation (2.3.2), C_i is the expansion coefficient in equation (2.3.2), which serves as the linear variational parameters and N is the total number of terms in the basis set. The generalized eigenvalue

equation [162] is written as

$$\underline{\underline{H}}\ \underline{C} = E\underline{\underline{S}}\ \underline{C} \tag{2.3.3}$$

where, $\underline{\underline{H}}$, $\underline{\underline{S}}$ and $\underline{C}$ are the Hamiltonian matrix, overlap matrix and eigen-vector respectively. By solving this equation we determine the energy eigenvalues E.

2.3.2 Variational Equation

The energy eigenvalues of two–body systems are determined by solving the variational equation,

$$\delta\left[\langle T\rangle + \langle V\rangle - E\langle S\rangle\right] = 0 \tag{2.3.4}$$

where the kinetic energy (K.E.) term, in spherical polar coordinates takes the form

$$\langle T\rangle = \frac{1}{2}\left(\frac{1}{m_1}+\frac{1}{m_2}\right)\int\left[\left(\frac{\partial\Psi}{\partial r}\right)^2 + \frac{1}{r^2}\left(\frac{\partial\Psi}{\partial\theta}\right)^2 + \frac{1}{r^2\sin^2\theta}\left(\frac{\partial\Psi}{\partial\phi}\right)^2\right] r^2\sin\theta d\theta d\phi dr \tag{2.3.5}$$

where m_1 and m_2 are the masses of the nucleus and the electron respectively. The potential energy (P.E.) term,

$$\langle V\rangle = \int V_{eff}\Psi^2 r^2\sin\theta d\theta d\phi dr \tag{2.3.6}$$

and the normalization or overlap term,

$$\langle S\rangle = \int \Psi^2 r^2\sin\theta d\theta d\phi dr \tag{2.3.7}$$

In equation (2.3.6) the effective potential energies (V_{eff}) which were derived in the previous section are listed below in atomic units (a.u.)

- **Classical weakly coupled plasma**

$$V_{eff} = -\frac{Z}{r}e^{-\frac{r}{\lambda_D}} + \xi r K_0\left(\frac{r}{\lambda_D}\right)\cos\theta \tag{2.3.8}$$

$$\text{where } \xi = \frac{Zv}{2}\sqrt{\frac{2}{\pi}}\sum_s \frac{1}{v_s\lambda_s^2} \tag{2.3.9}$$

is the coefficient of the NFWP and Z is the atomic number of the moving atom/ion.

- **Classical dusty plasma**

$$V_{eff} = -\frac{Z}{r}e^{-\frac{r}{\lambda_t}} + \xi r K_0\left(\frac{r}{\lambda_t}\right)\cos\theta + \chi e^{-\frac{r}{\lambda_t}}\cos\theta \tag{2.3.10}$$

The first two parts are the exponentially screened Coulomb potential (ESCP) and near field wake potential (NFWP) respectively, while the third part is called 'dusty potential' (DP). In this expression,

$$\xi = \frac{Zv}{2}\sqrt{\frac{2}{\pi}}\sum_s \frac{1}{v_s\lambda_s^2} \tag{2.3.11}$$

$$\text{and } \chi = \frac{Zv\nu_e}{2\nu_c^2\lambda_i^2} \tag{2.3.12}$$

are the coefficients of NFWP and DP respectively.

- **Quantum plasma**

$$V_{eff} = -\frac{Z}{r}e^{-\frac{r}{\lambda_Q}} + \xi r K_0\left(\frac{r}{\lambda_Q}\right)\cos\theta \tag{2.3.13}$$

These two terms in the RHS of equation (2.3.13) are clearly the exponentially screened Coulomb potential (ESCP) and the near field wake potential (NFWP) respectively. In this expression, we have used

$$\xi = \frac{Zv}{2}\sum_s \frac{1}{v_{ts}\lambda_s^2} \tag{2.3.14}$$

which is the coefficient of NFWP.

2.3.3 Matrix elements and basis integrals

We have estimated the energy eigenvalues of $1s_0$, $2s_0$, $2p_0$ and $2p_{\pm1}$ states of hydrogen atom moving under classical weakly coupled plasma, classical dusty plasma and quantum plasma. Here the subscript signifies the values of the azimuthal quantum number 'm'. A special emphasis has been given on C^{5+} ion moving under electron-hole quantum plasma due to its abundance in such plasma scenario. In this case we have estimated the energy eigenvalues of ns_0 $[n = 1-4]$; np_0, $np_{\pm1}$ $[n = 2-4]$; nd_0, $nd_{\pm1}$, $nd_{\pm2}$ $[n = 3-4]$ and nf_0, $nf_{\pm1}$, $nf_{\pm2}$, $nf_{\pm3}$ $[n = 4]$ states of C^{5+} ion. The matrix elements of the K.E., P.E. and overlap terms are given below for all the states mentioned above.

Matrix elements of ns_0

Following equation (2.3.1) the trial wavefunction is given by

$$\Psi(r,\theta,\phi) = Y_{00}(\theta,\phi)(a+b\cos\theta)\sum_{i=1}^{N} C_i r^{n_i} e^{-\rho_i r}$$

(i) Matrix element of K.E.

$$T_{ij} = \frac{1}{2}\left[\left(\frac{\partial\Psi}{\partial r}\right)^2 + \frac{1}{r^2}\left(\frac{\partial\Psi}{\partial\theta}\right)^2 + \frac{1}{r^2\sin^2\theta}\left(\frac{\partial\Psi}{\partial\phi}\right)^2\right]_{ij}$$

Now,

$$\begin{aligned}\left(\frac{\partial\Psi}{\partial r}\right)_i &= Y_{00}(\theta,\phi)(a+b\cos\theta)\left(n_i r^{n_i-1} - \rho_i r^{n_i}\right)e^{-\rho_i r}\\ \therefore \left(\frac{\partial\Psi}{\partial r}\right)^2_{ij} &= Y_{00}^2(\theta,\phi)(a+b\cos\theta)^2\left(n_i r^{n_i-1} - \rho_i r^{n_i}\right)\left(n_j r^{n_j-1} - \rho_j r^{n_j}\right)e^{-(\rho_i+\rho_j)r}\end{aligned}$$

By performing the angular integrals over θ and ϕ we obtain

$$\begin{aligned}T_{ij} &= \left(a^2+\frac{b^2}{3}\right)\left[n_i n_j A\left(n_i+n_j,\rho_i+\rho_j\right) - \left(n_i\rho_j + n_j\rho_i\right)A\left(n_i+n_j+1,\rho_i+\rho_j\right)\right.\\ &+ \left.\rho_i\rho_j A\left(n_i+n_j+2,\rho_i+\rho_j\right)\right] + \frac{2b^2}{3}A\left(n_i+n_j,\rho_i+\rho_j\right)\end{aligned}$$

The radial basis integral $A(n,\alpha)$ is defined below

$$A(n,\alpha) = \int_0^\infty x^n e^{-\alpha r}dx = \frac{\Gamma(n+1)}{\alpha^{n+1}} \qquad [\Gamma = \text{Euler's gamma function}]$$

(ii) Matrix element of P.E.

- **Classical WCP:**

$$\begin{aligned}V_{ij} &= -2Z\left(a^2+\frac{b^2}{3}\right)A\left(n_i+n_j+1,\rho_i+\rho_j+\frac{1}{\lambda_D}\right)\\ &\quad +\frac{4}{3}\xi abW\left(n_i+n_j+3,\rho_i+\rho_j,\frac{1}{\lambda_D}\right)\end{aligned}$$

In this case, the radial basis integral $W(\sigma,\alpha,\gamma)$ is given by

$$\begin{aligned}W(\sigma,\alpha,\gamma) &= \int_0^\infty x^{\sigma-1}e^{-\alpha x}K_\nu(\gamma x)dx\\ &= \frac{\sqrt{\pi}(2\gamma)^\nu}{(\alpha+\gamma)^{\sigma+\nu}}\frac{\Gamma(\sigma+\nu)\Gamma(\sigma-\nu)}{\Gamma(\sigma-\frac{1}{2})}\times_2 F_1\left(\sigma+\nu,\nu+\frac{1}{2};\sigma+\frac{1}{2};\frac{\alpha-\gamma}{\alpha+\gamma}\right)\end{aligned}$$

where, Re σ > | Re ν |, Re $(\alpha+\gamma) > 0$ and ${}_2F_1$ is the confluent hypergeometric function [156].

- **Classical dusty plasma:**

$$\begin{aligned} V_{ij} &= -2Z\left(a^2+\frac{b^2}{3}\right)A\left(n_i+n_j+1,\rho_i+\rho_j+\frac{1}{\lambda_t}\right)+ \\ &\quad \frac{4}{3}\xi abW\left(n_i+n_j+3,\rho_i+\rho_j,\frac{1}{\lambda_t}\right)+\frac{4}{3}\chi abA\left(n_i+n_j+2,\rho_i+\rho_j+\frac{1}{\lambda_t}\right) \end{aligned}$$

- **Quantum plasma:**

$$\begin{aligned} V_{ij} &= -2Z\left(a^2+\frac{b^2}{3}\right)A\left(n_i+n_j+1,\rho_i+\rho_j+\frac{1}{\lambda_Q}\right) \\ &\quad +\frac{4}{3}\xi abW\left(n_i+n_j+3,\rho_i+\rho_j,\frac{1}{\lambda_Q}\right) \end{aligned}$$

(iii) Matrix element of overlap term

$$S_{ij} = 2\left(a^2+\frac{b^2}{3}\right)A\left(n_i+n_j+2,\rho_i+\rho_j\right)$$

The common multiplying factor in T_{ij}, V_{ij} and S_{ij} has been ignored.

Matrix elements of np_0

Following equation (2.3.1) the trial wavefunction is given by

$$\Psi(r,\theta,\phi) = Y_{10}(\theta,\phi)(a+b\cos\theta)\sum_{i=1}^{N} C_i r^{n_i} e^{-\rho_i r}$$

Matrix element of K.E.

$$\begin{aligned} T_{ij} &= \left(\frac{a^2}{3}+\frac{b^2}{5}\right)\left[n_i n_j A\left(n_i+n_j,\rho_i+\rho_j\right)-\left(n_i\rho_j+n_j\rho_i\right)A\left(n_i+n_j+1,\rho_i+\rho_j\right)\right. \\ &\quad \left.+\rho_i\rho_j A\left(n_i+n_j+2,\rho_i+\rho_j\right)\right]+2\left(\frac{a^2}{3}+\frac{4b^2}{15}\right)A\left(n_i+n_j,\rho_i+\rho_j\right) \end{aligned}$$

Matrix element of P.E.

- **Classical WCP:**

$$V_{ij} = -2Z\left(\frac{a^2}{3}+\frac{b^2}{5}\right)A\left(n_i+n_j+1,\rho_i+\rho_j+\frac{1}{\lambda_D}\right)$$

$$+\frac{4}{5}\xi abW\left(n_i+n_j+3,\rho_i+\rho_j,\frac{1}{\lambda_D}\right)$$

- **Classical dusty plasma:**

$$\begin{aligned}V_{ij} &= -2Z\left(\frac{a^2}{3}+\frac{b^2}{5}\right)A\left(n_i+n_j+1,\rho_i+\rho_j+\frac{1}{\lambda_t}\right)+\\ &\frac{4}{5}\xi abW\left(n_i+n_j+3,\rho_i+\rho_j,\frac{1}{\lambda_t}\right)+\frac{4}{5}\chi abA\left(n_i+n_j+2,\rho_i+\rho_j+\frac{1}{\lambda_t}\right)\end{aligned}$$

- **Quantum plasma:**

$$\begin{aligned}V_{ij} &= -2Z\left(\frac{a^2}{3}+\frac{b^2}{5}\right)A\left(n_i+n_j+1,\rho_i+\rho_j+\frac{1}{\lambda_Q}\right)\\ &+\frac{4}{5}\xi abW\left(n_i+n_j+3,\rho_i+\rho_j,\frac{1}{\lambda_Q}\right)\end{aligned}$$

Matrix element of overlap term

$$S_{ij}=2\left(\frac{a^2}{3}+\frac{b^2}{5}\right)A\left(n_i+n_j+2,\rho_i+\rho_j\right)$$

Matrix elements of $np_{\pm1}$

Following equation (2.3.1) the trial wavefunction is given by

$$\Psi(r,\theta,\phi)=Y_{1,\pm1}(\theta,\phi)(a+b\cos\theta)\sum_{i=1}^{N}C_i r^{n_i}e^{-\rho_i r}$$

Matrix element of K.E.

$$\begin{aligned}T_{ij} &= 2\left(\frac{a^2}{3}+\frac{b^2}{15}\right)\left[n_in_jA\left(n_i+n_j,\rho_i+\rho_j\right)-\left(n_i\rho_j+n_j\rho_i\right)A\left(n_i+n_j+1,\rho_i+\rho_j\right)\right.\\ &\left.+\rho_i\rho_jA\left(n_i+n_j+2,\rho_i+\rho_j\right)\right]+4\left(\frac{a^2}{3}+\frac{b^2}{5}\right)A\left(n_i+n_j,\rho_i+\rho_j\right)\end{aligned}$$

Matrix element of P.E.

- **Classical WCP:**

$$\begin{aligned}V_{ij} &= -4Z\left(\frac{a^2}{3}+\frac{b^2}{15}\right)A\left(n_i+n_j+1,\rho_i+\rho_j+\frac{1}{\lambda_D}\right)\\ &+\frac{8}{15}\xi abW\left(n_i+n_j+3,\rho_i+\rho_j,\frac{1}{\lambda_D}\right)\end{aligned}$$

- **Classical dusty plasma:**

$$\begin{aligned} V_{ij} &= -4Z\left(\frac{a^2}{3}+\frac{b^2}{15}\right)A\left(n_i+n_j+1,\rho_i+\rho_j+\frac{1}{\lambda_t}\right)+ \\ &\quad \frac{8}{15}\xi abW\left(n_i+n_j+3,\rho_i+\rho_j,\frac{1}{\lambda_t}\right)+\frac{8}{15}\chi abA\left(n_i+n_j+2,\rho_i+\rho_j+\frac{1}{\lambda_t}\right) \end{aligned}$$

- **Quantum plasma:**

$$\begin{aligned} V_{ij} &= -4Z\left(\frac{a^2}{3}+\frac{b^2}{15}\right)A\left(n_i+n_j+1,\rho_i+\rho_j+\frac{1}{\lambda_Q}\right) \\ &\quad +\frac{8}{15}\xi abW\left(n_i+n_j+3,\rho_i+\rho_j,\frac{1}{\lambda_Q}\right) \end{aligned}$$

Matrix element of overlap term

$$S_{ij}=4\left(\frac{a^2}{3}+\frac{b^2}{15}\right)A\left(n_i+n_j+2,\rho_i+\rho_j\right)$$

Matrix elements of nd_0

Following equation (2.3.1) the trial wavefunction is given by

$$\Psi(r,\theta,\phi)=Y_{20}(\theta,\phi)(a+b\cos\theta)\sum_{i=1}^{N}C_i r^{n_i}e^{-\rho_i r}$$

Matrix element of K.E.

$$\begin{aligned} T_{ij} &= \left(\frac{a^2}{5}+\frac{11b^2}{105}\right)\left[n_in_jA\left(n_i+n_j,\rho_i+\rho_j\right)-\left(n_i\rho_j+n_j\rho_i\right)A\left(n_i+n_j+1,\rho_i+\rho_j\right)\right. \\ &+ \left.\rho_i\rho_jA\left(n_i+n_j+2,\rho_i+\rho_j\right)\right]+2\left(\frac{3a^2}{5}+\frac{38b^2}{105}\right)A\left(n_i+n_j,\rho_i+\rho_j\right) \end{aligned}$$

Matrix element of P.E. for quantum plasma

$$\begin{aligned} V_{ij} &= -2Z\left(\frac{a^2}{5}+\frac{11b^2}{105}\right)A\left(n_i+n_j+1,\rho_i+\rho_j+\frac{1}{\lambda_Q}\right) \\ &\quad +\frac{22}{105}\xi abW\left(n_i+n_j+3,\rho_i+\rho_j,\frac{1}{\lambda_Q}\right) \end{aligned}$$

Matrix element of overlap term

$$S_{ij}=2\left(\frac{a^2}{5}+\frac{11b^2}{105}\right)A\left(n_i+n_j+2,\rho_i+\rho_j\right)$$

Matrix elements of $nd_{\pm1}$

Following equation (2.3.1) the trial wavefunction is given by

$$\Psi(r,\theta,\phi) = Y_{2,\pm1}(\theta,\phi)(a+b\cos\theta)\sum_{i=1}^{N} C_i r^{n_i} e^{-\rho_i r}$$

Matrix element of K.E.

$$\begin{aligned} T_{ij} &= \left(\frac{a^2}{15}+\frac{b^2}{35}\right)\left[n_i n_j A\left(n_i+n_j,\rho_i+\rho_j\right)-\left(n_i\rho_j+n_j\rho_i\right)A\left(n_i+n_j+1,\rho_i+\rho_j\right)\right. \\ &\quad \left.+\rho_i\rho_j A\left(n_i+n_j+2,\rho_i+\rho_j\right)\right]+2\left(\frac{3a^2}{5}+\frac{11b^2}{105}\right)A\left(n_i+n_j,\rho_i+\rho_j\right) \end{aligned}$$

Matrix element of P.E. for quantum plasma

$$\begin{aligned} V_{ij} &= -2Z\left(\frac{a^2}{15}+\frac{b^2}{35}\right)A\left(n_i+n_j+1,\rho_i+\rho_j+\frac{1}{\lambda_Q}\right) \\ &\quad +\frac{4}{35}\xi abW\left(n_i+n_j+3,\rho_i+\rho_j,\frac{1}{\lambda_Q}\right) \end{aligned}$$

Matrix element of overlap term

$$S_{ij} = 2\left(\frac{a^2}{15}+\frac{b^2}{35}\right)A\left(n_i+n_j+2,\rho_i+\rho_j\right)$$

Matrix elements of $nd_{\pm2}$

Following equation (2.3.1) the trial wavefunction is given by

$$\Psi(r,\theta,\phi) = Y_{2,\pm2}(\theta,\phi)(a+b\cos\theta)\sum_{i=1}^{N} C_i r^{n_i} e^{-\rho_i r}$$

Matrix element of K.E.

$$\begin{aligned} T_{ij} &= \left(\frac{a^2}{15}+\frac{b^2}{105}\right)\left[n_i n_j A\left(n_i+n_j,\rho_i+\rho_j\right)-\left(n_i\rho_j+n_j\rho_i\right)A\left(n_i+n_j+1,\rho_i+\rho_j\right)\right. \\ &\quad \left.+\rho_i\rho_j A\left(n_i+n_j+2,\rho_i+\rho_j\right)\right]+2\left(\frac{a^2}{5}+\frac{2b^2}{35}\right)A\left(n_i+n_j,\rho_i+\rho_j\right) \end{aligned}$$

Matrix element of P.E. for quantum plasma

$$V_{ij} = -2Z\left(\frac{a^2}{15}+\frac{b^2}{105}\right)A\left(n_i+n_j+1,\rho_i+\rho_j+\frac{1}{\lambda_Q}\right)$$

$$+\frac{4}{105}\xi abW\left(n_i+n_j+3,\rho_i+\rho_j,\frac{1}{\lambda_Q}\right)$$

Matrix element of overlap term

$$S_{ij}=2\left(\frac{a^2}{15}+\frac{b^2}{105}\right)A\left(n_i+n_j+2,\rho_i+\rho_j\right)$$

Matrix elements of nf_0

Following equation (2.3.1) the trial wavefunction is given by

$$\Psi(r,\theta,\phi)=Y_{30}(\theta,\phi)(a+b\cos\theta)\sum_{i=1}^{N}C_i r^{n_i}e^{-\rho_i r}$$

Matrix element of K.E.

$$\begin{aligned}T_{ij} &= \left(\frac{a^2}{7}+\frac{23b^2}{315}\right)[n_in_jA\left(n_i+n_j,\rho_i+\rho_j\right)-\left(n_i\rho_j+n_j\rho_i\right)A\left(n_i+n_j+1,\rho_i+\rho_j\right)\\ &\quad+\rho_i\rho_jA\left(n_i+n_j+2,\rho_i+\rho_j\right)]+2\left(\frac{6a^2}{7}+\frac{149b^2}{315}\right)A\left(n_i+n_j,\rho_i+\rho_j\right)\end{aligned}$$

Matrix element of P.E. for quantum plasma

$$\begin{aligned}V_{ij} &= -2Z\left(\frac{a^2}{7}+\frac{23b^2}{315}\right)A\left(n_i+n_j+1,\rho_i+\rho_j+\frac{1}{\lambda_Q}\right)\\ &\quad+\frac{92}{315}\xi abW\left(n_i+n_j+3,\rho_i+\rho_j,\frac{1}{\lambda_Q}\right)\end{aligned}$$

Matrix element of overlap term

$$S_{ij}=2\left(\frac{a^2}{7}+\frac{23b^2}{315}\right)A\left(n_i+n_j+2,\rho_i+\rho_j\right)$$

Matrix elements of $nf_{\pm1}$

Following equation (2.3.1) the trial wavefunction is given by

$$\Psi(r,\theta,\phi)=Y_{3,\pm1}(\theta,\phi)(a+b\cos\theta)\sum_{i=1}^{N}C_i r^{n_i}e^{-\rho_i r}$$

Matrix element of K.E.

$$T_{ij} = \left(\frac{a^2}{21}+\frac{b^2}{45}\right)[n_in_jA\left(n_i+n_j,\rho_i+\rho_j\right)-\left(n_i\rho_j+n_j\rho_i\right)A\left(n_i+n_j+1,\rho_i+\rho_j\right)$$

$$+\rho_i\rho_j A\left(n_i+n_j+2,\rho_i+\rho_j\right)]+4\left(\frac{a^2}{7}+\frac{23b^2}{315}\right)A\left(n_i+n_j,\rho_i+\rho_j\right)$$

Matrix element of P.E. for quantum plasma

$$\begin{aligned}V_{ij} &= -2Z\left(\frac{a^2}{21}+\frac{b^2}{45}\right)A\left(n_i+n_j+1,\rho_i+\rho_j+\frac{1}{\lambda_Q}\right)\\ &\quad+\frac{4}{45}\xi abW\left(n_i+n_j+3,\rho_i+\rho_j,\frac{1}{\lambda_Q}\right)\end{aligned}$$

Matrix element of overlap term

$$S_{ij}=2\left(\frac{a^2}{21}+\frac{b^2}{45}\right)A\left(n_i+n_j+2,\rho_i+\rho_j\right)$$

Matrix elements of $nf_{\pm2}$

Following equation (2.3.1) the trial wavefunction is given by

$$\Psi(r,\theta,\phi)=Y_{3,\pm2}(\theta,\phi)(a+b\cos\theta)\sum_{i=1}^{N}C_i r^{n_i}e^{-\rho_i r}$$

Matrix element of K.E.

$$\begin{aligned}T_{ij} &= \left(\frac{a^2}{105}+\frac{b^2}{315}\right)[n_in_jA\left(n_i+n_j,\rho_i+\rho_j\right)-\left(n_i\rho_j+n_j\rho_i\right)A\left(n_i+n_j+1,\rho_i+\rho_j\right)\\ &\quad+\rho_i\rho_jA\left(n_i+n_j+2,\rho_i+\rho_j\right)]+2\left(\frac{2a^2}{35}+\frac{b^2}{45}\right)A\left(n_i+n_j,\rho_i+\rho_j\right)\end{aligned}$$

Matrix element of P.E. for quantum plasma

$$\begin{aligned}V_{ij} &= -2Z\left(\frac{a^2}{105}+\frac{b^2}{315}\right)A\left(n_i+n_j+1,\rho_i+\rho_j+\frac{1}{\lambda_Q}\right)\\ &\quad+\frac{4}{315}\xi abW\left(n_i+n_j+3,\rho_i+\rho_j,\frac{1}{\lambda_Q}\right)\end{aligned}$$

Matrix element of overlap term

$$S_{ij}=2\left(\frac{a^2}{105}+\frac{b^2}{315}\right)A\left(n_i+n_j+2,\rho_i+\rho_j\right)$$

Matrix elements of $nf_{\pm 3}$

Following equation (2.3.1) the trial wavefunction is given by

$$\Psi(r,\theta,\phi) = Y_{3,\pm 3}(\theta,\phi)(a + b\cos\theta)\sum_{i=1}^{N} C_i r^{n_i} e^{-\rho_i r}$$

Matrix element of K.E.

$$\begin{aligned} T_{ij} &= \left(\frac{a^2}{35} + \frac{b^2}{315}\right)[n_i n_j A(n_i + n_j, \rho_i + \rho_j) - (n_i\rho_j + n_j\rho_i) A(n_i + n_j + 1, \rho_i + \rho_j) \\ &\quad + \rho_i\rho_j A(n_i + n_j + 2, \rho_i + \rho_j)] + 4\left(\frac{3a^2}{35} + \frac{5b^2}{315}\right) A(n_i + n_j, \rho_i + \rho_j) \end{aligned}$$

Matrix element of P.E. for quantum plasma

$$\begin{aligned} V_{ij} &= -2Z\left(\frac{a^2}{35} + \frac{b^2}{315}\right) A\left(n_i + n_j + 1, \rho_i + \rho_j + \frac{1}{\lambda_Q}\right) \\ &\quad + \frac{4}{315}\xi abW\left(n_i + n_j + 3, \rho_i + \rho_j, \frac{1}{\lambda_Q}\right) \end{aligned}$$

Matrix element of overlap term

$$S_{ij} = 2\left(\frac{a^2}{35} + \frac{b^2}{315}\right) A(n_i + n_j + 2, \rho_i + \rho_j)$$

2.4 Results and Discussions

At first, we report the energy eigenvalues of $1s_0$ $2s_0$, $2p_0$ and $2p_{\pm 1}$ states of H atom moving under classical weakly coupled plasma, classical dusty plasma and quantum plasma for a particular plasma particle density and very few ion velocity (v). The energy eigenvalues of $1s_0$ $2s_0$, $2p_0$ and $2p_{\pm 1}$ states of free static hydrogen atom are also evaluated to observe the shift in the energy eigenvalues in the plasma conditions. In the next phase, the energy eigenvalues of ns_0 $[n = 1 - 4]$; np_0, $np_{\pm 1}$ $[n = 2 - 4]$; nd_0, $nd_{\pm 1}$, $nd_{\pm 2}$ $[n = 3 - 4]$ and nf_0, $nf_{\pm 1}$, $nf_{\pm 2}$, $nf_{\pm 3}$ $[n = 4]$ states of C^{5+} ion moving under electron–hole quantum plasma are given elaborately for different set of plasma densities and various ion velocities.

2.4.1 H atom in classical weakly coupled plasma

The plasma we consider is composed of free electrons and H^+ ions having equal number density $n = 10^{21} m^{-3}$. With a view to assessing the effects of plasma environment and the 'wake' potential through the ESCP and NFWP terms (equation–2.3.8) respectively, we have also carried out the energy calculation for a 'free' (no plasma in the surrounding) and

static H atom. For a free atom, we set $\lambda_D = \infty$ and for a static H atom, we set $v = 0$ in equation (2.3.8). Moreover, there is no velocity dependent distortion in the wavefunction for static H atom and hence, we set $a = 1,\ b = 0$ in equation (2.3.1). All the results are given in table (2.4.1). The present results for free and static H atom can be readily verified from Bohr's energy formula $E_n = -\mu_H \frac{1}{2n^2}$ (a.u.) where $\mu_H = \frac{m_H}{m_H + 1}$ is the reduced mass of hydrogen atom. In this expression, $m_H = 1836.152667$ a.u. is the mass of the nucleus *i.e.* of proton and n is the principal quantum number of the states. Under the plasma environment having density $n = 10^{21} m^{-3}$, the energy eigenvalues of static hydrogen atom ($v = 0$) become more positive with respect to the free case, exhibiting the effect of ESCP. It is evident from Table (2.4.1) that $2s_0$, $2p_0$ and $2p_{\pm 1}$ states are degenerate in the free case, but under plasma environment ($n = 10^{21} m^{-3}$ and $v = 0$), the energy of $2s_0$ state becomes more negative (*i.e.* more bound) than $2p_{0,\pm 1}$ states. This is the typical breaking of accidental degeneracy (*i.e.* the l–degeneracy corresponding to a given n) which occurs due to the presence of plasma surrounding, or in other words, the effect of ESCP. However, the $2p_0$ and $2p_{\pm 1}$ states are still degenerate, as is seen from table (2.4.1). When the H

Table 2.4.1: Energy eigenvalues (*a.u.*) of $1s_0$, $2s_0$, $2p_0$ and $2p_{\pm 1}$ states of H atom moving in classical plasma having number density $n = 10^{21} m^{-3}$ of electrons for different ion velocities v (m/s).

n	v	$1s_0$	$2s_0$	$2p_0$	$2p_{\pm 1}$
free	0	–0.499727	–0.124931	–0.124931	–0.124931
10^{21}	0	–0.499720	–0.124924	–0.124921	–0.124921
	1×10^4	–0.499682	–0.124822	–0.124782	–0.124854
	1×10^5	–0.499447	–0.123987	–0.121662	–0.124174
	3×10^5	–0.498917	–0.122123	–0.115341	–0.122698
	5×10^5	–0.498388	–0.120269	–0.109149	–0.121231
	7×10^5	–0.497859	–0.118425	–0.102968	–0.119809
	9×10^5	–0.497330	–0.116589	–0.097177	–0.118363

atom is moving ($v \neq 0$) through the plasma, the effect of NFWP on the energy eigenvalues comes into play. Due to the presence of the '$\cos\theta$' term in NFWP, the $|m|$–degeneracy is eliminated for each ion velocity (v) and thus, a Stark–like splitting of energy levels are

found. For example, table (2.4.1) shows, for $v = 10^4\ m/s$ and $n = 10^{21}m^{-3}$, the energy eigenvalues of $2p_0$ and $2p_{\pm1}$ states are –0.124782 a.u. and –0.124854 a.u. respectively. Similar feature is observed for other velocities also. It is evident that at higher velocities (say, $v \geqslant 10^5\ m/s$), the effect of NFWP becomes more prominent. For, $n = 10^{21}m^{-3}$, we have found maximum effect of NFWP at $v \simeq 9 \times 10^5\ m/s$ beyond which the thermal Mach number of the moving ion defined by the ratio $M_T = \frac{v}{v_s}(s = e,\ i)$ becomes close to unity or even higher. The thermal Mach number depends strictly on the density of plasma particles. The present methodology is valid when $M_T < 1$ and, therefore, for $v > 10^5\ m/s$ when $n = 10^{21}m^{-3}$, the expression for NFWP may not be completely valid.

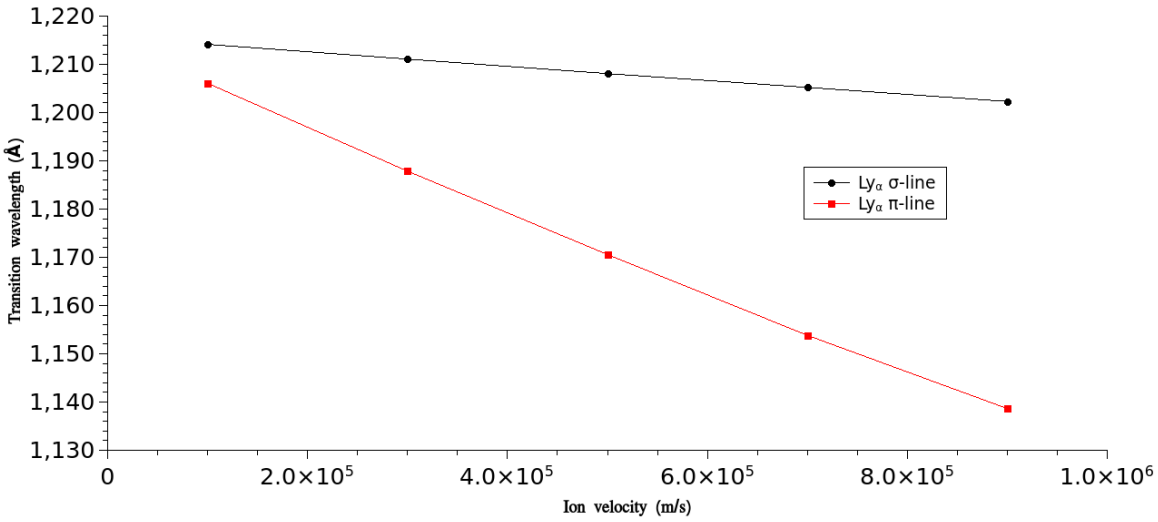

Figure 2.4.1: Transition wavelength of π and σ-components of Lyman-α lines of a moving hydrogen in classical plasma environment.

From the data given in Table (2.4.1), we can estimate the transition wavelength (λ) of π-line ($2p_0 \rightarrow 1s_0$) and σ-line ($2p_{\pm1} \rightarrow 1s_0$) corresponding to Lyman-α transition of hydrogen atom. In Figure (2.4.1), we have depicted the variation of λ with respect to ion velocity (v) under classical plasma environment. The conversion factor used here to obtain the transition wavelength λ (in Å) from the energy difference (ΔE in a.u.) between initial and final states is $\lambda = \frac{455.633494}{\Delta E}$. It is seen from Figure (2.4.1) that although λ values of both π and σ lines decrease as v increases, the rate of decrease of λ is faster in case of π-lines than of σ-lines. Thus, a 'blue-shift' of spectral lines corresponding to Lyman-α transition can be found under plasma environment if the ion velocity increases. In a real scenario, when an initially energized moving ion loses its kinetic energy due to various processes in plasma and consequently its velocity decreases, a 'red-shift' in both π and σ components of Lyman-α transition in weakly coupled classical plasma environment should be observed. This feature may find important application in the field of plasma diagnostics.

2.4.2 H atom in classical dusty plasma

Similar to classical plasma, the energy eigenvalues of $1s_0$, $2s_0$, $2p_0$ and $2p_{\pm1}$ states of hydrogen atom in dusty plasma environment are estimated using Ritz variational method and the results are given in table (2.4.2). For the sake of comparison, the results of 'free' and static H-atom are also given in table (2.4.2). We have chosen typical size of dust radius $r_d = 0.5$ nm, charge accumulated on dust grain $Z_d = 100$ a.u. and mass of dust grains $m_d = 10000 m_H$ in these calculations. The parameters of the model potential are chosen appropriately to mimic classical plasma environment. The densities of plasma electrons, ions (H^+) and dust particles are taken as $n_e = 10^{21}\ m^{-3}$, $n_i = 2 \times 10^{21}\ m^{-3}$ and $n_d = 10^{19}\ m^{-3}$ respectively. The temperatures of electron (T_e), ion (T_i) and dust (T_d) are taken as $T_d = T_i = 2T_e$ and where $T_e = 2.9 \times 10^4$ K. For these plasma parameters, the effective plasma screening length becomes $\lambda_t = 971.16$ a.u. or 51.39 nm.

Table 2.4.2: Energy eigenvalues ($a.u.$) of $1s_0$, $2s_0$, $2p_0$ and $2p_{\pm1}$ states of H atom moving in classical dusty plasma having number density $n_e = 10^{21} m^{-3}$ of electrons for different ion velocities v (m/s).

n_e	v	$1s_0$	$2s_0$	$2p_0$	$2p_{\pm1}$
free	0	–0.49972783	–0.12493196	–0.12493196	–0.12493196
10^{21}	0	–0.49869893	–0.12389767	–0.12397295	–0.12397295
	1.0×10^3	–0.49869808	–0.12389719	–0.12390410	–0.12397267
	1.0×10^4	–0.49869388	–0.12389288	–0.12389723	–0.12397038
	1.5×10^4	–0.49869165	–0.12389052	–0.12389342	–0.12396911
	2.0×10^4	–0.49868943	–0.12388816	–0.12388960	–0.12396784
	2.5×10^4	–0.49868720	–0.12388580	–0.12388579	–0.12396657
	3.0×10^4	–0.49868497	–0.12388344	–0.12388197	–0.12396530

As shown in table (2.4.2), for the static case ($v = 0$) due to the effect of ESCP part in the potential (2.3.10), the l-degeneracy is removed and as a result the energy of $2s_0$ state becomes different from those of $2p_0$ and $2p_{\pm1}$ states. While studying the variation of energy eigenvalues with respect to v, the thermal Mach number $M_T = \dfrac{v}{v_s}$ $(s = e, i, d)$ is kept below unity to maintain the validity of the model potential. For $v > 0$, the $|m|$ degeneracy of energy eigenvalues is removed due to the '$\cos\theta$' term in NFWP and DP parts in the effective

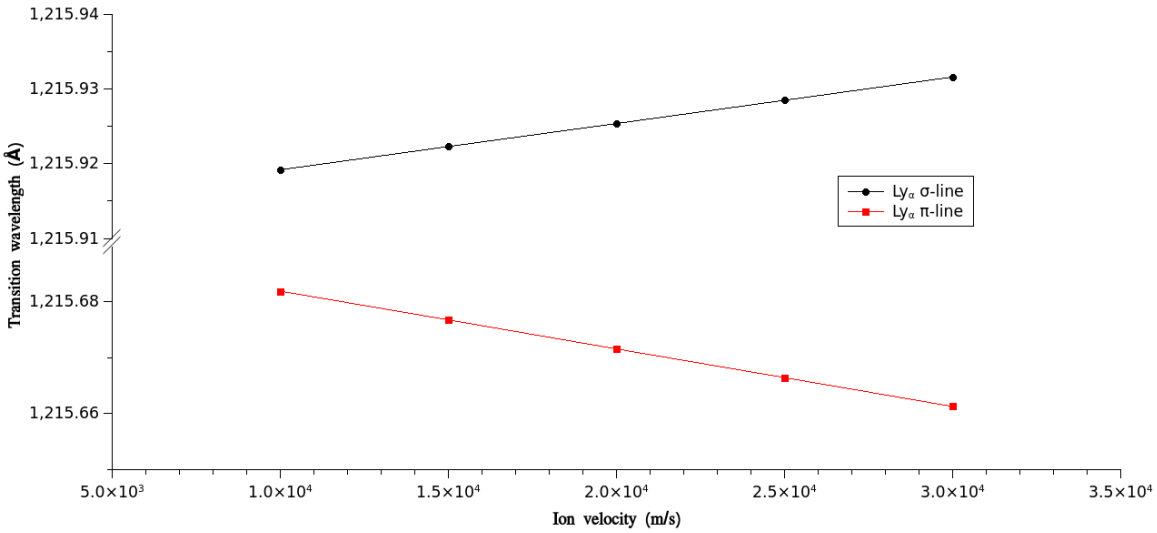

Figure 2.4.2: Transition wavelength of π and σ-components of Lyman-α lines of a moving hydrogen in classical dusty plasma environment.

potential (2.3.10). This feature is more or less similar to what was found in classical plasma environment. For instance, table (2.4.2) shows that the energy eigenvalues of the $2p_0$ and $2p_{\pm1}$ states are –0.12390410 a.u. and –0.12397267 a.u. respectively, indicating that the states are not degenerate at ion velocity $v = 10^3\ m/s$ and plasma electron density $n_e = 10^{21}\ m^{-3}$, thus giving rise to Stark-like splitting. This splitting becomes more prominent at velocities greater than $10^4\ m/s$, as is shown in table (2.4.2).

Similar to the classical plasma, we have estimated the transition wavelengths (λ) of π and σ components of Lyman-α transition of moving H atom for different v under classical dusty plasma environment and variation of λ with respect to v is shown in figure (2.4.2). It is remarkable that, unlike the classical plasma, the variation of λ show different behaviour for π and σ-lines. It can be seen from figure (2.4.2) that for π–line λ decreases ('blue-shift') as v increases whereas the σ–line shows red-shift.

2.4.3 H-like ion in quantum plasma

The energy eigenvalues of $1s_0$, $2s_0$, $2p_0$ and $2p_{\pm1}$ states of hydrogen atom moving in electron-hole quantum plasma are estimated variationally, as is done in previous cases, and the results are given in table (2.4.3). Number densities of electrons and holes are considered to be equal:$n_e = n_h = 10^{25}\ m^{-3}$. The effective masses of hole and electron are taken as $m_h = 0.39M_e$ and $m_e = 0.26M_e$ respectively [163, 164], where M_e is the rest mass of the electron. Table (2.4.3) shows that under quantum plasma environment the energy eigenvalues of static hydrogen atom ($v = 0$) increase from the free energy eigenvalues. It is also evident that under the same plasma condition ($n_e = 10^{25}m^{-3}$ and $v = 0$), the breaking of l-degeneracy takes place due to the effect of ESCP, similar to that observed in classical

Table 2.4.3: Energy eigenvalues ($a.u.$) of $1s_0$, $2s_0$, $2p_0$ and $2p_{\pm1}$ states of H atom moving in quantum plasma having electron number density $n_e = 10^{25}m^{-3}$ of electrons for different ion velocities v (m/s). The notation $P(\pm Q)$ stands for $P \times 10^{\pm Q}$.

n_e	v	$1s_0$	$2s_0$	$2p_0$	$2p_{\pm1}$
free	0	–0.499727	–0.124931	–0.124931	–0.124931
10^{25}	0	–0.346612	–0.200549(–1)	–0.129652(–1)	–0.129652(–1)
	1.0×10^4	–0.346600	–0.200511(–1)	–0.129595(–1)	–0.129632(–1)
	1.0×10^5	–0.346571	–0.200227(–1)	–0.129097(–1)	–0.129455(–1)
	1.2×10^5	–0.346565	–0.200164(–1)	–0.128986(–1)	–0.129418(–1)
	1.4×10^5	–0.346558	–0.200101(–1)	–0.128876(–1)	–0.129379(–1)
	1.6×10^5	–0.346552	–0.200038(–1)	–0.128765(–1)	–0.129340(–1)
	1.8×10^5	–0.346545	–0.199975(–1)	–0.128654(–1)	–0.129301(–1)

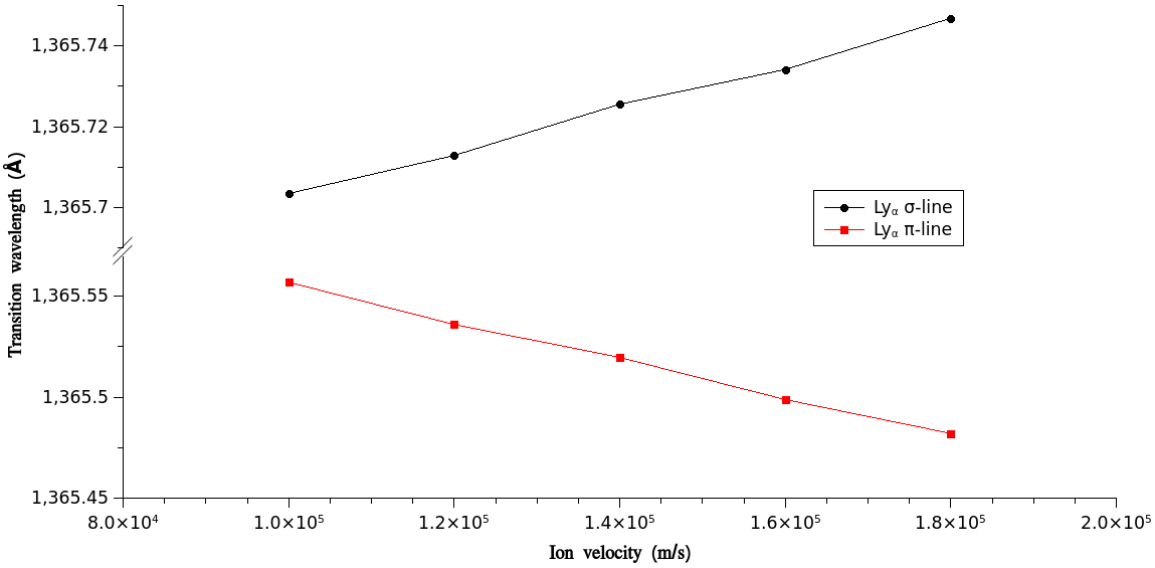

Figure 2.4.3: Transition wavelength of π and σ-components of Lyman-α lines of a moving hydrogen in quantum plasma environment.

plasma. For hydrogen atom moving with velocity $v = 10^4\ m/s$ the energy eigenvalues of all the states increases slowly. In this case, the energy eigenvalues of $2p_0$ and $2p_{\pm1}$ states become –0.0129595 a.u. and –0.0129632 a.u. respectively, which denotes the lifting of $|m|$-degeneracy and Stark-like splitting is observed in this case also. Similar features are observed for the higher velocities up to $v = 1.8 \times 10^5\ m/s$, as shown in table (2.4.3).

Figure (2.4.3) shows the variation of transition wavelengths (λ) of π and σ-lines corresponding to the Lyman-α transition of hydrogen atom with respect to different v under the quantum plasma environment. Similar features are observed as found in case of classical dusty plasma environment *i.e.* λ of the π-line decreases ('blue-shift) and for σ-line, it increases ('red-shift) as the ion velocity (v) increases.

C^{5+} ion

We have made an extensive study on the energy eigenvalues of ns_0 $[n = 1 - 4]$; np_0, $np_{\pm1}$ $[n = 2-4]$; nd_0, $nd_{\pm1}$, $nd_{\pm2}$ $[n = 3-4]$ and nf_0, $nf_{\pm1}$, $nf_{\pm2}$, $nf_{\pm3}$ $[n = 4]$ states of C^{5+} ion moving under quantum plasma environment considering the relevant parameters similar to real experimental scenario.

Table 2.4.4: Values of plasma screening lengths (λ_Q in a.u.) and the coefficients of the wake potential (ξ in a.u.) of C^{5+} moving in QP for different plasma particle densities n_s (in /c.c.) and ion velocities v (in cm./sec). The symbol $P(+Q)$ corresponds to $P \times 10^Q$.

n_s(/c.c.)	v(cm./sec)	λ_Q(a.u)	ξ(a.u.)
10^{19}	10^3	0.5856781(+01)	0.3826279(-05)
	10^5		0.3826279(-03)
	10^7		0.3826279(-01)
10^{20}	10^3	0.3990179(+01)	0.3826279(-05)
	10^5		0.3826279(-03)
	10^7		0.3826279(-05)
10^{21}	10^3	0.2718477(+01)	0.3826279(-05)
	10^5		0.3826279(-03)
	10^7		0.3826279(-01)
10^{22}	10^3	0.1852077(+01)	0.3826279(-05)
	10^5		0.3826279(-03)
	10^7		0.3826279(-01)
10^{23}	10^3	0.1261805(+01)	0.3826279(-05)
	10^5		0.3826279(-03)
	10^7		0.3826279(-01)

The effective masses of the plasma constituting electron (e) and hole (h) are 0.26 a.u. and 0.39 a.u. respectively [163, 164]. Such parameters carry physical significance if we

Table 2.4.5: Convergence of the energy eigenvalues ($a.u.$) of $1s_0$, $2p_{\pm1}$, $3d_{\pm2}$ and $4f_{\pm3}$ states of C^{5+} moving in QP. The plasma particle density $n_s = 10^{19}$/c.c. and the velocity of the ion $v = 10^3$cm./sec. N represents the total number of terms in the basis set.

N	$1s_0$	N	$2p_{\pm1}$	N	$3d_{\pm2}$	N	$4f_{\pm3}$
1	16.996 989 379	2	3.516 726 519	3	1.101 328 256	4	0.328 549 543
3	16.996 997 305	5	3.544 757 189	7	1.114 962 499	9	0.329 492 549
6	16.996 997 518	9	3.544 757 475	12	1.114 962 616	15	0.329 493 091
15	16.996 997 543	20	3.544 757 476	25	1.114 962 632	22	0.329 493 108
28	16.996 997 543	35	3.544 757 476	42	1.114 962 632	39	0.329 493 108
45	16.996 997 543	54	3.544 757 476	52	1.114 962 632	49	0.329 493 108

consider the ion to be embedded inside Si where the temperature is very low (0–20 K). For other types of environment, the parameters may differ. We have considered the plasma particle densities (n_e and n_h) within the range $10^{19} - 10^{23}$/c.c. and ion velocities v in the range $10^3 - 10^7$cm./sec. Table (2.4.4) shows the values of plasma screening lengths λ_Q (equation–2.2.48) and the coefficients of the wake potential ξ (equation–2.3.14) in equation for the C^{5+} ion moving in the quantum plasma for different parameters. For each density, v is chosen in such a manner that the thermal Mach number (M) remains below unity. Orbital distortion parameters a and b (equation–2.3.1) are optimized using Nelder-Mead (NM) algorithm [161]. We increase the number(N) of terms in the basis set expansion (2.3.2) which includes different powers of 'r' to achieve desired level of accuracy of the energy eigenvalues for all the states considered. The ρ values we use here are different for different powers of 'r' and taken in decreasing geometrical sequence. Table (2.4.5) displays the results for convergence of energy eigenvalues for $1s_0$, $2p_{\pm1}$, $3d_{\pm2}$ and $4f_{\pm3}$ states with plasma density (n_s) 10^{19}/c.c. and ion velocity (v) 10^3 cm./sec. It is evident from table (2.4.5) that the energy eigenvalues converge upto 9–th decimal place in each case. Similar convergence of energy values are obtained for all the calculations done here.

Tables (2.4.6), (2.4.7) and (2.4.8) show the energy eigenvalues of C^{5+} ion for $n = 1-4$ levels corresponding to different n_s and v. The first row of each table shows the free results *i.e.* without plasma medium, which agrees with the non-relativistic energy eigenvalues $-\frac{Z^2}{2n^2}$ (a.u.) of one-electron systems where $Z = 6$. The results presented in the tables (2.4.6), (2.4.7) and (2.4.8) show that the energies become more and more positive as plasma particle density and ion velocity increase.

The reason behind this behavior is that, as we increase n_s it decreases λ_Q which screens or scales down the effect of Coulomb potential largely. On the other hand, the wake coefficient ξ increases as v increases, which strengthens the positive NFWP resulting in the shift of energy levels towards continuum. In order to asses the effect of ESCP on the energy of C^{5+} ion in quantum plasma environment, we set $v = 0$ in our calculations and the results

Table 2.4.6: The energy eigenvalues -E (a.u.) of $1s_0$, $2s_0$, $2p_0$ and $2p_{\pm1}$ states of C^{5+} moving in QP having different sets of plasma particle (electron and hole) densities n_s (/c.c.) and ion velocities v (cm./sec).

		-E (a.u.)			
n_s (/c.c.)	v (cm./sec)	$1s_0$	$2s_0$	$2p_0$	$2p_1$
0	0	18.00000000	4.50000000	4.50000000	4.50000000
10^{19}	0	16.99701207	3.55780856	3.54476161	3.54476161
	10^3	16.99699754	3.55780693	3.54472655	3.54475747
	10^5	16.99699738	3.55780657	3.54472073	3.54475700
	10^7	16.99698206	3.55777061	3.54418783	3.54449515
10^{20}	0	16.54217234	3.16902746	3.14230776	3.14230777
	10^3	16.54214839	3.16902456	3.14229037	3.14224439
	10^5	16.54214822	3.16902418	3.14229621	3.14224287
	10^7	16.54213093	3.16898702	3.14223675	3.14215211
10^{21}	0	15.89053458	2.65209786	2.59865596	2.59865596
	10^3	15.89046598	2.65208981	2.59862497	2.59858157
	10^5	15.89046573	2.65208933	2.59862135	2.59858025
	10^7	15.89044045	2.65204099	2.59825988	2.59844818
10^{22}	0	14.96731440	1.99849293	1.89549274	1.89549274
	10^3	14.96727643	1.99848876	1.89542088	1.89549069
	10^5	14.96727627	1.99848850	1.89541666	1.89549053
	10^7	14.96726037	1.99846268	1.89483600	1.89547373
10^{23}	0	13.68055489	1.23890690	1.05303897	1.05303897
	10^3	13.68051129	1.23890275	1.05281193	1.05303710
	10^5	13.68051115	1.23890257	1.05280651	1.05303730
	10^7	13.68049712	1.23888478	1.05229719	1.05302671

are displayed in the first row of each density in the tables (2.4.6), (2.4.7) and (2.4.8). The energy eigenvalues in these cases show that for a fixed principle quantum number (n), the states with different angular momentum (l) are now non-degenerate *e.g.* from table (2.4.6), for $n_s = 10^{19}$/c.c. and $v = 0$, we see that the energies of $2s_0$ and $2p_0$(or $2p_{\pm1}$) states are -3.55780856 a.u. and -3.54476161 a.u. respectively, whereas they are degenerate in the free case with energy -4.5 a.u. Thus the ESCP lifts the 'l' degeneracy corresponding to a fixed value of n. Although the energy levels are still degenerate with respect to the 'm' values *i.e.* energies of $2p_0$ and $2p_{\pm1}$ are still the same as discussed in the above example. Same feature can be found from the tables (2.4.6), (2.4.7) and (2.4.8), for all n_s and $v = 0$. The increase in energy eigenvalues with the increase in v takes place in a much slower rate as compared to the same with respect to the increase of n_s. It is evident that the effect of static ($v = 0$) ESCP is more pronounced than the velocity dependent NFWP under the quantum plasma environment considered. The significant role of the NFWP is that it

Table 2.4.7: The energy eigenvalues -E (a.u.) of $3s_0$, $3p_0$, $3p_{\pm1}$, $3d_0$, $3d_{\pm1}$ and $3d_{\pm2}$ states of C^{5+} moving in QP having different sets of plasma particle (electron and hole) densities n_s (/c.c.) and ion velocities v (cm./sec).

		-E (a.u.)					
n_s	v	$3s_0$	$3p_0$	$3p_{\pm1}$	$3d_0$	$3d_{\pm1}$	$3d_{\pm2}$
0	0	2.00000000	2.00000000	2.00000000	2.00000000	2.00000000	2.00000000
10^{19}	0	1.14923194	1.13789722	1.13789723	1.11496287	1.11496287	1.11496287
	10^3	1.14923145	1.13788733	1.13789606	1.11496273	1.11496270	1.11496263
	10^5	1.14923096	1.13787887	1.13789537	1.11496174	1.11496190	1.11496236
	10^7	1.14918232	1.13709896	1.13759242	1.11486312	1.11488121	1.11493546
10^{20}	0	0.85275345	0.83113577	0.83113577	0.78686902	0.78686902	0.78686902
	10^3	0.85275269	0.83113114	0.83111901	0.78686882	0.78686878	0.78686868
	10^5	0.85275224	0.83113021	0.83111706	0.78686792	0.78686805	0.78686843
	10^7	0.85270789	0.83104578	0.83097475	0.78677385	0.78679108	0.78684275
10^{21}	0	0.51307024	0.47479205	0.47479205	0.39462864	0.39462864	0.39462864
	10^3	0.51306840	0.47478483	0.47477478	0.39462843	0.39462840	0.39462828
	10^5	0.51306792	0.47478106	0.47477341	0.39462775	0.39462784	0.39462810
	10^7	0.51302066	0.47440449	0.47463583	0.39455982	0.39457226	0.39460957
10^{22}	0	0.18762946	0.13082887	0.13082887		0.01136017	0.01136017
	10^3	0.18762878	0.13081719	0.13082853		0.01136002	0.01135996
	10^5	0.18762861	0.13081432	0.13082842		0.01135976	0.01135987
	10^7	0.18761157	0.13044258	0.13081701		0.01133326	0.01135103
10^{23}	0	0.00358750					
	10^3	0.00358738					
	10^5	0.00358736					
	10^7	0.00358535					

lifts the $|m|$ degeneracy of the states. For example, from table-2.4.6 we can find that for $n_s = 10^{19}$/c.c. and $v = 10^3$cm./sec, the energy eigenvalues of $2p_0$ and $2p_{\pm1}$ are -3.54472655 a.u. and -3.54475747 a.u. *i.e.* $2p_0$ and $2p_{\pm1}$ are non-degenerate by an amount 0.00003092 a.u. Similar results can be found for np_0, $np_{\pm1}$ $[n = 2-4]$; nd_0, $nd_{\pm1}$, $nd_{\pm2}$ $[n = 3-4]$ and nf_0, $nf_{\pm1}$, $nf_{\pm2}$, $nf_{\pm3}$ $[n = 4]$ states for all the cases with $n_s \neq 0$ and $v \neq 0$, as given in the tables (2.4.6), (2.4.7) and (2.4.8). The removal of $|m|$ degeneracy for $l \geq 1$ states arises due to the '$\cos\theta$' term in the velocity (v) dependent NFWP under the quantum plasma environment, which resembles with the *Stark-like splitting* of the energy levels.

Table 2.4.8: The energy eigenvalues -E (a.u.) of $4s_0$, $4p_0$, $4p_{\pm1}$, $4d_0$, $4d_{\pm1}$, $4d_{\pm2}$, $4f_0$, $4f_{\pm1}$, $4f_{\pm2}$ and $4f_{\pm3}$ states of C^{5+} moving in quantum plasmas having different set of plasma particle (electron and hole) densities n_s (/c.c.) and ion velocities v (cm./sec).

		-E_{4s} (a.u.)	-E_{4p} (a.u.)		-E_{4d} (a.u.)			-E_{4f} (a.u.)			
n_s	v	$\|m\|$=0	$\|m\|$=0	$\|m\|$=1	$\|m\|$=0	$\|m\|$=1	$\|m\|$=2	$\|m\|$=0	$\|m\|$=1	$\|m\|$=2	$\|m\|$=3
0	0	1.12500000	1.12500000	1.12500000	1.12500000	1.12500000	1.12500000	1.12500000	1.12500000	1.12500000	1.12500000
10^{19}	0	0.38627150	0.37710044	0.37710044	0.35842741	0.35842741	0.35842741	0.32949318	0.32949318	0.32949318	0.32949318
	10^3	0.38627133	0.37709676	0.37710000	0.35842735	0.35842734	0.35842731	0.32949313	0.32949313	0.32949312	0.32949310
	10^5	0.38627083	0.37708789	0.37709929	0.35842627	0.35842645	0.35842702	0.32949196	0.32949206	0.32949235	0.32949285
	10^7	0.38622101	0.37626956	0.37679442	0.35831828	0.35833810	0.35839757	0.32936955	0.32938029	0.32941613	0.32946744
10^{20}	0	0.19334518	0.17815971	0.17815971	0.14683884	0.14683884	0.14683884	0.09678684	0.09678684	0.09678684	0.09678684
	10^3	0.19334495	0.17815827	0.17815457	0.14683878	0.14683877	0.14683874	0.09678681	0.09678681	0.09678680	0.09678679
	10^5	0.19334458	0.17815633	0.17815294	0.14683800	0.14683813	0.14683852	0.09678618	0.09678623	0.09678639	0.09678666
	10^7	0.19330816	0.17808454	0.17803027	0.14675666	0.14677158	0.14681633	0.09672344	0.09672894	0.09674547	0.09677302
10^{21}	0	0.03820810	0.02020779	0.02020779							
	10^3	0.03820777	0.02020659	0.02020495							
	10^5	0.03820756	0.02020497	0.02020436							
	10^7	0.03818578	0.02004326	0.02014525							

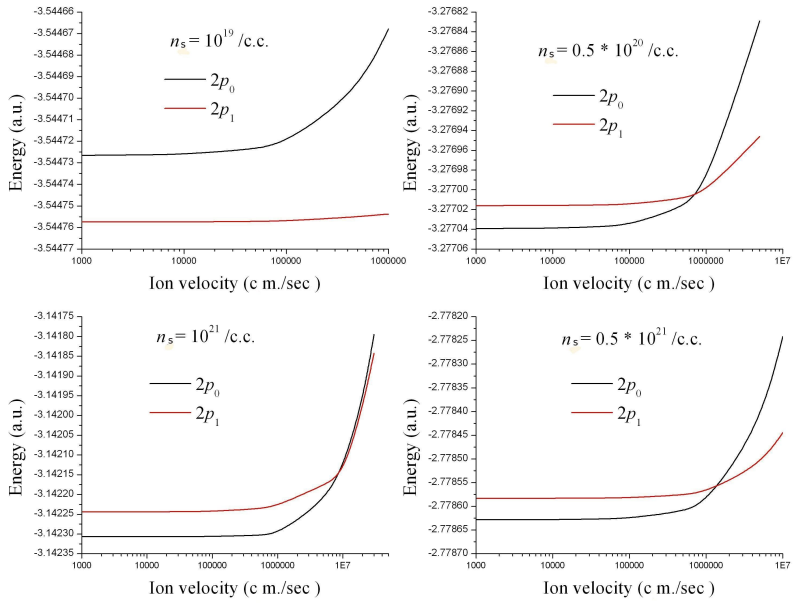

Figure 2.4.4: Plot of energy values (in a.u.) of $2p_0$ and $2p_1$ states of C^{5+} against ion velocity (in cm./sec) for different plasma particle densities n_s (/c.c).

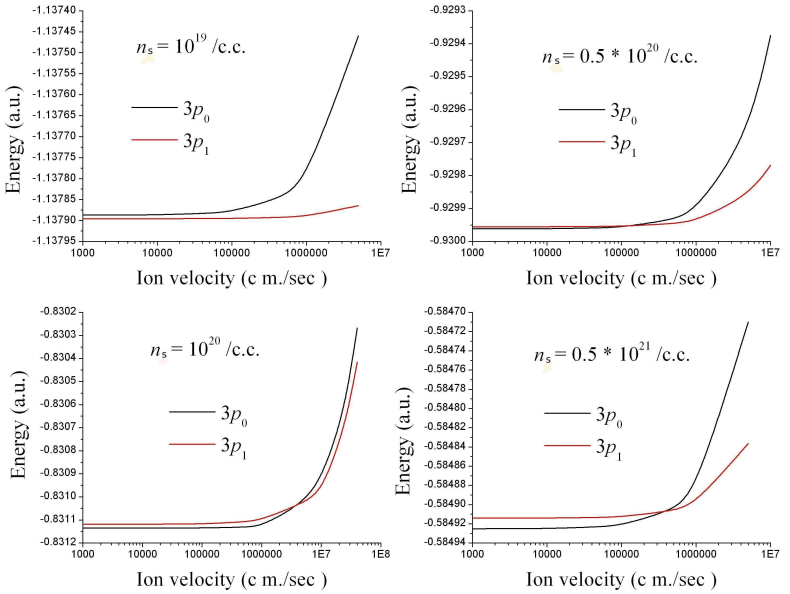

Figure 2.4.5: Plot of energy values (in a.u.) of $3p_0$ and $3p_1$ states of C^{5+} against ion velocity (in cm./sec) for different plasma particle densities n_s (/c.c).

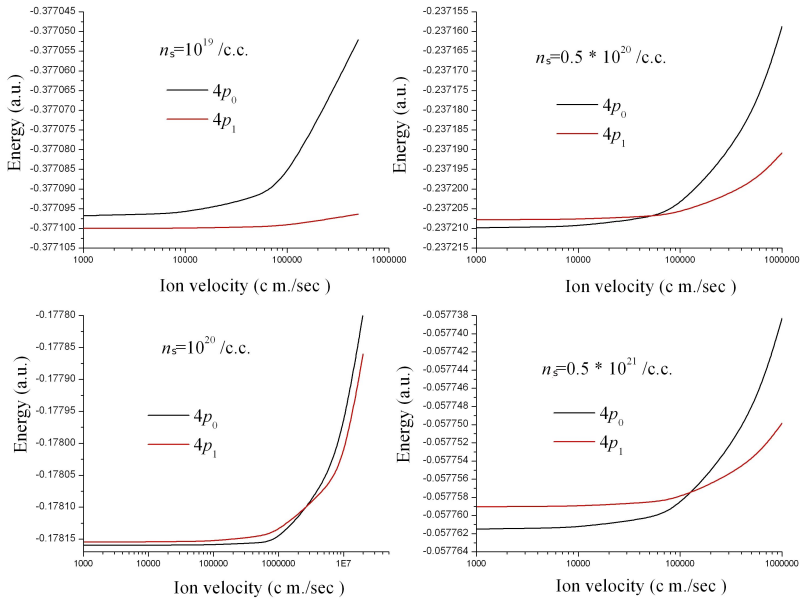

Figure 2.4.6: Plot of energy values (in a.u.) of $4p_0$ and $4p_1$ states of C^{5+} against ion velocity (in cm/sec) for different plasma particle densities n_s (/c.c).

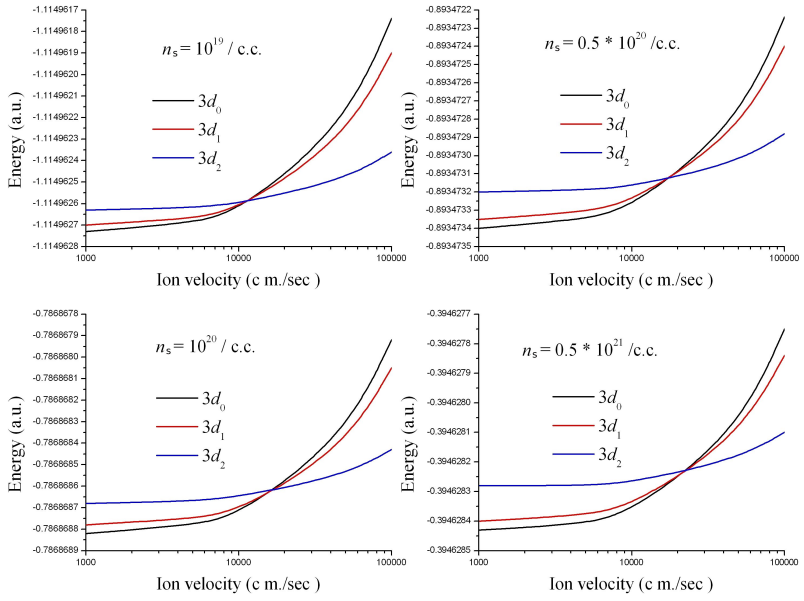

Figure 2.4.7: Plot of energy values (in a.u.) of $3d_0$, $3d_1$ and $3d_2$ states of C^{5+} against ion velocity (in cm/sec) for different plasma particle densities n_s (/c.c).

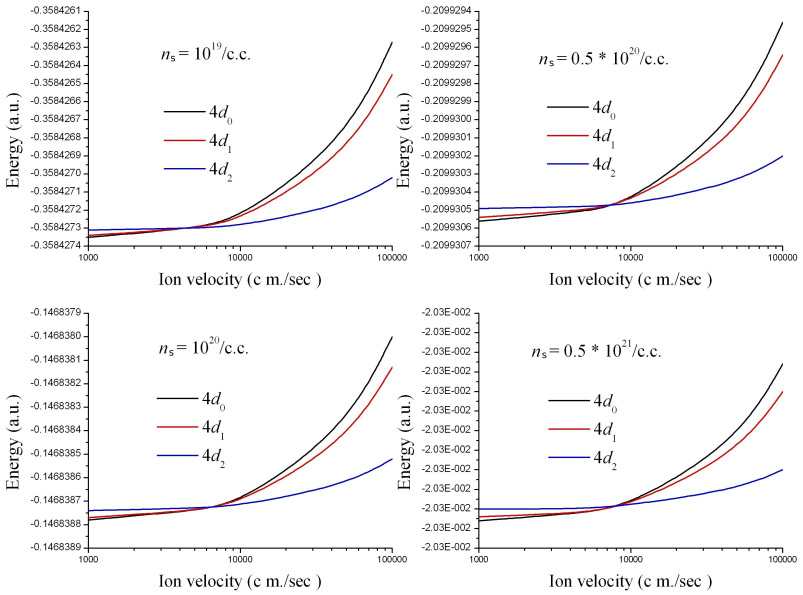

Figure 2.4.8: Plot of energy values (in a.u.) of $4d_0$, $4d_1$ and $4d_2$ states of C^{5+} against ion velocity (in cm/sec) for different plasma particle densities n_s (/c.c).

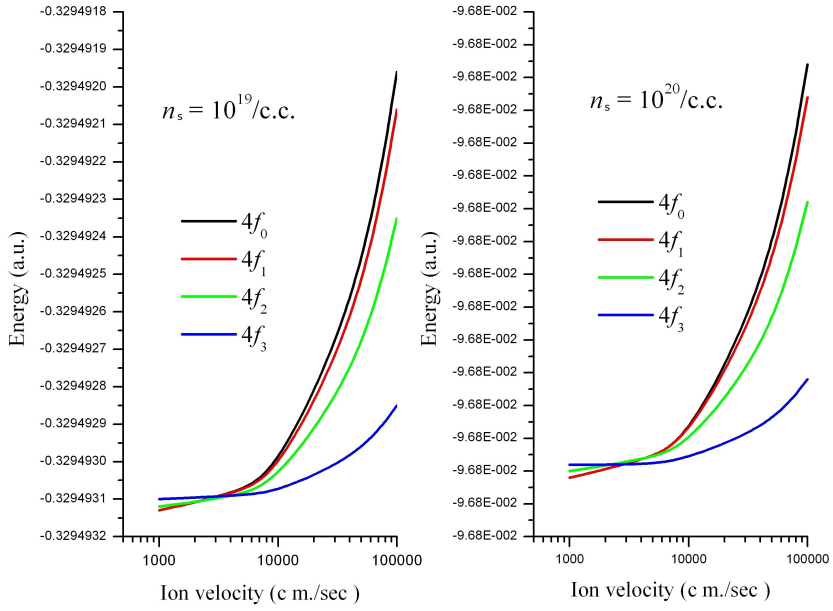

Figure 2.4.9: Plot of energy values (in a.u.) of $4f_0$, $4f_1$, $4f_2$ and $4f_3$ states of C^{5+} against ion velocity (in cm/sec) for different plasma particle densities n_s (/c.c).

The variation of energies of np_0, $np_{\pm1}$ $[n = 2-4]$; nd_0, $nd_{\pm1}$, $nd_{\pm2}$ $[n = 3-4]$ and nf_0, $nf_{\pm1}$, $nf_{\pm2}$, $nf_{\pm3}$ $[n = 4]$ states with v for few fixed values of n_s are shown in the figures (2.4.4), (2.4.5), (2.4.6), (2.4.7), (2.4.8) and (2.4.9), respectively. It is evident from figure (2.4.4) that corresponding to plasma density $n_s = 10^{19}$/c.c, $2p_{\pm1}$ states energetically lie below $2p_0$ state for the entire range of ion velocity (v) and thus no crossing of energy levels is being observed. But, when the density is higher than the previous one, the $2p_0$ state lies energetically below $2p_{\pm1}$ states for low ion velocity, whereas after a '*critical ion velocity*', $2p_{\pm1}$ states become more negative than the $2p_0$ state, and hence crossover is observed. Similar feature of crossover of np_0 and $np_{\pm1}$ $[n = 3-4]$ states is observed and shown in figures (2.4.5) and (2.4.6), respectively. Hence, '*incidental degeneracy*' of np_0 and $np_{\pm1}$ states occurs at the '*critical ion velocity*'. The crossing of energy levels and subsequent appearance of incidental degeneracy of d and f states occur for each densities considered, as shown in the figures (2.4.7), (2.4.8) and (2.4.9). The phenomenon of incidental degeneracy was reported earlier by Sen [165] in case of a hydrogen atom, confined in an impenetrable spherical shell. Table (2.4.9) shows the values of critical ion velocities at the crossing points of p, d and f states with some selective plasma densities. In comparison to our

Table 2.4.9: Variation of energy eigenvalues $-E$ $(a.u.)$ and critical ion velocity (cm./sec) at the 'crossing point' of energy eigenvalue vs ion velocity curves, for different angular momentum states with respect to plasma particle densities n_s (/c.c.). The symbol $P(+Q)$ corresponds to $P \times 10^Q$.

Crossover States	n_s	Critical ion velocity	Energy (-E) at crossing
$2p_0$,$2p_1$	0.5(+20)	7.22(+5)	3.27700464
	1.0(+20)	8.79(+6)	3.14214490
	0.5(+21)	1.36(+6)	2.77855694
$3p_0$,$3p_1$	0.5(+20)	1.19(+5)	0.92995292
	1.0(+20)	3.75(+6)	0.83103806
	0.5(+21)	3.72(+5)	0.58490697
$4p_0$,$4p_1$	0.5(+20)	5.78(+4)	0.23720661
	1.0(+20)	2.78(+6)	0.83103806
	0.5(+21)	1.27(+5)	0.05775748
$3d_0$,$3d_1$,$3d_2$	1.0(+19)	1.13(+4)	1.11496259
	0.5(+20)	1.77(+4)	0.89347312
	1.0(+20)	1.67(+4)	0.78686862
	0.5(+21)	2.24(+4)	0.39462823
$4d_0$,$4d_1$,$4d_2$	1.0(+19)	4.70(+3)	0.35842729
	0.5(+20)	7.31(+3)	0.20993047
	1.0(+20)	6.51(+3)	0.14683872
	0.5(+21)	7.96(+3)	0.02025229
$4f_0$,$4f_1$,$4f_2$,$4f_3$	1.0(+19)	3.09(+3)	0.32949309
	0.5(+20)	2.64(+3)	0.16679314
	1.0(+20)	2.84(+3)	0.09678679

present calculations, there were some contrasting results reported by Hu *et.al.* [152] while studying the variation of energy eigenvalues of moving C^{5+} ion under the quantum plasma environment using Ritz variational principle. For example, Hu *et. al.* [152] reported that for $n_e = 8.0 \times 10^{17}$/c.c. and ion velocity $v = 5 \times 10^5$ cm./sec, the ground state ($1s_0$) energy of C^{5+} becomes -25.60524 a.u. which is more negative than the ground state energy -18.0 a.u. for the free C^{5+} ion. According to their calculation [152], the contribution of NFWP is negative which make the total energy of moving ion in quantum plasma overbound as compared to the 'free' case. The present calculation shows that, according to equation (2.3.13) the effect of NFWP is positive and the ground state ($1s_0$) energy of the C^{5+} ion as -17.33679 a.u. for $n_e = 8.0 \times 10^{17}$/c.c. and $v = 5 \times 10^5$ cm./sec. Table (2.4.10) shows the comparisons between the energy eigenvalues calculated in the present method to those obtained by Hu *et. al.* [152].

Table 2.4.10: The energy eigenvalues $-E$ $(a.u.)$ of ns_0 $[n = 1-4]$; np_0, np_1 $[n = 2-4]$; nd_0, nd_1, nd_2 $[n = 3-4]$ and nf_0, nf_1, nf_2, nf_3 $[n = 4]$ states of C^{5+} ion moving with velocity v (cm./sec) in a quantum plasma environment having particle density $n_s = 8.0 \times 10^{+17}$/c.c. The symbol $P(+Q)$ corresponds to $P \times 10^Q$.

State	v	$-E$ (present work)	$-E$ (Hu *et. al.* [152])
$1s_0$	1.0(+04)	17.33681118	16.98306649
	1.0(+05)	17.33681098	17.25328413
	5.0(+05)	17.33681008	25.60522514
$2s_0$	1.0(+04)	3.86368685	3.54344882
	1.0(+05)	3.86368633	3.57641662
	5.0(+05)	3.86368405	4.40032501
$2p_0$	1.0(+04)	3.85782487	3.52966415
	1.0(+05)	3.85781925	3.53956809
	5.0(+05)	3.85779427	3.77474159
$2p_1$	1.0(+04)	3.85779514	3.52956493
	1.0(+05)	3.85779322	3.52966415
	5.0(+05)	3.85778469	3.53214473
$3s_0$	1.0(+04)	1.40534564	1.13800837
	1.0(+05)	1.40534488	1.14713322
	5.0(+05)	1.40534149	1.36260174
$3p_0$	1.0(+04)	1.40001207	1.12586272
	1.0(+05)	1.40000307	1.12861525
	5.0(+05)	1.39996310	1.19290815
$3p_1$	1.0(+04)	1.40000402	1.12583700
	1.0(+05)	1.40000094	1.12586272
	5.0(+05)	1.39998729	1.12655361

Continuation of Table (2.4.10)

State	v	$-E$ (present work)	$-E$ (Hu *et. al.* [152])
$3d_0$	1.0(+04)	1.38931351	1.10181765
	1.0(+05)	1.38931254	1.10203080
	5.0(+05)	1.38930820	1.10715733
$3d_1$	1.0(+04)	1.38931351	1.10181765
	1.0(+05)	1.38931272	1.06519697
	5.0(+05)	1.38930917	1.10223659
$3d_2$	1.0(+04)	1.38931351	1.10181765
	1.0(+05)	1.38931325	1.10193893
	5.0(+05)	1.38931206	1.10490827
$4s_0$	1.0(+04)	0.58332127	0.38038470
	1.0(+05)	0.58332038	0.38363334
	5.0(+05)	0.58331642	0.45895839
$4p_0$	1.0(+04)	0.57864913	0.36991115
	1.0(+05)	0.57863836	0.37089235
	5.0(+05)	0.57859047	0.39373940
$4p_1$	1.0(+04)	0.57864648	0.36990012
	1.0(+05)	0.57864279	0.36991115
	5.0(+05)	0.57862644	0.37015737
$4d_0$	1.0(+04)	0.56923669	0.34919409
	1.0(+05)	0.56923546	0.34926980
	5.0(+05)	0.56923001	0.35111057
$4d_1$	1.0(+04)	0.56923670	0.34919336
	1.0(+05)	0.56923570	0.33600587
	5.0(+05)	0.56923124	0.34934403
$4d_2$	1.0(+04)	0.56923675	0.34919373
	1.0(+05)	0.56923642	0.34923783
	5.0(+05)	0.56923493	0.35030319
$4f_0$	1.0(+04)	0.55490176	0.31860361
	1.0(+05)	0.55490031	0.31861941
	5.0(+05)	0.55489389	0.31900087
$4f_1$	1.0(+04)	0.55490177	0.31849924
	1.0(+05)	0.55490045	0.31860544
	5.0(+05)	0.55489459	0.31865101
$4f_2$	1.0(+04)	0.55490179	0.31860397
	1.0(+05)	0.55490086	0.31866130
	5.0(+05)	0.55489667	0.32004822
$4f_3$	1.0(+04)	0.55490185	0.31860361

Continuation of Table (2.4.10)

State	v	$-E$ (present work)	$-E$ (Hu *et. al.* [152])
	1.0(+05)	0.55490153	0.31863742
	5.0(+05)	0.55490014	0.31860397

The second contradiction appears from the work of Hu *et. al.* [152] is that, they reported the lifting of degeneracy of the energy levels with respect to the magnetic quantum number 'm' *i.e.* '*Zeeman–like splitting*', due to the presence of velocity dependent wake part in the potential. But we have found that the calculation of the matrix element of kinetic energy have some mistakes and for this reason they observed Zeeman–like splitting of the energy levels. On the contrary, we get the Stark–like splitting of the energy levels due to the '$\cos\theta$' term in the velocity dependent NFWP (2.3.13).

Chapter 3

Three–body exotic ions

Three–body exotic ions

When the nucleus or the electrons or both are replaced by the exotic particles like muon (μ), pion (π), kaon (K), tauons (τ), positron (e^+), anti-proton ($\bar{p}$) etc., then the atomic systems are called *exotic systems*. The binding energies of such exotic systems are very high in comparison to the binding energy of an atomic system because of the exotic particles which are much heavier than the electrons. Examples of two–body exotic systems are positronium (e^+e^-), true-muonium ($\mu^+\mu^-$), anti-hydrogen ($e^+\bar{p}$), $\pi^+\pi^-$, $p^+\mu^-$, $p^+\pi^-$, p^+K^- etc. and three–body systems are negative positronium $Ps^-(e^+e^-e^-)$, $p^+p^+\mu^-$, $p^+p^+\pi^-$, $p^+p^+K^-$ etc. Few–body exotic systems are generally formed in particle accelerators by trapping exotic particles via Coulomb field due to a nucleus. The exotic systems formed in this manner are in high excited states from which they cascade down to the lowest energy level either by emitting photons or via Auger transitions. Since the experiments producing the exotic systems deal with high speed projectiles into the matter, it produces different charge states within the medium which can form a plasma environment which may, in turn alter the effective potential experienced by the exotic ions, or in other words, a screening through the environment is generated. Thus the structure calculations of the exotic systems become important to predict the fundamental processes of forming those exotic systems as well as the plasma parameters of the medium. Here we will give a detail account on the structural properties of two- and three-body exotic systems under classical weakly coupled plasma (WCP).

3.1 Literature review

Saha *et. al.* [166] and Sil *et. al.* [167] investigated the structural properties of two–body exotic $e^+e^-, p^+\mu^-$ and $\mu^+\mu^-$ using the time-dependent variation-perturbation theory under the influence of WCP formed within a spherical box. For a fixed radius of the box, it is seen that the transition energy, oscillator strength and transition probability of the Lyman-series ($1s \rightarrow np;\ n = 2, 3, 4$) decreases as μ_D increases.
In comparison to the two–body exotic systems, the structure calculations of three–body exotic systems under WCP grabs attentions of a larger number of researchers around the globe [168–195]. Stability and negative charge affinity (electron affinity and negative muonic affinity) of Ps^-, H_2^+ and H_2 molecule were investigated under WCP environment [170, 173, 176] using correlated wavefunctions in the variational framework. Kar and Ho [174]showed that dipole polarizabilitiy of $^1S^e$ and $^3P^o$ states of H_2^+ increases as μ_D increases.

The study on the few-body "Borromean" systems adds another dimension to the field of investigation on the stability of such systems under WCP environment. An $N-$body bound system ($N \geq 3$) is called a Borromean system if it's all $(N-1)$, $(N-2)$,....., 3, $2-$ body sub-systems are unbound [196]. In 1935, Borromean binding was first observed

by Thomas [197] while comparing three-nucleon and two-nucleon bound state energies. 35 years later, in the context of nuclear scattering, Efimov [198] showed weak binding of symmetric three–body bosonic system while its two–body subsystem does not exist − which is famously known as "Efimov effect". Except the nuclear physics, Borromean systems are also encountered in different disciplines of science like atom and molecular physics, chemical physics, biology etc. [199]. In the beginning of this century some experiments were reported where Borromean bindings in ultra–cold gas was confirmed [200–202]. Under the WCP environment Borromean binding is explained with respect to the critical screening parameter μ_D^c of the interaction potential modeled by ESCP (1.0.1). Critical screening parameter μ_D^c is defined as the specific value of plasma screening parameter/strength μ_D (1.0.1) for which the system placed under the plasma environment destabilizes, or in other words, the binding energy of the system becomes zero. While studying the stability of the ground states of H atom, H_2^+ and molecular H_2 under WCP using Monte Carlo technique, Bertini *et.al* [171] found that $(\mu_D^c)_{\rm H} < (\mu_D^c)_{H_2^+} < (\mu_D^c)_{H_2}$ *i.e.* both H_2^+ and H_2 show Borromean binding. Apart from the ground state Kar and Ho [182,183] observed Borromean binding of H_2^+ ion with respect to the variation of μ_D for the $^3P^o$,$^1D^e$,$^3F^o$ and $^1F^e$ states using exponentially correlated wavefunction under the variational framework. The Borromean binding of symmetric three–body exotic systems like $p^+p^+\mu^-$, $d^+d^+\mu^-$, $t^+t^+\mu^-$ (d^+ = deuteron and t^+ = triton) and asymmetric three–body exotic systems like $p^+d^+\mu^-$, $p^+t^+\mu^-$, $d^+t^+\mu^-$ are also reported in literature [177–179] where the workers estimated the Borromean window (BW) which is defined as the difference between the μ_{CD} values of three–body and its two–body sub-systems. Now the question arises that, which kind of three–body systems can show BW? Pont and Serra [179] estimated BWs of various symmetric three–body systems to address this question. They reported [179] BWs of symmetric three–body systems for different mass ratios (q_m) which is defined as $q_m = \dfrac{m'}{m}$ where m' = mass of the non-identical particle and m = mass of any one of the remaining two identical particles. It can be seen from their work [179] that BW exists for $q_m \leq 1$ *i.e.* only positively charged three–body systems can show BW. An extensive study has been made by Pawlak *et. al.* [184] where the authors performed variational calculations using correlated wavefunction to find the BWs for a large span of q_m. Their work revealed that BW exists for $q_m \leq 1.668$ *i.e.* some of the negatively charged three–body systems like $\pi^+\mu^-\mu^-$, Ps^- etc. can also posses BWs. Jiang *et. al.* [186] estimated BWs for positively charged heavy molecular ions like $p^+d^+e^-, p^+t^+e^-, d^+d^+e^-, d^+t^+e^-, t^+t^+e^-, d^+t^+\mu^-, p^+t^+\mu^-, p^+d^+\mu^-, p^+p^+\mu^-, d^+d^+\mu^-$ and $t^+t^+\mu^-$ under WCP using Hylleraas-type wavefunction in the framework of Ritz variational principle.

The study of resonance states of exotic atoms/ions are of great importance for the plasma diagnostics purpose. Kar and co-workers [188–193] made some useful studies on the effect of WCP on the resonance $^1S^e$,$^{1,3}P^o$,$^1D^e$ and $^{1,3}P^e$ states of Ps^- ion using correlated wavefunctions by adopting complex coordinate rotation (CCR) method and stabilization

method. It can be seen from their studies that resonance energy increases while the resonance width decreases as the plasma screening μ_D increases. Similar kind of investigations are reported [194,195] on muonic three-body exotic systems like $p^+p^+\mu^-, d^+d^+\mu^-, d^+t^+\mu^-$ etc. under WCP modeled by ESCP.

In this chapter, we present an extensive calculation of energy eigenvalues of ground states of different three–body exotic systems using Ritz variation technique under free and classical WCP environment. In total, we have considered 22 number of three–body systems. The trial wavefunction is expanded in explicitly correlated multi-exponent Hylleraas type basis set. Resonance $^1S^e$ states of symmetric three-body exotic pYY negative atomic ions ($Y = \mu^-, \pi^-, K^-$) and ppY positive molecular ions are studied in details under the framework of stabilization method. The resonance states under consideration lie below $N = 2$ ionization threshold of the corresponding two–body sub–systems pY.

3.2 The present method

In this section the trial wavefunction is constructed for variational calculation. The variation equation of the three-body system is formulated for general angular momentum states. The basis set expansion of the trial function is established and the method of evaluating the basis integrals is explained in detail. For the determination of resonance parameters (energy and width) of three body systems, the stabilization method is explained in detail and subsequently applied to find the resonance parameters of hadronic three-body systems.

3.2.1 Wavefunction

As per the proposal of Bhatia and Temkin [30], we have considered the trial wavefunction of the three body system as sum of the product of radial and angular functions which is given by

$$\Psi = \sum_k{}'' \left(f_L^{k+} D_L^{k+} + f_L^{k-} D_L^{k-} \right) \tag{3.2.1}$$

where $f_L^{k\pm} = f_L^{k\pm}(r_1, r_2, \theta_{12} \text{ or } r_{12})$ and $D_L^{k\pm} = D_L^{k\pm}(\theta, \phi, \psi)$ are the radial and angular functions respectively. r_1, r_2 and r_{12} are the sides of the triangle formed by the three body system, θ_{12} is the angle between $\vec{r_1}$ and $\vec{r_2}$. θ, ϕ and ψ are the Eulerian angles [30] through which the triangle formed by r_1, r_2 and r_{12} can rotate in space. The choice of the Eulerian angles is only the matter of convenience of the problem. We have adopted the same set of Eulerian angles (θ, ϕ, ψ) as given by Bhatia and Temkin [30]. We can start from the rotations of space fixed axes (X, Y, Z) through Eulerian angles θ, ϕ and ψ such that we can reach at the body fixed axes (X', Y', Z') as shown in figure (3.2.1). There are three steps of the rotations which are described below:

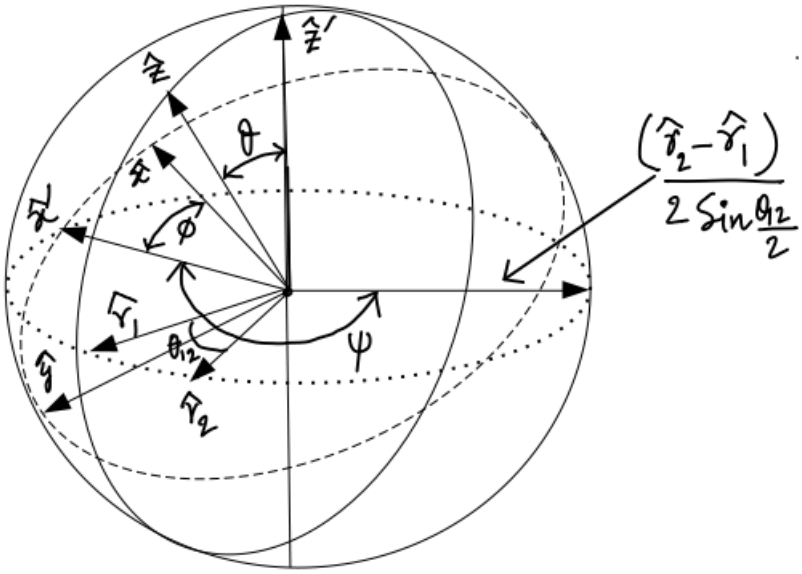

Figure 3.2.1: Diagram of Eulerian angles [30] connecting space fixed axes (X, Y, Z) with the body fixed axes (X', Y', Z').

i. Rotations are given in such a manner that $\vec{r}_1$ and $\vec{r}_2$ lie in the X′–Y′ plane (marked by dotted line in figure 3.2.1). First rotation is given with respect to Z–axis in the anti-clockwise direction by the angle ϕ so that X–axis ($\hat{x}$ in figure 3.2.1) coincides with the 'line-of-node' ($\hat{x}'$ in figure 3.2.1). The 'line-of-node' is the straight line where X–Y and X′–Y′ planes intersect each other.

ii. The second rotation is given with respect to line-of-node by an angle θ so that we get Z′–axis where the angle between Z and Z′ becomes θ, as shown in figure (3.2.1).

iii. The third rotation is given with respect to Z′–axis so that the axis in the direction $\dfrac{(\hat{r}_1 - \hat{r}_2)}{2\sin\dfrac{\theta_{12}}{2}}$ rotates through angle ψ in the clockwise direction and coincides on the line-of-node which gives rise to body fixed X′–axis. Y′–axis will be in the direction perpendicular to X′–axis which is not shown in figure (3.2.1).

The ranges of the Eulerian angles are : $0 \leq \theta \leq \pi$, $0 \leq \phi \leq 2\pi$ and $0 \leq \psi \leq 2\pi$.
In the equation (3.2.1), L is the *total angular momentum quantum number* of the coupled state of the particles of masses m_1 and m_2. If the individual angular momenta of the particles are l_1 and l_2, then according to the $LS-$coupling scheme, $L = (l_1 + l_2), (l_1 + l_2 - 1), ..., |l_1 - l_2|$. The double prime in the summation of the equation (3.2.1) signifies that the quantum number k takes every alternate positive integer values (even or odd). $D_L^{k\pm}$ are the real

symmetric top functions defined as

$$\begin{aligned} D_L^{k+} &= N_{Lk}\cos(k\psi)\sin^k\theta F_k \\ D_L^{k-} &= N_{Lk}\sin(k\psi)\sin^k\theta F_k \end{aligned} \tag{3.2.2}$$

The parameters N_{Lk} and F_k are given by

$$\begin{aligned} N_{Lk} &= \frac{(-1)^k}{2^k k!}\frac{1}{1+\delta_{0k}(\sqrt{2}-1)}\left[\frac{(2L+1)(L+k)!}{4\pi^2(L-k)!}\right]^{\frac{1}{2}} \qquad \text{and} \\ F_k &= {}_2F_1[L+k+1,-(L-k),k+1,\sin^2\theta/2] \end{aligned}$$

where ${}_2F_1$ is the hypergeometric function [156]. The real $D_L^{k\pm}$ functions are constructed from the complex Wigner D-functions [30, 203] which are basically eigenfunctions of total angular momentum operator L^2. The $D_L^{k\pm}$ functions obey the following identities [30]:

$$\frac{\partial D_L^{k+}}{\partial\psi} = -kD_L^{k-}; \qquad \frac{\partial D_L^{k-}}{\partial\psi} = kD_L^{k+} \tag{3.2.3}$$

The orthogonality conditions of the $D_L^{k\pm}$ functions are given below:

$$\begin{aligned} &\int D_L^{k+}D_L^{k'+}\sin\theta\ d\theta\ d\phi\ d\psi = \delta_{kk'} \\ &\int D_L^{k-}D_L^{k'-}\sin\theta\ d\theta\ d\phi\ d\psi = \delta_{kk'} \\ &\int D_L^{k+}D_L^{k'-}\sin\theta\ d\theta\ d\phi\ d\psi = 0 \end{aligned} \tag{3.2.4}$$

3.2.2 Variational equation

The Hamiltonian of the $(N+1)$ particle atom can be written as

$$\hat{H} = \hat{T} + \hat{V} \tag{3.2.5}$$

where, the kinetic energy (K.E.) operator $\hat{T}$ and the potential energy (P.E.) operator $\hat{V}$ are given by

$$\hat{T} = -\frac{1}{2M}\nabla_{R_0}^2 + \sum_{i=1}^{N}\left(-\frac{1}{2m_i}\nabla_{R_i}^2\right) \tag{3.2.6}$$

$$\hat{V} = -Z\sum_{i=1}^{N}\frac{1}{|R_0-R_i|} + \sum_{i=1}^{N}\sum_{j>i}^{N}\frac{1}{|R_i-R_j|} \tag{3.2.7}$$

Z is the atomic number of the atom. $\vec{R_0}$ and $\vec{R_i}$ are the position vectors of the nucleus of mass M and i-th particle $(i = 1, 2, ..., N)$ of mass m_i respectively. We seek the transformation of co-ordinates $\left(\vec{R_0}, \vec{R_1}, ..., \vec{R_N}\right) \rightarrow \left(\vec{R}, \vec{r_1}, ..., \vec{r_N}\right)$, where $\vec{r_i} = \vec{R_i} - \vec{R_0}$ is the position vector of i-th particle with respect to the nucleus and $\vec{R}$ is the position vector of center of mass (c.m.) of the system as given by

$$\vec{R} = \frac{1}{M_T}\left(M\vec{R_0} + \sum_{i=1}^{N} m_i\vec{R_i}\right) \tag{3.2.8}$$

where $M_T = M + \sum_{i=1}^{N} m_i$ = Total mass of the system. The X-components of the above equation and $\vec{r_i}$ are

$$X = \frac{1}{M_T}\left(MX_0 + m_1X_1 + ... + m_NX_N\right) \qquad and \qquad x_i = X_i - X_0 \tag{3.2.9}$$

From equation (3.2.9) the following derivatives are calculated

$$\frac{\partial X}{\partial X_i} = \frac{m_i}{M_T}, \qquad \frac{\partial X}{\partial X_0} = \frac{M}{M_T}, \qquad \frac{\partial x_i}{\partial X_i} = 1, \qquad \frac{\partial x_i}{\partial X_0} = -1$$

$$\begin{aligned} \therefore \frac{\partial}{\partial X_0} &= \frac{\partial X}{\partial X_0}\frac{\partial}{\partial X} + \frac{\partial x_1}{\partial X_0}\frac{\partial}{\partial x_i} + ... + \frac{\partial x_N}{\partial X_0}\frac{\partial}{\partial x_N} \\ &= \frac{M}{M_T}\frac{\partial}{\partial X} - \sum_{i=1}^{N}\frac{\partial}{\partial x_i} \end{aligned}$$

Evaluating $\frac{\partial}{\partial Y_0}$ and $\frac{\partial}{\partial Z_0}$ in the same manner we can rewrite $\vec{\nabla}_{R_0}$ and $\vec{\nabla}_{R_i}$ as

$$\vec{\nabla}_{R_0} = \frac{M}{M_T}\vec{\nabla}_R - \sum_{i=1}^{N}\vec{\nabla}_{r_i} \tag{3.2.10}$$

$$\vec{\nabla}_{R_i} = \frac{m_i}{M_T}\vec{\nabla}_R + \vec{\nabla}_{r_i} \tag{3.2.11}$$

$$\begin{aligned} \therefore \nabla^2_{R_0} &= \vec{\nabla}_{R_0}.\vec{\nabla}_{R_0} = \frac{M^2}{{M_T}^2}\nabla^2_R + \sum_{i=1}^{N}\sum_{j=1}^{N}\vec{\nabla}_{r_i}.\vec{\nabla}_{r_j} - 2\frac{M}{M_T}\sum_{i=1}^{N}\vec{\nabla}_R.\vec{\nabla}_{r_i} \qquad \text{and} \\ \nabla^2_{R_i} &= \vec{\nabla}_{R_i}.\vec{\nabla}_{R_i} = \frac{m_i^2}{{M_T}^2}\nabla^2_R + \nabla^2_{r_i} + 2\frac{m_i}{M_T}\vec{\nabla}_R.\vec{\nabla}_{r_i} \end{aligned}$$

Putting these relations into the equation (3.2.6) we get

$$\hat{T} = -\frac{1}{2M_T}\nabla_R^2 - \sum_{i=1}^{N}\frac{1}{2\mu_i}\nabla_{r_i}^2 - \frac{1}{M}\sum_{\substack{i=1\\i<j}}^{N}\sum_{j=1}^{N}\vec{\nabla}_{r_i}.\vec{\nabla}_{r_j} \tag{3.2.12}$$

Here $\frac{1}{\mu_i} = \frac{1}{M} + \frac{1}{m_i}$ is the reduced mass of the i-th particle. If a system of identical particles *i.e.* $m_i = m$ (say) is considered, then $\mu_i = \mu = \frac{mM}{(m+M)}$ and the K.E. operator will be

$$\hat{T} = -\frac{1}{2M_T}\nabla_R^2 - \frac{1}{2\mu}\sum_{i=1}^{N}\nabla_{r_i}^2 - \frac{1}{M}\sum_{\substack{i=1\\i<j}}^{N}\sum_{j=1}^{N}\vec{\nabla}_{r_i}.\vec{\nabla}_{r_j} \tag{3.2.13}$$

It can be noted that the K.E. operator consists of two parts:

1. K.E. of the centre of mass (c.m.) given by

$$\hat{T}_{c.m.} = -\frac{1}{2M_T}\nabla_R^2$$

2. Relative K.E. part which of the form

$$\hat{T}_r = -\sum_{i=1}^{N}\frac{1}{2\mu_i}\nabla_{r_i}^2 - \frac{1}{M}\sum_{\substack{i=1\\i<j}}^{N}\sum_{j=1}^{N}\vec{\nabla}_{r_i}.\vec{\nabla}_{r_j}$$

   The double summation term is known as *mass-polarization* term which occurs due to the motion of the nucleus having finite mass (M).

The 1st part *i.e.* the motion of c.m. can be separated due to the translation symmetry of the Hamiltonian $\hat{H}$. Thus the wavefunction of the (N+1) particle system is written as, $\Psi_{total} = \Psi_{c.m.}\Psi_r$ where $\Psi_{c.m.}$ and Ψ_r are the wavefunctions corresponding to the c.m. and relative co-ordinates respectively. The time independent Schrödinger equation is given by, $\hat{H}\Psi_{total} = E_{total}\Psi_{total}$, E_{total} being the total energy of the (N+1) particle system. Now using the method of separation of variables and considering $\hat{T}_{c.m.}\Psi_{c.m.} = E_{c.m.}\Psi_{c.m.}$ ($E_{c.m.}$ being the K.E. of c.m. which moves like a free particle), the time independent Schrödinger equation can be converted into the following form

$$\left(\hat{T}_r + \hat{V}\right)\Psi_r = (E_{total} - E_{c.m.})\,\Psi_r = E\Psi_r \tag{3.2.14}$$

E is the relative energy of the entire N-particle system with respect to the c.m. of the system.

In case of three-body systems ($N = 2$), the total number of degrees of freedom (D.O.F) of the system is 9. But due to the separation of the center of mass coordinates the remaining D.O.F is reduced to 6. The expectation value of $\hat{T}_r$ for the general three-body systems can be written as

$$\begin{aligned}
\langle \hat{T}_r \rangle &= \int \Psi_r^* \, \hat{T}_r \, \Psi_r \, d\tau_{\vec{r_1},\vec{r_2}} \\
&= -\frac{1}{2} \int \left[\frac{1}{\mu_1} \Psi_r^* \nabla_{r_1}^2 \Psi_r \; + \; \frac{1}{\mu_2} \Psi_r^* \nabla_{r_2}^2 \Psi_r \; + \; \frac{2}{M} \Psi_r^* \left(\vec{\nabla}_{r_1} . \vec{\nabla}_{r_2} \right) \Psi_r \right] d\tau_{\vec{r_1},\vec{r_2}} \\
&= +\frac{1}{2} \int \left[\frac{1}{\mu_1} \left(\vec{\nabla}_{r_1} \Psi_r \right)^2 \; + \; \frac{1}{\mu_2} \left(\vec{\nabla}_{r_2} \Psi_r \right)^2 \; + \; \frac{2}{M} \left(\vec{\nabla}_{r_1} \Psi_r . \vec{\nabla}_{r_2} \Psi_r \right) \right] d\tau_{\vec{r_1},\vec{r_2}} \\
&= \langle \hat{T}_r \rangle_1 \; + \; \langle \hat{T}_r \rangle_2 \; + \; \langle \hat{T}_r \rangle_3
\end{aligned}$$

where $\langle \hat{T}_r \rangle_1$, $\langle \hat{T}_r \rangle_2$ and $\langle \hat{T}_r \rangle_3$ in Cartesian co-ordinates is given by

$$\langle \hat{T}_r \rangle_1 = A \int \left\{ \left(\frac{\partial \Psi}{\partial x_1} \right)^2 + \left(\frac{\partial \Psi}{\partial y_1} \right)^2 + \left(\frac{\partial \Psi}{\partial z_1} \right)^2 \right\} d\tau_{\vec{r_1},\vec{r_2}} \qquad \therefore A = \frac{1}{2} \left(\frac{1}{M} + \frac{1}{m_1} \right) \tag{3.2.15}$$

$$\langle \hat{T}_r \rangle_2 = B \int \left\{ \left(\frac{\partial \Psi}{\partial x_2} \right)^2 + \left(\frac{\partial \Psi}{\partial y_2} \right)^2 + \left(\frac{\partial \Psi}{\partial z_2} \right)^2 \right\} d\tau_{\vec{r_1},\vec{r_2}} \qquad \therefore B = \frac{1}{2} \left(\frac{1}{M} + \frac{1}{m_2} \right) \tag{3.2.16}$$

$$\langle \hat{T}_r \rangle_3 = C \int \left\{ \frac{\partial \Psi}{\partial x_1} \frac{\partial \Psi}{\partial x_2} + \frac{\partial \Psi}{\partial y_1} \frac{\partial \Psi}{\partial y_2} + \frac{\partial \Psi}{\partial z_1} \frac{\partial \Psi}{\partial z_2} \right\} d\tau_{\vec{r_1},\vec{r_2}} \qquad \therefore C = \frac{1}{M} \tag{3.2.17}$$

To simplify the writing, we have used the notation Ψ instead of Ψ_r. In the above three relations (3.2.15), (3.2.16) and (3.2.17), the volume element is $d\tau_{\vec{r_1},\vec{r_2}} = dx_1 dy_1 dz_1 dx_2 dy_2 dz_2$. We now shift the coordinate system from the Cartesian $(x_1, y_1, z_1, x_2, y_2, z_2)$ to the polar co-ordinate $(r_1, r_2, \theta_{12}$ *or* $r_{12}, \theta, \phi, \psi)$ system. These two sets of coordinates are related to

each other by the following relations [30, 38]:

$$\begin{aligned}
x_1 &= r_1\left[\cos\phi\sin\left(\psi-\frac{\theta_{12}}{2}\right)+\cos\theta\sin\phi\cos\left(\psi-\frac{\theta_{12}}{2}\right)\right]\\
y_1 &= r_1\left[\sin\phi\sin\left(\psi-\frac{\theta_{12}}{2}\right)-\cos\theta\cos\phi\cos\left(\psi-\frac{\theta_{12}}{2}\right)\right]\\
x_2 &= r_2\left[\cos\phi\sin\left(\psi+\frac{\theta_{12}}{2}\right)+\cos\theta\sin\phi\cos\left(\psi+\frac{\theta_{12}}{2}\right)\right]\\
y_2 &= r_2\left[\sin\phi\sin\left(\psi+\frac{\theta_{12}}{2}\right)-\cos\theta\cos\phi\cos\left(\psi+\frac{\theta_{12}}{2}\right)\right]\\
z_1 &= -r_1\sin\theta\cos\left(\psi-\frac{\theta_{12}}{2}\right)\\
z_2 &= -r_2\sin\theta\cos\left(\psi+\frac{\theta_{12}}{2}\right)
\end{aligned} \tag{3.2.18}$$

Let us now consider the following transformation relations

$$\begin{aligned}
\frac{\partial\Psi}{\partial x_1} &= \frac{\partial\Psi}{\partial r_1}\frac{\partial r_1}{\partial x_1}+\frac{\partial\Psi}{\partial r_2}\frac{\partial r_2}{\partial x_1}+\frac{\partial\Psi}{\partial\theta_{12}}\frac{\partial\theta_{12}}{\partial x_1}+\frac{\partial\Psi}{\partial\theta}\frac{\partial\theta}{\partial x_1}+\frac{\partial\Psi}{\partial\phi}\frac{\partial\phi}{\partial x_1}+\frac{\partial\Psi}{\partial\psi}\frac{\partial\psi}{\partial x_1}\\
\frac{\partial\Psi}{\partial y_1} &= \frac{\partial\Psi}{\partial r_1}\frac{\partial r_1}{\partial y_1}+\frac{\partial\Psi}{\partial r_2}\frac{\partial r_2}{\partial y_1}+\frac{\partial\Psi}{\partial\theta_{12}}\frac{\partial\theta_{12}}{\partial y_1}+\frac{\partial\Psi}{\partial\theta}\frac{\partial\theta}{\partial y_1}+\frac{\partial\Psi}{\partial\phi}\frac{\partial\phi}{\partial y_1}+\frac{\partial\Psi}{\partial\psi}\frac{\partial\psi}{\partial y_1}\\
\frac{\partial\Psi}{\partial z_1} &= \frac{\partial\Psi}{\partial r_1}\frac{\partial r_1}{\partial z_1}+\frac{\partial\Psi}{\partial r_2}\frac{\partial r_2}{\partial z_1}+\frac{\partial\Psi}{\partial\theta_{12}}\frac{\partial\theta_{12}}{\partial z_1}+\frac{\partial\Psi}{\partial\theta}\frac{\partial\theta}{\partial z_1}+\frac{\partial\Psi}{\partial\phi}\frac{\partial\phi}{\partial z_1}+\frac{\partial\Psi}{\partial\psi}\frac{\partial\psi}{\partial z_1}\\
\frac{\partial\Psi}{\partial x_2} &= \frac{\partial\Psi}{\partial r_1}\frac{\partial r_1}{\partial x_2}+\frac{\partial\Psi}{\partial r_2}\frac{\partial r_2}{\partial x_2}+\frac{\partial\Psi}{\partial\theta_{12}}\frac{\partial\theta_{12}}{\partial x_2}+\frac{\partial\Psi}{\partial\theta}\frac{\partial\theta}{\partial x_2}+\frac{\partial\Psi}{\partial\phi}\frac{\partial\phi}{\partial x_2}+\frac{\partial\Psi}{\partial\psi}\frac{\partial\psi}{\partial x_2}\\
\frac{\partial\Psi}{\partial y_2} &= \frac{\partial\Psi}{\partial r_1}\frac{\partial r_1}{\partial y_2}+\frac{\partial\Psi}{\partial r_2}\frac{\partial r_2}{\partial y_2}+\frac{\partial\Psi}{\partial\theta_{12}}\frac{\partial\theta_{12}}{\partial y_2}+\frac{\partial\Psi}{\partial\theta}\frac{\partial\theta}{\partial y_2}+\frac{\partial\Psi}{\partial\phi}\frac{\partial\phi}{\partial y_2}+\frac{\partial\Psi}{\partial\psi}\frac{\partial\psi}{\partial y_2}\\
\frac{\partial\Psi}{\partial z_2} &= \frac{\partial\Psi}{\partial r_1}\frac{\partial r_1}{\partial z_2}+\frac{\partial\Psi}{\partial r_2}\frac{\partial r_2}{\partial z_2}+\frac{\partial\Psi}{\partial\theta_{12}}\frac{\partial\theta_{12}}{\partial z_2}+\frac{\partial\Psi}{\partial\theta}\frac{\partial\theta}{\partial z_2}+\frac{\partial\Psi}{\partial\phi}\frac{\partial\phi}{\partial z_2}+\frac{\partial\Psi}{\partial\psi}\frac{\partial\psi}{\partial z_2}
\end{aligned} \tag{3.2.19}$$

Since, $r_1^2 = x_1^2 + y_1^2 + z_1^2$ and $r_2^2 = x_2^2 + y_2^2 + z_2^2$, we can write

$$\begin{aligned}
&\frac{\partial r_1}{\partial x_1}=\frac{x_1}{r_1},\frac{\partial r_1}{\partial y_1}=\frac{y_1}{r_1},\frac{\partial r_1}{\partial z_1}=\frac{z_1}{r_1} \quad\text{and}\quad \frac{\partial r_1}{\partial x_2}=\frac{\partial r_1}{\partial y_2}=\frac{\partial r_1}{\partial z_2}=0\\
&\frac{\partial r_2}{\partial x_2}=\frac{x_2}{r_2},\frac{\partial r_2}{\partial y_2}=\frac{y_2}{r_2},\frac{\partial r_2}{\partial z_2}=\frac{z_2}{r_2} \quad\text{and}\quad \frac{\partial r_2}{\partial x_1}=\frac{\partial r_2}{\partial y_1}=\frac{\partial r_2}{\partial z_1}=0
\end{aligned} \tag{3.2.20}$$

For the determination of other coefficients we will use the relations between the space fixed axes (X,Y,Z) and the body fixed axes $(\mathrm{X}', \mathrm{Y}', \mathrm{Z}')$. The later set of axes is formed via rotation through the Eulerian triangles (θ, ϕ, ψ) as discussed in section (3.2.1). Bhatia and Temkin [30] assumed the Eulerian angles in such a way that the rotational symmetry of the Hamiltonian can be exploited and the six dimensional time-independent Schrödinger equation (3.2.14) can be dissolved into a three dimensional equation where the 3 generalized co-ordinates are r_1, r_2 and r_{12} (or θ_{12}). If we denote the unit vectors in the space fixed and body fixed axes as $(\hat{i}, \hat{j}, \hat{k})$ and $(\hat{i}', \hat{j}', \hat{k}')$ respectively, then following Bhatia and Temkin [30]

we can write

$$\begin{bmatrix} \hat{i}' \\ \hat{j}' \\ \hat{k}' \end{bmatrix} = \begin{bmatrix} \cos\phi & \sin\phi & 0 \\ -\cos\theta\sin\phi & \cos\theta\cos\phi & \sin\theta \\ \sin\theta\sin\phi & -\sin\theta\cos\phi & \cos\theta \end{bmatrix} \begin{bmatrix} \hat{i} \\ \hat{j} \\ \hat{k} \end{bmatrix} \tag{3.2.21}$$

The position vectors of m_1 and m_2 with respect to M are given by

$$\begin{aligned} \vec{r}_1 &= x_1\hat{i} + y_1\hat{j} + z_1\hat{k} && \text{in (X,Y,Z) system} \\ &= r_1 \sin\left(\psi - \frac{\theta_{12}}{2}\right)\hat{i}' - r_1\cos\left(\psi - \frac{\theta_{12}}{2}\right)\hat{j}' && \text{in (X}', \text{Y}', \text{Z}') \text{ system} \end{aligned} \tag{3.2.22}$$

$$\begin{aligned} \vec{r}_2 &= x_2\hat{i} + y_2\hat{j} + z_2\hat{k} && \text{in (X,Y,Z) system} \\ &= r_2 \sin\left(\psi + \frac{\theta_{12}}{2}\right)\hat{i}' - r_2\cos\left(\psi + \frac{\theta_{12}}{2}\right)\hat{j}' && \text{in (X}', \text{Y}', \text{Z}') \text{ system} \end{aligned} \tag{3.2.23}$$

According to the choice of the Eulerian angles [30], Z′ axis is perpendicular to the plane containing $\vec{r}_1$ and $\vec{r}_2$ and we can write the following relations:

$$\vec{r}_1.\hat{k}' = x_1\sin\theta\sin\phi - y_1\sin\theta\cos\phi + z_1\cos\theta = 0 \qquad \text{[using (3.2.21) and (3.2.22)]} \tag{3.2.24}$$

$$\vec{r}_2.\hat{k}' = x_2\sin\theta\sin\phi - y_2\sin\theta\cos\phi + z_2\cos\theta = 0 \qquad \text{[using (3.2.21) and (3.2.23)]} \tag{3.2.25}$$

Now using (3.2.21) and (3.2.22) we get

$$\vec{r}_1.\hat{i}' = r_1\sin\left(\psi - \frac{\theta_{12}}{2}\right) = x_1\cos\phi + y_1\sin\phi \quad \text{and} \tag{3.2.26}$$

$$\vec{r}_1.\hat{j}' = -r_1\cos\left(\psi - \frac{\theta_{12}}{2}\right) = -x_1\cos\theta\sin\phi + y_1\cos\theta\cos\phi + z_1\sin\theta \tag{3.2.27}$$

Similarly, using (3.2.21) and (3.2.23) we get

$$\vec{r}_2.\hat{i}' = r_1\sin\left(\psi + \frac{\theta_{12}}{2}\right) = x_2\cos\phi + y_2\sin\phi \quad \text{and} \tag{3.2.28}$$

$$\vec{r}_2.\hat{j}' = -r_2\cos\left(\psi + \frac{\theta_{12}}{2}\right) = -x_2\cos\theta\sin\phi + y_2\cos\theta\cos\phi + z_2\sin\theta \tag{3.2.29}$$

Equations (3.2.24) and (3.2.25) are used to find the terms $\frac{\partial\theta}{\partial x_1}, ..., \frac{\partial\theta}{\partial z_2}$ and $\frac{\partial\phi}{\partial x_1}, ..., \frac{\partial\phi}{\partial z_2}$, while using (3.2.26) and (3.2.28) we find $\frac{\partial\theta_{12}}{\partial x_1}, ..., \frac{\partial\theta_{12}}{\partial z_2}$ and $\frac{\partial\psi}{\partial x_1}, ..., \frac{\partial\psi}{\partial z_2}$. For example,

differentiating both sides of the equation (3.2.24) with respect to x_1 we can write

$$[(x_1 \sin\phi - y_1 \cos\phi)\cos\theta - z_1 \sin\theta]\frac{\partial\theta}{\partial x_1} + (x_1\cos\phi + y_1 \sin\phi)\sin\theta\frac{\partial\phi}{\partial x_1} = -\sin\theta\sin\phi$$

Now putting the values of x_1, y_1 and z_1 from equation (3.2.18), the above equation becomes

$$\cos\left(\psi - \frac{\theta_{12}}{2}\right)\frac{\partial\theta}{\partial x_1} + \sin\theta\sin\left(\psi - \frac{\theta_{12}}{2}\right)\frac{\partial\phi}{\partial x_1} = -\frac{1}{r_1}\sin\theta\sin\phi \tag{3.2.30}$$

Similarly, differentiating both sides of the equation (3.2.25) with respect to x_1 we get

$$\cos\left(\psi + \frac{\theta_{12}}{2}\right)\frac{\partial\theta}{\partial x_1} + \sin\theta\sin\left(\psi + \frac{\theta_{12}}{2}\right)\frac{\partial\phi}{\partial x_1} = 0 \tag{3.2.31}$$

Now solving the equations (3.2.30) and (3.2.31) we get

$$\begin{aligned}
\frac{\partial\theta}{\partial x_1} &= -\frac{1}{r_1\sin\theta_{12}}\sin\theta\sin\phi\sin\left(\psi + \frac{\theta_{12}}{2}\right)\\
\frac{\partial\phi}{\partial x_1} &= \frac{1}{r_1\sin\theta_{12}}\sin\phi\cos\left(\psi + \frac{\theta_{12}}{2}\right)
\end{aligned} \tag{3.2.32}$$

Similarly, using equations (3.2.24) and (3.2.25) the following formulation can be done

$$\begin{aligned}
\frac{\partial\theta}{\partial y_1} &= \frac{1}{r_1\sin\theta_{12}}\sin\theta\cos\phi\sin\left(\psi + \frac{\theta_{12}}{2}\right)\\
\frac{\partial\theta}{\partial z_1} &= -\frac{1}{r_1\sin\theta_{12}}\cos\theta\sin\left(\psi + \frac{\theta_{12}}{2}\right)\\
\frac{\partial\theta}{\partial x_2} &= \frac{1}{r_2\sin\theta_{12}}\sin\theta\sin\phi\sin\left(\psi - \frac{\theta_{12}}{2}\right)\\
\frac{\partial\theta}{\partial y_2} &= -\frac{1}{r_2\sin\theta_{12}}\sin\theta\cos\phi\sin\left(\psi - \frac{\theta_{12}}{2}\right)\\
\frac{\partial\theta}{\partial z_2} &= \frac{1}{r_2\sin\theta_{12}}\cos\theta\sin\left(\psi - \frac{\theta_{12}}{2}\right)\\
\frac{\partial\phi}{\partial y_1} &= -\frac{1}{r_1\sin\theta_{12}}\cos\phi\cos\left(\psi + \frac{\theta_{12}}{2}\right)\\
\frac{\partial\phi}{\partial z_1} &= \frac{1}{r_1\sin\theta_{12}\tan\theta}\cos\left(\psi + \frac{\theta_{12}}{2}\right)\\
\frac{\partial\phi}{\partial x_2} &= -\frac{1}{r_2\sin\theta_{12}}\sin\phi\cos\left(\psi - \frac{\theta_{12}}{2}\right)\\
\frac{\partial\phi}{\partial y_2} &= \frac{1}{r_2\sin\theta_{12}}\cos\phi\cos\left(\psi - \frac{\theta_{12}}{2}\right)\\
\frac{\partial\phi}{\partial z_2} &= -\frac{1}{r_2\sin\theta_{12}\tan\theta}\cos\left(\psi - \frac{\theta_{12}}{2}\right)
\end{aligned} \tag{3.2.33}$$

Proceeding in the same way, using equations (3.2.26) and (3.2.28) we can extract the following terms

$$
\begin{aligned}
\frac{\partial\theta_{12}}{\partial x_1} &= -\frac{1}{r_1}\cos\phi\cos\left(\psi-\frac{\theta_{12}}{2}\right)+\frac{1}{r_1}\cos\theta\sin\phi\sin\left(\psi-\frac{\theta_{12}}{2}\right)\\
\frac{\partial\theta_{12}}{\partial y_1} &= -\frac{1}{r_1}\sin\phi\cos\left(\psi-\frac{\theta_{12}}{2}\right)-\frac{1}{r_1}\cos\theta\cos\phi\sin\left(\psi-\frac{\theta_{12}}{2}\right)\\
\frac{\partial\theta_{12}}{\partial z_1} &= -\frac{1}{r_1}\sin\theta\sin\left(\psi-\frac{\theta_{12}}{2}\right)\\
\frac{\partial\theta_{12}}{\partial x_2} &= \frac{1}{r_2}\cos\phi\cos\left(\psi+\frac{\theta_{12}}{2}\right)-\frac{1}{r_2}\cos\theta\sin\phi\sin\left(\psi+\frac{\theta_{12}}{2}\right)\\
\frac{\partial\theta_{12}}{\partial y_2} &= \frac{1}{r_2}\sin\phi\cos\left(\psi+\frac{\theta_{12}}{2}\right)+\frac{1}{r_2}\cos\theta\cos\phi\sin\left(\psi+\frac{\theta_{12}}{2}\right)\\
\frac{\partial\theta_{12}}{\partial z_2} &= \frac{1}{r_2}\sin\theta\sin\left(\psi+\frac{\theta_{12}}{2}\right)\\
\frac{\partial\psi}{\partial x_1} &= \frac{1}{2r_1}\cos\phi\cos\left(\psi-\frac{\theta_{12}}{2}\right)-\frac{1}{2r_1}\cos\theta\sin\phi\sin\left(\psi-\frac{\theta_{12}}{2}\right)\\
&\quad-\frac{1}{r_1\sin\theta_{12}}\cos\theta\sin\phi\cos\left(\psi+\frac{\theta_{12}}{2}\right)\\
\frac{\partial\psi}{\partial y_1} &= \frac{1}{2r_1}\sin\phi\cos\left(\psi-\frac{\theta_{12}}{2}\right)+\frac{1}{2r_1}\cos\theta\cos\phi\sin\left(\psi-\frac{\theta_{12}}{2}\right)\\
&\quad+\frac{1}{r_1\sin\theta_{12}}\cos\theta\cos\phi\cos\left(\psi+\frac{\theta_{12}}{2}\right)\\
\frac{\partial\psi}{\partial z_1} &= \frac{1}{2r_1}\sin\theta\sin\left(\psi-\frac{\theta_{12}}{2}\right)-\frac{1}{r_1\sin\theta_{12}}\cos\theta\cot\theta\cos\left(\psi+\frac{\theta_{12}}{2}\right)\\
\frac{\partial\psi}{\partial x_2} &= \frac{1}{2r_2}\cos\phi\cos\left(\psi+\frac{\theta_{12}}{2}\right)-\frac{1}{2r_2}\cos\theta\sin\phi\sin\left(\psi+\frac{\theta_{12}}{2}\right)\\
&\quad+\frac{1}{r_2\sin\theta_{12}}\cos\theta\sin\phi\cos\left(\psi-\frac{\theta_{12}}{2}\right)\\
\frac{\partial\psi}{\partial y_2} &= \frac{1}{2r_2}\sin\phi\cos\left(\psi+\frac{\theta_{12}}{2}\right)+\frac{1}{2r_2}\cos\theta\cos\phi\sin\left(\psi+\frac{\theta_{12}}{2}\right)\\
&\quad-\frac{1}{r_2\sin\theta_{12}}\cos\theta\cos\phi\cos\left(\psi-\frac{\theta_{12}}{2}\right)\\
\frac{\partial\psi}{\partial z_2} &= \frac{1}{2r_2}\sin\theta\sin\left(\psi+\frac{\theta_{12}}{2}\right)+\frac{1}{r_2\sin\theta_{12}}\cos\theta\cot\theta\cos\left(\psi-\frac{\theta_{12}}{2}\right)
\end{aligned}
\tag{3.2.34}
$$

Now using the transformations (3.2.19) and the equations (3.2.32), (3.2.33) and (3.2.34), we can get the coefficients of different derivatives of Ψ which are given below

$$
\text{Coefficient of } \left(\frac{\partial\Psi}{\partial r_1}\right)^2 = \left(\frac{\partial r_1}{\partial x_1}\right)^2+\left(\frac{\partial r_1}{\partial y_1}\right)^2+\left(\frac{\partial r_1}{\partial z_1}\right)^2 = 1
$$

$$\text{Coefficient of } \left(\frac{\partial\Psi}{\partial\theta_{12}}\right)^2 = \left(\frac{\partial\theta_{12}}{\partial x_1}\right)^2 + \left(\frac{\partial\theta_{12}}{\partial y_1}\right)^2 + \left(\frac{\partial\theta_{12}}{\partial z_1}\right)^2 = \frac{1}{r_1^2}$$

$$\text{Coefficient of } \left(\frac{\partial\Psi}{\partial\theta}\right)^2 = \left(\frac{\partial\theta}{\partial x_1}\right)^2 + \left(\frac{\partial\theta}{\partial y_1}\right)^2 + \left(\frac{\partial\theta}{\partial z_1}\right)^2 = \frac{1}{r_1^2\sin^2\theta_{12}}\sin^2\left(\psi+\frac{\theta_{12}}{2}\right)$$

$$\begin{aligned}\text{Coefficient of } \left(\frac{\partial\Psi}{\partial\psi}\right)^2 &= \left(\frac{\partial\psi}{\partial x_1}\right)^2 + \left(\frac{\partial\psi}{\partial y_1}\right)^2 + \left(\frac{\partial\psi}{\partial z_1}\right)^2 \\ &= \frac{1}{4r_1^2} + \frac{1}{r_1^2\sin^2\theta_{12}}\cot^2\theta\cos^2\left(\psi+\frac{\theta_{12}}{2}\right)\end{aligned}$$

$$\text{Coefficient of } 2\frac{\partial\Psi}{\partial r_1}\frac{\partial\Psi}{\partial\theta_{12}} = \frac{\partial r_1}{\partial x_1}\frac{\partial\theta_{12}}{\partial x_1} + \frac{\partial r_1}{\partial y_1}\frac{\partial\theta_{12}}{\partial y_1} + \frac{\partial r_1}{\partial z_1}\frac{\partial\theta_{12}}{\partial z_1} = 0$$

$$\text{Coefficient of } 2\frac{\partial\Psi}{\partial r_1}\frac{\partial\Psi}{\partial\theta} = \frac{\partial r_1}{\partial x_1}\frac{\partial\theta}{\partial x_1} + \frac{\partial r_1}{\partial y_1}\frac{\partial\theta}{\partial y_1} + \frac{\partial r_1}{\partial z_1}\frac{\partial\theta}{\partial z_1} = 0$$

$$\text{Coefficient of } 2\frac{\partial\Psi}{\partial r_1}\frac{\partial\Psi}{\partial\psi} = \frac{\partial r_1}{\partial x_1}\frac{\partial\psi}{\partial x_1} + \frac{\partial r_1}{\partial y_1}\frac{\partial\psi}{\partial y_1} + \frac{\partial r_1}{\partial z_1}\frac{\partial\psi}{\partial z_1} = 0$$

$$\text{Coefficient of } 2\frac{\partial\Psi}{\partial\theta_{12}}\frac{\partial\Psi}{\partial\theta} = \frac{\partial\theta_{12}}{\partial x_1}\frac{\partial\theta}{\partial x_1} + \frac{\partial\theta_{12}}{\partial y_1}\frac{\partial\theta}{\partial y_1} + \frac{\partial\theta_{12}}{\partial z_1}\frac{\partial\theta}{\partial z_1} = 0$$

$$\text{Coefficient of } 2\frac{\partial\Psi}{\partial\theta_{12}}\frac{\partial\Psi}{\partial\psi} = \frac{\partial\theta_{12}}{\partial x_1}\frac{\partial\psi}{\partial x_1} + \frac{\partial\theta_{12}}{\partial y_1}\frac{\partial\psi}{\partial y_1} + \frac{\partial\theta_{12}}{\partial z_1}\frac{\partial\psi}{\partial z_1} = -\frac{1}{2r_1^2}$$

$$\text{Coefficient of } 2\frac{\partial\Psi}{\partial\theta}\frac{\partial\Psi}{\partial\psi} = \frac{\partial\theta}{\partial x_1}\frac{\partial\psi}{\partial x_1} + \frac{\partial\theta}{\partial y_1}\frac{\partial\psi}{\partial y_1} + \frac{\partial\theta}{\partial z_1}\frac{\partial\psi}{\partial z_1} = \frac{1}{2r_1^2\sin^2\theta_{12}}\cot\theta\sin\left(2\psi+\theta_{12}\right)$$

$$\begin{aligned}\therefore \langle\hat{T}_r\rangle_1 &= A\int\left[\left(\frac{\partial\Psi}{\partial r_1}\right)^2 + \frac{1}{r_1^2}\left(\frac{\partial\Psi}{\partial\theta_{12}}\right)^2 + \frac{1}{r_1^2\sin^2\theta_{12}}\sin^2\left(\psi+\frac{\theta_{12}}{2}\right)\left(\frac{\partial\Psi}{\partial\theta}\right)^2\right. \\ &\quad + \left\{\frac{1}{4r_1^2} + \frac{1}{r_1^2\sin^2\theta_{12}}\cot^2\theta\cos^2\left(\psi+\frac{\theta_{12}}{2}\right)\right\}\left(\frac{\partial\Psi}{\partial\psi}\right)^2 - \frac{1}{r_1^2}\frac{\partial\Psi}{\partial\theta_{12}}\frac{\partial\Psi}{\partial\psi} \\ &\quad \left. + \frac{1}{r_1^2\sin^2\theta_{12}}\cot\theta\sin\left(2\psi+\theta_{12}\right)\frac{\partial\Psi}{\partial\theta}\frac{\partial\Psi}{\partial\psi}\right] d\tau_{\vec{r_1},\vec{r_2}} \qquad (3.2.35)\end{aligned}$$

As the non-relativistic Hamiltonian is independent on the spin operator, Bhatia and Temkin [30] showed that the dependency of the wavefunction Ψ on the azimuthal angle ϕ can be discarded. That is why, in the above expression $\dfrac{\partial\Psi}{\partial\phi}$ is set to zero. Similarly, other two K.E. terms become

$$\begin{aligned}\langle\hat{T}_r\rangle_2 &= B\int\left[\left(\frac{\partial\Psi}{\partial r_2}\right)^2+\frac{1}{r_2^2}\left(\frac{\partial\Psi}{\partial\theta_{12}}\right)^2+\frac{1}{r_2^2\sin^2\theta_{12}}\sin^2\left(\psi-\frac{\theta_{12}}{2}\right)\left(\frac{\partial\Psi}{\partial\theta}\right)^2\right.\\&+\left\{\frac{1}{4r_2^2}+\frac{1}{r_2^2\sin^2\theta_{12}}\cot^2\theta\cos^2\left(\psi-\frac{\theta_{12}}{2}\right)\right\}\left(\frac{\partial\Psi}{\partial\psi}\right)^2+\frac{1}{r_2^2}\frac{\partial\Psi}{\partial\theta_{12}}\frac{\partial\Psi}{\partial\psi}\\&\left.+\frac{1}{r_2^2\sin^2\theta_{12}}\cot\theta\sin\left(2\psi-\theta_{12}\right)\frac{\partial\Psi}{\partial\theta}\frac{\partial\Psi}{\partial\psi}\right]d\tau_{\vec{r_1},\vec{r_2}}\end{aligned}\tag{3.2.36}$$

$$\begin{aligned}\langle\hat{T}_r\rangle_3 &= C\int\left[\cos\theta_{12}\frac{\partial\Psi}{\partial r_1}\frac{\partial\Psi}{\partial r_2}-\frac{1}{r_2}\sin\theta_{12}\frac{\partial\Psi}{\partial r_1}\frac{\partial\Psi}{\partial\theta_{12}}-\frac{1}{r_1}\sin\theta_{12}\frac{\partial\Psi}{\partial r_2}\frac{\partial\Psi}{\partial\theta_{12}}\right.\\&-\frac{1}{2r_2}\sin\theta_{12}\frac{\partial\Psi}{\partial r_1}\frac{\partial\Psi}{\partial\psi}+\frac{1}{2r_1}\sin\theta_{12}\frac{\partial\Psi}{\partial r_2}\frac{\partial\Psi}{\partial\psi}-\frac{1}{r_1r_2}\cos\theta_{12}\left(\frac{\partial\Psi}{\partial\theta_{12}}\right)^2\\&-\frac{1}{r_1r_2\sin^2\theta_{12}}\sin\left(\psi-\frac{\theta_{12}}{2}\right)\sin\left(\psi+\frac{\theta_{12}}{2}\right)\left(\frac{\partial\Psi}{\partial\theta}\right)^2\\&-\frac{1}{r_1r_2\sin^2\theta_{12}}\cot\theta\sin2\psi\frac{\partial\Psi}{\partial\theta}\frac{\partial\Psi}{\partial\psi}+\left\{\frac{1}{4r_1r_2}\cos\theta_{12}\right.\\&\left.\left.-\frac{1}{2r_1r_2\sin^2\theta_{12}}\cot^2\theta\left(\cos2\psi+\cos\theta_{12}\right)\right\}\left(\frac{\partial\Psi}{\partial\psi}\right)^2\right]d\tau_{\vec{r_1},\vec{r_2}}\end{aligned}\tag{3.2.37}$$

The expectation value of the potential is

$$\langle\hat{V}\rangle=\int V_{eff}|\Psi|^2\;d\tau_{\vec{r_1},\vec{r_2}}\tag{3.2.38}$$

where the V_{eff} is the effective potential of the three–body system.
The overlap term is given by,

$$\langle\hat{S}\rangle=\int|\Psi|^2\;d\tau_{\vec{r_1},\vec{r_2}}\tag{3.2.39}$$

In the above relations (3.2.35), (3.2.36), (3.2.37), (3.2.38) and (3.2.39), the volume element is $d\tau_{\vec{r_1},\vec{r_2}}=r_1^2dr_1r_2^2dr_2\sin\theta_{12}d\theta_{12}\sin\theta d\theta d\phi d\psi$. Since r_{12} and θ_{12} are connected by the relation

$$r_{12}^2=r_1^2+r_2^2-2r_1r_2\cos\theta_{12}\tag{3.2.40}$$

we may also write the volume element as $d\tau_{\vec{r_1},\vec{r_2}} = r_1 dr_1 r_2 dr_2 r_{12} dr_{12} \sin\theta d\theta d\phi d\psi$. The variational equation now can be written as,

$$\Delta\left[\langle\hat{T}_r\rangle + \langle\hat{V}\rangle - E\langle\hat{O}\rangle\right] = 0 \tag{3.2.41}$$

The symbol Δ signifies the variation of the parameters contained within the trial wavefunction Ψ.

Variational equation and wavefunction of general three–body system in $^{1,3}\mathbf{S}^e$ *states*

For the spherically symmetric ($^{1,3}\mathrm{S}^e$) state ($L = 0$ and $k = 0$), the wavefunction (3.2.1) becomes $\Psi = f_0^0 D_0^0 = f \pm \tilde{f}$, where $f = f\,(r_1, r_2, \theta_{12}\ or\ r_{12})$ and $\tilde{f} = \tilde{f}\,(r_2, r_1, \theta_{12}\ or\ r_{12})$. The upper '+' sign signifies the space symmetric wavefunction *i.e* for singlet state ($^1\mathrm{S}^e$) and the lower '−' sign signifies the space anti-symmetric wavefunction *i.e* for triplet state ($^3\mathrm{S}^e$). From equations (3.2.35), (3.2.36) and (3.2.37) K.E. terms for S-state becomes

$$\therefore \langle\hat{T}_r\rangle_1 = A\int\left[\left(\frac{\partial\Psi}{\partial r_1}\right)^2 + \frac{1}{r_1^2}\left(\frac{\partial\Psi}{\partial\theta_{12}}\right)^2\right] d\tau_{\vec{r_1},\vec{r_2}} \tag{3.2.42}$$

$$\langle\hat{T}_r\rangle_2 = B\int\left[\left(\frac{\partial\Psi}{\partial r_2}\right)^2 + \frac{1}{r_2^2}\left(\frac{\partial\Psi}{\partial\theta_{12}}\right)^2\right] d\tau_{\vec{r_1},\vec{r_2}} \tag{3.2.43}$$

$$\begin{aligned}\langle\hat{T}_r\rangle_3 = C\int\Bigg[&\cos\theta_{12}\frac{\partial\Psi}{\partial r_1}\frac{\partial\Psi}{\partial r_2} - \frac{1}{r_2}\sin\theta_{12}\frac{\partial\Psi}{\partial r_1}\frac{\partial\Psi}{\partial\theta_{12}} - \frac{1}{r_1}\sin\theta_{12}\frac{\partial\Psi}{\partial r_2}\frac{\partial\Psi}{\partial\theta_{12}}\\ &- \frac{1}{r_1 r_2}\cos\theta_{12}\left(\frac{\partial\Psi}{\partial\theta_{12}}\right)^2\Bigg] d\tau_{\vec{r_1},\vec{r_2}}\end{aligned} \tag{3.2.44}$$

For the convenience of calculation we write the K.E. (3.2.42), (3.2.43) and (3.2.44) in terms of r_{12} instead of θ_{12}. The relative radial distance is defined as, $r_{12}^2 = (x_1 - x_2)^2 + (y_1 - y_2)^2 + (z_1 - z_2)^2$. Thus, by using relations in (3.2.20) and

$$\begin{aligned}&\frac{\partial r_{12}}{\partial x_1} = \frac{x_1 - x_2}{r_{12}},\quad \frac{\partial r_{12}}{\partial y_1} = \frac{y_1 - y_2}{r_{12}},\quad \frac{\partial r_{12}}{\partial z_1} = \frac{z_1 - z_2}{r_{12}}\\ &\frac{\partial r_{12}}{\partial x_2} = -\frac{x_1 - x_2}{r_{12}},\quad \frac{\partial r_{12}}{\partial y_2} = -\frac{y_1 - y_2}{r_{12}},\quad \frac{\partial r_{12}}{\partial z_2} = -\frac{z_1 - z_2}{r_{12}}\end{aligned} \tag{3.2.45}$$

we can get

$$\begin{aligned}
\frac{\partial\Psi}{\partial x_1} &= \frac{\partial\Psi}{\partial r_1}\frac{\partial r_1}{\partial x_1} + \frac{\partial\Psi}{\partial r_{12}}\frac{\partial r_{12}}{\partial x_1} = \frac{x_1}{r_1}\frac{\partial\Psi}{\partial r_1} + \frac{x_1 - x_2}{r_{12}}\frac{\partial\Psi}{\partial r_{12}} \\
\frac{\partial\Psi}{\partial y_1} &= \frac{\partial\Psi}{\partial r_1}\frac{\partial r_1}{\partial y_1} + \frac{\partial\Psi}{\partial r_{12}}\frac{\partial r_{12}}{\partial y_1} = \frac{y_1}{r_1}\frac{\partial\Psi}{\partial r_1} + \frac{y_1 - y_2}{r_{12}}\frac{\partial\Psi}{\partial r_{12}} \\
\frac{\partial\Psi}{\partial z_1} &= \frac{\partial\Psi}{\partial r_1}\frac{\partial r_1}{\partial z_1} + \frac{\partial\Psi}{\partial r_{12}}\frac{\partial r_{12}}{\partial z_1} = \frac{z_1}{r_1}\frac{\partial\Psi}{\partial r_1} + \frac{z_1 - z_2}{r_{12}}\frac{\partial\Psi}{\partial r_{12}} \\
\frac{\partial\Psi}{\partial x_2} &= \frac{\partial\Psi}{\partial r_1}\frac{\partial r_1}{\partial x_2} + \frac{\partial\Psi}{\partial r_{12}}\frac{\partial r_{12}}{\partial x_2} = \frac{x_2}{r_1}\frac{\partial\Psi}{\partial r_1} + \frac{x_2 - x_1}{r_{12}}\frac{\partial\Psi}{\partial r_{12}} \\
\frac{\partial\Psi}{\partial y_2} &= \frac{\partial\Psi}{\partial r_1}\frac{\partial r_1}{\partial y_2} + \frac{\partial\Psi}{\partial r_{12}}\frac{\partial r_{12}}{\partial y_2} = \frac{y_2}{r_1}\frac{\partial\Psi}{\partial r_1} + \frac{y_2 - y_1}{r_{12}}\frac{\partial\Psi}{\partial r_{12}} \\
\frac{\partial\Psi}{\partial z_2} &= \frac{\partial\Psi}{\partial r_1}\frac{\partial r_1}{\partial z_2} + \frac{\partial\Psi}{\partial r_{12}}\frac{\partial r_{12}}{\partial z_2} = \frac{z_2}{r_1}\frac{\partial\Psi}{\partial r_1} + \frac{z_2 - z_1}{r_{12}}\frac{\partial\Psi}{\partial r_{12}}
\end{aligned} \tag{3.2.46}$$

Now using the above six relations the K.E. terms in equations (3.2.15), (3.2.16) and (3.2.17) can be converted into the following forms

$$\langle\hat{T}_r\rangle_1 = A\int\left\{\left(\frac{\partial\Psi}{\partial r_1}\right)^2 + \left(\frac{\partial\Psi}{\partial r_{12}}\right)^2 + 2\cos(r_1, r_{12})\frac{\partial\Psi}{\partial r_1}.\frac{\partial\Psi}{\partial r_{12}}\right\} d\tau_{\vec{r_1},\vec{r_2}}$$

$$\langle\hat{T}_r\rangle_2 = B\int\left\{\left(\frac{\partial\Psi}{\partial r_2}\right)^2 + \left(\frac{\partial\Psi}{\partial r_{12}}\right)^2 + 2\cos(r_2, r_{12})\frac{\partial\Psi}{\partial r_2}.\frac{\partial\Psi}{\partial r_{12}}\right\} d\tau_{\vec{r_1},\vec{r_2}}$$

$$\begin{aligned}
\langle\hat{T}_r\rangle_3 = C\int\Bigg\{&\cos(r_1, r_2)\frac{\partial\Psi}{\partial r_1}.\frac{\partial\Psi}{\partial r_2} - \cos(r_1, r_{12})\frac{\partial\Psi}{\partial r_1}.\frac{\partial\Psi}{\partial r_{12}} \\
&- \cos(r_2, r_{12})\frac{\partial\Psi}{\partial r_2}.\frac{\partial\Psi}{\partial r_{12}} - \left(\frac{\partial\Psi}{\partial r_{12}}\right)^2\Bigg\} d\tau_{\vec{r_1},\vec{r_2}}
\end{aligned}$$

Here we have defined

$$\cos(r_i, r_j) = \frac{r_i^2 + r_j^2 - r_k^2}{2\, r_i\, r_j} \tag{3.2.47}$$

where, the indices are used as $(i, j, k) \equiv (1, 2, 12)$. Now the total K.E. can be simplified as

$$\begin{aligned}
\langle\hat{T}_r\rangle &= \langle\hat{T}_r\rangle_1 + \langle\hat{T}_r\rangle_2 + \langle\hat{T}_r\rangle_3 \\
&= \int\Bigg[\frac{1}{2}\left(\frac{1}{M} + \frac{1}{m_1}\right)\left(\frac{\partial\Psi}{\partial r_1}\right)^2 + \frac{1}{2}\left(\frac{1}{M} + \frac{1}{m_2}\right)\left(\frac{\partial\Psi}{\partial r_2}\right)^2 \\
&+ \frac{1}{2}\left(\frac{1}{m_1} + \frac{1}{m_2}\right)\left(\frac{\partial\Psi}{\partial r_{12}}\right)^2 + \frac{1}{M}\cos(r_1, r_2)\frac{\partial\Psi}{\partial r_1}.\frac{\partial\Psi}{\partial r_2} \\
&+ \frac{1}{m_2}\cos(r_2, r_{12})\frac{\partial\Psi}{\partial r_2}.\frac{\partial\Psi}{\partial r_{12}} + \frac{1}{m_1}\cos(r_1, r_{12})\frac{\partial\Psi}{\partial r_1}.\frac{\partial\Psi}{\partial r_{12}}\Bigg] d\tau_{\vec{r_1},\vec{r_2}}
\end{aligned} \tag{3.2.48}$$

Using $\Psi = f \pm \tilde{f}$, the above expression takes the form

$$\begin{aligned}
\langle \hat{T}_r \rangle &= \int \left[\sum_{i=1}^{2} \frac{1}{2} \left(\frac{1}{M} + \frac{1}{m_i} \right) \left\{ \left(\frac{\partial f}{\partial r_i} \right)^2 + \left(\frac{\partial \tilde{f}}{\partial r_i} \right)^2 \pm 2 \frac{\partial f}{\partial r_i} \frac{\partial \tilde{f}}{\partial r_i} \right\} \right. \\
&+ \frac{1}{2} \left(\frac{1}{m_1} + \frac{1}{m_2} \right) \left\{ \left(\frac{\partial f}{\partial r_{12}} \right)^2 + \left(\frac{\partial \tilde{f}}{\partial r_{12}} \right)^2 \pm 2 \frac{\partial f}{\partial r_{12}} \frac{\partial \tilde{f}}{\partial r_{12}} \right\} \\
&+ \frac{1}{M} \cos(r_1, r_2) \left\{ \frac{\partial f}{\partial r_1} \frac{\partial f}{\partial r_2} + \frac{\partial \tilde{f}}{\partial r_1} \frac{\partial \tilde{f}}{\partial r_2} \pm \frac{\partial f}{\partial r_1} \frac{\partial \tilde{f}}{\partial r_2} \pm \frac{\partial f}{\partial r_2} \frac{\partial \tilde{f}}{\partial r_1} \right\} \\
&+ \frac{1}{m_1} \cos(r_1, r_{12}) \left\{ \frac{\partial f}{\partial r_1} \frac{\partial f}{\partial r_{12}} + \frac{\partial \tilde{f}}{\partial r_1} \frac{\partial \tilde{f}}{\partial r_{12}} \pm \frac{\partial f}{\partial r_1} \frac{\partial \tilde{f}}{\partial r_{12}} \pm \frac{\partial f}{\partial r_{12}} \frac{\partial \tilde{f}}{\partial r_1} \right\} \\
&+ \left. \frac{1}{m_2} \cos(r_2, r_{12}) \left\{ \frac{\partial f}{\partial r_2} \frac{\partial f}{\partial r_{12}} + \frac{\partial \tilde{f}}{\partial r_2} \frac{\partial \tilde{f}}{\partial r_{12}} \pm \frac{\partial f}{\partial r_2} \frac{\partial \tilde{f}}{\partial r_{12}} \pm \frac{\partial f}{\partial r_{12}} \frac{\partial \tilde{f}}{\partial r_2} \right\} \right] d\tau_{\vec{r_1}, \vec{r_2}}
\end{aligned} \tag{3.2.49}$$

The expectation values of the potential energy and overlap term are given by

$$\langle \hat{V} \rangle = \int V_{eff} \left(f^2 + \tilde{f}^2 \pm 2 f \tilde{f} \right) \, d\tau_{\vec{r_1}, \vec{r_2}} \tag{3.2.50}$$

$$\langle \hat{S} \rangle = \int \left(f^2 + \tilde{f}^2 \pm 2 f \tilde{f} \right) \, d\tau_{\vec{r_1}, \vec{r_2}} \tag{3.2.51}$$

As a sample calculation, we now consider a simplistic trial function for the ground state ($^1S^e$) as $f = e^{-\alpha r_1 - \beta r_2}$ (α, β being the non-linear parameters) for free Ps^- exotic ion, where the potential of the system is

$$V_{eff} = -\frac{1}{r_1} - \frac{1}{r_2} + \frac{1}{r_{12}} \quad \text{in a.u.} \tag{3.2.52}$$

The masses of the particles are $m_1 = m_2 = M = 1$ a.u. If we put the trial wavefunction f into the equation (3.2.49) we can get the K.E. as a function of α and β only. For this we have to calculate the integrals of the type

$$\int \left(\frac{\partial f}{\partial r_i} \right)^2 d\tau_{\vec{r_1}, \vec{r_2}} = \alpha^2 \int e^{-2\alpha r_1 - 2\beta r_2} r_1 dr_1 r_2 dr_2 r_{12} dr_{12} \int \sin\theta d\theta d\phi d\psi$$

Now,

$$\int \sin\theta d\theta d\phi d\psi = \int_0^{\pi} \sin\theta d\theta \int_0^{2\pi} d\phi \int_0^{2\pi} d\psi = 8\pi^2$$

$$\therefore \int \left(\frac{\partial f}{\partial r_i}\right)^2 d\tau_{\vec{r_1},\vec{r_2}} = 8\pi^2\alpha^2 \left[\int_0^\infty e^{-2\alpha r_1} r_1 dr_1 \int_0^{r_1} e^{-2\beta r_2} r_2 dr_2 \int_{r_1-r_2}^{r_2+r_2} r_{12} dr_{12} + \int_0^\infty e^{-2\beta r_2} r_2 dr_2 \int_0^{r_2} e^{-2\alpha r_1} r_1 dr_1 \int_{r_2-r_1}^{r_2+r_2} r_{12} dr_{12}\right] = 8\pi^2 \frac{1}{8\beta^3\alpha}$$

Here we have used the following standard integrals [156],

$$\int_0^R r^n e^{-\mu r} dr = \frac{n!}{\mu^{n+1}} - e^{-\mu R} \sum_{k=0}^{n} \frac{n!}{k!} \frac{R^k}{\mu^{n-k+1}} \tag{3.2.53}$$

$$\int_0^\infty r^n e^{-\mu r} dr = \frac{n!}{\mu^{n+1}} \tag{3.2.54}$$

Similarly we can do all the integrals appearing in (3.2.49), (3.2.50) and (3.2.51) to get the following results

$$\langle \hat{T}_r \rangle = 8\pi^2 \left[\left(\frac{\alpha^2+\beta^2}{4\alpha^3\beta^3}\right) + \frac{32\alpha\beta}{(\alpha+\beta)^6}\right]$$

$$\langle \hat{V} \rangle = -8\pi^2 \left[\frac{\alpha^4+3\alpha\beta^3+3\alpha^2\beta^2+3\alpha^3\beta+\beta^4}{4\alpha^3\beta^3(\alpha+\beta)^3} + \frac{11}{(\alpha+\beta)^5}\right]$$

$$\langle \hat{S} \rangle = 8\pi^2 \left[\frac{1}{4\alpha^3\beta^3} + \frac{16}{(\alpha+\beta)^6}\right]$$

The energy eigenvalue will be expressed as

$$E = \frac{\langle \hat{T}_r \rangle + \langle \hat{V} \rangle}{\langle \hat{S} \rangle} = E(\alpha, \beta)$$

Now α and β are to be varied to achieve the minimum value of E. For the sake of simplicity in calculation let us assume that $\alpha = \beta$ which gives

$$E = 2\left(\alpha^2 - \frac{11}{16}\alpha\right)$$

If E becomes minimum *w.r.t* α then

$$\frac{dE}{d\alpha} = 0 \implies 2\alpha - \frac{11}{16} = 0 \implies \alpha = \frac{11}{32}$$

Using this value of α the variational minimum value of energy will be, $E = -0.236328125$ a.u. This is surprising to see that this energy is lying above the first ionization energy (-0.25 a.u.) *i.e.* the ground state energy of positronium (Ps or e^+e^-) atom. In the literature [204], one can find that the lowest non-relativistic energy value of the ground state of Ps^- ion is $E = -0.2620050702$ a.u. In order to get better bound state energy eigenvalue we now

optimize the nonlinear parameters (α, β) using the Nelder–Mead algorithm [161]. This gives $E = -0.256574823$ a.u. with optimised non-linear parameters, $\alpha = 0.13691648$ a.u. and $\beta = 0.52658950$ a.u. So we can see that, Nelder–Mead optimization can bring the bound state energy very close ($\backsim$ 0.006 a.u. or 0.163 eV) to the best available non-relativistic result [204]. The energy eigenvalue can be made better by using the basis set expansion of the wavefunction where electron correlation is included explicitly. This is discussed in details in the following sub–section.

3.2.3 Basis set

The trial wave function of $^{1,3}S^e$ state $f(r_1, r_2, r_{12})$ is expanded in multi–exponent Hylleraas type basis set

$$f(r_1, r_2, r_{12}) = \sum_{k=1}^{s} r_1^{l_k}\ r_2^{m_k}\ r_{12}^{n_k}\ \left[\sum_{i=1}^{p} C_{kii}\eta_i(1)\eta_i(2) + \sum_{i=1}^{p}\sum_{j>i}^{p} C_{kij}\eta_i(1)\eta_j(2)\right] \tag{3.2.55}$$

1. The powers of r_1, r_2 and r_{12} satisfies $(l_k, m_k, n_k) \geq (0, 0, 0)$.
2. s is the number of elements in the set of the powers of r_1, r_2 and r_{12}.
3. $\eta_i(j) = e^{-\rho_i r_j}$ is the Slater-type orbital. ρ is the non-linear parameter.
4. p denotes the number of non-linear parameters.
5. C_{kij} are the linear variational parameter.
6. The dimension of the full multi-exponent basis, $N = \frac{p(p+1)}{2} \times s$

In our present calculations, ρ's are chosen in the following two ways:

1. Double exponent: In this case, $p = 2$ and initially we have to choose two different ρ's *i.e.* ρ_1 and ρ_2. We consider three distinct sets of (ρ_1,ρ_2) initially and then by using Nelder–Mead algorithm [161] we optimize ρ_1 and ρ_2, so that the corresponding bound state energy eigenvalue becomes minimum. The initial choices of non-linear parameters (ρ_1 and ρ_2) are done from the values of non-linear parameters in the Slater-type orbitals [162]. This process is then repeated by increasing the number (s) of the powers (l_k, m_k, n_k) of r_1, r_2 and r_{12} respectively. The following table (3.2.1) shows a numerical example of such optimization. From table (3.2.1) we see that, the energy eigenvalue of the ground state of Ps^- ion using 102 terms in the basis set is -0.262004780 a.u., which is comparable with the best available energy eigenvalue -0.2620050702 a.u. as obtained by Kar and Ho [204], where they [204] used 500 terms in their basis set. This shows a clear advantage of present method to achieve excellent level of accuracy in a considerably reduced basis size.

Table 3.2.1: Optimized values of $-E$, ρ_1 and ρ_2 of the ground state of Ps^- ion corresponding to different sets (s) of powers (l_k, m_k, n_k) of r_1, r_2 and r_{12} respectively and double exponent basis ($p = 2$). $N = \frac{p(p+1)}{2} \times s$ is the total number of terms in the basis set. All the quantities are given in a.u.

s	(l_k, m_k, n_k)	N	ρ_1	ρ_2	$-E$
3	(0,0,0) (1,0,0) (0,0,1)	9	0.12488560	0.50400779	0.259907886
7	(0,0,0) (1,0,0) (0,0,1) (2,0,0) (1,1,0) (1,0,1) (0,0,2)	21	0.11555350	0.45250487	0.261831394
13	(0,0,0) (1,0,0) (0,0,1) (2,0,0) (1,1,0) (1,0,1) (0,0,2) (3,0,0) (2,1,0) (2,0,1) (1,1,1) (1,0,2) (0,0,3)	39	0.12488560	0.50400779	0.261971409
22	(0,0,0) (1,0,0) (0,0,1) (2,0,0) (1,1,0) (1,0,1) (0,0,2) (3,0,0) (2,1,0) (2,0,1) (1,1,1) (1,0,2) (0,0,3) (4,0,0) (3,1,0) (3,0,1) (2,2,0) (2,1,1) (2,0,2) (1,1,2) (1,0,3) (0,0,4)	66	0.12488560	0.50400779	0.262003078
34	(0,0,0) (1,0,0) (0,0,1) (2,0,0) (1,1,0) (1,0,1) (0,0,2) (3,0,0) (2,1,0) (2,0,1) (1,1,1) (1,0,2) (0,0,3) (4,0,0) (3,1,0) (3,0,1) (2,2,0) (2,1,1) (2,0,2) (1,1,2) (1,0,3) (0,0,4) (5,0,0) (4,1,0) (4,0,1) (3,2,0) (3,1,1) (3,0,2) (2,2,1) (2,1,2) (2,0,3) (1,1,3) (1,0,4) (0,0,5)	102	0.12488560	0.50400779	0.262004780

2. Nine exponent: In this case, $p = 9$ and ρ's are taken in a geometrical sequence [205,206] following $\rho_i = \rho_{i-1}\gamma$ $[i = 2 - 9]$; γ being the geometrical ratio of the sequence. The higher ρ value is responsible for spanning the space near the nucleus whereas the lower one spans the space far away from the nucleus. Thus, wavefunction can be squeezed or diffused by changing the geometrical ratio γ while ρ_1 is kept constant throughout. If we take 22 distinct set of powers (*i.e.* $s = 22$ and hence, $N = 990$) and choose the limiting values of ρ as $\rho_1 = 0.06$ and $\rho_9 = 1.5$ *i.e.* $\gamma = 1.4953$, then the energy eigenvalue of the ground state of Ps^- ion turns out to be $-0.262\ 005\ 069$ a.u. which

agrees upto the 8–th decimal place of the lowest reported value of $E = -0.262\,005\,0702$ a.u. available in the literature [204].

In double exponent basis set, optimization is done for a particular bound state energy level (ground or excited) and one can get benchmark results for the bound states using explicitly correlated wavefunction. On the other hand, for nine–exponent basis set, optimization is not much required as the exponents are sufficient to span the entire space and in this case also benchmark results for ground and several exited states are simultaneously obtained. For same number of terms (N) in the basis set, the computational time for the nine–exponent basis set is much lesser than that of the double exponent basis set. The most significant advantage of the explicitly correlated nine exponent basis set is that it can be used in determining the resonance states by using stabilization procedure where the geometrical ratio γ is used as a parameter to plot the stabilization diagram (discussed in section 3.2.5).

The multi-exponent Hylleraas type basis set (3.2.55) can be recast as

$$f\left(r_1, r_2, r_{12}\right) = \sum_{i=1}^{N} C_i X_i\left(r_1, r_2, r_{12}\right) \tag{3.2.56}$$

The correspondence between the basis set expansion formula (3.2.55) and (3.2.56). For $s = 1$ and $p = 2$ (double-exponent) *i.e.* $N = 3$, the expanded form of equation (3.2.55) will be

$$f\left(r_1, r_2, r_{12}\right) = r_1^{l_1}\ r_2^{m_1}\ r_{12}^{n_1}\ \left[C_{111}\eta_1(1)\eta_1(2) + C_{112}\eta_1(1)\eta_2(2) + C_{122}\eta_2(1)\eta_2(2)\right] \tag{3.2.57}$$

Now, with $N = 3$, equation (3.2.56) assumes the form

$$f\left(r_1, r_2, r_{12}\right) = C_1X_1 + C_2X_2 + C_3X_3 \tag{3.2.58}$$

Comparing (3.2.57) and (3.2.58), we find

$$\begin{aligned} C_1 &= C_{111}, \quad C_2 = C_{112}, \quad C_3 = C_{122} \qquad \text{and} \\ X_1 &= r_1^{l_1}\ r_2^{m_1}\ r_{12}^{n_1}\eta_1(1)\eta_1(2), \quad X_2 = r_1^{l_1}\ r_2^{m_1}\ r_{12}^{n_1}\eta_1(1)\eta_2(2), \quad X_3 = r_1^{l_1}\ r_2^{m_1}\ r_{12}^{n_1}\eta_2(1)\eta_2(2) \end{aligned}$$

We have considered equation (3.2.56) for further calculation. Following the linear variation technique, we have solved the generalized eigenvalue equation [162]

$$\underline{\underline{H}}\ \underline{C} = E\underline{\underline{S}}\ \underline{C} \tag{3.2.59}$$

to get the minimized energy eigenvalues (E). Here $\underline{\underline{H}}$ and $\underline{\underline{S}}$ are the $N \times N$ dimensional Hamiltonian and overlap matrices respectively and $\underline{C}$ is the N dimensional column matrix or column vector whose elements are the expansion coefficients or linear variational parameters

$C_1, C_2, ..., C_N$.

In our present methodology, the basis functions X_i and the expansion coefficients C_i are taken to be real. Thus the matrix elements H_{ij} and S_{ij} $(i, j = 1, 2, ..., N)$ are symmetric. So we only calculate the upper triangular matrix elements of $\underline{\underline{H}}$ and $\underline{\underline{S}}$. Then by reflection symmetry we form the lower triangular matrix elements which saves computational time to calculate the integrals. It can be seen from equations (3.2.49), (3.2.50) and (3.2.51) the integrals we need to perform are of the following types

$$\begin{aligned}
\langle \mathcal{O}_1 f | \mathcal{O}_2 f \rangle &= \int (\mathcal{O}_1 f)\,(\mathcal{O}_2 f)\, d\tau \\
\langle \mathcal{O}_1 \tilde{f} | \mathcal{O}_2 \tilde{f} \rangle &= \int \left(\mathcal{O}_1 \tilde{f}\right)\left(\mathcal{O}_2 \tilde{f}\right) d\tau \\
\langle \mathcal{O}_1 f | \mathcal{O}_2 \tilde{f} \rangle &= \int (\mathcal{O}_1 f)\left(\mathcal{O}_2 \tilde{f}\right) d\tau
\end{aligned}$$

$\mathcal{O}_1$ and $\mathcal{O}_2$ are any linear operators. To illustrate the determination of the general form of matrix elements corresponding to each type of the integrals, we consider a simple example with $N = 2$ *i.e.* $f = C_1 X_1 + C_2 X_2$. Then,

$$\begin{aligned}
\langle \mathcal{O}_1 f | \mathcal{O}_2 f \rangle &= C_1 C_1 \int (\mathcal{O}_1 X_1)\,(\mathcal{O}_2 X_1)\, d\tau + C_1 C_2 \int (\mathcal{O}_1 X_1)\,(\mathcal{O}_2 X_2)\, d\tau \\
&\quad + C_2 C_1 \int (\mathcal{O}_1 X_2)\,(\mathcal{O}_2 X_1)\, d\tau + C_2 C_2 \int (\mathcal{O}_1 X_2)\,(\mathcal{O}_2 X_2)\, d\tau \\
&= C_1 C_1 \int (\mathcal{O}_1 X_1)\,(\mathcal{O}_2 X_1)\, d\tau + \frac{1}{2} C_1 C_2 \int [(\mathcal{O}_1 X_1)\,(\mathcal{O}_2 X_2) \\
&\quad + (\mathcal{O}_1 X_2)\,(\mathcal{O}_2 X_1)]\, d\tau + \frac{1}{2} C_2 C_1 \int [(\mathcal{O}_1 X_1)\,(\mathcal{O}_2 X_2) + (\mathcal{O}_1 X_2)\,(\mathcal{O}_2 X_1)]\, d\tau \\
&\quad + C_2 C_2 \int (\mathcal{O}_1 X_2)\,(\mathcal{O}_2 X_2)\, d\tau
\end{aligned}$$

The four integrals corresponding to the coefficients C_1C_1, C_1C_2, C_2C_1 and C_2C_2 are the (11), (12), (21) and (22)–th matrix elements. Thus generally the ij-th $(i, j = 1, 2, ..., N)$ matrix element will be,

$$\langle \mathcal{O}_1 f | \mathcal{O}_2 f \rangle_{ij} = \frac{1}{2} \int [(\mathcal{O}_1 X_i)\,(\mathcal{O}_2 X_j) + (\mathcal{O}_1 X_j)\,(\mathcal{O}_2 X_i)]\, d\tau \tag{3.2.60}$$

Similarly, by taking $\tilde{f} = \sum_{i=1}^{N} C_i \tilde{X}_i$, we write

$$\langle \mathcal{O}_1 \tilde{f} | \mathcal{O}_2 \tilde{f} \rangle_{ij} = \frac{1}{2} \int \left[\left(\mathcal{O}_1 \tilde{X}_i\right)\left(\mathcal{O}_2 \tilde{X}_j\right) + \left(\mathcal{O}_1 \tilde{X}_j\right)\left(\mathcal{O}_2 \tilde{X}_i\right)\right] d\tau \tag{3.2.61}$$

$$\langle \mathcal{O}_1 f | \mathcal{O}_2 \tilde{f} \rangle_{ij} = \frac{1}{2} \int \left[(\mathcal{O}_1 X_i)\left(\mathcal{O}_2 \tilde{X}_j\right) + (\mathcal{O}_1 X_j)\left(\mathcal{O}_2 \tilde{X}_i\right)\right] d\tau \tag{3.2.62}$$

After estimating the matrix elements of $\underline{\underline{H}}$ and $\underline{\underline{S}}$, we evaluate the eigenvalues (E) and the linear variational coefficients $C_1, C_2, ..., C_N$ from (3.2.59) by using EISPACK routine [207].

3.2.4 Basis integrals

For the calculation of each matrix element, a definite type of integral appears in the algebra which is called here as basis–integral. The necessary basis integral is of the form [208]

$$A(m,n,l;\alpha,\beta) = \int_{r_1=0}^{\infty}\int_{r_2=0}^{\infty}\int_{|r_1-r_2|}^{r_1+r_2} r_1^m r_2^n r_{12}^l e^{-\alpha r_1-\beta r_2} dr_1 dr_2 dr_{12} \tag{3.2.63}$$

with the conditions $m \geq 0$, $n \geq 0$, $l \geq 0$ and $\alpha, \beta > 0$. We can write (3.2.63) as

$$\begin{aligned} A(m,n,l;\alpha,\beta,\gamma) &= (-1)^{m+n+l}\left(\frac{\partial}{\partial\alpha}\right)^m\left(\frac{\partial}{\partial\beta}\right)^n\left(\frac{\partial}{\partial\gamma}\right)^l \\ &\int_{r_1=0}^{\infty}\int_{r_2=0}^{\infty}\int_{|r_1-r_2|}^{r_1+r_2} e^{-\alpha r_1-\beta r_2-\gamma r_{12}} dr_1 dr_2 dr_{12} \end{aligned} \tag{3.2.64}$$

After evaluating the explicit form of the integral (3.2.64) we will set $\gamma = 0$ to get the formula of the actual integral (3.2.63). Now

$$\begin{aligned} I(\alpha,\beta,\gamma) &= \int_{r_1=0}^{\infty}\int_{r_2=0}^{\infty}\int_{|r_1-r_2|}^{r_1+r_2} e^{-\alpha r_1-\beta r_2-\gamma r_{12}} dr_1 dr_2 dr_{12} \\ &= \int_{r_2=0}^{\infty} e^{-\beta r_2} dr_2 \int_{r_1=r_2}^{\infty} e^{-\alpha r_1} dr_1 \int_{(r_1-r_2)}^{r_1+r_2} e^{-\gamma r_{12}} dr_{12} + \\ &\quad \int_{r_1=0}^{\infty} e^{-\alpha r_1} dr_1 \int_{r_2=r_1}^{\infty} e^{-\beta r_2} dr_2 \int_{(r_2-r_1)}^{r_1+r_2} e^{-\gamma r_{12}} dr_{12} \\ &= \frac{1}{(\alpha+\beta)(\alpha+\gamma)(\alpha+\beta+2\gamma)} + \frac{1}{(\alpha+\beta)(\beta+\gamma)(\alpha+\beta+2\gamma)} \\ &= \frac{2}{(\alpha+\beta)(\beta+\gamma)(\alpha+\gamma)} \end{aligned} \tag{3.2.65}$$

$$\begin{aligned} \therefore \left(\frac{\partial}{\partial\gamma}\right)^l I(\alpha,\beta,\gamma) &= 2\left(\frac{\partial}{\partial\gamma}\right)^l \frac{1}{(\alpha+\beta)(\beta+\gamma)(\alpha+\gamma)} \\ &= \frac{2}{(\alpha+\beta)}\sum_{k=0}^{l}\binom{l}{k}\left[\left(\frac{\partial}{\partial\gamma}\right)^{l-k}\frac{1}{(\alpha+\gamma)}\right]\left[\left(\frac{\partial}{\partial\gamma}\right)^{k}\frac{1}{(\beta+\gamma)}\right] \\ &= \frac{2}{(\alpha+\beta)}(-1)^l\sum_{k=0}^{l}\binom{l}{k}\frac{(l-k)!}{(\alpha+\gamma)^{l-k+1}}\frac{k!}{(\beta+\gamma)^{k+1}} \end{aligned}$$

Here, we have used the Leibniz formula [156] for the derivative on $l-$th order of the product of two functions and $\binom{l}{k} = \frac{l!}{k!(l-k)!}$. Proceeding in the same way we can find

$\left(\frac{\partial}{\partial\beta}\right)^n\left(\frac{\partial}{\partial\gamma}\right)^l I(\alpha,\beta,\gamma)$ and $\left(\frac{\partial}{\partial\alpha}\right)^m\left(\frac{\partial}{\partial\beta}\right)^n\left(\frac{\partial}{\partial\gamma}\right)^l I(\alpha,\beta,\gamma)$ successively and then setting $\gamma = 0$ we obtain from equation (3.2.64)

$$\begin{aligned} A(m,n,l;\alpha,\beta) &= 2m!n!l!\sum_{i=0}^{m}\sum_{j=0}^{n}\sum_{k=0}^{l}\frac{(k+j)!(n+i-j)!(m+l-i-k)!}{i!j!k!(m-i)!(n-j)!(l-k)!} \\ &\quad \frac{1}{(\alpha+\beta)^{n+1+i-j}\,\alpha^{m+l+1-i-k}\beta^{j+k+1}} \end{aligned} \tag{3.2.66}$$

To verify the formula (3.2.66), let us perform an integral $A(1,1,1;\alpha,\beta)$ directly and then try to match the result from the summation formula (3.2.66). In the direct manner, the integral $A(1,1,1;\alpha,\beta)$ may be expanded as

$$\begin{aligned} A(1,1,1;\alpha,\beta) &= \int_{r_1=0}^{\infty}\int_{r_2=0}^{\infty}\int_{|r_1-r_2|}^{r_1+r_2} r_1 r_2 r_{12} e^{-\alpha r_1-\beta r_2} dr_1 dr_2 dr_{12} \\ &= \int_{r_1=0}^{\infty} r_1 e^{-\alpha r_1} dr_1 \int_{r_2=0}^{r_1} r_2 e^{-\beta r_2} dr_2 \int_{(r_1-r_2)}^{r_1+r_2} r_{12} dr_{12} \\ &+ \int_{r_2=0}^{\infty} r_2 e^{-\beta r_2} dr_2 \int_{r_1=0}^{r_2} r_1 e^{-\alpha r_1} dr_1 \int_{(r_2-r_1)}^{r_1+r_2} r_{12} dr_{12} \\ &= 2\int_{r_1=0}^{\infty} r_1^2 e^{-\alpha r_1} dr_1 \int_{r_2=0}^{r_1} r_2^2 e^{-\beta r_2} dr_2 \\ &+ 2\int_{r_2=0}^{\infty} r_2^2 e^{-\beta r_2} dr_2 \int_{r_1=0}^{r_2} r_1^2 e^{-\alpha r_1} dr_1 \\ &= I_1 + I_2 \end{aligned} \tag{3.2.67}$$

$$\begin{aligned} \text{where, } I_1 &= 2\int_{r_1=0}^{\infty} r_1^2 e^{-\alpha r_1} dr_1 \int_{r_2=0}^{r_1} r_2^2 e^{-\beta r_2} dr_2 \\ &= 2\int_{r_1=0}^{\infty} r_1^2 e^{-\alpha r_1} dr_1 \left[\frac{\partial^2}{\partial\beta^2}\int_{r_2=0}^{r_1} e^{-\beta r_2} dr_2\right] \\ &= 2\int_{r_1=0}^{\infty} r_1^2 e^{-\alpha r_1}\left(\frac{2}{\beta^3} - \frac{2}{\beta^3}e^{-\beta r_1} - \frac{2r_1}{\beta^2}e^{-\beta r_1} - \frac{r_1^2}{\beta}e^{-\beta r_1}\right) dr_1 \\ &= 8\left[\frac{1}{\alpha^3\beta^3} - \frac{1}{\beta^3(\alpha+\beta)^3} - \frac{3}{\beta^2(\alpha+\beta)^4} - \frac{6}{\beta(\alpha+\beta)^5}\right] \\ \text{and similarly, } I_2 &= 8\left[\frac{1}{\alpha^3\beta^3} - \frac{1}{\alpha^3(\alpha+\beta)^3} - \frac{3}{\alpha^2(\alpha+\beta)^4} - \frac{6}{\alpha(\alpha+\beta)^5}\right] \end{aligned}$$

Putting I_1 and I_2 in the equation (3.2.67) and simplifying we can get $A(1,1,1;\alpha,\beta) = \frac{8}{\alpha^3\beta^3}$. Now, by putting $m = n = l = 1$, the summation (3.2.66) yields the same result for the integral $A(1,1,1;\alpha,\beta)$. Integrals $A(m,n,l;\alpha,\beta)$ with different powers and non-linear parameters are checked in this way.

3.2.5 Stabilization method for resonance states

Ritz variation principle is not applicable in case of resonance states because these states lie within the continuum and there exists lower lying bound states of the same symmetry. Stabilization method is used to determine the resonance parameters *i.e.* resonance energy (E_r) and width (Γ_r) of a three-body exotic system (ion) XXY or XYY, where X and Y are constituent particles with positive and negative charges respectively. If a charged particle X (or Y) moving with a "suitable amount" of K.E., it may be captured by the XY system, a quasi-bound state of $XY + X$(or Y) *i.e.* XXY^* (or XYY^*) system is temporarily formed, which is known as "resonance state". These resonance states having finite life-time can decay via auto-ionization channel, $XXY^* \rightarrow XY + X$ or via cascading through different fluorescence decay channel like, $XXY^* \rightarrow XXY$(ground or lower excited state). We can take an example from the scattering theory of e^- with H atom where the wavefunction of the system XXY (or XYY) can be written as that of the composite system (e^- + H) *i.e.* ($e^- + e^- p^+$) [162],

$$\Psi_\pm(\vec{r_1},\vec{r_2}) = \sum_j \left[F_j^\pm(\vec{r_1})\,\psi_j(\vec{r_2}) \pm F_j^\pm(\vec{r_2})\,\psi_j(\vec{r_1})\right] + \sum_k C_k^\pm \chi_k^\pm(\vec{r_1},\vec{r_2}) \tag{3.2.68}$$

where, $\vec{r_1}$ and $\vec{r_2}$ are the positions of two identical particles X(or Y) with respect to the third particle Y(or X). In the above equation (3.2.68) the '+' sign stands for the singlet and '−' sign stands for the triplet states. In the first sum of the equation (3.2.68), 'j' represents the final atomic state of the target XY having wavefunction ψ_j and $F_j^\pm$ is the asymptotic form of the wavefunction for the outgoing particle X(or Y) after auto-ionization. This first part of the wavefunction $\Psi_\pm(\vec{r_1},\vec{r_2})$ is the "open channel" part. In the second sum of (3.2.68), $\chi_k^\pm$ is a square integrable correlation function and this part is the "closed channel" part of the wavefunction $\Psi_\pm(\vec{r_1},\vec{r_2})$. It is to be noted that $\chi_k^\pm$ are orthogonal to ψ_j. Using the Feshbach projection operator formalism [209, 210] we can write

$$\Psi_\pm = P\Psi_\pm + Q\Psi_\pm \tag{3.2.69}$$

P and Q are projection operators satisfying the condition, $P + Q = I$, I being the identity operator. Comparing (3.2.68) and (3.2.69) we see that $P\Psi_\pm$ contains open-channel subspace and $Q\Psi_\pm$ contains closed-channel subspace. Hence, the spectral density of states (DOS) $\rho(E)$ below the threshold of double-ionization consists of two parts : (1) DOS of open-channel $\rho^P(E)$ and (2) DOS of closed-channel $\rho^Q(E)$. $\rho^P(E)$ smoothly varies with energy E. $\rho^Q(E)$ is given by

$$\rho^Q(E) = -\frac{1}{\pi} Im\left[\sum_k \frac{1}{(E - E_k) + i\Gamma_k}\right]$$

$E = E_k - i\Gamma_k$ are the complex poles of the Green's function, where E_k and Γ_k are the resonance energy and width of the k-th resonance state. For an isolated resonance, Bowman [211] showed a Lorentzian shape of $\rho^Q(E)$ can be given as

$$\rho^Q(E) \simeq \frac{1}{\pi} \frac{\Gamma/2}{(E - E_r)^2 + \Gamma^2} \tag{3.2.70}$$

where E_r and Γ are the resonance energy and width. The equation (3.2.70) is similar to the Breit–Wigner formula for the resonance scattering cross-section [162].

We now move attention from the scattering picture to the quasi-bound state calculations where a significant work was done by Mandelshtam *et.al.* [212] by considering a box problem to calculate the resonance parameters. In their work [212], they argued that the DOS $\rho_L(E)$ is a function of box length L and shows a region of L where $\rho_L(E)$ assumes a Lorentzian shape. This region of L defines the Q-space. If the eigenvalues of a Hamiltonian $E_K(L)$ are known, the DOS is a simple count of states *i.e.* a histogram as given by

$$\rho_L(E) = \sum_k \delta\left[E_K(L) - E\right] \tag{3.2.71}$$

Here $E_K(L)$ are the box eigenvalues of the system XXY^* or XYY^*. $E_K(L)$ are calculated by repeated diagonalization of the Hamiltonian for different 'L' values. Mandelshtam *et.al.* [212] have shown that

$$\rho^Q(E) = \frac{1}{L_{max} - L_{min}} \int_{L_{min}}^{L_{max}} \rho_L(E) dL \tag{3.2.72}$$

This idea of calculating DOS $\rho^Q(E)$ is known as 'hard wall' technique as in this procedure the box length L is varied. But we are more interested in a more useful technique to calculate $\rho^Q(E)$ as done by Müller *et.al.* [213], where 'soft wall' strategy has been employed by varying the non-linear parameter γ in the wavefunction. The histogram form of DOS (3.2.71) can be expressed as

$$\rho_\gamma(E) = \sum_k \delta\left[E_K(\gamma) - E\right]$$

Müller *et.al.* [213] shows the equation (3.2.72) can be re-written as

$$\begin{aligned} \rho^Q(E) &= \frac{1}{\gamma_{max} - \gamma_{min}} \int_{\gamma_{min}}^{\gamma_{max}} \rho_\gamma(E) d\gamma \\ &= \frac{1}{\gamma_{max} - \gamma_{min}} \sum_k \int_{\gamma_{min}}^{\gamma_{max}} \delta\left[E_K(\gamma) - E\right] d\gamma \end{aligned} \tag{3.2.73}$$

Using the relation

$$\int \delta\left[a - f(x)\right] g(x) dx = g(x) \left|\frac{df}{dx}\right|^{-1}_{f(x)=a} \tag{3.2.74}$$

the equation (3.2.73) becomes

$$\rho^{Q}(E) = \frac{1}{\gamma_{max} - \gamma_{min}} \sum_{k} \left|\frac{dE_K(\gamma)}{d\gamma}\right|^{-1}_{E_K(\gamma)=E} \tag{3.2.75}$$

This formula is basically an average over the basis set expansion parameter (Γ) corresponding to a particular energy position. Instead of doing average, we select a plateau for an energy eigenroot and calculate DOS. The graph showing the variation of the k–th energy eigenroot versus γ produces the stabilization diagram. A specimen stabilization diagram is shown in figure (3.2.2). These roots form flat plateaus in the vicinity of avoided crossings which confirm the presence of the resonance states. The inverse of tangent at different points near the stabilization plateau for each energy eigenroot gives rise to the density of states (DOS) as

$$\rho^{Q}(E) = \left|\frac{\gamma^{i+1} - \gamma^{i-1}}{E_k(\gamma^{i+1}) - E_k(\gamma^{i-1})}\right| \tag{3.2.76}$$

The resonance parameters (E_r, Γ) are obtained by Lorentzian fitting of the DOS as

$$\rho^{Q}(E) = y_0 + \frac{A}{\pi} \frac{\Gamma/2}{(E - E_r)^2 + (\Gamma/2)^2} \tag{3.2.77}$$

where y_0 is the baseline background (basically open channel contribution), A is the total area under the curve from the baseline, E_r gives the peak position of the curve, and Γ represents the full width of the curve at half maxima. For example, the energy eigenroot no. 25 of $^1S^e$ state of exotic $p^+p^+\mu^-$ ion in the energy range -60 a.u. to -24 a.u. is depicted in figure (3.2.2), which shows three distinct plateaus in the vicinity of -30 a.u., -26 a.u. and -24 a.u. energies. This energy eigenroot shows one plateau around -30.2718 a.u. which is depicted in figure 3.2.3(a) and the numerically estimated DOS [using (3.2.76)] in the plateau region are plotted in figure 3.2.3(b). The DOSs for the full range of energies of the 25–th eigenroot are plotted in figure (3.2.4), which shows a histogram. It clearly shows three peaks at three different energies for first three resonances. It is also evident that the resonances are isolated as the separation of peaks are greater than the widths of the consecutive resonances. The next part is to consider DOS of each isolated resonance and to fit with respective Lorentzian profile (3.2.77). The estimated DOSs [hollow black circles] and the fitted Lorentzian [red lines] for the first resonance state are given in figure 3.2.5. The fitting yields resonance position E_r at -30.2718 a.u. and width $\Gamma = 5.963 \times 10^{-5}$ a.u.

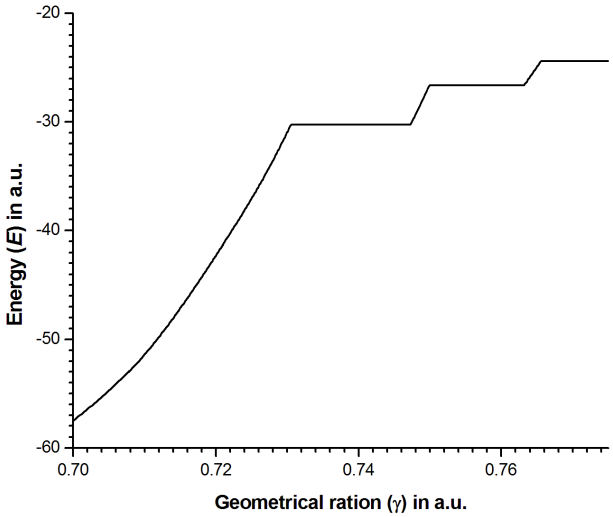

Figure 3.2.2: Stabilization diagram for eigenroot no. 25 of $^1S^e$ state of exotic $p^+p^+\mu^-$ ion.

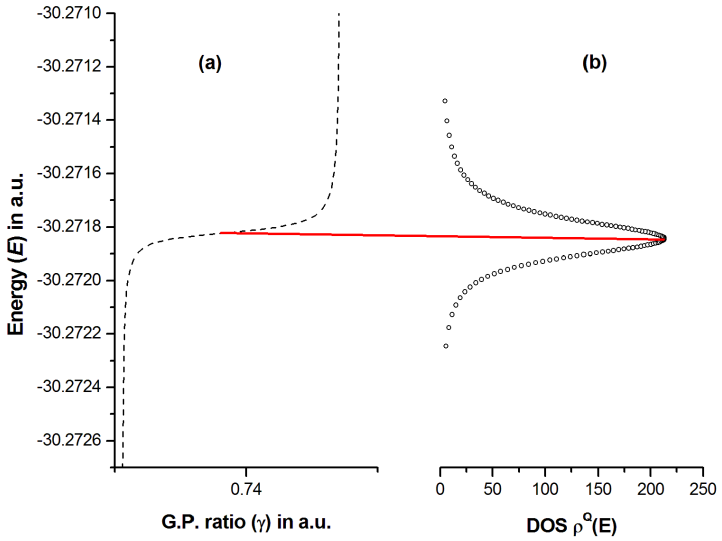

Figure 3.2.3: Plot of DOS corresponding to lowest plateau of eigenroot no. 25 of $^1S^e$ state of exotic $p^+p^+\mu^-$ ion.

Repeated calculations of DOS near the flat plateau of each of the eigenroots are done which result into Lorentzian fitted curves. For a particular resonance, the position and width are chosen with respect to the best fitting parameters such as least χ^2 fitting or correlation $R^2 \leq 1$.

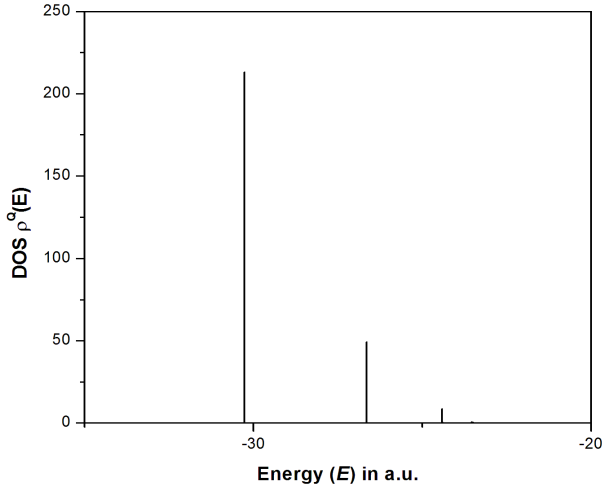

Figure 3.2.4: Plot of all DOS of eigenroot no. 25 with respect to the energy eigenvalues (E) of $^1S^e$ state of exotic $p^+p^+\mu^-$ ion.

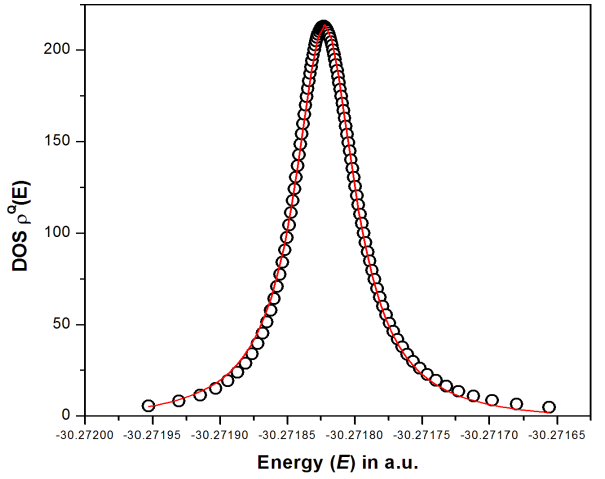

Figure 3.2.5: Lorentzian fit of relevant DOS of eigen root no. 25 of $^1S^e$ states of exotic $p^+p^+\mu^-$ ion. Hollow black circles show the estimated values of DOS and the red line shows the fitted Lorentzian.

3.3 Results and Discussions

The results of three–body exotic systems presented here are divided in two broad categories: bound and resonance states. In the former case we will discuss on the stability of the ions by calculating the energy eigenvalues of the ions in ground state ($^1S^e$) under free as well as classical WCP environment. In the later case we will discuss the resonance states of some of those ions under only free environment.

3.3.1 Bound state

The ground state energies of free three–body exotic XXY and XYY systems are given in the table (3.3.1), where 'X' denotes unit positively charged particles like p^+, d^+, t^+ and e^+ while, 'Y' denotes unit negatively charged elementary particles like μ^-, π^-, K^- and e^-.

Table 3.3.1: Ground state energy eigenvalues $-E$ (a.u.) of free three–body exotic XXY and XYY systems [X = p^+, d^+, and t^+, Y = μ^-, π^- and K^-], $Ps^-(e^+e^-e^-)$ ion and three–body molecular $H_2^+(p^+p^+e^-)$, $D_2^+(d^+d^+e^-)$ and $T_2^+(t^+t^+e^-)$ ions.

	$-E$(a.u.)						
Ions	Present work	Pawlak *et. al.* [178]	Sil *et. al.* [177]	Kar and Ho [214]	Bhattacharyya *et. al.* [215]	Frolov *et. al.* [216]	Bertini *et. al.* [171]
$p^+p^+\mu^-$	102.223497	102.223491	102.2235	102.2235036			
$p^+\mu^-\mu^-$	97.566984				97.56698459	97.56698343	
$d^+d^+\mu^-$	109.816924	109.815698	109.8165				
$d^+\mu^-\mu^-$	102.991910					102.9919106	
$t^+t^+\mu^-$	112.972830	112.971933	112.9718				
$t^+\mu^-\mu^-$	104.944115					104.9441154	
$p^+p^+\pi^-$	129.718073						
$p^+\pi^-\pi^-$	124.690674				124.69067407		
$d^+d^+\pi^-$	141.524534						
$d^+\pi^-\pi^-$	133.653701						
$t^+t^+\pi^-$	146.472365						
$t^+\pi^-\pi^-$	136.951552						
$p^+p^+K^-$	334.575377						
$p^+K^-K^-$	330.800637				330.80063677		
$d^+d^+K^-$	410.609734						
$d^+K^-K^-$	400.176959						
$t^+t^+K^-$	446.122899						
$t^+K^-K^-$	430.623711						
Ps^-	0.262005			0.2620050702			
H_2^+	0.596902						0.597136
D_2^+	0.598211						
T_2^+	0.598702						

The energy eigenvalues are determined variationally using nine–exponent ($p = 9$) Hylleraas basis set consisting of total $N = 990$ number of terms. The energy values converged atleast upto 6–th decimal place and those values are compared with other results from the literature [171, 177, 178, 188, 215, 216]. The comparison shows that the present method is quite efficient to produce precise energy values of such systems. We note that among the three–body systems listed in table (3.3.1), H_2^+, D_2^+ and T_2^+ do not belong to the exotic ion category.

We extend our methodology to calculate the ground state energy eigenvalues of the same set of three-body exotic systems under classical WCP where the effective potential is modeled by ESCP (equation–2.2.25) as

$$V_{eff}(r_1, r_2, r_{12}) = -\frac{1}{r_1}e^{-\mu_D r_1} - \frac{1}{r_2}e^{-\mu_D r_2} + \frac{1}{r_{12}}e^{-\mu_D r_{12}} \qquad \text{(in a.u.)} \qquad (3.3.1)$$

In this expression, μ_D is the plasma screening parameter which is the inverse of the plasma screening length λ_D (equation–2.2.6) *i.e.* $\mu_D = \dfrac{1}{\lambda_D}$. The first two terms in the potential (3.3.1) denote the attractive screened Coulomb potential between the X and Y particles, whereas the last term is the repulsive screened Coulomb potential between either two X or two Y particles. The energy eigenvalues of $p^+\mu^-\mu^-$, $p^+p^+\mu^-$, $d^+\mu^-\mu^-$, $d^+d^+\mu^-$, $t^+\mu^-\mu^-$ and $t^+t^+\mu^-$ systems are given in table (3.3.2); $p^+\pi^-\pi^-$, $p^+p^+\pi^-$, $d^+\pi^-\pi^-$, $d^+d^+\pi^-$, $t^+\pi^-\pi^-$ systems in table (3.3.3) and $t^+t^+\pi^-$; $p^+K^-K^-$, $p^+p^+K^-$, $d^+K^-K^-$, $d^+d^+K^-$, $t^+K^-K^-$ and $t^+t^+K^-$ systems in table (3.3.4).

Table 3.3.2: Ground state energy eigenvalues $-E$ (a.u.) of three-body exotic XXY and XYY systems [X = p^+, d^+, t^+, Y = μ^-] for different screening parameters (μ_D in a.u.) with the relative binding energies (R_X^μ in %).

	$-E$			$-E$			$-E$		
μ_D	$p^+\mu^-\mu^-$	$p^+p^+\mu^-$	R_p^μ	$d^+\mu^-\mu^-$	$d^+d^+\mu^-$	R_d^μ	$t^+\mu^-\mu^-$	$t^+t^+\mu^-$	R_t^μ
10.0	87.855345	92.568209	5.09	93.260418	100.145956	6.87	95.205930	103.296334	7.83
		92.568199[a]			100.144720[a]			103.295434[a]	
		92.5682[b]			100.1456[b]			103.2953[b]	
50.0	54.839746	60.038615	8.66	59.825553	67.257235	11.05	61.198210	70.280415	12.92
		60.038611[a]			67.255863[a]			70.279521[a]	
		60.0386[b]			67.2567[b]			70.2793[b]	
100.0	25.826355	30.782620	16.10	29.756288	36.948814	19.47	31.198210	39.591867	21.2
		30.782618[a]		36.947245[a]				39.591120[a]	
		30.7825[b]		36.9481[b]				39.5905[b]	
150.0	8.446984	11.937001	29.24	10.982746	16.485717	33.38	11.945982	18.532941	35.54
		11.937011[a]			16.484151[a]			18.532441[a]	
		11.9369[b]			16.4848[b]			18.5315[b]	
170.0	4.297395	6.944875	38.12	6.216664	10.706357	41.93	6.968302	12.460505	44.08
190.0	1.581640	3.296125	52.01	2.858609	6.191216	53.82	3.390177	7.621487	55.52
200.0	0.731816	1.960682	62.67	1.678362	4.390282	61.77	2.097041	5.646489	62.86
		1.960682[a]			4.389327[a]			5.646211[a]	
		1.9603[b]			4.3895[b]			5.6452[b]	
210.0	0.207350	0.948810	78.14	0.816355	2.886918	71.72	1.120501	3.960122	71.70
		0.948810[a]			2.886181[a]				
		0.9471[b]			2.8861[b]				
215.0	0.064944	0.565957	88.52						
217.0	0.030274	0.436440	93.06						
219.0	0.008277	0.320819	97.42						
220.0	0.001736	0.268351	99.35	0.260874	1.678541	84.46	0.450726	2.558335	82.38
		0.268355[a]			1.678029[a]			2.558159[a]	
					1.6768[b]			2.5569[b]	
220.2	0.000738	0.258291	99.17						
220.3	0.000273	0.253317	99.89						
220.36	0.000005	0.250349	99.99						
220.37	-0.000039								
223.0		0.133212		0.150990	1.373618	89.00			
		0.133223[a]							
224.0		0.095989		0.119785	1.277921	90.63			
		0.096009[a]							
225.0		0.063015		0.091167	1.185209	92.31	0.227221	1.963501	88.43
		0.063032[a]							
226.0		0.034623		0.065044	1.095491	94.06			
		0.034642[a]							
227.0		0.011481		0.058442	1.008779	94.2			
		0.011503[a]							
227.6		0.000821							

Continuation of Table (3.3.2)

	$-E$			$-E$			$-E$		
μ_D	$p^+\mu^-\mu^-$	$p^+p^+\mu^-$	R_p^μ	$d^+\mu^-\mu^-$	$d^+d^+\mu^-$	R_d^μ	$t^+\mu^-\mu^-$	$t^+t^+\mu^-$	R_t^μ
		0.000871[a]							
227.65		0.000093							
227.66		-0.000049							
228.0				0.041017	0.925084	95.56			
229.0				0.026588	0.844421	96.85			
230.0				0.015117	0.766808	98.02	0.073756	1.439475	94.88
					0.766510[a]				
231.0				0.006487	0.692261	99.06		1.343207	
232.0				0.000422	0.620805	99.93			
232.08				0.000035	0.615223	99.99			
232.09				-0.000013					
233.0							0.028768	1.159259	97.52
234.0							0.016915	1.071598	98.42
235.0					0.425236		0.007890	0.986826	99.20
					0.425125[a]				
236.0							0.001462	0.904956	99.84
236.2							0.000453	0.888931	99.95
236.29							0.000026	0.881759	99.99
236.3							-0.000020		
236.5					0.338356				
					0.338250[a]				
238.0					0.258924				
					0.258842[a]				
240.0					0.165098			0.606836	
					0.165049[a]			0.606762[a]	
242.0					0.086017			0.475709	
					0.085997[a]			0.475647[a]	
243.0					0.052549				
					0.052542[a]				
244.0					0.023686				
					0.023704[a]				
244.5					0.011245				
					0.011305[a]				
244.8					0.004596				
					0.004663[a]				
245.0					0.000590			0.302169	
					0.000670[a]			0.302164[a]	
245.03					0.000113				
245.04					-0.000069				
248.0								0.157711	
								0.157936[a]	
250.0								0.079315	
								0.079473[a]	
252.0								0.017483	
								0.017562[a]	
252.5								0.005217	
								0.005378[a]	
252.7								0.000837	
								0.001049[a]	
252.74								0.000008	
252.75								-0.000196	

[a] [178], [b] [177]

Table 3.3.3: Ground state energy eigenvalues $-E$ (a.u.) of three-body exotic XXY and XYY systems [X = p^+, d^+, t^+ , Y = π^-] for different screening parameters (μ_D in a.u.) with the relative binding energies (R_X^π in %).

	$-E$			$-E$			$-E$		
μ_D	$p^+\pi^-\pi^-$	$p^+p^+\pi^-$	R_p^π	$d^+\pi^-\pi^-$	$d^+d^+\pi^-$	R_d^π	$t^+\pi^-\pi^-$	$t^+t^+\pi^-$	R_t^π
50.0	80.425360	85.969490	6.45	88.937428	97.405083	8.69	92.081757	102.223361	9.92
100.0	47.215697	52.927045	10.79	54.588414	63.309187	13.77	57.341339	67.754111	15.37
150.0	23.821049	28.803607	17.33	29.617686	37.546979	21.19	31.826161	41.400552	23.13
200.0	8.925715	12.402317	28.03	12.869611	19.006120	32.29	14.437058	22.075746	34.60
210.0	6.862148	9.969063	31.16						
230.0	3.583539	5.904747	39.31	6.322564	11.005377	42.55			
250.0	1.387016	2.883109	51.89	3.290509	6.888817	52.23	4.153681	8.995895	53.83
260.0	0.677872	1.757214	61.42	2.154059	5.184217	58.45	2.870325	7.076785	59.44
270.0	0.220759	0.888919	75.16	1.262464	3.711794	65.99	1.829890	5.381642	65.99
275.0	0.085564	0.553326	84.52						
280.0	0.011735	0.286065	95.89	0.609687	2.470156	75.32	1.026418	3.908086	73.74
281.0	0.003820	0.241133	98.41						
281.2	0.002338	0.232497	98.99						
281.4	0.001015	0.223979	99.55						
281.5	0.000612	0.219764	99.72						
281.6	0.000002	0.215579	99.99						
281.61	-0.000058								
283.0		0.160262							
285.0		0.091848							
287.0		0.037260							
288.0		0.015642							
289.0		0.000179							
289.02		0.000007							
289.03		-0.000090							
290.0				0.187206	1.459767	87.17	0.453008	2.654741	82.93
295.0				0.055832	1.042335	94.64			
298.0				0.027442	0.820496	96.65			
299.0				0.017139	0.751392	97.72			
300.0				0.009212	0.684736	98.65	0.114300	1.621863	92.95
301.0				0.003686	0.620544	99.41			
302.0				0.000611	0.558837	99.89			
302.4				0.000053	0.534855	99.99			
302.45				0.000006	0.531886	99.99			
302.46				-0.000002					
305.0					0.388858		0.028253	1.188937	97.62
306.0							0.017897	1.109122	98.39
307.0							0.009856	1.031583	99.04
308.0							0.004158	0.956329	99.56
309.0							0.000847	0.883372	99.90
309.5							0.000081	0.847758	99.99
309.58							0.000006	0.842114	99.99
309.59							-0.000003		
310.0					0.157682			0.812723	
311.0					0.119531				
312.0					0.084133				
313.0					0.051501				
314.0					0.029496				
315.0					0.005910				
315.2					0.001680				
315.3					0.001361				

Continuation of Table (3.3.3)

	$-E$			$-E$			$-E$		
μ_D	$p^+\pi^-\pi^-$	$p^+p^+\pi^-$	R_p^π	$d^+\pi^-\pi^-$	$d^+d^+\pi^-$	R_d^π	$t^+\pi^-\pi^-$	$t^+t^+\pi^-$	R_t^π
315.37					0.000153				
315.38					-0.000014				
320.0								0.236205	
321.0								0.191857	
322.0								0.149967	
323.0								0.116501	
324.0								0.082026	
325.0								0.050882	
326.0								0.023476	
327.0								0.000776	
327.04								0.000012	
327.05								-0.000176	

Table 3.3.4: Ground state energy eigenvalues $-E$ (a.u.) of three-body exotic XXY and XYY systems [X = p^+, d^+, t^+ , Y = K^-] for different screening parameters (μ_D in a.u.) with the relative binding energies (R_X^K in %).

	$-E$			$-E$			$-E$		
μ_D	$p^+K^-K^-$	$p^+p^+K^-$	R_p^K	$d^+K^-K^-$	$d^+d^+K^-$	R_d^K	$t^+K^-K^-$	$t^+t^+K^-$	R_t^K
100.0	239.838364	244.007205	1.71	307.459282	318.599460	3.49	337.295789	353.626696	4.62
200.0	166.075945	170.608044	2.66	229.055514	241.066693	4.98	257.247701	274.688669	6.35
300.0	107.891316	112.326102	3.95	164.095730	176.332809	6.94	189.854114	207.722505	8.60
400.0	63.670079	67.522047	5.70	111.501363	123.127272	9.44	134.225608	151.556582	11.43
500.0	31.977129	34.866702	8.29	70.209125	80.428582	12.71	89.439333	105.257705	15.02
600.0	11.579834	13.284046	12.83	39.237733	47.399557	17.22	54.615579	68.060983	19.75
700.0	1.450568	1.951378	25.66	17.708389	23.354972	24.17	28.946063	39.334553	26.41
710.0	0.970778	1.362893	28.77						
720.0	0.585947	0.874168	32.97						
730.0	0.296183	0.486795	39.16						
740.0	0.101628	0.203732	50.12						
745.0	0.040922	0.102705	60.15						
750.0	0.005884	0.031387	81.25						
752.0	0.000367	0.011356	96.77						
752.2	0.000190	0.010504	98.19						
752.4	0.000068	0.008791	99.22						
752.6	0.000006	0.007123	99.92						
752.66	0.000001	0.006631	99.99						
752.67	-0.0000002								
753.0		0.003917							
754.0		0.002306							
754.1		0.001775							
754.2		0.001257							
754.3		0.000753							
754.4		0.000263							
754.45		0.000023							
754.46		-0.000025							
800.0				4.852758	7.762306	37.483	11.705996	18.566747	36.95
850.0				1.472341	3.032857	51.45	6.045429	11.044957	45.26
870.0				0.668722	1.715585	61.02			
880.0				0.383635	1.183266	67.58			
890.0				0.176330	0.737658	76.09			
900.0				0.047548	0.381782	87.54	2.263549	5.393579	58.03

Continuation of Table (3.3.4)

	$-E$			$-E$			$-E$		
μ_D	$p^+K^-K^-$	$p^+p^+K^-$	R_p^K	$d^+K^-K^-$	$d^+d^+K^-$	R_d^K	$t^+K^-K^-$	$t^+t^+K^-$	R_t^K
905.0				0.013001	0.238701	94.55			
906.0				0.008420	0.212937	96.04			
907.0				0.004550	0.188131	97.58			
908.0				0.001333	0.164286	99.19			
908.4				0.000214	0.155018	99.86			
908.48				0.000001	0.153183	99.99			
908.49				-0.000025					
910.0					0.119486				
912.0					0.078536				
913.0					0.059501				
914.0					0.041417				
916.0					0.025423				
917.0					0.013630				
918.0					0.003757				
918.4					0.000367				
918.44					0.000047				
918.45					-0.000032				
920.0							1.262584	3.657489	65.48
930.0							0.869294	2.903244	70.06
940.0							0.545767	2.225926	75.48
950.0							0.289334	1.626773	82.21
960.0							0.095004	1.107561	91.42
970.0							0.025565	0.670780	96.19
975.0							0.002600	0.484293	99.45
975.9							0.000172	0.453034	99.96
975.97							0.000002	0.450633	99.99
975.98							-0.000022		
980.0								0.319666	
985.0								0.177313	
990.0								0.057524	
993.0								0.022217	
994.0								0.008063	
994.6								0.000920	
994.68								0.000033	
994.69								-0.000076	

It can be seen from the tables (3.3.2)–(3.3.4) that, if μ_D increases, the energy eigenvalues of all the exotic systems increases gradually towards the limit of destabilization. Figures (3.3.1) to (3.3.3) show the nature of variation of the ground state energies of XXY and XYY systems with respect to μ_D. It is also evident from the tables (3.3.2)–(3.3.4) that the energy eigenvalues of XYY systems are higher than that of the XXY systems at any arbitrary screening parameter μ_D. The amount of boundness of the XYY systems with respect to XXY systems can be examined effectively by introducing a dimensionless quantity, called *relative binding energy* (R_X^Y) which is defined as $R_X^Y = \dfrac{E_{XXY} - E_{XYY}}{E_{XXY}} \times 100$, where E_{XXY} and E_{XYY} are the ground state energies of XXY and XYY systems respectively. In the tables (3.3.2) to (3.3.4), the values of R_X^Y show that XYY systems destabilizes more rapidly compared to the XXY systems. The variations of R_X^Y with respect to μ_D are also shown in

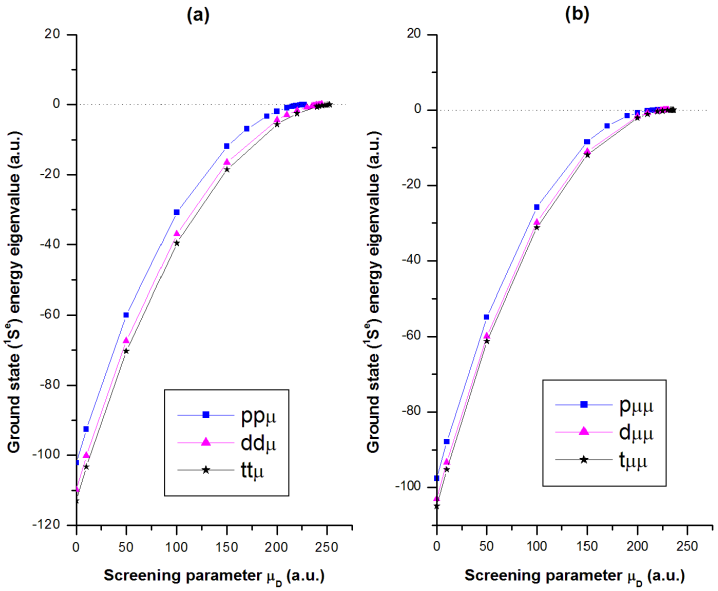

Figure 3.3.1: The variation of ground state ($^1S^e$) energy eigenvalue E (in a.u.) of exotic (a) $XX\mu^-$ ions and (b) $X\mu^-\mu^-$ ions $[X : p^+, d^+, t^+]$, with respect to the screening parameter μ_D (in a.u.).

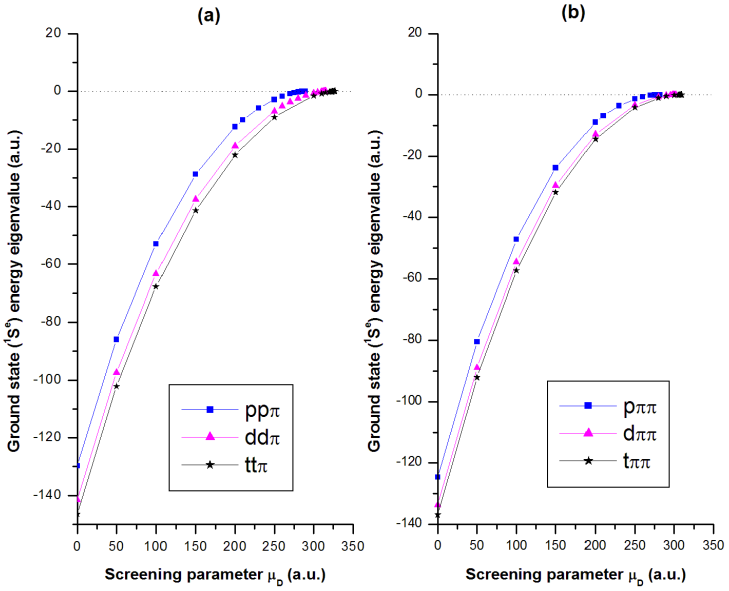

Figure 3.3.2: The variation of ground state ($^1S^e$) energy eigenvalue E (in a.u.) of exotic (a) $XX\pi^-$ ions and (b) $X\pi^-\pi^-$ ions $[X : p^+, d^+, t^+]$, with respect to the screening parameter μ_D (in a.u.).

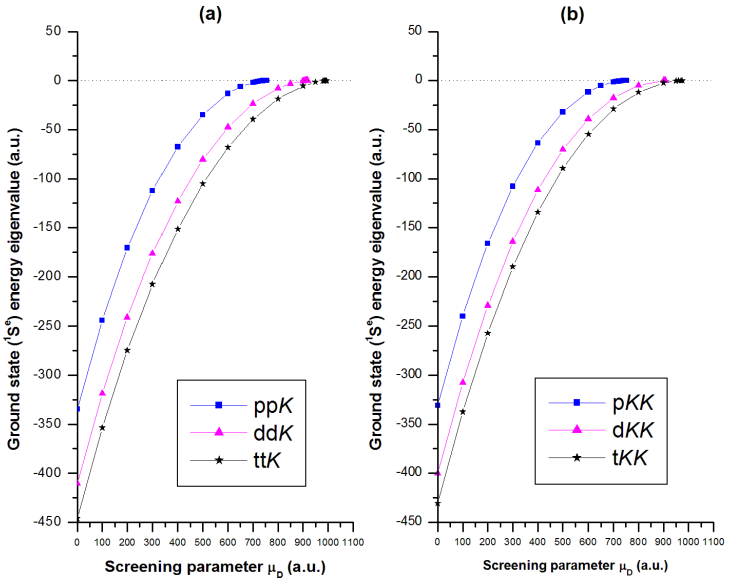

Figure 3.3.3: The variation of ground state ($^1S^e$) energy eigenvalue E (in a.u.) of exotic (a) XXK^- ions and (b) XK^-K^- ions $[X : p^+, d^+, t^+]$, with respect to the screening parameter μ_D (in a.u.).

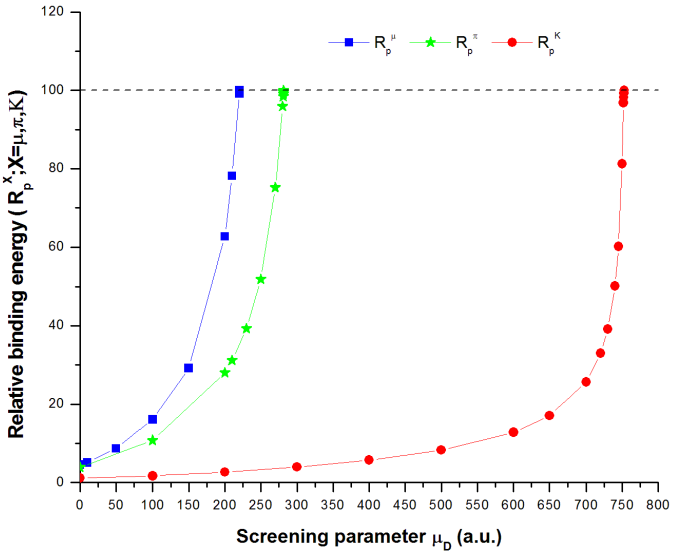

Figure 3.3.4: The variation of relative binding energies (R_p^Y) $[Y : \mu^-, \pi^-, K^-]$ (in %) with respect to the screening parameter μ_D (in a.u.).

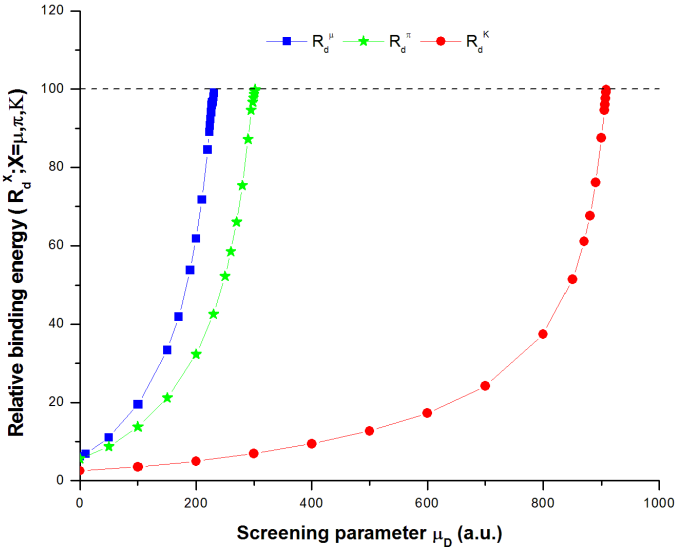

Figure 3.3.5: The variation of relative binding energies (R_d^Y) $[Y : \mu^-, \pi^-, K^-]$ (in %) with respect to the screening parameter μ_D (in a.u.).

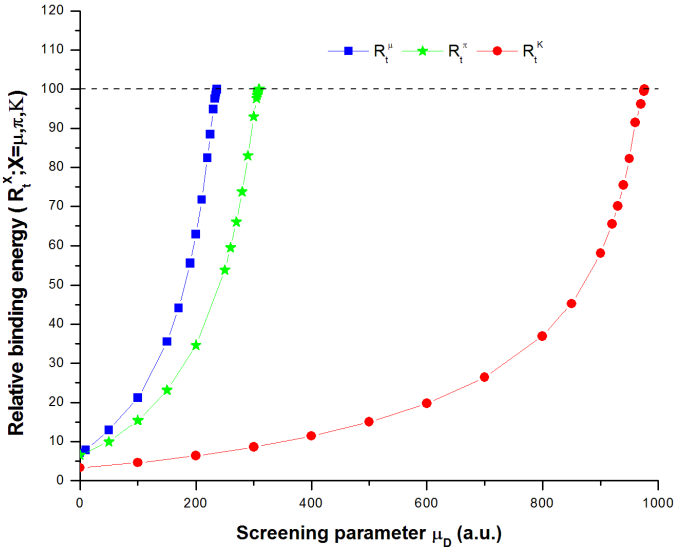

Figure 3.3.6: The variation of relative binding energies (R_t^Y) $[Y : \mu^-, \pi^-, K^-]$ (in %) with respect to the screening parameter μ_D (in a.u.).

figures (3.3.4) to (3.3.6). It is clear from the figures that R_X^Y increases slowly upto a certain value of μ_D and after that R_X^Y increases rapidly upto 100% until the XYY systems become unbound.

The energy eigenvalues of exotic $Ps^-(e^+e^-e^-)$ ion and non–exotic $H_2^+(p^+p^+e^-)$, $D_2^+(d^+d^+e^-)$ and $T_2^+(t^+t^+e^-)$ ions are given in table (3.3.5) for different values of μ_D.

Table 3.3.5: Ground state energy eigenvalues $-E$ (a.u.) of three–body $Ps^-(e^+e^-e^-)$, $H_2^+(p^+p^+e^-)$, $D_2^+(d^+d^+e^-)$ and $T_2^+(t^+t^+e^-)$ ions for different screening parameters μ_D (a.u.).

	$-E$			
μ_D	$Ps^-(e^+e^-e^-)$	$H_2^+(p^+p^+e^-)$	$D_2^+(d^+d^+e^-)$	$T_2^+(t^+t^+e^-)$
0.1	0.173618	0.503099	0.504402	0.504889
	0.1736181600[a]	0.503330[b]		
0.2	0.106409			
	0.1064096775[a]			
0.3	0.057553			
0.4	0.024698			
0.5	0.005965	0.226676	0.227817	0.228241
	0.0059656643[a]			
0.55	0.001421			
0.56	0.000871			
0.57	0.000481			
0.58	0.000191			
0.59	0.000029			
0.594	0.000001			
0.595	-0.000002			
0.7		0.135199	0.136214	0.136579
		0.135561[b]		
1.0		0.044832	0.045025	0.045288
1.2		0.011923	0.012187	0.012308
		0.012287[b]		
1.25		0.006808		
		0.007201[b]		
1.29		0.003672		
		0.003989[b]		
1.3			0.003222	0.003296
1.33		0.001339		
1.34		0.000882		
		0.001190[b]		
1.35		0.000476	0.000609	0.000657
		0.000750[b]		
1.36		0.000118	0.000236	0.000279
		0.000400[b]		
1.363		0.000019		

Continuation of Table (3.3.5)

	$-E$			
μ_D	$Ps^-(e^+e^-e^-)$	$H_2^+(p^+p^+e^-)$	$D_2^+(d^+d^+e^-)$	$T_2^+(t^+t^+e^-)$
1.364		-0.000019		
1.367			0.000004	
1.368			-0.000027	0.000011
1.369				-0.000020

[a] [188], [b] [171]

We now proceed to calculate borromean window (BW) of the relevant three–body systems. Table (3.3.6) displays the critical screening parameters (μ_D^c) of the three–body systems along with their two–body sub–systems. The μ_D^c values of the two–body sub-systems (XY) are estimated following the work of Gomes *et.al.* [217]. It is evident from table (3.3.6) that μ_D^c for the two–body sub-systems (XY) lie between the μ_D^c of XXY and XYY systems [$X : p^+, d^+, t^+$ and $Y : \mu^-, \pi^-, K^-$] *i.e.* $(\mu_D^c)_{XXY} > (\mu_D^c)_{XY} > (\mu_D^c)_{XYY}$. Thus all the XXY systems possess borromean window (BW) whereas XYY systems do not have BW, as shown in the last column of the table (3.3.6). The values of BW for the XXY systems, keeping Y fixed, show that, as the mass of X increases the BW also increases *e.g* $(BW)_{tt\mu} > (BW)_{dd\mu} > (BW)_{pp\mu}$.

Table 3.3.6: Critical screening parameters (μ_D^c) and borromean windows (BW) of the three–body XXY and XYY systems [X=p^+, d^+, t^+, e^+ , Y=μ^-, π^-, K^-, e^-]. μ_D^c of the two–body systems (XY) are taken from [217].

Two–body sub–system	μ_D^c	Three–body system	μ_D^c	BW
$p^+\mu^-$	221.26	$p^+p^+\mu^-$	227.65	6.39
			227.66[a]	
		$p^+\mu^-\mu^-$	220.36	0
$p^+\pi^-$	283.07	$p^+p^+\pi^-$	289.02	5.95
		$p^+\pi^-\pi^-$	281.6	0
p^+K^-	753.69	$p^+p^+K^-$	754.45	0.76
		$p^+K^-K^-$	752.66	0
$d^+\mu^-$	233.05	$d^+d^+\mu^-$	245.03	11.98
			245.03[a]	
		$d^+\mu^-\mu^-$	232.08	0
$d^+\pi^-$	302.67	$d^+d^+\pi^-$	315.37	12.70
		$d^+\pi^-\pi^-$	302.45	0
d^+K^-	910.58	$d^+d^+K^-$	918.44	7.86
		$d^+K^-K^-$	908.48	0
$t^+\mu^-$	237.26	$t^+t^+\mu^-$	252.74	15.48
			252.75[a]	
		$t^+\mu^-\mu^-$	236.29	0
$t^+\pi^-$	309.80	$t^+t^+\pi^-$	327.04	17.24

Continuation of Table (3.3.6)

Two–body sub–system	μ_D^c	Three–body system	μ_D^c	BW
		$t^+\pi^-\pi^-$	309.58	0
t^+K^-	978.31	$t^+t^+K^-$	994.68	16.37
		$t^+K^-K^-$	975.97	0
$p^+e^-(H)$	1.1899	$p^+p^+e^-(\mathrm{H}_2^+)$	1.363	0.1731
			1.365[b]	
			1.3734[c]	
d^+e^-	1.1903	$d^+d^+e^-(\mathrm{D}_2^+)$	1.367	0.1767
t^+e^-	1.1904	$t^+t^+e^-(\mathrm{T}_2^+)$	1.368	0.1776
$e^+e^-(Ps)$	0.5953	$e^+e^-e^-(\mathrm{Ps}^-)$	0.594	0

[a] [178], [b] [171] and [c] [218]

To compare the BWs of XXY systems we introduce a dimensionless quantity called *relative borromean window* (RBW), which is defined as $\mathrm{RBW} = \dfrac{(\mu_D^c)_{XXY} - (\mu_D^c)_{XY}}{(\mu_D^c)_{XXY}} \times 100\%$. The estimated RBWs for different mass relation parameters (q_m) are given in table (3.3.7) and the variation of RBW with respect to q_m is shown in figure (3.3.7).

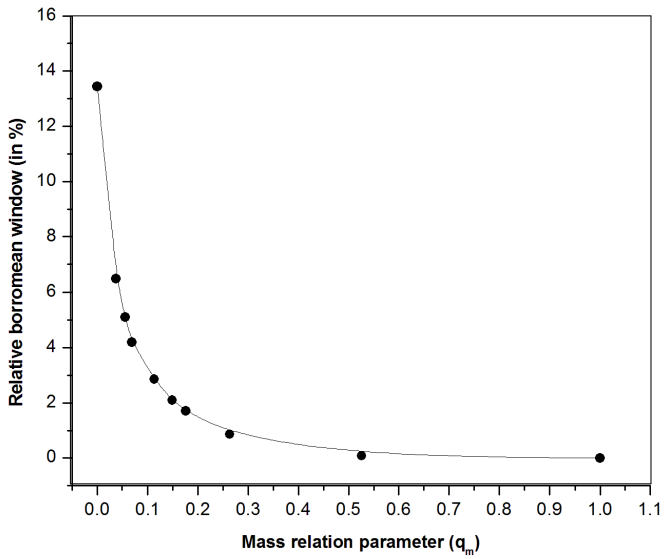

Figure 3.3.7: The variation of relative borromean window (RBW) with respect to the mass relation parameters (q_m).

Table 3.3.7: Relative borromean window (RBW) and the mass relation parameter (q_m) of the three-body exotic XXY and XYY systems [X=p^+, d^+, t^+, e^+ , Y=μ^-, π^-, K^-, e^-].

Three-body system	q_m	RBW	Three-body system	q_m	RBW
$t^+\mu^-\mu^-$	26.58497	0	$d^+d^+K^-$	0.26321	0.86
$t^+\pi^-\pi^-$	20.12551	0	$t^+t^+K^-$	0.17575	1.71
$d^+\mu^-\mu^-$	17.75169	0	$p^+p^+\pi^-$	0.14875	2.09
$d^+\pi^-\pi^-$	13.43849	0	$p^+p^+\mu^-$	0.11261	2.86
$p^+\mu^-\mu^-$	8.88025	0	$d^+d^+\pi^-$	0.06879	4.19
$p^+\pi^-\pi^-$	6.72258	0	$d^+d^+\mu^-$	0.05633	5.10
$t^+K^-K^-$	5.68979	0	$t^+t^+\pi^-$	0.04968	6.19
$d^+K^-K^-$	3.79927	0	$t^+t^+\mu^-$	0.03762	6.50
$p^+K^-K^-$	1.90062	0	$p^+p^+e^-(H_2^+)$	0.00054	12.70
$e^+e^-e^-(Ps^-)$	1.00000	0	$d^+d^+e^-(D_2^+)$	0.00027	12.95
$p^+p^+K^-$	0.52615	0.08	$t^+t^+e^-(T_2^+)$	0.00018	13.01

Both the table (3.3.7) and figure (3.3.7) show that, RBW = 0 for $q_m \geq 1$ and RBW increases rapidly as q_m tends to zero. For example, from table (3.3.7) one can find that RBW = 0.08% at $q_m = 0.52615$ (for $p^+p^+K^-$ system), which is small as compared to the highest estimated RBW = 13.01% (for T_2^+ system) at $q_m = 0.00018$. Hence, we have chosen systems in the range $0 < q_m < 0.5$, to get a smooth variation of RBW with respect to q_m. It is well established that negative ions are less stable than the positive ions *e.g.* H^-, He^- etc. ions are less stable than H^+, He^+ etc. We have also found that the binding energies of XYY systems ($q_m \geq 1$) are less than that of the XXY systems ($q_m < 1$) for free case. As we put those exotic systems in classical WCP and increase the screening parameter μ_D, XYY systems destabilize more rapidly than XXY systems and its two–body sub–systems (XY). This is the reason behind the non–possessing of the borromean bindings of the XYY ions.

3.3.2 Resonance state

We now extend our study to estimate the resonance parameters (resonance energy and width) of three-body exotic p^+p^+Y and p^+YY [$Y : \mu^-, \pi^-, K^-$] ions in the free environment *i.e.* all interaction potentials among the particles are purely Coulombic as given in equation (3.2.52). The energy eigenvalues of $^1S^e$ states of p^+p^+Y and p^+YY ions are calculated using nine–exponent (*i.e.* $p = 9$) Hylleraas type basis set containing $N = 675$ terms. For 200 different geometrical progression ratios (γ) in the basis set expansion, the Hamiltonian matrix has been repeatedly diagonalized to obtain energies corresponding to different eigenroots. The plot of each energy eigenroot versus γ produces the stabilization diagram from which we estimate the resonance parameters of p^+p^+Y and p^+YY ions.

A portion of the stabilization diagram for $^1S^e$ states of exotic $p^+p^+\mu^-$ ion is given in figure (3.3.8). In this diagram, we have plotted first 40 eigenroots of $^1S^e$ symmetry for 200 differ-

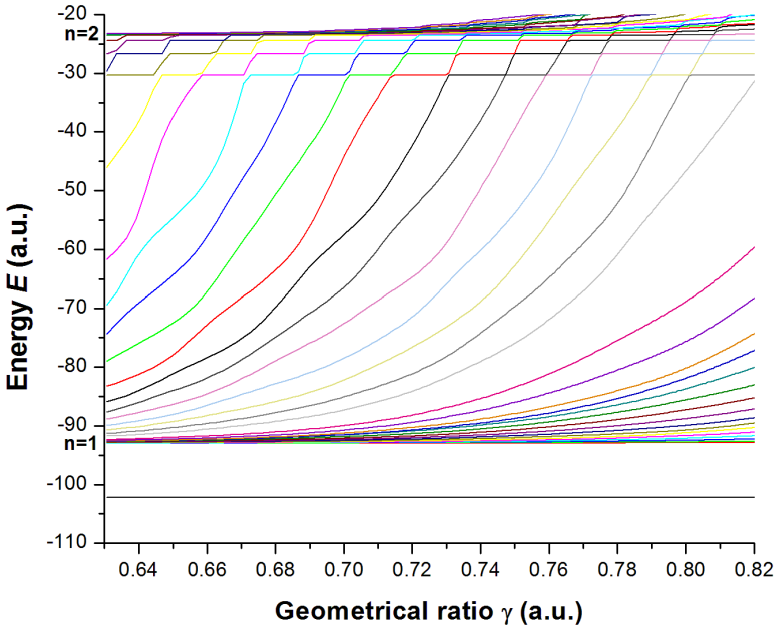

Figure 3.3.8: Stabilization diagram for the resonance $^1S^e$ states of exotic $p^+p^+\mu^-$ ion in free environment.

ent values of γ ranging from 0.63058 a.u. to 0.82353 a.u. From figure (3.3.8), one can see that there exist two classes of states:

i. Only one energy level below the first ionization threshold ($n = 1$) of $p^+\mu^-$ is formed at -92.920408 a.u. due to ground state ($1s^2$) configuration. This level remains invariant with the variation of γ. The energy eigenvalue of this level is $-102.223\ 503$ which is consistent with the value presented in table (3.3.1) for ground state of $p^+p^+\mu^-$ using 990 terms in the nine–exponent Hylleraas type basis set.

ii. Roots lying above $n = 1$ but below $n = 2$ ionization threshold of $p^+\mu^-$ are sensitive with the variation of γ and give rise to flat plateaus in the vicinity of avoided crossings of the energy eigenroots for some particular energy value. Such behaviour is a clear signature of resonance states.

Similar classes of states are also observed for other exotic systems: $p^+\mu^-\mu^-$, $p^+p^+\pi^-$, $p^+\pi^-\pi^-$, $p^+p^+K^-$ and $p^+K^-K^-$. An enlarged view of a portion of the stabilization diagram (figure 3.3.8) of $^1S^e$ state of exotic $p^+p^+\mu^-$ ion in the energy range -40.0 a.u. to -23.23 a.u. is given in figure (3.3.9).

From a closer look at figure (3.3.9), we see that, for a short range of γ, each

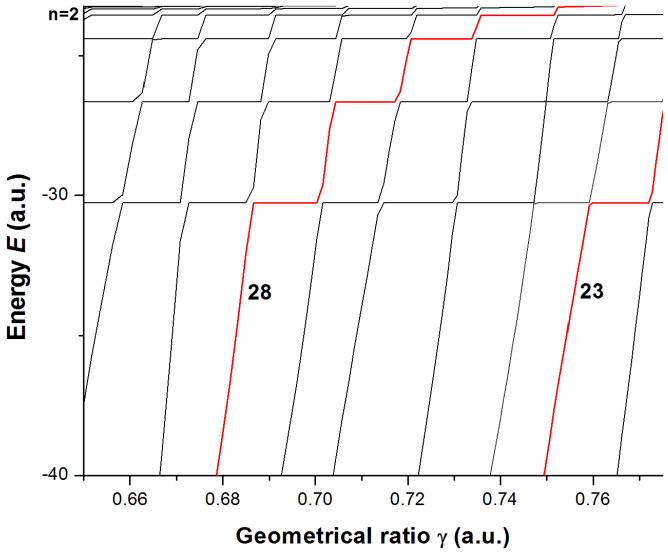

Figure 3.3.9: Enlarged view of the stabilization diagram for the resonance $^1S^e$ states of exotic $p^+p^+\mu^-$ ion below $n = 2$ ionization threshold of $p^+\mu^-$.

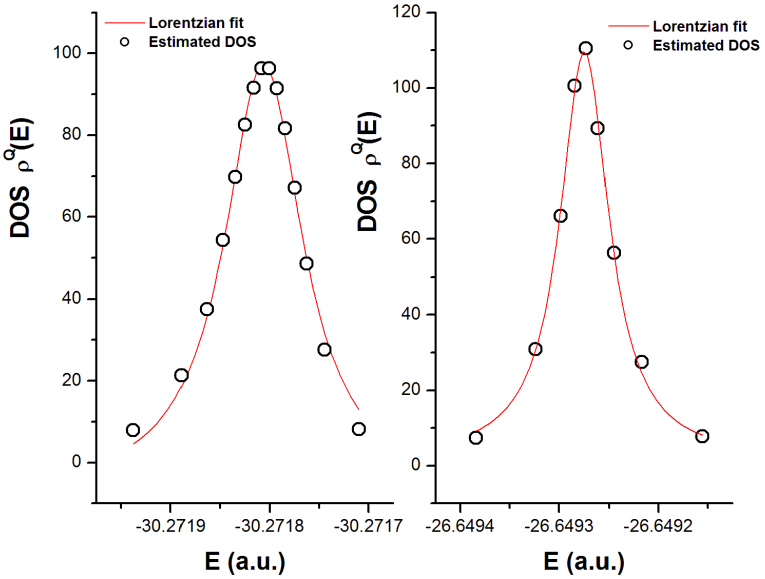

Figure 3.3.10: Calculated density (hollow black circles) and the fitted Lorentzian (solid line in red) for the resonance $^1S^e$ states of exotic $p^+p^+\mu^-$ ion having (a) Resonance energy $-E_r = 30.27180$(a.u.) and width $\Gamma = 5.963 \times 10^{-5}$(a.u.) and (b) Resonance energy $-E_r = 26.64933$(a.u.) and width $\Gamma = 1.03 \times 10^{-4}$(a.u.).

eigenroot becomes almost flat in the vicinity of avoided crossings in the neighborhood of a particular resonance state. The density of states $\rho^Q(E)$ is calculated by using equation (3.2.76) and then fitted by the Lorentzian profile given in the equation (3.2.77). Among

different fitting curves for each eigenroot corresponding to a particular resonance state, the fitting curve which gives least χ^2 value and where the square of correlation ($R^2 \leq 1$) leads to the desired resonance energy (E_r) and width (Γ), as described in the methodology section. For example, figure (3.3.10) shows fitted Lorentzians of the first two resonance $^1S^e$ states of $p^+p^+\mu^-$ ion corresponding to energy eigenroot numbers 23 and 28 respectively which give least χ^2 value and square of correlation $R^2 < 1$ in the fitting process. Table (3.3.8) shows all the resonance energies (E_r in a.u.) and widths (Γ in a.u.) of $^1S^e$ states of exotic p^+YY and p^+p^+Y ions [$Y = \mu^-, \pi^-, K^-$] below $n = 2$ ionization threshold of p^+Y atom. The results have been compared with those available in literature [219, 220] for p^+YY and p^+p^+Y [$Y = \mu^-, \pi^-$] ions. The comparison shows that resonance energies and widths are in very good agreement with the available results [219, 220]. To the best of our knowledge the present calculated resonance energies and widths of $p^+K^-K^-$ and $p^+p^+K^-$ ions are given for the first time in the literature. Table (3.3.8) shows that the widths of the negative ions (p^+YY) are higher than the corresponding three–body positive counterpart (p^+p^+Y), which indicates that the resonance states of the p^+p^+Y ions are more long lived against auto–ionization than the p^+YY ions.

Table 3.3.8: Resonance energies ($-E_r$ in a.u.) and widths (Γ in a.u.) of $^1S^e$ states of exotic p^+YY and p^+p^+Y [$Y = \mu^-, \pi^-, K^-$] ions below $n = 2$ ionization threshold of p^+Y atom of energy $E_{pY} = -\frac{m_p m_Y}{8(m_p+m_Y)}$ a.u., m_p and m_Y being the masses of p^+ and Y respectively. The notation $A[\pm B]$ stands for $A \times 10^{\pm B}$.

		$E_{p\mu} = -23.230\ 102$		$E_{p\pi} = -29.720\ 545$		$E_{pK} = -79.128\ 711$	
States	Parameters	$p^+\mu^-\mu^-$	$p^+p^+\mu^-$	$p^+\pi^-\pi^-$	$p^+p^+\pi^-$	$p^+K^-K^-$	$p^+p^+K^-$
1	$-E_r$	27.651 07	30.271 80 30.271 841 23[a]	35.414 51	38.399 77 38.399 777 312 3[b]	95.067 38	98.051 24
	Γ	27.608[-2]	5.963[-5] 6.353[-5][a]	30.258[-2]	9.220[-5] 5.443[-5][b]	31.004[-2]	8.68[-3]
2	$-E_r$	23.420 34	26.649 33 26.649 428 350[a]	29.965 33	33.400 63 33.400 857 338[b]	80.042 80	82.079 05
	Γ	1.902[-2]	1.030[-4] 1.108[-4][a]	2.788[-2]	3.274[-4] 7.068[-5][b]	3.131[-2]	4.35[-3]
3	$-E_r$		24.403 99 24.404 608 394[a]		30.698 68 30.698 940 424 1[b]	79.179 80	79.472 55
	Γ		2.065[-4] 8.146[-5][a]		2.153[-4] 3.509[-5][b]	8.40[-3]	6.486[-4]

[a] [219], [b] [220]

Chapter 4

Doubly excited states of two–electron atoms

Doubly excited states of two–electron atoms

The topic of doubly excited states (DESs) in two-electron atoms has been attracting significant attention since the early days of quantum chemical research as is still relevant in the present days, from both theoretical and experimental perspectives. Following the groundbreaking discovery of the two-electron one-photon peak by Madden and Codling [42, 43] while measuring the photo-absorption spectra of helium atom placed in the field of synchrotron radiation, the DESs of two-electron atoms are always in the focus of researcher in the field of atomic structure calculation. Precise knowledge of the structural characteristics of DESs of different two-electron atoms is essential for analyzing astrophysical data, diagnosing lines seen in the solar corona, detecting high temperature discharges and performing laboratory plasma diagnostics [49,51,221,222]. In this chapter, we give a detailed account of the works on DESs for the two-electron systems embedded in classical plasma environment. We investigate the structural properties of high lying doubly excited F^e states of 'free' two-electron systems by solving the Scrödinger equation using Ritz variation principle. This methodology is further extended to estimate the structural properties of the atoms placed within classical weakly coupled plasma (WCP) where the potential is modeled by exponential screened Coulomb potential (ESCP) (1.0.1). Under such plasma environment we have also estimated the transition energies of different dipole allowed transitions between various DESs.

4.1 Literature review

The complexity of the estimations of the structural properties of two-electron systems under WCP environment increases a notch higher than that of one-electron systems because of the presence of the non-central Coulombic repulsion potential modified by ESCP. The investigation of the effect of WCP on the ground state energy level ($1s^2;^1\,S^e$) of He-like systems was first introduced by Rogers [223] using radially correlated basis. Lam and Varshni [224] reported decrease of the ionization energy (known as *ionization potential depression* or *IPD*) of ground state of He atom with respect to the increase in plasma screening strength μ_D (equation (1.0.2)). They [224] also found the value of critical screening at which the ground state energy crosses the first ionization threshold *i.e.* the energy of $He^+(1s)$. A large number of spectral data (energy, stability or critical parameter, transition probabilities, oscillator strengths, static and dynamic multipolar polarizabilities etc.) for ground and singly excited states of two-electron atoms under weakly coupled plasma have been generated by different workers over the past decades [225–237]. These studies show that, like the one-electron systems, the increase in μ_D lessens the number of bound states and pushes the two-electron energy levels towards the continuum. From the radiative transition point of view, Ray and Mukherjee [227] showed that for He-like carbon the transition energy for principal quantum

number conserving transitions ($\Delta n = 0$) increases with the increase of μ_D whereas for principal quantum number non-conserving transitions ($\Delta n \neq 0$) transition energy decreases as μ_D decreases.

From the beginning of this century, many researchers have estimated the energy eigenvalues, transition energies, multi-pole polarizabilities etc. structural properties of doubly excited metastable bound P^e, D^o, F^e and G^o states of two-electron systems (He, Li^+, Be^{2+}, H^-) under WCP environment [238–244]. In these works several quantum-chemical approximation techniques like Ritz variation technique, B-spline method using Hylleraas-CI functions etc. are employed. Similar to the ground and singly excited states, the energy eigenvalues of metastable bound DESs increase with the increase of μ_D resulting in reduction of the number of metastable-bound states under second ionization threshold. Level crossing phenomena of some certain DESs have been observed for the transition $P^e \rightarrow D^o$ as μ_D increases [242]. Saha *et al.* [242] reported a mixture of both red and blue shift of the spectral lines for the transitions between various DESs. In a recent article Zhou *et al.* [244] described the variation of some geometric quantities of He-atom such as $\langle r \rangle$, $\langle r_{12} \rangle$, $\langle r_< \rangle$, $\langle r_> \rangle$, $\langle \cos\theta_{12} \rangle$ and $\langle \theta_{12} \rangle$ for the $^{1,3}P^e$ and $^{1,3}D^o$ states, with respect to μ_D.

Resonance parameters (energy and width) of doubly excited $^1S^e$ state was first calculated analytically by Wang and Winkler [245] for H^- ion under plasma environment. They modeled the plasma medium by Debye-Laughton potential which reduces to ESCP or Debye plasma potential by adjusting the parameters of that potential. Subsequently, Ho and co-workers published a series of papers [204, 214, 238, 239, 246–256] where they estimated the variation of resonance parameters of different doubly excited $^{1,3}S^e$, $^{1,3}P^o$, $^1D^e$, $^{1,3}P^e$, $^{1,3}D^o$, $^{1,3}F^e$ and $^{1,3}G^o$ states of two-electron systems like H^-, H^-, He, Li^+, C^{4+}, O^{6+} and Ne^{8+} using stabilization and complex co-ordinate rotation (CCR) techniques, under the WCP environment modeled by ESCP. They have shown that, as μ_D increases, resonance energy increases while resonance widths may increase or decrease depending upon the configurations of DESs. Other workers have also estimated the variation of resonance parameters of two-electron systems under Debye plasma environment where they have used different quantum-chemical techniques like time-dependent harmonic perturbation [257], stabilization method using explicitly correlated wave functions [258, 259], close-coupling approximation [260–262] etc. Besides the variations in the resonance parameters with respect to μ_D, transformation of Feshbach resonances to shape resonance was also observed [252, 262] for screening parameter μ_D greater than the critical value (μ_{DC}) of screening parameter at which the resonance energies crosses the one-electron threshold.

There are some relativistic calculations available in literature on DES of two-electron systems embedded in WCP [263–266]. Das *et al.* [263] used relativistic Fock-space multireference coupled-cluster theory to compute the transition energies and oscillator strengths of the dipole-allowed ($E1$) $^1S_0 \rightarrow ^1P_0$ transition of C^{4+}, Al^{11+} and Ar^{16+} ions at different plasma

screening μ_D. Xie *et. al.* [264] also studied the influence of the plasma on the magnetic-dipole ($M1$) and magnetic-quadrupole ($M2$) transition probabilities and oscillator strengths of the transitions between various configurations of C^{4+} using the multi-configuration Dirac-Hartree-Fock method. Chen *et. al.* [265] compares the relativistic Flexible Atomic Code (FAC) computations and multiconfiguration Dirac-Fock (MCDF) method in predicting the variation of the transition energies for the $1s^2(^1S) \rightarrow 1snp(^1P)[n = 2, 3]$ $E1$ transitions with respect to μ_D for C^{4+}, Ne^{8+}, Ar^{16+} and Kr^{34+} ions. Using MCDF method Ma *et. al.* [266] found that in the dielectronic recombination (DR) process, the total radiative rates and Auger rates of the intermediate two-electronic states decrease monotonically with increasing the plasma screening μ_D with an exception of Auger rate first increases and then decreases for the $2p^2(^1S^e)$ state with the increase of μ_D. In their work [266], both the blueshift and redshift phenomena are observed for the resonance energies with increasing μ_D.

Mukherjee and group investigated [267–270] the structural modification of two-electron systems under SCP described by ion-sphere potential (1.0.3) using different quantum-chemical approximation techniques like time-dependent perturbation theory, time dependent Hatree-Fock (HF) theory and Rayleigh-Ritz variation principle with Hylleraas-type correlated wavefunction. The IPD, pressure ionization, level-crossing phenomena etc. with respect to the IS-radius are the main findings of those studies. Belkhiri *et al.* [271] computed shifts of binding energies of different charge states of Al (Al^{11+} to Al^{7+}) and transition line shifts of Be-like iron (Fe^{22+}) and titenium atom by using different atomic packages like Los Almos Cowan Atomic Structure (CATS) code in HF or Hatree-Fock-Slater form, FAC and MARIA codes within ion-sphere potential. A series of theoretical works have been performed [272–276] in the relativistic framework using MCDF method, GRASP2K code including correlations via configuration-interaction, FAC etc. The SCP effect was considered through self-consistent ion-sphere potential or average atom ion-sphere potential to incorporate the effects of both temperature and density of the plasma medium. In those works the shift of He_β transition line of Cl^{15+} ion (in the X-ray region) was estimated to verify available experimental data. Chen [273] and Singh *et.al.* [275] reported "red-shift" of He_α and He_β lines for the He-like Cl^{15+}, Ar^{16+}, Ti^{20+} and Fe^{24+} ions with respect to the increase in plasma density. In a very recent article Chandra *et.al.* [277] reported the energies and probabilities of $2p^2(^3P_{0,1,2}) \rightarrow 1s2p(^1P_{0,1,2})$ satellite transition lines for the C^{4+}, Ne^{8+}, Al^{11+} and Ar^{16+} ions within the IS-model where the energy eigenvalues are computed by both non-relativistic variation technique using correlated Hylleraas-type basis and relativistic MCDF method using modified GRASP2K code. While the above studies are focused on the radiative transitions, Belkhiri *et.al.* [278] estimated the variation of auto-ionization rates as a function of plasma density under the ion-sphere model potential for the non-radiative transitions between different charge states of Al *i.e.* for the transitions $Al^{11+} \rightarrow Al^{12+}$, $Al^{10+} \rightarrow Al^{11+}$, $Al^{9+} \rightarrow Al^{10+}$ and $Al^{8+} \rightarrow Al^{9+}$, using FAC and GIPPER codes.

A large number of investigations [204, 241–245, 247, 249, 250, 253, 256, 258] have been carried out for the determination of various structural properties of DES of He-like systems in plasma environments for S, P and D states. The same applies to higher angular momentum F^e states are quite limited [239,240]. In these works the authors used CI–type basis functions to calculate energies of metastable bound $^{1,3}F^e$ states [239, 240] and the energy and width of $^{1,3}F^e$ resonance states below $n = 3$ ionization threshold [239] of He-atom placed within classical WCP environment modeled by ESCP. The authors simplified their calculations by approximating the screened electron-electron repulsion potential term by Taylor series expansion [239, 240]. In this chapter, we have extensively studied the structural properties of $^{1,3}F^e$ states of He-atom under pure Coulomb potential (free atom) and ESCP (plasma embedded atom) using trial wavefunction expanded in multi-exponent Hylleraas-type basis set. Energies of the metastable bound $^{1,3}F^e$ states are calculated using Ritz variation principle for different screening conditions of the potential. "Soft wall" strategy [206, 213, 279] of the stabilization method [212] is used to determine the resonance parameters of $^{1,3}F^e$ states of He-atom for various screening parameters of ESCP. We have calculated the matrix elements for both the attractive and repulsive parts of ESCP analytically by retaining the exact form of the potential terms.

4.2 The present method

In this section we will construct the wavefunction for the unnatural even parity F^e state of two-electron systems, followed by the general variational equation and the necessary basis integrals to estimate the structural properties of the two-electron systems.

4.2.1 Wavefunction

The DES $^{1,3}F^e$ of two electron systems can arise from the configurations such as $npn'f[n \geq 2$ and $n' \geq 4]$, $ndn'd[n \geq 3$ and $n' \geq 4$ for $^1F^e; n, n' \geq 3$ for $^3F^e]$, $ndn'g[n \geq 3$ and $n' \geq 5]$ etc. (indicated in table-1.0.1). We are going to construct the trial wavefunction by taking two basic pf and dd configurations explicitly and all other higher configurations will be incorporated through different powers of r_{12} in the trial wavefunction. The general form of the wavefunction of $^{1,3}F^e$ state of two-electron systems, is given by

$$\Psi = \Psi_{pf} + \Psi_{dd} \tag{4.2.1}$$

where, Ψ_{pf} and Ψ_{dd} are the wavefunctions representing the pf and dd configurations, respectively. We introduce the coupled angular function $Y^{l_1,l_2}_{L,M}$ where L = total angular momentum quantum number, M = total magnetic quantum number which is considered to be zero in the present case, l_1 and l_2 = individual angular momentum quantum numbers. Equation

(4.2.1) can then be written as

$$\Psi = \left[f\left(r_1, r_2, r_{12}\right) Y_{3,0}^{3,1} + g\left(r_1, r_2, r_{12}\right) Y_{3,0}^{2,2} \right] \pm \texttt{exchange} \tag{4.2.2}$$

where $f\left(r_1, r_2, r_{12}\right)$ and $g\left(r_1, r_2, r_{12}\right)$ are the radial parts of pf and dd configurations respectively. r_1 and r_2 are the distances of two electrons from the nucleus and r_{12} is the inter-electronic distance. The $\pm$ sign in equation (4.2.2) stands for either singlet or triplet state. The coupled angular function arising out of pf configuration can be written as,

$$Y_{3,0}^{3,1} = \frac{1}{\sqrt{2}} \left[y_3^1(1) y_1^{-1}(2) - y_3^{-1}(1) y_1^1(2) \right] \tag{4.2.3}$$

while the same for dd configuration is

$$Y_{3,0}^{2,2} = \frac{1}{\sqrt{10}} \left[y_2^2(1) y_2^{-2}(2) - y_2^{-2}(1) y_2^2(2) + 2y_2^1(1) y_2^{-1}(2) - 2y_2^{-1}(1) y_2^1(2) \right] \tag{4.2.4}$$

where, $y_l^m(i)[i = 1, 2]$ represents the spherical harmonics for the uncoupled states. In terms of individual angular coordinates (θ_1, ϕ_1) and (θ_2, ϕ_2) of two electrons, 'y' can be written as [158]

$$\begin{aligned}
y_1^{\pm1}(1) &= \mp\sqrt{\frac{3}{8\pi}} \sin\theta_1 e^{\pm i\phi_1} \\
y_3^{\pm1}(1) &= \mp\sqrt{\frac{21}{64\pi}} \sin\theta_1 \left(5\cos^2\theta_1 - 1\right) e^{\pm i\phi_1} \\
y_2^0(1) &= \sqrt{\frac{5}{16\pi}} \left(3\cos^2\theta_1 - 1\right) \\
y_2^{\pm1}(1) &= \mp\sqrt{\frac{15}{8\pi}} \sin\theta_1 \cos\theta_1 e^{\pm i\phi_1} \\
y_2^{\pm2}(1) &= \sqrt{\frac{15}{32\pi}} \sin^2\theta_1 e^{\pm 2i\phi_1}
\end{aligned} \tag{4.2.5}$$

Similarly, $y_1^{\pm1}(2), y_3^{\pm1}(2), y_2^0(2), y_2^{\pm1}(2)$ and $y_2^{\pm2}(2)$ can be written by replacing (θ_1, ϕ_1) by (θ_2, ϕ_2) in equation (4.2.5). Equations (4.2.3) and (4.2.4) can now be recast as

$$Y_{3,0}^{3,1} = \frac{3\sqrt{7}i}{16\pi} \left(5\cos^2\theta_1 - 1\right) \sin\theta_1 \sin\theta_2 \sin\left(\phi_2 - \phi_1\right) \tag{4.2.6}$$

and

$$Y_{3,0}^{2,2} = \frac{15i}{2\pi\sqrt{10}} \left[\frac{1}{4} \sin\theta_1 \sin\theta_2 \cos(\phi_1 - \phi_2) - \cos\theta_1 \cos\theta_2 \right] \times \sin\theta_1 \sin\theta_2 \sin(\phi_1 - \phi_2) \tag{4.2.7}$$

Let us now consider following relations between the polar angles $(\theta_1, \phi_1, \theta_2, \phi_2)$ and the Eulerian angles (θ, ϕ, ψ) [30]

$$\begin{aligned}
&\sin\theta_1 \sin\theta_2 \sin(\phi_2 - \phi_1) = \sin\theta_{12}\cos\theta \\
&\sin\theta_1 \sin\theta_2 \cos(\phi_2 - \phi_1) + \cos\theta_1 \cos\theta_2 = \cos\theta_{12} \\
&\cos\theta_1 = -\sin\theta\cos\left(\psi - \frac{\theta_{12}}{2}\right), \qquad \cos\theta_2 = -\sin\theta\cos\left(\psi + \frac{\theta_{12}}{2}\right)
\end{aligned} \tag{4.2.8}$$

Using these transformation relations, equations (4.2.6) and (4.2.7) becomes,

$$\begin{aligned}
Y_{3,0}^{3,1} &= N\left[-\sin\theta_{12}\frac{\left(5\cos^3\theta - 3\cos\theta\right)}{2} + \frac{5}{2}\sin\theta_{12}\cos\theta_{12}\sin^2\theta\cos\theta\cos 2\psi\right. \\
&+ \left.\frac{5}{2}\sin^2\theta_{12}\sin^2\theta\cos\theta\sin 2\psi\right] \qquad (4.2.9)
\end{aligned}$$

$$Y_{3,0}^{2,2} = M\left[-\sin\theta_{12}\cos\theta_{12}\frac{\left(5\cos^3\theta - 3\cos\theta\right)}{2} + \frac{5}{2}\sin\theta_{12}\sin^2\theta\cos\theta\cos 2\psi\right] \tag{4.2.10}$$

where, $N = \dfrac{3\sqrt{7}i}{16\pi}$ and $M = \dfrac{15i}{8\pi\sqrt{10}}$ are the normalization constants of $Y_{3,0}^{3,1}$ and $Y_{3,0}^{2,2}$. Using equation (3.2.2) we can get real angular momentum Wigner functions D_3^0, D_3^{2+} and D_3^{2-} as follows

$$\begin{aligned}
D_3^0 &= \frac{5\cos^3\theta - 3\cos\theta}{2} \\
D_3^{2+} &= \frac{\sqrt{15}}{2}\cos 2\psi \sin^2\theta\cos\theta \\
D_3^{2-} &= \frac{\sqrt{15}}{2}\sin 2\psi \sin^2\theta\cos\theta
\end{aligned} \tag{4.2.11}$$

Here we have not written the common factor $\sqrt{\dfrac{7}{8\pi^2}}$ in D_3^0, D_3^{2+} and D_3^{2-}. Using equation (4.2.11), the equations (4.2.9) and (4.2.10) can be modified as

$$Y_{3,0}^{3,1} = N\left[-\sin\theta_{12}D_3^0 + \frac{\sqrt{15}}{6}\sin 2\theta_{12}D_3^{2+} + \frac{\sqrt{15}}{6}\left(1 - \cos 2\theta_{12}\right)D_3^{2-}\right] \tag{4.2.12}$$

$$Y_{3,0}^{2,2} = M\left[-\sin\theta_{12}\cos\theta_{12}D_3^0 + \frac{\sqrt{5}}{3}\sin\theta_{12}D_3^{2+}\right] \tag{4.2.13}$$

On substitution of $Y_{3,0}^{3,1}$ and $Y_{3,0}^{2,2}$ into the equation (4.2.2) we get

$$\Psi = Nf\left[-\sin\theta_{12}D_3^0 + \frac{\sqrt{15}}{6}\sin 2\theta_{12}D_3^{2+} + \frac{\sqrt{15}}{6}\left(1 - \cos 2\theta_{12}\right)D_3^{2-}\right]$$

$$+ \quad Mg\left[-\sin\theta_{12}\cos\theta_{12}D_3^0+\sqrt{\frac{5}{3}}\sin\theta_{12}D_3^{2+}\right]\pm \texttt{exchange} \tag{4.2.14}$$

To find the exchange term we will consider the following operations [30] of exchange operator ϵ_{12} on $f(r_1,r_2,r_{12})$, $g(r_1,r_2,r_{12})$ and $D_L^{k\pm}(\theta,\phi,\psi)$ as

$$\begin{aligned}
\epsilon_{12}f(r_1,r_2,r_{12}) &= \tilde{f}(r_2,r_1,r_{12})\\
\epsilon_{12}g(r_1,r_2,r_{12}) &= \tilde{g}(r_2,r_1,r_{12})\\
\epsilon_{12}D_L^{k\pm}(\theta,\phi,\psi) &= \pm(-1)^{L+k}D_L^{k\pm}(\theta,\phi,\psi)
\end{aligned}$$

Now the equation (4.2.14) becomes,

$$\begin{aligned}
\Psi &= Nf\left[-\sin\theta_{12}D_3^0+\frac{\sqrt{15}}{6}\sin 2\theta_{12}D_3^{2+}+\frac{\sqrt{15}}{6}(1-\cos 2\theta_{12})D_3^{2-}\right]\\
&+ Mg\left[-\sin\theta_{12}\cos\theta_{12}D_3^0+\sqrt{\frac{5}{3}}\sin\theta_{12}D_3^{2+}\right]\\
&\pm N\tilde{f}\left[-\sin\theta_{12}(-1)^3D_3^0+\frac{\sqrt{15}}{6}\sin 2\theta_{12}(-1)^5D_3^{2+}+\frac{\sqrt{15}}{6}(1-\cos 2\theta_{12})(-1)^5D_3^{2-}\right]\\
&\pm M\tilde{g}\left[-\sin\theta_{12}\cos\theta_{12}(-1)^3D_3^0+\sqrt{\frac{5}{3}}\sin\theta_{12}(-1)^5D_3^{2+}\right]\\
&= N\left[-\sin\theta_{12}\left(f\mp\tilde{f}\right)D_3^0+\frac{\sqrt{15}}{6}\sin 2\theta_{12}\left(f\mp\tilde{f}\right)D_3^{2+}+\frac{\sqrt{15}}{6}(1-\cos 2\theta_{12})\left(f\mp\tilde{f}\right)D_3^{2-}\right]\\
&+ M\left[-\sin\theta_{12}\cos\theta_{12}(g\mp\tilde{g})D_3^0+\sqrt{\frac{5}{3}}\sin\theta_{12}(g\mp\tilde{g})D_3^{2+}\right]
\end{aligned} \tag{4.2.15}$$

Following the general form of the wavefunction (3.2.1) prescribed by Bhatia and Temkin [30], we can write Ψ for ${}^{1,3}\mathrm{F}^e$ state ($L=3$ and $k=0,\pm 2$) into the following form

$$\Psi = f_3^0D_3^0+f_3^{2+}D_3^{2+}+f_3^{2-}D_3^{2-} \tag{4.2.16}$$

where

$$\begin{aligned}
f_3^0 &= -\left(f\mp\tilde{f}\right)\sin\theta_{12}-\sqrt{\frac{10}{7}}(g\mp\tilde{g})\sin\theta_{12}\cos\theta_{12}\\
f_3^{2+} &= \frac{\sqrt{15}}{6}\left(f\mp\tilde{f}\right)\sin 2\theta_{12}+\sqrt{\frac{50}{21}}(g\mp\tilde{g})\sin\theta_{12}\\
f_3^{2-} &= \frac{\sqrt{15}}{6}\left(f\mp\tilde{f}\right)(1-\cos 2\theta_{12})
\end{aligned} \tag{4.2.17}$$

Here we have ignored the common factor N in equation (4.2.15), as it will not make any difference to the variational calculation and used $\frac{M}{N} = \sqrt{\frac{10}{7}}$. Upto this point it is not clear that which of the $\mp$ sign within the parentheses of f_3^0, f_3^{2+} and f_3^{2-} signifies the singlet and triplet states. In this regard Bhatia and Temkin [30] provided a very useful formula where the exchange operator acts on $f_L^{k\pm}$ functions as given below,

$$\begin{aligned} f_L^{k+}(r_2, r_1, r_{12}) = \epsilon_{12} f_L^{k+}(r_1, r_2, r_{12}) &= \pm(-1)^{L+k} f_L^{k+}(r_1, r_2, r_{12}) \\ f_L^{k-}(r_2, r_1, r_{12}) = \epsilon_{12} f_L^{k-}(r_1, r_2, r_{12}) &= \pm(-1)^{L+k+1} f_L^{k-}(r_1, r_2, r_{12}) \end{aligned} \tag{4.2.18}$$

The upper '+' sign and the lower '−' sign signify the singlet and triplet states respectively. Thus the exchange terms of the three radial functions f_3^0, f_3^{2+} and f_3^{2-} of $^{1,3}\mathrm{F}^e$ state now become,

$$\begin{aligned} f_3^0(r_2, r_1, r_{12}) &= \pm(-1)^{3+0} f_3^0(r_1, r_2, r_{12}) = \mp f_3^0(r_1, r_2, r_{12}) \\ f_3^{2+}(r_2, r_1, r_{12}) &= \pm(-1)^{3+2} f_3^{2+}(r_1, r_2, r_{12}) = \mp f_3^{2+}(r_1, r_2, r_{12}) \\ f_3^{2-}(r_2, r_1, r_{12}) &= \pm(-1)^{3+2+1} f_3^{2-}(r_1, r_2, r_{12}) = \pm f_3^{2-}(r_1, r_2, r_{12}) \end{aligned} \tag{4.2.19}$$

Thus, f_3^0 and f_3^{2+} are anti-symmetric for singlet case whereas f_3^{2-} is symmetric for singlet case. This guides us to write the correct forms of f_3^0, f_3^{2+} and f_3^{2-} from equation (4.2.17), which is consistent with the Pauli's exclusion principle. The equation (4.2.17) is now modified as,

$$\begin{aligned} f_3^0 &= -F_1 \sin\theta_{12} - \sqrt{\frac{10}{7}} G_1 \sin\theta_{12}\cos\theta_{12} \\ f_3^{2+} &= \frac{\sqrt{15}}{6} F_1 \sin 2\theta_{12} + \sqrt{\frac{50}{21}} G_1 \sin\theta_{12} \\ f_3^{2-} &= \frac{\sqrt{15}}{6} F_2 (1 - \cos 2\theta_{12}) \end{aligned} \tag{4.2.20}$$

where, $F_1 = (f \mp \tilde{f})$, $F_2 = (f \pm \tilde{f})$ and $G_1 = (g \mp \tilde{g})$. The upper sign corresponds to the singlet state and the lower sign to the triplet state.

4.2.2 Variational equation

In this subsection we will construct the variational equation of $^{1,3}\mathrm{F}^e$ states of two-electron systems by following the steps as described in section (3.2.2). In the present case, the three particles are two electrons ($m_1 = m_2 = 1$ a.u.) and the nucleus which is infinitely heavy with respect to the electrons. Here the nucleus will be static and the mass polarization term will not appear. Thus, in equations (3.2.35), (3.2.36) and (3.2.37) we put $A = B = \frac{1}{2}$

and $C = 0$ to write the general variational equation (3.2.41) of two-electron systems as:

$$\begin{aligned}
\Delta \int \Bigg[& \left(\frac{\partial\Psi}{\partial r_1}\right)^2 + \left(\frac{\partial\Psi}{\partial r_2}\right)^2 + \left(\frac{1}{r_1^2}+\frac{1}{r_2^2}\right)\left(\frac{\partial\Psi}{\partial\theta_{12}}\right)^2 \\
+ & \left\{\frac{1}{r_1^2\sin^2\theta_{12}}\sin^2\left(\psi+\frac{\theta_{12}}{2}\right) + \frac{1}{r_2^2\sin^2\theta_{12}}\sin^2\left(\psi-\frac{\theta_{12}}{2}\right)\right\}\left(\frac{\partial\Psi}{\partial\theta}\right)^2 \\
+ & \left\{\frac{1}{r_1^2\sin^2\theta_{12}}\cot^2\theta\cos^2\left(\psi+\frac{\theta_{12}}{2}\right) + \frac{1}{r_2^2\sin^2\theta_{12}}\cot^2\theta\cos^2\left(\psi-\frac{\theta_{12}}{2}\right)\right\}\left(\frac{\partial\Psi}{\partial\psi}\right)^2 \\
+ & \frac{1}{4}\left(\frac{1}{r_1^2}+\frac{1}{r_2^2}\right)\left(\frac{\partial\Psi}{\partial\psi}\right)^2 + \left(\frac{1}{r_2^2}-\frac{1}{r_1^2}\right)\frac{\partial\Psi}{\partial\theta_{12}}\frac{\partial\Psi}{\partial\psi} \\
+ & \left\{\frac{1}{r_1^2\sin^2\theta_{12}}\cot\theta\sin\left(2\psi+\theta_{12}\right) + \frac{1}{r_2^2\sin^2\theta_{12}}\cot\theta\sin\left(2\psi-\theta_{12}\right)\right\}\frac{\partial\Psi}{\partial\theta}\frac{\partial\Psi}{\partial\psi} \\
+ & 2\left(V_{eff}-E\right)|\Psi|^2\Bigg] d\tau_{\vec{r_1},\vec{r_2}} = 0
\end{aligned} \tag{4.2.21}$$

We now put Ψ of equation (4.2.16) with $D-$functions given by the equation (4.2.11) and perform integrations over the Eulerian angles (θ, ϕ, ψ). This modifies the variational equation (4.2.21) to take the following form:

$$\begin{aligned}
\Delta \int \Bigg\{ & \frac{1}{2}\left[\sum_{i=1}^{2}\left(\frac{\partial f_3^0}{\partial r_i}\right)^2 + \left(\frac{\partial f_3^{2+}}{\partial r_i}\right)^2 + \left(\frac{\partial f_3^{2-}}{\partial r_i}\right)^2\right] \\
+ & \frac{1}{2}\left(\frac{1}{r_1^2}+\frac{1}{r_2^2}\right)\left[\left(\frac{\partial f_3^0}{\partial\theta_{12}}\right)^2 + \left(\frac{\partial f_3^{2+}}{\partial\theta_{12}}\right)^2 + \left(\frac{\partial f_3^{2-}}{\partial\theta_{12}}\right)^2\right] \\
+ & \frac{1}{2}\left(\frac{1}{r_1^2}+\frac{1}{r_2^2}\right)\left[\left(f_3^{2+}\right)^2 + \left(f_3^{2-}\right)^2\right] + \left(\frac{1}{r_2^2}-\frac{1}{r_1^2}\right)\left[f_3^{2-}\frac{\partial f_3^{2+}}{\partial\theta_{12}} - f_3^{2+}\frac{\partial f_3^{2-}}{\partial\theta_{12}}\right] \\
+ & \frac{1}{\sin^2\theta_{12}}\left(\frac{1}{r_1^2}+\frac{1}{r_2^2}\right)\left[3\left(f_3^0\right)^2 + 2\left(f_3^{2+}\right)^2 + 2\left(f_3^{2-}\right)^2\right] + \frac{\sqrt{15}\cos\theta_{12}}{\sin^2\theta_{12}}\left(\frac{1}{r_1^2}+\frac{1}{r_2^2}\right) f_3^0 f_3^{2+} \\
+ & \frac{\sqrt{15}}{\sin\theta_{12}}\left(\frac{1}{r_2^2}-\frac{1}{r_1^2}\right) f_3^0 f_3^{2-} + 2\left(V_{eff}-E\right)\left[\left(f_3^0\right)^2 + \left(f_3^{2+}\right)^2 + \left(f_3^{2-}\right)^2\right]\Bigg\} d\tau = 0
\end{aligned} \tag{4.2.22}$$

where $d\tau = r_1^2\ r_2^2\ \sin\theta_{12}\ dr_1\ dr_2\ d\theta_{12}$. Using the explicit forms of f_3^0, f_3^{2+} and f_3^{2-} from equation (4.2.20), the variational equation (4.2.22) becomes

$$\begin{aligned}
\Delta \int \Bigg\{ & \sin^2\theta_{12}\left(1+\frac{5}{3}\cos^2\theta_{12}\right)\left|\nabla_s F_1\right|^2 + \frac{5}{3}\sin^4\theta_{12}\left|\nabla_s F_2\right|^2 \\
+ & 2\left(\frac{1}{r_1^2}+\frac{1}{r_2^2}\right)\sin\theta_{12}\cos\theta_{12}\left[\left(\frac{10}{3}\cos^2\theta_{12}-\frac{2}{3}\right)F_1\frac{\partial F_1}{\partial\theta_{12}} + \frac{10}{3}\sin^2\theta_{12}F_2\frac{\partial F_2}{\partial\theta_{12}}\right] \\
+ & \frac{10}{3}\left(\frac{1}{r_2^2}-\frac{1}{r_1^2}\right)\sin^3\theta_{12}\cos\theta_{12}\left(F_2\frac{\partial F_1}{\partial\theta_{12}} - F_1\frac{\partial F_2}{\partial\theta_{12}}\right) - \frac{40}{3}\left(\frac{1}{r_2^2}-\frac{1}{r_1^2}\right)\sin^2\theta_{12}F_1F_2 \\
+ & 2\left(\frac{1}{r_1^2}+\frac{1}{r_2^2}\right)\left[\left(\frac{5}{2}\cos^4\theta_{12}-\frac{11}{3}\cos^2\theta_{12}+\frac{23}{6}\right)F_1^2 + \left(-\frac{5}{2}\sin^4\theta_{12}+\frac{20}{3}\sin^2\theta_{12}\right)F_2^2\right]
\end{aligned}$$

$$
\begin{aligned}
&+ \frac{10}{7}\sin^2\theta_{12}\left(\frac{5}{3}+\cos^2\theta_{12}\right)\left|\nabla_s G_1\right|^2 + \frac{10}{7}\left(\frac{1}{r_1^2}+\frac{1}{r_2^2}\right)\left[\left(\cos^2 2\theta_{12} - 4\cos^2\theta_{12} + \frac{25}{3}\right)G_1^2\right] \\
&+ \frac{20}{7}\left(\frac{1}{r_1^2}+\frac{1}{r_2^2}\right)\sin\theta_{12}\cos\theta_{12}\left(\cos 2\theta_{12}+\frac{5}{3}\right)G_1\frac{\partial G_1}{\partial\theta_{12}} \\
&+ \frac{16}{3}\sqrt{\frac{10}{7}}\sin^2\theta_{12}\cos\theta_{12}\left(\nabla_s F_1.\nabla_s G_1\right) \\
&+ 2\sqrt{\frac{10}{7}}\left(\frac{1}{r_1^2}+\frac{1}{r_2^2}\right)\sin\theta_{12}\left(\frac{11}{3}\cos^2\theta_{12}-1\right)G_1\frac{\partial F_1}{\partial\theta_{12}} \\
&+ \frac{2}{3}\sqrt{\frac{10}{7}}\left(\frac{1}{r_1^2}+\frac{1}{r_2^2}\right)\sin\theta_{12}\left(13\cos^2\theta_{12}-5\right)F_1\frac{\partial G_1}{\partial\theta_{12}} \\
&+ \frac{10}{3}\sqrt{\frac{10}{7}}\left(\frac{1}{r_2^2}-\frac{1}{r_1^2}\right)\sin^3\theta_{12}\left(F_2\frac{\partial G_1}{\partial\theta_{12}} - G_1\frac{\partial F_2}{\partial\theta_{12}}\right) \\
&+ \frac{8}{3}\sqrt{\frac{10}{7}}\left(\frac{1}{r_1^2}+\frac{1}{r_2^2}\right)\cos\theta_{12}\left(5-\cos^2\theta_{12}\right)F_1G_1 - \frac{40}{3}\sqrt{\frac{10}{7}}\left(\frac{1}{r_2^2}-\frac{1}{r_1^2}\right)\cos\theta_{12}\sin^2\theta_{12}F_2G_1 \\
&+ 2\left(V_{eff}-E\right)\left[\sin^2\theta_{12}\left(1+\frac{5}{3}\cos^2\theta_{12}\right)F_1^2 + \frac{5}{3}\sin^4\theta_{12}F_2^2\right. \\
&+ \left.\left.\frac{10}{7}\sin^2\theta_{12}\left(\frac{5}{3}+\cos^2\theta_{12}\right)G_1^2 + \frac{16}{3}\sqrt{\frac{10}{7}}\sin^2\theta_{12}\cos\theta_{12}F_1G_1\right]\right\}d\tau = 0
\end{aligned}
\tag{4.2.23}
$$

where,

$$
\left|\nabla_s U\right|^2 = \left(\frac{\partial U}{\partial r_1}\right)^2 + \left(\frac{\partial U}{\partial r_2}\right)^2 + \left(\frac{1}{r_1^2}+\frac{1}{r_2^2}\right)\left(\frac{\partial U}{\partial\theta_{12}}\right)^2 \tag{4.2.24}
$$

is called the s-part of the variational equation which can be derived from (3.2.42), (3.2.43) and (3.2.44) with $A = B = \frac{1}{2}, C = 0$ and multiplying each term by a factor '2'. The expression for $\left|\nabla_s U\right|^2$ in terms of (r_1, r_2, r_{12}) can be formulated from the expression of kinetic energy term for $^{1,3}\mathrm{S}^e$ state (3.2.48) with $m_1 = m_2 = 1$, $M \to \infty$ and multiplying each term by a factor '2', which will give the following form,

$$
\begin{aligned}
\left|\nabla_s U\right|^2 &= \left(\frac{\partial U}{\partial r_1}\right)^2 + \left(\frac{\partial U}{\partial r_2}\right)^2 + 2\left(\frac{\partial U}{\partial r_{12}}\right)^2 + 2\cos(r_1, r_{12})\frac{\partial U}{\partial r_1}.\frac{\partial U}{\partial r_{12}} \\
&+ 2\cos(r_2, r_{12})\frac{\partial U}{\partial r_2}.\frac{\partial U}{\partial r_{12}}
\end{aligned}
\tag{4.2.25}
$$

where $\cos(r_1, r_{12}) = \dfrac{r_1^2 + r_{12}^2 - r_2^2}{2\, r_1\, r_{12}}$ and $\cos(r_2, r_{12}) = \dfrac{r_2^2 + r_{12}^2 - r_1^2}{2\, r_2\, r_{12}}$. Thus using (4.2.25) we can write s-parts $\left|\nabla_s F_1\right|^2$ and $\left|\nabla_s F_2\right|^2$ for pf terms and $\left|\nabla_s G_1\right|^2$ for dd terms. In equation (4.2.23) the s-part $\nabla_s F_1.\nabla_s G_1$ for pf-dd mixing terms is defined as,

$$
\nabla_s F_1.\nabla_s G_1 = \frac{\partial F_1}{\partial r_1}\frac{\partial G_1}{\partial r_1} + \frac{\partial F_1}{\partial r_2}\frac{\partial G_1}{\partial r_2} + \left(\frac{1}{r_1^2}+\frac{1}{r_2^2}\right)\frac{\partial F_1}{\partial\theta_{12}}\frac{\partial G_1}{\partial\theta_{12}} \tag{4.2.26}
$$

To find $\nabla_s F_1.\nabla_s G_1$ in (r_1, r_2, r_{12}) let us write,

$$\left|\nabla_s \left(F_1 + G_1\right)\right|^2 = \left|\nabla_s F_1\right|^2 + \left|\nabla_s G_1\right|^2 + 2\nabla_s F_1.\nabla_s G_1 \tag{4.2.27}$$

Using (4.2.24), L.H.S of the above equation (4.2.27) can be expanded as follows:

$$\begin{aligned}
\left|\nabla_s \left(F_1 + G_1\right)\right|^2 &= \left(\frac{\partial F_1}{\partial r_1} + \frac{\partial G_1}{\partial r_1}\right)^2 + \left(\frac{\partial F_1}{\partial r_2} + \frac{\partial G_1}{\partial r_2}\right)^2 + 2\left(\frac{\partial F_1}{\partial r_{12}} + \frac{\partial G_1}{\partial r_{12}}\right)^2 \\
&+ 2\cos(r_1, r_{12})\left(\frac{\partial F_1}{\partial r_1} + \frac{\partial G_1}{\partial r_1}\right).\left(\frac{\partial F_1}{\partial r_{12}} + \frac{\partial G_1}{\partial r_{12}}\right) \\
&+ 2\cos(r_2, r_{12})\left(\frac{\partial F_1}{\partial r_2} + \frac{\partial G_1}{\partial r_2}\right).\left(\frac{\partial F_1}{\partial r_{12}} + \frac{\partial G_1}{\partial r_{12}}\right) \\
&= \left|\nabla_s F_1\right|^2 + \left|\nabla_s G_1\right|^2 + 2\left[\frac{\partial F_1}{\partial r_1}\frac{\partial G_1}{\partial r_1} + \frac{\partial F_1}{\partial r_2}\frac{\partial G_1}{\partial r_2} + 2\frac{\partial F_1}{\partial r_{12}}\frac{\partial G_1}{\partial r_{12}}\right. \\
&+ \frac{1}{2}\cos(r_1, r_{12})\left(\frac{\partial F_1}{\partial r_1}\frac{\partial G_1}{\partial r_{12}} + \frac{\partial F_1}{\partial r_{12}}\frac{\partial G_1}{\partial r_1}\right) \\
&+ \left.\frac{1}{2}\cos(r_2, r_{12})\left(\frac{\partial F_1}{\partial r_2}\frac{\partial G_1}{\partial r_{12}} + \frac{\partial F_1}{\partial r_{12}}\frac{\partial G_1}{\partial r_2}\right)\right]
\end{aligned} \tag{4.2.28}$$

Comparing (4.2.27) and (4.2.28),

$$\begin{aligned}
\nabla_s F_1.\nabla_s G_1 &= \frac{\partial F_1}{\partial r_1}\frac{\partial G_1}{\partial r_1} + \frac{\partial F_1}{\partial r_2}\frac{\partial G_1}{\partial r_2} + 2\frac{\partial F_1}{\partial r_{12}}\frac{\partial G_1}{\partial r_{12}} \\
&+ \frac{1}{2}\cos(r_1, r_{12})\left(\frac{\partial F_1}{\partial r_1}\frac{\partial G_1}{\partial r_{12}} + \frac{\partial F_1}{\partial r_{12}}\frac{\partial G_1}{\partial r_1}\right) \\
&+ \frac{1}{2}\cos(r_2, r_{12})\left(\frac{\partial F_1}{\partial r_2}\frac{\partial G_1}{\partial r_{12}} + \frac{\partial F_1}{\partial r_{12}}\frac{\partial G_1}{\partial r_2}\right)
\end{aligned} \tag{4.2.29}$$

Using $F_1 = (f \mp \tilde{f})$, $F_2 = (f \pm \tilde{f})$ and $G_1 = (g \mp \tilde{g})$ the variational equation (4.2.23) assumes the following final form,

$$\begin{aligned}
\Delta &\int \left\{2\left(T_{pf} + T_{dd} + T_{pfdd}\right)\right. \\
&+ 2\left(V_{eff} - E\right)\left[\frac{8}{3}\sin^2\theta_{12}\left(f^2 + \tilde{f}^2\right) \mp 2\sin^2\theta_{12}\left(1 + \frac{5}{3}\cos 2\theta_{12}\right) f\tilde{f}\right. \\
&+ \frac{10}{7}\sin^2\theta_{12}\left(\frac{5}{3} + \cos^2\theta_{12}\right)\left(g^2 + \tilde{g}^2 \mp 2g\tilde{g}\right) \\
&+ \left.\left.\frac{16}{3}\sqrt{\frac{10}{7}}\sin^2\theta_{12}\cos\theta_{12}\left(fg + \tilde{f}\tilde{g} \mp f\tilde{g} \mp \tilde{f}g\right)\right]\right\} d\tau = 0
\end{aligned} \tag{4.2.30}$$

where, T_{pf}, T_{dd} and T_{pfdd} are the K.E. parts corresponding to the pf, dd and mixed $pf-dd$ configurations respectively and given by,

$$
\begin{aligned}
T_{pf} = {} & \frac{4}{3}\sin^2\theta_{12}\left[\left(\frac{\partial f}{\partial r_1}\right)^2+\left(\frac{\partial \tilde{f}}{\partial r_1}\right)^2+\left(\frac{\partial f}{\partial r_2}\right)^2+\left(\frac{\partial \tilde{f}}{\partial r_2}\right)^2\right. \\
& \mp 2\left(\frac{\partial f}{\partial r_1}\frac{\partial \tilde{f}}{\partial r_1}+\frac{\partial f}{\partial r_2}\frac{\partial \tilde{f}}{\partial r_2}\right)+2\left\{\left(\frac{\partial f}{\partial r_{12}}\right)^2+\left(\frac{\partial \tilde{f}}{\partial r_{12}}\right)^2\mp 2\frac{\partial f}{\partial r_{12}}\frac{\partial \tilde{f}}{\partial r_{12}}\right\} \\
& +\cos(r_1,r_{12})\left(\frac{\partial f}{\partial r_1}\frac{\partial f}{\partial r_{12}}+\frac{\partial \tilde{f}}{\partial r_1}\frac{\partial \tilde{f}}{\partial r_{12}}\mp\frac{\partial f}{\partial r_1}\frac{\partial \tilde{f}}{\partial r_{12}}\mp\frac{\partial \tilde{f}}{\partial r_1}\frac{\partial f}{\partial r_{12}}\right) \\
& \left.+\cos(r_2,r_{12})\left(\frac{\partial f}{\partial r_2}\frac{\partial f}{\partial r_{12}}+\frac{\partial \tilde{f}}{\partial r_2}\frac{\partial \tilde{f}}{\partial r_{12}}\mp\frac{\partial f}{\partial r_2}\frac{\partial \tilde{f}}{\partial r_{12}}\mp\frac{\partial \tilde{f}}{\partial r_2}\frac{\partial f}{\partial r_{12}}\right)\right] \\
& +\frac{5}{3}\sin^4\theta_{12}\left[2\left(\pm\frac{\partial f}{\partial r_1}\frac{\partial \tilde{f}}{\partial r_1}\pm\frac{\partial f}{\partial r_2}\frac{\partial \tilde{f}}{\partial r_2}\right)\pm 4\frac{\partial f}{\partial r_{12}}\frac{\partial \tilde{f}}{\partial r_{12}}\right. \\
& \left.\pm\cos(r_1,r_{12})\left(\frac{\partial f}{\partial r_1}\frac{\partial \tilde{f}}{\partial r_{12}}+\frac{\partial \tilde{f}}{\partial r_1}\frac{\partial f}{\partial r_{12}}\right)\pm\cos(r_2,r_{12})\left(\frac{\partial f}{\partial r_2}\frac{\partial \tilde{f}}{\partial r_{12}}+\frac{\partial \tilde{f}}{\partial r_2}\frac{\partial f}{\partial r_{12}}\right)\right] \\
& +\left(\frac{1}{r_1^2}+\frac{1}{r_2^2}\right)\frac{2}{3}\sin^2\theta_{12}\cos\theta_{12}\frac{r_1r_2}{r_{12}}\left[4\left(f\frac{\partial f}{\partial r_{12}}+\tilde{f}\frac{\partial \tilde{f}}{\partial r_{12}}\right)\mp\right. \\
& \left.(5\cos\theta_{12}-1)\left(f\frac{\partial \tilde{f}}{\partial r_{12}}+\tilde{f}\frac{\partial f}{\partial r_{12}}\right)\right]\pm\left(\frac{1}{r_2^2}-\frac{1}{r_1^2}\right)\frac{10}{3}\sin^4\theta_{12}\cos\theta_{12}\frac{r_1r_2}{r_{12}}\left(\tilde{f}\frac{\partial f}{\partial r_{12}}-f\frac{\partial \tilde{f}}{\partial r_{12}}\right) \\
& +\left(\frac{1}{r_1^2}+\frac{1}{r_2^2}\right)\left[\left(8-\frac{16}{3}\cos^2\theta_{12}\right)\left(f^2+\tilde{f}^2\right)\pm 2f\tilde{f}\left(\frac{1}{3}-5\cos^4\theta_{12}+2\cos^2\theta_{12}\right)\right] \\
& -\frac{20}{3}\sin^2\theta_{12}\left(\frac{1}{r_2^2}-\frac{1}{r_1^2}\right)\left(f^2-\tilde{f}^2\right) \qquad (4.2.31)
\end{aligned}
$$

$$
\begin{aligned}
T_{dd} = {} & \frac{5}{7}\sin^2\theta_{12}\left(\cos^2\theta_{12}+\frac{5}{3}\right)\left[\left(\frac{\partial g}{\partial r_1}\right)^2+\left(\frac{\partial \tilde{g}}{\partial r_1}\right)^2+\left(\frac{\partial g}{\partial r_2}\right)^2+\left(\frac{\partial \tilde{g}}{\partial r_2}\right)^2\right. \\
& \mp 2\left(\frac{\partial g}{\partial r_1}\frac{\partial \tilde{g}}{\partial r_1}+\frac{\partial g}{\partial r_2}\frac{\partial \tilde{g}}{\partial r_2}\right)+2\left\{\left(\frac{\partial g}{\partial r_{12}}\right)^2+\left(\frac{\partial \tilde{g}}{\partial r_{12}}\right)^2\mp 2\frac{\partial g}{\partial r_{12}}\frac{\partial \tilde{g}}{\partial r_{12}}\right\} \\
& +\cos(r_1,r_{12})\left(\frac{\partial g}{\partial r_1}\frac{\partial g}{\partial r_{12}}+\frac{\partial \tilde{g}}{\partial r_1}\frac{\partial \tilde{g}}{\partial r_{12}}\mp\frac{\partial g}{\partial r_1}\frac{\partial \tilde{g}}{\partial r_{12}}\mp\frac{\partial \tilde{g}}{\partial r_1}\frac{\partial g}{\partial r_{12}}\right) \\
& \left.+\cos(r_2,r_{12})\left(\frac{\partial g}{\partial r_2}\frac{\partial g}{\partial r_{12}}+\frac{\partial \tilde{g}}{\partial r_2}\frac{\partial \tilde{g}}{\partial r_{12}}\mp\frac{\partial g}{\partial r_2}\frac{\partial \tilde{g}}{\partial r_{12}}\mp\frac{\partial \tilde{g}}{\partial r_2}\frac{\partial g}{\partial r_{12}}\right)\right] \\
& +\frac{10}{7}\left(\frac{1}{r_1^2}+\frac{1}{r_2^2}\right)\sin^2\theta_{12}\cos\theta_{12}\left(\cos 2\theta_{12}+\frac{5}{3}\right)\frac{r_1r_2}{r_{12}}\left(g\frac{\partial g}{\partial r_{12}}+\tilde{g}\frac{\partial \tilde{g}}{\partial r_{12}}\mp g\frac{\partial \tilde{g}}{\partial r_{12}}\mp\tilde{g}\frac{\partial g}{\partial r_{12}}\right) \\
& +\frac{5}{7}\left(\frac{1}{r_1^2}+\frac{1}{r_2^2}\right)\left(\cos^2 2\theta_{12}-4\cos^2\theta_{12}+\frac{25}{3}\right)\left(g^2+\tilde{g}^2\mp 2g\tilde{g}\right) \qquad (4.2.32)
\end{aligned}
$$

and

$$
\begin{aligned}
T_{pfdd} = {} & \frac{8}{3}\sqrt{\frac{10}{7}}\sin^2\theta_{12}\cos\theta_{12}\left[\left(\frac{\partial f}{\partial r_1}\frac{\partial g}{\partial r_1}+\frac{\partial \tilde{f}}{\partial r_1}\frac{\partial \tilde{g}}{\partial r_1}\mp\frac{\partial f}{\partial r_1}\frac{\partial \tilde{g}}{\partial r_1}\mp\frac{\partial \tilde{f}}{\partial r_1}\frac{\partial g}{\partial r_1}\right)\right. \\
& +\left(\frac{\partial f}{\partial r_2}\frac{\partial g}{\partial r_2}+\frac{\partial \tilde{f}}{\partial r_2}\frac{\partial \tilde{g}}{\partial r_2}\mp\frac{\partial f}{\partial r_2}\frac{\partial \tilde{g}}{\partial r_2}\mp\frac{\partial \tilde{f}}{\partial r_2}\frac{\partial g}{\partial r_2}\right) \\
& +2\left(\frac{\partial f}{\partial r_{12}}\frac{\partial g}{\partial r_{12}}+\frac{\partial \tilde{f}}{\partial r_{12}}\frac{\partial \tilde{g}}{\partial r_{12}}\mp\frac{\partial f}{\partial r_{12}}\frac{\partial \tilde{g}}{\partial r_{12}}\mp\frac{\partial \tilde{f}}{\partial r_{12}}\frac{\partial g}{\partial r_{12}}\right) \\
& +\frac{1}{2}\cos(r_1,r_{12})\left\{\left(\frac{\partial f}{\partial r_1}\frac{\partial g}{\partial r_{12}}+\frac{\partial \tilde{f}}{\partial r_1}\frac{\partial \tilde{g}}{\partial r_{12}}\mp\frac{\partial f}{\partial r_1}\frac{\partial \tilde{g}}{\partial r_{12}}\mp\frac{\partial \tilde{f}}{\partial r_1}\frac{\partial g}{\partial r_{12}}\right)\right. \\
& \left.+\left(\frac{\partial g}{\partial r_1}\frac{\partial f}{\partial r_{12}}+\frac{\partial \tilde{g}}{\partial r_1}\frac{\partial \tilde{f}}{\partial r_{12}}\mp\frac{\partial g}{\partial r_1}\frac{\partial \tilde{f}}{\partial r_{12}}\mp\frac{\partial \tilde{g}}{\partial r_1}\frac{\partial f}{\partial r_{12}}\right)\right\} \\
& +\frac{1}{2}\cos(r_2,r_{12})\left\{\left(\frac{\partial f}{\partial r_2}\frac{\partial g}{\partial r_{12}}+\frac{\partial \tilde{f}}{\partial r_2}\frac{\partial \tilde{g}}{\partial r_{12}}\mp\frac{\partial f}{\partial r_2}\frac{\partial \tilde{g}}{\partial r_{12}}\mp\frac{\partial \tilde{f}}{\partial r_2}\frac{\partial g}{\partial r_{12}}\right)\right. \\
& \left.\left.+\left(\frac{\partial g}{\partial r_2}\frac{\partial f}{\partial r_{12}}+\frac{\partial \tilde{g}}{\partial r_2}\frac{\partial \tilde{f}}{\partial r_{12}}\mp\frac{\partial g}{\partial r_2}\frac{\partial \tilde{f}}{\partial r_{12}}\mp\frac{\partial \tilde{g}}{\partial r_2}\frac{\partial f}{\partial r_{12}}\right)\right\}\right] \\
& +\sqrt{\frac{10}{7}}\left(\frac{1}{r_1^2}+\frac{1}{r_2^2}\right)\sin^2\theta_{12}\left(\frac{11}{3}\cos^2\theta_{12}-1\right)\frac{r_1r_2}{r_{12}}\left(g\frac{\partial f}{\partial r_{12}}+\tilde{g}\frac{\partial \tilde{f}}{\partial r_{12}}\mp g\frac{\partial \tilde{f}}{\partial r_{12}}\mp\tilde{g}\frac{\partial f}{\partial r_{12}}\right) \\
& +\frac{1}{3}\sqrt{\frac{10}{7}}\left(\frac{1}{r_1^2}+\frac{1}{r_2^2}\right)\sin^2\theta_{12}\left(13\cos^2\theta_{12}-5\right)\frac{r_1r_2}{r_{12}}\left(f\frac{\partial g}{\partial r_{12}}+\tilde{f}\frac{\partial \tilde{g}}{\partial r_{12}}\mp f\frac{\partial \tilde{g}}{\partial r_{12}}\mp\tilde{f}\frac{\partial g}{\partial r_{12}}\right) \\
& +\frac{10}{3}\sqrt{\frac{10}{7}}\left(\frac{1}{r_2^2}-\frac{1}{r_1^2}\right)\sin^4\theta_{12}\frac{r_1r_2}{r_{12}}\left[\left(f\frac{\partial g}{\partial r_{12}}-\tilde{f}\frac{\partial \tilde{g}}{\partial r_{12}}\right.\right. \\
& \left.\left.\mp f\frac{\partial \tilde{g}}{\partial r_{12}}\pm\tilde{f}\frac{\partial g}{\partial r_{12}}\right)+\left(-g\frac{\partial f}{\partial r_{12}}+\tilde{g}\frac{\partial \tilde{f}}{\partial r_{12}}\mp g\frac{\partial \tilde{f}}{\partial r_{12}}\pm\tilde{g}\frac{\partial f}{\partial r_{12}}\right)\right] \\
& +\frac{4}{3}\sqrt{\frac{10}{7}}\left(\frac{1}{r_1^2}+\frac{1}{r_2^2}\right)\cos\theta_{12}\left(5-\cos^2\theta_{12}\right)\left(fg+\tilde{f}\tilde{g}\mp f\tilde{g}\mp\tilde{f}g\right) \\
& +\frac{20}{3}\sqrt{\frac{10}{7}}\left(\frac{1}{r_1^2}-\frac{1}{r_2^2}\right)\cos\theta_{12}\sin^2\theta_{12}\left(fg-\tilde{f}\tilde{g}\mp f\tilde{g}\pm\tilde{f}g\right) \qquad (4.2.33)
\end{aligned}
$$

4.2.3 Basis set

The trial radial functions $f(r_1,r_2,r_{12})$ and $g(r_1,r_2,r_{12})$ are expanded in multi-exponent Hylleraas type basis set as

$$f(r_1,r_2,r_{12}) = \sum_{k=1}^{s_1} r_1^{l_k+3}\ r_2^{m_k+1}\ r_{12}^{n_k}\ \left[\sum_{i=1}^{p_1} C_{kii}\eta_i(1)\eta_i(2)+\sum_{i=1}^{p_1}\sum_{j>i}^{p_1} C_{kij}\eta_i(1)\eta_j(2)\right] \qquad (4.2.34)$$

$$g(r_1,r_2,r_{12}) = \sum_{k=1}^{s_2} r_1^{l_k+2}\ r_2^{m_k+2}\ r_{12}^{n_k}\ \left[\sum_{i=1}^{p_2} D_{kii}\xi_i(1)\xi_i(2)+\sum_{i=1}^{p_2}\sum_{j>i}^{p_2} D_{kij}\xi_i(1)\xi_j(2)\right] \qquad (4.2.35)$$

The characteristics of different parameters used in the above two equations (4.2.34) and (4.2.35) are described below

1. $(l_k, m_k, n_k) \geq (0, 0, 0)$.
2. s_1 and s_2 are the numbers of elements in the sets of the powers of r_1, r_2 and r_{12} for pf and dd configurations respectively.
3. $\eta_i(j) = e^{-\rho_i r_j}$ and $\xi_i(j) = e^{-\nu_i r_j}$. where ρ_i and ν_i are the non-linear parameters for pf and dd configurations respectively.
4. p_1 and p_2 denote the number of non-linear parameters for pf and dd configurations respectively.
5. C_{kij} and D_{kij} are the linear variational parameters for pf and dd configurations respectively.
6. The dimensions of the multi-exponent basis of pf and dd configurations are $N_1 = \frac{p_1(p_1+1)}{2} \times s_1$ and $N_2 = \frac{p_2(p_2+1)}{2} \times s_2$ respectively. Hence the total dimension of the wavefunction Ψ is $N = N_1 + N_2$

The non-linear parameters ρ_i and ν_i are selected as described in subsection 3.2.3. The equations (4.2.34) and (4.2.35) can be rewritten as:

$$f(r_1, r_2, r_{12}) = \sum_{i=1}^{N_1} C_i X_i(r_1, r_2, r_{12}) \tag{4.2.36}$$

$$g(r_1, r_2, r_{12}) = \sum_{i=1}^{N_2} D_i Y_i(r_1, r_2, r_{12}) \tag{4.2.37}$$

It is evident from the equation (4.2.30) that the necessary integrals for the calculation of matrix elements of the Hamiltonian matrix $\underline{\underline{H}}$ and overlap matrix $\underline{\underline{S}}$ in the generalized eigenvalue equation (3.2.59) are of the following forms:

$$\langle \mathcal{O}_1 F | \mathcal{O}_2 G \rangle = \int (\mathcal{O}_1 F)(\mathcal{O}_2 G)\, d\tau \tag{4.2.38}$$

where the functions F and G are replaced by f, $\tilde{f}$, g and $\tilde{g}$, as required. Using the integral (4.2.38), the general form of matrix elements, where no mixing of pf and dd configurations

takes place, may be written as:

$$\begin{aligned}
\langle \mathcal{O}_1 f | \mathcal{O}_2 f \rangle_{ij} &= \frac{1}{2} \int \left[\left(\mathcal{O}_1 X_i \right) \left(\mathcal{O}_2 X_j \right) + \left(\mathcal{O}_1 X_j \right) \left(\mathcal{O}_2 X_i \right) \right] d\tau \\
\langle \mathcal{O}_1 \tilde{f} | \mathcal{O}_2 \tilde{f} \rangle_{ij} &= \frac{1}{2} \int \left[\left(\mathcal{O}_1 \tilde{X}_i \right) \left(\mathcal{O}_2 \tilde{X}_j \right) + \left(\mathcal{O}_1 \tilde{X}_j \right) \left(\mathcal{O}_2 \tilde{X}_i \right) \right] d\tau \\
\langle \mathcal{O}_1 f | \mathcal{O}_2 \tilde{f} \rangle_{ij} &= \frac{1}{2} \int \left[\left(\mathcal{O}_1 X_i \right) \left(\mathcal{O}_2 \tilde{X}_j \right) + \left(\mathcal{O}_1 X_j \right) \left(\mathcal{O}_2 \tilde{X}_i \right) \right] d\tau \\
\langle \mathcal{O}_1 g | \mathcal{O}_2 g \rangle_{ij} &= \frac{1}{2} \int \left[\left(\mathcal{O}_1 Y_i \right) \left(\mathcal{O}_2 Y_j \right) + \left(\mathcal{O}_1 Y_j \right) \left(\mathcal{O}_2 Y_i \right) \right] d\tau \\
\langle \mathcal{O}_1 \tilde{g} | \mathcal{O}_2 \tilde{g} \rangle_{ij} &= \frac{1}{2} \int \left[\left(\mathcal{O}_1 \tilde{Y}_i \right) \left(\mathcal{O}_2 \tilde{Y}_j \right) + \left(\mathcal{O}_1 \tilde{Y}_j \right) \left(\mathcal{O}_2 \tilde{Y}_i \right) \right] d\tau \\
\langle \mathcal{O}_1 g | \mathcal{O}_2 \tilde{g} \rangle_{ij} &= \frac{1}{2} \int \left[\left(\mathcal{O}_1 Y_i \right) \left(\mathcal{O}_2 \tilde{Y}_j \right) + \left(\mathcal{O}_1 Y_j \right) \left(\mathcal{O}_2 \tilde{Y}_i \right) \right] d\tau
\end{aligned} \tag{4.2.39}$$

Other relevant general forms of the matrix elements where the mixing of pf and dd configurations has been considered, are given by

$$\begin{aligned}
\langle \mathcal{O}_1 f | \mathcal{O}_2 g \rangle_{ij} &= \frac{1}{2} \int \left(\mathcal{O}_1 X_i \right) \left(\mathcal{O}_2 Y_j \right) d\tau \\
\langle \mathcal{O}_1 \tilde{f} | \mathcal{O}_2 \tilde{g} \rangle_{ij} &= \frac{1}{2} \int \left(\mathcal{O}_1 \tilde{X}_i \right) \left(\mathcal{O}_2 \tilde{Y}_j \right) d\tau \\
\langle \mathcal{O}_1 f | \mathcal{O}_2 \tilde{g} \rangle_{ij} &= \frac{1}{2} \int \left(\mathcal{O}_1 X_i \right) \left(\mathcal{O}_2 \tilde{Y}_j \right) d\tau \\
\langle \mathcal{O}_1 \tilde{f} | \mathcal{O}_2 g \rangle_{ij} &= \frac{1}{2} \int \left(\mathcal{O}_1 \tilde{X}_i \right) \left(\mathcal{O}_2 Y_j \right) d\tau
\end{aligned} \tag{4.2.40}$$

To visualize how the matrix looks like under the basis set expansion technique, let us take a sample calculation with $N_1 = N_2 = 2$ *i.e.* $f = C_1 X_1 + C_2 X_2$ and $g = D_1 Y_1 + D_2 Y_2$. Hence, we can write the Hamiltonian matrix $\underline{\underline{H}}$ as

$$\underline{\underline{H}} = \left[\begin{array}{cc|cc} H_{11} & H_{12} & H_{13} & H_{14} \\ H_{21} & H_{22} & H_{23} & H_{24} \\ \hline H_{31} & H_{32} & H_{33} & H_{34} \\ H_{41} & H_{42} & H_{43} & H_{44} \end{array}\right]$$

In this matrix H_{11}, H_{12}, H_{21} and H_{22} contain only pf terms, H_{33}, H_{34}, H_{43} and H_{44} contain only dd terms and $H_{13}, H_{14}, H_{23}, H_{24}, H_{31}, H_{32}, H_{41}$ and H_{42} contain $pf - dd$ mixed terms. Finally we solve the generalized eigenvalue equation [162]

$$\underline{\underline{H}}\ \underline{C} = E \underline{\underline{S}}\ \underline{C} \tag{4.2.41}$$

where $\underline{\underline{H}}$ is the Hamiltonian matrix, $\underline{\underline{S}}$ is the overlap matrix, $\underline{C}$ is the column vector and E is the energy eigenvalue.

4.2.4 Basis integrals

The integrals appearing in the present calculation are of two types:

(i) The first type of the integrals is given by

$$A(m,n,l;\alpha,\beta) = \int_{r_1=0}^{\infty}\int_{r_2=0}^{\infty}\int_{|r_1-r_2|}^{r_1+r_2} r_1^m r_2^n r_{12}^l e^{-\alpha r_1-\beta r_2} dr_1 dr_2 dr_{12} \tag{4.2.42}$$

with the conditions: $m \geq 0$, $n \geq 0$, $l \geq 0$ and $\alpha, \beta > 0$. This integral is evaluated as described previously in equation (3.2.66).

(ii) Another type of integral is of the form

$$\begin{aligned} A(-1,m,l;\alpha,\beta) &= \int_0^{\infty} r_1^{-1} e^{-\alpha r_1} dr_1 \int_0^{\infty} r_2^m e^{-\beta r_2} dr_2 \int_{|r_1-r_2|}^{r_1+r_2} r_{12}^l dr_{12} \\ &= \int_0^{\infty} r_1^{-1} e^{-\alpha r_1} dr_1 \int_0^{r_1} r_2^m e^{-\beta r_2} dr_2 \int_{r_1-r_2}^{r_1+r_2} r_{12}^l dr_{12} \\ &+ \int_0^{\infty} r_2^m e^{-\beta r_2} dr_2 \int_0^{r_2} {r_1}^{-1} e^{-\alpha r_1} dr_1 \int_{r_2-r_1}^{r_1+r_2} r_{12}^l dr_{12} \\ &= I_1 + I_2 \end{aligned} \tag{4.2.43}$$

where I_1 and I_2 are given by

$$\begin{aligned} I_1 &= \int_0^{\infty} r_1^{-1} e^{-\alpha r_1} dr_1 \int_0^{r_1} r_2^m e^{-\beta r_2} dr_2 \int_{r_1-r_2}^{r_1+r_2} r_{12}^l dr_{12} \\ &= \frac{1}{(l+1)} \int_0^{\infty} r_1^{-1} e^{-\alpha r_1} dr_1 \int_0^{r_1} r_2^m e^{-\beta r_2} dr_2 \left[(r_1+r_2)^{l+1} - (r_2-r_1)^{l+1}\right] \end{aligned} \tag{4.2.44}$$

$$\begin{aligned} I_2 &= \int_0^{\infty} r_2^m e^{-\beta r_2} dr_2 \int_0^{r_2} {r_1}^{-1} e^{-ar_1} dr_1 \int_{r_2-r_1}^{r_1+r_2} r_{12}^l dr_{12} \\ &= \frac{1}{(l+1)} \int_0^{\infty} r_2^m e^{-\beta r_2} dr_2 \int_0^{r_2} {r_1}^{-1} e^{-\alpha r_1} dr_1 \left[(r_1+r_2)^{l+1} - (r_2-r_1)^{l+1}\right] \end{aligned} \tag{4.2.45}$$

For convenience, we describe the evaluation of I_2 first. Let us take $l+1 = n$ and use the binomial expansion to get the following relation

$$(r_1+r_2)^n - (r_2-r_1)^n = 2\sum_{i=0}^{\frac{n-1}{2}} \frac{n!}{(n-2i-1)!\,(2i+1)!} r_2^{n-2i-1} r_1^{2i+1} \qquad (n = odd)$$

$$= 2\sum_{i=0}^{\frac{n-2}{2}} \frac{n!}{(n-2i-1)!\,(2i+1)!} r_2^{n-2i-1} r_1^{2i+1} \qquad (n = even) \tag{4.2.46}$$

For even l *i.e.* odd n, equation (4.2.45) becomes

$$I_2 = \frac{2}{n}\sum_{i=0}^{\frac{n-1}{2}} \frac{n!}{(n-2i-1)!\,(2i+1)!} \int_0^\infty r_2^{m+n-2i-1} e^{-\beta r_2} dr_2 \int_0^{r_2} {r_1}^{2i} e^{-\alpha r_1} dr_1 \tag{4.2.47}$$

Using the standard integral [156]

$$\int_0^R r^n e^{-\nu r} dr = \frac{n!}{\nu^{n+1}} - e^{-\nu R}\sum_{k=0}^{n} \frac{n!}{k!}\frac{R^k}{\nu^{n-k+1}}$$

equation (4.2.47) can be written as

$$\begin{aligned} I_2 &= \frac{2}{n}\sum_{i=0}^{\frac{n-1}{2}} \frac{n!(m+n-2i-1)!}{(2i+1)(n-2i-1)!}\frac{1}{\alpha^{2i+1}\beta^{m+n-2i}} \\ &- \frac{2}{n}\sum_{i=0}^{\frac{n-1}{2}}\sum_{j=0}^{2i} \frac{n!(m+n-j-1)!}{(2i+1)(n-2i-1)!(2i-j)!}\frac{1}{\alpha^{j+1}(\alpha+\beta)^{m+n-j}} \end{aligned} \tag{4.2.48}$$

When l is odd *i.e.* n is even, then I_2 will be given by,

$$\begin{aligned} I_2 &= \frac{2}{n}\sum_{i=0}^{\frac{n-2}{2}} \frac{n!(m+n-2i-1)!}{(2i+1)(n-2i-1)!}\frac{1}{\alpha^{2i+1}\beta^{m+n-2i}} \\ &- \frac{2}{n}\sum_{i=0}^{\frac{n-2}{2}}\sum_{j=0}^{2i} \frac{n!(m+n-j-1)!}{(2i+1)(n-2i-1)!(2i-j)!}\frac{1}{\alpha^{j+1}(\alpha+\beta)^{m+n-j}} \end{aligned} \tag{4.2.49}$$

Following the similar procedure we formulate I_1 for two different cases like, even l,

$$\begin{aligned} I_1 &= \frac{2}{n}\frac{(m+n)!}{\beta^{m+n+1}} ln\left(\frac{\alpha+\beta}{\alpha}\right) \\ &+ \frac{2}{n}\sum_{i=0,n>1}^{\frac{n-1}{2}-1} \frac{n!(m+2i+1)!}{(n-2i-1)(2i+1)!}\frac{1}{\alpha^{n-2i-1}\beta^{m+2i+2}} \\ &- \frac{2}{n}\sum_{i=0}^{\frac{n-1}{2}-1}\sum_{j=0}^{m+2i+1} \frac{(m+2i+1)!n!(m+n-j-1)!}{(m+2i+1-j)!(2i+1)!(n-2i-1)!}\frac{1}{(\alpha+\beta)^{m+n-j}\beta^{j+1}} \end{aligned}$$

$$- \frac{2}{n}\sum_{j=0}^{m+n-1}\frac{(m+n)!}{(m+n-j)}\frac{1}{(\alpha+\beta)^{m+n-j}\beta^{j+1}} \tag{4.2.50}$$

and odd l,

$$\begin{aligned} I_1 &= \frac{2}{n}\sum_{i=0}^{\frac{n-2}{2}}\frac{n!(m+2i+1)!}{(2i+1)!(n-2i-1)}\frac{1}{\alpha^{n-2i-1}\beta^{m+2i+2}} \\ &- \frac{2}{n}\sum_{i=0}^{\frac{n-2}{2}}\sum_{j=0}^{m+2i+1}\frac{n!(m+2i+1)!(m+n-j-1)!}{(2i+1)!(n-2i-1)!(m+2i+1-j)!}\frac{1}{\beta^{j+1}(\alpha+\beta)^{m+n-j}} \end{aligned} \tag{4.2.51}$$

4.3 Results and Discussions

In the first phase, we estimate the energy eigenvalues of metastable bound $^{1,3}\mathrm{F}^e$ states of several two-electron systems ($Z = 2 - 18$) under 'free' environment by sake of considering trial wavefunction consisting of only the pf-part. A slow convergence pattern of the energy eigenvalues of the metastable bound states (MBSs) is observed. In the next phase, the dd-part is included in the trial wavefunction. Similarly, the effect of the mixing of pf and dd-parts in the trial wavefunction is also demonstrated in case of the resonance $^{1,3}\mathrm{F}^e$ states of free He atom.

In the second part of this section we have studied the variation of different structural properties of $^{1,3}\mathrm{F}^e$ states of two-electron systems embedded under classical WCP environment. The variation of transition energies for the dipole allowed transitions $^{1,3}\mathrm{F}^e \rightarrow^{1,3} \mathrm{D}^o$ are studied with respect to screening lengths of classical WCP in a simplistic manner by only considering pf-part in the trial wavefunction. Then we have taken more appropriate trial wavefunction consisted of both pf and dd-parts for He atom embedded in classical WCP and done an extensive study on the variation of different structural properties of both metastable bound and resonance $^{1,3}\mathrm{F}^e$ states with respect to different plasma screening lengths.

4.3.1 Structural properties under free environment

The energy eigenvalues of $^{1,3}\mathrm{F}^e$ states of He atom are estimated by considering only the most dominant configuration pf-part of the wavefunction (4.2.34). The radial function $f(r_1, r_2, r_{12})$ is expanded using nine-exponent ($p = 9$) Hylleraas basis set with $N = 900$. Figure (4.3.1) shows the stabilization diagram of the first 40 energy eigenroots with respect to 288 different values of γ_1, where γ_1 is the common ratio in the geometrical sequence following $\rho_i = \rho_{i-1}\gamma_1$. There are two different classes of states in the figure:

1. Below $\mathrm{He}^+(2p)$ threshold energy -0.5 a.u., the energy eigenroots are insensitive to

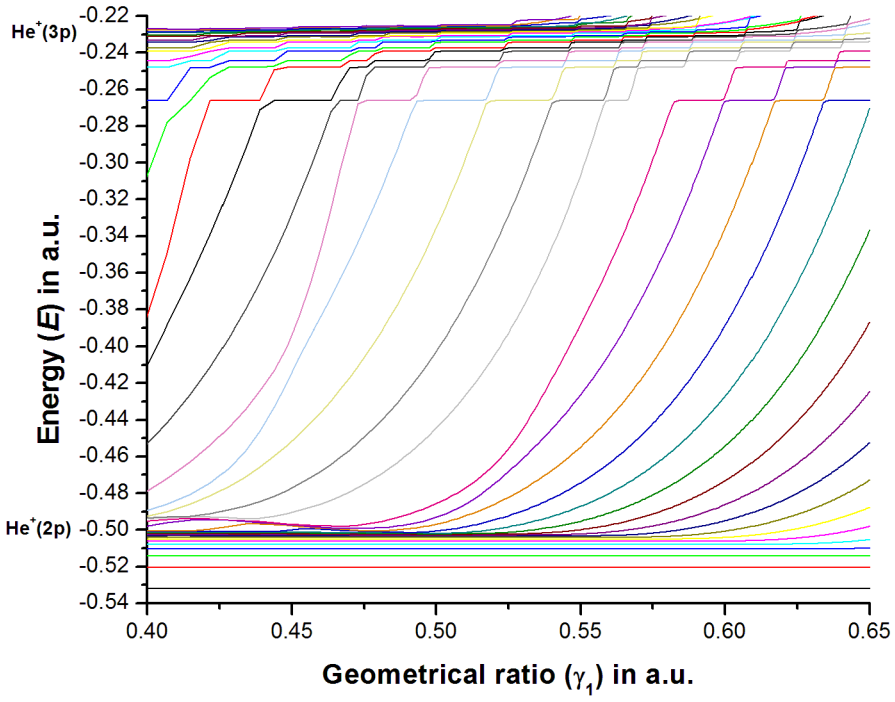

Figure 4.3.1: Stabilization diagram of ${}^3\mathrm{F}^e$ states of He atom upto $\mathrm{He}^+(3p)$ ionization threshold of energy -0.2222 a.u.

the variation in γ_1. These are metastable bound ${}^3\mathrm{F}^e$ states.

2. Above $\mathrm{He}^+(2p)$ threshold the energy of each eigenroot increases as γ_1 is increased. These eigenroots produce flat plateaus in the vicinity of avoided crossings which shows a clear signature of resonance states of ${}^3\mathrm{F}^e$ symmetry.

The investigation on the convergence of energy eigenvalues with respect to the size of the wavefunction of the metastable bound ${}^{1,3}\mathrm{F}^e$ states of He atom are given in table (4.3.1).

Table 4.3.1: Energy eigenvalues ($-E$ in a.u.) of metastable bound ${}^{1,3}\mathrm{F}^e$ states having configurations $2pnf$ $[n = 4 - 20]$ of free He atom for basis size $N = 450(s_1 = 10)$, $675(s_1 = 15)$ and $900(s_1 = 20)$.

		${}^1\mathrm{F}^e$			${}^3\mathrm{F}^e$
State	N	$-E$	*State*	N	$-E$
2p4f	450	0.5319942932	2p4f	450	0.5319856206
	675	0.5319943001		675	0.5319856301
	900	0.5319943002		900	0.5319856694
		0.5319954369509[a]			0.5319913263465[a]
2p5f	450	0.5203849389	2p5f	450	0.5203783809
	675	0.5203849437		675	0.5203784120

Continuation of Table (4.3.1)

		$^1F^e$			$^3F^e$
State	*N*	$-E$	*State*	*N*	$-E$
	900	0.5203849438		900	0.5203784183
		0.52038567104[a]			0.52038285928[a]
2p6f	450	0.5141127585	2p6f	450	0.5141083122
	675	0.5141127614		675	0.5141083351
	900	0.5141127621		900	0.5141083381
		0.51411321817[a]			0.51411142911[a]
2p7f	450	0.5103454370	2p7f	450	0.5103423957
	675	0.5103454391		675	0.5103424102
	900	0.5103454396		900	0.5103424135
		0.51034573804[a]			0.51034456468[a]
2p8f	450	0.5079073308	2p8f	450	0.5079052020
	675	0.5079073438		675	0.5079052108
	900	0.5079073441		900	0.5079052145
		0.50790754830[b]			0.5079067461[a]
2p9f	450	0.5062390572	2p9f	450	0.5062379263
	675	0.5062395124		675	0.5062379456
	900	0.5062395140		900	0.5062379673
		0.50623965811[b]			0.506239088[a]
2p10f	450	0.5050424416	2p10f	450	0.5050473631
	675	0.5050486254		675	0.5050474167
	900	0.5050486314		900	0.5050474726
		0.50504873915[b]			0.50504832108[b]
2p11f	450	0.5041085253	2p11f	450	0.5041654011
	675	0.5041686197		675	0.5041670098
	900	0.5041687782		900	0.5041677606
		0.504168863147[b]			0.50416854777[b]
2p12f	450	0.5033383724	2p12f	450	0.5034782360
	675	0.5034979961		675	0.5034899203
	900	0.5035003593		900	0.5034985413
		0.503500444342[b]			0.50350020079[b]
2p13f	450	0.5026656389	2p13f	450	0.5029345287
	675	0.5029675061		675	0.5029593264
	900	0.5029805595		900	0.5029758865
		0.502980780358[b]			0.50298058847[b]
2p14f	450	0.5020002734	2p14f	450	0.5024906614
	675	0.5025467159		675	0.5025275941
	900	0.5025670113		900	0.5025579394
		0.502568796718[b]			0.50256864290[b]
2p15f	450	0.4979800866	2p15f	450	0.5020901684
	675	0.5020136499		675	0.50219931652
	900	0.5022266858		900	0.50221121909

Continuation of Table (4.3.1)

		$^1F^e$			$^3F^e$
State	*N*	$-E$	*State*	*N*	$-E$
		0.502236675558[b]			0.50223655040[b]
2p16f	450	0.4886154512	2p16f	450	0.5017092551
	675	0.5016587221		675	0.5018079826
	900	0.5019354674		900	0.5018829299
		0.50196503430 34[b]			0.50196493112[b]
2p17f	450	0.4710085902	2p17f	450	0.5013595350
	675	0.5003490984		675	0.5013856792
	900	0.5016927483		900	0.5014888818
		0.501740032588[b]			0.50173994653[b]
2p18f	450	0.4401811708	2p18f	450	0.5006619355
	675	0.4973037549		675	0.5009365421
	900	0.5014930654		900	0.5010619401
		0.5015515739[b]			0.5015515014[b]
2p19f	450	0.3887485157	2p19f	450	0.4991539664
	675	0.4920110819		675	0.5001065942
	900	0.5007156652		900	0.5007815172
		0.501392[b]			0.5013921[b]
2p20f	450	0.3040516778	2p20f	450	0.4980315374
	675	0.4833901370		675	0.4981659745
	900	0.5006178973		900	0.4987499987

[a] [240],[b] [280]

The lowest bound energy values of the $^1F^e$ states are estimated using three different sets of the limiting values of nine-exponents (ρ_1, ρ_9) as $(0.13, 4.0)$, $(0.1, 4.0)$ and $(0.01, 4.0)$, whereas the same for $^3F^e$ states are estimated using four different sets of (ρ_1, ρ_9) as $(0.25, 4.0)$, $(0.1, 4.0)$, $(0.05, 4.0)$ and $(0.01, 4.0)$. Table (4.3.1) shows that the convergence of energy eigenvalues decreases from lower to upper metastable bound $^{1,3}F^e$ states. The energy values are compared with the available results in literature [240, 280] as shown in table (4.3.1). It can be seen from the table (4.3.1) that, the energy eigenvalues obtained by Kar *et. al.* [240] and Eiglsperger *et. al.* [280] are more negative than our present calculated values.

The energy eigenvalues and effective quantum number (n^*) of metastable bound $^{1,3}F^e$ states of Li^+ to Ar^{16+} $(Z = 3-18)$ are given in the table (4.3.2). The effective quantum numbers (n^*) are calculated from the equation from the quantum defect theory [281]

$$E = -\frac{1}{2}\left[\left(\frac{Z}{N_i}\right)^2 + \left(\frac{Z-1}{n^*}\right)^2\right] \tag{4.3.1}$$

where, E is the energy of the state below complete ionization and N_i is the inner electron quantum number. In the present case $N_i = 2$. Our results are compared with those available

in literature [282] which is also reflected in the table (4.3.2). The comparison shows similar features as that of the He atom. However, for some of the states, no such data are available in literature for comparison.

Table 4.3.2: Energy eigenvalues ($-E$ in a.u.) and effective quantum numbers (n^*) of metastable bound $^{1,3}F^e$ states having configurations $2pnf$ $[n = 4 - 20]$ of Li^+ to Ar^{16+} $(Z = 3 - 18)$ ions.

		$^1F^e$		$^3F^e$	
Ion	State	-E	n^*	-E	n^*
Li^+	2p4f	1.252511	3.960419	1.252420	3.961833
		1.252515231764[a]	3.960353617514[a]	1.252450638234[a]	3.961357068025[a]
	2p5f	1.206292	4.960108	1.206227	4.962092
		1.20629449566[a]	4.96003141641[a]	1.206251595683[a]	4.961340665488[a]
	2p6f	1.181305	5.959935	1.181262	5.962212
		1.181306379[a]	5.959861923[a]	1.1812794195[a]	5.96128922690[a]
	2p7f	1.166288	6.959901	1.166260	6.962262
		1.1662896[a]	6.95976635[a]	1.1662720[a]	6.96125015[a]
	2p8f	1.156566	7.959856	1.156546	7.962379
	2p9f	1.149904	8.961495	1.149899	8.962394
	2p10f	1.145151	9.962462	1.145151	9.962462
	2p11f	1.141650	10.959932	1.141642	10.962566
	2p12f	1.138982	11.959977	1.138976	11.962544
	2p13f	1.136908	12.959719	1.136903	12.962441
	2p14f	1.135263	13.959756	1.135259	13.962477
	2p15f	1.133936	14.960407	1.133933	14.962919
	2p16f	1.132852	15.959705	1.132849	15.962754
	2p17f	1.131953	16.960119	1.131951	16.962558
	2p18f	1.131200	17.960530	1.131199	17.961979
	2p19f	1.130563	18.960966	1.130558	18.969493
	2p20f	1.130111	19.781629	1.130038	19.924430
Be^{2+}	2p4f	2.285835	3.967789	2.285581	3.969553
		2.285840435960[a]	3.967751130897[a]	2.285639440599[a]	3.969146875345[a]
	2p5f	2.182357	4.967582	2.182182	4.969967
		2.182359664331[a]	4.967545627247[a]	2.182228822190[a]	4.969328681292[a]
	2p6f	2.126366	5.967482	2.126253	5.970152
		2.1263673969[a]	5.96744929071[a]	2.126285925[a]	5.9693738957[a]
	2p7f	2.092697	6.967443	2.092622	6.970263
		2.0926982[a]	6.96739779[a]	2.0926454[a]	6.9693829[a]
	2p8f	2.070889	7.967404	2.070837	7.970328
	2p9f	2.055960	8.967418	2.055923	8.970384
	2p10f	2.045295	9.967383	2.045268	9.970355
	2p11f	2.037412	10.967327	2.037390	10.970553
	2p12f	2.031421	11.967302	2.031404	11.970541
	2p13f	2.026761	12.967465	2.026748	12.970616

Continuation of Table (4.3.2)

		$^1F^e$		$^3F^e$	
Ion	State	-E	n^*	-E	n^*
	2p14f	2.023067	13.967243	2.023056	13.970575
	2p15f	2.020087	14.967481	2.020078	14.970835
	2p16f	2.017650	15.967389	2.017643	15.970556
	2p17f	2.015631	16.967305	2.015625	16.970563
	2p18f	2.013939	17.967616	2.013934	17.970839
	2p19f	2.012508	18.967597	2.012503	18.971390
	2p20f	2.011286	19.968077	2.011282	19.971616
B^{3+}	2p4f	3.631775	3.973172	3.631307	3.975008
		3.63178147087[a]	3.97314696448[a]	3.631390336345[a]	3.974681092280[a]
	2p5f	3.448482	4.973017	3.448167	4.975440
		3.44848492847[a]	4.97299437381[a]	3.44823320775[a]	4.97493037865[a]
	2p6f	3.349239	5.972957	3.349037	5.975650
		3.349240870[a]	5.972932525[a]	3.349084879[a]	5.975011116[a]
	2p7f	3.289536	6.972917	3.289402	6.975759
		3.2895368[a]	6.9729005[a]	3.2894359[a]	6.9750395[a]
	2p8f	3.250851	7.972906	3.250759	7.975822
	2p9f	3.224363	8.972896	3.224297	8.975878
	2p10f	3.205425	9.973543	3.205376	9.976583
	2p11f	3.189685	11.120984	3.189641	11.124768
	2p12f	3.178997	12.171951	3.178965	12.175559
	2p13f	3.170688	13.232561	3.170662	13.236328
	2p14f	3.164094	14.305068	3.164070	14.309461
	2p15f	3.158758	15.394183	3.158735	15.399430
	2p16f	3.154394	16.497405	3.154373	16.503302
	2p17f	3.150779	17.616189	3.150760	17.622684
	2p18f	3.147739	18.756824	3.147734	18.758887
	2p19f	3.145161	19.919983	3.145124	19.938287
	2p20f	3.142965	21.102377	3.142716	21.250158
C^{4+}	2p4f	5.290270	3.977107	5.289558	3.978900
		5.29027795753[a]	3.97708682340[a]	5.289661360120[a]	3.978639250204[a]
	2p5f	5.004636	4.976980	5.004162	4.979319
		5.00463919882[a]	4.97696418412[a]	5.00424519430[a]	4.97890824179[a]
	2p6f	4.849907	5.976937	4.849606	5.979510
		4.849908858[a]	5.976921310[a]	4.849665342[a]	5.979002189[a]
	2p7f	4.756793	6.976915	4.756594	6.979620
		4.75679392[a]	6.9769022[a]	4.75663661[a]	6.979040226[a]
	2p8f	4.696445	7.976907	4.696308	7.979690
	2p9f	4.655116	8.976907	4.655019	8.979715
	2p10f	4.625579	9.976920	4.625508	9.979742

Continuation of Table (4.3.2)

		$^1F^e$		$^3F^e$	
Ion	State	$-E$	n^*	$-E$	n^*
	2p11f	4.603741	10.976902	4.603687	10.979760
	2p12f	4.587141	11.976881	4.587099	11.979768
	2p13f	4.574225	12.977167	4.574192	12.980053
	2p14f	4.563980	13.977609	4.563954	13.980450
	2p15f	4.555713	14.978790	4.555691	14.981748
	2p16f	4.548938	15.982028	4.548919	15.985132
	2p17f	4.543310	16.988730	4.543294	16.991869
	2p18f	4.538579	18.000291	4.538565	18.003558
	2p19f	4.534542	19.023099	4.534529	19.026680
	2p20f	4.531002	20.079835	4.530991	20.083399
N^{5+}	2p4f	7.261297	3.980066	7.260319	3.981780
		7.26130514460[a]	3.98005218186[a]	7.26043935330[a]	3.981569320540[a]
	2p5f	6.850806	4.979961	6.850162	4.982172
		6.85080960411[a]	4.97994902415[a]	6.85025899833[a]	4.981839016900[a]
	2p6f	6.628362	5.979929	6.627954	5.982354
		6.628363930[a]	5.979917697[a]	6.628024153[a]	5.9819369788[a]
	2p7f	6.494464	6.979916	6.494196	6.982449
		6.4944651[a]	6.9799055[a]	6.4942457[a]	6.98197886[a]
	2p8f	6.407668	7.979909	6.407483	7.982521
	2p9f	6.348211	8.980044	6.348079	8.982700
	2p10f	6.305718	9.980115	6.305621	9.982795
	2p11f	6.274294	10.980322	6.274221	10.983007
	2p12f	6.250405	11.980607	6.250348	11.983331
	2p13f	6.230878	13.038673	6.230827	13.041814
	2p14f	6.216116	14.055261	6.216075	14.058425
	2p15f	6.204192	15.076329	6.204159	15.079471
	2p16f	6.194429	16.101480	6.194401	16.104728
	2p17f	6.186279	17.138800	6.186257	17.141878
	2p18f	6.179393	18.191342	6.179374	18.194520
	2p19f	6.173492	19.266428	6.173476	19.269607
	2p20f	6.168348	20.377538	6.168335	20.380595
O^{6+}	2p4f	9.544842	3.982365	9.543587	3.983983
		9.54485107280[a]	3.98235280803[a]	9.54371957137[a]	3.983812014932[a]
	2p5f	8.986986	4.982273	8.986164	4.984349
		8.98698988676[a]	4.98226347983[a]	8.98627272866[a]	4.984074551558[a]
	2p6f	8.684600	5.982251	8.684082	5.984515
		8.684602473[a]	5.982239697[a]	8.684160333[a]	5.9841724017[a]
	2p7f	8.502546	6.982246	8.502206	6.984609
		8.50254794[a]	6.98223230[a]	8.5022626[a]	6.98421535[a]

Continuation of Table (4.3.2)

		$^1F^e$		$^3F^e$	
Ion	State	-E	n^*	-E	n^*
	2p8f	8.384518	7.982239	8.384284	7.984669
	2p9f	8.303666	8.982246	8.303499	8.984717
	2p10f	8.245861	9.982475	8.245738	9.984973
	2p11f	8.203121	10.982612	8.203028	10.985127
	2p12f	8.170624	11.982929	8.170552	11.985458
	2p13f	8.145344	12.983282	8.145287	12.985829
	2p14f	8.125210	13.988255	8.125164	13.990825
	2p15f	8.107893	15.069069	8.107851	15.072002
	2p16f	8.094587	16.094123	8.094553	16.097016
	2p17f	8.083519	17.127359	8.083490	17.130333
	2p18f	8.074224	18.168157	8.074199	18.171217
	2p19f	8.066230	19.233382	8.066213	19.235851
	2p20f	8.059229	20.338356	8.059188	20.345399
F^{7+}	2p4f	12.140900	3.984194	12.139356	3.985721
		12.14090927076[a]	3.98418501875[a]	12.13950016801[a]	3.985578204205[a]
	2p5f	11.413173	4.984113	11.412168	4.986059
		11.41317664739[a]	4.98410609294[a]	11.41228577247[a]	4.985830437001[a]
	2p6f	11.018620	5.984096	11.017988	5.986213
		11.018622523[a]	5.984087511[a]	11.018073607[a]	5.9859262493[a]
	2p7f	10.781034	6.984122	10.780619	6.986332
		10.7810413[a]	6.9840831[a]	10.7806871[a]	6.985969246[a]
	2p8f	10.626979	7.984215	10.626684	7.986562
	2p9f	10.521423	8.984534	10.521219	8.986847
	2p10f	10.445916	9.985718	10.445777	9.987881
	2p11f	10.389938	10.990131	10.389834	10.992289
	2p12f	10.347096	12.003409	10.347009	12.005761
	2p13f	10.313940	13.014067	10.313879	13.016168
	2p14f	10.287695	14.024516	10.287646	14.026629
	2p15f	10.266389	15.044133	10.266342	15.046635
	2p16f	10.248509	16.096286	10.248468	16.098959
	2p17f	10.233047	17.209515	10.232999	17.213339
	2p18f	10.211977	19.181068	10.211908	19.188680
	2p19f	10.186256	22.856023	10.186170	22.872085
	2p20f	10.177034	24.798841	10.176961	24.816255
Ne^{8+}	2p4f	15.049466	3.985684	15.047626	3.987123
		15.04947593532[a]	3.98567656525[a]	15.04778041165[a]	3.987002559633[a]
	2p5f	14.129364	4.985612	14.128172	4.987436
		14.12936788309[a]	4.98560578775[a]	14.12829797405[a]	4.987243469809[a]
	2p6f	13.630421	5.985596	13.629671	5.987583

Continuation of Table (4.3.2)

		$^1F^e$		$^3F^e$	
Ion	State	$-E$	n^*	$-E$	n^*
		13.630422927[a]	5.985590933[a]	13.629763942[a]	5.9873363597[a]
	2p7f	13.329943	6.985595	13.329452	6.987662
		13.32994444[a]	6.98558854[a]	13.3295192[a]	6.98737884[a]
	2p8f	13.135092	7.985630	13.134756	7.987743
	2p9f	13.001597	8.985661	13.001357	8.987812
	2p10f	12.906154	9.985783	12.905978	9.987948
	2p11f	12.835548	10.986268	12.835416	10.988429
	2p12f	12.781773	11.988858	12.781669	11.991071
	2p13f	12.739992	12.990598	12.739911	12.992790
	2p14f	12.706857	13.992406	12.706793	13.994571
	2p15f	12.680121	14.994961	12.680068	14.997167
	2p16f	12.658004	16.010079	12.657957	16.012461
	2p17f	12.639445	17.042215	12.639406	17.044599
	2p18f	12.622479	18.184305	12.622428	18.188092
	2p19f	12.604086	19.725651	12.604043	19.729727
	2p20f	12.592190	20.959726	12.592141	20.965299
Na^{9+}	2p4f	18.270539	3.986919	18.268398	3.988277
		18.27054868630[a]	3.98691334478[a]	18.26856003131[a]	3.988174230763[a]
	2p5f	17.135558	4.986855	17.134175	4.988571
		17.13556233814[a]	4.98684914338[a]	17.13430934555[a]	4.988403784836[a]
	2p6f	16.520001	5.986841	16.519134	5.988703
		16.520002960[a]	5.986837049[a]	16.519231389[a]	5.9884933851[a]
	2p7f	16.149256	6.986839	16.148688	6.988777
		16.14925691[a]	6.98683603[a]	16.14875893[a]	6.98853510[a]
	2p8f	15.908826	7.986843	15.908437	7.988826
	2p9f	15.744092	8.986848	15.743816	8.988852
	2p10f	15.626317	9.986856	15.626114	9.988879
	2p11f	15.539211	10.986875	15.539057	10.988918
	2p12f	15.472528	11.994720	15.472856	11.989063
	2p13f	15.420942	12.998155	15.421353	12.989138
	2p14f	15.379978	14.003405	15.380494	13.989257
	2p15f	15.346841	15.012883	15.347535	14.989455
	2p16f	15.319621	16.028399	15.320534	15.990935
	2p17f	15.296921	17.053775	15.297692	17.015664
	2p18f	15.277685	18.096176	15.278779	18.031692
	2p19f	15.261007	19.173631	15.260964	19.176663
	2p20f	15.246294	20.303240	15.246355	20.298136
Mg^{10+}	2p4f	21.804116	3.987960	21.801669	3.989243
		21.80412595849[a]	3.98795494500[a]	21.80183895368[a]	3.989154246319[a]

Continuation of Table (4.3.2)

		$^1F^e$		$^3F^e$	
Ion	State	$-E$	n^*	$-E$	n^*
	2p5f	20.431755	4.987900	20.430180	4.989517
		20.43175918580[a]	4.98789617386[a]	20.43031995723[a]	4.989372864234[a]
	2p6f	19.687360	5.987890	19.686374	5.989640
		19.687362146[a]	5.987886177[a]	19.686476020[a]	5.9894590800[a]
	2p7f	19.238977	6.987890	19.238332	6.989710
		19.23897839[a]	6.98788616[a]	19.23840642[a]	6.989499690[a]
	2p8f	18.948178	7.987902	18.947737	7.989761
	2p9f	18.748924	8.987912	18.748610	8.989797
	2p10f	18.606463	9.987931	18.606232	9.989834
	2p11f	18.501095	10.987975	18.500921	10.989883
	2p12f	18.420940	11.988576	18.420806	11.990484
	2p13f	18.358596	12.988978	18.358489	12.990916
	2p14f	18.308896	13.994956	18.308811	13.996882
	2p15f	18.267538	15.037822	18.267466	15.039846
	2p16f	18.232922	16.116563	18.232876	16.118155
	2p17f	18.204634	17.194470	18.204563	17.197454
	2p18f	18.181584	18.253195	18.181526	18.256111
	2p19f	18.161895	19.331296	18.161838	19.334700
	2p20f	18.144794	20.441013	18.144739	20.444896
Al^{11+}	2p4f	25.650197	3.988848	25.647442	3.990063
	2p5f	24.017954	4.988793	24.016185	4.990319
	2p6f	23.132498	5.988785	23.131391	5.990436
	2p7f	22.599107	6.988786	22.598384	6.990501
	2p8f	22.253153	7.988813	22.252658	7.990566
	2p9f	22.016098	8.988837	22.015745	8.990618
	2p10f	21.846601	9.988900	21.846342	9.990694
	2p11f	21.721220	10.989122	21.721025	10.990919
	2p12f	21.625579	11.993058	21.625427	11.994879
	2p13f	21.551393	12.994549	21.551273	12.996378
	2p14f	21.492519	13.996722	21.492424	13.998532
	2p15f	21.445031	14.999273	21.444953	15.001102
	2p16f	21.406172	16.002219	21.406106	16.004098
	2p17f	21.373949	17.006348	21.373892	17.008295
	2p18f	21.346587	18.025782	21.346539	18.027734
	2p19f	21.323359	19.051988	21.323317	19.054005
	2p20f	21.302666	20.130941	21.302629	20.133038
Si^{12+}	2p4f	29.808779	3.989615	29.805714	3.990768
	2p5f	27.894154	4.989564	27.892189	4.991009
	2p6f	26.855415	5.989556	26.854187	5.991118

Continuation of Table (4.3.2)

		$^1F^e$		$^3F^e$	
Ion	State	-E	n^*	-E	n^*
	2p7f	26.229645	6.989560	26.228843	6.991181
	2p8f	25.823763	7.989567	25.823215	7.991221
	2p9f	25.545631	8.989574	25.545241	8.991251
	2p10f	25.346763	9.989584	25.346476	9.991278
	2p11f	25.199667	10.989620	25.199451	10.991316
	2p12f	25.087774	11.990110	25.087606	11.991824
	2p13f	25.000743	12.990352	25.000611	12.992064
	2p14f	24.931698	13.990664	24.931592	13.992382
	2p15f	24.876004	14.991052	24.875918	14.992767
	2p16f	24.830405	15.992084	24.830333	15.993826
	2p17f	24.792037	17.010200	24.791975	17.012006
	2p18f	24.759949	18.029525	24.759899	18.031259
	2p19f	24.730700	19.138353	24.730647	19.140552
	2p20f	24.706440	20.231656	24.706399	20.233665
P^{13+}	2p4f	34.279865	3.990284	34.276486	3.991379
	2p5f	32.060355	4.990236	32.058194	4.991607
	2p6f	30.856109	5.990230	30.854760	5.991710
	2p7f	30.130594	6.990231	30.129713	6.991767
	2p8f	29.659995	7.990235	29.659393	7.991802
	2p9f	29.337504	8.990243	29.337076	8.991831
	2p10f	29.106914	9.990249	29.106599	9.991852
	2p11f	28.936353	10.990264	28.936115	10.991876
	2p12f	28.806642	11.990433	28.806457	11.992060
	2p13f	28.705727	12.990535	28.705581	12.992168
	2p14f	28.625668	13.990657	28.625552	13.992278
	2p15f	28.561089	14.990823	28.560995	14.992439
	2p16f	28.508229	15.991303	28.508151	15.992931
	2p17f	28.464302	16.994948	28.464236	16.996601
	2p18f	28.426749	18.021466	28.426693	18.023139
	2p19f	28.395128	19.047073	28.395079	19.048800
	2p20f	28.366136	20.159605	28.366097	20.161235
S^{14+}	2p4f	39.063452	3.990872	39.059758	3.991916
	2p5f	36.516557	4.990827	36.514199	4.992130
	2p6f	35.134583	5.990821	35.133111	5.992229
	2p7f	34.301950	6.990823	34.300989	6.992283
	2p8f	33.761851	7.990826	33.761195	7.992314
	2p9f	33.391724	8.990828	33.391257	8.992337
	2p10f	33.127066	9.990830	33.126723	9.992351
	2p11f	32.931304	10.990831	32.931044	10.992365

Continuation of Table (4.3.2)

		$^1F^e$		$^3F^e$	
Ion	State	-E	n^*	-E	n^*
	2p12f	32.782444	11.990841	32.782244	11.992373
	2p13f	32.666619	12.990845	32.666462	12.992376
	2p14f	32.574731	13.990845	32.574604	13.992391
	2p15f	32.500609	14.990873	32.500506	14.992416
	2p16f	32.439946	15.991035	32.439860	15.992598
	2p17f	32.389652	16.991738	32.389581	16.993286
	2p18f	32.346881	18.008851	32.346819	18.010461
	2p19f	32.310679	19.029190	32.310626	19.030814
	2p20f	32.278212	20.108901	32.278167	20.110527
Cl^{15+}	2p4f	44.159541	3.991393	44.155530	3.992389
	2p5f	41.262760	4.991351	41.260203	4.992593
	2p6f	39.690835	5.991345	39.689240	5.992686
	2p7f	38.743714	6.991348	38.742674	6.992737
	2p8f	38.129331	7.991352	38.128620	7.992770
	2p9f	37.708279	8.991378	37.707774	8.992812
	2p10f	37.407184	9.991480	37.406812	9.992929
	2p11f	37.184473	10.991578	37.184192	10.993036
	2p12f	37.015107	11.991786	37.014891	11.993241
	2p13f	36.883273	12.992484	36.883102	12.993949
	2p14f	36.778449	13.995845	36.778312	13.997313
	2p15f	36.694092	14.997323	36.693981	14.998786
	2p16f	36.625059	15.999056	36.624966	16.000544
	2p17f	36.567812	17.001815	36.567733	17.003332
	2p18f	36.519640	18.009615	36.519572	18.011167
	2p19f	36.478161	19.037881	36.478103	19.039445
	2p20f	36.442081	20.091848	36.442022	20.093717
Ar^{16+}	2p4f	49.568131	3.991858	49.563803	3.992810
	2p5f	46.298963	4.991818	46.296208	4.993004
	2p6f	44.524864	5.991814	44.523147	5.993092
	2p7f	43.455887	6.991816	43.454767	6.993141
	2p8f	42.762436	7.991821	42.761671	7.993173
	2p9f	42.287194	8.991830	42.286649	8.993201
	2p10f	41.947327	9.991958	41.946927	9.993339
	2p11f	41.695944	10.992045	41.695642	10.993433
	2p12f	41.504770	11.992248	41.504538	11.993633
	2p13f	41.356011	12.992546	41.355828	12.993935
	2p14f	41.237637	13.996279	41.237489	13.997683
	2p15f	41.142415	14.997749	41.142295	14.999150
	2p16f	41.064482	15.999591	41.064383	16.000994

Continuation of Table (4.3.2)

		$^1F^e$		$^3F^e$	
Ion	State	-E	n^*	-E	n^*
	2p17f	40.999872	17.002176	40.999787	17.003622
	2p18f	40.945690	18.006010	40.945617	18.007484
	2p19f	40.898984	19.030762	40.898919	19.032313
	2p20f	40.858603	20.073679	40.858545	20.075302

[a] [282]

For the determination of the resonance parameters *i.e.* energy (E_r) and width (Γ) of $^3F^e$ states below $He^+(3p)$ threshold of free He atom, we have used stabilization method. The resonance parameters are estimated by calculating density of states (DOS) $\rho^Q(E)$ from equation (3.2.76) and fitting those $\rho^Q(E)$ by Lorentzian profile given in equation (3.2.77). E_r and Γ for first four $^3F^e$ states below $He^+(3p)$ energy threshold are given in table (4.3.3) and compared with the results available in literature [281, 283–286]. The comparison shows that the present calculated E_r values are slightly more positive than the one obtained in previous works [281, 283–286]. Thus the trial wavefunction containing only pf terms fails to achieve the desired accuracy.

The reason behind the loss of precision in both the metastable bound and the resonance state calculations is due to the non-inclusion of the dd-part (Ψ_{dd}) explicitly in the wavefunction (4.2.1), as the mere basis-set expansion of Ψ_{pf} cannot include the dd–configuration in the radial part explicitly. Thus, for the further analysis we will use the general wavefunction (4.2.1) of F^e states where both pf and dd parts are expanded in Hylleraas basis-set. The variational upper-bound of energy eigenvalues of the metastable bound $^3F^e$ states having configurations $2pnf[n > 4]$ are estimated using following two techniques:

1. In the first method we have taken double exponent basis set expansions (4.2.34) and (4.2.35), with $p_1 = p_2 = 2$ which implies that we have considered two sets of non-linear parameters (ρ_1,ρ_2) and (ν_1,ν_2) for pf and dd–configurations, respectively. These non-linear parameters are optimized using Nelder-Mead algorithm [161]. The details of the optimization procedure is described in the subsection 3.2.3. Table (4.3.4) shows the optimized energy eigenvalues and non-linear parameters for $2pnf[n = 4 - 6]$ configurations of $^3F^e$ states of He atom for different basis size (N). For further improvement of our present results, we have fixed the optimized non-linear parameters ρ_1, ρ_2, ν_1 and ν_2 for the highest value of N as given in the table (4.3.4) and then increased N to achieve the desired level of accuracy in the energy eigenvalues. The 2nd and 3rd columns of table (4.3.5) show the energy eigenvalues of $^3F^e(2pnf; n = 4 - 9)$ states for $N = 750$ and $N = 900$ terms in the basis set respectively. The energy eigenvalues of $2pnf(n = 4 - 6)$ are converged upto 11-th decimal place whereas the same for $2pnf(n = 7 - 9)$ states show convergence upto 8-th decimal place. The process of

Table 4.3.3: Positions ($-E_r$ in a.u.) and widths (Γ in a.u.) of first four resonance states of ($^3F^e$) below $He^+(3p)$ threshold. The notation $P[-Q]$ stands for $P \times 10^{-Q}$.

	Present work		Other works	
States	$-E_r$	Γ	$-E_r$	Γ
$^3F^e(1)$	0.26607	8.34[-5]	0.31069[a]	1.98[-3][a]
			0.3111[b]	2.131[-3][b]
			0.310725[c]	1.95 [-3][c]
			0.309915[d]	
			0.310749[d]	
$^3F^e(2)$	0.24801	4.30[-5]	0.262825[a]	4.5[-4][a]
			0.2628[b]	4.77[-4][b]
			0.26283[c]	4.4[-4][c]
			0.26264[d]	
			0.262598[e]	
$^3F^e(3)$	0.24426	6.12[-7]	0.25826[a]	1.68[-4][a]
			0.2583[b]	1.83[-4][b]
			0.258275[c]	1.5[-4][c]
			0.258205[d]	
			0.258199[e]	
$^3F^e(4)$	0.23434	1.57[-5]	0.246805[a]	2.1[-4][a]
			0.2468[b]	2.27[-4][b]
			0.246715[c]	
			0.246653[d]	

[a] [283], [b] [284], [c] [285], [d] [286] and [e] [281]

diagonalization using double–exponent basis is quite involving and time consuming because, in this process, one have to pick a particular energy-root (or configuration) to optimize at a lower basis and then carry out further calculation at a higher basis, say for example, $N = 750$ or 900.

2. As an alternative to the previous method, one-shot diagonalization using nine–exponent basis ($p_1 = p_2 = 9$) is used to estimate the energy eigenvalues of metastable bound $^3F^e$ states. Two types of nine–exponent basis sets have been considered – *symmetric* and *asymmetric*. In symmetric basis, the number of powers of (r_1, r_2, r_{12}) in the basis set expansions (4.2.34) and (4.2.35), are equal *i.e.* $s_1 = s_2$, while for the later case $s_1 > s_2 (= 2)$ is considered. The 4-th and 5-th columns of table (4.3.5) show the convergence behavior of the energy eigenvalues of $^3F^e(2pnf, n = 4-18)$ states for symmetric basis corresponding to $N = 900(s_1 = s_2 = 10)$ and $N = 1530(s_1 = s_2 = 17)$

Table 4.3.4: Optimized values of $-E, \rho_1, \rho_2, \nu_1$ and ν_2 of $^3\mathrm{F}^e$ states having configurations $2pnf[n = 4, 5, 6]$ of He-atom corresponding to different sets of powers (l_k, m_k, n_k) of r_1, r_2 and r_{12} respectively and double exponent basis $(p_1 = p_2 = 2)$ *viz.* equations (4.2.34) and (4.2.35). $N = \frac{p_1(p_1+1)}{2} \times s_1 + \frac{p_2(p_2+1)}{2} \times s_2$ is the total number of terms in the basis set, s_1 and s_2 being the number of powers of pf and dd configurations respectively.

Configuration	s_1 or s_2	(l_k, m_k, n_k)	N	ρ_1 in a.u.	ρ_2 in a.u.	ν_1 in a.u.	ν_2 in a.u.	$-E$ in a.u.
$2p4f$	2	(0,0,0) (0,0,1)	12	0.27285213	0.99130236	0.42856797	0.71593340	0.531 925 191
	4	(0,0,0) (0,0,1) (1,0,0) (0,1,0)	24	0.27285213	0.99130236	0.42856797	0.71593340	0.531 961 962
	6	(0,0,0) (0,0,1) (1,0,0) (0,1,0) (2,0,0) (0,0,2)	36	0.27285213	0.99130236	0.42856797	0.71593340	0.531 983 591
$2p5f$	4	(0,0,0) (0,0,1) (1,0,0) (0,1,0)	24	0.19710246	0.99359515	0.37164322	0.67202703	0.520 281 804
	7	(0,0,0) (0,0,1) (1,0,0) (0,1,0) (2,0,0) (0,0,2) (0,2,0)	42	0.19710246	0.99359515	0.37164322	0.67202703	0.520 344 952
	10	(0,0,0) (0,0,1) (1,0,0) (0,1,0) (2,0,0) (0,0,2) (0,2,0) (1,0,1) (0,1,1)	60	0.21089071	1.02849419	0.37122904	0.68213090	0.520 368 928
$2p6f$	4	(0,0,0) (0,0,1) (1,0,0) (0,1,0)	24	0.05447293	0.74887306	0.58679505	0.81490751	0.478 427 876
	7	(0,0,0) (0,0,1) (1,0,0) (0,1,0) (2,0,0) (0,0,2) (0,2,0)	42	0.17285213	0.99130236	0.42856797	0.71593340	0.514 054 194
	10	(0,0,0) (0,0,1) (1,0,0) (0,1,0) (2,0,0) (0,0,2) (0,2,0) (1,0,1) (0,1,1)	60	0.17285213	0.99130236	0.42856797	0.71593340	0.514 064 715

Table 4.3.5: Energy eigenvalues ($-E$ in a.u.) of metastable bound $^3\mathrm{F}^e$ ($2pnf, n \geq 4$) states for different choice of basis sets using different number of terms in the basis sets.

Configuration	Double Exponent		Nine Exponent			
			Symmetric Basis		Asymmetric Basis	
	N =750	N =900	N =900	N =1530	N =1350	N =1530
$2p4f$	0.5319913263468	0.5319913263485	0.5319913258284	0.5319913263513	0.5319913261595	0.53199132616450
$2p5f$	0.5203828592813	0.5203828592853	0.5203828589216	0.5203828613614	0.5203828591643	0.52038285929302
$2p6f$	0.5141114291154	0.5141114291191	0.5141114286873	0.5141114291166	0.5141114290354	0.51411142927528
$2p7f$	0.5103445646194	0.5103445656885	0.5103445628175	0.5103445646815	0.5103445646439	0.51034456470790
$2p8f$	0.5079067459561	0.5079067462723	0.5079066925246	0.5079067606712	0.5079067461492	0.50790674627610
$2p9f$	0.5062390860001	0.5062390884513	0.5062386665548	0.5062390870716	0.5062390885034	0.50623908868559
$2p10f$			0.5050451459782	0.5050483116213	0.5050483206789	0.50504832666688
$2p11f$			0.5041441160851	0.5041683759270	0.5041685601914	0.50416856783908
$2p12f$			0.5034118118494	0.5034990626971	0.5035001039946	0.50350020569843
$2p13f$			0.5028320754932	0.5029766752202	0.5029778169414	0.50298059371759
$2p14f$			0.5022960514768	0.5025584256797	0.5025686165973	0.50256887024567
$2p15f$			0.5012313201500	0.5022112271052	0.5022365435680	0.50223659253604
$2p16f$			0.5007079126835	0.5018827805313	0.5019648269563	0.50196521180896
$2p17f$			0.5004688559343	0.5014894480147	0.5017168163780	0.50174013288428
$2p18f$			0.5003084861460	0.5005964256713	0.5015196531527	0.50155210736964
$2p19f$					0.5013095900752	0.50139603567465
$2p20f$					0.5012392360422	0.50126368214833
$2p21f$					0.5010961347848	0.50115434103934
$2p22f$					0.5009902068174	0.50105114035136

respectively. Similarly the last two columns of table (4.3.5) show the convergence behavior of the energy eigenvalues of $^3\mathrm{F}^e(2pnf, n = 4 - 22)$ states for asymmetric basis corresponding to $N = 1350(s_1 = 28, s_2 = 2)$ and $N = 1530(s_1 = 32, s_2 = 2)$ respectively. It is clear from the table (4.3.5) that the asymmetric nine-exponent basis with $N = 1530$ yields lower variational energy eigenvalues for most of the configurations.

The lowest energy eigenvalues obtained in the present work along with those available in literature [240, 280, 281, 286] are given in table (4.3.6). The values of effective quantum number n^* are also given in table (4.3.6).

Table 4.3.6: Comparison of energy eigenvalues ($-E$ in a.u.) and effective quantum number (n^*) of metastable bound $2pnf\ ^3\mathrm{F}^e$ $[n = 4 - 22]$ states of helium.

	Present work		Other works	
n	$-E$	n^*	$-E$	n^*
4	0.5319913263513	3.9534	0.5319913263465[c]	3.953382897[c]
			0.531968[a]	3.95483[a]
			0.531985[b]	
			0.5319913251[d]	
5	0.5203828613614	4.9528	0.5203828592839[c]	4.953382897[c]
			0.520367[a]	4.95477[a]
			0.520375[b]	
			0.5203828583[d]	
6	0.5141114292752	5.9525	0.5141114291180[c]	5.952501354[c]
			0.514101[a]	5.95476[a]
			0.514105[b]	
			0.5141114284[d]	
7	0.5103445647079	6.9523	0.510344564686[c]	6.95230621[c]
			0.51034456422[d]	
8	0.5079067462761	7.9522	0.5079067461[c]	7.9521782[c]
			0.50790674595[d]	
9	0.5062390886855	8.9521	0.506239088[c]	8.952090[c]
			0.50623908834[d]	
10	0.5050483266668	9.9520	0.50504832108[d]	
11	0.5041685678390	10.9520	0.50416854777[d]	
12	0.5035002056984	11.9519	0.50350020079[d]	
13	0.5029805937175	12.9519	0.50298058847[d]	
14	0.5025688702456	13.9513	0.50256864290[d]	
15	0.5022365925360	14.9517	0.50223655040[d]	
16	0.5019652118089	15.9507	0.50196493112[d]	
17	0.5017401328842	16.9509	0.50173994653[d]	
18	0.5015521073696	17.9483	0.5015515014[d]	
19	0.5013960356746	18.9250	0.5013921[d]	
20	0.5012636821483	19.8914		
21	0.5011543410393	20.8122		

Continuation of Table (4.3.6)

	Present work		Other works	
n	$-E$	n^*	$-E$	n^*
22	0.5010511403513	21.8099		

[a] [281], [b] [286], [c] [240], [d] [280]

Kar and Ho [240] used 2200 terms in their wavefunction expanded in purely exponential correlated basis set to obtain the energy eigenvalues for ${}^3\mathrm{F}^e(2pnf, n = 4-9)$ states. The only calculation available for ${}^3\mathrm{F}^e(2pnf, n = 10-19)$ states is due to Eiglsperger *et. al.* [280] where they considered 16,000 terms in the wavefunction expanded in Coulomb-Sturmenium basis set. A comparison with other theoretical results as shown in table (4.3.6) reveals that the present energy eigenvalues are lowest yet obtained. It is remarkable that the energy eigenvalues using only 900 terms in the symmetric double exponent basis set are better than those available in the literature. Therefore, one obvious benefit of the current approach is the significant decrease in the number of terms in the basis set. The explicit inclusion of the *dd* configuration, expanded in the Hylleraas basis set, is what makes the current wavefunction a much more improved one as compared to the ones used by other workers. For instance, the energy value of the $2p4f({}^3\mathrm{F}^e)$ state as calculated by using 900 terms in the nine-exponent wavefunction without *dd* configuration is -0.53198567 a.u. as given in table (4.3.1), while the energy improves to -0.53199132 a.u. for the same state upon the inclusion of *dd* configuration. Thus, the inclusion of the *dd* configuration contributes 0.001% to the energy value of the $2p4f({}^3\mathrm{F}^e)$ state. This contribution decreases as we move towards the $\mathrm{He}^+(2p)$ threshold, *e.g.* it decreases to 0.0002% for the $2p9f$ state.

The accuracy of the wavefunction is tested by estimating the expectation values of inter-electronic angles $< \theta_{12} >$, different one and two-particle moments like $\langle r_1 \rangle$, $\langle r_1^2 \rangle$, $\langle r_{12} \rangle$ and $\langle r_{12}^2 \rangle$ and the *virial factor* (ξ) defined as,

$$\xi = 1 - \left| \frac{\langle V \rangle}{2\langle T \rangle} \right| \tag{4.3.2}$$

where, $\langle V \rangle$ and $\langle T \rangle$ are the expectation values of potential and kinetic energies respectively. All the mentioned expectation values are quoted in table (4.3.7). It can be seen from table (4.3.7) that the moments $\langle r_1 \rangle$, $\langle r_1^2 \rangle$, $\langle r_{12} \rangle$ and $\langle r_{12}^2 \rangle$ gradually increase as we move towards the higher excited states. The angle $\langle \theta_{12} \rangle$ is estimated approximately by taking cosine inverse of $\langle \cos\theta_{12} \rangle$ and expressed in degrees. Table (4.3.7) shows that $\langle \theta_{12} \rangle$ decreases very slowly from $2p4f$ to $2p22f$ states. It is well known fact that for a perfectly central potential, $\xi = 0$. From the second column of table (4.3.7) it can be seen that, $\xi \sim 10^{-11}$ for $2p4f$ configuration and the values of ξ increases gradually for the higher excited states. This indicates that, the nature of the overall potential of the two-electron atom remains nearly central as we investigate the lower states and the potential gradually looses its central

nature as the higher excited states are considered.

For the investigations on the resonance $^3F^e$ states of He-atom, we have diagonalized the

Table 4.3.7: The virial-factor ξ, expectation values of inter-electronic angles (in degree), different one and two-particle moments of metastable bound $2pnf\ ^3F^e$ $[n = 4 - 22]$ states of He below $He^+(2p)$ threshold. The notation $P[\pm Q]$ stands for $P \times 10^{\pm Q}$. All values are given in atomic units.

n	ξ	$\langle r_1 \rangle$	$\langle r_1^2 \rangle$	$\langle r_{12} \rangle$	$\langle r_{12}^2 \rangle$	$\langle \theta_{12} \rangle$
4	1.28 [-11]	9.96 [+0]	1.73 [+2]	1.77 [+1]	3.47 [+2]	90.761
5	5.45 [-11]	1.66 [+1]	5.42 [+2]	3.09 [+1]	1.08 [+3]	90.388
6	6.87 [-11]	2.48 [+1]	1.26 [+3]	4.72 [+1]	2.53 [+3]	90.223
7	4.35 [-12]	3.45 [+1]	2.50 [+3]	6.66 [+1]	5.00 [+3]	90.140
8	3.56 [-10]	4.57 [+1]	4.45 [+3]	8.89 [+1]	8.89 [+3]	90.094
9	1.62 [-10]	5.84 [+1]	7.33 [+3]	1.14 [+2]	1.47 [+4]	90.065
10	1.12 [-09]	7.25 [+1]	1.14 [+4]	1.43 [+2]	2.28 [+4]	90.048
11	2.30 [-09]	8.82 [+1]	1.69 [+4]	1.74 [+2]	3.39 [+4]	90.036
12	4.59 [-08]	1.05 [+2]	2.43 [+4]	2.08 [+2]	4.85 [+4]	90.027
13	1.03 [-07]	1.24 [+2]	3.37 [+4]	2.46 [+2]	6.74 [+4]	90.021
14	2.43 [-07]	1.44 [+2]	4.57 [+4]	2.86 [+2]	9.13 [+4]	90.017
15	2.52 [-07]	1.66 [+2]	6.05 [+4]	3.29 [+2]	1.21 [+5]	90.014
16	3.76 [-06]	1.89 [+2]	7.88 [+4]	3.76 [+2]	1.58 [+5]	90.011
17	1.88 [-05]	2.14 [+2]	1.01 [+5]	4.25 [+2]	2.02 [+5]	90.009
18	1.43 [-05]	2.41 [+2]	1.28 [+5]	4.79 [+2]	2.56 [+5]	90.008
19	2.59 [-04]	2.66 [+2]	1.59 [+5]	5.30 [+2]	3.19 [+5]	90.008
20	1.51 [-03]	3.11 [+2]	2.32 [+5]	6.19 [+2]	4.65 [+5]	90.014
21	1.13 [-04]	3.55 [+2]	2.81 [+5]	7.07 [+2]	5.61 [+5]	90.006
22	9.03 [-04]	3.90 [+2]	3.65 [+5]	7.78 [+2]	7.30 [+5]	90.009

Hamiltonian matrix 1840 times using symmetric nine-exponent Hylleraas basis set with $N = 1530$ for different values of γ_1 ranging from 0.456 to 0.732 keeping γ_2 constant at 0.6, where γ_1 and γ_2 are the common ratios in the geometrical sequences $\rho_i = \rho_{i-1}\gamma_1$ ($pf-$part) and $\nu_i = \nu_{i-1}\gamma_2$ ($dd-$part), respectively. The highest value of the ρ sequence *i.e.* ρ_9 is fixed at 8.0 while ρ_1 of any set differs from that of the previous one by 0.001. The plot of each energy eigenroot versus γ_1 produces the stabilization diagram. A portion of the stabilization diagram in the energy range -0.325 a.u. to -0.225 a.u. is given in figure (4.3.2) where one can see flat plateaus in the vicinity of avoided crossings which signify the existence of resonance states. For instance, it is evident from figure (4.3.2) that the resonance positions are in the vicinity of -0.310 a.u., -0.264 a.u., -0.258 a.u. ... etc.

The determination of the actual resonance parameters is a two-step process. First, we take an energy eigenroot and numerically estimate the spectral DOS $\rho^Q(E)$ following equation (3.2.76) at different energies. For a better understanding we consider the energy eigen root no. 13 in the energy range -0.330 a.u. to -0.300 a.u. where one of the plateaus lies around -0.310 a.u. as depicted in figure–4.3.3(a) and the numerically estimated DOS at the corresponding energies are plotted in figure–4.3.3(b). The figure–4.3.3(b) shows a peak of the DOS right at the center of the platue (following the red line) which locates the resonance energy position. As one root may produce plateau at different energies, corresponding peaks of DOS will occur at those points. The DOS peaks of root no. 13

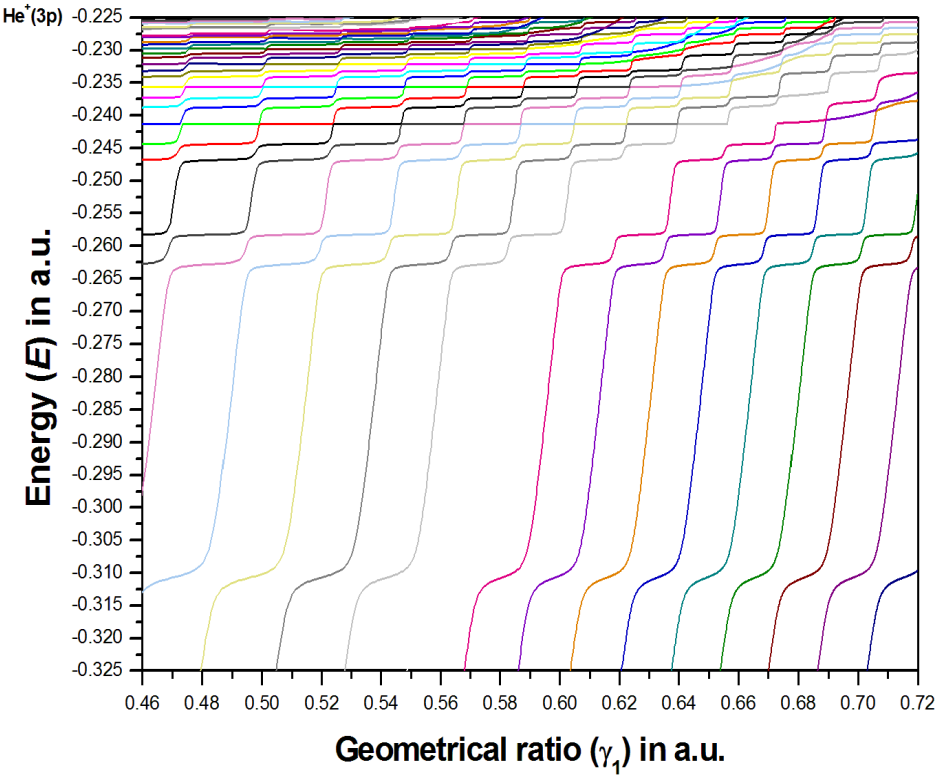

Figure 4.3.2: Enlarged view of stabilization diagram for $^3F^e$ states of He atom in the energy range -0.325 a.u. to -0.225 a.u. which shows several resonance states below $He^+(3p)$ threshold.

in the full range of energy is given in figure (4.3.4). It clearly shows three peaks at three different energies for first three resonances. It is also evident that the resonances are isolated as the separation of peaks are greater than the widths of the consecutive resonances. The next part is to consider DOS of each isolated resonance and to fit it with Lorentzian profile [equation (3.2.77)] to extract the desired position and width of the resonance in energy scale. As an example, the estimated DOSs [hollow black circles] and the fitted Lorentzian [red lines] for the second and third resonances (figure–4.3.4) of root no. 13 are shown in figure (4.3.5). The fitting to the first curve yields resonance position E_r at -0.26284 a.u. and width $\Gamma = 0.00045$ a.u. Similar fitting for the second curve yields resonance position E_r at -0.25826 a.u. and width $\Gamma = 0.00017$ a.u. Repeated calculations of DOS near the flat plateau of each of the eigenroots for the resonance state and subsequent Lorentzians are carried out for a particular resonance. The position and width of a particular resonance state is chosen with respect to the best fitting parameters, as discussed in section (3.2.5).

In table (4.3.8), the convergence behavior of first twelve $^3F^e$ resonance states below

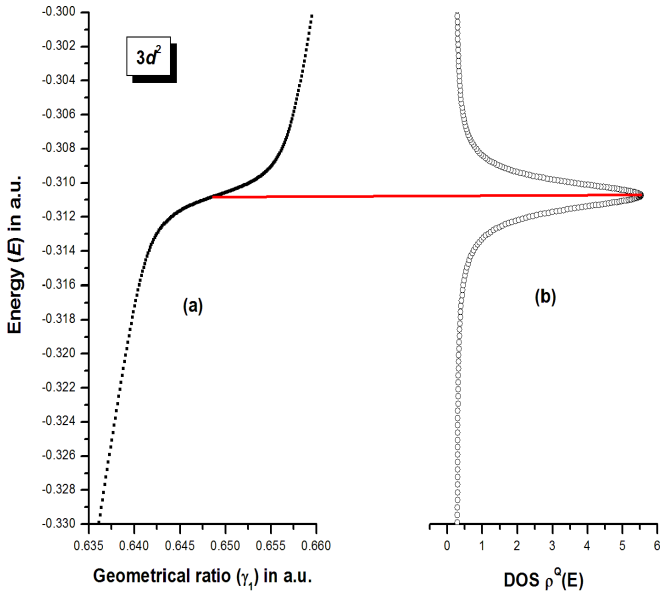

Figure 4.3.3: Plot of DOS corresponding to lowest platue of eigen root no. 13 of $^3F^e$ state of He-atom.

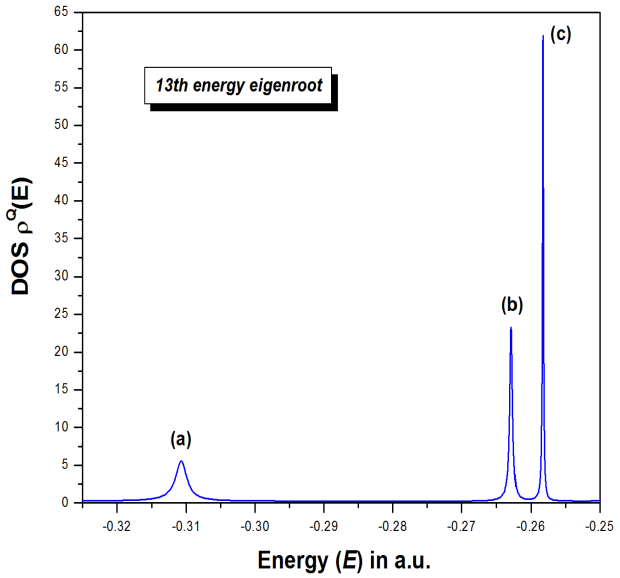

Figure 4.3.4: Plot of DOS in the full energy range of eigen root no. 13 of $^3F^e$ state of He-atom below $He^+(3p)$ threshold.

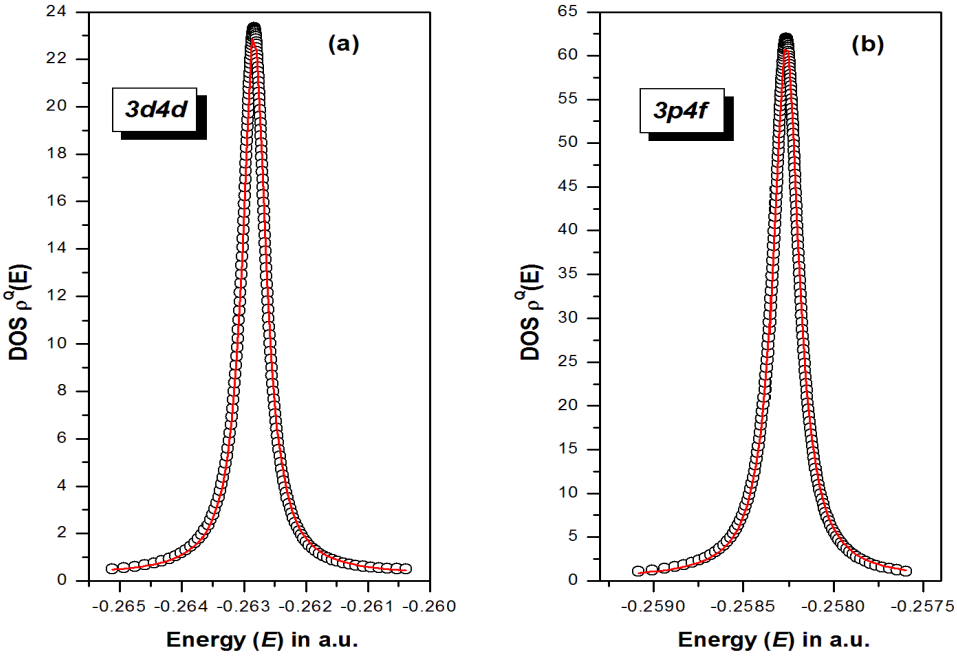

Figure 4.3.5: Plot of DOSs of second and third resonance states originated from energy eigenroot no. 13 of ${}^3\mathrm{F}^e$ state of He atom below $\mathrm{He}^+(3p)$ threshold.

$\mathrm{He}^+(3p)$ threshold are shown.

Table 4.3.8: Convergence behavior for the position ($-E_r$ in a.u.) and width (Γ in a.u.) of ${}^3\mathrm{F}^e$ resonance states below $\mathrm{He}^+(3p)$ threshold. The notation $P[\pm Q]$ stands for $P \times 10^{\pm Q}$.

State	N	$-E_r$	Γ
1	900	0.31077	1.98 [-3]
	1530	0.31075	1.98 [-3]
2	900	0.26284	4.5 [-4]
	1530	0.26284	4.5 [-4]
3	900	0.25827	1.7 [-4]
	1530	0.25826	1.7 [-4]
4	900	0.24681	2.1 [-4]
	1530	0.24680	2.4 [-4]
5	900	0.24439	1.1 [-4]
	1530	0.24438	1.2 [-4]
6	900	0.24130	8.5 [-9]
	1530	0.24130	6.9 [-11]
7	900	0.23871	1.2 [-4]
	1530	0.23871	1.1 [-4]
8	900	0.23730	7.0 [-5]
	1530	0.23730	7.0 [-5]

Continuation of Table (4.3.8)

State	N	$-E_r$	Γ
9	900	0.23559	5.3 [-11]
	1530	0.23560	3.1 [-12]
10	900	0.23403	8.0 [-5]
	1530	0.23404	6.0 [-5]
11	900	0.23315	4.0 [-5]
	1530	0.23315	4.0 [-5]
12	900	0.23207	5.8 [-9]
	1530	0.23210	5.6 [-10]

It is clear from table (4.3.8) that the values of resonance parameters (E_r, Γ) are converged upto at least 4th decimal place when the numbers of terms (N) in the wavefunction are increased from 900 to 1530. Resonance energy (E_r) and width (Γ) of first 19 number of $^3F^e$ states below $He^+(3p)$ threshold using 1530 terms in the Hylleraas basis set are summarized in table (4.3.9).

Table 4.3.9: Positions ($-E_r$ in a.u.), widths (Γ in a.u.), effective quantum number (n^*), the energy gap between the threshold and resonance energy values (ϵ_r), relative energies (R_ϵ) and relative widths (R_Γ) of resonance states of ($^3F^e$) below $He^+(3p)$ threshold. Present results are compared with the available theoretical estimates. The notation $P[\pm Q]$ stands for $P \times 10^{\pm Q}$.

Class	States	$-E_r$	Γ	n^*	ϵ_r	R_ϵ	R_Γ	Other works	
								$-E_r$	Γ
A	1	0.31075	1.98 [-3]	2.37654	0.08853			0.31069[a]	1.98 [-3][a]
								0.3111[b]	2.131 [-3][b]
								0.310725[c]	1.95 [-3][c]
								0.309915[d]	
								0.310749[e]	
	2	0.26284	4.5 [-4]	3.50854	0.04062	2.18	4.40	0.262825[a]	4.5 [-4][a]
								0.2628[b]	4.77 [-4][b]
								0.26283[c]	4.4 [-4][c]
								0.26264[d]	
								0.262598[e]	
	3	0.24680	2.4 [-4]	4.51039	0.02458	1.65	1.87	0.246805[a]	2.1 [-4][a]
								0.2468[b]	2.27 [-4][b]
								0.246715[e]	
								0.246653[d]	
	4	0.23871	1.1 [-4]	5.50686	0.01649	1.49	2.18	0.238705[a]	1.1 [-4][a]
								0.238645[d]	
								0.238597[e]	
	5	0.23404	6.0 [-5]	6.50455	0.01182	1.39	1.83	0.234035[a]	6.6 [-5][a]
								0.233963[e]	
	6	0.23110	4.0 [-5]	7.50469	0.00878	1.34	1.50		

Continuation of Table (4.3.9)

Class	States	$-E_r$	Γ	n^*	ϵ_r	R_ϵ	R_Γ	Other works	
								$-E_r$	Γ
	7	0.22914	3.0 [-5]	8.50162	0.00692	1.26	1.33		
	8	0.22754	7.0 [-5]	9.69661	0.00532	1.30	0.42		
B	1	0.25826	1.7 [-4]	3.72483	0.03604			0.25826[a]	1.68 [-4][a]
								0.2583[b]	1.83 [-4][b]
								0.258275[c]	1.5 [-4][c]
								0.258205[d]	
								0.258199[e]	
	2	0.24438	1.2 [-4]	4.75031	0.02216	1.62	1.42	0.244385[a]	1.1 [-4][a]
								0.2444[b]	1.14 [-4][b]
								0.244345[d]	
								0.244341[e]	
	3	0.23730	7.0 [-5]	5.75859	0.01508	1.47	1.71	0.237295[a]	6.6 [-5][a]
								0.237265[d]	
								0.237255[e]	
	4	0.23315	4.0 [-5]	6.76424	0.01093	1.38	1.75	0.233155[a]	
								0.233113[e]	
	5	0.23051	3.0 [-5]	7.76723	0.00829	1.32	1.34		
	6	0.22885	1.7 [-4]	8.68562	0.00663	1.25	0.18		
C	1	0.24130	6.9 [-11]	5.11942	0.01908			0.2413[a]	
								0.2413[b]	1.61 [-11][b]
								0.24124[d]	
								0.241293[e]	
	2	0.23560	3.1 [-12]	6.11354	0.01338	1.43	22.26	0.2356[a]	
								0.235535[d]	
								0.235563[e]	
	3	0.23211	5.6 [-10]	7.11468	0.00988	1.35	0.01	0.2321[a]	
	4	0.22982	4.3 [-9]	8.11226	0.00759	1.31	0.13		
	5	0.22824	1.9 [-8]	9.14566	0.00598	1.27	0.23		

[a] [283], [b] [284], [c] [285], [d] [286], [e] [281]

The present calculated resonance parameters are compared with the results available in the literature [281, 283–286]. The comparison shows excellent agreement between the present resonance parameters below $He^+(3p)$ threshold with other works. Moreover, it has been found that the effect of the inclusion of dd configurations varies from 14% to 3% for the energy positions of first six resonances. For instance, the energy position of the first resonance below $He^+(3p)$ threshold excluding dd configurations is –0.26607 a.u. (table 4.3.3) while the same using the mixed (pf and dd) wavefunction (equation 4.2.1) is –0.31077 a.u. (table 4.3.9). The resonance energy of $3p4f(^3F^e)$ state lies above the $3d^2(^3F^e)$ state, and

for this reason, we may infer that it is not possible to include dd configuration by just increasing the powers of r_{12} in the pf configuration. This insight will be useful while calculating the resonance parameters of such higher symmetry states in future. It is worthwhile to mention that Ho and Bhatia [36] constructed the general D^o wavefunction as a combination of pd and df configurations and opined that such mixing is necessary to facilitate better convergence of energy of metastable bound $2pnd$ states. However, Bhattacharyya *et. al.* [287] showed that sufficient accuracy of the enery eigenvalues of $2pnd$ states may be achieved by considering only pd configurations. Moreover it appears from the calculation of Saha *et. al.* [288] that the parameters of the resonances of D^o below $He^+(3p)$ threshold estimated using only pd configurations are more or less in agreement with those estimated using general D^o wavefunction of Ho and Bhatia [36]. Thus in contrast to the D^o states, the mixing of pf and dd configurations in the F^e wavefunction (4.2.1) not only leads to the better convergence of the metastable bound states, but also extremely necessary to get a complete picture about the accurate structure of resonance states above $He^+(2p)$ threshold for the even parity F state of He atom.

As the individual angular momenta do not commute with the two-electron Hamiltonian, the labels denoting them may only act as an indicator of the dominant contributions to various excited states. The $^3F^e$ resonances below $He^+(3p)$ threshold can arise from three possible dominant configurations: $3dnd$ $[n \geq 3]$, $3pnf$ $[n \geq 4]$ and $3dng$ $[n \geq 5]$. Bachau *et. al.* [284] estimated the percentage contribution of the major configurations to few lower lying resonances of this symmetry by projecting the closed channel wavefunction expanded in hydrogenic basis. The resonances estimated in the present work are categorized in three classes as A, B and C for the dominant configurations $3dnd$ $[n \geq 3]$, $3pnf$ $[n \geq 4]$ and $3dng$ $[n \geq 5]$ respectively by comparing with the previous results [283, 284]. Such classification are supported by systematic estimation of the following parameters:

i. Effective quantum number (n^*), given in equation (4.3.1).

ii. Energy difference, $[\epsilon_r(n) = E_{th} - E_r$, between the threshold energy (E_{th}) and the estimated resonance energy (E_r) of $n-$th resonance state.

iii. Energy difference ratio $R_\epsilon = \dfrac{\epsilon_r(n-1)}{\epsilon_r(n)}$.

iv. Width ratio $R_\Gamma = \dfrac{\Gamma(n-1)}{\Gamma(n)}$, $\Gamma(n)$ being the width of $n-$th resonance state.

It is noticeable that

1. For $3dnd$ $[n \geq 3]$ (class A) and $3pnf$ $[n \geq 4]$ (class B) states, $n^* < n$, while for $3dng$ $[n \geq 5]$ (class C) states, $n^* > n$.

2. In general, the resonances of class A are broader than class B for the same outer electron principle quantum number (n). The width of the resonance states gradually

decreases for higher excited states for both class A and class B. The present method determines extremely narrow width of the class C resonances. In fact, Kar and Ho [283] also reported the positions of first three dg resonances without any estimate of widths. The only estimate of width of the $3d5g$ state is of the order of nano–eV [284]. Thus the higher members of the dg series should have much lesser width making its determination extremely challenging.

3. As the dg resonances (class C) show apparently very feeble width, these states may de-excite to lower lying $3d4f$ ($^3\mathrm{D}^o$) states via dipole transition. We, therefore, predict the transition energies of 269 meV, 424 meV, 519 meV, 606 meV and 625 meV corresponding to the transition $3dng(^3\mathrm{F}^e) \rightarrow 3d4f(^3\mathrm{D}^o)$ $[n = 5 - 9]$ respectively. The energy eigenvalue of the $3d4f(^3\mathrm{D}^o)$ state is taken as -0.25118 a.u. [288]. The conversion factor $1a.u. = 27.21138$ eV has been used [289].

4. For the $3dnd$ (class A) and $3pnf$ (class B) states, although the effective quantum numbers and R_ϵ shows more or less a systematic pattern (gradual decrements for higher excited states), R_Γ shows an irregularity for few states as is evident from table (4.3.9). Such inconsistency for R_Γ may be resolved with more accurate parameters calculated with larger number of terms in the basis set. This kind of analysis based on R_ϵ and R_Γ was done earlier by Bylicki *et. al.* [290, 291] in case of high–lying $^1\mathrm{S}^e$, $^1\mathrm{P}^o$, $^1\mathrm{D}^e$, $^1\mathrm{D}^o$ and $^1\mathrm{F}^e$ resonances of negative hydrogen ion.

The expectation values of repulsive potential $\langle V_r \rangle$, attractive potential $\langle -V_a \rangle$, their ratio $\eta = \dfrac{\langle V_r \rangle}{\langle -V_a \rangle}$, $< \theta_{12} >$, $\langle r_1 \rangle$, $\langle r_1^2 \rangle$, $\langle r_{12} \rangle$ and $\langle r_{12}^2 \rangle$ for different $^3\mathrm{F}^e$ resonances states of He below $\mathrm{He}^+(3p)$ threshold are listed in table (4.3.10). For this purpose, we have to construct the resonance wavefunction appropriately. We have chosen γ_1 value for a particular energy eigenroot at which the corresponding spectral DOS reaches its maxima. The finding on the expectations are as follows:

1. Table (4.3.10) shows that for each class of states, η gradually decreases as the resonance states come closer to the $\mathrm{He}^+(3p)$ threshold. Thus the repulsive part of the potential decreases in comparison to the attractive part of the potential. For instance, in case of class A, $\eta \sim 15\%$ for the first state and $\eta \sim 2.5\%$ for the eighth state. Similarly for class B, $\eta \sim 11.2\%$ for the first state and $\eta \sim 3.3\%$ for the sixth state. This in turn supports the fact of gradual decreasing nature of width of the resonances.

2. On the other hand $\langle r_1 \rangle$ and $\langle r_{12} \rangle$ increases for the energetically higher excited states for each class of states. It shows that the system becomes more and more diffuse for higher excited states, in fact it appears that the electrons are moving away from each other as well as from the nucleus.

Table 4.3.10: The expectation values of repulsive potential $\langle V_r \rangle$, attractive potential $\langle -V_a \rangle$ [their ratio $\eta = \frac{\langle V_r \rangle}{\langle -V_a \rangle}$], inter-electronic angles $< \theta_{12} >$(in degree) and different one and two-particle moments *e.g.* $\langle r_1 \rangle$, $\langle r_1^2 \rangle$, $\langle r_{12} \rangle$, $\langle r_{12}^2 \rangle$ for different $^3\mathrm{F}^e$ resonances states of He below $\mathrm{He}^+(3p)$ threshold. The notation $P[\pm Q]$ stands for $P \times 10^{\pm Q}$. All values are given in atomic units.

Class	States	$\langle V_r \rangle$	$\langle -V_a \rangle$	η	$\langle r_1 \rangle$	$\langle r_1^2 \rangle$	$\langle r_{12} \rangle$	$\langle r_{12}^2 \rangle$	$\langle \theta_{12} \rangle$
A	1	1.10 [-1]	7.54 [-1]	1.46 [-1]	6.84 [+0]	6.56 [+1]	1.08 [+1]	1.46 [+2]	97.776
	2	6.67 [-2]	5.98 [-1]	1.12 [-1]	1.07 [+1]	1.61 [+2]	1.83 [+1]	3.77 [+2]	103.335
	3	4.34 [-2]	5.39 [-1]	8.03 [-2]	1.65 [+1]	4.39 [+2]	2.94 [+1]	9.73 [+2]	104.469
	4	2.99 [-2]	5.09 [-1]	5.88 [-2]	2.39 [+1]	1.02 [+3]	4.42 [+1]	2.19 [+3]	105.469
	5	2.18 [-2]	4.91 [-1]	4.44 [-2]	3.28 [+1]	2.05 [+3]	6.21 [+1]	4.32 [+3]	105.932
	6	1.66 [-2]	4.79 [-1]	3.46 [-2]	4.33 [+1]	3.69 [+3]	8.30 [+1]	7.71 [+3]	106.243
	7	1.30 [-2]	4.72 [-1]	2.76 [-2]	5.54 [+1]	6.19 [+3]	1.07 [+2]	1.28 [+4]	106.413
	8	1.11 [-2]	4.68 [-1]	2.37 [-2]	6.97 [+1]	1.03 [+4]	1.34 [+2]	2.05 [+4]	89.384
B	1	6.50 [-2]	5.84 [-1]	1.11 [-1]	1.11 [+1]	1.71 [+2]	1.74 [+1]	3.34 [+2]	89.435
	2	4.12 [-2]	5.31 [-1]	7.76 [-2]	1.75 [+1]	5.05 [+2]	2.97 [+1]	9.93 [+2]	88.397
	3	2.85 [-2]	5.04 [-1]	5.66 [-2]	2.53 [+1]	1.17 [+3]	4.53 [+1]	2.31 [+3]	87.902
	4	2.09 [-2]	4.88 [-1]	4.28 [-2]	3.48 [+1]	2.33 [+3]	6.41 [+1]	4.61 [+3]	87.667
	5	1.59 [-2]	4.77 [-1]	3.34 [-2]	4.57 [+1]	4.16 [+3]	8.58 [+1]	8.27 [+3]	87.424
	6	1.63 [-2]	4.78 [-1]	3.41 [-2]	5.34 [+1]	6.16 [+3]	1.02 [+2]	1.23 [+4]	90.249
C	1	4.07 [-2]	5.24 [-1]	7.77 [-2]	1.67 [+1]	4.45 [+2]	2.73 [+1]	8.17 [+2]	79.635
	2	2.83 [-2]	4.99 [-1]	5.65 [-2]	2.51 [+1]	1.14 [+3]	4.37 [+1]	2.16 [+3]	78.277
	3	2.06 [-2]	4.85 [-1]	4.26 [-2]	3.52 [+1]	2.41 [+3]	6.37 [+1]	4.62 [+3]	77.478
	4	1.58 [-2]	4.75 [-1]	3.31 [-2]	4.68 [+1]	4.42 [+3]	8.68 [+1]	8.56 [+3]	77.139
	5	1.26 [-2]	4.69 [-1]	2.68 [-2]	5.99 [+1]	7.46 [+3]	1.13 [+2]	1.46 [+4]	76.877

3. From the last column of the table (4.3.10), it can be seen that the inter-electronic angle $< \theta_{12} >$ increases for the upper excited states of class A, while it decreases for the upper excited states of class B and class C. To be specific, $< \theta_{12} >$ varies in the range 97^0 to 106^0, 89^0 to 87^0 and 79^0 to 76^0 for class A, class B and class C states respectively.

Thus along with the quantities n^*, ϵ_k, R_ϵ and R_Γ as mentioned in table (4.3.9), the properties listed in table (4.3.10) are also significant for classification of the resonance states below $\mathrm{He}^+(3p)$ threshold.

Let us now consider the resonance states above $\mathrm{He}^+(3p)$ threshold. A portion of the stabilization diagram in the energy range -0.225 a.u. to -0.125 a.u. *i.e.* lying between $\mathrm{He}^+(3p)$ and $\mathrm{He}^+(4p)$ thresholds is depicted in figure (4.3.6). Figure (4.3.6) clearly reveals that presence of several resonances in this energy regime. Resonance energy (E_r) and width (Γ) of first thirty $^3\mathrm{F}^e$ resonance states below $\mathrm{He}^+(4p)$ threshold are summarized in table (4.3.11). The $^3\mathrm{F}^e$ resonances below $\mathrm{He}^+(4p)$ threshold can arise from $4dnd$ [$n \geq 4$], $4pnf$ [$n \geq 4$], $4fnf$ [$n \geq 4$], $4dng$ [$n \geq 5$] and $4fnh$ [$n \geq 6$] dominant configurations. Different structural parameters like n^*, $\langle V_r \rangle$, $\langle -V_a \rangle$, $\eta = \dfrac{\langle V_r \rangle}{\langle -V_a \rangle}$, $< \theta_{12} >$, $\langle r_1 \rangle$, $\langle r_1^2 \rangle$, $\langle r_{12} \rangle$ and $\langle r_{12}^2 \rangle$ of the respective resonance states are also given in table (4.3.11) with a view to classifying them according to the dominant configurations. In contrast to the resonance states below $\mathrm{He}^+(3p)$, any systemic trend of the structural parameters are hardly found for

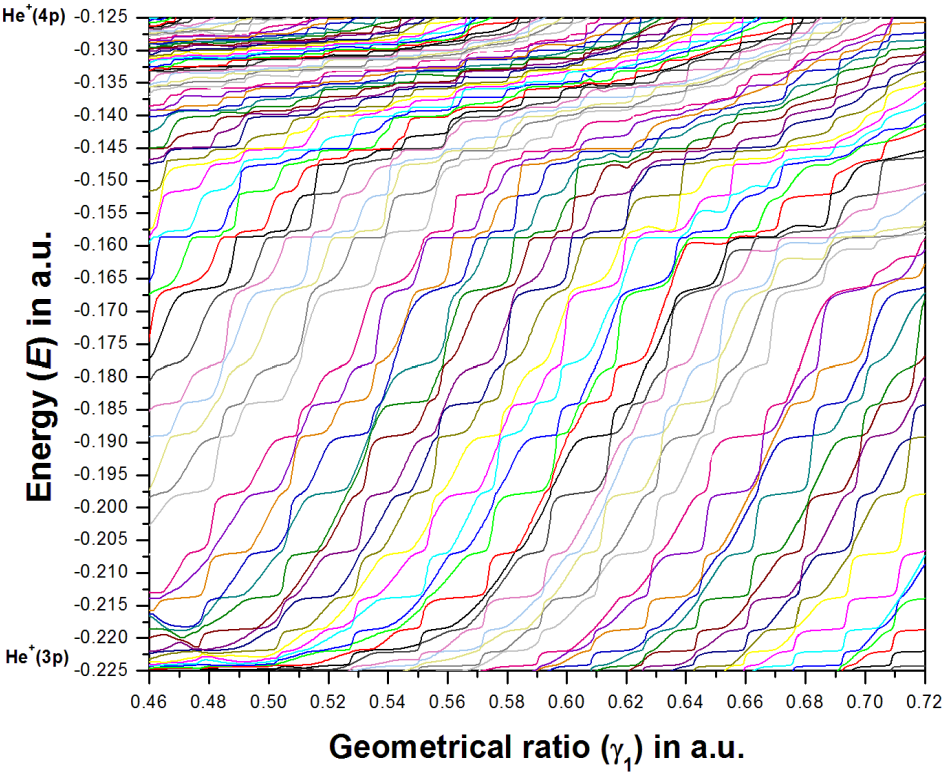

Figure 4.3.6: Stabilization plot for $^3F^e$ states of He atom in the energy range -0.225 a.u. to -0.125 a.u. showing a series of resonance states below $He^+(4p)$ threshold.

the resonance states below $He^+(4p)$ threshold. Thus we have listed the resonances according to their energy values (from lower to higher), without classifying them on the basis of the dominant configurations. The Resonance energies (E_r) and widths (Γ) of the resonance states lying between $He^+(4p-7p)$ thresholds are given in table (4.3.12).

Table 4.3.12: Positions ($-E_r$ in a.u.), widths (Γ in a.u.), effective quantum number (n^*) for different $^3F^e$ resonances states of He below $He^+(5p)$, $He^+(6p)$ and $He^+(7p)$ threshold. The notation $P[\pm Q]$ stands for $P \times 10^{\pm Q}$. All values are given in atomic units.

	Below $He^+(5p)$			Below $He^+(6p)$			Below $He^+(7p)$		
States	$-E_r$	Γ	n^*	$-E_r$	Γ	n^*	$-E_r$	Γ	n^*
1	0.12385	6.2 [-5]	3.37676	0.07941	6.0 [-5]	4.57825	0.05346	2.5 [-4]	6.28851
2	0.12187	1.5 [-5]	3.45568	0.07723	4.3 [-4]	4.80298	0.05297	2.6 [-4]	6.41403
3	0.12058	2.3 [-4]	3.51017	0.07604	3.8 [-4]	4.94052	0.05104	3.3 [-4]	6.99328
4	0.11920	3.8 [-4]	3.57142	0.07557	1.3 [-4]	4.99819	0.05082	3.8 [-4]	7.06976
5	0.11898	2.5 [-4]	3.58149	0.07445	3.0 [-4]	5.14420	0.05024	1.0 [-4]	7.28408
6	0.11760	5.1 [-4]	3.64662	0.07292	2.8 [-4]	5.36604	0.05005	1.4 [-4]	7.35864

Continuation of Table (4.3.12)

	Below $He^+(5p)$			Below $He^+(6p)$			Below $He^+(7p)$		
States	$-E_r$	Γ	n^*	$-E_r$	Γ	n^*	$-E_r$	Γ	n^*
7	0.11656	6.5 [-4]	3.69812	0.07175	7.1 [-4]	5.55650	0.04859	1.2 [-4]	8.01995
8	0.11427	6.7 [-5]	3.81968	0.06709	7.4 [-4]	6.58395	0.04686	1.5 [-4]	9.09566
9	0.11312	6.7 [-4]	3.88543	0.06686	3.0 [-4]	6.65059	0.04516	1.6 [-4]	10.72893
10	0.11224	3.5 [-4]	3.93810	0.06494	2.1 [-4]	7.29929	0.04290	1.7 [-4]	15.49066
11	0.11085	5.5 [-4]	4.02584	0.06438	2.9 [-4]	7.52733			
12	0.10926	7.0 [-4]	4.13378	0.06263	1.3 [-4]	8.40695			
13	0.10822	1.3 [-4]	4.20926	0.06228	2.6 [-4]	8.62296			
14	0.10638	1.2 [-4]	4.35359	0.06139	8.0 [-5]	9.25731			
15	0.10539	2.6 [-4]	4.43765	0.06007	5.2 [-4]	10.52404			
16	0.10394	2.6 [-4]	4.57007	0.05819	7.0 [-4]	13.77655			
17	0.10227	2.0 [-4]	4.73832	0.05717	3.6 [-4]	17.59841			
18	0.10191	2.2 [-4]	4.77709	0.05564	1.2 [-4]	76.94837			
19	0.10008	8.4 [-5]	4.99002						
20	0.09803	2.1 [-4]	5.26651						
21	0.09753	8.8 [-5]	5.34064						
22	0.09572	2.5 [-4]	5.63901						
23	0.09285	2.0 [-4]	6.23831						
24	0.09044	3.3 [-4]	6.91880						
25	0.08871	1.4 [-4]	7.57706						
26	0.08775	8.7 [-5]	8.03167						
27	0.08691	1.1 [-4]	8.50578						
28	0.085845	6.8 [-5]	9.24895						
29	0.085052	1.2 [-4]	9.94840						
30	0.084614	1.9 [-4]	10.40989						
31	0.083472	7.6 [-5]	12.00038						
32	0.082917	1.4 [-4]	13.09232						
33	0.08171	2.1 [-4]	17.09963						

So far, we have studied resonance parameters and different expectation values of $^3F^e$ states of free He atom. To get a proper visualization of the resonance states, we estimate the two particle radial probability density $\rho(r_1, r_2)$. As an example, we discuss the classes of states A, B and C in this light. Two particle radial probability density is defined as

$$\rho(r_1, r_2) = \int_{r_{12}=|r_1 \sim r_2|}^{r_1+r_2} r_{12} dr_{12} \int_{\theta=0}^{\pi} \int_{\phi=0}^{2\pi} \int_{\psi=0}^{2\pi} |\Psi|^2 \sin\theta d\theta d\phi d\psi \tag{4.3.3}$$

Ψ is defined in equation (4.2.16). For the $^3F^e$ resonance states of He having configurations $3d^2$ (class A), $3p4f$ (class B) and $3d5g$ (class C) lying below $He^+(3p)$ threshold, $\rho(r_1, r_2)$ are plotted in figure (4.3.7). The density plot for $3d^2$ configuration exhibits similar behavior as the two-electron ground state [292] showing a maximum along the symmetry line $r_1 = r_2$.

Table 4.3.11: Positions ($-E_r$ in a.u.), widths (Γ in a.u.), effective quantum number (n^*), the ratio between expectation values of repulsive potential $\langle V_r \rangle$, attractive potential $\langle -V_a \rangle$ [$\eta = \dfrac{\langle V_r \rangle}{\langle -V_a \rangle}$], inter-electronic angles $< \theta_{12} >$(in degree) and different one and two-particle moments *e.g.* $\langle r_1 \rangle$, $\langle r_1^2 \rangle$, $\langle r_{12} \rangle$, $\langle r_{12}^2 \rangle$ for different $^3\mathrm{F}^e$ resonances states of He below $\mathrm{He}^+(4p)$ threshold. The notation $P[\pm Q]$ stands for $P \times 10^{\pm Q}$. All values are given in atomic units.

States	$-E_r$	Γ	n^*	η	$\langle r_1 \rangle$	$\langle r_1^2 \rangle$	$\langle r_{12} \rangle$	$\langle r_{12}^2 \rangle$	$\langle \theta_{12} \rangle$
1	0.22207	1.8 [-4]	2.26956	3.28 [-2]	5.73 [+1]	7.72 [+3]	1.09 [+2]	1.54 [+4]	89.085
2	0.2187	2.1 [-4]	2.31001	4.02 [-2]	4.76 [+1]	5.47 [+3]	9.02 [+1]	1.09 [+4]	89.448
3	0.21389	3.1 [-4]	2.37169	4.76 [-2]	4.02 [+1]	3.98 [+3]	7.56 [+1]	7.96 [+3]	90.454
4	0.20705	3.7 [-4]	2.46857	5.50 [-2]	3.40 [+1]	2.91 [+3]	6.29 [+1]	5.79 [+3]	88.530
5	0.19788	5.3 [-4]	2.61927	6.33 [-2]	2.92 [+1]	2.19 [+3]	5.34 [+1]	4.38 [+3]	89.512
6	0.18903	5.4 [-4]	2.79443	1.04 [-1]	1.67 [+1]	7.45 [+2]	2.95 [+1]	1.58 [+3]	104.178
7	0.18404	2.4 [-4]	2.91012	8.64 [-2]	2.21 [+1]	1.33 [+3]	3.96 [+1]	2.68 [+3]	94.377
8	0.17834	1.2 [-3]	3.06167	1.27 [-1]	1.49 [+1]	5.32 [+2]	2.39 [+1]	1.07 [+3]	91.943
9	0.16668	9.2 [-4]	3.46354	9.77 [-2]	1.99 [+1]	1.06 [+3]	3.42 [+1]	2.11 [+3]	89.631
10	0.15878	6.0 [-5]	3.84729	1.10 [-1]	1.82 [+1]	6.79 [+2]	3.06 [+1]	1.45 [+3]	100.183
11	0.15778	2.6 [-4]	3.90553	1.07 [-1]	1.79 [+1]	5.09 [+2]	3.15 [+1]	1.23 [+3]	110.336
12	0.15224	5.9 [-4]	4.28431	1.08 [-1]	2.04 [+1]	8.34 [+2]	3.34 [+1]	1.67 [+3]	90.229
13	0.1476	3.0 [-4]	4.70360	1.24 [-1]	1.81 [+1]	4.57 [+2]	2.83 [+1]	9.18 [+2]	90.594
14	0.14685	1.2 [-4]	4.78364	1.02 [-1]	2.21 [+1]	9.99 [+2]	3.76 [+1]	2.05 [+3]	93.799
15	0.1455	4.0 [-5]	4.93864	9.21 [-2]	2.24 [+1]	7.48 [+2]	3.88 [+1]	1.70 [+3]	103.584
16	0.14514	9.0 [-5]	4.98259	1.19 [-1]	1.93 [+1]	5.33 [+2]	2.93 [+1]	1.01 [+3]	85.276
17	0.1434	5.0 [-4]	5.21286	9.03 [-1]	2.19 [+1]	1.01 [+3]	3.82 [+1]	2.11 [+3]	95.959
18	0.14075	4.4 [-4]	5.63436	9.13 [-2]	2.55 [+1]	1.08 [+3]	4.30 [+1]	2.21 [+3]	92.365
19	0.13998	2.4 [-4]	5.77735	9.49 [-2]	2.58 [+1]	1.06 [+3]	4.26 [+1]	2.08 [+3]	88.699
20	0.13925	1.7 [-4]	5.92348	7.72 [-2]	2.97 [+1]	1.47 [+3]	5.40 [+1]	3.35 [+3]	109.571
21	0.13877	3.6 [-4]	6.02584	8.38 [-2]	2.80 [+1]	1.31 [+3]	4.88 [+1]	2.79 [+3]	97.637
22	0.13747	9.0 [-5]	6.33215	7.27 [-2]	3.48 [+1]	2.48 [+3]	6.18 [+1]	4.91 [+3]	88.794
23	0.13564	5.0 [-5]	6.85510	5.97 [-2]	3.97 [+1]	2.75 [+3]	7.47 [+1]	6.24 [+3]	115.556
25	0.13314	8.0 [-5]	7.83741	6.02 [-2]	4.52 [+1]	3.91 [+3]	8.15 [+1]	7.88 [+3]	92.945
26	0.13154	1.0 [-4]	8.74371	5.39 [-2]	5.54 [+1]	6.14 [+3]	1.01 [+2]	1.23 [+4]	89.327
27	0.13032	2.0 [-4]	9.69458	5.54 [-2]	6.19 [+1]	8.14 [+3]	1.14 [+2]	1.63 [+4]	88.458
28	0.12878	2.9 [-4]	11.50109	4.97 [-2]	7.26 [+1]	1.16 [+4]	1.35 [+2]	2.32 [+4]	89.766
29	0.12766	2.1 [-4]	13.71021	4.86 [-2]	7.24 [+1]	1.18 [+4]	1.35 [+2]	2.35 [+4]	88.858
30	0.12588	1.8 [-4]	23.83656	5.90 [-2]	5.76 [+1]	8.03 [+3]	1.07 [+2]	1.62 [+4]	96.553

In contrast, the density plot for $3p4f$ configuration exhibits a lesser probability density along the symmetry line. In fact the maximum probability density appears at two different regions on the either sides of the symmetry line. In case of $3d5g$ state the probability density vanishes along the symmetry line and therefore two distinct regions having finite probability density are observed. Thus the structures of two particle radial probability densities for three classes of states below $\mathrm{He}^+(3p)$ are quite distinct.

4.3.2 Structural properties under classical weakly coupled plasma

For the investigation on the effect of classical weakly coupled plasma (WCP) on the metastable bound $2pnf(n = 4-6)$ $^{1,3}\mathrm{F}^e$ states of two electron systems– He, Li^+ and Be^{2+}, the effective potential is modeled by exponential screened Coulomb potential (ESCP) as given in equation (3.3.1). In the begining, we start with only the pf part in the wavefunction (4.2.16). The wavefunction is expanded in nine–exponent ($p_1 = 9$) Hylleraas basis set. The energy

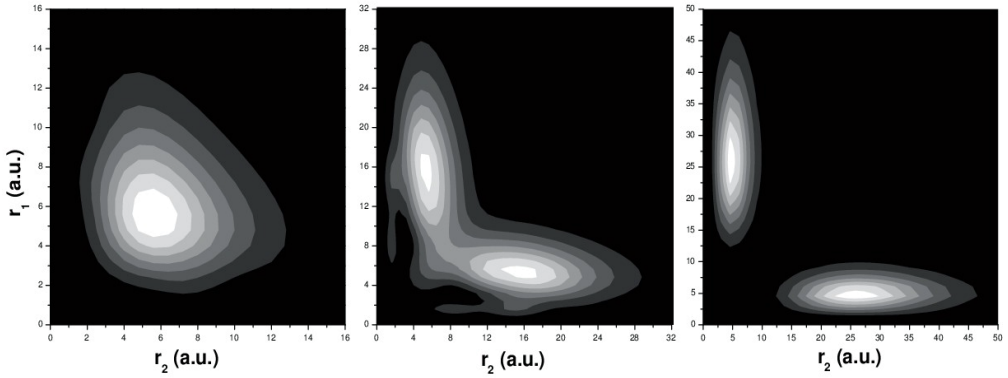

Figure 4.3.7: Two particle radial probability density $\rho(r_1, r_2)$ for three $^3\mathrm{F}^e$ resonance states of He atom with the dominant $3d^2$ (left), $3p4f$ (middle) and $3d5g$ (right) configurations.

eigenvalues of $2pnf(n = 4 - 6)$ $^{1,3}\mathrm{F}^e$ states of He atom for $N_1 = 675$ are given in the table (4.3.13) for different values of plasma screening length λ_D (1.0.2) ranging from 100 a.u. to 10 a.u. The present estimated energy eigenvalues are compared with some data available in literature [240,283]. The comparison reveals that except for the $2p4f$ state at $\lambda_D = 100$ a.u., the calculated energy eigenvalues are lowest yet obtained which establishes the efficiency of the present method as well as the completeness of the wavefunction only on pf–part in case of metastable bound $^{1,3}\mathrm{F}^e$ states. The last two columns of table (4.3.13) show the energy eigenvalues of $2s$ and $2p$ states of He^+ for the whole range of λ_D. The energy eigenvalues of $2s$ and $2p$ are calculated by solving the variational equation of one-electron systems given by

$$\delta \int \left\{ \left(\frac{\partial f}{\partial r} \right)^2 + \frac{l(l+1)}{r^2} - E + Z \frac{e^{-\frac{r}{\lambda_D}}}{r} \right\} dr = 0 \tag{4.3.4}$$

'l' being the angular momentum of the one-electron state. The radial function $f(r)$ is expanded in terms of exponential basis set as

$$f(r) = \sum_i C_i e^{-\rho_i r} \tag{4.3.5}$$

We have used 101 ($i = 100$) terms in the basis set and the exponents are taken in a geometrical sequence $\rho_i = \rho_{i-1}\gamma$, γ is the geometrical ratio. The energy eigenvalues (E) are determined by solving the generalized eigenvalue equation (3.2.59). It is found from table (4.3.13) that $2s$ and $2p$ energies are different from each other for each λ_D which is a direct consequence of non-Coulomb central potential (3.3.1) and the $2s$ state remains more bound

Table 4.3.13: Variation of energy eigenvalues ($-E$ in a.u.) for the $2pnf[n = 4-6]$ $^{1,3}\mathrm{F}^e$ states of He and $2s$, $2p$ states of He^+ with respect to the screening length λ_D (a.u.).

	$^1\mathrm{F}^e$			$^3\mathrm{F}^e$				
λ_D	$2p4f$	$2p5f$	$2p6f$	$2p4f$	$2p5f$	$2p6f$	$\mathrm{He}^+(2s)$	$\mathrm{He}^+(2p)$
100	0.503055	0.492022	0.486401	0.503047	0.492017	0.486397	0.480296	0.480247
	0.502956[a]	0.491928[a]	0.4863145[a]	0.502952[a]	0.4919255[a]	0.486313[a]		
	0.50306068[b]			0.503052113[b]				
90	0.499965	0.489058	0.483572	0.499957	0.489052	0.483569	0.478143	0.478083
80	0.496136	0.485400	0.480100	0.496128	0.485394	0.480097	0.475462	0.475386
70	0.491267	0.480775	0.475736	0.491259	0.480770	0.475733	0.472031	0.471932
	0.491074[a]	0.4805995[a]	0.4755835[a]	0.4910705[a]	0.480597[a]	0.4755805[a]		
60	0.484869	0.474742	0.470087	0.484862	0.474737	0.470085	0.467484	0.467350
50	0.476090	0.466543	0.462494	0.476083	0.466539	0.462493	0.461173	0.460981
	0.4757375[a]	0.4662415[a]	0.4622235[a]	0.4757335[a]	0.466237[a]	0.462197[a]		
	0.476090624[b]			0.476087092[b]				
40	0.463300	0.454773	0.451782	0.463293	0.454770	0.451781	0.451823	0.451525
	0.462784[a]	0.454351[a]		0.46278[a]	0.454334[a]			
30	0.442973	0.436545	0.435913	0.442968	0.436543	0.435913	0.436545	0.436025
	0.4421585[a]			0.4421485[a]				
20	0.406087	0.405856	0.405709	0.406086	0.405856	0.405709	0.407104	0.405970
	0.4060876[b]			0.4060871[b]				
10	0.322848	0.322699	0.321485	0.322848	0.322699	0.321485	0.327085	0.322761

[a] [283], [b] [240]

than $2p$ state as λ_D decreases *i.e.*, as effect of plasma increases.

From table (4.3.13) it can also be seen that, as λ_D decreases the energies of $2pnf$ ($^{1,3}\mathrm{F}^e$, $n = 4-6$) states are pushed towards the continuum which is the outcome of the fact that ESCP becomes more and more positive with respect to the decrease in λ_D. It is worthwhile to mention that $^1\mathrm{F}^e$ states are more bound than $^3\mathrm{F}^e$ states for each configurations but at a very low value of λ_D, both $^1\mathrm{F}^e$ and $^3\mathrm{F}^e$ states become nearly degenerate. For example, from table (4.3.13), it can be seen that the energy eigenvalue of $2p4f$ ($^1\mathrm{F}^e$) state remains more bound than $2p4f$ ($^3\mathrm{F}^e$) state in the range $\lambda_D = 100$ a.u. to $\lambda_D = 20$ a.u. At $\lambda_D = 10$ a.u., both the states become (almost) degenerate with energy value -0.322848 a.u. At these low values of λ_D, plasma screening increases and the two-electron energy levels become greatly affected by the continuum embedded states through configuration interactions. Another interesting feature to be noted from table (4.3.13) is that, at a definite low value of λ_D, $2pnf$ ($^{1,3}\mathrm{F}^e$, $n = 4-6$) states cross the energy threshold value of $\mathrm{He}^+(2s)$ but they still remain below the $\mathrm{He}^+(2p)$ threshold. For example, at $\lambda_D = 40$ a.u., $2p6f$ ($^1\mathrm{F}^e$) state energetically just crosses $\mathrm{He}^+(2s)$ threshold energy but lies below $\mathrm{He}^+(2p)$ threshold. This particular value of λ_D decreases for the lower states like $2p5f$ and $2p4f$ of $^1\mathrm{F}^e$ symmetry. Identical behavior is observed for $^3\mathrm{F}^e$ states also. At sufficiently low values of λ_D (i.e.

high screening), the energy values of He atom come very close to the one-electron (He^+) continuum and tend to merge into the $2p$ threshold of the respective one-electron (He^+) system. In tables (4.3.14) and (4.3.15) the energy values of $2pnf$ ($^{1,3}F^e$, $n = 4 - 6$) states of Li^+ and Be^{2+} are given respectively, along with their respective one-electron $2s$ and $2p$ threshold energies. All the features observed in case of He atom are also noted for Li^+ and Be^{2+} ions.

Table 4.3.14: Variation of energy eigenvalues ($-E$ in a.u.) for the $2pnf[n = 4 - 6]$ $^{1,3}F^e$ states of Li^+ and $2s$, $2p$ states of Li^{2+} with respect to the screening length (λ_D in a.u.).

	$^1F^e$			$^3F^e$				
λ_D	$2p4f$	$2p5f$	$2p6f$	$2p4f$	$2p5f$	$2p6f$	$Li^{2+}(2s)$	$Li^{2+}(2p)$
100	1.203600	1.158000	1.133734	1.203510	1.157937	1.133693	1.095298	1.095248
90	1.198297	1.152835	1.128727	1.198207	1.152772	1.128687	1.092033	1.091973
80	1.191703	1.146433	1.122542	1.191614	1.146371	1.122503	1.087964	1.087887
70	1.183284	1.138288	1.114706	1.183195	1.138227	1.114668	1.082748	1.082648
60	1.172159	1.127578	1.104457	1.172071	1.127517	1.104420	1.075823	1.075687
50	1.156775	1.112862	1.090478	1.156688	1.112803	1.090442	1.066182	1.065987
40	1.134107	1.091381	1.070283	1.134022	1.091326	1.070251	1.051840	1051537
30	1.097393	1.057098	1.038579	1.097312	1.057048	1.038553	1.028251	1.027719
20	1.027813	0.993914	0.982019	1.027745	0.993879	0.982008	0.982227	0.981057
10	0.848931	0.846906	0.844900	0.848912	0.845428	0.841774	0.852947	0.848554

Table 4.3.15: Variation of energy eigenvalues ($-E$ in a.u.) for the $2pnf[n = 4 - 6]$ $^{1,3}F^e$ states of Be^{2+} and $2s$, $2p$ states of Be^{3+} with respect to the screening length (λ_D in a.u.).

	$^1F^e$			$^3F^e$				
λ_D	$2p4f$	$2p5f$	$2p6f$	$2p4f$	$2p5f$	$2p6f$	$Be^{3+}(2s)$	$Be^{3+}(2p)$
100	2.216939	2.114095	2.058854	2.216686	2.113923	2.058745	1.960298	1.960249
90	2.216938	2.114095	2.051646	2.209165	2.106546	2.051536	1.955923	1.955862
80	2.200052	2.097554	2.042712	2.199800	2.097382	2.042603	1.950465	1.950388
70	2.188072	2.085861	2.031351	2.187821	2.085691	2.031243	1.943464	1.943364
60	2.172202	2.070428	2.016417	2.171952	2.070259	2.016311	1.934159	1.934022
50	2.150179	2.049114	1.995905	2.150086	2.048951	1.995806	1.921186	1.920990
40	2.117577	2.017784	1.965994	2.117332	2.017621	1.965895	1.901848	1.901543
30	2.064350	1.967188	1.918278	2.064110	1.967033	1.918192	1.869937	1.869400
20	1.961936	1.871780	1.830341	1.961713	1.871646	1.830273	1.807292	1.806102
10	1.685196	1.628246	1.623064	1.685048	1.628199	1.619216	1.628414	1.623879

In order to have a comparative study on the modification of doubly excited energy levels of

two–electron systems, we have displayed the energy level diagram containing three different DESs - $2p4p$ (P^e), $2p4d$ (D^o) and $2p4f$ (F^e) of He-atom along with $2s$ and $2p$ states of He^+ ion for $\lambda_D = 100,\ 50,\ 30$ and 20 a.u. in figure (4.3.8). We have taken the energy values of

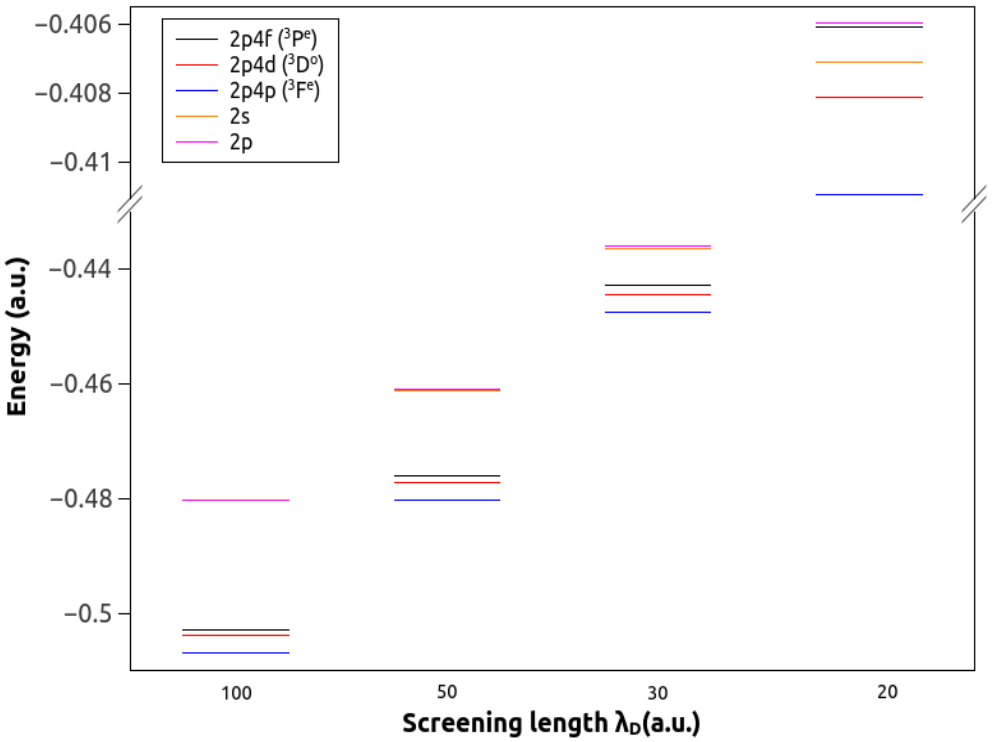

Figure 4.3.8: Energy positions of $2p4f$ ($^3F^e$), $2p4d$ ($^3D^o$) and $2p4p$ ($^3P^e$) states of He atom and $2s,\ 2p$ energy levels of He^+ ion for $\lambda_D = 100,\ 50,\ 30$ and 20 a.u.

$2p4p$ ($^3P^e$) and $2p4d$ ($^3D^o$) states of He atom embedded in classical WCP environment from literature [293, 294]. We note that the energy relationship between the DESs is $E_{2p4f} > E_{2p4d} > E_{2p4p}$. Figure (4.3.8) also shows the removal of l-degeneracy between $2s$ and $2p$ states of He^+ ion at low values of λ_D where the energy of $2s$ is lower than $2p$ state. It is interesting to note from figure (4.3.8) that, down to $\lambda_D = 30$ a.u. the three DESs are energetically lower than both $He^+(2s)$ and $He^+(2p)$ thresholds. At $\lambda_D = 20$ a.u., the $2p4f$ level crosses the $He^+(2s)$ threshold whereas $2p4d$ and $2p4p$ levels remain below $He^+(2s)$ threshold. Hence, at a low value of λ_D, the $2p4f$ ($^3F^e$) level of He merges to the one-electron (He^+) continuum.

Tables (4.3.16)–(4.3.18) show the energies of $2pnf$ ($^{1,3}F^e$) $\rightarrow$ $2pmd$ ($^{1,3}D^o$) dipole transitions $[n = 4-6;\ m = 3-6]$ for He, Li^+ and Be^{2+} respectively, as a function of λ_D.

Table 4.3.16: Absolute values of the $2pnf(^{1,3}\mathrm{F}^e) \rightarrow 2pn'd(^{1,3}D^o)[n = 4-6;\ n' = 3-6]$ transition energies (in meV) of He atom under WCP.

	Screening length (λ_D) in a.u.								
Transition	100	90	80	70	60	50	40	30	20
$^1\mathrm{F}^e \rightarrow\ ^1\mathrm{D}^o$									
$2p4f \rightarrow 2p3d$	854.25	851.72	848.21	843.20	835.57	823.21	801.09	754.79	623.78
$\rightarrow 2p4d$	71.70	72.01	72.44	73.01	73.81	75.06	76.97	79.81	77.62
$\rightarrow 2p5d^*$	264.68	360.44	381.82	413.23					
$\rightarrow 2p6d^*$	433.29								
$2p5f \rightarrow 2p3d$	1154.46	1148.52	1140.35	1128.69	1111.15	1082.97	1033.10	929.71	630.08
$\rightarrow 2p4d$	371.91	368.81	364.58	358.50	349.40	334.82	308.98	254.73	83.92
$\rightarrow 2p5d^*$	35.53	63.63	89.69	127.74					
$\rightarrow 2p6d^*$	133.06								
$2p6f \rightarrow 2p3d$	1307.43	1297.78	1284.57	1265.82	1237.82	1193.17	1114.51	946.91	634.08
$\rightarrow 2p4d$	524.89	518.07	508.80	495.63	476.06	445.02	390.38	271.94	87.92
$\rightarrow 2p5d$	188.50	85.62	54.53	9.39					
$\rightarrow 2p6d$	19.89								
$^3\mathrm{F}^e \rightarrow\ ^3\mathrm{D}^o$									
$2p4f \rightarrow 2p3d$	734.25	732.05	729.02	724.65	718.03	707.29	688.04	647.69	532.15
$\rightarrow 2p4d$	21.93	22.59	23.48	24.75	26.60	29.49	34.28	42.84	55.08
$\rightarrow 2p5d^*$	288.62	284.67	279.28	271.66					
$\rightarrow 2p6d^*$	445.89								
$2p5f \rightarrow 2p3d$	1034.40	1028.79	1021.08	1010.07	993.54	966.98	919.97	822.52	538.40
$\rightarrow 2p4d$	322.07	319.32	315.55	310.17	302.12	289.18	266.21	217.67	61.33
$\rightarrow 2p5d$	11.53	12.07	12.79	13.77					
$\rightarrow 2p6d^*$	145.74								
$2p6f \rightarrow 2p3d$	1187.31	1177.99	1165.24	1147.14	1120.14	1077.10	1001.31	839.68	542.41
$\rightarrow 2p4d$	474.99	468.52	459.71	447.24	428.72	399.29	347.55	234.83	65.34
$\rightarrow 2p5d$	164.44	161.26	156.95	150.84					
$\rightarrow 2p6d$	7.17								

* pf level lies energetically lower than the pd level

Table 4.3.17: Absolute values of the $2pnf(^{1,3}\mathrm{F}^e) \rightarrow 2pn'd(^{1,3}D^o)[n = 4-6;\ n' = 3-6]$ transition energies (in meV) of Li^+ ion under WCP.

	Screening length (λ_D) in a.u.								
Transition	100	90	80	70	60	50	40	30	20
$^1\mathrm{F}^e \rightarrow\ ^1\mathrm{D}^o$									
$2p4f \rightarrow 2p3d$	3229.53	3226.99	3223.50	3218.43	3210.71	3198.09	3175.37	3127.69	2997.69
$\rightarrow 2p4d$	190.39	190.91	191.65	192.69	194.25	196.75	201.14	209.82	230.55
$\rightarrow 2p5d^*$	1148.05	1143.86	1138.06	1129.78	1117.30	1097.24			
$\rightarrow 2p6d^*$	1848.71	1840.33	1828.78	1812.33	1787.67				
$2p5f \rightarrow 2p3d$	4470.37	4464.07	4455.36	4442.83	4423.82	4393.02	4338.01	4224.17	3920.13
$\rightarrow 2p4d$	1431.23	1427.99	1423.51	1417.09	1407.36	1391.68	1363.78	1306.30	1152.99
$\rightarrow 2p5d$	92.79	93.22	93.80	94.62	95.81	97.69			
$\rightarrow 2p6d^*$	607.87	603.24	596.92	587.93	574.56				
$2p6f \rightarrow 2p3d$	5130.68	5120.08	5105.47	5084.53	5052.98	5002.12	4912.11	4728.10	4243.81

Continuation of Table (4.3.17)

Transition	Screening length (λ_D) in a.u.								
	100	90	80	70	60	50	40	30	20
$\rightarrow 2p4d$	2091.54	2084.00	2073.62	2058.79	2036.52	2000.78	1937.88	1810.23	1476.67
$\rightarrow 2p5d$	753.10	749.23	743.90	736.32	724.96	706.79			
$\rightarrow 2p6d$	52.44	52.77	53.18	53.77	54.59				
$^3F^e \rightarrow {}^3D^o$									
$2p4f \rightarrow 2p3d$	2839.04	2836.78	2833.64	2829.13	2822.23	2810.97	2790.70	2748.17	2632.07
$\rightarrow 2p4d$	44.19	44.97	46.07	47.64	49.99	53.78	60.47	73.87	107.00
$\rightarrow 2p5d^*$	1216.58	1212.10	1205.91	1197.05	1183.72	1162.29			
$\rightarrow 2p6d^*$	1885.17	1876.47	1864.50	1847.42	1821.85				
$2p5f \rightarrow 2p3d$	4079.14	4073.13	4064.77	4052.77	4034.61	4005.14	3952.52	3843.81	3553.62
$\rightarrow 2p4d$	1284.29	1281.32	1277.19	1271.28	1262.37	1247.95	1222.29	1169.51	1028.54
$\rightarrow 2p5d$	23.52	24.25	25.21	26.59	28.65	31.88			
$\rightarrow 2p6d^*$	645.07	640.12	633.38	623.78	609.48				
$2p6f \rightarrow 2p3d$	4738.85	4728.51	4714.25	4693.84	4663.11	4613.62	4526.00	4347.08	3876.64
$\rightarrow 2p4d$	1944.00	1936.71	1926.67	1912.35	1890.87	1856.42	1795.77	1672.79	1351.57
$\rightarrow 2p5d$	683.23	679.64	674.69	667.67	657.15	640.35			
$\rightarrow 2p6d^*$	14.64	15.27	16.10	17.29	19.02				

* pf level lies energetically lower than the pd level

Table 4.3.18: Absolute values of the $2pnf(^{1,3}F^e) \rightarrow 2pn'd(^{1,3}D^o)[n = 4-6;\ n' = 3-6]$ transition energies (in meV) of Be^{2+} ion under WCP.

Transition	Screening length (λ_D) in a.u.								
	100	90	80	70	60	50	40	30	20
$^1F^e \rightarrow {}^1D^o$									
$2p4f \rightarrow 2p3d$	6948.14	6945.64	6942.18	6937.13	6929.45	6916.18	6894.02	6845.82	6713.53
$\rightarrow 2p4d$	309.27	309.91	310.81	312.08	314.03	317.18	322.84	334.38	364.21
$\rightarrow 2p5d^*$	2649.02	2644.54	2638.32	2629.38	2615.82	2593.85			
$\rightarrow 2p6d^*$	4217.37	4208.40	4196.01	4178.25	4151.41				
$2p5f \rightarrow 2p3d$	9746.64	9740.19	9731.29	9718.44	9698.86	9666.27	9609.52	9489.74	9166.80
$\rightarrow 2p4d$	3107.77	3104.46	3099.92	3093.38	3083.44	3067.28	3038.34	2978.29	2817.48
$\rightarrow 2p5d$	149.48	150.02	150.80	151.92	153.59	156.24			
$\rightarrow 2p6d^*$	1418.87	1413.85	1406.90	1396.94	1382.00				
$2p6f \rightarrow 2p3d$	11249.80	11238.81	11223.59	11201.73	11168.58	11114.14	11018.80	10820.54	10294.42
$\rightarrow 2p4d$	4610.93	4603.07	4592.22	4576.68	4553.16	4515.14	4447.62	4309.09	3945.09
$\rightarrow 2p5d$	1652.63	1648.63	1643.10	1635.21	1623.30	1604.11			
$\rightarrow 2p6d$	84.29	84.76	85.40	86.35	87.71				
$^3F^e \rightarrow {}^3D^o$									
$2p4f \rightarrow 2p3d$	6267.78	6265.49	6262.34	6257.71	6250.67	6509.08	6218.23	6174.16	6053.13
$\rightarrow 2p4d$	68.33	69.63	70.35	72.00	74.54	77.13	86.03	101.20	140.68
$\rightarrow 2p5d^*$	2758.91	2754.21	2747.67	2738.34	2724.12	2705.26			
$\rightarrow 2p6d^*$	4274.57	4265.36	4252.62	4234.40	4206.86				
$2p5f \rightarrow 2p3d$	9064.10	9057.90	9049.27	9036.81	9017.88	8987.00	8931.50	8815.76	8503.97
$\rightarrow 2p4d$	2864.65	2862.04	2857.28	2851.10	2841.75	2829.15	2799.30	2742.80	2591.53
$\rightarrow 2p5d$	37.41	38.20	39.26	40.76	43.08	46.77			
$\rightarrow 2p6d^*$	1478.25	1472.95	1465.69	1455.30	1439.65				

Continuation of Table (4.3.18)

Transition	Screening length (λ_D) in a.u.								
	100	90	80	70	60	50	40	30	20
$2p6f \rightarrow 2p3d$	10565.57	10554.80	10539.88	10518.41	10485.88	10433.15	10339.04	10144.79	9629.79
$\rightarrow 2p4d$	4366.12	4358.94	4347.90	4332.71	4309.75	4275.30	4206.84	4071.83	3717.34
$\rightarrow 2p5d$	1538.88	1535.10	1529.87	1522.37	1511.08	1492.91			
$\rightarrow 2p6d$	23.22	23.95	24.93	26.31	28.35				

* pf level lies energetically lower than the pd level

The energy eigenvalues of $2pmd$ ($^{1,3}D^o$ $m = 3-6$) states of WCP embedded He, Li^+ and Be^{2+} are taken from the work of Saha *et. al.* [294]. The transition energies given in the tables are the absolute values of the difference between the $2pnf$ ($^{1,3}F^e$) and $2pmd$ ($^{1,3}D^o$) levels because for a given λ_D the energy values of $2pnf$ ($^{1,3}F^e$) levels can be higher or lower with respect to the energy of $2pmd$ ($^{1,3}D^o$) levels. For instance, in the case of $^1F^e$ state of He, $2p4f$ state lies energetically higher than $2p3d$ ($^1D^o$) and $2p4d$ ($^1D^o$) states but lower than the $2p5d$ ($^1D^o$) and $2p6d$ ($^1D^o$) states. The conversion factor 1 a.u. of energy = 27.21138 eV [289] has been used. Saha *et. al.* [294] reported an initial blue shift (increase in the transition energy) followed by a red shift (decrease in the transition energy) for $2pmd$ ($^3D^o$) $\rightarrow$ $2p3p$ ($^3P^e$) transitions, with respect to the decrease in λ_D. In contrast, we find either a blue shift or a red shift for a particular transition scheme. For instance, the $2p4f$ ($^3F^e$) $\rightarrow$ $2p3d$ ($^3D^o$) line for Be^{2+} gets a gradual red shift with respect to decreasing λ_D and a blue shift is observed for the $2p4f$ ($^3F^e$) $\rightarrow$ $2p4d$ ($^3D^o$) of the same ion under similar conditions. Such features are evident from figure (4.3.9) where the $2p4f(^{1,3}F^e) \rightarrow 2pnd(^{1,3}D^o)$ $[n = 3-6]$ transition energies of Be^{2+} are plotted as a function of screening length (λ_D).

The structure calculations of $^{1,3}F^e$ states of two electron systems under classical WCP are very limited [240, 283] in the literature. In references [240, 283], the following two approximations were made for the sake of simplicity in solving the basis integrals involved in CI-method:

1. The screened electron-electron repulsion in the potential (1.0.1) is approximated by expanding it in a Taylor series as

$$\frac{e^{-r_{12}/\lambda_D}}{r_{12}} \approx \sum_{i=0}^{M} (-1)^i \frac{r_{12}^{i-1}}{\lambda_D^i i!}$$

where M is the upper limit of the terms in the Taylor series expansion.

2. The inter-electronic distance is approximated by $r_{12} \approx r_1 + r_2$, which indicates that the electrons are assumed to be situated in the opposite sides of the nucleus which is clearly a special case and, not a general picture.

So it is necessary to make an investigation using whole analytic form of the screened potential as well as proper correlation in the wavefunction. In this subsection we have already

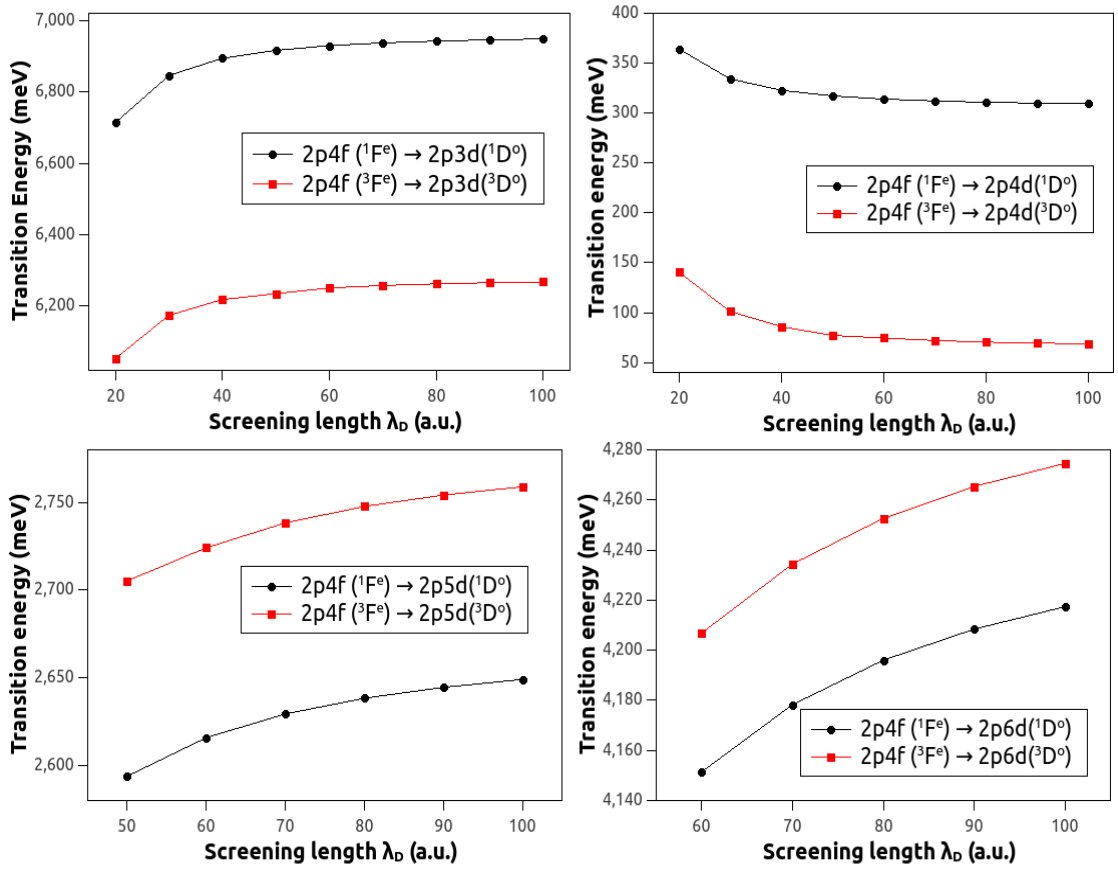

Figure 4.3.9: Modification of transition energies (in meV) for dipole transitions $2p4f\ (^{1,3}\mathrm{F}^e) \rightarrow 2pmd(^{1,3}\mathrm{D}^o)$ $[m = 3 - 6]$ of Be^{2+} ion embedded in classical WCP.

discussed the influence of ESCP on the energy eigenvalues of metastable bound $^{1,3}\mathrm{F}^e$ states of two-electron systems like He, Li^+ and Be^{2+}, where the whole analytic form of the screened potential has been used without any approximation. But the wavefunction we have used consists only pf configuration, for which we have compromised the numerical accuracy in the order of 0.001%. Under such circumstances we have executed a precise investigation on the structural properties of metastable bound and resonance $^{1,3}\mathrm{F}^e$ states under the ESCP where the entire analytic form of the screened potential retaining its original form (1.0.1) and considered a complete wavefunction containing both pf and dd configurations which are expanded in explicitly correlated nine–exponent Hylleraas basis set.

For the investigations on the metastable bound and resonance $^{1,3}\mathrm{F}^e$ states of He atom under ESCP, we have diagonalized the Hamiltonian matrix 432 times using symmetric nine–exponent Hylleraas basis set with $N = 900$ for different values of γ_1 so that the lowest value of ρ can vary from 0.005 a.u. to 0.545 a.u. in a step size of 0.00125 a.u. and kept γ_2 constant, where γ_1 (4.2.34) and γ_2 (4.2.35) are the common ratios in the geometrical sequences $\rho_i = \rho_{i-1}\gamma_1$ ($pf-$part) and $\nu_i = \nu_{i-1}\gamma_2$ ($dd-$part), respectively. We have selected

432 different γ_1 values which produce 432 sets of energy eigenvalues (E). The highest value of the ρ sequence *i.e.* ρ_9 is fixed at 8.0 while ρ_1 of any set differs from that of the previous set by 0.001. This process is executed for various plasma conditions by choosing different values of λ_D. The lowest bound energies of metastable bound $^3\mathrm{F}^e$ and $^1\mathrm{F}^e$ states for different λ_D are given in tables (4.3.19) and (4.3.20) respectively. In the first row of the tables the energy eigenvalues of $\mathrm{He}^+(2p)$ states are given, below which all the energy eigenvalues of metastable bound $^{1,3}\mathrm{F}^e$ states lie. It can be seen that the energy values of the MBSs gradually become more and more positive as λ_D decreases and as a result the number of states decrease with the decrease of λ_D. For example, in table (4.3.19) we see that there are 12 $^3\mathrm{F}^e$ MBSs in free case ($\lambda_D = \infty$), and the number reduces to 7 for $\lambda_D = 100$ a.u. and 1 for $\lambda_D = 20$ a.u. Below $\lambda_D = 20$ a.u. there is no MBS of $^3\mathrm{F}^e$ symmetry of He-atom. The present energy eigenvalues of MBSs are compared with that reported by Kar and Ho [239, 240]. The comparison reveals that under the plasma scenario $\lambda_D \leq 100$ a.u. our present calculated energy values are lowest yet obtained. Thus we have achieved better accuracy in the determination of the energy eigenvalues of metastable bound $^{1,3}\mathrm{F}^e$ states under plasma using 900 terms in the multi-exponent Hylleraas type basis set which is smaller than the number of terms used in the correlated CI-type basis sets ($1160 - 1296$ terms) [239] and ($1800 - 2200$ terms) [240] and as a consequence, the computational time is substantially reduced. The reason behind this advantage lies in the fact that we use an exact analytic form of the matrix element of the potential part.

Structural properties like electron-electron repulsive potential $\langle V_r \rangle$, electron-nucleus attractive potential $\langle V_a \rangle$ and their ratio $\eta = \left| \frac{\langle V_a \rangle}{\langle V_r \rangle} \right|$, $\langle \cos\theta_{12} \rangle$, $\langle \theta_{12} \rangle$, $\langle r_1 \rangle$, $\langle r_1^2 \rangle$, $\langle r_{12} \rangle$ and $\langle r_{12}^2 \rangle$ of $^3\mathrm{F}^e$ and $^1\mathrm{F}^e$ MBSs of He atom for different λ_D are shown in the tables (4.3.21) and (4.3.22), respectively. It is to be mentioned that in case of free atom we have estimated the inter-electronic angles $\langle \theta_{12} \rangle$ by taking the cosine inverse of $\langle \cos\theta_{12} \rangle$ (tables 4.3.21 and 4.3.22). However, in the present case, $\langle \theta_{12} \rangle$ is determined by the following relation [295]

$$\langle \theta_{12} \rangle \approx \frac{\pi}{2} - \frac{3\pi}{2} \langle \cos\theta_{12} \rangle \tag{4.3.6}$$

Tables (4.3.21) and (4.3.22) show that both $\langle r_1 \rangle$ and $\langle r_{12} \rangle$ increase when λ_D decreases for $^{1,3}\mathrm{F}^e$ states. This shows that as λ_D decreases, the size of the atom expands.

Table 4.3.21: Expectation values of repulsive potential $\langle V_r \rangle$, attractive potential $\langle V_a \rangle$, ratio of attractive to repulsive potential η, inter-electronic angles $\langle \theta_{12} \rangle$ (in degree) using (4.3.6), different one and two-particle moments of metastable bound $2pnf$ $^3\mathrm{F}^e$ $[n = 4 - 15]$ states of He atom below $\mathrm{He}^+(2p)$ threshold for different screening length λ_D of classical weakly coupled plasma. The notation $P[\pm Q]$ stands for $P \times 10^{\pm Q}$. All values are given in atomic units.

States	λ_D	$\langle V_r \rangle$	$\langle V_a \rangle$	η	$\langle r_1 \rangle$	$\langle r_1^2 \rangle$	$\langle r_{12} \rangle$	$\langle r_{12}^2 \rangle$	$\langle \theta_{12} \rangle$
$2p4f$	∞	6.38[-2]	-1.12[+0]	17.65	9.96[+0]	1.72[+2]	1.76[+1]	3.47[+2]	93.59
	100	5.39[-2]	-1.08[+0]	20.17	1.00[+1]	1.78[+2]	1.79[+1]	3.57[+2]	93.47

Continuation of Table 4.3.21

States	λ_D	$\langle V_r \rangle$	$\langle V_a \rangle$	η	$\langle r_1 \rangle$	$\langle r_1^2 \rangle$	$\langle r_{12} \rangle$	$\langle r_{12}^2 \rangle$	$\langle \theta_{12} \rangle$
	70	4.97[-2]	-1.07[+0]	21.53	1.02[+1]	1.83[+2]	1.81[+1]	3.67[+2]	93.36
	50	4.41[-2]	-1.04[+0]	23.74	1.04[+1]	1.93[+2]	1.86[+1]	3.88[+2]	93.17
	40	3.93[-2]	-1.02[+0]	26.15	1.07[+1]	2.06[+2]	1.91[+1]	4.13[+2]	92.95
	30	3.13[-2]	-9.96[-1]	31.78	1.14[+1]	2.39[+2]	2.05[+1]	4.79[+2]	92.52
	25	2.48[-2]	-9.69[-1]	38.96	1.23[+1]	2.86[+2]	2.24[+1]	5.73[+2]	92.09
	20	1.41[-2]	-9.28[-1]	65.49	1.59[+1]	5.32[+2]	2.94[+1]	1.06[+3]	91.25
$2p5f$	∞	4.07[-2]	-1.08[+0]	26.56	1.66[+1]	5.41[+2]	3.09[+1]	1.08[+3]	91.82
	100	3.08[-2]	-1.04[+0]	33.79	1.71[+1]	5.79[+2]	3.19[+1]	1.15[+3]	91.69
	70	2.67[-2]	-1.02[+0]	38.36	1.77[+1]	6.19[+2]	3.30[+1]	1.23[+3]	91.56
	50	2.13[-2]	-1.00[+0]	46.93	1.88[+1]	7.03[+2]	3.52[+1]	1.40[+3]	91.35
	40	1.67[-2]	-9.83[-1]	58.64	2.02[+1]	8.27[+2]	3.81[+1]	1.65[+3]	91.12
	30	8.98[-3]	-9.51[-1]	105.83	2.56[+1]	1.37[+3]	4.88[+1]	2.74[+3]	90.65
$2p6f$	∞	2.81[-2]	-1.05[+0]	37.48	2.48[+1]	1.26[+3]	4.72[+1]	2.52[+3]	91.05
	100	1.84[-2]	-1.01[+0]	55.18	2.64[+1]	1.43[+3]	5.04[+1]	2.87[+3]	90.90
	70	1.44[-2]	-1.00[+0]	69.09	2.81[+1]	1.64[+3]	5.39[+1]	3.28[+3]	90.77
	50	9.42[-3]	-9.78[-1]	103.87	3.22[+1]	2.17[+3]	6.21[+1]	4.34[+3]	90.55
	40	5.01[-3]	-9.60[-1]	191.34	4.06[+1]	3.52[+3]	7.89[+1]	7.05[+3]	90.31
$2p7f$	∞	2.06[-2]	-1.04[+0]	50.39	3.44[+1]	2.50[+3]	6.65[+1]	5.00[+3]	90.66
	100	1.10[-2]	-1.00[+0]	90.45	3.86[+1]	3.14[+3]	7.48[+1]	6.28[+3]	90.50
	70	7.34[-3]	-9.86[-1]	134.26	4.37[+1]	4.04[+3]	8.50[+1]	8.08[+3]	90.36
	50	2.53[-3]	-9.65[-1]	381.10	6.40[+1]	8.91[+3]	1.25[+2]	1.78[+4]	90.13
$2p8f$	∞	1.57[-2]	-1.03[+0]	65.32	4.56[+1]	4.45[+3]	8.89[+1]	8.90[+3]	90.44
	100	6.43[-3]	-9.92[-1]	154.20	5.53[+1]	6.51[+3]	1.08[+2]	1.30[+4]	90.27
	70	2.95[-3]	-9.77[-1]	331.09	7.15[+1]	1.09[+4]	1.40[+2]	2.18[+4]	90.14
$2p9f$	∞	1.24[-2]	-1.02[+0]	82.20	5.83[+1]	7.33[+3]	1.14[+2]	1.46[+4]	90.31
	100	3.38[-3]	-9.86[-1]	291.23	8.00[+1]	1.37[+4]	1.57[+2]	2.74[+4]	90.13
$2p10f$	∞	9.99[-3]	-1.02[+0]	102.05	7.31[+1]	1.15[+4]	1.43[+2]	2.31[+4]	90.21
	100	1.33[-3]	-9.82[-1]	733.41	1.25[+2]	3.38[+4]	2.48[+2]	6.76[+4]	90.05
$2p11f$	∞	7.99[-3]	-1.01[+0]	127.19	9.15[+1]	1.81[+4]	1.80[+2]	3.63[+4]	90.14
$2p12f$	∞	6.15[-3]	-1.01[+0]	164.69	1.17[+2]	3.00[+4]	2.33[+2]	6.00[+4]	90.08
$2p13f$	∞	6.75[-3]	-1.01[+0]	149.84	1.33[+2]	4.07[+4]	2.64[+2]	8.15[+4]	90.14
$2p14f$	∞	5.08[-3]	-1.00[+0]	198.36	1.83[+2]	7.49[+4]	3.63[+2]	1.49[+5]	90.09
$2p15f$	∞	7.02[-3]	-1.00[+0]	142.97	2.12[+2]	1.11[+5]	4.22[+2]	2.23[+5]	90.20

[a] [239]

Table 4.3.19: Energy eigenvalues (E in a.u.) of metastable bound $2pnf\ ^3\mathrm{F}^e$ $[n \geq 4]$ states of He below $\mathrm{He}^+(2p)$ threshold and $2p$ state of He^+ ion for different screening length λ_D (a.u.) of classical weakly coupled plasma.

States	∞	100	70	50	40 λ_D	30	25	20	15	12
$\mathrm{He}^+(2p)$	-0.5	-0.480247	-0.471931	-0.460980	-0.451525	-0.436025	-0.423853	-0.405969	-0.377135	-0.349478
$2p4f$	-0.531991	-0.503052	-0.491264	-0.476087	-0.463297	-0.442971	-0.427595	-0.406086		
	-0.5319915[a]	-0.502952[a]	-0.4910705[a]	-0.4757335[a]	-0.46278[a]	-0.442148[a]	-0.426497[a]			
	-0.531991326[b]	-0.503052113[b]		-0.476087092[b]				-0.4060871[b]		
$2p5f$	-0.520383	-0.492020	-0.480773	-0.466541	-0.454771	-0.436544				
	-0.520383[a]	-0.491925[a]	-0.480597[a]	-0.466237[a]	-0.454334[a]					
$2p6f$	-0.514111	-0.486399	-0.475734	-0.462493	-0.451781					
	-0.514111[a]	-0.486313[a]	-0.475580[a]	-0.462197[a]						
$2p7f$	-0.510344	-0.483338	-0.473276	-0.461041						
$2p8f$	-0.507906	-0.481645	-0.472187							
$2p9f$	-0.506238	-0.480744								
$2p10f$	-0.505044	-0.480330								
$2p11f$	-0.504144									
$2p12f$	-0.503410									
$2p13f$	-0.502832									
$2p14f$	-0.502296									
$2p15f$	-0.501224									

[a] [239], [b] [240]

Table 4.3.20: Energy eigenvalues (E in a.u.) of metastable bound $2pnf$ $^1\mathrm{F}^e$ $[n \geq 4]$ states of He below $\mathrm{He}^+(2p)$ threshold and $2p$ state of He^+ ion for different screening length λ_D (a.u.) of classical weakly coupled plasma.

States	∞	100	70	50	40 λ_D	30	25	20	15	12
$\mathrm{He}^+(2p)$	-0.5	-0.480247	-0.471931	-0.460980	-0.451525	-0.436025	-0.423853	-0.405969	-0.377135	-0.349478
$2p4f$	-0.531995	-0.503056	-0.491268	-0.476090	-0.463300	-0.442973	-0.427597	-0.406087		
	-0.5319955[a]	-0.502956[a]	-0.491074[a]	-0.4757375[a]	-0.462784[a]	-0.4421585[a]	-0.426532[a]			
	-0.531995436[b]	-0.503056068[b]		-0.476090624[b]				-0.4060876[b]		
$2p5f$	-0.520385	-0.492023	-0.480775	-0.466543	-0.454773	-0.436545				
	-0.5203855[a]	-0.491928[a]	-0.4805995[a]	-0.4662415[a]	-0.454351[a]					
$2p6f$	-0.514113	-0.486401	-0.475736	-0.462494	-0.451781					
	-0.514113[a]	-0.4863145[a]	-0.4755835[a]	-0.4622235[a]						
$2p7f$	-0.510345	-0.483339	-0.473276	-0.461042						
$2p8f$	-0.507907	-0.481645	-0.472187							
$2p9f$	-0.506239	-0.480745								
$2p10f$	-0.505045	-0.480330								
$2p11f$	-0.504144									
$2p12f$	-0.503411									
$2p13f$	-0.502832									
$2p14f$	-0.502296									
$2p15f$	-0.501230									

[a] [239], [b] [240]

Table 4.3.22: Expectation values of repulsive potential $\langle V_r \rangle$, attractive potential $\langle V_a \rangle$, ratio of attractive to repulsive potential $\eta = \left| \frac{\langle V_a \rangle}{\langle V_r \rangle} \right|$, inter-electronic angles $\langle \theta_{12} \rangle$ (in degree) using (4.3.6), different one and two-particle moments of metastable bound $2pnf\ ^1\mathrm{F}^e$ $[n = 4 - 15]$ states of He atom below $\mathrm{He}^+(2p)$ threshold for different screening length λ_D of classical weakly coupled plasma. The notation $P[\pm Q]$ stands for $P \times 10^{\pm Q}$. All values are given in atomic units.

States	λ_D	$\langle V_r \rangle$	$\langle V_a \rangle$	η	$\langle r_1 \rangle$	$\langle r_1^2 \rangle$	$\langle r_{12} \rangle$	$\langle r_{12}^2 \rangle$	$\langle \theta_{12} \rangle$
$2p4f$	∞	6.39[-2]	-1.12[+0]	17.64	9.96[+0]	1.72[+2]	1.76[+1]	3.46[+2]	93.46
	100	5.39[-2]	-1.08[+0]	20.15	1.00[+1]	1.77[+2]	1.78[+1]	3.57[+2]	93.36
	70	4.97[-2]	-1.07[+0]	21.52	1.02[+1]	1.83[+2]	1.81[+1]	3.67[+2]	93.25
	50	4.41[-2]	-1.04[+0]	23.73	1.04[+1]	1.93[+2]	1.86[+1]	3.87[+2]	93.07
	40	3.93[-2]	-1.02[+0]	26.14	1.07[+1]	2.06[+2]	1.91[+1]	4.13[+2]	92.87
	30	3.13[-2]	-9.96[-1]	31.76	1.14[+1]	2.39[+2]	2.05[+1]	4.79[+2]	92.45
	25	2.49[-2]	-9.69[-1]	38.93	1.23[+1]	2.86[+2]	2.24[+1]	5.73[+2]	92.05
	20	1.41[-2]	-9.28[-1]	65.43	1.59[+1]	5.32[+2]	2.94[+1]	1.06[+3]	91.23
$2p5f$	∞	4.07[-2]	-1.08[+0]	26.55	1.66[+1]	5.41[+2]	3.09[+1]	1.08[+3]	91.73
	100	3.08[-2]	-1.04[+0]	33.76	1.71[+1]	5.79[+2]	3.19[+1]	1.15[+3]	91.61
	70	2.67[-2]	-1.02[+0]	38.33	1.77[+1]	6.18[+2]	3.30[+1]	1.23[+3]	91.49
	50	2.13[-2]	-1.00[+0]	46.90	1.88[+1]	7.03[+2]	3.52[+1]	1.40[+3]	91.29
	40	1.67[-2]	-9.83[-1]	58.59	2.02[+1]	8.27[+2]	3.81[+1]	1.65[+3]	91.08
	30	8.99[-3]	-9.51[-1]	105.71	2.56[+1]	1.37[+3]	4.88[+1]	2.74[+3]	90.63
$2p6f$	∞	2.82[-2]	-1.05[+0]	37.46	2.48[+1]	1.26[+3]	4.72[+1]	2.52[+3]	90.99
	100	1.84[-2]	-1.01[+0]	55.14	2.64[+1]	1.43[+3]	5.04[+1]	2.87[+3]	90.85
	70	1.44[-2]	-1.00[+0]	69.04	2.81[+1]	1.64[+3]	5.39[+1]	3.28[+3]	90.73
	50	9.43[-3]	-9.78[-1]	103.78	3.22[+1]	2.17[+3]	6.21[+1]	4.34[+3]	90.52
	40	5.02[-3]	-9.60[-1]	191.11	4.06[+1]	3.52[+3]	7.88[+1]	7.05[+3]	90.29
$2p7f$	∞	2.06[-2]	-1.04[+0]	50.37	3.44[+1]	2.50[+3]	6.65[+1]	5.00[+3]	90.61
	100	1.10[-2]	-1.00[+0]	90.38	3.86[+1]	3.14[+3]	7.48[+1]	6.28[+3]	90.46
	70	7.35[-3]	-9.86[-1]	134.16	4.37[+1]	4.04[+3]	8.50[+1]	8.08[+3]	90.34
	50	2.53[-3]	-9.65[-1]	380.59	6.40[+1]	8.91[+3]	1.25[+2]	1.78[+4]	90.13
$2p8f$	∞	1.57[-2]	-1.03[+0]	65.29	4.56[+1]	4.44[+3]	8.89[+1]	8.90[+3]	90.41
	100	6.44[-3]	-9.92[-1]	154.09	5.52[+1]	6.51[+3]	1.08[+2]	1.30[+4]	90.25
	70	2.95[-3]	-9.77[-1]	330.77	7.14[+1]	1.09[+4]	1.40[+2]	2.18[+4]	90.13
$2p9f$	∞	1.24[-2]	-1.02[+0]	82.17	5.83[+1]	7.33[+3]	1.14[+2]	1.46[+4]	90.29
	100	3.39[-3]	-9.86[-1]	291.01	8.00[+1]	1.37[+4]	1.57[+2]	2.74[+4]	90.12
$2p10f$	∞	9.99[-3]	-1.02[+0]	102.02	7.31[+1]	1.15[+4]	1.43[+2]	2.31[+4]	90.20
	100	1.34[-3]	-9.82[-1]	732.32	1.25[+2]	3.38[+4]	2.48[+2]	6.76[+4]	90.04
$2p11f$	∞	7.99[-3]	-1.01[+0]	127.14	9.14[+1]	1.81[+4]	1.80[+2]	3.63[+4]	90.12
$2p12f$	∞	6.15[-3]	-1.01[+0]	164.66	1.17[+2]	3.00[+4]	2.33[+2]	6.00[+4]	90.07
$2p13f$	∞	6.74[-3]	-1.01[+0]	150.09	1.33[+2]	4.07[+4]	2.64[+2]	8.15[+4]	90.13
$2p14f$	∞	5.07[-3]	-1.00[+0]	198.97	1.83[+2]	7.49[+4]	3.64[+2]	1.49[+5]	90.08
$2p15f$	∞	6.76[-3]	-1.00[+0]	147.92	2.15[+2]	1.13[+5]	4.27[+2]	2.26[+5]	90.17

[a] [239]

In the last phase, we focus on the resonance energy and width of $^{1,3}F^e$ states under WCP. Tables (4.3.23) and (4.3.24) show the resonance energies (E_r) and widths (Γ) respectively for the resonance $^3F^e$ states below the $He^+(3p)$ threshold with respect to different values of λ_D and the present results are compared with only available values from literature [239].

Similar to the MBSs the number of resonance $^3F^e$ states decrease with respect to the decrease of λ_D. In tables (4.3.23) and (4.3.24), the resonance $^3F^e$ states are associated with the dominant electronic configurations $3dnd$ $[n \geq 3]$, $3pnf$ $[n \geq 4]$ and $3dng$ $[n \geq 5]$ as described below:

i. $3dnd$ $[3 \leq n \leq 10]$ configurations signify $^3F^e(1)$, $^3F^e(2)$, $^3F^e(4)$, $^3F^e(7)$, $^3F^e(10)$, $^3F^e(13)$, $^3F^e(16)$ and $^3F^e(19)$ states.

ii. $3pnf$ $[4 \leq n \leq 10]$ configurations signify $^3F^e(3)$, $^3F^e(5)$, $^3F^e(8)$, $^3F^e(11)$, $^3F^e(14)$, $^3F^e(17)$ and $^3F^e(20)$ states.

iii. $3dng$ $[5 \leq n \leq 9]$ configurations signify $^3F^e(6)$,$^3F^e(9)$,$^3F^e(12)$,$^3F^e(15)$ and $^3F^e(18)$ states.

It can be observed from table (4.3.24) that the width (Γ) decreases with the decrease of λ_D for most of the states except the $3dng$ $[5 \leq n \leq 9]$ states. In this context we have explored the changes of the structural properties of resonance $^3F^e$ states of He atom below $He^+(3p)$ threshold, similar to the metastable bound $^3F^e$ states with respect to λ_D, which is presented in table (4.3.25). Resonance $^3F^e$ states show similar features for the variation of $\langle V_a\rangle$, $\langle V_r\rangle$, η, $\langle r_1\rangle$, $\langle r_1^2\rangle$, $\langle r_{12}\rangle$ and $\langle r_{12}^2\rangle$ with the changes in λ_D as noted in case of metastable bound $^3F^e$ states. Table (4.3.25) also shows that, inter-electronic angle $\langle\theta_{12}\rangle$ values decrease with the decrease of λ_D for both $3dnd$ and $3pnf$ states whereas it increase as λ_D decreases for $3dng$ states. Therefore, it can be concluded that there is a direct relationship between changes in the inter-electronic angle $\langle\theta_{12}\rangle$ and width Γ, with respect to λ_D. Moreover, the data presented in tables (4.3.24) and (4.3.25) suggest that, the small acute inter-electronic angles correspond to very feeble resonance widths (higher autoionizing lifetime), as observed for $3dng$ states. As a result, $3dng$ states are extremely stable against autoionization in the free case and become more prone to autoionization when λ_D decreases.

Table 4.3.25: Expectation values of repulsive potential $\langle V_r\rangle$, attractive potential $\langle V_a\rangle$, ratio of attractive to repulsive potential $\eta = \left|\frac{\langle V_a\rangle}{\langle V_r\rangle}\right|$, inter-electronic angles $\langle\theta_{12}\rangle$ (in degree) using (4.3.6), different one and two-particle moments $\langle r_1\rangle$, $\langle r_1^2\rangle$, $\langle r_{12}\rangle$ and $\langle r_{12}^2\rangle$ of resonance $^3F^e$ states of He atom below $He^+(3p)$ threshold under classical weakly coupled plasma. All values are given in atomic units. The notation $P[\pm Q]$ stands for $P \times 10^{\pm Q}$.

States	λ_D	$\langle V_r\rangle$	$\langle V_a\rangle$	η	$\langle r_1\rangle$	$\langle r_1^2\rangle$	$\langle r_{12}\rangle$	$\langle r_{12}^2\rangle$	$\langle\theta_{12}\rangle$
$^3F^e(1)$	∞	1.11[-1]	-7.49[-1]	6.75	6.70[+0]	5.70[+1]	1.04[+1]	1.28[+2]	126.85
	100	1.01[-1]	-7.10[-1]	7.01	6.63[+0]	5.46[+1]	1.03[+1]	1.24[+2]	127.06
	70	9.74[-2]	-6.93[-1]	7.12	6.62[+0]	5.42[+1]	1.03[+1]	1.23[+2]	126.86
	50	9.23[-2]	-6.71[-1]	7.26	6.61[+0]	5.39[+1]	1.02[+1]	1.22[+2]	126.69
	40	8.84[-2]	-6.49[-1]	7.35	6.59[+0]	5.27[+1]	1.02[+1]	1.20[+2]	127.12

Continuation of Table (4.3.25)

States	λ_D	$\langle V_r \rangle$	$\langle V_a \rangle$	η	$\langle r_1 \rangle$	$\langle r_1^2 \rangle$	$\langle r_{12} \rangle$	$\langle r_{12}^2 \rangle$	$\langle \theta_{12} \rangle$
	30	8.13[-2]	-6.18[-1]	7.60	6.62[+0]	5.38[+1]	1.02[+1]	1.22[+2]	126.68
	25	7.60[-2]	-5.93[-1]	7.79	6.64[+0]	5.42[+1]	1.03[+1]	1.23[+2]	126.64
	20	6.86[-2]	-5.55[-1]	8.09	6.71[+0]	5.51[+1]	1.04[+1]	1.25[+2]	126.77
	15	5.69[-2]	-4.94[-1]	8.68	6.88[+0]	5.83[+1]	1.07[+1]	1.32[+2]	126.50
	12	4.63[-2]	-4.32[-1]	9.33	7.14[+0]	6.34[+1]	1.11[+1]	1.44[+2]	126.52
$^3F^e(2)$	∞	6.67[-2]	-5.96[-1]	8.93	1.07[+1]	1.59[+2]	1.82[+1]	3.74[+2]	152.41
	100	5.70[-2]	-5.57[-1]	9.76	1.08[+1]	1.62[+2]	1.83[+1]	3.80[+2]	152.03
	70	5.30[-2]	-5.40[-1]	10.17	1.09[+1]	1.66[+2]	1.85[+1]	3.87[+2]	151.71
	50	4.79[-2]	-5.17[-1]	10.80	1.10[+1]	1.71[+2]	1.88[+1]	3.99[+2]	151.04
	40	4.35[-2]	-4.98[-1]	11.43	1.12[+1]	1.79[+2]	1.91[+1]	4.15[+2]	150.50
	30	3.65[-2]	-4.66[-1]	12.77	1.16[+1]	1.95[+2]	1.99[+1]	4.47[+2]	149.18
	25	3.11[-2]	-4.41[-1]	14.18	1.20[+1]	2.13[+2]	2.07[+1]	4.85[+2]	148.05
	20	2.33[-2]	-4.03[-1]	17.30	1.30[+1]	2.56[+2]	2.25[+1]	5.75[+2]	146.73
$^3F^e(3)$	∞	6.50[-2]	-5.83[-1]	8.96	1.10[+1]	1.70[+2]	1.73[+1]	3.34[+2]	87.32
	100	5.53[-2]	-5.43[-1]	9.81	1.11[+1]	1.73[+2]	1.74[+1]	3.39[+2]	86.99
	70	5.13[-2]	-5.26[-1]	10.24	1.12[+1]	1.76[+2]	1.76[+1]	3.45[+2]	86.83
	50	4.63[-2]	-5.04[-1]	10.89	1.13[+1]	1.82[+2]	1.79[+1]	3.56[+2]	86.22
	40	4.19[-2]	-4.84[-1]	11.56	1.15[+1]	1.89[+2]	1.82[+1]	3.71[+2]	85.84
	30	3.48[-2]	-4.53[-1]	12.99	1.20[+1]	2.08[+2]	1.90[+1]	4.05[+2]	84.46
	25	2.93[-2]	-4.27[-1]	14.57	1.25[+1]	2.31[+2]	1.99[+1]	4.50[+2]	82.68
	20	2.08[-2]	-3.89[-1]	18.69	1.39[+1]	3.01[+2]	2.25[+1]	5.81[+2]	77.07
$^3F^e(4)$	∞	4.32[-2]	-5.38[-1]	12.46	1.65[+1]	4.41[+2]	2.95[+1]	9.81[+2]	158.78
	100	3.37[-2]	-4.99[-1]	14.79	1.67[+1]	4.58[+2]	3.00[+1]	1.01[+3]	155.89
	70	2.97[-2]	-4.82[-1]	16.24	1.72[+1]	4.86[+2]	3.09[+1]	1.07[+3]	156.97
	50	2.47[-2]	-4.60[-1]	18.61	1.78[+1]	5.29[+2]	3.21[+1]	1.16[+3]	155.25
	40	2.05[-2]	-4.41[-1]	21.45	1.86[+1]	5.85[+2]	3.37[+1]	1.27[+3]	153.64
	30	1.38[-2]	-4.10[-1]	29.54	2.09[+1]	7.57[+2]	3.80[+1]	1.62[+3]	151.75
$^3F^e(5)$	∞	4.12[-2]	-5.30[-1]	12.88	1.74[+1]	5.05[+2]	2.97[+1]	9.95[+2]	82.44
	100	3.19[-2]	-4.92[-1]	15.40	1.77[+1]	5.23[+2]	3.01[+1]	1.02[+3]	78.25
	70	2.76[-2]	-4.74[-1]	17.17	1.83[+1]	5.61[+2]	3.13[+1]	1.10[+3]	79.77
	50	2.26[-2]	-4.52[-1]	20.01	1.91[+1]	6.20[+2]	3.28[+1]	1.21[+3]	76.79
	40	1.83[-2]	-4.33[-1]	23.58	2.02[+1]	7.01[+2]	3.48[+1]	1.36[+3]	72.94
	30	1.14[-2]	-4.02[-1]	35.09	2.34[+1]	9.83[+2]	4.09[+1]	1.90[+3]	62.83
$^3F^e(6)$	∞	4.04[-2]	-5.23[-1]	12.93	1.68[+1]	4.55[+2]	2.75[+1]	8.35[+2]	40.86
	100	3.04[-2]	-4.83[-1]	15.89	1.73[+1]	4.85[+2]	2.85[+1]	8.96[+2]	42.11
	70	2.59[-2]	-4.65[-1]	17.98	1.79[+1]	5.31[+2]	2.98[+1]	9.85[+2]	43.44
	50	2.00[-2]	-4.43[-1]	22.13	1.92[+1]	6.26[+2]	3.24[+1]	1.17[+3]	45.81
	40	1.40[-2]	-4.21[-1]	30.12	2.25[+1]	9.20[+2]	3.89[+1]	1.75[+3]	53.29
$^3F^e(7)$	∞	2.98[-2]	-5.08[-1]	17.01	2.39[+1]	1.02[+3]	4.42[+1]	2.20[+3]	161.74
	100	2.04[-2]	-4.69[-1]	22.95	2.49[+1]	1.12[+3]	4.62[+1]	2.40[+3]	159.20
	70	1.66[-2]	-4.52[-1]	27.17	2.61[+1]	1.23[+3]	4.86[+1]	2.64[+3]	159.15
	50	1.20[-2]	-4.31[-1]	35.91	2.84[+1]	1.49[+3]	5.31[+1]	3.16[+3]	157.30

Continuation of Table (4.3.25)

States	λ_D	$\langle V_r \rangle$	$\langle V_a \rangle$	η	$\langle r_1 \rangle$	$\langle r_1^2 \rangle$	$\langle r_{12} \rangle$	$\langle r_{12}^2 \rangle$	$\langle \theta_{12} \rangle$
	40	8.87[-3]	-4.13[-1]	46.62	3.08[+1]	1.81[+3]	5.78[+1]	3.81[+3]	150.06
$^3F^e(8)$	∞	2.85[-2]	-5.03[-1]	17.67	2.53[+1]	1.17[+3]	4.53[+1]	2.31[+3]	80.32
	100	1.90[-2]	-4.64[-1]	24.32	2.65[+1]	1.29[+3]	4.75[+1]	2.54[+3]	75.03
	70	1.51[-2]	-4.47[-1]	29.51	2.81[+1]	1.46[+3]	5.05[+1]	2.87[+3]	73.93
	50	1.14[-2]	-4.29[-1]	37.65	3.01[+1]	1.72[+3]	5.52[+1]	3.44[+3]	89.70
	40	6.73[-3]	-4.08[-1]	60.73	3.57[+1]	2.44[+3]	6.53[+1]	4.78[+3]	58.94
$^3F^e(9)$	∞	2.80[-2]	-4.99[-1]	17.76	2.52[+1]	1.16[+3]	4.40[+1]	2.20[+3]	34.77
	100	1.79[-2]	-4.59[-1]	25.59	2.71[+1]	1.36[+3]	4.78[+1]	2.58[+3]	38.17
	70	1.37[-2]	-4.42[-1]	32.17	2.92[+1]	1.60[+3]	5.20[+1]	3.06[+3]	40.89
	50	6.80[-3]	-4.18[-1]	61.46	3.96[+1]	3.12[+3]	7.32[+1]	6.15[+3]	69.33
$^3F^e(10)$	∞	2.17[-2]	-4.90[-1]	22.52	3.29[+1]	2.05[+3]	6.21[+1]	4.33[+3]	163.34
	100	1.25[-2]	-4.51[-1]	35.86	3.55[+1]	2.41[+3]	6.73[+1]	5.06[+3]	159.16
	70	8.99[-3]	-4.35[-1]	48.40	3.89[+1]	2.93[+3]	7.41[+1]	6.12[+3]	159.57
	50	4.71[-3]	-4.14[-1]	88.03	4.91[+1]	4.87[+3]	9.33[+1]	9.76[+3]	96.51
$^3F^e(11)$	∞	2.09[-2]	-4.87[-1]	23.27	3.47[+1]	2.32[+3]	6.39[+1]	4.60[+3]	76.04
	100	1.14[-2]	-4.48[-1]	38.99	3.82[+1]	2.84[+3]	7.08[+1]	5.61[+3]	73.67
	70	7.94[-3]	-4.32[-1]	54.41	4.24[+1]	3.52[+3]	7.88[+1]	6.94[+3]	65.72
$^3F^e(12)$	∞	2.08[-2]	-4.84[-1]	23.20	3.48[+1]	2.36[+3]	6.30[+1]	4.52[+3]	30.16
	100	1.11[-2]	-4.45[-1]	39.99	3.96[+1]	3.12[+3]	7.28[+1]	6.04[+3]	37.76
	70	6.24[-3]	-4.28[-1]	68.58	4.97[+1]	5.04[+3]	9.30[+1]	9.84[+3]	45.72
$^3F^e(13)$	∞	1.64[-2]	-4.78[-1]	29.07	4.36[+1]	3.76[+3]	8.36[+1]	7.82[+3]	162.69
	100	7.54[-3]	-4.40[-1]	58.37	5.00[+1]	4.97[+3]	9.62[+1]	1.02[+4]	160.82
	70	4.50[-3]	-4.25[-1]	94.44	5.81[+1]	6.81[+3]	1.12[+2]	1.40[+4]	158.04
$^3F^e(14)$	∞	1.59[-2]	-4.77[-1]	29.87	4.57[+1]	4.16[+3]	8.56[+1]	8.24[+3]	73.07
	100	7.80[-3]	-4.41[-1]	56.58	5.18[+1]	5.46[+3]	9.87[+1]	1.09[+4]	93.25
	70	3.70[-3]	-4.23[-1]	114.22	6.48[+1]	8.56[+3]	1.23[+2]	1.69[+4]	57.61
$^3F^e(15)$	∞	1.54[-2]	-4.75[-1]	30.69	4.77[+1]	4.60[+3]	8.87[+1]	8.93[+3]	30.34
	100	4.92[-3]	-4.35[-1]	88.43	6.93[+1]	9.94[+3]	1.33[+2]	1.98[+4]	88.76
$^3F^e(16)$	∞	1.36[-2]	-4.72[-1]	34.67	5.47[+1]	6.13[+3]	1.05[+2]	1.25[+4]	143.56
$^3F^e(17)$	∞	1.32[-2]	-4.72[-1]	35.67	5.67[+1]	6.63[+3]	1.08[+2]	1.32[+4]	87.60
$^3F^e(18)$	∞	1.06[-2]	-4.66[-1]	43.76	6.99[+1]	1.01[+4]	1.34[+2]	2.03[+4]	89.12
$^3F^e(19)$	∞	1.46[-2]	-4.78[-1]	32.76	6.41[+1]	9.26[+3]	1.23[+2]	1.85[+4]	90.23
$^3F^e(20)$	∞	1.72[-2]	-4.82[-1]	28.01	5.17[+1]	6.17[+3]	9.84[+1]	1.23[+4]	91.24

The resonance parameters (E_r and Γ) of $^1F^e$ states below $He^+(3p)$ threshold for different λ_D are given in the tables (4.3.26) and (4.3.27) respectively. These tables reveal similar features as discussed in case of $^3F^e$ states. Structural properties like $\langle V_r \rangle$, $\langle V_a \rangle$, $\langle \theta_{12} \rangle$ and different moments– $\langle r_1 \rangle$, $\langle r_1^2 \rangle$, $\langle r_{12} \rangle$ and $\langle r_{12}^2 \rangle$ of resonance $^1F^e$ states below $He^+(3p)$ threshold are also estimated for different λ_D, as shown in table (4.3.28).

Table 4.3.23: Resonance energy E_r (a.u.) of $^3F^e$ states of He atom below $He^+(3p)$ threshold and energy eigenvalue of $3p$ state of He^+ ion for different screening length λ_D (a.u.) of classical weakly coupled plasma.

	λ_D									
States	∞	100	70	50	40	30	25	20	15	12
$He^+(3p)$	-0.222222	-0.202835	-0.194885	-0.184610	-0.175918	-0.162017	-0.151409	-0.136315	-0.113232	-0.092587
$^3F^e(1)$	-0.31072	-0.28159	-0.26947	-0.25385	-0.24059	-0.21926	-0.20291	-0.17953	-0.14352	-0.11113
	-0.31069[a]	-0.28135[a]	-0.269175[a]	-0.253315[a]	-0.23978[a]	-0.217945[a]	-0.2011[a]	-0.176905[a]	-0.139385[a]	-0.10523[a]
$^3F^e(2)$	-0.26283	-0.23404	-0.22239	-0.20750	-0.19505	-0.17546	-0.16080	-0.14047		
	-0.262825[a]	-0.23388[a]	-0.22211[a]	-0.206995[a]	-0.194305[a]	-0.17426[a]	-0.159195[a]	-0.138115[a]		
$^3F^e(3)$	-0.25826	-0.22956	-0.21801	-0.20327	-0.19098	-0.17171	-0.15734	-0.13759		
	-0.25826[a]	-0.229345[a]	-0.217605[a]	-0.202535[a]	-0.1899[a]	-0.16996[a]	-0.155015[a]			
$^3F^e(4)$	-0.24681	-0.21852	-0.20739	-0.19338	-0.18188	-0.16426				
	-0.246805[a]	-0.218385[a]	-0.20712[a]	-0.192915[a]	-0.18122[a]	-0.16309[a]				
$^3F^e(5)$	-0.24438	-0.21621	-0.20524	-0.19145	-0.18018	-0.16300				
	-0.244385[a]	-0.21604[a]	-0.20485[a]	-0.19077[a]	-0.179205[a]					
$^3F^e(6)$	-0.2412	-0.21318	-0.20213	-0.18840	-0.17724					
	-0.2413[a]	-0.2129[a]	-0.2017[a]	-0.1876[a]	-0.1762[a]					
$^3F^e(7)$	-0.23871	-0.21104	-0.20046	-0.18741	-0.17691					
	-0.238705[a]	-0.210905[a]	-0.20022[a]	-0.186985[a]						
$^3F^e(8)$	-0.23730	-0.20979	-0.19936	-0.18655	-0.17631					
	-0.237295[a]	-0.209605[a]	-0.199015[a]	-0.18593[a]						
$^3F^e(9)$	-0.23560	-0.20815	-0.19776	-0. 18513						
	-0.2356[a]	-0.2079[a]	-0.19735[a]							
$^3F^e(10)$	-0.23403	-0.20705	-0.19705	-0.18494						
	-0.234035[a]	-0.20693[a]	-0.196835[a]							

[a] [239]

Continuation of table (4.3.23)

	λ_D									
States	∞	100	70	50	40	30	25	20	15	12
$^3F^e(11)$	-0.23314	-0.20636	-0.19650							
	-0.233155[a]	-0.206175[a]	-0.19618[a]							
$^3F^e(12)$	-0.23207	-0.20526	-0.19559							
	-0.2321[a]	-0.2052[a]	-0.19525[a]							
$^3F^e(13)$	-0.23108	-0.20483	-0.19543							
$^3F^e(14)$	-0.23071	-0.20443	-0.19518							
$^3F^e(15)$	-0.22975	-0.20340								
$^3F^e(16)$	-0.22906									
$^3F^e(17)$	-0.22882									
$^3F^e(18)$	-0.22743									
$^3F^e(19)$	-0.22624									
$^3F^e(20)$	-0.22401									

[a] [239]

Table 4.3.24: Resonance width Γ (a.u.) of $^3F^e$ states of He below $He^+(3p)$ threshold for different screening length λ_D (a.u.) of classical weakly coupled plasma. The notation $P[\pm Q]$ stands for $P \times 10^{\pm Q}$.

	λ_D									
States	∞	100	70	50	40	30	25	20	15	12
$^3F^e(1)$	1.97[-3]	1.98[-3]	1.95[-3]	1.93[-3]	1.88[-3]	1.83[-3]	1.77[-3]	1.66[-3]	1.47[-3]	1.23[-3]
	1.98[-3][a]	1.975[-3][a]	1.965[-3][a]	1.945[-3][a]	1.925[-3][a]	1.88[-3][a]	1.835[-3][a]	1.76[-3][a]	1.61[-3][a]	1.4[-3][a]
$^3F^e(2)$	4.50[-4]	4.49[-4]	4.37[-4]	4.31[-4]	4.12[-4]	3.80[-4]	3.46[-3]	2.79[-4]		
	4.515[-4][a]	4.47[-4][a]	4.425[-4][a]	4.33[-4][a]	4.205[-4][a]	3.905[-4][a]	3.575[-4][a]	3.01[-4][a]		
$^3F^e(3)$	1.67[-4]	1.60[-3]	1.46[-4]	1.37[-4]	1.14[-4]	8.58[-5]	6.52[-5]	4.21[-5]		
	1.68[-4][a]	1.57[-4][a]	1.465[-4][a]	1.29[-4][a]	1.115[-4][a]	8.25[-5][a]	0.615[-4][a]			
$^3F^e(4)$	2.08[-4]	1.99[-4]	1.92[-4]	1.83[-4]	1.68[-4]	1.14[-4]				
	2.065[-4][a]	2.005[-4][a]	1.945[-4][a]	1.805[-4][a]	1.635[-4][a]	1.305[-4][a]				
$^3F^e(5)$	1.12[-4]	1.04[-4]	8.10[-5]	6.63[-5]	5.04[-5]	4.09[-5]				
	1.06[-4][a]	9.25[-5][a]	8.1[-5][a]	6.4[-5][a]	5.05[-5][a]					
$^3F^e(6)$	1.29[-9]	2.49[-8]	5.08[-7]	1.48[-6]	2.37[-6]					
$^3F^e(7)$	1.09[-4]	9.55[-5]	9.26[-5]	7.43[-5]	4.48[-5]					
	1.105[-4][a]	1.035[-4][a]	9.45[-5][a]	7.75[-5][a]						
$^3F^e(8)$	6.61[-5]	5.24[-5]	3.94[-5]	3.64[-5]	2.75[-5]					
	6.6[-5][a]	5.2[-5][a]	4.15[-5][a]	3.0[-5][a]						
$^3F^e(9)$	1.18[-8]	1.73[-7]	1.22[-5]	1.73[-5]						
$^3F^e(10)$	5.96[-5]	5.37[-5]	4.39[-5]	1.41[-5]						
	6.6[-5][a]	5.95[-5][a]								

[a] [239]

Continuation of table (4.3.24)

	λ_D									
States	∞	100	70	50	40	30	25	20	15	12
$^3F^e(11)$	5.37[-5]	2.71[-5]	1.07[-5]							
$^3F^e(12)$	2.45[-7]	2.91[-6]	1.16[-5]							
$^3F^e(13)$	1.84[-4]	1.11[-4]	4.36[-5]							
$^3F^e(14)$	1.61[-4]	3.05[-5]	1.16[-5]							
$^3F^e(15)$	4.06[-6]	9.0 [-5]								
$^3F^e(16)$	6.53[-5]									
$^3F^e(17)$	1.06[-4]									
$^3F^e(18)$	7.46[-5]									
$^3F^e(19)$	1.60[-4]									
$^3F^e(20)$	1.83[-4]									

[a] [239]

Table 4.3.26: Resonance energy E_r (a.u.) of $^1F^e$ states of He atom below $He^+(3p)$ threshold and energy eigenvalue of $3p$ state of He^+ ion for different screening length λ_D (a.u.) of classical weakly coupled plasma.

	λ_D									
States	∞	100	70	50	40	30	25	20	15	12
$He^+(3p)$	-0.22222	-0.202835	-0.194885	-0.18461	-0.1759181	-0.162017	-0.151409	-0.136315	-0.113232	-0.092587
$^1F^e(1)$	-0.26853	-0.23968	-0.22798	-0.21299	-0.20040	-0.18051	-0.16554	-0.14459		
	-0.268535[a]	-0.23953[a]	-0.22769[a]	-0.21245[a]	-0.19961[a]	-0.179235[a]	-0.16384[a]	-0.14222[a]		
$^1F^e(2)$	-0.26096	-0.23215	-0.22050	-0.20559	-0.19312	-0.17350	-0.15885	-0.13862		
	-0.26096[a]	-0.231955[a]	-0.220125[a]	-0.204905[a]	-0.192105[a]	-0.17185[a]	-0.156635[a]			
$^1F^e(3)$	-0.24883	-0.22050	-0.20931	-0.19519	-0.18356	-0.16558	-0.15244			
	-0.248835[a]	-0.22035[a]	-0.209025[a]	-0.194695[a]	-0.182855[a]	-0.16451[a]				
$^1F^e(4)$	-0.24571	-0.21747	-0.20636	-0.19242	-0.18101	-0.16356				
	-0.24571[a]	-0.21727[a]	-0.20599[a]	-0.191765[a]	-0.18007[a]					
$^1F^e(5)$	-0.24130	-0.21317	-0.20214	-0.18842	-0.17749					
	-0.24131[a]	-0.21293[a]	-0.20173[a]	-0.18765[a]	-0.17685[a]					
$^1F^e(6)$	-0.23967	-0.21194	-0.20129	-0.18811	-0.17722					
	-0.239665[a]	-0.21180[a]	-0.20104[a]							
$^1F^e(7)$	-0.23802	-0.21041	-0.19990	-0.18696	-0.17660					
	-0.23803[a]	-0.210235[a]	-0.19961[a]	-0.18625[a]	-0.17615[a]					
$^1F^e(8)$	-0.23560	-0.20813	-0.19777	-0.18526						
	-0.23560[a]	-0.20792[a]	-0.197365[a]	-0.18475[a]						
$^1F^e(9)$	-0.23457	-0.20751	-0.19727	-0.18508						
	-0.23458[a]									
$^1F^e(10)$	-0.23358	-0.20667	-0.19675	-0.18481						
	-0.233595[a]	-0.20650[a]	-0.1963[a]							

[a] [239]

Continuation of table (4.3.26)

	λ_D									
States	∞	100	70	50	40	30	25	20	15	12
$^1F^e(11)$	-0.23201	-0.20508	-0.19563							
	-0.2321[a]	-0.2052[a]	-0.1948[a]							
$^1F^e(12)$	-0.23106	-0.20456								
	-0.2314[a]	-0.2045[a]								
$^1F^e(13)$	-0.23078	-0.20350								
		-0.2035[a]								
$^1F^e(14)$	-0.22925									
$^1F^e(15)$	-0.22778									
$^1F^e(16)$	-0.22670									
$^1F^e(17)$	-0.22518									

[a] [239]

Table 4.3.27: Resonance width Γ (a.u.) of $^1F^e$ states of He atom below $He^+(3p)$ threshold for different screening length λ_D (a.u.) of classical weakly coupled plasma. The notation $P[\pm Q]$ denotes $P \times 10^{\pm Q}$.

	λ_D									
States	∞	100	70	50	40	30	25	20	15	12
$^1F^e(1)$	1.99[-7]	1.95[-7]	1.91[-7]	1.84[-7]	1.68[-7]	1.32[-7]	1.04[-7]	5.76[-8]		
	3.9[-7][a]	3.80[-7][a]	3.66[-7][a]	3.39[-7][a]	2.92[-7][a]					
$^1F^e(2)$	4.75[-5]	4.68[-5]	4.52[-5]	4.24[-5]	3.94[-5]	3.31[-5]	2.76[-5]	1.83[-5]		
	9.68[-5][a]	9.39[-5][a]	9.10[-5][a]	8.58[-5][a]	8.00[-5][a]					
$^1F^e(3)$	6.20[-8]	4.26[-8]	2.47[-8]	6.20[-9]	5.92[-9]	2.71[-10]	2.38[-12]			
$^1F^e(4)$	2.92[-5]	2.72[-5]	2.36[-5]	1.93[-5]	1.73[-5]	1.52[-5]				
	5.41[-5][a]	5.04[-5][a]	4.69[-5][a]	4.07[-5][a]	3.42[-5][a]					
$^1F^e(5)$	1.23[-7]	2.03[-7]	8.10[-7]	1.30[-6]	7.97[-6]					
$^1F^e(6)$	5.49[-4]	1.38[-4]	3.38[-6]	2.15[-6]	9.69[-7]					
$^1F^e(7)$	1.35[-5]	1.29[-5]	1.14[-5]	1.13[-5]	4.88[-6]					
$^1F^e(8)$	1.87[-11]	1.01[-10]	1.63[-6]	6.86[-5]						
$^1F^e(9)$	4.37[-5]	2.48[-5]	2.26[-5]	1.74[-5]						
$^1F^e(10)$	3.62[-5]	2.04[-5]	1.24[-5]	3.83[-6]						

[a] [239]

Continuation of table (4.3.27)

	λ_D									
States	∞	100	70	50	40	30	25	20	15	12
$^1F^e(11)$	1.09[-10]	2.99[-7]	9.69[-6]							
$^1F^e(12)$	5.84[-5]	4.83[-7]								
$^1F^e(13)$	3.96[-4]	2.66[-5]								
$^1F^e(14)$	3.59[-5]									
$^1F^e(15)$	1.57[-5]									
$^1F^e(16)$	1.37[-5]									
$^1F^e(17)$	9.44[-5]									

[a] [239]

Table 4.3.28: Expectation values of repulsive potential $\langle V_r \rangle$, attractive potential $\langle V_a \rangle$, ratio of attractive to repulsive potential $\eta = \left| \frac{\langle V_a \rangle}{\langle V_r \rangle} \right|$, inter-electronic angles $\langle \theta_{12} \rangle$ (in degree) using (4.3.6), different one and two-particle moments $\langle r_1 \rangle$, $\langle r_1^2 \rangle$, $\langle r_{12} \rangle$ and $\langle r_{12}^2 \rangle$ of resonance $^1\mathrm{F}^e$ states of He atom below $\mathrm{He}^+(3p)$ threshold under classical weakly coupled plasma. All values are given in atomic units. The notation $P[\pm Q]$ stands for $P \times 10^{\pm Q}$.

States	λ_D	$\langle V_r \rangle$	$\langle V_a \rangle$	η	$\langle r_1 \rangle$	$\langle r_1^2 \rangle$	$\langle r_{12} \rangle$	$\langle r_{12}^2 \rangle$	$\langle \theta_{12} \rangle$
$^1\mathrm{F}^e(1)$	∞	6.55[-2]	-6.02[-1]	9.18	1.01[+1]	1.37[+2]	1.68[+1]	3.07[+2]	135.10
	100	5.60[-2]	-5.63[-1]	10.04	1.01[+1]	1.38[+2]	1.68[+1]	3.10[+2]	134.91
	70	5.22[-2]	-5.46[-1]	10.45	1.01[+1]	1.40[+2]	1.69[+1]	3.14[+2]	134.74
	50	4.74[-2]	-5.24[-1]	11.05	1.02[+1]	1.43[+2]	1.71[+1]	3.20[+2]	134.47
	40	4.34[-2]	-5.05[-1]	11.64	1.03[+1]	1.46[+2]	1.73[+1]	3.27[+2]	134.21
	30	3.71[-2]	-4.75[-1]	12.78	1.06[+1]	1.54[+2]	1.77[+1]	3.43[+2]	133.78
	25	3.24[-2]	-4.50[-1]	13.88	1.08[+1]	1.62[+2]	1.81[+1]	3.61[+2]	133.49
	20	2.59[-2]	-4.15[-1]	16.03	1.13[+1]	1.81[+2]	1.90[+1]	3.99[+2]	133.32
$^1\mathrm{F}^e(2)$	∞	7.01[-2]	-5.92[-1]	8.44	1.00[+1]	1.32[+2]	1.58[+1]	2.76[+2]	108.87
	100	6.04[-2]	-5.52[-1]	9.14	1.01[+1]	1.34[+2]	1.59[+1]	2.81[+2]	108.47
	70	5.64[-2]	-5.36[-1]	9.49	1.02[+1]	1.37[+2]	1.60[+1]	2.85[+2]	107.96
	50	5.12[-2]	-5.13[-1]	10.02	1.03[+1]	1.42[+2]	1.63[+1]	2.94[+2]	107.26
	40	4.68[-2]	-4.94[-1]	10.55	1.05[+1]	1.47[+2]	1.65[+1]	3.04[+2]	106.16
	30	3.96[-2]	-4.62[-1]	11.67	1.09[+1]	1.62[+2]	1.72[+1]	3.32[+2]	104.11
	25	3.38[-2]	-4.37[-1]	12.89	1.14[+1]	1.80[+2]	1.80[+1]	3.67[+2]	101.59
	20	2.49[-2]	-3.97[-1]	15.97	1.26[+1]	2.37[+2]	2.03[+1]	4.77[+2]	95.63
$^1\mathrm{F}^e(3)$	∞	4.19[-2]	-5.39[-1]	12.86	1.58[+1]	4.03[+2]	2.81[+1]	8.75[+2]	140.41
	100	3.25[-2]	-5.00[-1]	15.37	1.61[+1]	4.18[+2]	2.86[+1]	9.05[+2]	139.72
	70	2.88[-2]	-4.83[-1]	16.76	1.63[+1]	4.33[+2]	2.90[+1]	9.36[+2]	139.14
	50	2.42[-2]	-4.62[-1]	19.05	1.68[+1]	4.62[+2]	2.99[+1]	9.95[+2]	138.28
	40	2.05[-2]	-4.44[-1]	21.66	1.74[+1]	4.99[+2]	3.10[+1]	1.06[+3]	137.66
	30	1.47[-2]	-4.14[-1]	28.17	1.88[+1]	5.95[+2]	3.38[+1]	1.26[+3]	137.76
	25	1.03[-2]	-3.90[-1]	37.80	2.07[+1]	7.47[+2]	3.76[+1]	1.58[+3]	140.57
$^1\mathrm{F}^e(4)$	∞	4.32[-2]	-5.34[-1]	12.36	1.62[+1]	4.22[+2]	2.77[+1]	8.60[+2]	103.51
	100	3.36[-2]	-4.95[-1]	14.72	1.66[+1]	4.44[+2]	2.83[+1]	9.01[+2]	102.08
	70	2.97[-2]	-4.78[-1]	16.09	1.69[+1]	4.66[+2]	2.90[+1]	9.41[+2]	100.27
	50	2.47[-2]	-4.56[-1]	18.47	1.76[+1]	5.11[+2]	3.02[+1]	1.02[+3]	96.76
	40	2.04[-2]	-4.37[-1]	21.44	1.86[+1]	5.78[+2]	3.20[+1]	1.15[+3]	92.85
	30	1.36[-2]	-4.07[-1]	29.82	2.10[+1]	7.59[+2]	3.64[+1]	1.49[+3]	79.96
$^1\mathrm{F}^e(5)$	∞	4.04[-2]	-5.23[-1]	12.93	1.68[+1]	4.56[+2]	2.75[+1]	8.35[+2]	39.67
	100	3.03[-2]	-4.83[-1]	15.93	1.74[+1]	4.91[+2]	2.86[+1]	9.04[+2]	40.59
	70	2.57[-2]	-4.65[-1]	18.07	1.80[+1]	5.38[+2]	3.00[+1]	9.97[+2]	41.81
	50	1.98[-2]	-4.42[-1]	22.28	1.94[+1]	6.40[+2]	3.27[+1]	1.19[+3]	44.57
	40	8.91[-3]	-4.15[-1]	46.58	2.88[+1]	1.53[+3]	5.34[+1]	3.18[+3]	133.47
$^1\mathrm{F}^e(6)$	∞	2.90[-2]	-5.08[-1]	17.52	2.32[+1]	9.53[+2]	4.26[+1]	2.01[+3]	143.51
	100	1.97[-2]	-4.69[-1]	23.73	2.40[+1]	1.03[+3]	4.43[+1]	2.18[+3]	141.86
	70	1.62[-2]	-4.53[-1]	27.86	2.49[+1]	1.11[+3]	4.60[+1]	2.35[+3]	140.92

Continuation of Table (4.3.28)

States	λ_D	$\langle V_r \rangle$	$\langle V_a \rangle$	η	$\langle r_1 \rangle$	$\langle r_1^2 \rangle$	$\langle r_{12} \rangle$	$\langle r_{12}^2 \rangle$	$\langle \theta_{12} \rangle$
	50	1.21[-2]	-4.32[-1]	35.59	2.65[+1]	1.28[+3]	4.92[+1]	2.69[+3]	138.82
	40	1.41[-2]	-4.22[-1]	29.74	2.21[+1]	8.79[+2]	3.82[+1]	1.67[+3]	51.32
$^1F^e(7)$	∞	2.95[-2]	-5.05[-1]	17.12	2.39[+1]	1.02[+3]	4.29[+1]	2.07[+3]	100.93
	100	1.98[-2]	-4.66[-1]	23.46	2.53[+1]	1.16[+3]	4.54[+1]	2.33[+3]	95.65
	70	1.62[-2]	-4.50[-1]	27.71	2.63[+1]	1.26[+3]	4.74[+1]	2.53[+3]	95.86
	50	1.15[-2]	-4.28[-1]	37.22	2.90[+1]	1.55[+3]	5.25[+1]	3.10[+3]	88.78
	40	7.69[-3]	-4.10[-1]	53.33	3.32[+1]	2.11[+3]	6.08[+1]	4.20[+3]	81.39
$^1F^e(8)$	∞	2.80[-2]	-4.99[-1]	17.77	2.52[+1]	1.16[+3]	4.40[+1]	2.19[+3]	32.73
	100	1.80[-2]	-4.59[-1]	25.48	2.71[+1]	1.37[+3]	4.78[+1]	2.59[+3]	35.04
	70	1.38[-2]	-4.42[-1]	32.02	2.91[+1]	1.59[+3]	5.18[+1]	3.04[+3]	37.80
	50	5.38[-3]	-4.16[-1]	77.29	4.25[+1]	3.54[+3]	8.05[+1]	7.23[+3]	123.43
$^1F^e(9)$	∞	2.12[-2]	-4.90[-1]	23.09	3.20[+1]	1.93[+3]	6.01[+1]	4.03[+3]	145.03
	100	1.21[-2]	-4.51[-1]	37.05	3.44[+1]	2.25[+3]	6.49[+1]	4.67[+3]	142.75
	70	8.96[-3]	-4.36[-1]	48.62	3.69[+1]	2.61[+3]	6.88[+1]	5.41[+3]	140.87
	50	7.31[-3]	-4.19[-1]	57.28	3.74[+1]	2.77[+3]	6.98[+1]	5.42[+3]	56.30
$^1F^e(10)$	∞	2.15[-2]	-4.88[-1]	22.70	3.32[+1]	2.09[+3]	6.11[+1]	4.20[+3]	98.36
	100	1.21[-2]	-4.49[-1]	36.97	3.63[+1]	2.53[+3]	6.72[+1]	5.07[+3]	93.32
	70	8.61[-3]	-4.33[-1]	50.36	3.99[+1]	3.08[+3]	7.42[+1]	6.16[+3]	87.63
	50	4.51[-3]	-4.13[-1]	91.55	4.95[+1]	4.95[+3]	9.33[+1]	9.89[+3]	82.99
$^1F^e(11)$	∞	2.12[-2]	-4.85[-1]	22.80	3.50[+1]	2.40[+3]	6.33[+1]	4.61[+3]	30.81
	100	7.51[-3]	-4.40[-1]	58.68	4.79[+1]	4.55[+3]	9.17[+1]	9.34[+3]	138.97
	70	5.00[-3]	-4.26[-1]	85.22	5.31[+1]	5.65[+3]	1.01[+2]	1.14[+4]	116.89
$^1F^e(12)$	∞	1.63[-2]	-4.77[-1]	29.20	4.39[+1]	3.81[+3]	8.24[+1]	7.64[+3]	94.78
	100	7.21[-3]	-4.39[-1]	60.89	5.20[+1]	5.40[+3]	9.79[+1]	1.07[+4]	76.15
$^1F^e(13)$	∞	1.62[-2]	-4.77[-1]	29.47	4.42[+1]	3.87[+3]	8.31[+1]	7.76[+3]	96.62
	100	3.96[-3]	-4.32[-1]	109.24	7.34[+1]	1.10[+4]	1.39[+2]	2.17[+4]	38.90
$^1F^e(14)$	∞	1.32[-2]	-4.72[-1]	35.70	5.39[+1]	5.94[+3]	1.02[+2]	1.19[+4]	95.96
$^1F^e(15)$	∞	1.06[-2]	-4.66[-1]	44.05	6.76[+1]	9.49[+3]	1.30[+2]	1.90[+4]	91.57
$^1F^e(16)$	∞	9.74[-3]	-4.65[-1]	47.74	7.58[+1]	1.21[+4]	1.46[+2]	2.43[+4]	91.49
$^1F^e(17)$	∞	1.59[-2]	-4.79[-1]	30.11	5.82[+1]	7.98[+3]	1.11[+2]	1.59[+4]	90.31

Chapter 5

Concluding remarks and future scope

Concluding remarks and future scope

Research on few–body atomic systems under plasma environment is covered in detail in this dissertation. The findings of the present work expose several interesting structural properties of few–body systems under various plasma conditions and open up new directions for future research. Three types of plasma environments have been considered: (i) Classical weakly coupled plasma (WCP), (ii) classical dusty plasma (DP) and (iii) quantum plasma (QP). In each case variational equation has been formed and energy eigenvalues of the atomic systems considered are estimated by solving the generalized eigenvalue equation. All calculations are carried out in quadruple precision to ensure the accuracy of the obtained data. In what follows we draw conclusion on the results of present study along with the some of the possible future applications of the findings in the concerned field of research.

At the beginning, model potentials 'felt' by a hydrogenic ion while moving through classical WCP, classical DP and QP are developed considering the plasma as a dielectric medium. The model potentials are valid as long as the atom is moving at such a velocity (v) that the thermal Mach number lies below unity. The physical parameters of plasma, like particle number density, temperature etc. are incorporated in the screening terms of model potential experienced by atoms when placed inside the plasma medium. For the cases of classical WCP and QP, the potentials consist of two parts: (a) exponentially screened Coulomb potential (ESCP) and (b) near field wake potential (NFWP) which depends on ion velocity (v). For classical DP, in addition to ESCP and NFWP, an additional term dependent on velocity and dust grain size arises, which is known as "dust potential". Ritz variational principle is used to examine the impact of such model potentials on the energy eigenvalues of $1s_0$, $2s_0$, $2p_0$ and $2p_{\pm1}$ states of moving hydrogen atom using distorted trial wavefunctions and solving the generalized eigenvalue equation. It is observed that, under plasma environment, the energy eigenvalues of H–atom or H–like ions increase with respect to free (no plasma) and static ($v = 0$) case and they increase further if velocity of the atom increases. $l-$degeneracy is removed in presence of plasma and the velocity of hydrogen atom causes the removal of $|m|-$degeneracy giving rise to 'Stark-like' splitting of the energy levels. The variation of transition energies of π and σ components of Lyman–α transitions of plasma embedded hydrogen atom are also estimated for different velocities of the ion. In all the cases the π–lines exhibit blue-shift as velocity of the atom increases whereas the σ–lines exhibit blue-shift only in classical weakly coupled plasma and show red-shift in both classical dusty plasma and quantum plasma environments. The present methodology is extended to study the influence of quantum plasma potential on the modification of energy eigenvalues of different states of moving C^{5+} ion for different densities of the electron-hole quantum plasma environment. At the instance of an ion moving in a quantum plasma environment, the level crossing phenomena and incidental degeneracy are detected with respect to the

ion velocity. Future researchers are expected to explore the structural properties of various ions in a quantum plasma environment using the current form of the potential. The present methodology can be extended to study the variation of transition rate of H–like systems with respect to ion velocity, which will carry immense application in case of fast ion diagnostics in research works related to different thermonuclear fusion reactors. Such studies are being conducted with a great deal of effort as part of the ITER project and its auxiliary initiatives, such as the JET tokamak and ASDEX upgrade. Research on the modulation of spectral line features (intensity, profile, broadening, etc.) can help with the measurement of various plasma parameters, such as energies of plasma ions (using Lyman lines), fluctuations in the electron density (using Balmer lines) etc.

In the subsequent work, the ground state ($1s^2;^1\mathrm{S}^e$) energies of three–body systems are estimated using a flexible multi–exponent Hylleraas type basis–set under Ritz variation method for various screening parameters of the potential (ESCP) under classical WCP environment. Motion of all the three particles is incorporated in the variational equation. Different three–body systems are considered which include exotic systems of XXY, XYY [X = p^+, d^+, and t^+, Y = μ^-, π^- and K^-] and $\mathrm{Ps}^-(e^+e^-e^-)$ ions and molecular–like $\mathrm{H}_2^+(p^+p^+e^-)$, $\mathrm{D}_2^+(d^+d^+e^-)$ and $\mathrm{T}_2^+(t^+t^+e^-)$ ions. Some of the energy values are compared with the available results from literature and it is found that the present results can be treated as benchmark for future references. We have also estimated the energy eigenvalues of the ground state ($1s$) of the two–body subsystems of respective three–body ions in ESCP. For both three–body and its two–body subsystems, the ground state energies gradually become positive and move towards the destabilization limit (zero energy) as the plasma screening is increased. It is found that the positively charged three–body systems show the feature of 'borromean bindings' which means the three–body systems exists whereas their two–body subsystems destabilize for a range of values of plasma screening strength. This range of plasma screening strength is called 'borromean window' which increases as the mass of the positively charged particle increases. We have also estimated the resonance parameters (energy and width) of free p^+YY and p^+p^+Y [$Y = \mu^-, \pi^-, K^-$] ions below $n = 2$ ionization threshold of the respective two–body subsystems using stabilization method. The current findings are consistent with those found in literature. For the first time ever in the literature, the resonance parameters for $p^+K^-K^-$ and $p^+p^+K^-$ ions are provided. It is seen that the present method is capable to produce reasonably accurate bound state energies and resonance parameters with a smaller number of terms in the basis set expansion as compared to other existing methods. The present method can be extended in assessing the effect of surrounding environment of exotic systems and other external confinements. It can be used to investigate bound state properties of asymmetric three–body exotic systems like $p^+d^+\mu^-$, $p^+d^+\pi^-$, $d^+t^+\mu^-$ etc. Borromean bindings of such systems can also be estimated. For experimental cases, if any such experimental setup is designed, then present work may

provide the initial guiding data.

The last phase of this thesis deals with different structural properties of high-lying doubly excited $^{1,3}F^e$ states of free and plasma embedded two–electron systems. These doubly excited states (DES) are classified in two categories viz. metastable bound and resonance states. For metastable bound $^{1,3}\mathrm{F}^e$ states, Ritz variational method is employed and for resonance states, the stabilization method is adopted. The $^{1,3}\mathrm{F}^e$ states primarily originate from pf configuration. Therefore in the first place we have considered the trial wavefunction consisting only of the most dominant pf configuration, which is expanded in explicitly correlated multi-exponent Hylleraas type basis set. We have calculated the energy eigenvalues of metastable bound $^{1,3}\mathrm{F}^e$ states of free two-electron systems having atomic number $Z = 2 - 18$. Only a few of the results could be compared with those available in literature. From the comparison, it is seen that, although the estimated energy values shows reasonably good agreement with the available results but the convergence is quite slow. The next dominant contribution to $^{1,3}\mathrm{F}^e$ states come from dd configuration and the explicit inclusion of the dd term in the wavefunction along with the pf term improves the convergence of energy eigenvalues of metastable bound states. Consequently we have produced benchmark results for metastable bound $^{1,3}\mathrm{F}^e$ states of He atom which will be useful for future references. In case of resonance states, we have adopted the 'soft–wall' strategy of stabilization method to predict the resonance energy and width of nearly 100 resonance states of $^3\mathrm{F}^e$ state of free He atom upto $n = 7$ ionization threshold. It is seen that, the influence of the explicit inclusion of pf and dd configurations together in the wavefunction in defining the resonance state characteristics is quite pronounced. Various structural properties like one– and two–particle moments, virial factors, inter–electronic angles etc. are estimated for both metastable–bound as well as resonance $^{1,3}\mathrm{F}^e$ states. The present method could be applied to other resonance states with different symmetries where explicit configuration mixing is required. We next consider metastable bound $^{1,3}\mathrm{F}^e$ states of He, Li^+ and Be^{2+} ions embedded in classical WCP represented by ESCP. Instead of using Taylor series expansion of screened electron-electron repulsion term, we have developed a closed analytic form of the electron–electron screening term in the Hamiltonian for $^{1,3}\mathrm{F}^e$ states. The trial wavefunction in this case also is initially constructed in basis set expansion technique keeping the pf term explicit. It is observed that, when the plasma screening strength increases energy levels become more positive and as a result the number of bound states decreases. Transition wavelengths for the dipole transitions $2pnf\ (^{1,3}\mathrm{F}^e) \rightarrow 2pn'd\ (^{1,3}\mathrm{D}^o)[n = 4 - 6;\ n' = 3 - 6]$ exhibit a gradual blue or red shift with the variation of plasma screening. The study on complex atomic spectra, such as those from laboratory plasma experiments or astrophysical observations, may extract theoretical support from such findings. For the betterment of the accuracy of our estimated data, we have considered the mixing of both pf and dd configurations in the trial wavefunction for the determination of the structural properties of

meta-stable bound and resonance $^{1,3}F^e$ states of He atom placed in classical WCP environment. Most of the energy eigenvalues of the meta-stable bound $^{1,3}F^e$ states are the lowest yet obtained. Stabilization method has been used to estimate the resonance parameters of $^{1,3}F^e$ states (below $He^+(4p)$ threshold) of He atom for different plasma screening. Like the bound states, resonance energies increase and the number of such states decrease with the decrease as plasma screening strength increases. New features are found on the variation of resonance widths of those states with respect to plasma screening. It is observed that the widths of the resonance states with the dominant configurations $3dnd$ $[3 \leq n \leq 10]$ and $3pnf$ $[4 \leq n \leq 10]$ decreases with the increase of plasma screening strength whereas the resonance states having dominant configuration $3dng$ $[5 \leq n \leq 9]$ it increases. In this context, we have demonstrated that width will decrease if the inter-electronic angle increases with respect to increase of plasma screening strength. For the first time in the literature, the variations of other structural properties, such as attractive and repulsive potential, one- and two-particle moments, etc. are also examined for the metastable bound and resonance $^{1,3}F^e$ states of the He atom embedded in classical WCP. We anticipate that future researchers in related areas will take into consideration the current technique as an alternative approach for structural computations of such high-lying DES.

The real verification of this theoretical results requires highly advanced experimental techniques. At present, in some cases, a meaningful comparison of theoretical and experimental results could not be done due to scarcity of appropriate experimental data. With the advent of technology in performing high resolution experiments and in recording precise astrophysical data, this is quite likely to be possible in future.

Bibliography

[1] E. Schrödinger. An undulatory theory of the mechanics of atoms and molecules. *Physical review*, 28:1049, 1926.

[2] N. Bohr. I. On the constitution of atoms and molecules. *The London, Edinburgh, and Dublin Philosophical Magazine and Journal of Science*, 26:1, 1913.

[3] J. C. Slater. The structure of the Helium atom: I. *Proceedings of the National Academy of Sciences of the United States of America*, 13:423, 1927.

[4] D. R. Hartree. *The wave mechanics of an atom with a non-Coulomb central field. Part I. Theory and methods*, volume 24. Cambridge university press, 1928.

[5] D. R. Hartree. *The wave mechanics of an atom with a non-coulomb central field. Part II. Some results and discussion*, volume 24. Cambridge University Press, 1928.

[6] E. A. Hylleraas. Über den grundzustand des heliumatoms. *Zeitschrift für Physik*, 48:469, 1928.

[7] E. A. Hylleraas. Neue berechnung der energie des heliums im grundzustande, sowie des tiefsten terms von ortho-helium. *Zeitschrift für Physik*, 54:347, 1929.

[8] E. A. Hylleraas and B. Undheim. Numerische berechnung der 2S-terme von ortho-und par-helium. *Zeitschrift für Physik*, 65:759, 1930.

[9] M. Born and J. R. Oppenheimer. On the quantum theory of molecules. *Ann. Physik*, 84:457, 1927.

[10] T. Lyman. The Spectrum of Helium in the Extreme Ultra-violet. *Astrophys. J.*, 60:1, 1924.

[11] S. D. Bergeson et al. Measurement of the He Ground State Lamb Shift via the Two-Photon $1^1S - 2^1S$ Transition. *Physical review letters*, 80:3475, 1998.

[12] C. Pekeris. 1^1S and 2^3S states of helium. *Physical Review*, 115:1216, 1959.

[13] G. Drake. High precision variational calculations for the $1s^2\ ^1$S state of H^- and the $1s^2\ ^1$S, $1s2s\ ^1$S and $1s2s\ ^3$S states of helium. *Nuclear Instruments and Methods in Physics Research Section B: Beam Interactions with Materials and Atoms*, 31:7, 1988.

[14] K. Frankowski and C. Pekeris. Logarithmic terms in the wave functions of the ground state of two-electron atoms. *Physical Review*, 146:46, 1966.

[15] A. J. Thakkar and T. Koga. Ground-state energies for the helium isoelectronic series. *Physical Review A*, 50:854, 1994.

[16] G. W. Drake. High precision theory of atomic helium. *Physica Scripta*, 1999:83, 1999.

[17] G. W. Drake, M. M. Cassar, and R. A. Nistor. Ground-state energies for helium, H-, and Ps-. *Physical Review A*, 65:054501, 2002.

[18] V. I. Korobov. Nonrelativistic ionization energy for the helium ground state. *Physical Review A*, 66:024501, 2002.

[19] C. Schwartz. Experiment and theory in computations of the He atom ground state. *International Journal of Modern Physics E*, 15:877, 2006.

[20] H. Nakashima and H. Nakatsuji. Solving the Schrödinger equation for helium atom and its isoelectronic ions with the free iterative complement interaction (ICI) method. *The Journal of chemical physics*, 127, 2007.

[21] M. B. Ruiz. Hylleraas–Configuration Interaction calculations on the 1^1S ground state of helium atom. *Journal of Coordination Chemistry*, 68:3340, 2015.

[22] J. S. Sims, B. Padhy, and M. B. Ruiz. Exponentially correlated Hylleraas-configuration interaction nonrelativistic energy of the ^{1}S ground state of the helium atom. *International journal of quantum chemistry*, 121:e26470, 2021.

[23] V. Korobov and A. Yelkhovsky. Ionization potential of the helium atom. *Physical Review Letters*, 87:193003, 2001.

[24] H. Nakashima and H. Nakatsuji. Solving the electron-nuclear Schrödinger equation of helium atom and its isoelectronic ions with the free iterative-complement-interaction method. *The Journal of chemical physics*, 128:154107, 2008.

[25] A. M. Frolov. Numerical evaluations of the isotopic shifts and lowest-order QED corrections for the ground 1^1S-states of the ^{3}He and ^{4}He atoms. *Chemical Physics Letters*, 619:61, 2015.

[26] S. Alexander and R. Coldwell. Properties of the finite-mass helium ground state. *Molecular Physics*, 115:598, 2017.

[27] E. Wigner. Einige folgerungen aus der Schrödingerschen theorie für die termstrukturen. *Zeitschrift für Physik*, 43:624, 1927.

[28] G. Breit. Separation of angles in the two-electron problem. *Physical Review*, 35:569, 1930.

[29] G. Breit. The fine structure of He as a test of the spin interactions of two electrons. *Physical Review*, 36:383, 1930.

[30] A. Bhatia and A. Temkin. Symmetric Euler-angle decomposition of the two-electron fixed-nucleus problem. *Reviews of Modern Physics*, 36:1050, 1964.

[31] A. Bhatia. Transitions $(1s2p)^3P^o - (2p^2)^3P^e$ in He and $(2s2p)^3P^o - (2p^2)^3P^e$ in H^-. *Physical Review A*, 2:1667, 1970.

[32] A. Bhatia. Odd-parity D states in He. *Physical Review A*, 6:2498, 1972.

[33] A. Bhatia. Autoionization states of Li, Be^+, B^{2+}, and C^{3+}. *Physical Review A*, 18:2523, 1978.

[34] A. Bhatia and Y. Ho. Complex-coordinate calculations of doubly excited $^{1,3}D^e$ resonant states of Ps^-. *Physical Review A*, 48:264, 1993.

[35] Y. Ho and A. Bhatia. P-wave shape resonances in positronium ions. *Physical Review A*, 47:1497, 1993.

[36] Y. Ho and A. Bhatia. Doubly-excited states in helium-like systems. *Journal of Physics B: Atomic, Molecular and Optical Physics*, 30:3597, 1997.

[37] A. Bhatia and Y. Ho. Calculations of doubly excited states in helium-like systems using Hylleraas functions. *Journal of Physics B: Atomic, Molecular and Optical Physics*, 31:3307, 1998.

[38] T. K. Mukherjee and P. K. Mukherjee. Variational equation of states of arbitrary angular momentum for two-particle systems. *Physical Review A*, 50:850, 1994.

[39] P. Feldman and R. Novick. Autoionizing states in the alkali atoms with microsecond lifetimes. *Physical Review Letters*, 11:278, 1963.

[40] H. Berry, I. Martinson, L. Curtis, and L. Lundin. Lifetimes of some doubly excited levels in neutral helium. *Physical Review A*, 3:1934, 1971.

[41] H. Berry, J. Desesquelles, and M. Dufay. Energies and lifetimes of doubly excited states in He I. *Physical Review A*, 6:600, 1972.

[42] R. Madden and K. Codling. New autoionizing atomic energy levels in He, Ne, and Ar. *Physical Review Letters*, 10:516, 1963.

[43] R. Madden and K. Codling. Two-Electron Excitation States in Helium. *The Astrophysical Journal*, 141:364, 1965.

[44] P. Hicks and J. Comer. Ejected electron spectroscopy of autoionizing states excited by low energy electron impact. *Journal of Physics B: Atomic and Molecular Physics*, 8:1866, 1975.

[45] P. Hammond. Highly excited states: New experimental windows in photoexcitation. *Journal of electron spectroscopy and related phenomena*, 144:13, 2005.

[46] M. Coreno et al. A new system for photon induced fluorescence spectroscopy applied to the study of doubly excited states of helium. *Journal of electron spectroscopy and related phenomena*, 144:39, 2005.

[47] J. Saha, S. Bhattacharyya, P. Mukherjee, and T. Mukherjee. On the diagnosis of fluorescence active autoionizing states of helium. *Chemical Physics Letters*, 517:223, 2011.

[48] S. Kasthurirangan et al. Observation of $2p3d(^1P^o) \rightarrow 1s3d(^1D^e)$ Radiative Transition in He-like Si, S, and Cl Ions. *Physical review letters*, 111:243201, 2013.

[49] A. Doschek et al. Heliumlike calcium emission observed during a solar flare. *The Astrophysical Journal*, 164:165, 1971.

[50] G. W. F. Drake and A. Dalgarno. A $1/Z$ expansion study of the $2s2p^1P$ and ^3P autoionizing resonances of the helium isoelectronic sequence. *Proceedings of the Royal Society of London. A. Mathematical and Physical Sciences*, 320:549, 1971.

[51] S. M. Kahn. Recent progress in X-ray spectroscopy of astrophysical plasmas. *Physica Scripta*, 1999:23, 1999.

[52] A. Bhatia and A. Temkin. Decomposition of the Schrödinger equation for two identical particles and a third particle of finite mass. *Physical Review*, 137:A1335, 1965.

[53] T. K. Mukherjee and P. K. Mukherjee. Variational equation of states of arbitrary angular momenta for three-particle systems. *Physical Review A*, 51:4276, 1995.

[54] O. Ciricosta et al. Direct Measurements of the Ionization Potential Depression in a Dense Plasma. *Phys. Rev. Lett.*, 109:065002, 2012.

[55] D. J. Hoarty et al. Observations of the Effect of Ionization-Potential Depression in Hot Dense Plasma. *Phys. Rev. Lett.*, 110:265003, 2013.

[56] S. M. Vinko et al. Investigation of femtosecond collisional ionization rates in a solid-density aluminium plasma. *Nature Communications*, 6:6397, 2015.

[57] O. Ciricosta et al. Measurements of continuum lowering in solid-density plasmas created from elements and compounds. *Nature Communications*, 7:11713, 2016.

[58] S. Korsholm et al. Collective thomson scattering capabilities to diagnose fusion plasmas. *Nuclear Instruments and Methods in Physics Research Section A: Accelerators, Spectrometers, Detectors and Associated Equipment*, 623:677, 2010.

[59] M. Van Zeeland, W. Heidbrink, and J. Yu. Fast ion Dα imaging in the DIII-D tokamak. *Plasma Physics and Controlled Fusion*, 51:055001, 2009.

[60] M. Nocente et al. MeV range particle physics studies in tokamak plasmas using gamma-ray spectroscopy. *Plasma Physics and Controlled Fusion*, 62:014015, 2019.

[61] ITER - the way to new energy, http://www.iter.org.

[62] ITER Newsline. https://www.iter.org/newsline/102/1396.

[63] ITER Newsline. https://www.iter.org/newsline/-/3799.

[64] R. Neu, A. Kallenbach, and H. Zohm. 5 - ASDEX Upgrade. In *Magnetic Fusion Energy*, pp. 93. Woodhead Publishing, 2016.

[65] P. Rebut. The JET preliminary tritium experiment. *Plasma Physics and Controlled Fusion*, 34:1749, 1992.

[66] I. Langmuir. Oscillations in ionized gases. *Proceedings of the National Academy of Sciences of the United States of America*, 14:627, 1928.

[67] L. Tonks and I. Langmuir. Oscillations in Ionized Gases. *Phys. Rev.*, 33:195, 1929.

[68] P. M. Bellan. *Fundamentals of Plasma Physics*. Cambridge University Press, 2006.

[69] J. P. Freidberg. *Plasma Physics and Fusion Energy*. Cambridge University Press, 2007.

[70] S. Pfalzner. *An Introduction to Inertial Confinement Fusion*. Series in Plasma Physics. CRC Press, 2006.

[71] R. Hawryluk et al. Principal physics developments evaluated in the ITER design review. *Nuclear Fusion*, 49:065012, 2009.

[72] P. Stubbe and T. Hagfors. The Earth's ionosphere: A wall-less plasma laboratory. *Surveys in Geophysics*, 18:57, 1997.

[73] N. R. Council. *Space Plasma Physics: The Study of Solar-System Plasmas*. The National Academies Press, Washington, DC, 1978.

[74] B. De Pontieu et al. The origins of hot plasma in the solar corona. *Science*, 331:55, 2011.

[75] B. M. Smirnov. *Theory of Gas Discharge Plasma*. Springer International Publishing, 2015.

[76] B. A. Remington, R. P. Drake, and D. D. Ryutov. Experimental astrophysics with high power lasers and Z pinches. *Reviews of Modern Physics*, 78:755, 2006.

[77] G. Shpatakovskaya. Semiclassical model of a one-dimensional quantum dot. *Journal of Experimental and Theoretical Physics*, 102:466, 2006.

[78] N. Rani, M. Yadav, and Y. Mathur. The nonlinear wave in semiconductor quantum plasma for laser beam in a self-consistent plasma channel. *Physics Letters A*, 384:126188, 2020.

[79] R. J. Goldston and P. H. Rutherford. *Introduction to Plasma Physics*. Routledge and CRC Press, 1995.

[80] P. M. Bellan. *Fundamentals of Plasma Physics*. Cambridge University Press, 2004.

[81] S. Ichimaru. Strongly coupled plasmas: high-density classical plasmas and degenerate electron liquids. *Rev. Mod. Phys.*, 54:1017, 1982.

[82] V. Fortov, I. Iakubov, and A. Khrapak. *Physics of Strongly Coupled Plasma*. International Series of Monographs on Physics. Oxford University Press, Oxford, 2006.

[83] P. Debye and E. Hückel. De la theorie des electrolytes. i. abaissement du point de congelation et phenomenes associes. *Physikalische Zeitschrift*, 24:185, 1923.

[84] L. H. Thomas. The calculation of atomic fields. *Mathematical Proceedings of the Cambridge Philosophical Society*, 23:542, 1927.

[85] E. Fermi. Eine statistische Methode zur Bestimmung einiger Eigenschaften des Atoms und ihre Anwendung auf die Theorie des periodischen Systems der Elemente. *Zeitschrift für Physik*, 48:73, 1928.

[86] B. F. Rozsnyai. Relativistic Hartree-Fock-Slater Calculations for Arbitrary Temperature and Matter Density. *Phys. Rev. A*, 5:1137, 1972.

[87] D. Salzmann. Calculation of the electric potential around two identical atoms or ions. *Phys. Rev. A*, 49:3729, 1994.

[88] B. J. B. Crowley. Average-atom quantum-statistical cell model for hot plasma in local thermodynamic equilibrium over a wide range of densities. *Phys. Rev. A*, 41:2179, 1990.

[89] M. W. C. Dharma-wardana and F. Perrot. Density-functional theory of hydrogen plasmas. *Phys. Rev. A*, 26:2096, 1982.

[90] D. A. Liberman. Self-consistent field model for condensed matter. *Phys. Rev. B*, 20:4981, 1979.

[91] D. A. Liberman. Inferno: A better model of atoms in dense plasmas. *Journal of Quantitative Spectroscopy and Radiative Transfer*, 27:335, 1982.

[92] P. Shukla and B. Eliasson. Screening and wake potentials of a test charge in quantum plasmas. *Physics Letters A*, 372:2897, 2008.

[93] P. K. Shukla. Shielding of a slowly moving test charge in dusty plasmas. *Physics of Plasmas*, 1:1362, 1994.

[94] A. Hasegawa, K. Mima, and M. Duong-van. Plasma Distribution Function in a Superthermal Radiation Field. *Phys. Rev. Lett.*, 54:2608, 1985.

[95] D. Summers and R. M. Thorne. The modified plasma dispersion function. *Physics of Fluids B: Plasma Physics*, 3:1835, 1991.

[96] D. A. Bryant. Debye length in a kappa-distribution plasma. *Journal of Plasma Physics*, 56:87, 1996.

[97] L. G. Stanton and M. S. Murillo. Unified description of linear screening in dense plasmas. *Phys. Rev. E*, 91:033104, 2015.

[98] G. Ecker and W. Weizel. Zustandssumme und effektive Ionisierungsspannung eines Atoms im Inneren des Plasmas. *Annalen der Physik*, 452:126, 1956.

[99] C. R. Smith. Bound States in a Debye-Hückel Potential. *Phys. Rev.*, 134:A1235, 1964.

[100] G. J. Iafrate and L. B. Mendelsohn. High-Order Perturbation Theory for the Bound States of an Electron in a Screened Coulomb Potential. *Phys. Rev.*, 182:244, 1969.

[101] H. Muller-Kirsten and N. Vahedi-Faridi. Large coupling expansions for eigenenergies and Regge trajectories of the Yukawa potential. *Journal of Mathematical Physics*, 14:1291, 1973.

[102] J. McEnnan, L. Kissel, and R. H. Pratt. Analytic perturbation theory for screened Coulomb potentials: Nonrelativistic case. *Phys. Rev. A*, 13:532, 1976.

[103] B. Saha, P. K. Mukherjee, and G. H. F. Diercksen. Energy levels and structural properties of compressed hydrogen atom under Debye screening. *Astronomy and Astrophysics*, 396:337, 2002.

[104] S. Lumb, S. Lumb, and V. Prasad. Photoexcitation and ionization of a hydrogen atom confined by a combined effect of a spherical box and Debye plasma. *Physics Letters A*, 379:1263, 2015.

[105] G. M. Harris. Attractive Two-Body Interactions in Partially Ionized Plasmas. *Phys. Rev.*, 125:1131, 1962.

[106] J. B. Krieger. Electron Shielding in Heavily Doped Semiconductors. *Phys. Rev.*, 178:1337, 1969.

[107] C. S. Lam and Y. P. Varshni. Energies of s Eigenstates in a Static Screened Coulomb Potential. *Phys. Rev. A*, 4:1875, 1971.

[108] K. M. Roussel and R. F. O'Connell. Variational solution of Schrodinger's equation for the static screened Coulomb potential. *Phys. Rev. A*, 9:52, 1974.

[109] S. L. Garavelli and F. A. Oliveira. Analytical solution for a Yukawa-type potential. *Phys. Rev. Lett.*, 66:1310, 1991.

[110] C. Stubbins. Bound states of the Hulthen and Yukawa potentials. *Phys. Rev. A*, 48:220, 1993.

[111] S. Paul and Y. K. Ho. Hydrogen atoms in Debye plasma environments. *Physics of Plasmas*, 16:063302, 2009.

[112] J. K. Saha, T. K. Mukherjee, P. K. Mukherjee, and B. Fricke. Hyperpolarizability of hydrogen atom under spherically confined Debye plasma. *The European Physical Journal D*, 62:205, 2011.

[113] V. Bonch-Bruevich and V. Glasko. Energy levels in a Debye field. *Opt. Spectry.(USSR)(English Transl.)*, 14, 1963.

[114] C. A. Rouse. Screened Coulomb Solutions of the Schrödinger Equation. *Phys. Rev.*, 159:41, 1967.

[115] F. J. Rogers, H. C. Graboske, and D. J. Harwood. Bound Eigenstates of the Static Screened Coulomb Potential. *Phys. Rev. A*, 1:1577, 1970.

[116] Y. Y. Qi, J. G. Wang, and R. K. Janev. Static dipole polarizability of hydrogenlike ions in Debye plasmas. *Phys. Rev. A*, 80:032502, 2009.

[117] D. Bielinska-Waz, J. Karwowski, B. Saha, and P. K. Mukherjee. Relativistic effects in hydrogenlike atoms embedded in Debye plasmas. *Phys. Rev. E*, 69:016404, 2004.

[118] M. Pawlak and M. Bylicki. Stark resonances of the Yukawa potential: Energies and widths, crossings and avoided crossings. *Phys. Rev. A*, 83:023419, 2011.

[119] M. K. Bahar and A. Soylu. The hydrogen atom in plasmas with an external electric field. *Physics of Plasmas*, 21:092703, 2014.

[120] K. Scheibner, J. Weisheit, and N. Lane. Plasma screening effects on proton-impact excitation of positive ions. *Physical Review A*, 35:1252, 1987.

[121] Y.-D. Jung. Orientation phenomena for electron-ion collisional excitations in strongly coupled plasmas. *The European Physical Journal D-Atomic, Molecular, Optical and Plasma Physics*, 7:249, 1999.

[122] D. Ray. Influence of a dense plasma on the fine-structure levels of a hydrogenic ion. *Physical Review E*, 62:4126, 2000.

[123] B. F. Rozsnyai. Photoabsorption in hot plasmas based on the ion-sphere and ion-correlation models. *Physical Review A*, 43:3035, 1991.

[124] S. Skupsky. X-ray line shift as a high-density diagnostic for laser-imploded plasmas. *Physical Review A*, 21:1316, 1980.

[125] H. Nguyen et al. Atomic structure and polarization line shift in dense and hot plasmas. *Physical Review A*, 33:1279, 1986.

[126] J. Seidel, S. Arndt, and W. Kraeft. Energy spectrum of hydrogen atoms in dense plasmas. *Physical Review E*, 52:5387, 1995.

[127] U. Gupta and A. K. Rajagopal. Density functional formalism at finite temperatures with some applications. *Physics Reports*, 87:259, 1982.

[128] S. Bhattacharyya, A. Sil, S. Fritzsche, and P. Mukherjee. Effect of strongly coupled plasma on the spectra of hydrogenlike carbon, aluminium and argon. *The European Physical Journal D*, 46:1, 2008.

[129] A. Sil, B. Saha, and P. Mukherjee. Effect of dense plasma on the spectral properties of hydrogenic ions. *International journal of quantum chemistry*, 104:903, 2005.

[130] X. Li and F. Rosmej. Quantum-number–dependent energy level shifts of ions in dense plasmas: A generalized analytical approach. *Europhysics Letters*, 99:33001, 2012.

[131] Z.-B. Chen et al. Influence of dense plasma on the energy levels and transition properties in highly charged ions. *Physics of Plasmas*, 25:032108, 2018.

[132] Z.-B. Chen et al. Single-photon photoionization of highly charged ions under warm-and hot-dense plasmas using a unified description of screening. *Journal of Quantitative Spectroscopy and Radiative Transfer*, 253:107170, 2020.

[133] N. Mukherjee, C. N. Patra, and A. K. Roy. Confined hydrogenlike ions in plasma environments. *Physical Review A*, 104:012803, 2021.

[134] S. Balberg and S. L. Shapiro. The properties of matter in white dwarfs and neutron stars. *arXiv preprint astro-ph/0004317*, 2000.

[135] S. de Vega, J. D. Cox, and F. J. G. de Abajo. Plasmons in doped finite carbon nanotubes and their interactions with fast electrons and quantum emitters. *Physical Review B*, 94:075447, 2016.

[136] B. J. Falaye et al. Hydrogen atom in a laser-plasma. *Laser Physics Letters*, 13:116003, 2016.

[137] S. Regan et al. Diagnosing implosions at the National Ignition Facility with x-ray spectroscopy. In *AIP Conference Proceedings*, volume 1438, pp. 49. American Institute of Physics, 2012.

[138] U. Zastrau et al. Warm dense aluminum plasma generated by the free-electron-laser FLASH. In *AIP Conference Proceedings*, volume 1438, pp. 61. American Institute of Physics, 2012.

[139] R. Dutt. Bound s-state energies for the exponential cosine screened Coulomb potential in Ecker-Weizel approximations. *Physics Letters A*, 73:310, 1979.

[140] P. P. Ray and A. Ray. Continuum and discrete s states for the exponential cosine screened coulomb potential by the Ecker-Weizel approximation. *Physics Letters A*, 78:443, 1980.

[141] C. Lai. Energies of the exponential cosine screened Coulomb potential. *Physical Review A*, 26:2245, 1982.

[142] A. Chatterjee. Bound-state energies of the generalized exponential cosine-screened Coulomb potential. *Physical Review A*, 34:2470, 1986.

[143] S. M. Ikhdair and R. Sever. Bound state energies for the exponential cosine screened Coulomb potential. *Zeitschrift für Physik D Atoms, Molecules and Clusters*, 28:1, 1993.

[144] A. K. Roy. Studies on some exponential-screened Coulomb potentials. *International Journal of Quantum Chemistry*, 113:1503, 2013.

[145] S. Lumb, S. Lumb, D. Munjal, and V. Prasad. Intense field induced excitation and ionization of an atom confined in a dense quantum plasma. *Physica Scripta*, 90:095603, 2015.

[146] H. Hu, Z. Chen, and W. Chen. Radiative transition of hydrogen-like ions in quantum plasma. *Radiation Effects and Defects in Solids*, 171:890, 2016.

[147] Y. Qi, J. Wang, and R. Janev. Photoionization of hydrogen-like ions in dense quantum plasmas. *Physics of Plasmas*, 24:062110, 2017.

[148] G. Zhao, L. Liu, J. Wang, and R. Janev. Spectral properties of hydrogen-like ions in finite-temperature quantum plasmas. *Physics of Plasmas*, 24:053509, 2017.

[149] S. K. Nayek, S. Mondal, and J. K. Saha. Structural properties of hydrogen-like ions (Z= 1–18) under quantum and classical plasma environment. *Atomic Data and Nuclear Data Tables*, 137:101379, 2021.

[150] D.-N. Ly, N.-T. D. Hoang, and V.-H. Le. Highly accurate energies of a plasma-embedded hydrogen atom in a uniform magnetic field. *Physics of Plasmas*, 28:063301, 2021.

[151] H. Hu et al. Shielding effect of quantum plasma. *Physics of Plasmas*, 26:082108, 2019.

[152] H. Hu, F. Li, and C. Jiang. Binding energy levels of a slowly moving ion in quantum plasmas. *Physical Review E*, 85:056406, 2012.

[153] H. Hu et al. Radiative transitions of excited ions moving slowly in plasmas. *Physics of Plasmas*, 21:122113, 2014.

[154] E. L. L. P. Pitaevskii. *Physical Kinetics.* Course of theoretical physics. Butterworth-Heinemann, 1981.

[155] D. Pines. Classical and quantum plasmas. *Journal of Nuclear Energy. Part C, Plasma Physics, Accelerators, Thermonuclear Research*, 2:5, 1961.

[156] D. Zwillinger. *Table of Integrals, Series, and Products.* Elsevier, Burlington, 2007.

[157] E. Fichard and V. Franco. Differential properties of Meijer's G-function. *Journal of Physics A: Mathematical and General*, 13:2331, 1980.

[158] G. B. Arfken, H. J. Weber, and F. E. Harris. *Mathematical Methods for Physicists*. Academic Press, Boston, seventh edition, 2013.

[159] R. Varma, P. Shukla, and V. Krishan. Electrostatic oscillations in the presence of grain-charge perturbations in dusty plasmas. *Physical Review E*, 47:3612, 1993.

[160] P. K. Shukla, L. Stenflo, and R. Bingham. Shielding of a slowly moving test charge in a quantum plasma. *Physics Letters A*, 359:218, 2006.

[161] J. A. Nelder and R. Mead. A simplex method for function minimization. *The computer journal*, 7:308, 1965.

[162] B. H. Bransden and C. J. Joachain. *Physics of Atoms and Molecules*. Delhi: Pearson Education, 2004.

[163] R. Dexter and B. Lax. Effective masses of holes in silicon. *Physical Review*, 96:223, 1954.

[164] C. Hu. Electrons and Holes in Semiconductors. In *Modern Semiconductor Devices for Integrated Circuits*, pp. 351. Pearson/Prentice Hall, New Jersey, 1st edition, 2010.

[165] K. Sen. Shell-confined hydrogen atom. *The Journal of chemical physics*, 122:194324, 2005.

[166] B. Saha and P. Mukherjee. Effect of Debye plasma on the structural properties of compressed positronium atom. *Physics Letters A*, 302:105, 2002.

[167] A. Sil, B. Saha, and P. Mukherjee. Effect of Debye plasma on compressed exotic atoms. *Physics Letters A*, 324:308, 2004.

[168] J. Goy, J.-M. Richard, and S. Fleck. Weakly bound three-body systems with no bound subsystems. *Physical Review A*, 52:3511, 1995.

[169] D. Bressanini, G. Morosi, L. Bertini, and M. Mella. Stability of few-body systems and quantum Monte-Carlo methods. *Few-Body Systems*, 31:199, 2002.

[170] B. Saha, T. Mukherjee, and P. Mukherjee. Electron affinity of positronium embedded in Debye plasma. *Chemical physics letters*, 373:218, 2003.

[171] L. Bertini, M. Mella, D. Bressanini, and G. Morosi. Borromean binding in H_2 with Yukawa potential: A nonadiabatic quantum Monte Carlo study. *Physical Review A*, 69:042504, 2004.

[172] S. Kar and Y. Ho. Positron annihilation in the dense plasma-embedded Ps^-. *Chemical physics letters*, 424:403, 2006.

[173] P. Mukherjee, S. Fritzsche, and B. Fricke. Stability of H_2^+ molecular ion under Debye plasma. *Physics Letters A*, 360:287, 2006.

[174] S. Kar and Y. Ho. Bound states and dipole polarizability of hydrogen molecular ion H_2^+ in weakly coupled hot plasmas. *Physics Letters A*, 368:476, 2007.

[175] S. Bhattacharyya et al. Electron affinity of exotic systems under Debye plasma. *International Journal of Quantum Chemistry*, 107:946, 2007.

[176] S. Bhattacharyya, A. Sil, T. Mukherjee, and P. Mukherjee. Exotic affinities under Debye plasma. *Physics of plasmas*, 14:024503, 2007.

[177] A. N. Sil, M. Pawlak, P. K. Mukherjee, and M. Bylicki. The influence of Debye plasma on the ground state energies of exotic systems. *Journal of Quantitative Spectroscopy and Radiative Transfer*, 109:873, 2008.

[178] M. Pawlak, M. Bylicki, J. K. Saha, and P. K. Mukherjee. Borromean states of three-particle exotic systems with screened Coulomb interactions. *Journal of Physics B: Atomic, Molecular and Optical Physics*, 42:215701, 2009.

[179] F. Pont and P. Serra. Stability diagrams of plasma-embedded three-unit-charge systems: Borromean states and the Efimov effect. *Physical Review A*, 79:032508, 2009.

[180] A. Ghoshal and Y. Ho. Borromean bindings in muonic molecular ions with screened Coulomb potentials. *Journal of Physics B: Atomic, Molecular and Optical Physics*, 43:115007, 2010.

[181] S. Sen, P. Mandal, and P. Mukherjee. Positronium formation in Debye plasma. *The European Physical Journal D*, 62:379, 2011.

[182] S. Kar and Y. Ho. Borromean binding in H_2^+ with screened Coulomb potentials. *Chemical Physics Letters*, 506:282, 2011.

[183] S. Kar and Y. Ho. Borromean windows for H_2^+ with screened Coulomb potentials. *Physical Review A*, 86:014502, 2012.

[184] M. Pawlak, M. Bylicki, and P. K. Mukherjee. On the limit of existence of Borromean binding in three-particle systems with screened Coulomb interactions. *Journal of Physics B: Atomic, Molecular and Optical Physics*, 47:095701, 2014.

[185] A. Poszwa, M. K. Bahar, and A. Soylu. The nuclear size and mass effects on muonic hydrogen-like atoms embedded in Debye plasma. *Physics of Plasmas*, 23:103515, 2016.

[186] Z.-S. Jiang, X.-D. Song, L. Zhou, and S. Kar. Borromean Windows for Three-Particle Systems under Screened Coulomb Interactions. *Communications in Theoretical Physics*, 67:542, 2017.

[187] J. Karwowski. Three-Particle Non-Born-Oppenheimer Systems. In *Theoretical and Quantum Chemistry at the Dawn of the 21st Century*, pp. 527. Apple Academic Press, 2018.

[188] S. Kar and Y. Ho. Ground state and resonance state of Ps^- in plasmas with various Debye lengths. *Physical Review A*, 71:052503, 2005.

[189] S. Kar and Y. Ho. Doubly excited $^{1,3}P^o$ resonance states of Ps^- in weakly coupled plasmas. *Physical Review A*, 73:032502, 2006.

[190] S. Kar and Y. Ho. D-wave resonances in three-body system Ps^- with pure Coulomb and screened Coulomb (Yukawa) potentials. *Few-Body Systems*, 45:43, 2009.

[191] S. Kar and Y. Ho. Doubly excited $^{1,3}P^e$ resonance states of the positronium negative ion with Coulomb and screened Coulomb potentials. *Few-Body Systems*, 46:173, 2009.

[192] Y. Ho and S. Kar. Complex-scaling calculations for doubly excited resonances in Ps^- interacting with screened Coulomb (Yukawa) potentials. *Few-Body Systems*, 53:437, 2012.

[193] Y. Ho and S. Kar. High-lying doubly excited resonances in Ps^- interacting with screened Coulomb potentials. *Chinese Journal of Physics*, 54:574, 2016.

[194] S. Kar and Y. Ho. Bound states and resonance states of the plasma-embedded p p μ molecular ion. *Physical Review A*, 75:062509, 2007.

[195] S. Kar and Y. Ho. Bound states and resonance states of the plasma-embedded tdμ and ddμ molecular ions. *The European Physical Journal D*, 48:157, 2008.

[196] J.-M. Richard. Critically bound four-body molecules. *Physical Review A*, 67:034702, 2003.

[197] L. H. Thomas. The interaction between a neutron and a proton and the structure of H^3. *Physical review*, 47:903, 1935.

[198] V. Efimov. Energy levels arising from resonant two-body forces in a three-body system. *Physics Letters B*, 33:563, 1970.

[199] X. Cui and W. Yi. Universal borromean binding in spin-orbit-coupled ultracold fermi gases. *Physical Review X*, 4:031026, 2014.

[200] T. Kraemer et al. Evidence for Efimov quantum states in an ultracold gas of caesium atoms. *Nature*, 440:315, 2006.

[201] S. E. Pollack, D. Dries, and R. G. Hulet. Universality in three-and four-body bound states of ultracold atoms. *Science*, 326:1683, 2009.

[202] M. Zaccanti et al. Observation of an Efimov spectrum in an atomic system. *Nature Physics*, 5:586, 2009.

[203] E. Wigner. *Group Theory*. Academic Press, New York and London, 1959.

[204] S. Kar and Y. Ho. Doubly-excited $2s^2\ {}^1S^e$ resonance state of helium embedded in Debye plasmas. *Chemical physics letters*, 402:544, 2005.

[205] M. Bylicki. Spectrum of doubly excited resonances in. *Journal of Physics B: Atomic, Molecular and Optical Physics*, 30:189, 1997.

[206] J. K. Saha and T. K. Mukherjee. Doubly excited bound and resonance $({}^3P^e)$ states of helium. *Physical Review A*, 80:022513, 2009.

[207] B. T. Smith et al. *Matrix Eigensystem Routines - EISPACK Guide*. Lecture Notes in Computer Science. Springer-Verlag, Berlin Heidelberg, 2 edition, 1976.

[208] J.-L. Calais and P.-O. Löwdin. A simple method of treating atomic integrals containing functions of r_{12}. *Journal of Molecular Spectroscopy*, 8:203, 1962.

[209] H. Feshbach. Unified theory of nuclear reactions. *Annals of Physics*, 5:357, 1958.

[210] H. Feshbach. A unified theory of nuclear reactions. II. *Annals of Physics*, 19:287, 1962.

[211] J. M. Bowman. Collision lifetime approach to recombination and a new derivation of RRKM theory. *The Journal of Physical Chemistry*, 90:3492, 1986.

[212] V. Mandelshtam, T. Ravuri, and H. Taylor. Calculation of the density of resonance states using the stabilization method. *Physical review letters*, 70:1932, 1993.

[213] J. Müller, X. Yang, and J. Burgdörfer. Calculation of resonances in doubly excited helium using the stabilization method. *Physical Review A*, 49:2470, 1994.

[214] S. Kar and Y. Ho. Electron affinity of the hydrogen atom and a resonance state of the hydrogen negative ion embedded in Debye plasmas. *New Journal of Physics*, 7:141, 2005.

[215] S. Bhattacharyya, J. Saha, P. Mukherjee, and T. Mukherjee. Three-body negative ions under Coulomb interaction. *Physica Scripta*, 85:065305, 2012.

[216] A. Frolov, V. Smith Jr, and J. Komasa. On the algebraic solution of the non-relativistic three-body problem: bound states. *Journal of Physics A: Mathematical and General*, 26:6507, 1993.

[217] O. A. Gomes, H. Chacham, and J. R. Mohallem. Variational calculations for the bound-unbound transition of the Yukawa potential. *Physical Review A*, 50:228, 1994.

[218] Y. Ho. Recent advances in the theoretical methods and computational schemes for investigations of resonances in few-body atomic systems. *Few-Body Systems*, 54:31, 2013.

[219] S. Kar and Y. Ho. Bound states and resonance states of the plasma-embedded p p μ molecular ion. *Physical Review A*, 75:062509, 2007.

[220] S. Kilic, J.-P. Karr, and L. Hilico. Coulombic and radiative decay rates of the resonances of the exotic molecular ions p p μ, p p π, d d μ, d d π, and d t μ. *Physical Review A*, 70:042506, 2004.

[221] A. B. Walker Jr and H. R. Rugge. Observation of autoionizing states in the solar corona. *The Astrophysical Journal*, 164:181, 1971.

[222] J. S. Parker et al. High-energy cutoff in the spectrum of strong-field nonsequential double ionization. *Physical Review Letters*, 96:133001, 2006.

[223] F. J. Rogers. Statistical mechanics of Coulomb gases of arbitrary charge. *Phys. Rev. A*, 10:2441, 1974.

[224] C. S. Lam and Y. P. Varshni. Ionization energy of the helium atom in a plasma. *Phys. Rev. A*, 27:418, 1983.

[225] Z. Wang and P. Winkler. Pair-function calculations for two-electron systems in model plasma environments. *Phys. Rev. A*, 52:216, 1995.

[226] P. Winkler. Detachment energies for a negative hydrogen ion embedded in a variety of Debye plasmas. *Phys. Rev. E*, 53:5517, 1996.

[227] D. Ray and P. K. Mukherjee. Magnetic multipole transitions of a stripped carbon ion in a variety of Debye plasmas. *Journal of Physics B: Atomic, Molecular and Optical Physics*, 31:3479, 1998.

[228] P. K. Mukherjee, J. Karwowski, and G. H. Diercksen. On the influence of the Debye screening on the spectra of two-electron atoms. *Chemical Physics Letters*, 363:323, 2002.

[229] B. Saha, P. Mukherjee, D. Bielinska-Waz, and J. Karwowski. Time-dependent perturbation calculations for transition properties of two-electron atoms under Debye plasma. *Journal of Quantitative Spectroscopy and Radiative Transfer*, 78:131, 2003.

[230] S. Kar and Y. Ho. Effect of debye plasmas on the dispersion coefficients c6 for interactions among h and he atoms. *Chemical Physics Letters*, 449:246, 2007.

[231] S. Kar and Y. K. Ho. Multipole polarizabilities of helium and the hydrogen negative ion with Coulomb and screened Coulomb potentials. *Phys. Rev. A*, 80:062511, 2009.

[232] S. Kar and Y. K. Ho. Dispersion coefficients for interactions between helium atoms in Debye plasmas. *Phys. Rev. A*, 81:062506, 2010.

[233] Y.-C. Lin, C.-Y. Lin, and Y. K. Ho. Spectral data of helium atoms with screened Coulomb potentials using the B-spline approach. *Phys. Rev. A*, 85:042516, 2012.

[234] P. Serra and S. Kais. Ground-state stability and criticality of two-electron atoms with screened Coulomb potentials using the B-splines basis set. *Journal of Physics B: Atomic, Molecular and Optical Physics*, 45:235003, 2012.

[235] S. Kar. Dynamic dipole polarizability of the helium atom with Debye-Hückel potentials. *Phys. Rev. A*, 86:062516, 2012.

[236] S. Kar, Y.-S. Wang, W.-Q. Li, and X.-D. Sun. Dynamic polarizability of two-electron ions under Debye screening. *International Journal of Quantum Chemistry*, 115:1573, 2015.

[237] M.-A. Martínez-Sánchez et al. Ionization of many-electron atoms by the action of two plasma models. *Physical Review E*, 103:043202, 2021.

[238] S. Kar and Y. K. Ho. Doubly excited $^{1,3}P^e$ meta-stable bound states and resonance states of helium in weakly coupled plasmas. *Journal of Physics B: Atomic, Molecular and Optical Physics*, 40:1403, 2007.

[239] S. Kar and Y. K. Ho. Unnatural parity states of helium with screened Coulomb potentials. *International Journal of Quantum Chemistry*, 108:1491, 2008.

[240] S. Kar and Y. K. Ho. Doubly excited nonautoionizing P, D, and F states of helium with Coulomb and screened Coulomb potentials. *Phys. Rev. A*, 79:062508, 2009.

[241] J. K. Saha, S. Bhattacharyya, T. K. Mukherjee, and P. K. Mukherjee. $2pnp(^{1,3}P^e)$ states of neutral He and Li^+ ions under Debye plasma screening. *Journal of Physics B: Atomic, Molecular and Optical Physics*, 42:245701, 2009.

[242] J. K. Saha, S. Bhattacharyya, T. Mukherjee, and P. Mukherjee. $^{1,3}D^o$ and $^{1,3}P^e$ states of two electron atoms under Debye plasma screening. *Journal of Quantitative Spectroscopy and Radiative Transfer*, 111:675, 2010.

[243] L. Jiao and Y. Ho. Doubly-excited $2p^2\ ^3P^e$ state of the hydrogen negative ion in Debye plasmas. *Journal of Quantitative Spectroscopy and Radiative Transfer*, 144:27, 2014.

[244] C. Zhou, Y. Yu, S. Yang, and H. Qiao. Geometric quantities of lower doubly excited bound states of helium. *Chinese Physics B*, 2021.

[245] Z. Wang and P. Winkler. Analytic solution to the resonance problem of screened Coulomb potentials. *International Journal of Quantum Chemistry*, 36:89, 1989.

[246] S. Kar and Y. K. Ho. Autoionizing $^1S^e$ resonance of H^- in Debye plasma environments. *Phys. Rev. E*, 70:066411, 2004.

[247] S. Kar and Y. K. Ho. Doubly excited $2s2p\ ^{1,3}P^o$ resonance states of helium in dense plasmas. *Phys. Rev. A*, 72:010703, 2005.

[248] S. Kar and Y. Ho. Doubly excited inter-shell P-wave resonances of helium in weakly coupled plasmas. *Journal of Physics B: Atomic, Molecular and Optical Physics*, 39:2445, 2006.

[249] S. Kar and Y. Ho. The ground state and doubly-excited $^{1,3}P^o$ states of hot-dense plasma-embedded Li^+ ions. *The European Physical Journal D*, 44:1, 2007.

[250] S. Kar and Y. Ho. Isotope shift for the $^1D^e$ autodetaching resonance in H^- and D^-. *Journal of Physics B: Atomic, Molecular and Optical Physics*, 42:055001, 2009.

[251] S. Kar and Y. Ho. Effect of screened Coulomb potentials on the resonance states of two-electron highly stripped atoms using the stabilization method. *Journal of Physics B: Atomic, Molecular and Optical Physics*, 42:044007, 2009.

[252] S. Kar and Y. Ho. Resonances in electron–hydrogen scattering in Debye plasmas. *Journal of Physics B: Atomic, Molecular and Optical Physics*, 44:015001, 2010.

[253] S. Kar and Y. Ho. Doubly excited $^{1,3}P^e$ resonance states of helium and the hydrogen negative ion interacting with Coulomb and screened Coulomb potentials. *Physical Review A*, 83:042506, 2011.

[254] S. Chakraborty and Y. Ho. Complex-rotation treatment on high-lying doubly-excited resonances in H^- interacting with screened Coulomb potentials. *Chemical physics letters*, 438:99, 2007.

[255] L. Jiao and Y. Ho. Doubly excited P-wave resonance states of H^- in Debye plasmas. *Physics of Plasmas*, 20:083303, 2013.

[256] L. G. Jiao and Y. K. Ho. Complex-scaling calculations for resonance states of he with screened Coulomb potentials. *International Journal of Quantum Chemistry*, 113:2569, 2013.

[257] A. Sil and P. Mukherjee. Effect of Debye plasma on the doubly excited states of highly stripped ions. *International journal of quantum chemistry*, 102:1061, 2005.

[258] S. Kar et al. Doubly-excited $^{1,3}D^e$ resonance states of two-electron positive ions Li^+ and Be^{2+} in Debye plasmas. *Physics of Plasmas*, 21:012105, 2014.

[259] X.-Q. Hu et al. Doubly excited $^3P^e$ resonance states of two-electron positive ions in Debye plasmas. *Physics of Plasmas*, 22:112107, 2015.

[260] A. Basu. $2s^2\ ^1S^e$ resonance of H^- in a Debye plasma. *Europhysics Letters*, 88:53001, 2009.

[261] A. Basu. P-wave auto-detaching resonances of H^- below the $n = 2$ threshold in a Debye plasma medium. *Journal of Physics B: Atomic, Molecular and Optical Physics*, 43:115202, 2010.

[262] A. Basu. Lowest lying $^1D^e$ resonance of H^- in Debye plasma. *The European Physical Journal D*, 61:51, 2011.

[263] M. Das et al. Application of relativistic coupled cluster linear response theory to helium-like ions embedded in plasma environment. *Journal of Physics B: Atomic, Molecular and Optical Physics*, 44:165701, 2011.

[264] L. Xie et al. Energy levels and multipole transition properties of C^{4+} ion in Debye plasmas. *The European Physical Journal D*, 66:1, 2012.

[265] Z.-B. Chen, K. Ma, H.-W. Hu, and K. Wang. Relativistic effects on the energy levels and radiative properties of He-like ions immersed in Debye plasmas. *Physics of Plasmas*, 25:072120, 2018.

[266] Y. Ma et al. KLL dielectronic recombination of hydrogenlike carbon ion in Debye plasmas. *Journal of Quantitative Spectroscopy and Radiative Transfer*, 241:106731, 2020.

[267] A. Sil and P. Mukherjee. Spectral properties of helium-like ions under strongly coupled plasma conditions. *International journal of quantum chemistry*, 106:465, 2006.

[268] A. N. Sil et al. Spectra of heliumlike carbon, aluminium and argon under strongly coupled plasma. *The European Physical Journal D*, 55:645, 2009.

[269] J. K. Saha, T. Mukherjee, P. Mukherjee, and B. Fricke. Effect of strongly coupled plasma on the magnetic dipolar and quadrupolar transitions of two-electron ions. *Physics of Plasmas*, 20:042703, 2013.

[270] S. Bhattacharyya, J. Saha, and T. Mukherjee. Nonrelativistic structure calculations of two-electron ions in a strongly coupled plasma environment. *Physical Review A*, 91:042515, 2015.

[271] M. Belkhiri, C. J. Fontes, and M. Poirier. Influence of the plasma environment on atomic structure using an ion-sphere model. *Physical Review A*, 92:032501, 2015.

[272] X.-F. Li et al. Transition energies, transition probabilities and weighted oscillator strengths of He-like Al in hot and dense plasmas. *Physica Scripta*, 92:075401, 2017.

[273] Z.-B. Chen. Calculation of the energies and oscillator strengths of Cl^{15+} in hot dense plasmas. *Journal of Quantitative Spectroscopy and Radiative Transfer*, 237:106615, 2019.

[274] X. Li and F. Rosmej. Analytical approach to level delocalization and line shifts in finite temperature dense plasmas. *Physics Letters A*, 384:126478, 2020.

[275] A. Singh et al. Plasma screening effects on the atomic structure of He-like ions embedded in strongly coupled plasma. *Physics Letters A*, 384:126369, 2020.

[276] K. Ma, Y. Chu, and Z. Chen. Analytical Calculation of Cl^{15+} Ion Immersed in Dense Plasmas. *Few-Body Systems*, 61:1, 2020.

[277] R. Chandra et al. Satellite lines of helium-like ions in strongly coupled plasma environment. *Journal of Quantitative Spectroscopy and Radiative Transfer*, 272:107830, 2021.

[278] M. Belkhiri and C. J. Fontes. Influence of the plasma environment on auto-ionization. *Journal of Physics B: Atomic, Molecular and Optical Physics*, 49:175002, 2016.

[279] S. S. Tan and Y. K. Ho. Determination of resonance energy and width by calculation of the density of reesonance states using the stabilisation method. *Chinese Journal of Physics*, 35:701, 1997.

[280] J. Eiglsperger, B. Piraux, and J. Madronero. Spectral representation of the three-body Coulomb problem. I. Nonautoionizing doubly excited states of high angular momentum in helium. *Physical Review A*, 81:042527, 2010.

[281] L. Lipsky, R. Anania, and M. Conneely. Energy levels and classifications of doubly-excited states in two-electron systems with nuclear charge, Z= 1, 2, 3, 4, 5, below the N= 2 and N= 3 thresholds. *Atomic data and nuclear data tables*, 20:127, 1977.

[282] S. Kar, Y. Wang, W.-Q. Li, and X.-D. Sun. Doubly Excited Nonautoionizing F and G States of Two-Electron Ions. *Few-Body Systems*, 56:651, 2015.

[283] S. Kar and Y. Ho. Unnatural parity states of helium with screened Coulomb potentials. *International Journal of Quantum Chemistry*, 108:1491, 2008.

[284] H. Bachau, F. Martin, A. Riera, and M. Yanez. Resonance parameters and properties of helium-like doubly excited states: $2 \leq Z \leq 10$. *Atomic data and nuclear data tables*, 48:167, 1991.

[285] Y. Ho and J. Callaway. Doubly excited states of helium atoms between the $N = 2$ and $N = 3$ He^+ thresholds. *Journal of Physics B: Atomic and Molecular Physics (1968-1987)*, 18:3481, 1985.

[286] J. Callaway. Two-electron excited states of helium. *Physics Letters A*, 66:201, 1978.

[287] S. Bhattacharyya, T. Mukherjee, J. Saha, and P. Mukherjee. Ritz variational calculation for two-electron–one-photon transitions in helium. *Physical Review A*, 78:032505, 2008.

[288] J. K. Saha, S. Bhattacharyya, and T. K. Mukherjee. Metastable bound $^{1,3}D^o$ states below $N = 3$ ionization threshold of He^+. *The Journal of Chemical Physics*, 132:134107, 2010.

[289] "atomic spectra database." nist. https://www.nist.gov/pml/atomic-spectra-database.

[290] M. Bylicki and C. A. Nicolaides. Theoretical resolution of the H^- resonance spectrum up to the $n = 4$ threshold. I. States of $^1P^o$, $^1D^o$, and $^1F^o$ symmetries. *Physical Review A*, 61:052508, 2000.

[291] M. Bylicki and C. A. Nicolaides. Theoretical resolution of the H^- resonance spectrum up to the $n = 4$ threshold. II. States of ^1S and ^1D symmetries. *Physical Review A*, 61:052509, 2000.

[292] A. Sadhukhan, S. Dutta, and J. K. Saha. Critical stability and quantum phase transition of screened two-electron system. *International Journal of Quantum Chemistry*, 119:e26042, 2019.

[293] J. K. Saha, S. Bhattacharyya, T. Mukherjee, and P. Mukherjee. $2pnp$ ($^{1,3}P^e$) states of neutral He and Li^+ ions under Debye plasma screening. *Journal of Physics B: Atomic, Molecular and Optical Physics*, 42:245701, 2009.

[294] J. K. Saha, S. Bhattacharyya, T. Mukherjee, and P. Mukherjee. $^{1,3}D^o$ and $^{1,3}P^e$ states of two electron atoms under Debye plasma screening. *Journal of Quantitative Spectroscopy and Radiative Transfer*, 111:675, 2010.

[295] T. Koga, H. Matsuyama, and A. J. Thakkar. Interelectronic angles: Rounding out a geometric picture of the helium atom. *Chemical Physics Letters*, 512:287, 2011.

Published Papers and Participation in Conferences

Exotic systems under screened Coulomb interactions: a study on Borromean windows

2014 Phys. Scr. 89 015401

(http://iopscience.iop.org/1402-4896/89/1/015401)

IOP Publishing | Royal Swedish Academy of Sciences Physica Scripta
Phys. Scr. **89** (2014) 015401 (13pp) doi:10.1088/0031-8949/89/01/015401

Exotic systems under screened Coulomb interactions: a study on Borromean windows

Sayantan Dutta[1], **Jayanta K Saha**[2], **Sukhamoy Bhattacharyya**[3,5], **Prasanta K Mukherjee**[4] **and Tapan K Mukherjee**[2]

[1] Belgharia Texmaco Estate School, Belgharia, Kolkata 700 056, India
[2] Narula Institute of Technology, Nilgunj Road, Agarpara, Kolkata 700 109, India
[3] Department of Physics, Auburn University, AL 36849, USA
[4] Ramakrishna Mission Vivekananda University Belur Math, Howrah 711202, India

E-mail: drtapanmukherjee@gmail.com

Received 17 July 2013, revised 6 November 2013
Accepted for publication 6 November 2013
Published 13 December 2013

Abstract

An extensive calculation of Borromean windows (BWs) for 22 different configurations of three-body exotic systems have been done using an explicitly correlated Hylleraas type basis set. From the variation of BWs with mass relation parameter (q) as observed from our calculations, a physical argument is being placed to interpret the existence of a BW for only $q < 1$ configurations.

Keywords: three-body system, screened Coulomb interaction, Borromean window, variational method

(Some figures may appear in colour only in the online journal)

1. Introduction

The bound (i.e. stable) state of an N-body system is termed as a Borromean state if all possible subsystems, i.e. $(N-1)$, $(N-2)$, ..., 3, 2 body systems become unbound [1]. This type of state is very interesting and indeed special because the natural process of forming an N-body system is by adding the constituent particles one by one. The possibility of the existence of such a state was first noticed long ago by Thomas [2] and then by Effimov [3] in the field of nuclear physics. After almost 35 years, the theoretical predictions on such states in ultra-cold gases have been experimentally verified by Kraemer *et al* [4] and Pollack *et al* [5]. The evidence of such states in different disciplines of science e.g. atomic physics [6–10], molecular physics [11–13], nuclear physics [2, 3, 14], chemical physics [15] and biology [16] is now available in the literature. The majority of the theoretical investigations on Borromean states deal with the systems in which net interactions within all pairs of particles are attractive. But in case of three-body systems, interaction between a pair of particles is always repulsive and thus provides an interesting case to study Borromean binding. In the last decade, considerable advancement [6–10, 13] has been made to study Borromean states of three-body systems under a screened Coulomb environment represented by the Yukawa type potential

$$V(r) = \frac{e^{-\lambda r}}{r}, \tag{1}$$

where λ is the screening parameter. A plasma environment can simulate such an interaction where the screening parameter becomes a function of the plasma temperature and density. However, such a screened Coulomb potential may be obtained in other physical situations also [17]. With the increase in screening parameter (λ), the energy eigenvalues of the three-body and the corresponding two-body subsystem become more and more positive [6, 7], leading to the complete fragmentation of the systems. The screening parameter (λ) at which an N-body system destabilizes under the screened Coulomb interaction is defined as the critical screening parameter (λ^c). The range of the screening parameter, in which the three-body system is bound despite the two-body subsystem being unbound, is termed as a Borromean window (BW). In other words, the BW is the difference between the critical screening parameters of the three-body and the corresponding two body subsystem. It is true that for pure Coulomb interactions, bound states of H_2^+ and H^- do not

[5] Permanent Address: Dept. of Physics, Acharya Prafulla Chandra College, New Barrackpore, Kolkata-700131, India.

fit the Borromean definition simply because they do not show Borromean binding. But in case of screened Coulomb interactions, it is seen [9, 10, 13, 18] that for a certain range of screening parameter (λ), the three-body H_2^+ exists in spite of the fact that the two-body sub-system H does not exist. In contrast, H^- and H destabilize for the same screening parameter. Thus H_2^+ shows Borromean binding whereas H^- does not under screened Coulomb interactions. For example, Bertini *et al* [13] studied the stability of the ground state of H_2^+ and H^- under a screened Coulomb interaction and found that both the systems show Borromean binding for a specific range of screening parameters. Kar and Ho found that the BW exists also for bound P, D, F and G states of an H_2^+ system in a screened Coulomb environment [9, 10, 18]. Due to the astrophysical abundance of the H_2^+ ion, experimental investigations [19–21] have been done to study the various structural properties of this ion. A few theoretical works [6–8] are available on the existence of Borromean binding for muonic molecular ions e.g. $pp\mu$, $dd\mu$, $tt\mu$ etc in the screened Coulomb potential. It is worthwhile mentioning that structures of Coulombic three-body ions have been theoretically studied [22–28] for a long time as the x-rays emitted from these ions provide very useful information about nuclear structure [29] and the muon catalyzed fusion processes [29–31] in stellar bodies. Such exotic two-body ions (XY) may be formed in experiments during the passage of hadrons through matter or dense plasma, although they have low lifetimes. The exotic two-body systems $p\mu(1S)$ and $p\mu(2S)$ have been observed experimentally [32–34]. The hardronic hydrogen atoms pY in the ground 1 s state have a very short lifetime (e.g. $\sim 10^{-16}$ s for $p\pi$ and $\sim 10^{-18}$ s for pK) due to prompt nuclear absorption via the strong interaction. Such two-body complexes can further capture a third particle through collisional processes to form a three body system XXY or XYY if the effective collisional volume is sufficiently small which is true for such massive systems. Usually the third particle is captured in a very high angular momentum state and then, by a de-excitation mechanism, it cascades down to a lower lying state via dipole radiation, which in turn increases the lifetime of the three-body system. It has been found that a small fraction of kaons [35], pions [36] and also antiprotons [37, 38] stopped in helium media survive for a longer time. Moreover, recent experimental measurements show that the structural properties of such exotic systems are gradually coming into reach due to the advancements in optical technologies and laser sources [39–42].

Whether a system can be observed in a bound state or not depends on the masses of constituent particles and on their mutual interactions as well. The mass relation parameter (q) of a symmetric three-body system is defined as the ratio between the mass of the particle that is attracting the other two (e.g. μ for the $pp\mu$ system) and the mass of the one repelling each particle. Pawlak *et al* [7] show that the width of BW depends on the mass relation parameter (q) but as their work is limited to only three exotic systems $pp\mu$, $dd\mu$ and $tt\mu$, they cannot answer the following subsequent questions :

1. What is the critical value of the mass relation parameter (q) of a symmetric three-body system at which BW just opens?
2. What is the asymptotic value of the BW for the mass relation parameter (q) of a symmetric three-body system that approaches zero?

These questions need to be addressed in the context of the study of BWs, as they would provide the knowledge of the entire range of BWs by considering the two limiting cases along with the study in the intermediate region. In this work, we have made an effort to answer these questions by an extensive calculation for 22 different three-body exotic systems with an improved wave function. Moreover, we have been able to elaborate on some of the physical arguments explaining why $q > 1$ configurations are disfavored for the existence of BW when compared to $q < 1$ ones. In particular, we have estimated the ground state energy eigenvalues of a number of exotic XXY (total charge is positive; $q < 1$) and XYY (total charge is negative; $q > 1$) systems $Y = \mu$, π, K and $X = p$, d, t under screened Coulomb interactions. The present calculations have been done under the framework of the Rayleigh–Ritz variational method using explicitly correlated Hylleraas type basis set. It is interesting to note that XXY systems show Borromean binding whereas XYY systems destabilize before the two body XY destabilization limit, although XY is the two-body subsystem for both XXY and XYY systems. A quantitative analysis shows that as the screening becomes stronger, the binding energy of XXY systems becomes greater than XYY systems. From the study of the variation of relative BW with the mass relation parameter (q) of the respective exotic systems, it is seen that relative BW opens for $q < 1$ and the asymptotic value of the relative BW is 13 as $q \to 0$. The details of this methodology are given in section 2, followed by a discussion on the results in section 3; the conclusion is given in section 4.

2. Methodology

The modified potential of a three-body system in the presence of a screened Coulomb environment can be expressed as

$$V = -\frac{e^{-\lambda r_1}}{r_1} - \frac{e^{-\lambda r_2}}{r_2} + \frac{e^{-\lambda r_{12}}}{r_{12}}, \tag{2}$$

where λ is the screened Coulomb parameter. r_{12} is the distance between the two identical particles and r_1 and r_2 are the distances of the identical particles from the central particle sitting at origin (e.g. for XYY and YXX systems, the central particles are X and Y respectively).

For the spherically symmetric ground state, the three-body general variational equation [43] for arbitrary angular momentum reduces to

$$\delta \int \left[\frac{1}{2}\left(\frac{1}{m_1}+\frac{1}{m_3}\right)\left(\frac{\partial\Psi}{\partial r_1}\right)^2 + \frac{1}{2}\left(\frac{1}{m_2}+\frac{1}{m_3}\right)\left(\frac{\partial\Psi}{\partial r_2}\right)^2 + \frac{1}{2}\left(\frac{1}{m_1}+\frac{1}{m_2}\right)\left(\frac{\partial\Psi}{\partial r_{12}}\right)^2 + \frac{1}{m_3}\left(\frac{r_1^2+r_2^2-r_{12}^2}{2r_1r_{12}}\right)\frac{\partial\Psi}{\partial r_1}\frac{\partial\Psi}{\partial r_2} + \frac{1}{m_2}\left(\frac{r_2^2-r_1^2+r_{12}^2}{2r_2r_{12}}\right)\frac{\partial\Psi}{\partial r_2}\frac{\partial\Psi}{\partial r_{12}} + \frac{1}{m_1}\left(\frac{r_1^2-r_2^2+r_{12}^2}{2r_1r_{12}}\right) \times \frac{\partial\Psi}{\partial r_1}\frac{\partial\Psi}{\partial r_{12}} + (V-E)\,\Psi^2 \right] dV_{r_1,r_2,r_{12}} = 0 \tag{3}$$

Table 1. The ground state energy eigenvalues (in au) of exotic XYY and XXY systems $\{X\colon p, d, t; Y\colon \mu\}$ for the different screening parameter (λ in au). Relative binding energies (R_X^μ) (percentage) between XXY and XYY systems $X\colon p, d, t; Y\colon \mu$ are given for the different screening parameter (λ in au).

λ	$-E$ (au)		R_p^μ	$-E$ (au)		R_d^μ	$-E$ (au)		R_t^μ
	$pp\mu$	$pp\mu$		$dd\mu$	$dd\mu$		$tt\mu$	$tt\mu$	
0.0	97.566 984	102.223 497	4.55	102.991 910	109.816 924	6.21	104.944 115	112.972 830	7.11
	97.566 984 59[a]	102.223 491[c]		102.991 910 6[b]	109.815 698[c]		104.944 115 4[b]	112.971 933[c]	
	97.566 983 43[b]	102.223 5[d]			109.816 5[d]			112.971 8[d]	
		102.223 503 6[e]							
10.0	87.855 345	92.568 209	5.09	93.260 418	100.145 956	6.87	95.205 930	103.296 334	
		92.568 199[c]			100.144 720[c]			103.295 434[c]	7.83
		92.568 2[d]			100.145 6[d]			103.295 3[d]	
50.0	54.839 746	60.038 615	8.66	59.825 553	67.257 235	11.05	61.198 210	70.280 415	12.92
		60.038 611[c]			67.255 863[c]			70.279 521[c]	
		60.038 6[d]			67.256 7[d]			70.279 3[d]	
100.0	25.826 355	30.782 620	16.10	29.756 288	36.948 814	19.47	31.198 210	39.591 867	21.20
		30.782 618[c]			36.947 245[c]			39.591 120[c]	
		30.782 5[d]			36.948 1[d]			39.590 5[d]	
150.0	8.446 984	11.937 011	29.24	10.982 746	16.485 717	33.38	11. 945 982	18.532 941	35.54
		11.937 011[c]			16.484 151[c]			18.532 441[c]	
		11.936 9[d]			16.484 8[d]			18.531 5[d]	
170.0	4.297 395	6.944 875	38.12	6.216 664	10.706 357	41.93	6.968 302	12.460 505	44.08
190.0	1.581 640	3.296 125	52.01	2.858 609	6.191 216	53.82	3.390 177	7.621 487	55.52
200.0	0.731 816	1.960 682	62.67	1.678 362	4.390 282	61.77	2.097 041	5.646 489	62.86
		1.960 682[c]			4.389 327[c]			5.646 211[c]	
		1.960 3[d]			4.389 5[d]			5.645 2[d]	
210.0	0.207 350	0.948 810	78.14	0.816 355	2.886 918	71.72	1.120 501	3.960 122	71.70
		0.948 810[c]			2.886 181[c]				
		0.947 1[d]			2.886 1[d]				
215.0	0.064 944	0.565 957	88.52						
217.0	0.030 274	0.436 440	93.06						
219.0	0.008 277	0.320 819	97.42						
220.0	0.001 736	0.268 351	99.35	0.260 874	1.678 541	84.46	0.450 726	2.558 334 99	82.38
		0.268 355[c]			1.678 029[c]			2.558 159[c]	
					1.676 8[d]			2.556 9[d]	
220.2	0.000 738	0.258 291	99.17						
220.3	0.000 273	0.253 317	99.89						
220.36	0.000 005	0.250 349	99.99						
220.37	−0.000 039								
223.0		0.133 212		0.150 990	1.373 618	89.00			
		0.133 223[c]							
224.0		0.095 989		0.119 785	1.277 921	90.63			
		0.096 009[c]							
225.0		0.063 015		0.091 167	1.185 209	92.31	0.227 221	1.963 501	88.43
		0.063 032[c]							
226.0		0.034 623		0.065 044	1.095 491	94.06			
		0.034 642[c]							
227.0		0.011 481		0.058 442	1.008 779	94.20			
		0.011 503[c]							
227.6		0.000 821							
		0.000 871[c]							
227.65		0.000 093							
227.66		−0.000 049							
228.0				0.041 017	0.925 084	95.56			
229.0				0.026 588	0.844 421	96.85			
230.0				0.015 117	0.766 808	98.02	0.073 756	1.439 475	94.88
					0.766 510[c]				
231.0				0.006 487	0.692 261	99.06		1.343 207	
232.0				0.000 422	0.620 805	99.93			
232.08				0.000 035	0.615 223	99.99			
232.09				−0.000 013					
233.0							0.028 768	1.159 259	97.52
234.0							0.016 915	1.071 598	98.42
235.0					0.425 236		0.007 890	0.986 826	99.20
					0.425 125[c]				
236.0							0.001 462	0.904 956	99.84
236.2							0.000 453	0.888 931	99.95
236.29							0.000 026	0.881 759	99.99

Table 1. Continued.

λ	$-E$ (au) $p\mu\mu$	$-E$ (au) $pp\mu$	R_p^μ	$-E$ (au) $d\mu\mu$	$-E$ (au) $dd\mu$	R_d^μ	$-E$ (au) $t\mu\mu$	$-E$ (au) $tt\mu$	R_t^μ
236.3							−0.000 020		
236.5					0.338 356				
					0.338 250[c]				
238.0					0.258 924				
					0.258 842[c]				
240.0					0.165 098			0.606 836	
					0.165 049[c]			0.606 762[c]	
242.0					0.086 017			0.475 709	
					0.085 997[c]			0.475 647[c]	
243.0					0.052 549				
					0.052 542[c]				
244.0					0.023 686				
					0.023 704[c]				
244.5					0.011 245				
					0.011 305[c]				
244.8					0.004 596				
					0.004 663[c]				
245.0					0.000 590			0.302 169	
					0.000 670[c]			0.302 164[c]	
245.03					0.000 113[c]				
245.04					−0.000 069[c]				
248.0								0.157 711	
								0.157 936[c]	
250.0								0.079 315	
								0.079 473[c]	
252.0								0.017 483	
								0.017 562[c]	
252.5								0.005 217	
								0.005 378[c]	
252.7								0.000 837	
								0.001 049[c]	
252.74								0.000 008	
252.75								−0.000 196	

[a] Bhattacharyya *et al* [48].
[b] Frolov *et al* [49].
[c] Pawlak *et al* [7].
[d] Sil *et al* [6].
[e] Kar *et al* [51].

subject to the normalization condition

$$\int \Psi^2 \, \mathrm{d}V_{r_1,r_2,r_{12}} = 1, \tag{4}$$

where the symbol used in equations (3) and (4) are the same as in [43]. Here, m_3 is the mass of the central particle whereas m_1 and m_2 are the masses of the identical particles of the symmetric three-body systems under consideration. The masses of μ, π, K, p, d and t are taken as $m_\mu = 206.768\,262 m_\mathrm{e}$, $m_\pi = 273.132\,426 m_\mathrm{e}$, $m_K = 966.101\,694\,9 m_\mathrm{e}$, $m_\mathrm{p} = 1\,836.152\,667\,5 m_\mathrm{e}$, $m_d = 3\,670.482\,965\,4 m_\mathrm{e}$ and $m_t = 5\,496.921\,526\,9 m_\mathrm{e}$ respectively, where m_e is the mass of the electron. We have taken $m_\mathrm{e} = 1$ as the atomic unit used throughout the calculations.

The correlated wave function considered for our calculation is given by

$$\begin{aligned}\Psi(r_1, r_2, r_{12}) = & \\ \times \sum_{i=1}^{9} \eta_i(1)\,\eta_i(2) & \left[\sum_{l>0}\sum_{m>0}\sum_{n\geqslant 0} C_{lmn} r_1^l r_2^m r_{12}^n + \text{exchange}\right] \\ + \sum_{\substack{i=1 \\ i\neq j}}^{9}\sum_{j=1}^{9} & \left[\eta_i(1)\,\eta_j(2)\sum_{l>0}\sum_{m>0}\sum_{n\geqslant 0} C_{lmn} r_1^l r_2^m r_{12}^n + \text{exchange}\right],\end{aligned} \tag{5}$$

where

$$\eta_j(i) = \mathrm{e}^{-\sigma_j r_i}, \tag{6}$$

where σs are the nonlinear parameters. The effect of the radial correlation is incorporated through different σs in the wave function, whereas the angular correlation effect is taken care of through different powers of r_{12}. In a multi-exponent basis set, if there are x number of nonlinear parameters, the number of terms in the radially correlated basis is $\frac{x(x+1)}{2}$ and therefore, the dimension of the full basis (M) including angular correlation will be $[\frac{x(x+1)}{2} \times y]$, where y is the number of terms involving r_{12}. For a fixed number of bases, x and y should be chosen in such a manner that the effect of the radial as well as the angular correlation are properly taken care of. To this end, to make the basis of a tractable size, we include nine different values of σ in our method, which form a geometrical sequence: $\sigma_i = \sigma_{i-1}\gamma$, γ being the geometrical ratio [44]. Thus, in this calculation, the number of terms in the radially correlated basis is 45 and with 22 terms involving different powers of r_{12}, the dimension of the full basis (N) becomes 990. A discussion on the choice of the specific number of nonlinear parameters was given in our earlier article [45]. For each screening parameter, the linear variational parameters used in

Table 2. The ground state energy eigenvalues (in au) of exotic XYY and YXX systems $\{X\colon p, d, t; Y\colon \pi\}$ for the different screening parameter (λ in au). Relative binding energies (R_X^{π}) (in au) between XXY and XYY systems $\{X\colon p, d, t; Y\colon \pi\}$ are given for the different screening parameter (λ in au).

λ	$-E$ (au)			$-E$ (au)			$-E$ (au)		
(au)	$pp\pi$	$ppp\pi$	R_p	$dd\pi$	$ddd\pi$	R_d	$tt\pi$	$ttt\pi$	R_t
0.0	124.690 674	129.718 073	3.87	133.653 701	141.524 534	5.56	136.951 552	146.472 365	6.50
	124.690 674 07[a]								
50.0	80.425 360	85.969 490	6.45	88.937 428	97.405 083	8.69	92.081 757	102.223 361	9.92
100.0	47.215 697	52.927 045	10.79	54.588 414	63.309 187	13.77	57.341 339	67.754 111	15.37
150.0	23.821 049	28.803 607	17.33	29.617 686	37.546 979	21.19	31.826 161	41.400 552	23.13
200.0	8.925 715	12.402 317	28.03	12.869 611	19.006 120	32.29	14.437 058	22.075 746	34.60
210.0	6.862 148	9.969 063	31.16						
230.0	3.583 539	5.904 747	39.31	6.322 564	11.005 377	42.55			
250.0	1.387 016	2.883 109	51.89	3.290 509	6.888 817	52.23	4.153 681	8.995 895	53.83
260.0	0.677 872	1.757 214	61.42	2.154 059	5.184 217	58.45	2.870 325	7.076 785	59.44
270.0	0.220 759	0.888 919	75.16	1.262 464	3.711 794	65.99	1.829 890	5.381 642	65.99
275.0	0.085 564	0.553 326	84.52						
280.0	0.011 735	0.286 065	95.89	0.609 687	2.470 156	75.32	1.026 418	3.908 086	73.74
281.0	0.003 820	0.241 133	98.41						
281.2	0.002 338	0.232 497	98.99						
281.4	0.001 015	0.223 979	99.55						
281.5	0.000 612	0.219 764	99.72						
281.6	0.000 002	0.215 579	99.99						
281.61	−0.000 058								
283.0		0.160 262							
285.0		0.091 848							
287.0		0.037 260							
288.0		0.015 642							
289.0		0.000 179							
289.02		0.000 007							
289.03		−0.000 090							
290.0				0.187 206	1.459 767	87.17	0.453 008	2.654 741	82.93
295.0				0.055 832	1.042 335	94.64			
298.0				0.027 442	0.820 496	96.65			
299.0				0.017 139	0.751 392	97.72			
300.0				0.009 212	0.684 736	98.65	0.114 300	1.621 863	92.95
301.0				0.003 686	0.620 544	99.41			
302.0				0.000 611	0.558 837	99.89			
302.4				0.000 053	0.534 855	99.99			
302.45				0.000 006	0.531 886	99.99			
302.46				−0.000 002					
305.0					0.388 858		0.028 253	1.188 937	97.62
306.0							0.017 897	1.109 122	98.39
307.0							0.009 856	1.031 583	99.04
308.0							0.004 158	0.956 329	99.56
309.0							0.000 847	0.883 372	99.90
309.5							0.000 081	0.847 758	99.99
309.58							0.000 006	0.842 114	99.99
309.59							−0.000 003		
310.0					0.157 682			0.812 723	
311.0					0.119 531				
312.0					0.084 133				
313.0					0.051 501				
314.0					0.029 496				
315.0					0.005 910			0.494 559	
315.2					0.001 680				
315.3					0.001 361				
315.37					0.000 153				
315.38					−0.000 014				
320.0								0.236 205	
321.0								0.191 857	
322.0								0.149 967	
323.0								0.116 501	
324.0								0.082 026	
325.0								0.050 882	
326.0								0.023 476	
327.0								0.000 776	
327.04								0.000 012	
327.05								−0.000 176	

[a] Bhattacharyya *et al* [48].

Table 3. The ground state energy eigenvalues (in au) of exotic XYY and YXX systems $\{X\colon p, d, t; Y\colon K\}$ for the different screening parameter (λ in au). Relative binding energies (R_X^K) (in percentage) between XXY and XYY systems $\{X\colon p, d, t; Y\colon K\}$ are given for the different screening parameter (λ in au).

	$-\boldsymbol{E}$ (au)			$-E$ (au)			$-E$ (au)		
λ	pKK	ppK	R_p	dKK	ddK	R_d	tKK	ttK	R_t
0.0	330.800 637	334.575 377	1.12	400.176 959	410.609 734	2.54	430.623 711	446.122 899	3.32
	330.800 636 77[a]								
100.0	239.838 364	244.007 205	1.71	307.459 282	318.599 460	3.49	337.295 789	353.626 696	4.62
200.0	166.075 945	170.608 044	2.66	229.055 514	241.066 693	4.98	257.247 701	274.688 669	6.35
300.0	107.891 316	112.326 102	3.95	164.095 730	176.332 809	6.94	189.854 114	207.722 505	8.60
400.0	63.670 079	67.522 047	5.70	111.501 363	123.127 272	9.44	134.225 608	151.556 582	11.43
500.0	31.977 129	34.866 702	8.29	70.209 125	80.428 582	12.71	89.439 333	105.257 705	15.02
600.0	11.579 834	13.284 046	12.83	39.237 733	47.399 557	17.22	54.615 579	68.060 983	19.75
700.0	1.450 568	1.951 378	25.66	17.708 389	23.354 972	24.17	28.946 063	39.334 553	26.41
710.0	0.970 778	1.362 893	28.77						
720.0	0.585 947	0.874 168	32.97						
730.0	0.296 183	0.486 795	39.16						
740.0	0.101 628	0.203 732	50.12						
745.0	0.040 922	0.102 705	60.15						
750.0	0.005 884	0.031 387	81.25						
752.0	0.000 367	0.011 356	96.77						
752.2	0.000 190	0.010 504	98.19						
752.4	0.000 068	0.008 791	99.22						
752.6	0.000 006	0.007 123	99.92						
752.66	0.000 001	0.006 631	99.99						
752.67	−0.000 000 2								
753.0		0.003 917							
754.0		0.002 306							
754.1		0.001 775							
754.2		0.001 257							
754.3		0.000 753							
754.4		0.000 263							
754.45		0.000 023							
754.46		−0.000 025							
800.0				4.852 758	7.762 306	37.483	11.705 996	18.566 747	36.95
850.0				1.472 341	3.032 857	51.45	6.045 429	11.044 957	45.26
870.0				0.668 722	1.715 585	61.02			
880.0				0.383 635	1.183 266	67.58			
890.0				0.176 330	0.737 658	76.09			
900.0				0.047 548	0.381 782	87.54	2.263 549	5.393 579	58.03
905.0				0.013 001	0.238 701	94.55			
906.0				0.008 420	0.212 937	96.04			
907.0				0.004 550	0.188 131	97.58			
908.0				0.001 333	0.164 286	99.19			
908.4				0.000 214	0.155 018	99.86			
908.48				0.000 001	0.153 183	99.99			
908.49				−0.000 025					
910.0					0.119 486				
912.0					0.078 536				
913.0					0.059 501				
914.0					0.041 417				
916.0					0.025 423				
917.0					0.013 630				
918.0					0.003 757				
918.4					0.000 367				
918.44					0.000 047				
918.45					−0.000 032				
920.0							1.262 584	3.657 489	65.48
930.0							0.869 294	2.903 244	70.06
940.0							0.545 767	2.225 926	75.48
950.0							0.289 334	1.626 773	82.21
960.0							0.095 004	1.107 561	91.42
970.0							0.025 565	0.670 780	96.19
975.0							0.002 600	0.484 293	99.45
975.9							0.000 172	0.453 034	99.96
975.97							0.000 002	0.450 633	99.99
975.98							−0.000 022		
980.0								0.319 666	

Table 3. Continued.

	$-E$ (au)			$-E$ (au)			$-E$ (au)		
λ	pKK	ppK	R_p	dKK	ddK	R_d	tKK	ttK	R_t
985.0								0.177 313	
990.0								0.057 524	
993.0								0.022 217	
994.0								0.008 063	
994.6								0.000 920	
994.68								0.000 033	
994.69								−0.000 076	

[a] Bhattacharyya *et al* [48].

Table 4. Ground state energy eigenvalues (in au) of H_2^+, D_2^+, T_2^+ and Ps^- for various screening parameters (λ in au).

	$-E$(au)			
λ	Ps^-	H_2^+	D_2^+	T_2^+
0.0	0.262 005	0.596 902	0.598 211	0.0.598 702
	0.262 005 070 2[a]	0.597 136[b]		
0.1	0.173 618	0.503 099	0.504 402	0.504 889
	0.173 618 160 0[a]	0.503 330[b]		
0.2	0.106 409			
	0.106 409 677 5[a]			
0.3	0.057 553			
0.4	0.024 698			
0.5	0.005 965	0.226 676	0.227 817	0.228 241
	0.005 965 664 3[a]			
0.55	0.001 421			
0.56	0.000 871			
0.57	0.000 481			
0.58	0.000 191			
0.59	0.000 029			
0.594	0.000 001			
0.595	−0.000 002			
0.7		0.135 199	0.136 214	0.136 579
		0.135 561[b]		
1.0		0.044 832	0.045 025	0.045 288
1.2		0.011 923	0.012 187	0.012 308
		0.012 287[b]		
1.25		0.006 808		
		0.007 201[b]		
1.29		0.003 672		
		0.003 989[b]		
1.3			0.003 222	0.003 296
1.33		0.001 339		
	0.001 597[b]			
1.34		0.000 882		
		0.001 190[b]		
1.35		0.000 476	0.000 609	0.000 657
		0.000 750[b]		
1.36		0.000 118	0.000 236	0.000 279
		0.000 400[b]		
1.363		0.000 019		
1.364		−0.000 019		
1.367			0.000 004	
1.368			−0.000 027	0.000 011
1.369				−0.000 020

[a] Kar and Ho [50].
[b] Bertini *et al* [13].

equation (5) along with energy eigenvalues E are determined by solving the generalized eigenvalues equation [46]

$$\underline{\underline{H}}\,\underline{C} = E\,\underline{\underline{S}}\,\underline{C}, \tag{7}$$

where $\underline{\underline{H}}$ is the Hamiltonian matrix, $\underline{\underline{S}}$ is the overlap matrix, $\underline{C}$ is the column matrix consisting of linear variational parameters and E is the energy eigenvalue. In order to set the highest and lowest σ value in the set of nine nonlinear

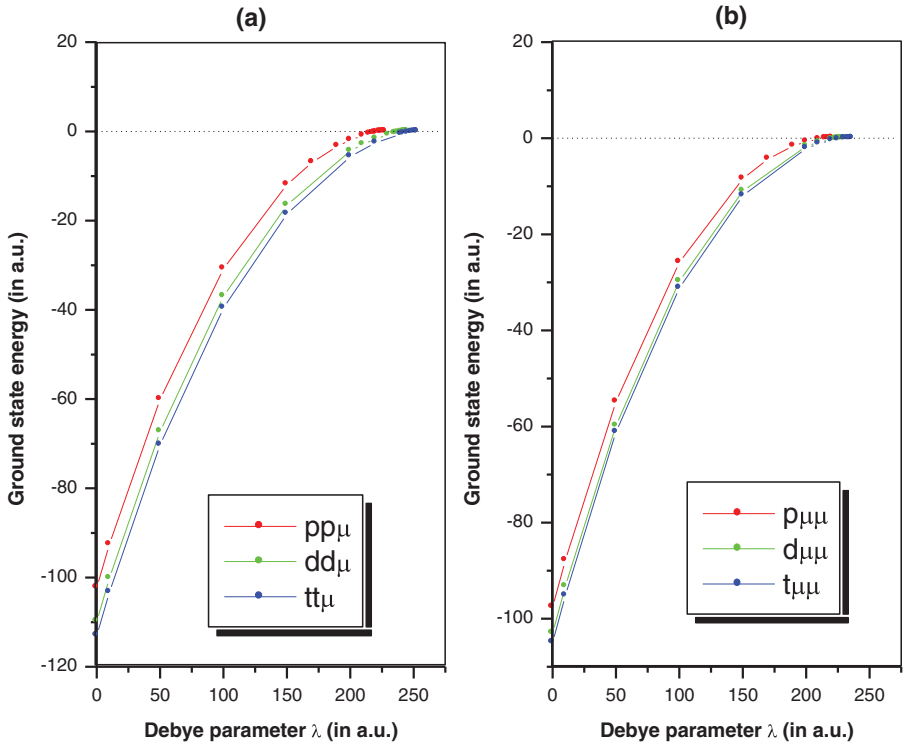

Figure 1. The variation of the ground state energies of $pp\mu$, $dd\mu$ and $tt\mu$ versus different screening parameter (λ) is given in (a) and those of $p\mu\mu$, $d\mu\mu$ and $t\mu\mu$ versus the different screening parameter (λ) are given in (b).

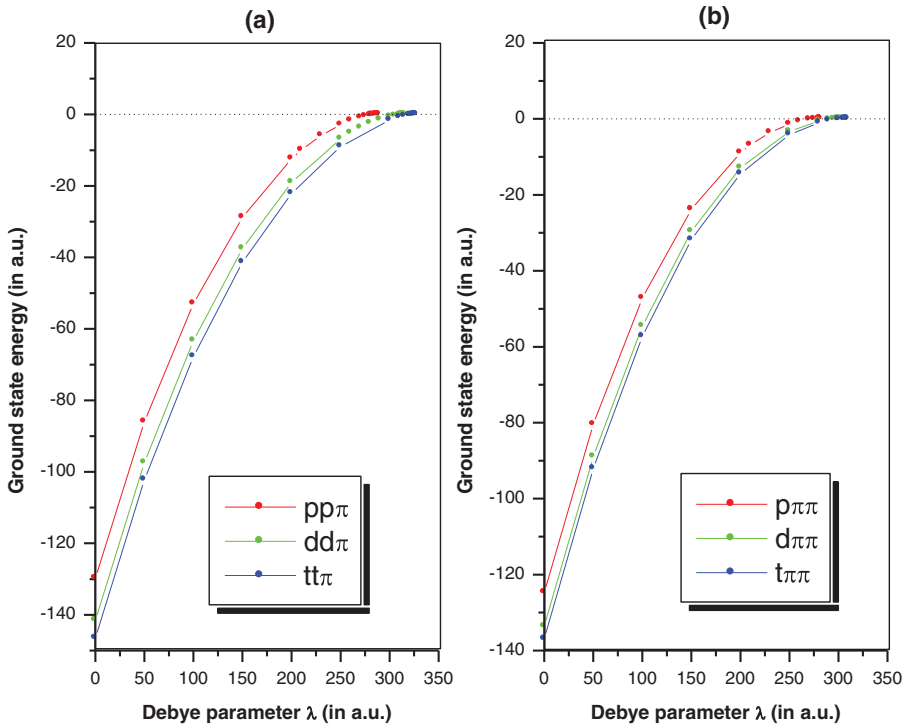

Figure 2. The variation of the ground state energies of $pp\pi$, $dd\pi$ and $tt\pi$ versus the different screening parameter (λ) is given in (a) and that of $p\pi\pi$, $d\pi\pi$ and $t\pi\pi$ versus the different screening parameter (λ) is given in (b).

parameters, we optimize the ground state energy eigenvalues using the Nelder–Mead procedure [47] with two nonlinear parameters. The higher value of the optimized set is taken as the highest value of the set of nine nonlinear parameters and it is fixed for all the sets. All calculations are carried out in quadruple precision to ensure better numerical stability for the extended multi-exponent Hylleraas basis set.

3. Results and discussion

For different screening parameter (λ), the ground state energy eigenvalues of exotic XYY and YXX systems $\{X: p, d, t\}$ taking Y as μ, π and K are given in tables 1–3 respectively. Table 4 displays the ground state energy eigenvalues of H_2^+, D_2^+, T_2^+ and Ps^- for various screening parameters (λ). The

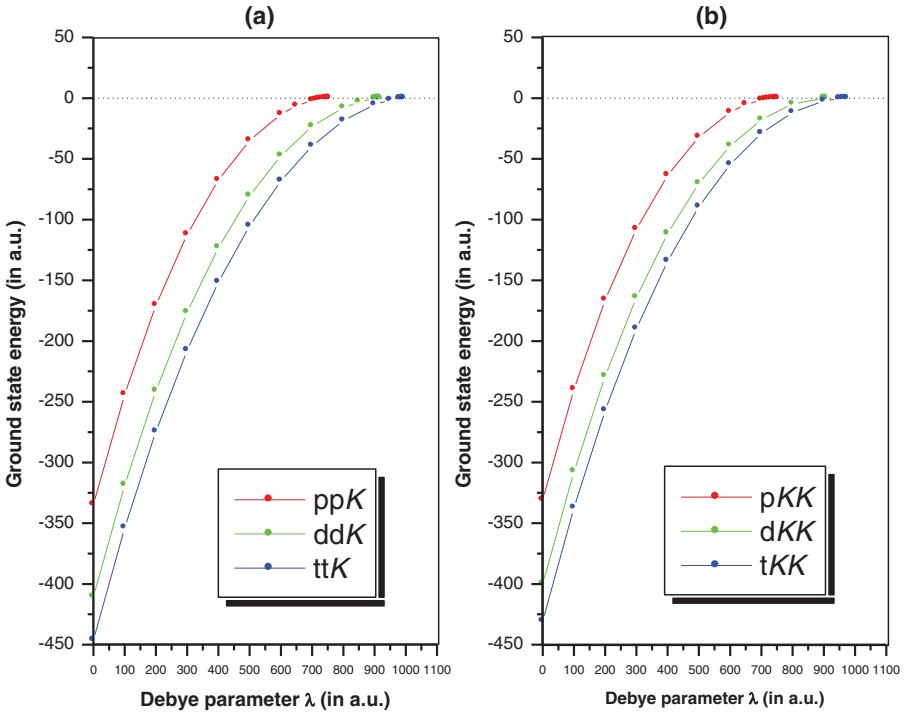

Figure 3. The variation of the ground state energies of ppK, ddK and ttK versus the different screening parameter (λ) is given in (a) and that of pKK, dKK and tKK versus different screening parameter (λ) is given in (b).

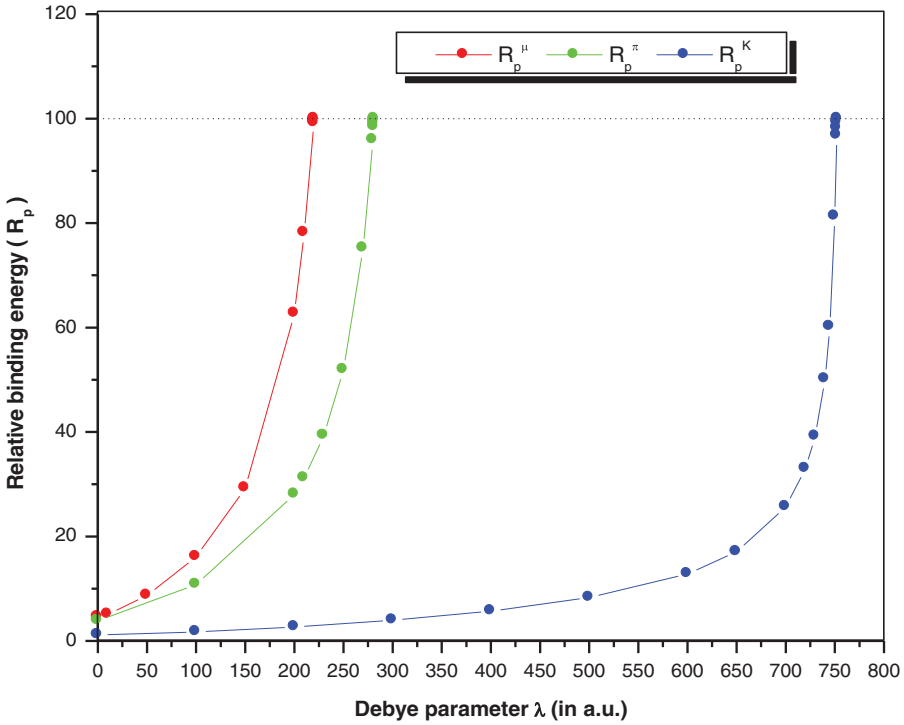

Figure 4. The variation of the relative binding energy (R_p^Y) ($Y = \mu, \pi, K$) with various screening parameters (λ).

screening parameter (λ) is primarily set at zero corresponding to a free system and then gradually increased in a systematic manner up to the limit of destabilization of the corresponding three-body system. The results reflect that for both unscreened and screened cases, our values are in good agreement with the other available theoretical results [6, 7, 13, 48–51] included in tables 1–4. For example, it is evident from table 1 that in the low screening region, the ground state energy eigenvalues of $pp\mu$, $dd\mu$ and $tt\mu$ systems are more negative than those reported by Pawlak *et al* [7] and Sil *et al* [6], whereas in the higher screening region, this feature is not obtained. It may be noted that this method may produce better results for the energy eigenvalues for the entire range of screening by adjusting the nonlinear parameters and size of the basis set. Nevertheless, the accuracy obtained in this work is adequate for the study of BW of the respective three-body exotic

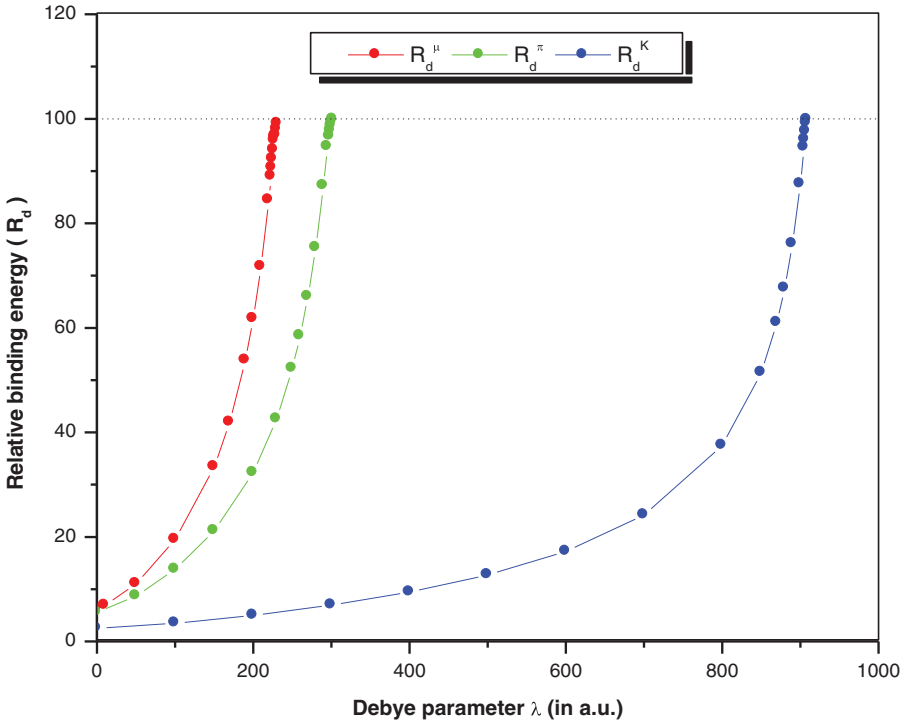

Figure 5. The variation of the relative binding energy (R_d^Y) ($Y = \mu, \pi, K$) with various screening parameters (λ).

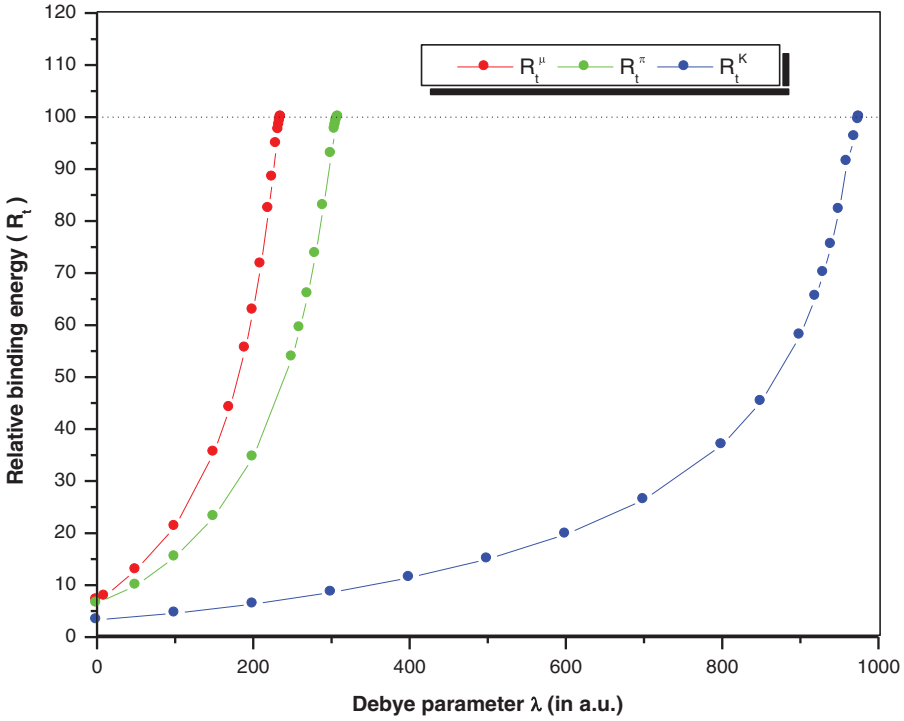

Figure 6. The variation of the relative binding energy (R_t^Y) ($Y = \mu, \pi, K$) with various screening parameters (λ).

systems. To the best of our knowledge, the results given in table 1 for $p\mu\mu$, $d\mu\mu$ and $t\mu\mu$ systems and the results displayed in tables 2 and 3 are reported here for the first time in the literature.

The ground state eigenenergies of XXY and XYY ($X = p, d, t$; $Y = \mu$) for different screening parameters (λ) are plotted in figures 1(a) and (b) respectively. In both figures, the dotted line represents the zero energy (i.e. the complete fragmentation limit) and all the three body systems gradually approach it with an increasing screening parameter (λ), due to the weakening of the Coulomb potential. A similar feature has been observed for XXY and XYY ($X = p, d, t$) systems taking $Y = \pi$ and K given in figures 2(a), (b) and 3(a), (b) respectively.

It is evident from tables 1–3 that the energy eigenvalues of XXY systems are more negative compared to XYY systems for any arbitrary screening parameter (λ). In order to estimate the amount of boundedness of XXY systems compared to

Table 5. Critical screening parameters and BWs of exotic three-body systems. Critical screening parameters (λ^c) of two-body systems are taken from [52].

Two-body sub-system	λ^C	Three-body system	λ^C	BW
$p\mu$	221.26	$pp\mu$	227.65	6.39
			227.66[a]	
		$p\mu\mu$	220.36	0
$p\pi$	283.07	$pp\pi$	289.02	5.95
		$p\pi\pi$	281.6	0
pK	753.69	ppK	754.45	0.76
		pKK	752.66	0
$d\mu$	233.05	$dd\mu$	245.03	11.98
			245.03[a]	
		$d\mu\mu$	232.08	0
$d\pi$	302.67	$dd\pi$	315.37	12.70
		$d\pi\pi$	302.45	0
dK	910.58	ddK	918.44	7.86
		dKK	908.48	0
$t\mu$	237.26	$tt\mu$	252.74	15.48
			252.75[a]	
		$t\mu\mu$	236.29	0
$t\pi$	309.80	$tt\pi$	327.04	17.24
		$t\pi\pi$	309.58	0
tK	978.31	ttK	994.68	16.37
		tKK	975.97	0
pe	1.1899	H_2^+	1.363	0.1731
			1.365[b]	
			1.3734[c]	
de	1.1903	D_2^+	1.367	0.1767
te	1.1904	T_2^+	1.368	0.1776
ee	0.5953	Ps^-	0.594	0

[a] Pawlak *et al* [7].
[b] Bertini *et al* [13].
[c] Ho [53].

XYY systems, we introduce a dimensionless quantity, the relative binding energy (R_X^Y), which is defined as the ratio between the difference of the ground state energies of XXY and XYY systems and the ground state energy of the XXY system. In tables 1–3, the estimated relative binding energy (R_X^Y) (given in percentage) between XXY and XYY systems are presented for a range of screening parameter (λ) and it is evident that, in each case, XYY systems destabilize more rapidly compared to XXY systems. We have depicted the variation of the relative binding energy (R_p^Y) ($Y = \mu, \pi, K$) with a screening parameter (λ) in figure 4. It is clear from figure 4 that R_p^Y ($Y = \mu, \pi, K$) increases slowly up to a certain value of the screening parameter (λ) and then increases rapidly to 100% until the XYY system becomes unbound. The variation of R_d^Y ($Y = \mu, \pi, K$) and R_t^Y ($Y = \mu, \pi, K$) with screening parameter (λ) presented in figures 5 and 6 respectively show a similar kind of pattern.

The estimated critical screening parameters (λ^c) of all three body systems along with the critical screening parameters of the respective two-body subsystems [52] are displayed in table 5. The radius of a muonic atom ($p\mu$) is 186 times smaller than that of the radius of a hydrogen atom and the ionization potential (IP) of a muonic atom ($p\mu$) is 186 times larger than the IP of a hydrogen atom [46]. Thus, it is expected that the critical screening parameters for exotic systems with heavier masses will be much larger compared to the critical screening parameters of normal atomic systems. The Debye length is likely to be very small

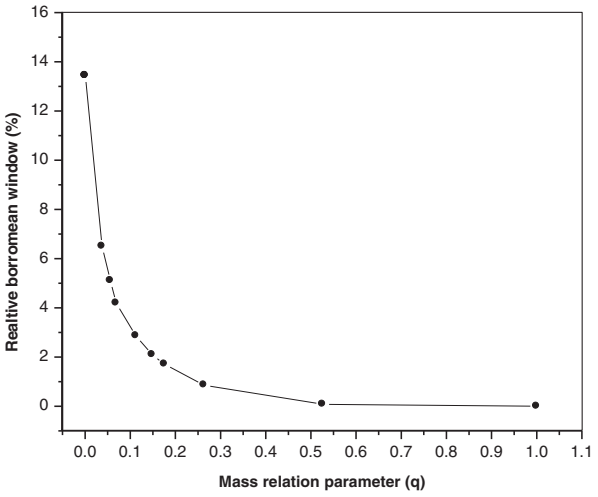

Figure 7. The variation of the relative BW (%) versus the mass relation parameter (q).

in such circumstances, as obtained from our calculations. Considering the screening by plasma environment, the densities involved in such calculations may be found in the interior of Zovian planets, where they may even exceed the solid state density. It is also evident that the critical screening parameter for the two-body system (XY) lies between the critical screening parameter of the XXY and XYY three-body systems i.e. $\lambda^c_{XXY} > \lambda^c_{XY} > \lambda^c_{XYY}$. Thus, all XXY systems show Borromean bindings, whereas all XYY systems destabilize before the corresponding two-body (XY) destabilization limit. Hence the BW for all XYY systems is zero. The estimated BW for all XXY systems is also given in the last column of table 5. The values of BW for XXY systems keeping a fixed Y shows that as the mass of the nucleus increases, the BW also increases. For example, $\mathrm{BW}_{tt\mu} > \mathrm{BW}_{dd\mu} > \mathrm{BW}_{pp\mu}$, which is in agreement with Pawlak *et al* [7]. Here we introduce a dimensionless quantity 'relative BW' which is defined as $\frac{\lambda^c_{XXY} - \lambda^c_{XY}}{\lambda^c_{XXY}} \times 100\%$ in order to make a comparison among the BWs of the XXY systems. The estimated relative BWs for different mass relation parameters (q) are given in table 6 and the corresponding variation is displayed in figure 7. It is evident from table 6 and figure 7 that the relative BW is zero for $q \geqslant 1$ and it increases as q approaches zero. It is clear that the relative BW slowly increases with q in the region 1–0.5 and then increases rapidly as q tends towards zero. It is worthwhile mentioning that for $q = 0.52615$ the relative BW is 0.08%, which is small compared to the highest relative BW of 13.01% for $q = 0.000\,18$ corresponding to T_2^+. Therefore, we have chosen systems in between $0 < q < 0.5$ to get a smooth variation of relative BW with q.

We have shown for the first time that BW exists if we add a positively charged particle X to the XY system ($m_X > m_Y$), as q becomes less than 1 for the XXY system; whereas BW does not exist when we add a negatively charged particle Y to the XY system, as q becomes greater than 1 for XYY systems. For example, the relative BW is 2.86 (for $q = 0.11261$) if we add a proton to the $p\mu$ system whereas the BW does not exist if we add a muon to the $p\mu$ system, for which. $q = 8.880\,25$ The reason behind the existence of BWs for systems with a $q > 1$ configuration is given below.

Table 6. Relative BWs for different exotic systems under screened Coulomb interactions.

System	Mass relation parameter (q)	Relative BW
$t\mu\mu$	26.584 97	0
$t\pi\pi$	20.125 51	0
$d\mu\mu$	17.751 69	0
$d\pi\pi$	13.438 49	0
$p\mu\mu$	8.880 25	0
$p\pi\pi$	6.722 58	0
tKK	5.689 79	0
dKK	3.799 27	0
pKK	1.900 62	0
eee	1.000 00	0
ppK	0.526 15	0.08
ddK	0.263 21	0.86
ttK	0.175 75	1.71
$pp\pi$	0.148 75	2.09
$pp\mu$	0.112 61	2.86
$dd\pi$	0.068 79	4.19
$dd\mu$	0.056 33	5.10
$tt\pi$	0.049 68	6.19
$tt\mu$	0.037 62	6.50
H_2^+	0.000 54	12.70
D_2^+	0.000 27	12.95
T_2^+	0.000 18	13.01

It is well known that the stability of negatively charged ions is less than the stability of positive ions, e.g. H^-, Ps^-, He^- etc ions are less stable. We have also found that the binding energies of the XYY (total charge is negative; $q > 1$) systems are less than that of the binding energies of XXY (total charge is positive; $q < 1$) systems for free case. When we switch on the screening parameter (λ), both the systems destabilize as the binding energy reduces compared to the free case due to a weakening of the Coulomb potential. With the gradual increment of the screening parameter (λ), the faster destabilization of XYY systems compared to XXY systems yields a lesser value of the critical screening parameter of XYY systems compared to XXY systems. Hence, it is expected that a BW does not exist for XYY systems ($q > 1$). These extensive calculations confirm the above mentioned fact for ten different $q \geqslant 1$ configurations.

4. Conclusion

It can be concluded that the BW opens for $q < 1$ configurations of three-body exotic systems and the asymptotic value of the relative BW is 13.6 for T_2^+. The novelty of our method lies in the choice of a flexible multi-exponent Hylleraas basis for three-body systems where all three particles are moving. We hope that the results presented in this communication will be useful for future studies in related disciplines.

Acknowledgments

The authors are grateful to the Department of Atomic Energy, BRNS, Government of India, for the financial assistance under Grant number 2011/37P/15/BRNS/0074. SB is grateful to USIEF to the Fulbright-Nehru fellowship (2012–2013) for the stay at Auburn, USA. The authors express heartfelt thanks to Professor M Bylicki, Instytut Fizyki, Uniwersytet MikoÃlaja Kopernika, Grudziadzka 5, PL-87-100 Torun, Poland for the stimulating discussions regarding the choice of basis set.

References

[1] Richard J M 2003 *Phys. Rev.* A **67** 034702 and references therein
[2] Thomas L H 1935 *Phys. Rev.* **47** 903
[3] Efimov V 1970 *Phys. Lett.* B **33** 563
[4] Kraemer T *et al* 2006 *Nature* **440** 315
[5] Pollack S E, Dries D and Hulet R G 2009 *Science* **326** 1683
[6] Sil A N, Pawlak M, Mukherjee P K and Bylicki M 2008 *J. Quant. Spectrosc. Radiat. Transfer* **109** 873
[7] Pawlak M, Byliciki M, Saha J K and Mukherjee P K 2009 *J. Phys. B: At. Mol. Opt. Phys.* **42** 215701
[8] Ghoshal A and Ho Y K 2010 *J. Phys. B: At. Mol. Opt. Phys.* **43** 115007
[9] Kar S and Ho Y K 2011 *Chem. Phys. Lett.* **506** 282
[10] Ghoshal A and Ho Y K 2011 *Int. J. Quantum Chem.* **111** 4288
[11] Li Y, Zhang W J, Gou Q D, Song H W and Shi T Y 2010 *Phys. Rev.* A **82** 022515
[12] Pont F and Serra P 2009 *Phys. Rev.* A **79** 032508
[13] Bertini L, Mella M, Bressanini D and Morosi G 2004 *Phys. Rev.* A **69** 042504
[14] Lemasson A *et al* 2010 *Phys. Rev.* C **82** 044617
[15] Meyer C D *et al* 2010 *Chemistry* **16** 12570
[16] Han D R, Pal S, Liu Y and Yan H 2010 *Nature Nano* **5** 712
[17] Ho Y K and Kar S 2008 *Few Body Syst.* **44** 253 and references therein
[18] Kar S and Ho Y K 2012 *Phys. Rev.* A **86** 014502
[19] Sturrus W G, Hessels E A, Arcuni P W and Lundeen S R 1991 *Phys. Rev.* A **44** 3032
[20] Jacobson P L, Komara R A, Sturrus W G and Lundeen S R 2000 *Phys. Rev.* A **62** 012509
[21] Picón A, Jaron-Becker A and Becker A 2012 *Phys. Rev. Lett.* **109** 163002
[22] Hylleraas E A 1947 *Phys. Rev.* **71** 491
[23] Kolos W, Roothaan C J and Sack R A 1960 *Rev. Mod. Phys.* **32** 178
[24] Ho Y K 1983 *J. Phys. B: At. Mol. Phys.* **16** 1503
Ho Y K 1993 *Phys. Rev.* A **48** 4780
Kar S and Ho Y K 2006 *Chem. Phys. Lett.* **424** 403
[25] Bhatia A K and Drachman R J 1983 *Phys. Rev.* A **28** 2523
[26] Drake G W F, Cassar M M and Nistor R A 2002 *Phys. Rev.* A **65** 054501
[27] Frolov A M 2004 *Phys. Rev.* A **69** 022505
[28] Lin C D 1995 *Phys. Rep.* **257** 1
[29] Cohen-Tannoudji C, Diu B and Laloë F 2005 *Quantum Mechanics* vol 1 (New York: Wiley) p 811
[30] Cohen J C 1993 *Review of Fundamental Processes and Applications of Atoms and Ions* (Singapore: World Scientific) p 61
[31] Froelich P 1992 *Adv. Phys.* **41** 405
[32] Pohl R *et al* 2006 *Phys. Rev. Lett.* **97** 193402
[33] Pohl R *et al* 2001 *Hyperfine Interact.* **138** 35
[34] Kottmann F *et al* 2001 *Hyperfine Interact.* **138** 55
[35] Yamazaki T *et al* 1989 *Phys. Rev. Lett.* **63** 1590
[36] Nakamura S N *et al* 1992 *Phys. Rev.* A **45** 6202
[37] Iwasaki M *et al* 1991 *Phys. Rev. Lett.* **67** 1246
[38] Nakamura S N *et al* 1994 *Phys. Rev.* A **49** 4457
[39] Hentschel M *et al* 2001 *Nature* **414** 509
[40] Sansone G *et al* 2006 *Science* **314** 443
[41] Goulielmakis E *et al* 2008 *Science* **320** 1614
[42] Corkum P B and Krausz F 2007 *Nature Phys.* **3** 381

[43] Mukherjee T K and Mukherjee P K 1995 *Phys. Rev.* A **51** 4276
[44] Bylicki M 1997 *J. Phys. B: At. Mol. Opt. Phys.* **30** 189
[45] Saha J K, Bhattacharyya S, Mukherjee T K and Mukherjee P K 2009 *J. Phys. B: At. Mol. Opt. Phys.* **42** 245701
[46] Bransden B H and Joachain C J 2004 *Physics of Atoms and Molecules* 2nd edn (Delhi: Pearson Education) pp 133 and 176
[47] Nelder J A and Mead R 1965 *Comput. J.* **7** 308
[48] Bhattacharyya S, Saha J K, Mukherjee P K and Mukherjee T K 2012 *Phys. Scr.* **85** 065305
[49] Frolov A M, Vedene H S Jr and Komasa J 1993 *J. Phys. A: Math. Gen.* **26** 6507
[50] Kar S and Ho Y K 2005 *Phys. Rev.* A **71** 052503
[51] Kar S and Ho Y K 2007 *Phys. Rev.* A **75** 062509
[52] Gomes O A, Chacham H and Mohallem J R 1994 *Phys. Rev.* A **50** 228
[53] Ho Y K 2013 *Few Body Syst.* **54** 31

Precise energy eigenvalues of hydrogen-like ion moving in quantum plasmas

S. Dutta, Jayanta K. Saha, and T. K. Mukherjee

Citation: Physics of Plasmas **22**, 062103 (2015); doi: 10.1063/1.4921739
View online: http://dx.doi.org/10.1063/1.4921739
View Table of Contents: http://scitation.aip.org/content/aip/journal/pop/22/6?ver=pdfcov
Published by the AIP Publishing

Precise energy eigenvalues of hydrogen-like ion moving in quantum plasmas

S. Dutta,[1] Jayanta K. Saha,[2] and T. K. Mukherjee[3]
[1]*Belgharia Texmaco Estate School, Kolkata 700 056, India*
[2]*Indian Association for the Cultivation of Science, Kolkata 700032, India*
[3]*Narula Institute of Technology, Kolkata 700109, India*

(Received 27 December 2014; accepted 14 May 2015; published online 2 June 2015)

The analytic form of the electrostatic potential felt by a slowly moving test charge in quantum plasma is developed. It has been shown that the electrostatic potential is composed of two parts: the Debye-Huckel screening term and the near-field wake potential. The latter depends on the velocity of the test charge as well as on the number density of the plasma electrons. Rayleigh-Ritz variational calculation has been done to estimate precise energy eigenvalues of hydrogen-like carbon ion under such plasma environment. A detailed analysis shows that the energy levels gradually move to the continuum with increasing plasma electron density while the level crossing phenomenon has been observed with the variation of ion velocity. © *2015 AIP Publishing LLC*.
[http://dx.doi.org/10.1063/1.4921739]

I. INTRODUCTION

The study of the changes in structural properties of foreign atoms or ions in different external environments[1–14] is a subject matter of immense interest for the last few decades as it provides a deep insight into several interesting phenomena in astrophysics and plasma physics. There exists a bulk of studies discussed in detail by Sil *et al.*,[15] on the behavioral changes in the structural properties of few-body systems embedded in an external plasma environment. These are useful for laboratory and astrophysical plasma diagnostics determination. The most important part of such studies is to model the environment by an effective potential that the foreign atom/ion or the test charge will feel inside or moving through that medium. It is well-known according to the Debye-Huckel theory[16,17] of weak electrolytes that a static atom/ion feels screened Coulomb type potential while placed within a collision-less high temperature classical plasma. In this case, the screening parameter is a function of electron number density (n_e) and temperature (T) of the plasma and thus different plasma situations can be simulated by suitably tuning the screening parameter.[4] In contrast, when the temperature (T) of the plasma electrons approaches the "*Fermi temperature*" $T_F = E_F/k_B$ [E_F and k_B are the "*Fermi energy*" of the electrons and the Boltzmann constant, respectively], the equilibrium plasma electron distribution function changes from the Maxwell-Boltzmann to the Fermi-Dirac distribution. Under such condition, the quantum degeneracy effects start playing a significant role as the thermal de Broglie wavelength for the plasma electrons becomes equal or comparable to the average inter-electronic distance.[18] Quantum plasmas are generally made of electrons and ions or holes. The studies on quantum plasma have become important in several branches of applied physics, especially in nano-science[19–21] as well as in laboratory plasma experiments[22–25] and in astrophysical scenario.[26–28]

Pine[29] has treated an arbitrary collision-less quantum plasma environment as a dielectric medium and derived the analytic form of dielectric function using the Random Phase Approximation (RPA) method. Using such dielectric function, Shukla *et al.*[30] showed that the effective potential felt by a slowly moving test charge has two components: the usual near field Debye-Huckel screening term and the far-field wake potential. Far field wake potential decays as the inverse cube of the distance between the origin of the test charge and the location of the observer. It is interesting to note that for far field, the effective potential of a moving "*test charge*" in an isotropic collision-less classical plasma also falls off as the inverse cube of the distance between the observer and the test charge.[31] The effect of far field wake potential is very small on the binding energy of the atom. Thus, it is very much important to investigate the effect of near field wake potential on the binding energy of the atom/ion. The only attempt in this context was made by Hu *et al.*[32] They[32] have found that the near field wake potential is proportional to $\frac{1}{r^2}$ and $\cos\theta$; r being the radial distance between the moving ion and the observer, while θ is the angle between the radius vector and the velocity vector of the ion. They[32] have used Meijer's G function in deriving the analytic form of the near field wake potential, where this G function violates the condition used in its definition.[33] These results in some anomalous findings in the binding energy calculations, e.g., variationally over-bound energy levels with respect to the energy levels of the free atom and the removal of degeneracy of the energy levels with respect to the magnetic quantum number "m." Even if we assume that their form of the potential to be correct, the energy levels should undergo a Stark-like shift due to the "$\cos\theta$" term in the potential and due to obvious reason there is no possibility of getting Zeeman-like splitting without any perturbation, e.g., magnetic field which breaks the azimuthal symmetry of the system.

To examine the influence of near field wake potential on the structural properties of a moving atom/ion in quantum plasma, the analytic form of the potential has been derived in the present work using the correct form of Meijer's G function[33] and its identities. The present potential is proportional

to $rK_0\left(\frac{r}{\lambda_q}\right)$ [$K_0(x)$ being the zeroth order Macdonald function or Modified Bessel's function of the second kind[34] and λ_q is the Debye parameter] and $\cos\theta$. Subsequently, we have applied Rayleigh-Ritz variation method to obtain the binding energies of all states lying between $1s$ and $4f$ configurations of hydrogen-like carbon ion moving through Electron-Hole-Droplet (EHD) quantum plasma. In contrast to the findings of Hu *et al.*,[32] no overbound result has been observed. Moreover, the splitting of energy levels with respect to $|m|$, has been observed and it is purely Stark-like shifting due to the presence of an oscillatory term in the potential. The details of the present methodology are given in Sec. II, followed by the results and discussion in Sec. III, and finally the conclusion is given in Sec. IV.

II. METHOD

A. Near-field potential felt by a slowly moving "*test charge*" in quantum plasma

The field ($\vec{D}$) of a charge q moving with a velocity $\vec{v}$ in a dielectric medium is given by the equation[18]

$$\vec{\nabla}.\vec{D} = 4\pi q\delta(\vec{r} - \vec{v}t). \tag{1}$$

Considering the quantum plasma environment as a linear dielectric medium, we have the relation $\vec{D} = \epsilon\vec{E}$; where the electric field $\vec{E}$ is derived from the scalar potential φ by using $\vec{E} = -\vec{\nabla}\varphi$. Equation (1), then, may be written as

$$-\vec{\nabla}\epsilon.\vec{\nabla}\varphi - \epsilon\nabla^2\varphi = 4\pi q\delta(\vec{r} - \vec{v}t). \tag{2}$$

After a Fourier transformation, we obtain

$$\varphi(k) = \frac{4\pi q}{(2\pi)^{\frac{3}{2}}}\frac{e^{-i\vec{k}.\vec{v}t}}{k^2\epsilon(k)}. \tag{3}$$

The potential $\varphi(r)$ can be obtained by inverse Fourier transform[18] of Eq. (3) and may be expressed as

$$\varphi(\vec{r}) = \frac{q}{2\pi^2}\int\frac{e^{i\vec{k}.\vec{r}}}{k^2\epsilon(\vec{k},\omega)}d^3\vec{k}. \tag{4}$$

The dielectric function $\epsilon(k,\omega)$ for low frequency perturbation ($\omega \ll kv_{ts}$) was derived by Pines[29] as

$$\epsilon(\vec{k},\omega) = 1 + \sum_{s=e,h}\frac{K_{Fs}^2}{k^2}\left(1 + i\frac{\pi}{2}\frac{\omega}{kv_{ts}}\right), \tag{5}$$

where $v_{ts} = \frac{\hbar}{m_s}(3\pi^2 n_s)^{\frac{1}{3}}$ is the thermal velocity. The subscript s used in the expression for thermal velocity (v_{ts}) corresponds to the species of the plasma. For electron-hole droplet plasma, the species corresponds to either electron (e) or hole (h); m_s and n_s are the effective mass and density, respectively, of the species s. In the present calculation, we have taken $m_h = 0.39M_e$ and $m_e = 0.26M_e$;[35,36] where M_e is the rest mass of an electron. The Fermi-Thomas screening wave number K_{Fs} is defined as $K_{Fs} = \frac{\sqrt{3}\omega_{ps}}{v_{ts}}$, where the plasma oscillation frequency (ω_{ps}) is given by $\omega_{ps} = \left(\frac{4\pi n_s e^2}{m_s}\right)^{\frac{1}{2}}$. It should be mentioned that the Debye length $\lambda_s = \frac{1}{K_{Fs}}$. Equation (5) can be rearranged as

$$\epsilon(\vec{k},\omega) = \frac{1 + k^2\lambda_q^2}{k^2\lambda_q^2}\left[1 + i\frac{\pi}{2}\frac{\omega\lambda_q^2}{k\left(1 + k^2\lambda_q^2\right)}\sum\frac{1}{v_{ts}\lambda_s^2}\right], \tag{6}$$

where $\frac{1}{\lambda_q^2} = \sum_{s=e,h}\frac{1}{\lambda_s^2}$. Pines[29] obtained Eq. (5) after performing complex integration where the pole position was at $\omega = -\vec{k}.\vec{v}$.[30,37] The velocity ($v$) of the ions is chosen in such a way that the thermal Mach number[37] remains less than unity. For $v < v_{ts}$, we can get

$$\frac{1}{\epsilon(\vec{k},\omega)} \approx \frac{k^2\lambda_q^2}{1 + k^2\lambda_q^2} + i\frac{\pi}{2}\frac{k\lambda_q^4}{\left(1 + k^2\lambda_q^2\right)^2}\vec{k}.\vec{v} \times \sum_{s=e,h}\frac{1}{v_{ts}\lambda_s^2}. \tag{7}$$

Combining Eqs. (4) and (7), we obtain

$$\varphi = \varphi_1 + \varphi_2, \tag{8}$$

where

$$\varphi_1 = \frac{q}{2\pi^2}\int\frac{\lambda_q^2}{1 + k^2\lambda_q^2}e^{i\vec{k}.\vec{r}}d^3\vec{k}. \tag{9}$$

In the spherical polar coordinates (k, σ, τ), the volume element is given as $d^3\vec{k} = k^2\sin\sigma d\sigma d\tau dk$. After integrating over σ and τ, Eq. (9) reduces to

$$\varphi_1 = \frac{2q\lambda_q^2}{\pi r}\int_o^\infty\frac{k}{1 + k^2\lambda_q^2}\sin krdk = \frac{q}{r}e^{-\frac{r}{\lambda_q}}. \tag{10}$$

φ_1 as expressed in Eq. (10) is the well-known Debye-Huckel screening potential.[4,16]

The second term of Eq. (8) is given by

$$\varphi_2 = i\frac{\pi}{2}\frac{q}{2\pi^2}\int\frac{\lambda_q^4}{k\left(1 + k^2\lambda_q^2\right)^2}\vec{k}.\vec{v}\sum_{s=e,h}\frac{1}{v_{ts}\lambda_s^2} \times e^{i\vec{k}.\vec{r}}d^3\vec{k}. \tag{11}$$

Performing integration over the azimuthal angle (τ), Eq. (11) reduces to

$$\varphi_2 = \frac{i}{2}qv\lambda_q^4\sum_{s=e,h}\frac{1}{v_{ts}\lambda_s^2}\int_o^\infty\frac{k^2}{\left(1 + k^2\lambda_q^2\right)^2} \times \int_0^\pi\cos(\sigma + \theta)e^{ikr\cos\sigma}\sin\sigma d\sigma, \tag{12}$$

where θ is the angle between $\vec{r}$ and $\vec{v}$, and $(\theta + \sigma)$ is the angle between $\vec{k}$ and $\vec{v}$. The polar angle part of the integral can be written as

$$\int_0^{\pi} \cos(\sigma+\theta) e^{ikr\cos\sigma} \sin\sigma d\sigma = \cos\theta \cdot I_1 - \sin\theta \cdot I_2, \quad (13)$$

where

$$I_1 = \int_0^{\pi} \cos\sigma e^{ikr\cos\sigma} \sin\sigma d\sigma = -\frac{2}{i} j_1(kr) \quad (14)$$

and

$$I_2 = \int_0^{\pi} \sin\sigma e^{ikr\cos\sigma} \sin\sigma d\sigma = \frac{\pi}{2}\left[j_0(kr) + j_2(kr)\right], \quad (15)$$

where $j_l(x)$ is the spherical Bessel function of first kind. Neglecting the imaginary part, Eq. (12) becomes

$$\varphi_2 = -qv\lambda_q^4 \sum_{s=e,h} \frac{1}{v_{ts}\lambda_s^2} \cos\theta \int_0^{\infty} \frac{k^2 j_1(kr)}{\left(1+k^2\lambda_q^2\right)^2} dk. \quad (16)$$

Using the following two identities:[33]

$$j_\nu(z) z^\mu = 2^\mu G_{02}^{10}\left(\frac{\mu}{2} + \frac{\nu}{2}, \frac{\mu}{2} - \frac{\nu}{2} \middle| \frac{z^2}{4}\right) \quad (17)$$

and[38]

$$\frac{z^\beta}{(1+az^b)^\alpha} = \frac{a^{-\frac{\beta}{b}}}{\Gamma(\alpha)} G_{11}^{11}\left(\begin{matrix} 1-\alpha+\frac{\beta}{b} \\ \frac{\beta}{b} \end{matrix} \middle| az^b\right). \quad (18)$$

Eq. (16) can be written as

$$\varphi_2 = -\frac{qv\lambda_q^3}{2} \sum_{s=e,h} \frac{1}{v_{ts}\lambda_s^2} \cos\theta \int_0^{\infty} G_{11}^{11}\left(\begin{matrix} -\frac{1}{2} \\ \frac{1}{2} \end{matrix} \middle| \lambda_q^2 k^2\right) \times G_{02}^{10}\left(\frac{1}{2}, -\frac{1}{2} \middle| \frac{k^2 r^2}{4}\right) d(k^2), \quad (19)$$

where $G_{pq}^{mn}\left(\begin{matrix} a_1,\ldots,a_p \\ b_1,\ldots,b_q \end{matrix} \middle| x\right)$ is the Meijer's G function[33] defined as

$$G_{pq}^{mn}\left(\begin{matrix} a_1,\ldots,a_p \\ b_1,\ldots,b_q \end{matrix} \middle| x\right) = \frac{1}{2\pi i} \int \frac{\prod_{j=1}^{m}\Gamma(b_j - s)\prod_{j=1}^{n}\Gamma(1-a_j+s)}{\prod_{j=m+1}^{q}\Gamma(1-b_j+s)\prod_{j=n+1}^{p}\Gamma(a_j-s)} \times x^s ds, \quad (20)$$

with the constraints $0 \le m \le q$ and $0 \le n \le p$. $\Gamma(n)$ is the Euler Gamma function. Using the identities[33] given below

$$\int_0^{\infty} G_{uv}^{st}\left(\begin{matrix} c_1,\ldots,c_u \\ d_1,\ldots,d_v \end{matrix} \middle| \xi x\right) G_{pq}^{mn}\left(\begin{matrix} a_1,\ldots,a_p \\ b_1,\ldots,b_q \end{matrix} \middle| \eta x\right) dx = \frac{1}{\xi} G_{p+vq+u}^{t+ms+n}\left(\begin{matrix} a_1,\ldots,a_n,-d_1,\ldots,-d_v,a_{n+1},\ldots,a_p \\ b_1,\ldots,b_m,-c_1,\ldots,-c_u,b_{m+1},\ldots,b_q \end{matrix} \middle| \frac{\eta}{\xi}\right), \quad (21)$$

$$x^k G_{pq}^{mn}\left(\begin{matrix} a_1,\ldots,a_p \\ b_1,\ldots,b_q \end{matrix} \middle| x\right) = G_{pq}^{mn}\left(\begin{matrix} a_1+k,\ldots,a_p+k \\ b_1+k,\ldots,b_q+k \end{matrix} \middle| x\right), \quad (22)$$

$$G_{pq}^{mn}\left(\begin{matrix} a_1,\ldots,a_p \\ b_1,\ldots,b_{q-1},a_1 \end{matrix} \middle| x\right) = G_{p-1\,q-1}^{m\,n-1}\left(\begin{matrix} a_2,\ldots,a_p \\ b_1,\ldots,b_q-1 \end{matrix} \middle| x\right). \quad (23)$$

Eq. (19) gets modified to

$$\varphi_2 = -\frac{qv\lambda_q^2}{r} \sum_{s=e,h} \frac{1}{v_{ts}\lambda_s^2} G_{02}^{20}\left(\begin{matrix} - \\ 1,1 \end{matrix} \middle| \frac{r^2}{4\lambda_q^2}\right) \cos\theta. \quad (24)$$

It is interesting to note that the Meijer's G function,[33] appearing in the above equation converges if and only if the argument, i.e., $\frac{r^2}{4\lambda_q^2}$ becomes less than unity, i.e., $r < 2\lambda_q$. To obtain the final form of the potential φ_2, we have used the following identity:[33]

$$2^{\mu-1} G_{02}^{20}\left(\frac{\mu}{2} + \frac{\nu}{2}, \frac{\mu}{2} - \frac{\nu}{2} \middle| \frac{x^2}{4}\right) = x^\mu K_\nu(x). \quad (25)$$

The final form of near-field wake potential φ_2 is given by

$$\varphi_2 = -\frac{qv}{2} \sum_{s=e,h} \frac{1}{v_{ts}\lambda_s^2} r K_0\left(\frac{r}{\lambda_q}\right) \cos\theta, \quad (26)$$

where $K_\nu(x)$ is the Macdonald function or modified Bessel function of second kind. It is interesting to note that similar kind of radial dependence of the potential was obtained by Frolov[39] in the case of short-range interaction between two point electric charges.

B. Structure calculation of slowly moving hydrogen-like ion in quantum plasma

The modified non-relativistic Hamiltonian of a slowly moving hydrogen-like ion in the presence of an external quantum plasma environment can be given by [a.u. is used throughout]

$$H = -\frac{1}{2}\nabla^2 + V_{eff}(r,\theta), \quad (27)$$

where the near-field effective potential $V_{eff}(r,\theta)$ is composed of two parts as

$$V_{eff}(r,\theta) = V_d(r) + V_w(r,\theta). \quad (28)$$

Here, $V_d(r)$ is the Debye-Huckel screening potential given by

$$V_d(r) = -\frac{Z}{r} e^{-\mu r}, \quad (29)$$

where Z is the atomic number of the moving ion and μ is the Debye screening parameter related to the Debye length as $\mu = \frac{1}{\lambda_q}$.

The near-field wake potential $V_w(r,\theta)$ is given by

$$V_w(r,\theta) = \zeta r K_0\left(\frac{r}{\lambda_q}\right) \cos\theta, \quad (30)$$

where the wake field coefficient (ζ) is defined as

TABLE I. Convergence of the energy eigenvalues (a.u.) of $1s_0$, $2p_1$, $3d_2$, and $4f_3$ states of C^{5+} moving in quantum plasma. The number density (n_e) of electrons is taken as 10^{19}/c.c. while the speed of the ion (v) is 10^3 cm/s. N represents the total number of terms in the basis set.

N	$1s_0$	N	$2p_1$	N	$3d_2$	N	$4f_3$
1	16.996 989 379	2	3.516 726 519	3	1.101 328 256	4	0.328 549 543
3	16.996 997 305	5	3.544 757 189	7	1.114 962 499	9	0.329 492 549
6	16.996 997 518	9	3.544 757 475	12	1.114 962 616	15	0.329 493 091
15	16.996 997 543	20	3.544 757 476	25	1.114 962 632	22	0.329 493 108
28	16.996 997 543	35	3.544 757 476	42	1.114 962 632	39	0.329 493 108
45	16.996 997 543	54	3.544 757 476	52	1.114 962 632	49	0.329 493 108

$$\zeta = \frac{Zv}{2}\sum\nolimits_{s=e,h}\frac{1}{v_{ts}\lambda_s^2}.$$

The variational equation for any arbitrary angular momentum state of one electron system is given by

$$\delta\int\left[\left(\frac{\partial\Psi}{\partial r}\right)^2+\frac{1}{r^2}\left(\frac{\partial\Psi}{\partial\theta}\right)^2+\frac{1}{r^2\sin^2\theta}\left(\frac{\partial\Psi}{\partial\phi}\right)^2+2(V_{eff}-E)\Psi^2\right]dv_{r,\theta,\phi}=0. \quad (31)$$

The wavefunction Ψ is subjected to the normalization condition

$$\int\Psi^2 dv_{r,\theta,\phi}=1. \quad (32)$$

The trial wavefunction is taken as

$$\Psi(r,\theta,\phi)=f(r)A_{l,m}(\theta,\phi), \quad (33)$$

where the radial part $f(r)$ is given by

$$f(r)=\sum_{i=1}^{N}C_i\chi_i(r), \quad (34)$$

TABLE II. The energy eigenvalues $-E$ (a.u.) of $1s_0$ states of C^{5+} moving in quantum plasma having different set of electron number density (n_e/c.c.) and ion velocity (v cm/s).

		$-E_{1s}$ (a.u.)
n_e (/c.c.)	v (cm/s)	$\|m\|=0$
0	0	18.00000000
8.0×10^{17}	0	17.33681121
	10^3	17.33681120
	10^4	17.33681118
		16.98306649[a]
	10^5	17.33681098
		17.25328413[a]
	5.0×10^5	17.33681008
		25.60522514[a]
10^{19}	0	16.99701207
	10^3	16.99699754
	10^5	16.99699738
	10^7	16.99698206
10^{20}	0	16.54217234
	10^3	16.54214839
	10^5	16.54214822
	10^7	16.54213093
10^{21}	0	15.89053458
	10^3	15.89046598
	10^5	15.89046573
	10^7	15.89044045
10^{22}	0	14.96731440
	10^3	14.96727643
	10^5	14.96727627
	10^7	14.96726037
10^{23}	0	13.68055489
	10^3	13.68051129
	10^5	13.68051115
	10^7	13.68049712

[a]Reference 32.

TABLE III. The energy eigenvalues $-E$ (a.u.) of $2s_0$, $2p_0$, and $2p_1$ states of C^{5+} moving in quantum plasma having different set of electron number density (n_e/c.c.) and ion velocity (v cm/s).

		$-E_{2s}$ (a.u.)	$-E_{2p}$ (a.u.)	
n_e (/c.c.)	v (cm/s)	$\|m\|=0$	$\|m\|=0$	$\|m\|=1$
0	0	4.50000000	4.50000000	4.50000000
8.0×10^{17}	0	3.86368690	3.85785292	3.85785292
	10^3	3.86368689	3.85782543	3.85779533
	10^4	3.86368685	3.85782487	3.85779514
		3.54344882[a]	3.52966416[a]	3.52956493[a]
	10^5	3.86368633	3.85781925	3.85779322
		3.57641662[a]	3.53956809[a]	3.52966416[a]
	5.0×10^5	3.86368405	3.85779427	3.85778469
		4.40032501[a]	3.77474159[a]	3.53214473[a]
10^{19}	0	3.55780856	3.54476161	3.54476161
	10^3	3.55780693	3.54472655	3.54475747
	10^5	3.55780657	3.54472073	3.54475700
	10^7	3.55777061	3.54418783	3.54449515
10^{20}	0	3.16902746	3.14230776	3.14230777
	10^3	3.16902456	3.14229037	3.14224439
	10^5	3.16902418	3.14229621	3.14224287
	10^7	3.16898702	3.14223675	3.14215211
10^{21}	0	2.65209786	2.59865596	2.59865596
	10^3	2.65208981	2.59862497	2.59858157
	10^5	2.65208933	2.59862135	2.59858025
	10^7	2.65204099	2.59825988	2.59844818
10^{22}	0	1.99849293	1.89549274	1.89549274
	10^3	1.99848876	1.89542088	1.89549069
	10^5	1.99848850	1.89541666	1.89549053
	10^7	1.99846268	1.89483600	1.89547373
10^{23}	0	1.23890690	1.05303897	1.05303897
	10^3	1.23890275	1.05281193	1.05303710
	10^5	1.23890257	1.05280651	1.05303730
	10^7	1.23888478	1.05229719	1.05302671

[a]Reference 32.

with $\chi_i(r) = r^{n_i} e^{-\alpha_i r}$. The trial angular part is given by

$$A_{lm}(\theta, \phi) = (\gamma + \beta \cos\theta) Y_{lm}(\theta, \phi), \tag{35}$$

where $Y_{lm}(\theta, \phi)$ is the spherical harmonics.

In order to calculate the matrix elements of the Hamiltonian, we have used the following integral:[33]

$$\int_0^\infty x^{\mu-1} e^{-\alpha x} K_\nu(\beta x) dx = \frac{\sqrt{\pi}(2\beta)^\nu}{(\alpha+\beta)^{\mu+\nu}} \frac{\Gamma(\mu+\nu)\Gamma(\mu-\nu)}{\Gamma\left(\mu-\frac{1}{2}\right)} \times F\left(\mu+\nu, \nu+\frac{1}{2}, \mu+\frac{1}{2}; \frac{\alpha-\beta}{\alpha+\beta}\right), \tag{36}$$

where F is the confluent Hypergeometric function and Re $\mu >$ | Re ν | and Re $(\alpha+\beta) > 0$.

Finally, we have solved the generalized eigenvalue equation[40] given as

$$\underline{\underline{H}}\,\underline{C} = E\underline{\underline{S}}\,\underline{C}, \tag{37}$$

where $\underline{\underline{H}}$ is the Hamiltonian matrix, $\underline{\underline{S}}$ is the overlap matrix, E's are the energy eigenroots, and $\underline{C}$'s are the linear variational coefficients. The non-linear parameters α_i's, β, and γ are optimized by using Nelder-Mead procedure.[41] The convergence behavior of the energy eigenvalues has been checked by increasing the number of terms in the wave function to ensure the accuracy of the present method. All calculations are carried out in quadruple precision.

III. RESULTS AND DISCUSSIONS

We have calculated the energy eigenvalues of ns_0 [the principal quantum number, $n = 1-4$ and the subscript denotes the values of the azimuthal quantum number]; np_0, np_1 [$n = 2-4$]; nd_0, nd_1, nd_2 [$n = 3-4$]; and nf_0, nf_1, nf_2, nf_3 [$n = 4$] states of C^{5+} ion. The plasma electron densities (n_e) are chosen within the range of $10^{19} - 10^{23}$/c.c., where for each value of plasma density (n_e), the ion velocities (v) are within the range of $10^3 - 10^7$ cm/s. Table I displays the results for convergence of energy eigenvalues for $1s_0$, $2p_1$, $3d_2$, and $4f_3$ states corresponding to plasma density (n_e) 10^{19}/c.c. and ion velocity (v) 10^3 cm/s. It is evident from Table I that the energy eigenvalues converge up to 9th decimal place in each case. Similar convergence of energy values is obtained for all the calculations done in the present work.

TABLE IV. The energy eigenvalues $-E$ (a.u.) of $3s_0$, $3p_0$, $3p_1$, $3d_0$, $3d_1$, and $3d_2$ states of C^{5+} moving in quantum plasmas having different set of electron number density (n_e/c.c.) and ion velocity (v cm/s).

		$-E_{3s}$ (a.u.)	$-E_{3p}$ (a.u.)		$-E_{3d}$ (a.u.)		
n_e (/c.c.)	v (cm/s)	$\|m\| = 0$	$\|m\| = 0$	$\|m\| = 1$	$\|m\| = 0$	$\|m\| = 1$	$\|m\| = 2$
0	0	2.00000000	2.00000000	2.00000000	2.00000000	2.00000000	2.00000000
8.0×10^{17}	0	1.40534572	1.40002099	1.40002099	1.38931372	1.38931372	1.38931372
	10^3	1.40534571	1.40001296	1.40000432	1.38931361	1.38931359	1.38931354
	10^4	1.40534564	1.40001207	1.40000402	1.38931351	1.38931351	1.38931351
		1.13800837[a]	1.12586273[a]	1.12583700[a]	1.10181766[a]	1.10181766[a]	1.10181766[a]
	10^5	1.40534488	1.40000307	1.40000094	1.38931254	1.38931272	1.38931325
		1.14713322[a]	1.12861525[a]	1.12586273[a]	1.10203080[a]	1.06519697[a]	1.10193893[a]
	5.0×10^5	1.40534149	1.39996310	1.39998729	1.38930820	1.38930917	1.38931206
		1.36260175[a]	1.19290816[a]	1.12655361[a]	1.10715733[a]	1.10223660[a]	1.10490827[a]
10^{19}	0	1.14923194	1.13789722	1.13789723	1.11496287	1.11496287	1.11496287
	10^3	1.14923145	1.13788733	1.13789606	1.11496273	1.11496270	1.11496263
	10^5	1.14923096	1.13787887	1.13789537	1.11496174	1.11496190	1.11496236
	10^7	1.14918232	1.13709896	1.13759242	1.11486312	1.11488121	1.11493546
10^{20}	0	0.85275345	0.83113577	0.83113577	0.78686902	0.78686902	0.78686902
	10^3	0.85275269	0.83113114	0.83111901	0.78686882	0.78686878	0.78686868
	10^5	0.85275224	0.83113021	0.83111706	0.78686792	0.78686805	0.78686843
	10^7	0.85270789	0.83104578	0.83097475	0.78677385	0.78679108	0.78684275
10^{21}	0	0.51307024	0.47479205	0.47479205	0.39462864	0.39462864	0.39462864
	10^3	0.51306840	0.47478483	0.47477478	0.39462843	0.39462840	0.39462828
	10^5	0.51306792	0.47478106	0.47477341	0.39462775	0.39462784	0.39462810
	10^7	0.51302066	0.47440449	0.47463583	0.39455982	0.39457226	0.39460957
10^{22}	0	0.18762946	0.13082887	0.13082887		0.01136017	0.01136017
	10^3	0.18762878	0.13081719	0.13082853		0.01136002	0.01135996
	10^5	0.18762861	0.13081432	0.13082842		0.01135976	0.01135987
	10^7	0.18761157	0.13044258	0.13081701		0.01133326	0.01135103
10^{23}	0	0.00358750					
	10^3	0.00358738					
	10^5	0.00358736					
	10^7	0.00358535					

[a]Reference 32.

TABLE V. The energy eigenvalues $-E$ (a.u.) of $4s_0$, $4p_0$, $4p_1$, $4d_0$, $4d_1$, $4d_2$, $4f_0$, $4f_1$, $4f_2$, and $4f_3$ states of C^{5+} moving in quantum plasmas having different set of electron number density (n_e/c.c.) and ion velocity (v cm/s).

		$-E_{4s}$ (a.u.)	$-E_{4p}$ (a.u.)		$-E_{4d}$ (a.u.)			$-E_{4f}$ (a.u.)			
n_e (/c.c.)	v (cm/s)	$\|m\|=0$	$\|m\|=0$	$\|m\|=1$	$\|m\|=0$	$\|m\|=1$	$\|m\|=2$	$\|m\|=0$	$\|m\|=1$	$\|m\|=2$	$\|m\|=3$
0	0	1.12500000	1.12500000	1.12500000	1.12500000	1.12500000	1.12500000	1.12500000	1.12500000	1.12500000	1.12500000
8.0×10^{17}	0	0.58332137	0.57865346	0.57865346	0.56923686	0.56923686	0.56923686	0.55490196	0.55490196	0.55490196	0.55490196
	10^3	0.58332136	0.57865021	0.57864684	0.56923680	0.56923680	0.56923678	0.55490190	0.55490190	0.55490189	0.55490187
	10^4	0.58332127	0.57864913	0.57864648	0.56923669	0.56923670	0.56923675	0.55490176	0.55490177	0.55490179	0.55490185
		0.38038470[a]	0.36991115[a]	0.36990013[a]	0.34919409[a]	0.34919336[a]	0.34919373[a]	0.31860361[a]	0.31849924[a]	0.31860398[a]	0.31860361[a]
	10^5	0.58332038	0.57863836	0.57864279	0.56923546	0.56923570	0.56923642	0.55490031	0.55490045	0.55490086	0.55490153
		0.38363334[a]	0.37089236[a]	0.36991115[a]	0.34926980[a]	0.33600588[a]	0.34923783[a]	0.31861941[a]	0.31860545[a]	0.31866131[a]	0.31863742[a]
	5.0×10^5	0.58331642	0.57859047	0.57862644	0.56923001	0.56923124	0.56923493	0.55489389	0.55489459	0.55489667	0.55490014
		0.45895839[a]	0.39373940[a]	0.37015737[a]	0.35111057[a]	0.34934404[a]	0.35030319[a]	0.31900087[a]	0.31865102[a]	0.32004822[a]	0.31860398[a]
10^{19}	0	0.38627150	0.37710044	0.37710044	0.35842741	0.35842741	0.35842741	0.32949318	0.32949318	0.32949318	0.32949318
	10^3	0.38627133	0.37709676	0.37710000	0.35842735	0.35842734	0.35842731	0.32949313	0.32949313	0.32949312	0.32949310
	10^5	0.38627083	0.37708789	0.37709929	0.35842627	0.35842645	0.35842702	0.32949196	0.32949206	0.32949235	0.32949285
	10^7	0.38622101	0.37626956	0.37679442	0.35831828	0.35833810	0.35839757	0.32936955	0.32938029	0.32941613	0.32946744
10^{20}	0	0.19334518	0.17815971	0.17815971	0.14683884	0.14683884	0.14683884	0.09678684	0.09678684	0.09678684	0.09678684
	10^3	0.19334495	0.17815827	0.17815457	0.14683878	0.14683877	0.14683874	0.09678681	0.09678681	0.09678680	0.09678679
	10^5	0.19334458	0.17815633	0.17815294	0.14683800	0.14683813	0.14683852	0.09678618	0.09678623	0.09678639	0.09678666
	10^7	0.19330816	0.17808454	0.17803027	0.14675666	0.14677158	0.14681633	0.09672344	0.09672894	0.09674547	0.09677302
10^{21}	0	0.03820810	0.02020779	0.02020779							
	10^3	0.03820777	0.02020659	0.02020495							
	10^5	0.03820756	0.02020497	0.02020436							
	10^7	0.03818578	0.02004326	0.02014525							

[a]Reference 32.

For different sets of plasma densities (n_e) and ion velocities (v), Tables II–V display the energy eigenvalues of $n=1$ to $n=4$ states, respectively. The energy eigenvalues obtained by Hu *et al.*[32] are also included in Tables II–V for a comparison with the present work. The energy eigenvalues of free ions are given in the first row of each table. From the numbers quoted in Tables II–V, it is evident that as the plasma density (n_e) increases for a given ion velocity (v), the energy eigenvalues become more and more positive leading towards destabilization of the ion and as the ion velocity increases for a given plasma density (n_e), the energy eigenvalues become more and more positive but with a much slower rate compared to the preceding one. Thus, it can be argued that the effect of static screening (which depends only on n_e) of the plasma environment on the energy eigenvalue is much more pronounced as compared to that of the wake field, where the later arises due to the velocity (v) of the ion and also depends on plasma electron density (n_e). In contrast, Hu *et al.*[32] showed that the energy of each state considered by them became over-bound (i.e., more negative than the energy of the free ion) when the ion velocity (v) reached a sufficiently high value. For example, Hu *et al.*[32] reported that for $n_e = 8.0 \times 10^{23}$ m^{-3} and ion velocity $v = 5000$ m/s, the ground state ($1s_0$) energy of C^{5+} becomes -25.60522514 a.u. which is more negative than the ground state energy -18.0 a.u. for the free C^{5+} ion. In this regard, Hu *et al.*[32] opined that such over-boundedness occurred because of the choice of angular part of the wave function. But the angular part of the wavefunction cannot be responsible for such over-boundedness as it violates the basic variational principle. No such over-boundedness is observed in the present calculations. For example, we have obtained the ground state ($1s_0$) energy of -17.33681008 a.u. for C^{5+} ion, where $n_e = 8.0 \times 10^{23}$ m^{-3} and $v = 5000$ m/s.

It can also be noted from Tables III–V that the usual breaking of accidental degeneracy (i.e., l degeneracy corresponding to a given n) occurs with respect to the plasma electron density (n_e). This is a well-known phenomenon in presence of Debye-Huckel potential and can be found in different studies.[15] The degeneracy of energy eigenvalues with respect to the absolute value of magnetic quantum number, i.e., $|m|$ is removed for each ion velocity (v) because of the presence of $\cos\theta$ term in the near-field wake potential as seen in Tables III–V. For example, Table III shows that for ion velocity (v) 10^3 cm/s and plasma electron density (n_e) 10^{19}/c.c., the energy eigenvalues of $2p_0$ and $2p_1$ states are -3.54472655 a.u. and -3.54475747 a.u., respectively. This is purely Stark-like splitting. Such kind of splitting is observed for different choice of plasma densities for p, d, and f states as can be seen from Tables III–V. In contrast, Hu *et al.*[32] reported Zeeman-like splitting, i.e., the lifting of degeneracy of the energy levels with respect to magnetic quantum no. "m."

The variation of energies of ($2p_0$, $2p_1$) states for two different plasma densities (n_e) is depicted in two sub-graphs of Figure 1. It is evident from Figure 1 that corresponding to plasma density $n_e = 10^{19}$/c.c., $2p_1$ state lies energetically below $2p_0$ state for the entire range of ion velocity (v), and thus no crossing of energy levels is being observed. But, for density higher than the previous one, it is to be noted that $2p_0$ state energetically lies below than that of $2p_1$ state when the ion velocity is low and after a critical ion velocity $2p_1$ state becomes more negative than that of $2p_0$ state. Hence, depending on the plasma electron density incidental degeneracy of np_0 and np_1 states occurs at a particular critical ion velocity. Such crossing of energy levels and subsequent appearance of incidental degeneracy occur for all other angular momentum states (i.e., d and f) as shown in Figures 2 and 3. It is clear

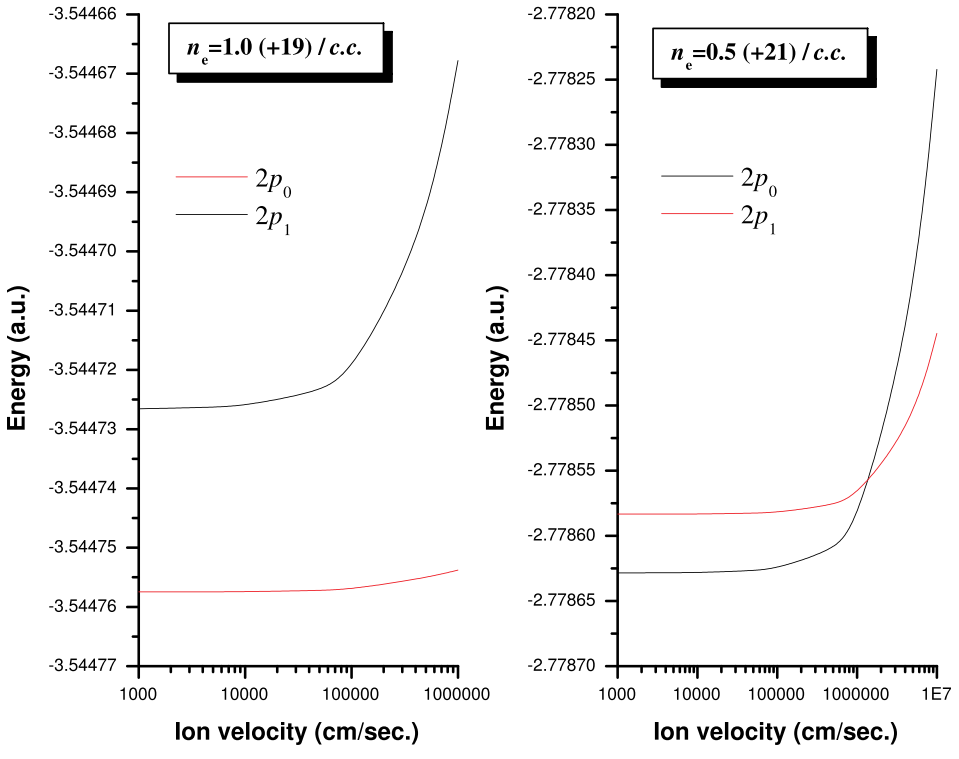

FIG. 1. Plot of energy values (in a.u.) of $2p_0$ and $2p_1$ states of C^{5+} against ion velocity (in cm/s) for plasma electron densities $n_e = 10^{19}$ (/c.c.) and $n_e = 0.5 \times 10^{21}$ (/c.c.).

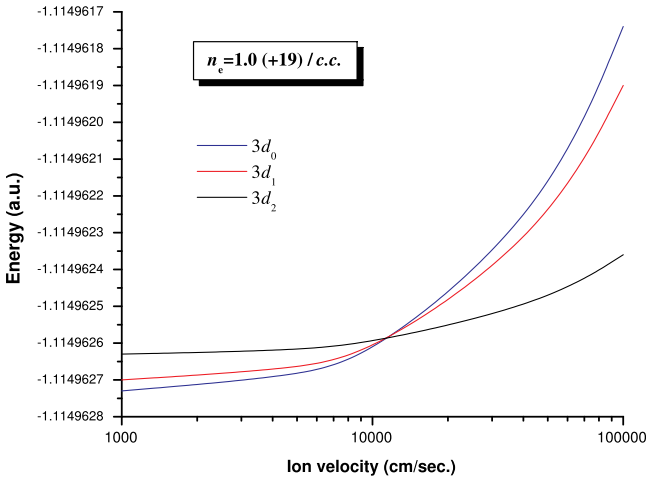

FIG. 2. Plot of energy values (in a.u.) of $3d_0$, $3d_1$, and $3d_2$ states of C^{5+} against ion velocity (in cm/s) for plasma electron density $n_e = 10^{19}$ (/c.c.).

from Figures 2 and 3 that contrary to *np* states, crossover of energy eigenvalues appears at low plasma density ($n_e = 10^{19}$/c.c.). The plasma density, critical velocity, and energy at which crossover of states occurs, are given in Table VI. Such incidental degeneracy was reported earlier by Sen[42] in case of shell confined hydrogen atom. Thus, Figures 1–3 give a good insight into the combined effect of static screening and near field wake potential on different angular momentum states of a slowly moving ion in quantum plasma.

IV. CONCLUSION

The electrostatic potential for a moving ion under quantum plasma is derived where the thermal Mach number remains less than unity. Subsequently, the effect of such potential on the change of the energy eigenvalues of different states of hydrogen-like carbon ion is studied under the framework of Rayleigh-Ritz variational method. Level crossing phenomenon and incidental degeneracy are observed for the first time in case of an ion moving in the quantum plasma environment. The present form of the potential will help future workers to investigate the structural properties of different ions under quantum plasma environment.

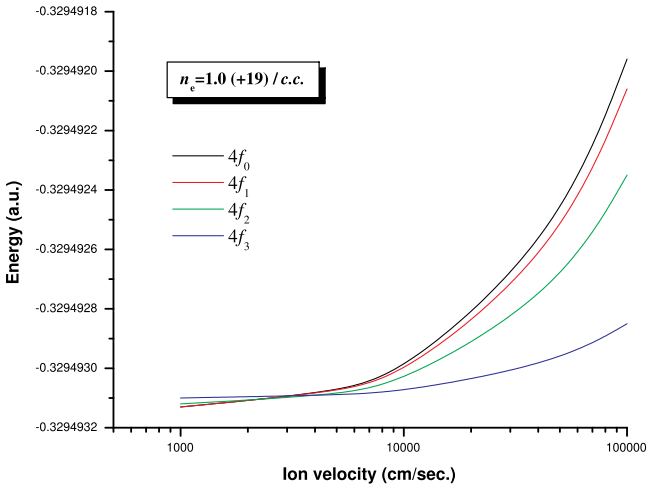

FIG. 3. Plot of energy values (in a.u.) of $4f_0$, $4f_1$, $4f_2$, and $4f_3$ states of C^{5+} against ion velocity (in cm/s) for plasma electron density $n_e = 10^{19}$ (/c.c.).

TABLE VI. For different plasma electron density (/c.c.), Critical ion velocity (cm/s) and energy eigenvalue ($-E$ in a.u.) at the crossing of different angular momentum states. The symbol $P(+Q)$ corresponds to $P \times 10^{Q}$.

Name of the crossover states	Plasma density (/c.c.)	Critical ion velocity (cm/s)	Energy at crossing ($-E$) (a.u.)
$2p_0$, $2p_1$	0.5(+20)	7.22(+5)	3.27700464
	1.0(+20)	8.79(+6)	3.14214490
	0.5(+21)	1.36(+6)	2.77855694
$3p_0$, $3p_1$	0.5(+20)	1.19(+5)	0.92995292
	1.0(+20)	3.75(+6)	0.83103806
	0.5(+21)	3.72(+5)	0.58490697
$4p_0$, $4p_1$	0.5(+20)	5.78(+4)	0.23720661
	1.0(+20)	2.78(+6)	0.83103806
	0.5(+21)	1.27(+5)	0.05775748
$3d_0$, $3d_1$, $3d_2$	1.0(+19)	1.13(+4)	1.11496259
	0.5(+20)	1.77(+4)	0.89347312
	1.0(+20)	1.67(+4)	0.78686862
	0.5(+21)	2.24(+4)	0.39462823
$4d_0$, $4d_1$, $4d_2$	1.0(+19)	4.70(+3)	0.35842729
	0.5(+20)	7.31(+3)	0.20993047
	1.0(+20)	6.51(+3)	0.14683872
	0.5(+21)	7.96(+3)	0.02025229
$4f_0$, $4f_1$, $4f_2$, $4f_3$	1.0(+19)	3.09(+3)	0.32949309
	0.5(+20)	2.64(+3)	0.16679314
	1.0(+20)	2.84(+3)	0.09678679

ACKNOWLEDGMENTS

Authors express heartfelt thanks to Professor H. Hu for helpful discussions. T.K.M. gratefully acknowledges financial support under Grant No. 37(3)/14/27/2014-BRNS from the Department of Atomic Energy, BRNS, Government of India. Authors are grateful to Dr. S. K. Das or careful proofreading of the manuscript.

[1]P. Jiang, S. Kar, and Y. Zhou, Phys. Plasmas **20**, 012126 (2013).
[2]L. G. Jiao and Y. K. Ho, Phys. Rev. A **87**, 052508 (2013).
[3]J. P. Santos, A. M. Costa, J. P. Marques, M. C. Martins, P. Indelicato, and F. Parente, Phys. Rev. A **82**, 062516 (2010).
[4]J. K. Saha, S. Bhattacharyya, P. K. Mukherjee, and T. K. Mukherjee, J. Phys. B **42**, 245701 (2009).
[5]F. Rosmej, K. Bennadji, and V. S. Lisitsa, Phys. Rev. A **84**, 032512 (2011).
[6]M. Das, M. Das, R. K. Chaudhuri, and S. Chattopadhyay, Phys. Rev. A **85**, 042506 (2012).
[7]K. D. Lawson, I. H. Coffey, K. M. Aggarwal, F. P. Keeman, and JET-EFDA Contributors, J. Phys. B **46**, 035701 (2013).
[8]R. Cabrera-Trujillo and S. A. Cruz, Phys. Rev. A **87**, 012502 (2013).
[9]Y. Zhang, Q. Liu, and T. Shi, J. Phys. B **45**, 085101 (2012).
[10]B. L. Burrows and M. Cohen, Phys. Rev. A **88**, 052511 (2013).
[11]S. Bhattacharyya, J. K. Saha, P. K. Mukherjee, and T. K. Mukherjee, Phys. Scr. **87**, 065305 (2013).
[12]K. Coutinho, S. Canuto, P. K. Mukherjee, and B. Fricke, in *Advances in the Theory of Atomic and Molecular Systems, Dynamics, Spectroscopy, Clusters and Nanostructures*, Progress in Theoretical Chemistry and Physics, edited by P. Piecuch *et al.* (Springer, New York, 2009), Vol. 20, p. 183.
[13]V. K. Dolmatov, J. L. King, and J. C. Oglesby, J. Phys. B **45**, 105102 (2012).
[14]C. Y. Lin and Y. K. Ho, J. Phys. B **45**, 145001 (2012).
[15]A. N. Sil, S. Canuto, and P. K. Mukherjee, Adv. Quantum Chem. **58**, 115 (2009).

[16]P. Debye and E. Huckel, Z. Phys. **24**, 185 (1923).
[17]A. I. Akhiezer, I. A. Akhiezer, R. A. Polovin, A. G. Sitenko, and K. N. Stepanov, *Plasma Electrodynamics*, Linear Response Theory (Pergamon, Oxford, 1975), Vol. 1.
[18]E. M. Lifshitz and L. P. Pitaevskii, *Physical Kinetics* (Butterworth-Heinemann, UK, 1981).
[19]A. Markowich, C. Ringhofer, and C. Schmeiser, *Semiconductor Equations* (Springer, Vienna, 1990).
[20]G. V. Shpatakovskaya, J. Exp. Theor. Phys. **102**, 466 (2006).
[21]L. K. Ang and P. Zhang, Phys. Rev. Lett. **98**, 164802 (2007).
[22]S. X. Hu and C. H. Keitel, Phys. Rev. Lett. **83**, 4709 (1999).
[23]S. H. Glenzer, O. L. Landen, P. Neumayer, R. W. Lee, K. Widmann, S. W. Pollaine, and R. J. Wallace, Phys. Rev. Lett. **98**, 065002 (2007).
[24]V. M. Malkin, N. J. Fisch, and J. S. Wurtele, Phys. Rev. E **75**, 026404 (2007).
[25]Y. I. Salamin, S. X. Hu, K. Z. Hatsagortsyan, and C. H. Keitel, Phys. Rep. **427**, 41 (2006).
[26]M. Opher, L. O. Silva, D. E. Dauger, V. K. Decyk, and J. M. Dawson, Phys. Plasmas **8**, 2454 (2001).
[27]O. G. Benvenuto and M. A. De Vito, Mon. Not. R. Astron. Soc. **362**, 891 (2005).
[28]G. Chabrier, D. Saumon, and A. Y. Potekhin, J. Phys. A **39**, 4411 (2006).
[29]D. Pines, J. Nucl. Energy **2**, 5 (1961).
[30]P. K. Shukla, L. Stenflo, and R. Bingham, Phys. Lett. A **359**, 218 (2006).
[31]D. Montgomery, G. Joyce, and R. Sugihara, Plasma Phys. **10**, 681 (1968).
[32]H. Hu, F. Li, and C. Jiang, Phys. Rev. E **85**, 056406 (2012).
[33]L. S. Gradshteyn and I. M. Ryzhik, *Table of Integrals, Series and Products*, 7th ed. (Academic, New York, 1994).
[34]M. Abramowitz and I. A. Stegun, *Handbook of Mathematical Functions* (Dover, New York, 1972).
[35]R. N. Dexter and B. Lax, Phys. Rev. **96**, 223 (1954).
[36]See http://www.eecs.berkeley.edu/∼hu/Chenming-Hu_ch1.pdf for the electron and hole effective masses (p. 13).
[37]A. V. Ivlev, S. A. Khrapak, S. K. Zhdanov, and G. E. Morfill, Phys. Rev. Lett. **92**, 205007 (2004).
[38]E. E. Fichard and V. Franco, J. Phys. A **13**, 2331 (1980).
[39]A. M. Frolov, Can. J. Phys. **92**, 1094 (2014).
[40]B. H. Bransden and C. J. Joachain, *Physics of Atoms and Molecules*, 2nd ed. (Pearson Education, Delhi, 2004), pp. 133.
[41]J. A. Nelder and R. Mead, Comput. J. **7**, 308 (1965).
[42]K. D. Sen, J. Chem. Phys. **122**, 194324 (2005).

I R A M P
6(2), Dec. 2015, pp. 73-82

ISSN: 2229-3159

Binding Energies of Hydrogenlike Carbon under Maxwellian Dusty Plasma Environment

S. DUTTA[1], J. K. SAHA[2], S. BHATTACHARYYA[3,*] AND T. K. MUKHERJEE[4]

[1]*Belgharia Texmaco Estate School, Belgharia, Kolkata-700056, India*
[2]*Dept. of Physics, Aliah University, Newtown, Kolkata-700156, India*
[3]*Dept. of Physics, Acharya Prafulla Chandra College, New Barrackpore, Kolkata-700131, India*
[4]*Dept. of Physics, Narula Institute of Technology, Agarpara, Kolkata-700109, India*
**E-mail: sukhamoy.b@gmail.com*

ABSTRACT: The analytic form of the electrostatic potential felt by a slowly moving test charge in Maxwellian dusty plasma is developed. It has been shown that the electrostatic potential is composed of three parts: i) the Debye-Hückel screening term, ii) the near-field wake potential and iii) the dust charge perturbation effect. The last two terms depend on the velocity of the test charge, the number density of the plasma electrons and the dust grain parameters. Precise energy eigenvalues of hydrogen-like carbon ion under such plasma environment has been estimated by employing Rayleigh-Ritz variational calculation. The form of the potential facilitates the removal of *l*-degeneracy and |*m*|-degeneracy in the energy levels. A detailed analysis shows that the energy levels gradually move to the continuum with increasing plasma electron density and the variation of ion velocity. Incidental degeneracy of the energy levels and level crossing phenomena have been observed with the variation of plasma electron density.

Keywords: Dusty plasma, variational method, one-electron atom

I. INTRODUCTION

In recent years, dusty plasmas are attracting considerable attention in the field of plasma physics research. In addition to electrons, ions, neutrals as present in ordinary plasmas, dusty plasmas contain massive particles of nanometer to micrometer size. The dust grains may be metallic, conducting, or made of ice particulates. Plasma with dust particles or grains can be termed as either 'dust in plasma' or 'dusty plasma' depending on the relative values of three characteristic lengths : i) the dust grain radius (r_d), ii) the average inter-grain distance (a) and iii) the Debye radius (λ_D). For $r_d < \lambda_D < a$, charged dust particles are considered as a collection of isolated screened grains, which corresponds to 'dust in plasma'. For the condition $r_d < a < \lambda_D$ dust particles participate in the collective behavior and in that case the plasma is said to be 'dusty plasma'. Dusty plasmas are most abundant in astrophysical objects like in the planetary rings, in cometary tails or in interstellar clouds [1, 2]. Dusty plasmas are also formed in laboratory based experiments like dc and rf- discharges, plasma processing reactors, fusion plasma devices, solid-fuel combustion products *etc.* [3]. Dusty plasmas play important role in formation of plasma crystals as under some plasma conditions dust grains can order themselves into crystal-like structure [4, 5].

There are a number of theoretical studies of plasma wave modulation, transport phenomena of the particles, ion drag forces, phase transitions, crystallization of dust grains under dusty plasma environment [6-13]. But the effect of dusty plasma on the structural properties of atoms is rather scanty [14]. The most important part of such studies is to develop an appropriate model interatomic potential from a pure electrostatic view which can mimic the conditions of such plasma environment. Unlike the plasma modeled by exponentially screened Coulomb potential, the model potential for dusty plasma contains a complex character [14-18]. The closed form of the far-field potential felt by a

slowly moving test charge through unmagnetized dusty plasma in the spherical polar co-ordinate was first derived by Shukla [15]. It is shown that the effective potential consists of three parts: exponentially screened Coulomb part, far-field wake potential part and dust charge fluctuation term. Shukla *et al.* [16] developed another form of the far-field potential of a slowly moving test charge in a plasma that consisted of positive dust grains and electrons. The dust grain charge fluctuations and collisions among neutral atoms, electrons and dust grains were taken into account. In the work of Moslem *et al.* [17], the Debye–Hückel screening potential and oscillatory wake field potential distribution around a test charge particle moving in the dusty plasma medium were derived by solving the linearized Vlasov equation along with the Poisson equation. Ali *et al.* [18] also used Vlasov-Poisson equation to formulate the electrostatic potential caused by a test charge in unmagnetized non-Maxwellian dusty plasma where the plasma particles are : superthermal hot electrons, cold fluid electrons, neutralizing cold cations and charge fluctuating isolated dust grains.

The aim of the present paper is to formulate the near field potential felt by an atom/ion moving slowly through unmagnetized dusty plasma and apply the potential to find the binding energies of one-electron ion. The binding energies of moving hydrogen-like carbon (C^{5+}) ion under different conditions of the classical dusty plasma are estimated by using variational method. It is observed that the *l*-degeneracy of the hydrogenic energy levels corresponding to a principal quantum number is lifted under this potential. Moreover, a partial removal of the *m*-degeneracy is also observed. In particular, we have calculated the energy values of C^{5+} ion in $1s_0$, $2s_0$, $2p_0$ and $2p_1$ states by varying the velocity of the ion and the plasma electron density as well. The details of the formulation of the inter-atomic potential for slowly moving test charge under dusty plasma is given in the Sec. II, the details of the variational method used for the atomic structure calculation is given in Sec. III, computational results are given in Sec. IV and final conclusion in Sec. V.

II. NEAR-FIELD POTENTIAL FELT BY A SLOWLY MOVING "TEST CHARGE" IN CLASSICAL DUSTY PLASMA

The field ($\vec{D}$) of a charge q moving with a velocity $\vec{u}$ in a dielectric medium is given by the Poisson's equation [20],

$$\vec{\nabla}.\vec{D} = \frac{q}{\varepsilon_0}\delta(\vec{r} - \vec{u}t) \tag{1}$$

where $\vec{D} = -D\vec{\nabla}\varphi$, D being the dielectric constant of the medium and φ being the potential in the medium. Using the relation and making a Fourier transform followed by an inverse Fourier transform, we obtain the expression for the potential as [20]

$$\varphi(\vec{r}) = \frac{q}{8\pi^3\varepsilon_0}\int \frac{e^{j\vec{k}.\vec{r}}}{k^2 D\left(\vec{k}, -\vec{k}\cdot\vec{u}\right)} d^3\vec{k} \tag{2}$$

Here $j = \sqrt{-1}$ and ε_0 is the permittivity of free space. The dielectric constant of the medium is given by,

$$D\left(\vec{k}, -\vec{k}\cdot\vec{u}\right) = 1 + \chi_e + \chi_i + \chi_d \tag{3}$$

where, $\chi_s\big|_{s=e,i,d}$ is the electric susceptibility for the plasma species 's' ($s=e,i,d$ corresponding to electron, ion and dust, respectively).

Considering the Maxwell-Boltzmann distribution for the plasma particles, the electric susceptibility due to the thermal motion of plasma electrons and ions is given by [20],

$$\chi_s\big|_{s=e,i} = \frac{1}{k^2\lambda_s^2}\left(1 - j\sqrt{\frac{\pi}{2}}\frac{\vec{k}.\vec{u}}{kv_{ts}}\right) \tag{4}$$

The electric susceptibility due to dust grain charging and thermal motion is given as [15],

$$\chi_d = \frac{1}{k^2\lambda_d^2}\left(1 - j\sqrt{\frac{\pi}{2}}\frac{\vec{k}.\vec{u}}{kv_{td}}\right) + \frac{1}{k^2\lambda_i^2}\frac{\nu_{ed}}{\nu_c + j\vec{k}.\vec{u}}$$

$\lambda_s = \frac{\varepsilon_0 m_s T_s}{n_s q_s^2}$ is the Debye screening length of the plasma species 's'. T_s, m_s, q_s and n_s are absolute temperature, mass, charge and equilibrium number density respectively of species 's'. The thermal speed of the plasma species 's' is given by, $v_{ts} = \sqrt{\frac{K_B T_s}{m_s}}$ where K_B is the Boltzmann constant.

If we consider that the dust grain contains negative charges only, then the quasi-charge neutrality condition within the effective Debye-sphere of the plasma becomes, $n_i q_i = n_e q_e + n_d q_d$. For $\nu_c >> \left|\vec{k}\cdot\vec{u}\right|$, electric susceptibility due to the dust grain becomes,

$$\chi_d \approx \frac{1}{k^2\lambda_d^2}\left(1 - j\sqrt{\frac{\pi}{2}}\frac{\vec{k}.\vec{u}}{kv_{td}}\right) + \frac{\nu_{ed}}{k^2\lambda_i^2\nu_c} - j\frac{\nu_{ed}\left(\vec{k}.\vec{u}\right)}{k^2\lambda_i^2\nu_c^2} \tag{5}$$

Using (4) and (5), one can obtain the modified form of (3) as,

$$D\left(\vec{k},-\vec{k}\cdot\vec{u}\right) = 1 + \frac{1}{k^2}\left(\sum_{s=e,i,d}\frac{1}{\lambda_s^2} + \frac{\nu_{ed}}{\nu_c\lambda_i^2}\right) - j\sqrt{\frac{\pi}{2}}\frac{\vec{k}.\vec{u}}{k^3}\sum_{s=e,i,d}\frac{1}{v_{ts}\lambda_s^2} - j\frac{\nu_{ed}\left(\vec{k}.\vec{u}\right)}{k^2\lambda_i^2\nu_c^2}$$

$$= 1 + \frac{1}{k^2\lambda_t^2} - j\sqrt{\frac{\pi}{2}}\frac{\vec{k}.\vec{u}}{k^3}\sum_{s=e,i,d}\frac{1}{v_{ts}\lambda_s^2} - j\frac{1}{k^2\lambda_i^2}\frac{\nu_{ed}\left(\vec{k}.\vec{u}\right)}{\nu_c^2}$$

$$= \frac{1+k^2\lambda_t^2}{k^2\lambda_t^2}\left[1 - j\frac{k^2\lambda_t^2}{1+k^2\lambda_t^2}\left\{\sqrt{\frac{\pi}{2}}\frac{\vec{k}.\vec{u}}{k^3}\sum_{s=e,i,d}\frac{1}{v_{ts}\lambda_s^2} + \frac{1}{k^2\lambda_i^2}\frac{\nu_{ed}\left(\vec{k}.\vec{u}\right)}{\nu_c^2}\right\}\right] \tag{6}$$

where

$$\frac{1}{\lambda_t^2} = \sum_{s=e,i,d}\frac{1}{\lambda_s^2} + \frac{\nu_{ed}}{\nu_c\lambda_i^2} \tag{7}$$

For very slowly moving atom/ion i.e. $v_{ts} >> u$, which means the thermal Mach number (defined as the ratio of ion velocity and thermal velocity of plasma particles) remains below unity, the inverse of dielectric function becomes,

$$\frac{1}{D\left(\vec{k},-\vec{k}\cdot\vec{u}\right)} \approx \frac{k^2\lambda_t^2}{1+k^2\lambda_t^2}\left[1 + j\frac{k^2\lambda_t^2}{1+k^2\lambda_t^2}\left\{\sqrt{\frac{\pi}{2}}\frac{\vec{k}.\vec{u}}{k^3}\sum_{s=e,i,d}\frac{1}{v_{ts}\lambda_s^2} + \frac{1}{k^2\lambda_i^2}\frac{\nu_e\left(\vec{k}.\vec{u}\right)}{\nu_c^2}\right\}\right]$$

$$= \frac{k^2\lambda_t^2}{1+k^2\lambda_t^2} + j\sigma_1\frac{k^2}{\left(1+k^2\lambda_t^2\right)^2}\cos\left(\eta+\theta\right) + j\sigma_2\frac{k^3}{\left(1+k^2\lambda_t^2\right)^2}\cos\left(\eta+\theta\right) \tag{8}$$

where, $$\sigma_1 = \sqrt{\frac{\pi}{2}} u \lambda_t^4 \sum_{s=e,i,d} \frac{1}{\nu_{ts} \lambda_s^2} \text{ and } \sigma_2 = \frac{u \nu_{ed} \lambda_t^4}{\lambda_i^2 \nu_c^2} \quad (9)$$

Here, θ is the angle between $\vec{r}$ and $\vec{u}$ and $(\theta + \eta)$ is the angle between $\vec{k}$ and $\vec{u}$. Using equation (8) one can dissolve equation (2) into three parts that may be given as follows:

$$\varphi = \varphi_1 + \varphi_2 + \varphi_3$$

where we define the first part as

$$\varphi_1 = \frac{q}{8\pi^3 \varepsilon_0} \int \frac{\lambda_t^2}{1 + k^2 \lambda_t^2} e^{i\vec{k}.\vec{r}} d^3\vec{k} = \frac{q}{4\pi\varepsilon_0 r} e^{-r/\lambda_t} \quad (10)$$

The method of solving the integral can be found in ref. [21]. Thus the potential φ_1 is of the form of Debye-Hückel potential [22], where λ_t signifies the effective or total *Debye length* of the plasma. The inverse of *Debye length* is known as *Debye parameter* or simply *screening parameter* (μ) *i.e.* $\mu = 1/\lambda_t$. The second part of the potential φ is

$$\varphi_2 = j \frac{q\sigma_1}{8\pi^3 \varepsilon_0} \int \frac{k^2 e^{jkr\cos\eta}}{\left(1 + k^2 \lambda_t^2\right)^2} \cos(\eta + \theta) \sin\eta d\eta d\tau dk \quad (11)$$

Here we have used the volume element $d^3\vec{k} = k^2 \sin\eta d\eta d\tau dk$ in spherical polar coordinate (k, η, τ). One can get the imaginary solution of the angular part of the integral (11) as,

$$\int_{\tau=0}^{2\pi} \int_{\eta=0}^{\pi} e^{jkr\cos\eta} \cos(\eta + \theta) \sin\eta d\eta d\tau = \frac{4\pi \cos\theta}{j} \left(\frac{\cos kr}{kr} - \frac{\sin kr}{k^2 r^2} \right) \quad (12)$$

Now using (12), equation (11) reduces to

$$\varphi_2 = -\frac{q\sigma_1 \cos\theta}{2\pi^2 \varepsilon_0} \int_{k=0}^{\infty} \frac{k^2 j_1(kr)}{\left(1 + k^2 \lambda_t^2\right)^2} dk \quad (13)$$

Here $j_1(kr)$ is the spherical Bessel function of first order [19]. The solution of integral (13) can be done using the standard Meijer's G function [19] and the solution technique described in [21], where in the limit $r < 2\lambda_t$ the above integral becomes

$\int_{k=0}^{\infty} \frac{k^2 j_1(kr)}{\left(1 + k^2 \lambda_t^2\right)^2} dk = \frac{1}{2\lambda_t^4} r K_0\left(r/\lambda_t\right)$, K_0(x) being the Macdonald function or modified Bessel function of second kind [19].

Using the above result and putting σ_1 from equation (9) one can get from equation (13) as,

$$\varphi_2 = -CrK_0\left(r/\lambda_t\right)\cos\theta \quad (14)$$

This potential is called the *near field wake potential* and $C = \frac{qu}{4\pi\varepsilon_0\sqrt{2\pi}}\sum_{s=e,i,d}\frac{1}{v_{ts}\lambda_s^2}$ is the wake-coefficient.

Let us now consider the third part of potential,

$$\varphi_3 = j\frac{q\sigma_2}{8\pi^3\varepsilon_0}\int\frac{k^3 e^{jkr\cos\eta}}{\left(1+k^2\lambda_t^2\right)^2}\cos(\eta+\theta)\sin\eta d\eta d\tau dk \tag{15}$$

Here, the angular part of the integration is same as the angular part in wake potential. So, by using equation (12) one can rearrange equation (15) in the following way,

$$\varphi_3 = \frac{q\sigma_2\cos\theta}{2\pi^2\varepsilon_0 r^2}\int_{k=0}^{\infty}\frac{k\left(kr\cos kr-\sin kr\right)}{\left(1+k^2\lambda_t^2\right)^2}dk \tag{16}$$

Let us now consider a standard integral [23],

$$\int_{k=0}^{\infty}\frac{k\sin kr}{\left(1+k^2\lambda_t^2\right)^2}dk = \frac{\pi r}{4\lambda_t^3}e^{-r/\lambda_t} \tag{17}$$

$$\therefore \int_{k=0}^{\infty}\frac{k^2\cos kr}{\left(1+k^2\lambda_t^2\right)^2}dk = \frac{\partial}{\partial r}\int_{k=0}^{\infty}\frac{k\sin kr}{\left(1+k^2\lambda_t^2\right)^2}dk = \frac{\pi}{4\lambda_t^3}\left(1-\frac{r}{\lambda_t}\right)e^{-r/\lambda_t} \tag{18}$$

Using the integrals (17) and (18) and the value of σ_2 from equation (9), equation (16) takes the following form,

$$\varphi_3 = -De^{-r/\lambda_t}\cos\theta \tag{19}$$

where, $D = \frac{q}{4\pi\varepsilon_0}\frac{uv_{ed}}{2\lambda_i^2 v_c^2}$. This potential is due to dust perturbation part and will vanish if the moving test charge is static *i.e.* $u = 0$ and/or the electron-dust collision is absent i.e. $v_{ed} = 0$.

III. CALCULATION OF ENERGY LEVELS OF HYDROGENLIKE ION

To estimate the modified non-relativistic energy eigenvalues of slowly moving hydrogen-like ion in the presence of an external classical dusty plasma environment, Rayleigh-Ritz variation calculation has been done (a.u. is used hereafter). The expectation value of kinetic energy is given by,

$$\langle T\rangle = \int\left[\left(\frac{\partial\Psi}{\partial r}\right)^2+\frac{1}{r^2}\left(\frac{\partial\Psi}{\partial\theta}\right)^2+\frac{1}{r^2\sin^2\theta}\left(\frac{\partial\Psi}{\partial\omega}\right)^2\right]d^3\vec{r} \tag{20}$$

Where $d^3\vec{r} = r^2\sin\theta d\theta d\omega dr$ is the volume element in spherical polar (r,θ,ω) co-ordinate ($0\le r\le\infty$, $0\le\theta\le\pi$, $0\le\omega\le 2\pi$). The effective potential energy of the atom can be written as,

$$V_{eff} = -\frac{q}{r}e^{-r/\lambda_t}+CrK_0\left(r/\lambda_t\right)\cos\theta+De^{-r/\lambda_t}\cos\theta \tag{21}$$

Thus the expectation value of potential energy is given by,

$$\langle V \rangle = \int V_{eff} \Psi^2 d^3\vec{r} \tag{22}$$

The normalization term is given by,

$$\langle N \rangle = \int \Psi^2 d^3\vec{r} \tag{23}$$

The trial wavefunction is taken as, $\Psi = R_{nl}(\alpha r) Y_{lm}(\theta,\omega) A(\theta)$, where $R_{nl}(\alpha r)$ is the radial part of hydrogenic wavefunction [24] with 'α' as variation parameter, $Y_{lm}(\theta,\omega)$ is the spherical harmonics [24] and $A(\theta) = (\gamma + \beta\cos\theta)$ is the orbital distortion part [21] with 'γ' and 'β' as variation parameters. For the static ion ($u = 0$), wake and dusty potentials will be absent and in this case we set γ = 1 and β = 0.

Let us now consider the one-electron auxiliary integral for radial part,

$$W_1(p,\rho) = \int_{r=0}^{\infty} r^p e^{-\rho r} dr = \frac{p!}{\rho^{p+1}} \tag{24}$$

and the integral necessary to evaluate the expectation value of wake potential,

$$U_1(p,v,\rho,\xi) = \int_{r=0}^{\infty} r^{p-1} e^{-\rho r} K_v(\xi r) dr$$

$$= \frac{\sqrt{\pi}(2\xi)^v}{(\rho+\xi)^{p+v}} \frac{\Gamma(p+v)\Gamma(p-v)}{\Gamma\left(p+\frac{1}{2}\right)} {}_2F_1\left(p+v, v+\tfrac{1}{2}; p+\tfrac{1}{2}; \frac{\rho-\xi}{\rho+\xi}\right) \tag{25}$$

where, ${}_2F_1(a,b;c;x)$ is the confluent Hypergeometric function and $\mathrm{Re}(p) > |\mathrm{Re}(v)|$ and $\mathrm{Re}(\rho+\xi) > 0$ [23]. The expectation values using (20),(22) and (23) for the $1s_0$, $2s_0$, $2p_0$ and $2p_1$ states are given as follows.

$1s_0$ – state

Using the trial wavefunction as $\Psi(r,\theta,\omega) = e^{-\alpha r} A(\theta)$, the expectation values can be derived as

$$\langle T \rangle = \left(\gamma^2 + \frac{\beta^2}{3}\right)\alpha^2 W_1(2,2\alpha) + \frac{2\beta^2}{3} W_1(0,2\alpha)$$

$$\langle V \rangle = -2q\left(\gamma^2 + \frac{\beta^2}{3}\right) W_1(1,2\alpha+\mu) + \frac{4}{3} C\gamma\beta U_1(4,0,2\alpha,\mu) + \frac{4}{3} D\gamma\beta W_1(2,2\alpha+\mu)$$

$$\langle N \rangle = 2\left(\gamma^2 + \frac{\beta^2}{3}\right) W_1(2,2\alpha)$$

$2s_0$ – state

Using the trial wavefunction as $\Psi(r,\theta,\omega) = (1-\alpha r)e^{-\alpha r} A(\theta)$, the expectation values can be derived as

$$\langle T\rangle = \alpha^2\left(\gamma^2+\frac{\beta^2}{3}\right)\left[4W_1(2,2\alpha)-4\alpha W_1(3,2\alpha)+\alpha^2 W_1(4,2\alpha)\right]+\frac{2\beta^2}{3}\left[W_1(0,2\alpha)-2\alpha W_1(1,2\alpha)+\alpha^2 W_1(2,2\alpha)\right]$$

$$\langle V\rangle = -2q\left(\gamma^2+\frac{\beta^2}{3}\right)\left[W_1(1,2\alpha+\mu)-2\alpha W_1(2,2\alpha+\mu)+\alpha^2 W_1(3,2\alpha+\mu)\right]$$

$$+\frac{4}{3}C\gamma\beta\left[U_1(4,0,2\alpha,\mu)-2\alpha U_1(5,0,2\alpha,\mu)+\alpha^2 U_1(6,0,2\alpha,\mu)\right]$$

$$+\frac{4}{3}D\gamma\beta\left[W_1(2,2\alpha+\mu)-2\alpha W_1(3,2\alpha+\mu)+\alpha^2 W_1(4,2\alpha+\mu)\right]$$

$$\langle N\rangle = 2\left(\gamma^2+\frac{\beta^2}{3}\right)\left[W_1(2,2\alpha)-2\alpha W_1(3,2\alpha)+\alpha^2 W_1(4,2\alpha)\right]$$

$2p_0$ – state

Using the trial wavefunction as, $\Psi(r,\theta,\omega)=re^{-\alpha r}\cos\theta A(\theta)$, the expectation values can be derived as

$$\langle T\rangle = \left(\frac{\gamma^2}{3}+\frac{\beta^2}{5}\right)\left[W_1(2,2\alpha)-2\alpha W_1(3,2\alpha)+\alpha^2 W_1(4,2\alpha)\right]+2\left(\frac{\gamma^2}{3}+\frac{4\beta^2}{15}\right)W_1(2,2\alpha)$$

$$\langle V\rangle = -2q\left(\frac{\gamma^2}{3}+\frac{\beta^2}{5}\right)W_1(3,2\alpha+\mu)+\frac{4}{5}C\gamma\beta U_1(6,0,2\alpha,\mu)+\frac{4}{5}D\gamma\beta W_1(4,2\alpha+\mu)$$

$$\langle N\rangle = 2\left(\frac{\gamma^2}{3}+\frac{\beta^2}{5}\right)W_1(4,2\alpha)$$

$2p_1$ – state

Using the trial wavefunction as, $\Psi(r,\theta,\omega)=-re^{-\alpha r}\sin\theta e^{j\omega}A(\theta)$ the expectation values can be derived as

$$\langle T\rangle = 2\left(\frac{\gamma^2}{3}+\frac{\beta^2}{15}\right)\left[W_1(2,2\alpha)-2\alpha W_1(3,2\alpha)+\alpha^2 W_1(4,2\alpha)\right]+4\left(\frac{\gamma^2}{3}+\frac{\beta^2}{5}\right)W_1(2,2\alpha)$$

$$\langle V\rangle = -4q\left(\frac{\gamma^2}{3}+\frac{\beta^2}{15}\right)W_1(3,2\alpha+\mu)+\frac{8}{15}C\gamma\beta U_1(6,0,2\alpha,\mu)+\frac{8}{15}D\gamma\beta W_1(4,2\alpha+\mu)$$

$$\langle N\rangle = 4\left(\frac{\gamma^2}{3}+\frac{\beta^2}{15}\right)W_1(4,2\alpha)$$

The variational energy eigenvalue is now given as,

$$E=\frac{\langle T\rangle+\langle V\rangle}{\langle N\rangle}=E_{nlm}(\alpha,\beta,\gamma) \tag{26}$$

The parameters (α,β,γ) have been optimized using Nelder-Mead algorithm [25].

IV. RESULTS AND DISCUSSION

The energy values of $1s_0$, $2s_0$, $2p_0$ and $2p_1$ states of C^{5+} ion are given in the table 1 where, the electron densities (n_e) are taken in such a way that the dust radius (r_d) remains smaller than the effective Debye length (λ_t) and different ion velocities are considered for which the thermal Mach number remains below unity. We have chosen typical size of dust radius as $r_d = 0.5\ nm$, charge accumulated on dust grain $q_d = 100q_e$ and mass of dust grains as $m_d = 12000m_H$, where m_H is the mass of hydrogen atom.

In the table 1, the first row corresponding to each state indicates the energy eigenvalue of the free static C^{5+} ion. For a fixed value of ion velocity (u) the energy eigenvalues for all the states decreases as n_e increases. Similar feature can be seen as the ion velocity (u) increases for a fixed electron density n_e. But the amount of decrease of energy in the former case is much greater than the later one. Thus the effect of static screening or Debye-Hückel part *i. e.* first part of the effective potential (21), which is a function of plasma electron density (n_e) and dust parameters, is more pronounced than the effect of the second and the third part of the effective potential (21) namely, wake-part and dusty-part, where the later two parts are dependent on ion velocity u and plasma electron density (n_e).

As shown in the table, for the static case ($u = 0$) due to the effect of Debye-Hückel part in the potential, the l-degeneracy gets removed at each density and as a result the energies of $2s_0$, $2p_0$ and $2p_1$ states become different.

Table 1
The energy eigenvalues $-E$ (a.u.) of $1s_0$, $2s_0$, $2p_0$ and $2p_1$ states of C^{5+} ion moving in dusty plasma estimated with different sets of electron number density (n_e in m^{-3}) and ion velocity (u in ms^{-1})

State	n_e (m^{-3})	u (ms^{-1})	$-E$ (a.u.)	*State*	n_e (m^{-3})	u (ms^{-1})	$-E$ (a.u.)
	-	-	18.0		-	-	4.5
		0	17.98216023			0	4.482196542
		100	17.98216023			100	4.482162312
		500	17.98216022		10^{20}	500	4.482161888
	10^{20}	1000	17.98216020			1000	4.482161358
		5000	17.98216008			5000	4.482157116
I_{s0}		10000	17.98215992	$2p_0$		10000	4.482151815
		0	17.44281241			0	3.957701449
		100	17.44281012			100	3.957652599
	10^{23}	500	17.44280094		10^{23}	500	3.957476414
		1000	17.44278948			1000	3.957276511
		5000	17.44271391			5000	3.955684605
		10000	17.44263049			10000	3.953694721
	-	-	4.5		-	-	4.5
		0	4.482198883			0	4.482196542
		100	4.482175960			100	4.482137215
	10^{20}	500	4.482175932		10^{20}	500	4.482137073
		1000	4.482175898			1000	4.482136897
		5000	4.482175675			5000	4.482135483
$2s_0$		10000	4.482175602	$2p_1$		10000	4.482133716
		0	3.961873870			0	3.957701449
		100	3.961868049			100	3.957656795
		500	3.961844765			500	3.957598066
	10^{23}	1000	3.961815660		10^{23}	1000	3.957524654
		5000	3.961664635			5000	3.956990871
		10000	3.961452745			10000	3.956327567

Because of the *cos* θ term in the near field wake part and the dusty part in the effective potential, the degeneracy of energy eigenvalues with respect to the absolute value of magnetic quantum number (|*m*|) is lifted (corresponding to given *n* and *l*). For example, from the table 1, it can be seen that for ion velocity u = 1000 m/s and plasma electron density $n_e = 10^{23}$ m^{-3} the energy eigenvalues of $2p_0$ and $2p_1$ states are -3.95727651 a.u. and -3.95752465 a.u., which indicates that both the states are no longer degenerate. It is also noteworthy that for $n_e=10^{20}$ m^{-3} the $2p_0$ state energetically lies below $2p_1$, while for $n_e=10^{23}$ m^{-3}, the $2p_0$ state energetically moves above to the $2p_1$ state, giving rise to the level-crossing phenomenon. Thus one may opine that the relative positions of the states corresponding to same *n* and *l*-values and different |*m*| values depend on the plasma density of the dusty plasma environment. Moreover, it can also be argued that two different levels can be made degenerate *i.e.* incidental degeneracy [21] may occur by tuning the plasma parameters.

If the dust charge perturbation term is removed from the effective potential (by setting $v_{ed}= 0$), the energy of $1s_0$ state for $n_e = 10^{23}\ m^{-3}$ and $u = 1000\ ms^{-1}$, becomes -17.44377726 a.u., whereas with dust potential under the same plasma conditions and ion velocity, the energy of $1s_0$ state becomes -17.44278948 a.u. (as shown in table 1). Thus in the presence of dust potential part, the energy of $1s_0$ state becomes more positive by an amount of 9.8778×10^{-4} a.u.

V. CONCLUSION

The electrostatic potential for a moving ion under classical dusty plasma is derived where the thermal Mach number remains less than unity and dust grain radius is smaller than the effective screening length of the plasma. Subsequently, the effect of such potential on the change of the energy eigenvalues of different states of hydrogen-like carbon ion is studied under the framework of Rayleigh-Ritz variational method. The removal of accidental (*l*) degeneracy and absolute magnetic quantum number (|*m*|) degeneracy are reported in case of an ion moving in the dusty plasma environment. Level-crossing phenomenon has been observed between $2p_0$ and $2p_1$ states with the variation of plasma electron density. The present form of the potential may be useful for calculating spectral properties of other ions within dusty plasma surrounding. The energy eigenvalues reported here may serve as benchmark for future theoretical research and also for experimental measurements under such plasma environment.

Acknowledgements

S.B. acknowledges the financial support under grant number PSW-160/14-15(ERO) from University Grants Commission, Govt. of India. T.K.M. is grateful to the Department of Atomic Energy, BRNS, Government of India for financial support under Grant No. 37(3)/14/27/ 2014-BRNS.

References

[1] C. K. Goertz, Rev. Geophys. **27** (1989) 271.

[2] I. L. Spitzer, *Physical Processes in the Intersteller Medium*, Wiley, New York (1978).

[3] P. K. Shukla, A. A. Mamun, *Introduction to Dusty Plasma Physics,* IOP Publishing, Bristol (2002).

[4] J. H. Chu, Lin. I, Phys. Rev. Lett. **72** (1994) 4009.

[5] H. C. Lee, D. Y. Chen, B. Rosenstein, Phys. Rev. E. **56** (1997) 4596.

[6] S. A. Khrapak, A. G. Khrapak, A. V. Ivlev, H. M. Thomas, Phys. Plas. **21** (2004) 123705.

[7] G. C. Das, R. Deka, M. P. Bora, Phys. Plas. **23**, (2016) 042308.

[8] I. Denysenko, M. Y. Yu, K. Ostrikov, N. A. Azarenkov, L. Stenflo, Phys. Plas. **11** (2004) 4959.

[9] I. H. Hutchinson, Phys. Plas. **18** (2011) 032111.

[10] S. A. Khrapak, Phys. Plas. **20** (2013) 013703.

[11] G. Lapenta, Phys. Plas. **6** (1999) 1442.

[12] K. Avinash, A. Bhattacharjee, R. Merlino, Phys. Plas. **10** (2003) 2663.

[13] I. L. Semenov, A. G. Zagorodny, I. V. Krivtsun, Phys. Plas. **20** (2013) 013701.

[14] H. Hu, F. Li, Phys. Plas. **20** (2013) 023701.

[15] P. K. Shukla, Phys. Plas. **1** (1994) 1362.

[16] P. K. Shukla, L. Stenflo, Plas. Phys. Rep. **27** (2001) 904.

[17] W. M. Moslem, R. Sabry, P. K. Shukla, J. Plas. Phys. **77** (2011) 663.

[18] S. Ali, S. Khan, Phys. Plas. **20** (2013) 072106.

[19] M. Abramowitz, I. A. Stegun, *Handbook of Mathematical Functions*, Dover, New York (1972).

[20] E. M. Lifshitz, L. P. Pitaevskii, *Physical Kinetics*, Butterworth-Heinemann, UK (1981).

[21] S. Dutta, Jayanta K. Saha, T. K. Mukherjee, Phys. Plas. **22** (2015) 062103.

[22] P. Debye, E. Hückel, Z. Phys. **24** (1923) 185.

[23] L. S. Gradshteyn, I. M. Ryzhik, *Table of Integrals, Series and Products*, 7th ed. Academic, NewYork (1994).

[24] B. H. Bransden, C. J. Joachain, *Physics of Atoms and Molecules*, 2nd ed. Pearson Education, Delhi (2004).

[25] J. A. Nelder, R. Mead, Comput. J. **7** (1965) 308.

Received: 2 September 2017 | Revised: 29 November 2017 | Accepted: 11 December 2017

DOI: 10.1002/qua.25577

FULL PAPER

WILEY International Journal of QUANTUM CHEMISTRY

Ritz variational method for the high-lying nonautoionizing doubly excited $^{1,3}F^e$ states of two-electron atoms

Sayantan Dutta[1] | Amar N. Sil[2] | Jayanta K. Saha[3] | Tapan K. Mukherjee[4]

[1]Belgharia Texmaco Estate School, Belgharia, Kolkata 700056, India

[2]Department of Physics, Jogamaya Devi College, Kolkata 700026, India

[3]Department of Physics, Aliah University, IIA/27, Newtown, Kolkata 700156, India

[4]Department of Physics, Narula Institute of Technology, Agarpara, Kolkata 700109, India

Correspondence
Jayanta K. Saha, Department of Physics, Aliah University, IIA/27, Newtown, Kolkata 700156, India.
Emails: jsaha84@gmail.com, jksaha.phys@aliah.ac.in

Funding information
Department of Atomic Energy, BRNS, Govt. of India, Grant/Award Number: 37(3)/14/27/2014-BRNS

Abstract

Energy eigenvalues of nonautoionizing doubly excited $^{1,3}F^e$ states originating from 2pnf ($n=4-20$) configuration of two-electron atoms $Z=3-18$ have been calculated by expanding the basis set in explicitly correlated Hylleraas coordinates under the framework of Ritz variational method. A detailed discussion on the evaluation of correlated basis integrals is given. The energy eigenvalues of a number of these doubly excited states are being reported for the first time especially for the high lying states. The effective quantum numbers (n^*) for the states mentioned above have been calculated by using the theory of quantum defect.

KEYWORDS

doubly excited states, Hylleraas coordinates, two-electron atoms, variational method

1 | INTRODUCTION

In a two-electron atoms/ions, the states where both the electrons are promoted to excited orbitals are termed as doubly excited states (DESs). These states are embedded in the one-electron continuum and thus are less bound compared to the singly excited states where one electron is in the 1s orbital and the other one is in arbitrary excited orbital. The DESs of two-electron atoms have become a subject of immense interest immediate after the pioneering observation of two-electron-one-photon peak by Madden and Codling[1] while recording photo-absorption spectra of helium atom placed in the field of synchrotron radiation. Bulk of theoretical studies[2–4] using different quantum chemical methods are employed afterwards to investigate the structural features of such states. Accurate determination of the structural properties of the DESs of different two-electron atoms are, therefore, necessary for astrophysical data analysis,[5] diagnosis of lines observed in solar corona,[6] high temperature discharges[7] as well as in laboratory plasma diagnostics.[8]

Depending on the angular momentum coupling scheme and parity conservation rules, these DES can be classified into two general groups as autoionizing and nonautoionizing.[9] There are two different channels of decay of those states namely radiative channel where the DES decays to a lower excited state by emitting a photon, while in the autoionization channel the DES decays to an ion by ejecting the other electron. The radiative channel is predominant for the nonautoionizing states. Electron-electron correlation plays an important role in forming these kinds of states and thus Ritz variational method with the trial wave function expanded in explicitly correlated Hylleraas type basis is proven to be the best procedure for theoretical estimation of energy levels and other structural properties of such states. Although, there exists a large number of investigations in the literature related to structural and spectral features of DESs having low total angular momentum (upto $L=2$),[10–23] but the same for other high angular momentum states are rather scanty.[14,24–29] For a two-electron atom, the lowest lying doubly excited nonautoionizing F state ($L=3$) of even parity originates from 2p4f configuration. Another important aspect of this state is that it is an unnatural parity bound state, that is, it's parity is determined by $\pi=(-1)^{L+1}$ instead of using the formula $\pi=(-1)^L$. The work done particularly on these states so far is very much countable. To be specific, Lipsky and collaborators[24] adopted truncated diagonalization method with CI-type basis for few ($^{1,3}F^e$) states of two-electron atoms ($Z=2-5$). Callaway[25] estimated the first three states of helium having 2pnf ($^{1,3}F^e$) configuration using CI-type wavefunction in the framework of Stabilization method based on hard wall strategy. Kar and Ho[27] also used large number of configurations in their CI-type basis for first three states

of 2pnf configuration of helium atom. The energy eigenvalues of 2pnf ($n=4-9$) $^{1,3}F^e$ states of helium have been reported by Kar and Ho[28] using exponentially correlated CI-type basis set. In a separate article, Kar et al.[29] used similar type of wavefunction and extended the calculations for the energy levels of other iso-electronic ions ($Z=3-12$).

In this communication, we have made an attempt to estimate the energy eigenvalues of 2pnf $^{1,3}F^e$ states ($n=4-20$) of two-electron systems ($Z=3-18$) using trial wave function expanded in multiexponent Hylleraas type basis set. We have already used such type of wavefunction to determine the structural parameters of different S, P, and D states of free and confined two-electron systems.[2,30–41] It is worthwhile to mention that using Hylleraas basis the energy values of 2pnf $^{1,3}F^e$ states $[n=8-20]$ of two electron atoms with $Z>10$ are being reported for the first time. The effective quantum number (n^*) of the outer electron for each of these states has also been calculated using the theory of quantum defect.

2 | METHOD

2.1 | Wavefunction

The coupled angular wavefunction for $^{1,3}F^e$ state having total angular momentum $L=3$ and magnetic quantum number $M=0$ in terms of the individual angular wavefunctions for *pf* (having angular momentum quantum numbers $l_1=3$ and $l_2=1$) configuration can be written as,

$$Y_{L;M}^{l_1,l_2}=Y_{3;0}^{3,1}=\frac{1}{\sqrt{2}}\left[y_3^1(1)y_1^{-1}(2)-y_3^{-1}(1)y_1^1(2)\right] \tag{1}$$

where, Y and y represents the spherical harmonics for the coupled and uncoupled states, respectively. Using the standard expressions for spherical harmonics for the uncoupled states (y) in terms of individual angular coordinates (θ_1,ϕ_1) and (θ_2,ϕ_2), Equation 1 dissolves as,

$$Y_{3;0}^{3,1}=\frac{3i}{\pi}\sqrt{\frac{21}{768}}(5\cos^2\theta_1-1)\sin\theta_1\sin\theta_2\sin(\phi_2-\phi_1) \tag{2}$$

With the symmetric Euler-angle (θ,ϕ,ψ) decomposition technique,[42] following two transformation relations originate:

$$\sin\theta_1\sin\theta_2\sin(\phi_2-\phi_1)=\sin\theta_{12}\cos\theta \tag{3}$$

$$\cos\theta_1=-\sin\theta\cos\left(\psi-\frac{1}{2}\theta_{12}\right) \tag{4}$$

Here, θ_{12} is the angle between $\vec{r_1}$ and $\vec{r_2}$. Using these two transformation relations (3) and (4) and discarding the multiplicative coefficient $\frac{3i}{\pi}\sqrt{\frac{21}{768}}$ Equation 2 takes the form,

$$\begin{aligned}Y_{3;0}^{3,1}&=\sin\theta_{12}\left(\frac{3\cos\theta-5\cos^3\theta}{2}\right)+\frac{5}{2}\sin^2\theta\cos\theta\cos2\psi\sin\theta_{12}\cos\theta_{12}+\frac{5}{2}\sin^2\theta\cos\theta\sin2\psi\sin^2\theta_{12}\\&=-\sin\theta_{12}D_3^0+\frac{\sqrt{15}}{6}\sin2\theta_{12}D_3^{2+}+\frac{\sqrt{15}}{6}(1-\cos2\theta_{12})D_3^{2-}\end{aligned} \tag{5}$$

where D_3^0, D_3^{2+}, and D_3^{2-} are the real angular momentum Wigner functions which depend on the Eulerian angles (θ,ϕ,ψ) and assume the following forms,[42]

$$D_3^0=\frac{5\cos^3\theta-3\cos\theta}{2}$$

$$D_3^{2+}=\frac{\sqrt{15}}{2}\cos2\psi\sin^2\theta\cos\theta$$

$$D_3^{2-}=\frac{\sqrt{15}}{2}\sin2\psi\sin^2\theta\cos\theta$$

The total wavefunction of the system of two electrons can be written as,

$$\Psi=f(r_1,r_2,r_{12})Y_{3;0}^{3,1}(\theta_1,\phi_1;\theta_2,\phi_2)\pm\text{exchange} \tag{6}$$

where, $f(r_1,r_2,r_{12})$ is the radial part of the wavefunction which explicitly depends on the inter-electronic distance r_{12}. Following the work of Bhatia and Temkin,[42] one may take the $^{1,3}F^e$ state wave function of even parity due to (*pf*) configuration of a two electron atom as,

$$\Psi=f_3^0D_3^0+f_3^{2+}D_3^{2+}+f_3^{2-}D_3^{2-} \tag{7}$$

Using the value of $Y_{3;0}^{3,1}$ into the Equation 6 and then comparing with Equation 7 one can get,

$f_3^0=-(f\mp\tilde{f})\sin\theta_{12}$, $f_3^{2+}=\frac{\sqrt{15}}{6}(f\mp\tilde{f})\sin2\theta_{12}$, and $f_3^{2-}=\frac{\sqrt{15}}{6}(f\pm\tilde{f})(1-\cos2\theta_{12})$. The upper sign corresponds to the singlet state and the lower sign to the triplet state. The symbols used here are the same as in Ref. 43. The singlet and triplet states are ensured by using following exchange properties on angular and radial wavefunctions,

$$\hat{\varepsilon}_{12} D_L^{k\pm}(\theta,\phi,\psi) = \pm(-1)^{L+k} D_L^{k\pm}(\theta,\phi,\psi) \tag{8}$$

and

$$\begin{aligned} f_L^{k+}(r_2,r_1,r_{12}) &= \pm(-1)^{L+k} f_L^{k+}(r_1,r_2,r_{12}) \\ f_L^{k-}(r_2,r_1,r_{12}) &= \pm(-1)^{L+k+1} f_L^{k-}(r_1,r_2,r_{12}) \end{aligned} \tag{9}$$

where $\hat{\varepsilon}_{12}$ is the two-electron permutation operator. The trial radial wave function $f(r_1, r_2, r_{12})$ can be written as,

$$f(r_1,r_2,r_{12}) = \left[\sum_{i=1}^{p} \eta_i(1)\eta_i(2) + \sum_{i=1}^{p}\sum_{j=1}^{p} \eta_i(1)\eta_j(2)\right] g(1,2) \tag{10}$$

In the second sum $i<j$ and $\eta_i(j)=e^{-\rho_i r_j}$, ρ being the nonlinear parameter. p denotes the number of nonlinear parameters which are taken in a geometrical sequence following $\rho_i=\rho_{i-1}\gamma$; γ being the geometrical sequence. The function $g(1, 2)$ containing correlation terms, is expanded into Hylleraas basis set as follows,

$$g(1,2) = r_1^3 r_2 \sum_{l\geq 0}\sum_{m\geq 0}\sum_{n\geq 0} C_{lmn} r_1^l r_2^m r_{12}^n \tag{11}$$

The effect of the radial correlation is incorporated through different ρ's in the wave function whereas, the angular correlation effect is taken care of through different powers of r_{12}. The dimension of the full multiexponent basis (N) is $\left[\frac{p(p+1)}{2}\times s\right]$, where s is the number of terms involving r_{12} and p is the number of exponents. For a fixed number of basis, p and s should be chosen in such a manner that the effect of radial as well as angular correlation is properly incorporated in the wavefunction. In the present calculation, we have taken $p = 9$, that is, a 9-exponent basis set and considering $s = 10, 15, 20$, the expansion length of the wavefunction becomes $N = 450, 675, 900$ terms, respectively. The aim of the choice of the basis set is to span the entire radial space adequately so that the desirable accuracy of the energy levels can be achieved even for very high excited states. Specifically, the higher ρ values are responsible for spanning the space near to the nucleus whereas the lower one spans the space far away from the nucleus. Thus spatial range of the basis can be tuned in a flexible manner by changing the geometrical ratio γ keeping ρ_1 constant throughout. To have a preliminary idea about the highest and lowest nonlinear parameters in the set of p number of nonlinear parameter, we optimize the energy eigen value of the corresponding angular momentum state with two nonlinear parameters using Nelder–Mead procedure.[44]

2.2 | Variational equation

The reduced variational equation for the even parity F state is obtained from the general variational equation of arbitrary angular momentum of a two electron system[43] as,

$$\begin{aligned} &\delta\int\Bigg(\frac{1}{2}\left[\sum_{i=1}^{2}\left(\frac{\partial f_3^0}{\partial r_i}\right)^2+\left(\frac{\partial f_3^{2+}}{\partial r_i}\right)^2+\left(\frac{\partial f_3^{2-}}{\partial r_i}\right)^2\right]+\frac{1}{2}\left(\frac{1}{r_1^2}+\frac{1}{r_2^2}\right)\left[\left(\frac{\partial f_3^0}{\partial \theta_{12}}\right)^2+\left(\frac{\partial f_3^{2+}}{\partial \theta_{12}}\right)^2+\left(\frac{\partial f_3^{2-}}{\partial \theta_{12}}\right)^2\right] \\ &+\frac{1}{2}\left(\frac{1}{r_1^2}+\frac{1}{r_2^2}\right)\left[(f_3^{2+})^2+(f_3^{2-})^2\right]+\left(\frac{1}{r_2^2}-\frac{1}{r_1^2}\right)\left[f_3^{2-}\frac{\partial f_3^{2+}}{\partial \theta_{12}}-f_3^{2+}\frac{\partial f_3^{2-}}{\partial \theta_{12}}\right] \\ &+\frac{1}{\sin^2\theta_{12}}\left(\frac{1}{r_1^2}+\frac{1}{r_2^2}\right)\left[3(f_3^0)^2+2(f_3^{2+})^2+2(f_3^{2-})^2\right]+\frac{\sqrt{15}\cos\theta_{12}}{\sin^2\theta_{12}}\left(\frac{1}{r_1^2}+\frac{1}{r_2^2}\right)f_3^0 f_3^{2+} \\ &+\frac{\sqrt{15}}{\sin\theta_{12}}\left(\frac{1}{r_2^2}-\frac{1}{r_1^2}\right)f_3^0 f_3^{2-}+2(V-E)\left[(f_3^0)^2+(f_3^{2+})^2+(f_3^{2-})^2\right]\Bigg)d\tau=0 \end{aligned} \tag{12}$$

where, $d\tau = r_1^2\ r_2^2\ \sin\theta_{12}\ dr_1\ dr_2\ d\theta_{12}$; $0 \leq r_1 \leq \infty$, $0 \leq r_2 \leq \infty$; and $0 \leq \theta_{12} \leq \pi$. The potential energy function of two electron atom is expressed as

$$V = -\frac{Z}{r_1} - \frac{Z}{r_2} + \frac{1}{r_{12}} \tag{13}$$

where Z is the atomic number.

After choosing the proper trial radial wave function, the energy eigenvalues are obtained by solving the generalized eigenvalue equation involving the Hamiltonian and overlap matrices given by

$$\underline{\underline{H}}\ \underline{C} = E\underline{\underline{S}}\ \underline{C} \tag{14}$$

where $\underline{\underline{H}}$ and $\underline{\underline{S}}$ are Hamiltonian and overlap matrices, respectively. Atomic units are used throughout. All calculations are carried out in quadruple precision to have a better numerical accuracy.

2.3 | Evaluation of basis integral

The following result[45] is used in our calculations in performing the integrals involving independent coordinates r_1, r_2 and r_{12}.

$$\begin{aligned}A(m,n,l;a_1,a_2)&=\int_{r_1=0}^{\infty}\int_{r_2=0}^{\infty}\int_{|r_1-r_2|}^{r_1+r_2} r_1^m r_2^n r_{12}^l e^{-a_1r_1-a_2r_2}dr_1dr_2dr_{12}\\&=2(m!n!l!)\sum_{i=0}^{m}\sum_{j=0}^{n}\sum_{k=0}^{l}\frac{(i+j)!(m-i+k)!(n-j+l-k)!}{i!j!k!(m-i)!(l-k)!(n-j)!}\\&\times\frac{1}{(a_1+a_2)^{i+j+1}a_1^{m+1-i+k}a_2^{n+l+1-j-k}}\end{aligned}\tag{15}$$

Here, $m \geq 0$, $n \geq 0$, $l \geq 0$, and $a_1, a_2 > 0$.

We have also used the following formula for r_1^{-1} with even and odd powers of r_{12}.

$$\begin{aligned}A(-1,n,l;a_1,a_2)&=\int_0^{\infty} r_1^{-1}e^{-a_1r_1}dr_1\int_0^{\infty} r_2^m e^{-a_2r_2}dr_2\int_{|r_1-r_2|}^{r_1+r_2} r_{12}^l dr_{12}\\&=\int_0^{\infty} r_1^{-1}e^{-a_1r_1}dr_1\int_0^{r_1} r_2^m e^{-a_2r_2}dr_2\int_{r_1-r_2}^{r_1+r_2} r_{12}^l dr_{12}\\&+\int_0^{\infty} r_2^m e^{-a_2r_2}dr_2\int_0^{r_2} {r_1}^{-1}e^{-a_1r_1}dr_1\int_{r_2-r_1}^{r_1+r_2} r_{12}^l dr_{12}\\&=I_1+I_2\end{aligned}\tag{16}$$

where,

$$\begin{aligned}I_2&=\int_0^{\infty} r_2^m e^{-a_2r_2}dr_2\int_0^{r_2} {r_1}^{-1}e^{-a_1r_1}dr_1\int_{r_2-r_1}^{r_1+r_2} r_{12}^l dr_{12}\\&=\frac{1}{(l+1)}\int_0^{\infty} r_2^m e^{-a_2r_2}dr_2\int_0^{r_2} {r_1}^{-1}e^{-a_1r_1}dr_1\left[(r_1+r_2)^{l+1}-(r_2-r_1)^{l+1}\right]\end{aligned}\tag{17}$$

Considering $l+1=n$ and using standard Binomial expansion one can get

$$\begin{aligned}(r_1+r_2)^n-(r_2-r_1)^n&=2\sum_{i=0}^{\frac{n-1}{2}}\frac{n!}{(n-2i-1)!(2i+1)!}r_2^{n-2i-1}r_1^{2i+1}(n=odd)\\&=2\sum_{i=0}^{\frac{n-2}{2}}\frac{n!}{(n-2i-1)!(2i+1)!}r_2^{n-2i-1}r_1^{2i+1}(n=even)\end{aligned}\tag{18}$$

When l is even, that is, n is odd, Equation 17 reduces to

$$I_2=\frac{2}{n}\sum_{i=0}^{\frac{n-1}{2}}\frac{n!}{(n-2i-1)!(2i+1)!}\int_0^{\infty} r_2^{m+n-2i-1}e^{-a_2r_2}dr_2\int_0^{r_2} {r_1}^{2i}e^{-a_1r_1}dr_1\tag{19}$$

Let us now use the following standard integral[46]

$$\int_0^R r^n e^{-\mu r}dr=\frac{n!}{\mu^{n+1}}-e^{-\mu R}\sum_{k=0}^{n}\frac{n!}{k!}\frac{R^k}{\mu^{n-k+1}}$$

Equation 19 now dissolves as,

$$\begin{aligned}I_2&=\frac{2}{n}\sum_{i=0}^{\frac{n-1}{2}}\frac{n!(m+n-2i-1)!}{(2i+1)(n-2i-1)!}\frac{1}{a_1^{2i+1}a_2^{m+n-2i}}\\&-\frac{2}{n}\sum_{i=0}^{\frac{n-1}{2}}\sum_{j=0}^{2i}\frac{n!(m+n-j-1)!}{(2i+1)(n-2i-1)!(2i-j)!}\frac{1}{a_1^{j+1}(a_1+a_2)^{m+n-j}}\end{aligned}\tag{20}$$

When l is odd, that is, n is even, the limits of the outer sum of Equation 20 will be $i = 0$ to $\frac{n-2}{2}$, otherwise the expression for integral I_2 will be the same as in Equation 20. In a similar fashion, I_1 integral for even l reduces to

$$
\begin{aligned}
I_1 &= \frac{2}{n}\frac{(m+n)!}{a_2^{m+n+1}}\ln\left(\frac{a_1+a_2}{a_1}\right) \\
&+ \frac{2}{n}\sum_{i=0,n>1}^{\frac{n-1}{2}-1}\frac{n!(m+2i+1)!}{(n-2i-1)(2i+1)!}\frac{1}{a_1^{n-2i-1}a_2^{m+2i+2}} \\
&- \frac{2}{n}\sum_{i=0}^{\frac{n-1}{2}-1}\sum_{j=0}^{m+2i+1}\frac{(m+2i+1)!n!(m+n-j-1)!}{(m+2i+1-j)!(2i+1)!(n-2i-1)!}\frac{1}{(a_1+a_2)^{m+n-j}a_2^{j+1}} \\
&- \frac{2}{n}\sum_{j=0}^{m+n-1}\frac{(m+n)!}{(m+n-j)}\frac{1}{(a_1+a_2)^{m+n-j}a_2^{j+1}}
\end{aligned}
\tag{21}
$$

and when l is odd,

$$
\begin{aligned}
I_1 &= \frac{2}{n}\sum_{i=0}^{\frac{n-2}{2}}\frac{n!(m+2i+1)!}{(2i+1)!(n-2i-1)}\frac{1}{a_1^{n-2i-1}a_2^{m+2i+2}} \\
&- \frac{2}{n}\sum_{i=0}^{\frac{n-2}{2}}\sum_{j=0}^{m+2i+1}\frac{n!(m+2i+1)!(m+n-j-1)!}{(2i+1)!(n-2i-1)!(m+2i+1-j)!}\frac{1}{a_2^{j+1}(a_1+a_2)^{m+n-j}}
\end{aligned}
\tag{22}
$$

3 | RESULTS AND DISCUSSIONS

The numerical values of the integral $A(a,b,c;\alpha,\beta)$ estimated using the formulae (16), (20), (21), and (22) corresponding to the different sets of $(-1,b,c)$ with the conditions $b \geq 0, c \geq 0$ are displayed in Table 1. In the first three columns of Table 1, different powers of r_1, r_2, and r_{12}, that is, a, b, and c are given. For each set of (a,b,c), the nonlinear parameters (α, β) in the preceding column of Table 1 are varied from very low to high values. It is to be noted that for each set, we have considered both the conditions $\alpha>\beta$ and $\beta>\alpha$ as well as $b>c$ and $c>b$ into account. The values of integrals are given in the last column of Table 1. It is worthwhile to mention that the results match exactly with those obtained from the standard symbolic computation software *Maple*, which ensure the numerical accuracy of the expression for $A(-1,b,c;\alpha,\beta)$ over the complete range of nonlinear parameters.

Table 2 shows the convergence behavior of the energy eigenvalues of 2pnf [n=4−20] $^{1,3}F^e$ states of Li^+ with respect to the total number of terms $N = 450$, 675, and 900 in the 9-exponent basis set. To determine the limiting values of the 9-exponents, that is, the highest and lowest ρ of the geometrical sequence, we have used a double exponent basis and optimized the energy eigenvalues of 2pnf [n=4−20] $^{1,3}F^e$ states using Nelder–Mead algorithm[44] upto $N \leq 57$. For Li^+ we have obtained three sets of limiting values of the nonlinear parameters as (0.25,1.5), (0.1,1.5), and (0.05,1.5). The first set is optimized for 2p4f state and the third one is for 2p20f state. In the 9-exponent basis set, the intermediate ρ values are generated in a geometrical progression as described in the methodology. The lower boundness of the states 2pnf [n=4−20] depends on the sets of nonlinear parameters. In Table 2, (0.25,1.5) set gives 2pnf [n=4−6], (0.1,1.5) set gives 2pnf [n=7−14], and (0.05,1.5) set gives 2pnf [n=15−20] states as lower bounds. From Table 2 one can find that the energy eigenvalues of 2p4f to 2p7f are converged upto eighth decimal place, 2p8f to 2p12f are converged upto 6th decimal place, 2p13f and 2p14f are converged upto fifth decimal place, and the rest of the configurations are converged upto fourth or third decimal place. It is evident that if the number of terms N in the basis set is further increased then the convergence behavior will be better. But the accuracy provided by the experiments in spectroscopic measurements, such as measurement of transition energies, is maximum of the order of *meV*. For this reason we have limited our study of convergence upto $N = 900$ terms to complete our whole study without so much time consumption but with reasonable accuracy. Similar features are seen for the other ions (Z=4−18) also.

The energy eigenvalues of 2pnf [n=4−20] $^{1,3}F^e$ state of Be^{2+} to Ar^{16+} ions for $N = 900$ are given in the Table 3. We have compared our results with those reported by Kar et al.[29] for 2pnf [n=4−7] $^{1,3}F^e$ state of Li^+ to Mg^{10+} ions. The comparison shows that their[29] results are more bound at the sixth decimal place for the singlet states and the fifth decimal place for the triplet states. In contrast, the present energy values are lower bound than that of the values obtained by Lipsky et al.[24] for the ions Z=2−5. For example, Lipsky et al.[24] obtained the energy value of 2p4f ($^1F^e$) state as −1.252331 a.u., whereas the present energy value of that state is −1.252511 a.u., which is more negative at the forth decimal place of the former result. It is worthwhile to mention here that, the general wavefunction for F^e state is of the form,

$$\Psi_F = \psi_{pf} + \varphi_{dd} \tag{23}$$

where, ψ_{pf} and φ_{dd} are the wavefunctions corresponding to *pf* and *dd* configurations. The reason of our upper bound-ness of the energies in comparison to that of obtained by Kar et al.,[29] lies in the fact that in our basis set expansion, we did not incorporated the terms containing 3d4d and it is higher orbital configuration for singlet state and $3d^2$ and it is higher orbital configuration for triplet state. Since $3d^2$

TABLE 1 Values of the integral $A(-1, b, c; \alpha, \beta)$ with $b \geq 0$, $c \geq 0$

a	B	c	α	β	$A(-1, b, c; \alpha, \beta)$
−1	3	1	0.001	0.0007	0.28559528767775331707[+21]
			1.0	0.05	0.15360000000000000000[+09]
			20.0	5.5	0.47686757610943117397[−03]
			3.5	17.0	0.96589203802113271165[−05]
			100.0	350.0	0.91390492056881061462[−13]
−1	5	4	0.001	0.0007	0.26402051936417828650[+41]
			1.0	0.05	0.74328146657279995997[+19]
			20.0	5.5	0.14386689860441544219[−02]
			3.5	17.0	0.30459951447336372127[−06]
			100.0	350.0	0.49414345416949721222[−21]
−1	8	3	0.001	0.0007	0.58191730025066474307[+49]
			1.0	0.05	0.32701328916480000000[+24]
			20.0	5.5	0.52167519715284150325[−02]
			3.5	17.0	0.55942949732896543776[−07]
			100.0	350.0	0.28886756507090846543[−24]
−1	6	10	0.001	0.0007	0.19197770405852866241[+71]
			1.0	0.05	0.54864986187432244132[+36]
			20.0	5.5	0.54776907438776790329[+00]
			3.5	17.0	0.36023828054357135428[−05]
			100.0	350.0	0.57274425067467716692[−30]
−1	7	7	0.001	0.0007	0.38172873195468099110[+62]
			1.0	0.05	0.57144154565308317696[+31]
			20.0	5.5	0.68786695213944311113[−01]
			3.5	17.0	0.19282009528632468693[−06]
			100.0	350.0	0.43369363418665017720[−28]
−1	4	4	0.001	0.0007	0.20696368991201417656[+37]
			1.0	0.05	0.41295053537279907736[+17]
			20.0	5.5	0.88024390534495116558[−03]
			3.5	17.0	0.72936362878251620218[−06]
			100.0	350.0	0.22573006227254058873[−19]

The notation $x[y]$ stands for $x \times 10^y$.

configuration lies energetically below than that of 3d4d configuration, convergence behavior of the present energy eigenvalues for the singlet states are better than the triplet states in comparison to the values obtained by Kar et al.[29] To the best of our knowledge, there are no other results for the nonautoionizing $^{1,3}F^e$ state energies of two-electron ions from Al^{11+} to Ar^{16+} in the literature for a comparison with our results. Also for the first time, we have estimated the energies of the 2pnf [n=8−20] configurations of $^{1,3}F^e$ state for Li^+ to Ar^{16+} ions. The effective quantum numbers n^* of 2pnf [n=4−20] $^{1,3}F^e$ states for Z=3−18 have also been calculated by using the relation

$$E = -\frac{1}{2}\left[\left(\frac{Z}{N}\right)^2 + \left(\frac{Z-1}{n^*}\right)^2\right] \tag{24}$$

where, E is the energy of the state below total ionization and N is the inner electron quantum number.

TABLE 2 Energy eigenvalues (– E in a.u.) of 2pnf [n=4−20] $^{1,3}F^e$ states of Li^+ ion for different number of terms N in the basis set

State	Singlet N	– E	State	Triplet N	– E
2p4f	450	1.2525115270	2p4f	450	1.2524200395
	675	1.2525115295		675	1.2524200469
	900	1.2525115302		900	1.2524200510
		1.252515231764[a]			1.252450638234[a]
2p5f	450	1.2062924486	2p5f	450	1.2062275184
	675	1.2062924503		675	1.2062275237
	900	1.2062924507		900	1.2062275269
		1.20629449566[a]			1.206251595683[a]
2p6f	450	1.1813051756	2p6f	450	1.1812625589
	675	1.1813051766		675	1.1812625626
	900	1.1813051769		900	1.1812625648
		1.181306379[a]			1.1812794195[a]
2p7f	450	1.1662888800	2p7f	450	1.1662602853
	675	1.1662888817		675	1.1662602879
	900	1.1662888819		900	1.1662602894
		1.1662896[a]			1.1662720[a]
2p8f	450	1.1565611795	2p8f	450	1.1565468468
	675	1.1565665106		675	1.1565468549
	900	1.1565666592		900	1.1565468560
2p9f	450	1.1499036594	2p9f	450	1.1498995194
	675	1.1499040107		675	1.1498995341
	900	1.1499041490		900	1.1498995413
2p10f	450	1.1451513000	2p10f	450	1.1451515933
	675	1.1451516717		675	1.1451516053
	900	1.1451517819		900	1.1451516107
2p11f	450	1.1416507793	2p11f	450	1.1416427056
	675	1.1416508072		675	1.1416427383
	900	1.1416508095		900	1.1416427425
2p12f	450	1.1389823573	2p12f	450	1.1389760839
	675	1.1389827634		675	1.1389764955
	900	1.1389827676		900	1.1389765008
2p13f	450	1.1369050101	2p13f	450	1.1369000251
	675	1.1369081272		675	1.1369031663
	900	1.1369081476		900	1.1369031921
2p14f	450	1.1352498253	2p14f	450	1.1352456879
	675	1.1352631325		675	1.1352591226
	900	1.1352631857		900	1.1352591778
2p15f	450	1.1339035029	2p15f	450	1.1339000066

(Continues)

TABLE 2 (Continued)

State	Singlet N	− E	State	Triplet N	− E
	675	1.1339367518		675	1.1339334791
	900	1.1339369311		900	1.1339336684
2p16f	450	1.1327738003	2p16f	450	1.1327707800
	675	1.1328515228		675	1.1328488095
	900	1.1328520996		900	1.1328493770
2p17f	450	1.1318011954	2p17f	450	1.1317984937
	675	1.1319520646		675	1.1319498125
	900	1.1319533127		900	1.1319511390
2p18f	450	1.1309511106	2p18f	450	1.1309484992
	675	1.1311979116		675	1.1311959750
	900	1.1312008804		900	1.1311990709
2p19f	450	1.1302005884	2p19f	450	1.1301974746
	675	1.1305543930		675	1.1305527634
	900	1.1305634926		900	1.1305584725
2p20f	450	1.1284727319	2p20f	450	1.1284716986
	675	1.1299948987		675	1.1299933567
	900	1.1305628999		900	1.1300384361

[a]Reference [29]

TABLE 3 Nonrelativistic energy eigenvalues − E (a.u.) and effective quantum numbers (n^*) for the 2pnf [n=4−20] $^{1,3}F^e$ states of helium-like (Z=4−18) ions

Ion	State	$-E_{singlet}$ (a.u.)	n^*	$-E_{triplet}$ (a.u.)	n^*
Be^{2+}	2p4f	2.285835	3.967789	2.285581	3.969553
		2.285840435960[a]	3.967751130897[a]	2.285639440599[a]	3.969146875345[a]
	2p5f	2.182357	4.967582	2.182182	4.969967
		2.182359664331[a]	4.967545627247[a]	2.182228822190[a]	4.969328681292[a]
	2p6f	2.126366	5.967482	2.126253	5.970152
		2.1263673969[a]	5.96744929071[a]	2.126285925[a]	5.9693738957[a]
	2p7f	2.092697	6.967443	2.092622	6.970263
		2.0926982[a]	6.96739779[a]	2.0926454[a]	6.9693829[a]
	2p8f	2.070889	7.967404	2.070837	7.970328
	2p9f	2.055960	8.967418	2.055923	8.970384
	2p10f	2.045295	9.967383	2.045268	9.970355
	2p11f	2.037412	10.967327	2.037390	10.970553
	2p12f	2.031421	11.967302	2.031404	11.970541
	2p13f	2.026761	12.967465	2.026748	12.970616
	2p14f	2.023067	13.967243	2.023056	13.970575
	2p15f	2.020087	14.967481	2.020078	14.970835
	2p16f	2.017650	15.967389	2.017643	15.970556

(Continues)

TABLE 3 (Continued)

Ion	State	$-E_{singlet}$ (a.u.)	n^*	$-E_{triplet}$ (a.u.)	n^*
	2p17f	2.015631	16.967305	2.015625	16.970563
	2p18f	2.013939	17.967616	2.013934	17.970839
	2p19f	2.012508	18.967597	2.012503	18.971390
	2p20f	2.011286	19.968077	2.011282	19.971616
B^{3+}	2p4f	3.631775	3.973172	3.631307	3.975008
		3.63178147087[a]	3.97314696448[a]	3.631390336345[a]	3.974681092280[a]
	2p5f	3.448482	4.973017	3.448167	4.975440
		3.44848492847[a]	4.97299437381[a]	3.44823320775[a]	4.97493037865[a]
	2p6f	3.349239	5.972957	3.349037	5.975650
		3.349240870[a]	5.972932525[a]	3.349084879[a]	5.975011116[a]
	2p7f	3.289536	6.972917	3.289402	6.975759
		3.2895368[a]	6.9729005[a]	3.2894359[a]	6.9750395[a]
	2p8f	3.250851	7.972906	3.250759	7.975822
	2p9f	3.224363	8.972896	3.224297	8.975878
	2p10f	3.205425	9.973543	3.205376	9.976583
	2p11f	3.189685	11.120984	3.189641	11.124768
	2p12f	3.178997	12.171951	3.178965	12.175559
	2p13f	3.170688	13.232561	3.170662	13.236328
	2p14f	3.164094	14.305068	3.164070	14.309461
	2p15f	3.158758	15.394183	3.158735	15.399430
	2p16f	3.154394	16.497405	3.154373	16.503302
	2p17f	3.150779	17.616189	3.150760	17.622684
	2p18f	3.147739	18.756824	3.147734	18.758887
	2p19f	3.145161	19.919983	3.145124	19.938287
	2p20f	3.142965	21.102377	3.142716	21.250158
C^{4+}	2p4f	5.290270	3.977107	5.289558	3.978900
		5.29027795753[a]	3.97708682340[a]	5.289661360120[a]	3.978639250204[a]
	2p5f	5.004636	4.976980	5.004162	4.979319
		5.00463919882[a]	4.97696418412[a]	5.00424519430[a]	4.97890824179[a]
	2p6f	4.849907	5.976937	4.849606	5.979510
		4.849908858[a]	5.976921310[a]	4.849665342[a]	5.979002189[a]
	2p7f	4.756793	6.976915	4.756594	6.979620
		4.75679392[a]	6.9769022[a]	4.75663661[a]	6.979040226[a]
	2p8f	4.696445	7.976907	4.696308	7.979690
	2p9f	4.655116	8.976907	4.655019	8.979715
	2p10f	4.625579	9.976920	4.625508	9.979742
	2p11f	4.603741	10.976902	4.603687	10.979760
	2p12f	4.587141	11.976881	4.587099	11.979768
	2p13f	4.574225	12.977167	4.574192	12.980053

(Continues)

TABLE 3 (Continued)

Ion	State	$-E_{singlet}$ (a.u.)	n^*	$-E_{triplet}$ (a.u.)	n^*
	2p14f	4.563980	13.977609	4.563954	13.980450
	2p15f	4.555713	14.978790	4.555691	14.981748
	2p16f	4.548938	15.982028	4.548919	15.985132
	2p17f	4.543310	16.988730	4.543294	16.991869
	2p18f	4.538579	18.000291	4.538565	18.003558
	2p19f	4.534542	19.023099	4.534529	19.026680
	2p20f	4.531002	20.079835	4.530991	20.083399
N^{5+}	2p4f	7.261297	3.980066	7.260319	3.981780
		7.26130514460[a]	3.98005218186[a]	7.26043935330[a]	3.981569320540[a]
	2p5f	6.850806	4.979961	6.850162	4.982172
		6.85080960411[a]	4.97994902415[a]	6.85025899833[a]	4.981839016900[a]
	2p6f	6.628362	5.979929	6.627954	5.982354
		6.628363930[a]	5.979917697[a]	6.628024153[a]	5.9819369788[a]
	2p7f	6.494464	6.979916	6.494196	6.982449
		6.4944651[a]	6.9799055[a]	6.4942457[a]	6.98197886[a]
	2p8f	6.407668	7.979909	6.407483	7.982521
	2p9f	6.348211	8.980044	6.348079	8.982700
	2p10f	6.305718	9.980115	6.305621	9.982795
	2p11f	6.274294	10.980322	6.274221	10.983007
	2p12f	6.250405	11.980607	6.250348	11.983331
	2p13f	6.230878	13.038673	6.230827	13.041814
	2p14f	6.216116	14.055261	6.216075	14.058425
	2p15f	6.204192	15.076329	6.204159	15.079471
	2p16f	6.194429	16.101480	6.194401	16.104728
	2p17f	6.186279	17.138800	6.186257	17.141878
	2p18f	6.179393	18.191342	6.179374	18.194520
	2p19f	6.173492	19.266428	6.173476	19.269607
	2p20f	6.168348	20.377538	6.168335	20.380595
O^{6+}	2p4f	9.544842	3.982365	9.543587	3.983983
		9.54485107280[a]	3.98235280803[a]	9.54371957137[a]	3.983812014932[a]
	2p5f	8.986986	4.982273	8.986164	4.984349
		8.98698988676[a]	4.98226347983[a]	8.98627272866[a]	4.984074551558[a]
	2p6f	8.684600	5.982251	8.684082	5.984515
		8.684602473[a]	5.982239697[a]	8.684160333[a]	5.9841724017[a]
	2p7f	8.502546	6.982246	8.502206	6.984609
		8.50254794[a]	6.98223230[a]	8.5022626[a]	6.98421535[a]
	2p8f	8.384518	7.982239	8.384284	7.984669
	2p9f	8.303666	8.982246	8.303499	8.984717
	2p10f	8.245861	9.982475	8.245738	9.984973

(Continues)

TABLE 3 (Continued)

Ion	State	$-E_{singlet}$ (a.u.)	n^*	$-E_{triplet}$ (a.u.)	n^*
	2p11f	8.203121	10.982612	8.203028	10.985127
	2p12f	8.170624	11.982929	8.170552	11.985458
	2p13f	8.145344	12.983282	8.145287	12.985829
	2p14f	8.125210	13.988255	8.125164	13.990825
	2p15f	8.107893	15.069069	8.107851	15.072002
	2p16f	8.094587	16.094123	8.094553	16.097016
	2p17f	8.083519	17.127359	8.083490	17.130333
	2p18f	8.074224	18.168157	8.074199	18.171217
	2p19f	8.066230	19.233382	8.066213	19.235851
	2p20f	8.059229	20.338356	8.059188	20.345399
F^{7+}	2p4f	12.140900	3.984194	12.139356	3.985721
		12.14090927076[a]	3.98418501875[a]	12.13950016801[a]	3.985578204205[a]
	2p5f	11.413173	4.984113	11.412168	4.986059
		11.41317664739[a]	4.98410609294[a]	11.41228577247[a]	4.985830437001[a]
	2p6f	11.018620	5.984096	11.017988	5.986213
		11.018622523[a]	5.984087511[a]	11.018073607[a]	5.9859262493[a]
	2p7f	10.781034	6.984122	10.780619	6.986332
		10.7810413[a]	6.9840831[a]	10.7806871[a]	6.985969246[a]
	2p8f	10.626979	7.984215	10.626684	7.986562
	2p9f	10.521423	8.984534	10.521219	8.986847
	2p10f	10.445916	9.985718	10.445777	9.987881
	2p11f	10.389938	10.990131	10.389834	10.992289
	2p12f	10.347096	12.003409	10.347009	12.005761
	2p13f	10.313940	13.014067	10.313879	13.016168
	2p14f	10.287695	14.024516	10.287646	14.026629
	2p15f	10.266389	15.044133	10.266342	15.046635
	2p16f	10.248509	16.096286	10.248468	16.098959
	2p17f	10.233047	17.209515	10.232999	17.213339
	2p18f	10.211977	19.181068	10.211908	19.188680
	2p19f	10.186256	22.856023	10.186170	22.872085
	2p20f	10.177034	24.798841	10.176961	24.816255
Ne^{8+}	2p4f	15.049466	3.985684	15.047626	3.987123
		15.04947593532[a]	3.98567656525[a]	15.04778041165[a]	3.987002559633[a]
	2p5f	14.129364	4.985612	14.128172	4.987436
		14.12936788309[a]	4.98560578775[a]	14.12829797405[a]	4.987243469809[a]
	2p6f	13.630421	5.985596	13.629671	5.987583
		13.630422927[a]	5.985590933[a]	13.629763942[a]	5.9873363597[a]
	2p7f	13.329943	6.985595	13.329452	6.987662
		13.32994444[a]	6.98558854[a]	13.3295192[a]	6.98737884[a]

(Continues)

TABLE 3 (Continued)

Ion	State	$-E_{singlet}$ (a.u.)	n^*	$-E_{triplet}$ (a.u.)	n^*
	2p8f	13.135092	7.985630	13.134756	7.987743
	2p9f	13.001597	8.985661	13.001357	8.987812
	2p10f	12.906154	9.985783	12.905978	9.987948
	2p11f	12.835548	10.986268	12.835416	10.988429
	2p12f	12.781773	11.988858	12.781669	11.991071
	2p13f	12.739992	12.990598	12.739911	12.992790
	2p14f	12.706857	13.992406	12.706793	13.994571
	2p15f	12.680121	14.994961	12.680068	14.997167
	2p16f	12.658004	16.010079	12.657957	16.012461
	2p17f	12.639445	17.042215	12.639406	17.044599
	2p18f	12.622479	18.184305	12.622428	18.188092
	2p19f	12.604086	19.725651	12.604043	19.729727
	2p20f	12.592190	20.959726	12.592141	20.965299
Na^{9+}	2p4f	18.270539	3.986919	18.268398	3.988277
		18.27054868630[a]	3.98691334478[a]	18.26856003131[a]	3.988174230763[a]
	2p5f	17.135558	4.986855	17.134175	4.988571
		17.13556233814[a]	4.98684914338[a]	17.13430934555[a]	4.988403784836[a]
	2p6f	16.520001	5.986841	16.519134	5.988703
		16.520002960[a]	5.986837049[a]	16.519231389[a]	5.9884933851[a]
	2p7f	16.149256	6.986839	16.148688	6.988777
		16.14925691[a]	6.98683603[a]	16.14875893[a]	6.98853510[a]
	2p8f	15.908826	7.986843	15.908437	7.988826
	2p9f	15.744092	8.986848	15.743816	8.988852
	2p10f	15.626317	9.986856	15.626114	9.988879
	2p11f	15.539211	10.986875	15.539057	10.988918
	2p12f	15.472528	11.994720	15.472856	11.989063
	2p13f	15.420942	12.998155	15.421353	12.989138
	2p14f	15.379978	14.003405	15.380494	13.989257
	2p15f	15.346841	15.012883	15.347535	14.989455
	2p16f	15.319621	16.028399	15.320534	15.990935
	2p17f	15.296921	17.053775	15.297692	17.015664
	2p18f	15.277685	18.096176	15.278779	18.031692
	2p19f	15.261007	19.173631	15.260964	19.176663
	2p20f	15.246294	20.303240	15.246355	20.298136
Mg^{10+}	2p4f	21.804116	3.987960	21.801669	3.989243
		21.80412595849[a]	3.98795494500[a]	21.80183895368[a]	3.989154246319[a]
	2p5f	20.431755	4.987900	20.430180	4.989517
		20.43175918580[a]	4.98789617386[a]	20.43031995723[a]	4.989372864234[a]
	2p6f	19.687360	5.987890	19.686374	5.989640

(Continues)

TABLE 3 (Continued)

Ion	State	$-E_{singlet}$ (a.u.)	n^*	$-E_{triplet}$ (a.u.)	n^*
		19.687362146[a]	5.987886177[a]	19.686476020[a]	5.9894590800[a]
	2p7f	19.238977	6.987890	19.238332	6.989710
		19.23897839[a]	6.98788616[a]	19.23840642[a]	6.989499690[a]
	2p8f	18.948178	7.987902	18.947737	7.989761
	2p9f	18.748924	8.987912	18.748610	8.989797
	2p10f	18.606463	9.987931	18.606232	9.989834
	2p11f	18.501095	10.987975	18.500921	10.989883
	2p12f	18.420940	11.988576	18.420806	11.990484
	2p13f	18.358596	12.988978	18.358489	12.990916
	2p14f	18.308896	13.994956	18.308811	13.996882
	2p15f	18.267538	15.037822	18.267466	15.039846
	2p16f	18.232922	16.116563	18.232876	16.118155
	2p17f	18.204634	17.194470	18.204563	17.197454
	2p18f	18.181584	18.253195	18.181526	18.256111
	2p19f	18.161895	19.331296	18.161838	19.334700
	2p20f	18.144794	20.441013	18.144739	20.444896
Al^{11+}	2p4f	25.650197	3.988848	25.647442	3.990063
	2p5f	24.017954	4.988793	24.016185	4.990319
	2p6f	23.132498	5.988785	23.131391	5.990436
	2p7f	22.599107	6.988786	22.598384	6.990501
	2p8f	22.253153	7.988813	22.252658	7.990566
	2p9f	22.016098	8.988837	22.015745	8.990618
	2p10f	21.846601	9.988900	21.846342	9.990694
	2p11f	21.721220	10.989122	21.721025	10.990919
	2p12f	21.625579	11.993058	21.625427	11.994879
	2p13f	21.551393	12.994549	21.551273	12.996378
	2p14f	21.492519	13.996722	21.492424	13.998532
	2p15f	21.445031	14.999273	21.444953	15.001102
	2p16f	21.406172	16.002219	21.406106	16.004098
	2p17f	21.373949	17.006348	21.373892	17.008295
	2p18f	21.346587	18.025782	21.346539	18.027734
	2p19f	21.323359	19.051988	21.323317	19.054005
	2p20f	21.302666	20.130941	21.302629	20.133038
Si^{12+}	2p4f	29.808779	3.989615	29.805714	3.990768
	2p5f	27.894154	4.989564	27.892189	4.991009
	2p6f	26.855415	5.989556	26.854187	5.991118
	2p7f	26.229645	6.989560	26.228843	6.991181
	2p8f	25.823763	7.989567	25.823215	7.991221
	2p9f	25.545631	8.989574	25.545241	8.991251

(Continues)

TABLE 3 (Continued)

Ion	State	$-E_{singlet}$ (a.u.)	n^*	$-E_{triplet}$ (a.u.)	n^*
	2p10f	25.346763	9.989584	25.346476	9.991278
	2p11f	25.199667	10.989620	25.199451	10.991316
	2p12f	25.087774	11.990110	25.087606	11.991824
	2p13f	25.000743	12.990352	25.000611	12.992064
	2p14f	24.931698	13.990664	24.931592	13.992382
	2p15f	24.876004	14.991052	24.875918	14.992767
	2p16f	24.830405	15.992084	24.830333	15.993826
	2p17f	24.792037	17.010200	24.791975	17.012006
	2p18f	24.759949	18.029525	24.759899	18.031259
	2p19f	24.730700	19.138353	24.730647	19.140552
	2p20f	24.706440	20.231656	24.706399	20.233665
P^{13+}	2p4f	34.279865	3.990284	34.276486	3.991379
	2p5f	32.060355	4.990236	32.058194	4.991607
	2p6f	30.856109	5.990230	30.854760	5.991710
	2p7f	30.130594	6.990231	30.129713	6.991767
	2p8f	29.659995	7.990235	29.659393	7.991802
	2p9f	29.337504	8.990243	29.337076	8.991831
	2p10f	29.106914	9.990249	29.106599	9.991852
	2p11f	28.936353	10.990264	28.936115	10.991876
	2p12f	28.806642	11.990433	28.806457	11.992060
	2p13f	28.705727	12.990535	28.705581	12.992168
	2p14f	28.625668	13.990657	28.625552	13.992278
	2p15f	28.561089	14.990823	28.560995	14.992439
	2p16f	28.508229	15.991303	28.508151	15.992931
	2p17f	28.464302	16.994948	28.464236	16.996601
	2p18f	28.426749	18.021466	28.426693	18.023139
	2p19f	28.395128	19.047073	28.395079	19.048800
	2p20f	28.366136	20.159605	28.366097	20.161235
S^{14+}	2p4f	39.063452	3.990872	39.059758	3.991916
	2p5f	36.516557	4.990827	36.514199	4.992130
	2p6f	35.134583	5.990821	35.133111	5.992229
	2p7f	34.301950	6.990823	34.300989	6.992283
	2p8f	33.761851	7.990826	33.761195	7.992314
	2p9f	33.391724	8.990828	33.391257	8.992337
	2p10f	33.127066	9.990830	33.126723	9.992351
	2p11f	32.931304	10.990831	32.931044	10.992365
	2p12f	32.782444	11.990841	32.782244	11.992373
	2p13f	32.666619	12.990845	32.666462	12.992376
	2p14f	32.574731	13.990845	32.574604	13.992391

(Continues)

TABLE 3 (Continued)

Ion	State	$-E_{singlet}$ (a.u.)	n^*	$-E_{triplet}$ (a.u.)	n^*
	2p15f	32.500609	14.990873	32.500506	14.992416
	2p16f	32.439946	15.991035	32.439860	15.992598
	2p17f	32.389652	16.991738	32.389581	16.993286
	2p18f	32.346881	18.008851	32.346819	18.010461
	2p19f	32.310679	19.029190	32.310626	19.030814
	2p20f	32.278212	20.108901	32.278167	20.110527
Cl^{15+}	2p4f	44.159541	3.991393	44.155530	3.992389
	2p5f	41.262760	4.991351	41.260203	4.992593
	2p6f	39.690835	5.991345	39.689240	5.992686
	2p7f	38.743714	6.991348	38.742674	6.992737
	2p8f	38.129331	7.991352	38.128620	7.992770
	2p9f	37.708279	8.991378	37.707774	8.992812
	2p10f	37.407184	9.991480	37.406812	9.992929
	2p11f	37.184473	10.991578	37.184192	10.993036
	2p12f	37.015107	11.991786	37.014891	11.993241
	2p13f	36.883273	12.992484	36.883102	12.993949
	2p14f	36.778449	13.995845	36.778312	13.997313
	2p15f	36.694092	14.997323	36.693981	14.998786
	2p16f	36.625059	15.999056	36.624966	16.000544
	2p17f	36.567812	17.001815	36.567733	17.003332
	2p18f	36.519640	18.009615	36.519572	18.011167
	2p19f	36.478161	19.037881	36.478103	19.039445
	2p20f	36.442081	20.091848	36.442022	20.093717
Ar^{16+}	2p4f	49.568131	3.991858	49.563803	3.992810
	2p5f	46.298963	4.991818	46.296208	4.993004
	2p6f	44.524864	5.991814	44.523147	5.993092
	2p7f	43.455887	6.991816	43.454767	6.993141
	2p8f	42.762436	7.991821	42.761671	7.993173
	2p9f	42.287194	8.991830	42.286649	8.993201
	2p10f	41.947327	9.991958	41.946927	9.993339
	2p11f	41.695944	10.992045	41.695642	10.993433
	2p12f	41.504770	11.992248	41.504538	11.993633
	2p13f	41.356011	12.992546	41.355828	12.993935
	2p14f	41.237637	13.996279	41.237489	13.997683
	2p15f	41.142415	14.997749	41.142295	14.999150
	2p16f	41.064482	15.999591	41.064383	16.000994
	2p17f	40.999872	17.002176	40.999787	17.003622
	2p18f	40.945690	18.006010	40.945617	18.007484
	2p19f	40.898984	19.030762	40.898919	19.032313
	2p20f	40.858603	20.073679	40.858545	20.075302

[a]Reference 29

4 | CONCLUSIONS

Explicitly correlated multiexponent Hylleraas type basis in the framework of Ritz variational principle can yield reasonably accurate energy eigenvalues for $^{1,3}F^e$ metastable bound states due to (*pf*) configuration of two-electron atoms ($Z=3-18$). The form of the wavefunction written as a linear combination of the product of correlated radial part and spherical top functions as an angular part is employed in the present work for the first time. The variational equation and related basis integrals are thus relatively different than the previous works. Multiexponent nature of the radial wavefunction is also an important aspect of the present method which has the potential to apply for the resonant states of the same symmetry in the purview of modified stabilization method.[32,33] The estimated data are in good agreement with the few available theoretical data. Although, the accuracy of the present data is less than Kar and Wang,[29] but it can be increased by incorporating *dd* configurations explicitly as well as by increasing the number of terms in the expansion of the radial wavefunction. We hope that the present treatment may be considered as an alternative method for structural computations of such high-lying DES for the future researchers in the related disciplines. A meaningful comparison between the theoretical and experimental energy values are not possible at present due to the unavailability of the experimental data. This situation thus warrants high resolution experimental measurement for $^{1,3}F^e$ states of two electron atoms.

ACKNOWLEDGMENT

TKM acknowledges the financial support from the Department of Atomic Energy, BRNS, Govt. of India under grant number 37(3)/14/27/2014-BRNS.

ORCID

Jayanta K. Saha http://orcid.org/0000-0002-1159-1905

REFERENCES

[1] R. P. Madden, K. Codling, *Phys. Rev. Lett.* **1963**, *10*, 516.
[2] J. K. Saha, S. Bhattacharyya, T. K. Mukherjee, P. K. Mukherjee, *Chem. Phys. Lett.* **2009**, *478*, 292.
[3] G. Tanner, K. Richter, J. M. Rost, *Rev. Mod. Phys.* **2000**, *72*, 497.
[4] C. D. Lin, *Phys. Rev. A* **1984**, *29*, 1019.
[5] V. Kharchenko, A. Bhardwaj, A. Dalgarno, D. R. Schulz, P. C. Stancil, *J. Geophys. Res.* **2008**, *113*, A08229.
[6] A. B. C. Walker, Jr, H. R. Rugge, *Astrophys. J.* **1971**, *164*, 181.
[7] A. H. Gabriel, C. Jordan, *Nature* **1969**, *221*, 94.
[8] T. Fujimoto, T. Kato, *Astrophys. J.* **1981**, *246*, 994.
[9] G. W. F. Drake, A. Dalgarno, *Phys. Rev. A* **1970**, *1*, 1325.
[10] a) E. Holøien, *J. Chem. Phys.* **1958**, *29*, 676; b) E. Holøien, *Phys. Norv.* **1961**, *1*, 53.
[11] A. K. Bhatia, *Phys. Rev. A* **1970**, *2*, 1667.
[12] T. K. Mukherjee, P. K. Mukherjee, *Phys. Rev. A* **2004**, *69*, 064501.
[13] Y. K. Ho, A. K. Bhatia, *Phys. Rev. A* **1993**, *47*, 2628.
[14] J. Eiglsperger, B. Piraux, J. Madronero, *Phys. Rev. A* **2010**, *81*, 042528.
[15] H. Doyle, M. Openheimer, G. W. F. Drake, *Phys. Rev. A* **1972**, *5*, 26.
[16] a) A. K. Bhatia, *Phys. Rev. A* **1972**, *6*, 2498; b) A. K. Bhatia, *Phys. Rev. A* **1972**, *6*, 120.
[17] A. K. Bhatia, *Phys. Rev. A* **1977**, *15*, 1315.
[18] S. R. Samanta, M. A. Ali, *J. Phys. B* **1977**, *10*, 2073.
[19] R. Bruch, G. Paul, J. Andra, L. Lipsky, *Phys. Rev. A* **1975**, *12*, 1808.
[20] H. W. van der Hart, J. E. Hansen, *J. Phys. B* **1993**, *26*, 641.
[21] M. Zitnik, K. Bucar, M. Stuhec, F. Penent, R. I. Hall, P. Lablanquie, *Phys. Rev. A* **2002**, *65*, 032520.
[22] S. Bhattacharyya, T. K. Mukherjee, J. K. Saha, P. K. Mukherjee, *Phys. Rev. A* **2008**, *78*, 032505.
[23] S. Kar, Z. Jiang, *At. Data Nucl. Data Tables* **2015**, *102*, 42.
[24] L. Lipsky, R. Anania, *At. Data Nucl. Data Tables* **1977**, *20*, 127.
[25] J. Callaway, *Phys. Lett. A* **1978**, *66*, 201.
[26] Y. K. Ho, J. Callaway, *J. Phys. B At. Mol. Phys.* **1985**, *18*, 3481.
[27] S. Kar, Y. K. Ho, *Int. J. Quantum Chem.* **2008**, *108*, 1491.
[28] S. Kar, Y. K. Ho, *Phys. Rev. A* **2009**, *79*, 062508.

[29] S. Kar, Y. Wang, W. Qi Li, X. D. Sun, *Few Body Syst.* **2015**, *56*, 651.

[30] J. K. Saha, S. Bhattacharyya, T. K. Mukherjee, P. K. Mukherjee; *J. Phys. B* **2009**, *42(24)*, 245701.

[31] J. K. Saha, S. Bhattacharyya, T. K. Mukherjee, P. K. Mukherjee; *J. Quant. Spectrosc. Radiat. Transf.* **2010**, *111(5)*, 675.

[32] J. K. Saha, S. Bhattacharyya, T. K. Mukherjee, *J. Chem. Phys.* **2010**, *132(13)*, 134107.

[33] J. K. Saha, S. Bhattacharyya, T. K. Mukherjee, P. K. Mukherjee; *Int. J. Quantum Chem.* **2010**, *111*, 1819.

[34] S. Bhattacharyya, J. K. Saha, T. K. Mukherjee, P. K. Mukherjee; *Phys. Scr.* **2012**, *85*, 065305.

[35] J. K. Saha, S. Bhattacharyya, T. K. Mukherjee; *Int. Rev. At. Mol. Phys.* **2012**, *3*, 1.

[36] S. Kasthurirangan, J. K. Saha, A. Agnihotri, S. Bhattacharyya, D. Misra, A. Kumar, P. K. Mukherjee, J. P. Santos, A. M. Costa, P. Indelicato, T. K. Mukherjee, L. C. Tribedi, *Phys. Rev. Lett.* **2013**, *111(24)*, 243201.

[37] S. Dutta, J. K. Saha, S. Bhattacharyya, T. K. Mukherjee, *Phys. Scr.* **2014**, *89(1)*, 015401.

[38] S. Bhattacharyya, J. K. Saha, T. K. Mukherjee; *Phys. Rev. A* **2015**, *91(4)*, 042515.

[39] J. K. Saha, S. Bhattacharyya, T. K. Mukherjee; *Commun. Theor. Phys.* **2016**, *65(3)*, 347.

[40] J. K. Saha, S. Bhattacharyya, T. K. Mukherjee; *Phys. Plasmas* **2016**, *23*, 092704.

[41] J. K. Saha, S. Bhattacharyya, T K. Mukherjee; *Int. J. Quantum Chem.* **2016**, *116*, 1802.

[42] A. K. Bhatia, A. Temkin, *Rev. Mod. Phys.* **1964**, *36*, 1050.

[43] T. K. Mukherjee, P. K. Mukherjee, *Phys. Rev. A* **1994**, *50*, 850.

[44] J. A. Nelder, R. Mead, *Comput. J.* **1965**, *7*, 308.

[45] J .L. Calais, P. O. Lowdin, *J. Mol. Spectrosc.* **1962**, *8*, 203.

[46] L. S. Gradshteyn, I. M. Ryzhik, *Table of Integrals, Series and Products*, 7th ed., Academic, New York **1994**.

How to cite this article: Dutta S, Sil AN, Saha JK, Mukherjee TK. Ritz variational method for the high-lying nonautoionizing doubly excited $^{1,3}F^e$ states of two-electron atoms. *Int J Quantum Chem*. 2017;e25577. https://doi.org/10.1002/qua.25577

Received: 6 February 2019 | Revised: 23 April 2019 | Accepted: 9 May 2019

DOI: 10.1002/qua.25981

FULL PAPER

International Journal of QUANTUM CHEMISTRY WILEY

Extensive investigations for metastable-bound and resonance $^3F^e$ states of He atom

Sayantan Dutta[1] | Amar N. Sil[2] | Jayanta K. Saha[3] | Tapan K. Mukherjee[4]

[1]Belgharia Texmaco Estate School, Kolkata, India

[2]Department of Physics, Jogamaya Devi College, Kolkata, India

[3]Department of Physics, Aliah University, Kolkata, India

[4]Department of Physics, Narula Institute of Technology, Kolkata, India

Correspondence
Jayanta K. Saha, Department of Physics, Aliah University, Kolkata, India.
Email: jksaha.phys@aliah.ac.in

Tapan K. Mukherjee, Department of Physics, Narula Institute of Technology, Kolkata, India.
Email: tapan.mukherjee@nit.ac.in

Funding information
DHESTB, Grant/Award Number: 249

Abstract

Evaluation of energy eigenvalues of first 19 metastable bound doubly excited states (DESs) arising from even parity *F* states of He atom are done within the framework of the Ritz variational principle. The wavefunction of the given state is constructed from different combinations of *pf* and *dd* configurations. The radial parts of the wavefunctions for both the configurations are expanded in Hylleraas type basis set. The nonlinear parameters of the Slater-type orbitals representing both the electrons are taken in geometrical sequence that span the radial space properly. The present calculated energies for the metastable bound states are lowest yet obtained. The resonance parameters that is, energy position and width of a large number of resonance states lying above $He^+(2p)$ threshold are evaluated by using stabilization method. The resonance parameters calculated in this work are in good agreement with the available theoretical results for the resonance states lying below $He^+(3p)$ threshold. The parameters for a large number of resonance states lying between $He^+(3p)$ and $He^+(7p)$ thresholds are being reported for the first time. The effective quantum numbers of all the states considered in the present work are estimated by using quantum defect theory. Different structural properties for example, the one- and two-particle moments, virial factors, expectation values of interelectronic angles, two-particle radial probability densities, and so forth are estimated for both metastable-bound as well as resonance states. The present results can be used as a benchmark for future references.

PACS: 31.15.ac, 31.15.V-, 31.15.xt, 32.80.Zb, 32.80.Ee

KEYWORDS

autoionization, doubly excited states, electron correlation, He atom, Hylleraas coordinate, variational method

1 | INTRODUCTION

Structural properties of two-electron atoms have drawn attention to many theoreticians as well as experimentalists. In the beginning of this century, Tanner et al[1] published a review article on the studies of two-electron atoms. Investigations on two-electron atoms are of immense interest in recent years due to the nonseparability of the dynamical equation of motion.[2–26] It provides a fundamental testing ground for various quantum chemical approximation methods for example, Feshbach projection operator formalism,[27–29] close-coupling approximation method,[30,31] multiconfigurational Hatree-Fock method,[32,33] hyperspherical close-coupling method based on numerical basis set,[34,35] complex-coordinate-rotation (CCR) method with a finite numerical basis set built on the solutions of discretized one particle Hamiltonian,[36] CCR method with minor

operational modifications,[26,37] stabilization method,[6,10,38–40] and so forth. According to the conventional classification scheme,[41] DESs may be classified on the basis of stability into two general groups as metastable bound states (nonautoionizing) and resonance states (autoionizing) depending on the angular momentum coupling scheme and parity conservation rule. With spin-orbit induced *LS*-mixing the metastable bound states will have opportunity to auto-ionize, although radiative decay will be much more probable.[41,42] Feldman and Novick[43] have provided the selection rule for autoionization where the nonradiative transition of doubly excited state (DES) to a state of ionized configuration of He takes place. The metastable bound states exhibit fluorescence decay where one electron of DES jumps to an energetically lower state giving rise to emission of a photon. On the basis of the criteria as provided by Saha et al.[14] the DESs are now classified into three groups, namely metastable-bound, pure resonance, and fluorescence-active resonance states.[14,44–47] The autoionization decay rate for the fluorescence active resonance states are very small compared to that of pure resonance states of a particular symmetry.[4] Dominance of fluorescence decay over autoinization for such states was established by previous studies.[14,44–47]

There exists numerous investigations in the literature related to structural and spectral features of DESs of two-electron atoms up to *D* state, among which few references are given.[4,5,7,12,15,48–56] In contrast, the same studies for F^e states are rather scanty.[8,9,11,16,24,57–61] The estimations of the energy eigenvalues of metastable bound $^{1,\,3}F^e$ states of the He atom were done by a group of theoreticians[8,9,11,58,59] by using different quantum chemical approximation methods. Among these calculations, Kar and Ho[9] obtained the lowest energies values for first six metastable bound states using purely exponentially correlated CI-type wavefunction with 2200 terms in their basis set. Eiglsperger et al[11] reported energy eigenvalues of more number of metastable bound states of He by using almost 16 000 terms in their wavefunction expanded in Coulomb-Strumenium basis. It is to be noted that energy values of first five metastable bound states are less accurate than those obtained by Kar and Ho.[9] Eiglsperger et al[11] opined that their methodology leads to the increase of precision of the energy eigenvalues for the states approaching toward the $He^+(2p)$ threshold. By analyzing the results of the above works, it appears that it is difficult to obtain precise energies for both lower and higher lying metastable bound $^{1,\,3}F^e$ states by using one particular method, although several efforts were made in this direction since the pioneering work of Lipsky et al.[58]

A group of authors[8,57–61] studied the properties of resonance $^{1,\,3}F^e$ states of the He atom. Lipsky et al[58] and Callaway[59] reported only resonance energy values, whereas Herrick and Sinanoglu,[57] Ho and Callaway[60] and Bachau et al[61] reported both resonance energies and width. Maximum number of resonance states were reported by Kar and Ho[8] using correlated CI type basis set in the framework of stabilization method, though widths of few states were not reported. The width of only one such state is available in the literature, due to the calculation of Bachau et al.[61] All such studies are limited to the resonance $^{1,\,3}F^e$ states below $He^+(3p)$ threshold.

We have therefore, made an extensive study on the structural properties of $^3F^e$ state of He atom where the Ritz variational principle is being used for metastable bound states below $He^+(2p)$ threshold. We have adopted stabilization method with "soft wall" strategy[39,40] for the calculation of resonance parameters of resonance $^3F^e$ states above $He^+(2p)$ threshold. The wavefunction used by Dutta et al[24] is being modified in the present work by introducing *dd* configuration. Explicitly correlated multiexponent Hylleraas type basis set is being used in the present communication. We have obtained better energy values than that of the previous studies[8,9,11,58,59] for both lower and higher lying metastable bound $^3F^e$ states of He. Moreover, the parameters of a large number of resonance states up to $He^+(7p)$ threshold have also been estimated. In the present work, the resonance parameters for the states with extremely narrow widths below $He^+(3p)$ threshold along with the states lying between $He^+(3p)$ and $He^+(7p)$ thresholds, are being reported for the first time. The one- and two-particle moments, virial factors, expectation values of inter-electronic angles, two-particle radial probability densities, and so forth are estimated to justify the classification scheme as given by previous studies.[8,61] The details of the methodology is given in Section 2 followed by the discussion on the results in Section 3 and finally concluded in Section 4.

2 | METHOD

The variational equation for the even parity *F* state is obtained from the general variational equation of arbitrary angular momentum of a two-electron system[62,63] where the translational and rotational symmetry of the Hamiltonian are being exploited to reduce the nine-dimensional variational equation to a three-dimensional one. The three coordinates of two-electron atom are the sides of the triangle (r_1, r_2, r_{12}) formed by the two electrons and the nucleus of two-electron atom where the rotation of the triangle in space can be defined by three Eulerian angles (θ, ϕ, ψ). Following the work of Bhatia and Temkin,[62] we can write the wave function of $^{1,\,3}F^e$ state of a two-electron atom as,

$$\Psi = f_3^0 D_3^0 + f_3^{2^+} D_3^{2^+} + f_3^{2^-} D_3^{2^-} \tag{1}$$

where $D_l^{k\pm}(\theta,\phi,\psi)$ are the real angular momentum Wigner functions.[24,62] $D_l^{k\pm}$ are the eigenfunctions of the two-electronic angular momentum operator $\hat{L}^2$, that is, $\hat{L}^2 D_l^{k\pm} = l(l+1)D_l^{k\pm}$ (in a.u.), *l* being the angular momentum quantum number. The symbols are same as used by Bhatia and Temkin.[62] The radial parts of the wavefunction are given by

$$f_3^0 = -F_1 \sin\theta_{12} - \sqrt{\frac{10}{7}} G_1 \sin\theta_{12}\cos\theta_{12}$$
$$f_3^{2+} = \frac{\sqrt{15}}{6} F_1 \sin 2\theta_{12} + \sqrt{\frac{50}{21}} G_1 \sin\theta_{12} \quad (2)$$
$$f_3^{2-} = \frac{\sqrt{15}}{6} F_2 (1 - \cos 2\theta_{12})$$

Here θ_{12} is the angle between $\vec{r_1}$ and $\vec{r_2}$. Each of the terms in the wavefunction Ψ has its own physical significance. By transforming the real angular momentum functions (D) in the individual polar coordinates of the two electrons, it can be shown that the terms associated with F_1 and F_2 represent *pf* configuration. The radial parts for *pf* configuration are $F_1 = (f \mp \tilde{f})$ and $F_2 = (f \pm \tilde{f})$, with the condition $\tilde{f} = f(r_2, r_1)$. The upper sign corresponds to the singlet state and the lower sign to the triplet state.

The trial radial wave function corresponding to *pf* configuration is expanded in Hylleraas basis set as

$$f = \sum_{i=1}^{A_1} r_1^{l_i+3} r_2^{m_i+1} r_{12}^{n_i} \left[\sum_{k_1=1}^{p} C_{ik_1k_1} \eta_{k_1}(1)\eta_{k_1}(2) + \sum_{k_1=1}^{p}\sum_{k_2=1}^{p} C_{ik_1k_2} \eta_{k_1}(1)\eta_{k_2}(2) \right] \quad (3)$$

with the following conditions:

1. The powers of r_1, r_2, and r_{12} satisfy $(l_i, m_i, n_i) \geq (0, 0, 0)$.
2. A_1 is the number of elements in the set of the powers of r_1, r_2, and r_{12}.
3. $\eta_i(j) = e^{-\rho_i r_j}$ is the Slater-type orbital. ρ is the nonlinear parameter.
4. p denotes the number of nonlinear parameters.
5. In the double sum of Equation (3) $k_1 < k_2$.
6. $C_{ik_1k_2}$'s are the linear variational parameter.

Similarly, it can be shown that the terms associated with G_1 in Equation (2) represent *dd* configuration where $G_1 = (g \mp \tilde{g})$ and $\tilde{g}$ $g(r_2, r_1)$. The trial radial wave function corresponding to *dd* configuration is expanded in Hylleraas basis set as

$$g = \sum_{i=1}^{A_2} r_1^{l_i+2} r_2^{m_i+2} r_{12}^{n_i} \left[\sum_{k_1=1}^{p} D_{ik_1k_1} \zeta_{k_1}(1)\zeta_{k_1}(2) + \sum_{k_1=1}^{p}\sum_{k_2=1}^{p} D_{ik_1k_2} \zeta_{k_1}(1)\zeta_{k_2}(2) \right] \quad (4)$$

The parameters A_2 and $D_{ik_1k_2}$ have the same meaning as of A_1 and $C_{ik_1k_2}$ of Equation (3). The Slater-type orbital $\zeta_i(j)$ is given by, $\zeta_i(j) = e^{-\sigma_i r_j}$, where σ is the nonlinear parameter for the *dd* configuration.

In the present calculation both $A_1 = A_2$ (symmetric basis set) and $A_1 \neq A_2$ (asymmetric basis set) are considered. The effect of the radial correlation is incorporated through different ρ's and σ's in the wave function whereas, the angular correlation effect is taken care of through different powers of r_{12}. The number of terms in the basis set expansions for the trial radial wave functions f and g are $N_1 = \frac{p(p+1)}{2} \times A_1$ and $N_2 = \frac{p(p+1)}{2} \times A_2$, respectively. The total dimension of the multiexponent basis is $N = N_1 + N_2$. Three different types of basis sets as considered in the present work are given below:

1. Symmetric double-exponent basis: The expansion length of the wavefunction are taken as N = 750 and 900 with p = 2. In the first case $A_1 = A_2$ = 125 while $A_1 = A_2$ = 150 is considered for the latter.
2. Symmetric nine-exponent basis: The expansion length of the wavefunction are taken as N = 900 and 1530 with p = 9. In the first case $A_1 = A_2$ = 10 while $A_1 = A_2$ = 17 is considered for the latter.
3. Asymmetric nine-exponent basis: The expansion length of the wavefunction are taken as N = 1350 and 1530 with p = 9. In the first case A_1 = 28 and A_2 = 2, while A_1 = 32 and A_2 = 2 is considered for the latter.

For the calculation of metastable bound state energies all the combinations of basis set (a, b, c) are used while for the resonance states, only the choice (b) is considered. The reason behind such choice of the basis sets is to span the entire radial space in a flexible manner so that the desirable accuracy of the energy levels can be achieved for bound as well as resonance states. The efficacy of each of the three basis sets are discussed in details in Section 3.

In case of nine-exponent basis sets the nonlinear parameters for *pf* and *dd* configurations are taken in a geometrical sequence following $\rho_i = \rho_{i-1}\gamma_1$ and $\sigma_i = \sigma_{i-1}\gamma_2$, respectively. γ_1 and γ_2 are the geometrical ratio of the sequences. The higher ρ values are responsible for spanning the

space near the nucleus whereas the lower one spans the space far away from the nucleus. Thus, wavefunction can be squeezed or diffused by changing the geometrical ratios γ_1 or γ_2 by keeping ρ_1 or σ_1 constant throughout.[10]

The energy eigenvalues are obtained by solving the generalized eigenvalue equation involving the Hamiltonian (*H*) and overlap (*S*) matrices given by

$$\underline{\underline{H}}\,\underline{C} = E\underline{\underline{S}}\,\underline{C} \tag{5}$$

where *C* is the column vector consisting of the linear variational parameters. Atomic units are used throughout.

The linear variational parameters $C_{ik_1k_2}$ and $D_{ik_1k_2}$, as obtained from Equation (5) are used to determine a number of expectation values for example, repulsive potential $\langle V_r \rangle$, attractive potential $\langle -V_a \rangle$, interelectronic angles $\langle \theta_{12} \rangle$, and different one and two-particle moments such as $\langle r_1 \rangle$, $\langle r_1^2 \rangle$, $\langle r_{12} \rangle$, $\langle r_{12}^2 \rangle$ of metastable bound as well as resonance $^3F^e$ states of *He* atom.

3 | RESULTS AND DISCUSSIONS

Repeated diagonalization of the Hamiltonian matrix in the symmetric nine exponent Hylleraas basis set with *N* = 1530 is done in the present work for different values of γ_1 keeping γ_2 constant. We have computed first 250 energy eigenroots for 1840 different values of γ_1 ranging from 0.456 to 0.732. The highest value of the ρ sequence that is, ρ_9 is fixed at 8.0 while ρ_1 of any set differs from that of the previous one by 0.001. All calculations are carried out in quadruple precision. The plot of each energy eigenroot vs γ_1 produces the stabilization diagram in Figure 1. The closer look at Figure 1 reveals the fact that there exists two classes of states:

1. Roots which are lying below $He^+(2p)$ threshold, are insensitive to the variation in γ_1. These $^3F^e$ states are metastable bound that is, stable against autoionization.
2. Roots lying above *He* + (2*p*) threshold are sensitive to the variation in γ_1 and gives rise to flat plateaus in the vicinity of avoided crossings. It therefore confirms the presence of $^3F^e$ resonance states above *He* + (2*p*) threshold.

Detailed structural features of both metastable bound and resonance states are discussed in the following subsections.

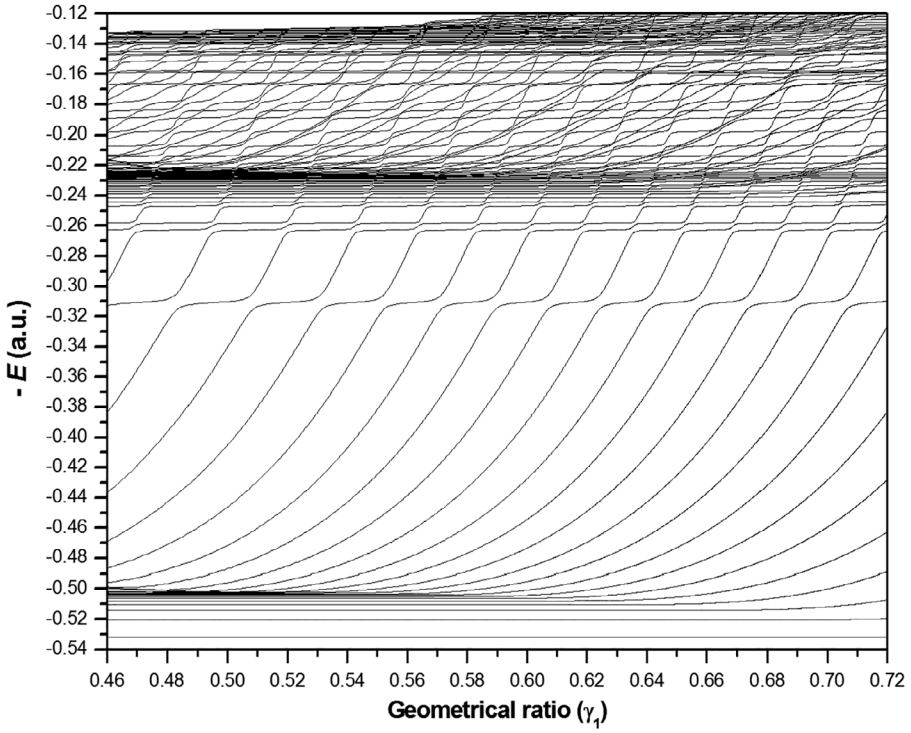

FIGURE 1 Stabilization plot of first 100 diagonalized energy eigenroots using *N* = 1530 terms in the symmetric nine exponent basis set for $^3F^e$ states of neutral He atom in the energy range −0.54 a.u. to −0.12 a.u. showing existence of both metastable bound and resonance states

3.1 | Metastable bound states

To estimate the upper-bound energies for metastable bound $^3F^e$ states below *He* + (2*p*) threshold we have adopted three different types of basis sets as discussed in Section 2. The energy eigenvalues using such basis sets along with their convergence behavior are given in Table 1. The energy eigenvalues of 2*pnf*[*n* = 4–9] $^3F^e$ states are obtained under the framework of the Ritz variational principle employing symmetric double exponent basis. For each *n*, the nonlinear parameters (ρ_1, ρ_2) and (σ_1, σ_2) of *pf* and *dd* configurations respectively, are optimized using Nelder-Mead algorithm.[64] A close look at the Table 1 shows that the energy values converge to 11th place after the decimal for the first three states (2*pnf*; *n* = 4–6) and eighth decimal place for the later three metastable bound states (2*pnf*; *n* = 7–9).

As a second choice we have opted for one-shot diagonalization using symmetric and asymmetric nine-exponent basis set. In Table 1 the fourth and fifth columns show the convergence behavior of the energy eigenvalues of $^3F^e$(2*pnf*, 4 ≤ *n* ≤ 18) states using symmetric nine-exponent basis, whereas the last two columns show the same for $^3F^e$(2*pnf*, 4 ≤ *n* ≤ 22) states by using asymmetric nine-exponent basis set. It is evident from Table 1 that the choice of asymmetric nine exponent basis set with *N* = 1530 is better than that of symmetric basis for obtaining the lowest energy values for all the metastable bound states except 2*p*4*f* and 2*p*5*f*. The energy eigenvalues for assymetric basis set converge up to 9 or 10 decimal places for the low-lying metastable bound states and the nature of the convergence gradually degrades for the high-lying metastable bound states.

The previous studies[9,11] reported the energy values in the range 10 to 13 decimal places. The lowest energy values obtained in the present work are compared with other theoretical results[9,11,58,59] in Table 2. The effective quantum numbers n^* as given in Table 2 for each of the states calculated by using the following relation

$$E = -\frac{1}{2}\left[\left(\frac{Z}{N_i}\right)^2 + \left(\frac{Z-1}{n^*}\right)^2\right] \tag{6}$$

where *E* is the energy of the state, *Z* is the atomic number, and N_i is the inner electron quantum number. It is evident that, the quantum defect that is, $\delta n = n - n^*$ remains nearly same ($\delta n \sim 0.05$) for the first 15 states and then increases gradually for the next 4 excited states. Kar and Ho[9]

TABLE 1 Energy eigenvalues (−*E* in a.u.) of metastable bound $^3F^e$ (2*pnf*, *n* ≥ 4) states for different choice of basis sets using different number of terms in the basis sets

			Nine exponent			
	Triple exponent		Symmetric basis		Asymmetric basis	
Configuration	*N* = 750	*N* = 900	*N* = 900	*N* = 1530	*N* = 1350	*N* = 1530
2*p*4*f*	0.5319913263468	0.5319913263485	0.5319913258284	0.5319913263513	0.5319913261595	0.53199132616450
2*p*5*f*	0.5203828592813	0.5203828592853	0.5203828589216	0.5203828613614	0.5203828591643	0.52038285929302
2*p*6*f*	0.5141114291154	0.5141114291191	0.5141114286873	0.5141114291166	0.5141114290354	0.51411142927528
2*p*7*f*	0.5103445646194	0.5103445656885	0.5103445628175	0.5103445646815	0.5103445646439	0.51034456470790
2*p*8*f*	0.5079067459561	0.5079067462723	0.5079066925246	0.5079067606712	0.5079067461492	0.50790674627610
2*p*9*f*	0.5062390860001	0.5062390884513	0.5062386665548	0.5062390870716	0.5062390885034	0.50623908868559
2*p*10*f*			0.5050451459782	0.5050483116213	0.5050483206789	0.50504832666688
2*p*11*f*			0.5041441160851	0.5041683759270	0.5041685601914	0.50416856783908
2*p*12*f*			0.5034118118494	0.5034990626971	0.5035001039946	0.50350020569843
2*p*13*f*			0.5028320754932	0.5029766752202	0.5029778169414	0.50298059371759
2*p*14*f*			0.5022960514768	0.5025584256797	0.5025686165973	0.50256887024567
2*p*15*f*			0.5012313201500	0.5022112271052	0.5022365435680	0.50223659253604
2*p*16*f*			0.5007079126835	0.5018827805313	0.5019648269563	0.50196521180896
2*p*17*f*			0.5004688559343	0.5014894480147	0.5017168163780	0.50174013288428
2*p*18*f*			0.5003084861460	0.5005964256713	0.5015196531527	0.50155210736964
2*p*19*f*					0.5013095900752	0.50139603567465
2*p*20*f*					0.5012392360422	0.50126368214833
2*p*21*f*					0.5010961347848	0.50115434103934
2*p*22*f*					0.5009902068174	0.50105114035136

TABLE 2 Comparison of energy eigenvalues (−*E* in a.u.) and effective quantum number (n^*) of metastable bound $2pnf\ ^3F^e$ [n = 4−22] states of helium

	Present work		Other works	
n	$-E$	n^*	$-E$	n^*
4	0.5319913263513	3.9534	0.5319913263465[a]	3.953382897[a]
			0.531968[b]	3.95483[b]
			0.531985[c]	
			0.5319913251[d]	
5	0.5203828613614	4.9528	0.5203828592839[a]	4.953382897[a]
			0.520367[b]	4.95477[b]
			0.520375[c]	
			0.5203828583[d]	
6	0.5141114292752	5.9525	0.5141114291180[a]	5.952501354[a]
			0.514101[b]	5.95476[b]
			0.514105[c]	
			0.5141114284[d]	
7	0.5103445647079	6.9523	0.510344564686[a]	6.95230621[a]
			0.51034456422[d]	
8	0.5079067462761	7.9522	0.5079067461[a]	7.9521782[a]
			0.50790674595[d]	
9	0.5062390886855	8.9521	0.506239088[a]	8.952090[a]
			0.50623908834[a]	
10	0.5050483266668	9.9520	0.50504832108[d]	
11	0.5041685678390	10.9520	0.50416854777[d]	
12	0.5035002056984	11.9519	0.50350020079[d]	
13	0.5029805937175	12.9519	0.50298058847[d]	
14	0.5025688702456	13.9513	0.50256864290[d]	
15	0.5022365925360	14.9517	0.50223655040[d]	
16	0.5019652118089	15.9507	0.50196493112[d]	
17	0.5017401328842	16.9509	0.50173994653[d]	
18	0.5015521073696	17.9483	0.5015515014[d]	
19	0.5013960356746	18.9250	0.5013921[d]	
20	0.5012636821483	19.8914		
21	0.5011543410393	20.8122		
22	0.5010511403513	21.8099		

[a]Kar and Ho[9]; 2200 parameter purely exponential correlated basis set.
[b]Lipsky et al [58]; truncated diagonalization method with CI-type basis set.
[c]Callaway[59]; 240 parameter uncorrelated CI-type wavefunction.
[d]Eigelsperger et al [11]; 16000 parameter Coulomb-Sturmenium basis set.

used 2200 terms in their wavefunction to obtain the lowest bound energy eigenvalues for $^3F^e(2pnf, n = 4–9)$ states. The only calculation available for $^3F^e(2pnf, n$ = 10-19) states is due to Eiglsperger et al[11] where 16 000 terms in the wavefunction were used. A comparison with other theoretical results as shown in Table 2 reveals that the present energy eigenvalues are lowest yet obtained. It is remarkable that the energy eigenvalues using only 900 terms in the symmetric double exponent basis set (as shown in Table 1) are better than those available in the literature. Even 750 terms in the symmetric double exponent basis set yields better energy eigenvalues than that of Kar and Ho[9] for the $2p4f$ state. Thus, the substantial reduction of the number of terms in the basis set is a clear advantage of the present method. The superiority of the present wavefunction over the other studies lies in the explicit inclusion of the *dd* configuration, expanded in the Hylleraas basis set. For instance, the energy position for the $2p4f$ state as calculated by using 900 terms in the 9 exponent wavefunction without *dd* configuration is −0.53198567 a.u. while the energy position improves to −0.53199132 a.u. for the same state upon the inclusion of *dd* configuration. Thus, the inclusion of the *dd* configuration contributes 0.001% to the energy value of the $2p4f$ state. This contribution decreases as we move toward the *He* + (2*p*) threshold, for example, it decreases to 0.0002% for the $2p9f$ state.

TABLE 3 The virial-factor ξ, expectation values of interelectronic angles (in degree), different one and two-particle moments of metastable bound $2pnf\ ^3F^e$ [n = 4–22] states of *He* below *He* + (2*p*) threshold

n	ξ	$\langle r_1 \rangle$	$\langle r_1^2 \rangle$	$\langle r_{12} \rangle$	$\langle r_{12}^2 \rangle$	$\langle \theta_{12} \rangle$
4	1.28 [−11]	9.96 [+0]	1.73 [+2]	1.77 [+1]	3.47 [+2]	90.761
5	5.45 [−11]	1.66 [+1]	5.42 [+2]	3.09 [+1]	1.08 [+3]	90.388
6	6.87 [−11]	2.48 [+1]	1.26 [+3]	4.72 [+1]	2.53 [+3]	90.223
7	4.35 [−12]	3.45 [+1]	2.50 [+3]	6.66 [+1]	5.00 [+3]	90.140
8	3.56 [−10]	4.57 [+1]	4.45 [+3]	8.89 [+1]	8.89 [+3]	90.094
9	1.62 [−10]	5.84 [+1]	7.33 [+3]	1.14 [+2]	1.47 [+4]	90.065
10	1.12 [−09]	7.25 [+1]	1.14 [+4]	1.43 [+2]	2.28 [+4]	90.048
11	2.30 [−09]	8.82 [+1]	1.69 [+4]	1.74 [+2]	3.39 [+4]	90.036
12	4.59 [−08]	1.05 [+2]	2.43 [+4]	2.08 [+2]	4.85 [+4]	90.027
13	1.03 [−07]	1.24 [+2]	3.37 [+4]	2.46 [+2]	6.74 [+4]	90.021
14	2.43 [−07]	1.44 [+2]	4.57 [+4]	2.86 [+2]	9.13 [+4]	90.017
15	2.52 [−07]	1.66 [+2]	6.05 [+4]	3.29 [+2]	1.21 [+5]	90.014
16	3.76 [−06]	1.89 [+2]	7.88 [+4]	3.76 [+2]	1.58 [+5]	90.011
17	1.88 [−05]	2.14 [+2]	1.01 [+5]	4.25 [+2]	2.02 [+5]	90.009
18	1.43 [−05]	2.41 [+2]	1.28 [+5]	4.79 [+2]	2.56 [+5]	90.008
19	2.59 [−04]	2.66 [+2]	1.59 [+5]	5.30 [+2]	3.19 [+5]	90.008
20	1.51 [−03]	3.11 [+2]	2.32 [+5]	6.19 [+2]	4.65 [+5]	90.014
21	1.13 [−04]	3.55 [+2]	2.81 [+5]	7.07 [+2]	5.61 [+5]	90.006
22	9.03 [−04]	3.90 [+2]	3.65 [+5]	7.78 [+2]	7.30 [+5]	90.009

Note: The notation P[±Q] stands for $P \times 10^{\pm Q}$. All values are given in atomic units.

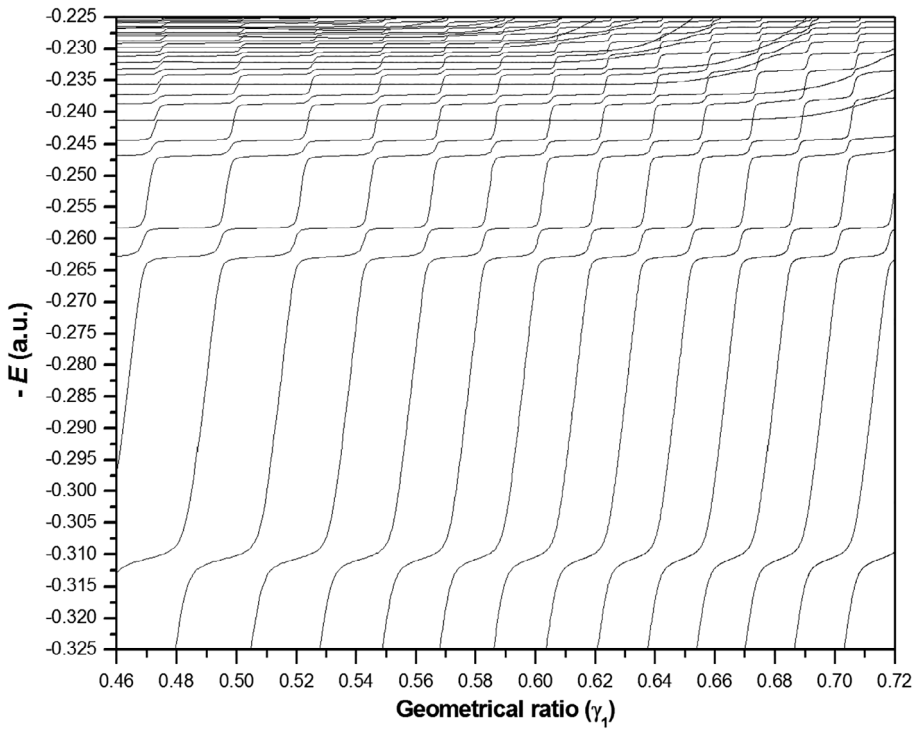

FIGURE 2 Stabilization plot for $^3F^e$ states of He in the energy range −0.325 a.u. to −0.225 a.u. showing series of resonances below *He* + (3*p*) threshold using N = 1530 number of terms in the symmetric nine exponent Hyllerass-type wavefunction

The wavefunction with 9 exponent basis corresponding to the best energy values have been used to calculate the expectation values of $\langle \theta_{12} \rangle$, $\langle r_1 \rangle$, $\langle r_1^2 \rangle$, $\langle r_{12} \rangle$ and $\langle r_{12}^2 \rangle$ as given in Table 3. It can be seen from Table 3 that the one- and two-particle moments for $2pnf$ (n = 4–22) increase gradually while the interelectronic angle $\langle \theta_{12} \rangle$ decreases very slowly within 1°. In order to check the accuracy of the wavefunction the virial-factor, defined as

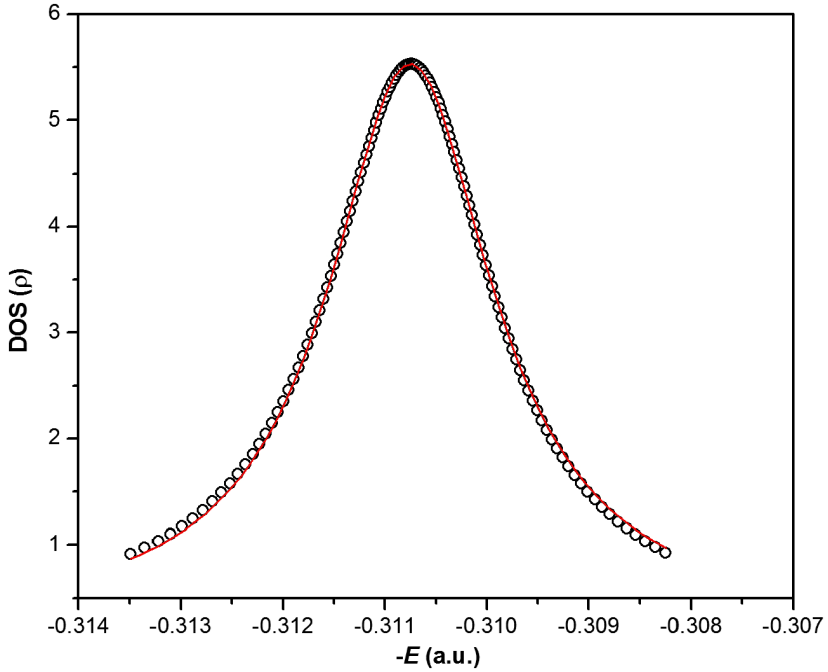

FIGURE 3 Calculated DOS (hollow circles) and the fitted Lorentzian (red line) for the first $^3F^e$ resonance states of He atom below $He^+(3p)$ threshold

$$\xi = 1 - \frac{\langle V \rangle}{2\langle T \rangle} \tag{7}$$

has been estimated; where $\langle V \rangle$ and $\langle T \rangle$ are the expectation values of potential and kinetic energies, respectively. It is evident from the value of ξ that the accuracy of the metastable bound state quantum properties for $2p4f$ configuration is at least of the order of 10^{-11} a.u. and gradually decreases for the higher excited states.

3.2 | Resonance states

A portion of the stabilization diagram in the energy range −0.325 a.u. to −0.225 a.u., that is, lying between $He + (2p)$ and $He + (3p)$ thresholds is given in Figure 2 where a series of resonance states can be seen. The inverse of tangent at different points near the stabilization plateau for each energy eigenroot gives rise to the density of states (DOS) as

$$\rho_n(E) = \left| \frac{\gamma_1^{i+1} - \gamma_1^{i-1}}{E_n(\gamma_1^{i+1}) - E_n(\gamma_1^{i-1})} \right| \tag{8}$$

Finally, the resonance parameters (E_r, Γ) are obtained by Lorentzian fitting of the DOS as

$$\rho_n(E) = y_0 + \frac{A}{\pi} \frac{\Gamma/2}{(E - E_r)^2 + (\Gamma/2)^2} \tag{9}$$

where y_0 is the baseline background, A is the total area under the curve from the baseline, E_r gives the position of the center of the peak of the curve, and Γ represents the full width of the peak of the curve at half height. All plots and fitting procedure are carried out in Microcal Origin software package and least χ^2 fitting is being taken. As an example, the resonance parameters E_r = −0.31075 a.u. and Γ = 0.00198 a.u. are obtained from 13th root is shown in Figure 3 where the hollow black circles and the red line represent the estimated DOS and the best fit Lorentzian, respectively.

In Table 4, the convergence behavior of first 12 $^3F^e$ resonance states below $He^+(3p)$ threshold are shown. The sensitivity of the resonance parameters (E_r, Γ) to the parameter N is as follows. From Table 4 it can be seen that the values of resonance parameters (E_r, Γ) for N = 900 and N = 1530, remain unchanged up to at least fourth decimal place. A comparison between the present calculated resonance parameters (E_r, Γ) and those of the other works[8,58–61] for the states lying below $He^+(3p)$ threshold is given in Table 5. It is evident from the comparison that the values of the present resonance parameters below $He^+(3p)$ threshold are in excellent agreement with those available in the literature.

TABLE 4 Convergence behavior for the position ($-E_r$ in a.u.) and width (Γ in a.u.) of $^3F^e$ resonance states below $He^+(3p)$ threshold

State	N	$-E_r$	Γ
1	900	0.31077	1.98 [−3]
	1530	0.31075	1.98 [−3]
2	900	0.26284	4.5 [−4]
	1530	0.26284	4.5 [−4]
3	900	0.25827	1.7 [−4]
	1530	0.25826	1.7 [−4]
4	900	0.24681	2.1 [−4]
	1530	0.24680	2.4 [−4]
5	900	0.24439	1.1 [−4]
	1530	0.24438	1.2 [−4]
6	900	0.24130	8.5 [−9]
	1530	0.24130	6.9 [−11]
7	900	0.23871	1.2 [−4]
	1530	0.23871	1.1 [−4]
8	900	0.23730	7.0 [−5]
	1530	0.23730	7.0 [−5]
9	900	0.23559	5.3 [−11]
	1530	0.23560	3.1 [−12]
10	900	0.23403	8.0 [−5]
	1530	0.23404	6.0 [−5]
11	900	0.23315	4.0 [−5]
	1530	0.23315	4.0 [−5]
12	900	0.23207	5.8 [−9]
	1530	0.23210	5.6 [−10]

Note: The notation $P[\pm Q]$ stands for $P \times 10^{\pm Q}$.

The individual angular momentum does not commute with the two-electron Hamiltonian. As a result, the assignment of the individual angular momentum to the electrons is the indicator of the dominant configuration in the wavefunction of the two-electron atom. Previous studies[8,61] classified the $^3F^e$ resonance states below $He^+(3p)$ threshold according to dominant configurations $3dnd$ [$n \geq 3$], $3pnf$ [$n \geq 4$], and $3dng$ [$n \geq 5$] that are denoted as classes A, B, and C, respectively as shown in Table 5. It is relevant to mention that the effective quantum numbers (n^*) are less than the outer electron quantum number (n) for classes A and B, whereas n^* is greater than n for class C states. A comparison between the widths of the resonance states of classes A and B having the same outer electron quantum number (n) shows that the width of the states in class A is greater than that of class B states. For example, the width of $3d4d$ (class A) is 0.00045 a.u. while that for $3p4f$ (class B) is 0.00017 a.u. as given in Table 5. The energy distance from the threshold [$\epsilon_k = E_{th} - E_k$] and the ratios $R_\epsilon = \frac{\epsilon_{k-1}}{\epsilon_k}$ and $R_\Gamma = \frac{\Gamma_{k-1}}{\Gamma_k}$[2,3] show a certain pattern for each of the classes with a few exceptions for states near the $He^+(3p)$ threshold. The reason behind these exceptions may be due to appreciable contributions from more than one configuration.

It is interesting to note that the present method enables to compute extremely narrow widths for a series of states (class C) as shown in Table 5. The only available estimation for the width of $3d5g$ state (class C) done by Bachau et al[61] shows that the autoionization lifetime is almost 10^6 times greater than that of other resonance states lying below $He + (3p)$ threshold. The present reported width of the state is in good agreement with that of Bachau et al.[61] The narrow widths of the resonance states (class C) indicate that the fluorescence decay may dominate over autoionization. Detailed investigations are needed in this direction for arriving at a definite conclusion. In this context, it is to be mentioned that presence of such fluorescence active resonance states for $^1P^o$ symmetry arising from pd configuration was reported earlier.[14,44–47]

The expectation values of repulsive potential $\langle V_r \rangle$, attractive potential $\langle -V_a \rangle$, their ratio $\left[\eta = \frac{\langle V_r \rangle}{\langle -V_a \rangle}\right]$, interelectronic angles $\langle \theta_{12} \rangle$ (in degree) and different one and two-particle moments for example, $\langle r_1 \rangle$, $\langle r_1^2 \rangle$, $\langle r_{12} \rangle$, $\langle r_{12}^2 \rangle$ for different $^3F^e$ resonances states below $He + (3p)$ threshold are listed in Table 6. The expectation values of the aforementioned quantities are calculated by using the resonance wavefunction corresponding to the resonance position of the root having least χ^2. Table 6 shows that for each class of states, η gradually decreases as the resonance states come closer to the $He + (3p)$ threshold. Thus the repulsive part of the potential decreases in comparison to the attractive part. This explains the fact of gradual decreasing width of resonance states as the repulsion between two electrons is responsible for autoionization. On the other hand the one- and

TABLE 5 Positions ($-E_r$ in a.u.), widths (Γ in a.u.), effective quantum number (n^*), the energy gap between the threshold and resonance energy values (ϵ_k), relative energies (R_ϵ) and relative widths (R_Γ) of resonance states of ($^3F^e$) below *He* + (3*p*) threshold

								Other works	
Class	**n**	$-E_r$	Γ	n^*	$\in_k$	$R_\in$	R_Γ	$-E_r$	Γ
A	3	0.31075	1.98 [−3]	2.37654	0.08853			0.31069[a]	1.98 [−3][a]
								0.3111[b]	2.131 [−3][b]
								0.310725[c]	1.95 [−3][c]
								0.309915[d]	
								0.310749[e]	
	4	0.26284	4.5 [−4]	3.50854	0.04062	2.18	4.40	0.262825[a]	4.5 [−4][a]
								0.2628[b]	4.77 [−4][b]
								0.26283[c]	4.4 [−4][c]
								0.26264[d]	
								0.262598[e]	
	5	0.24680	2.4 [−4]	4.51039	0.02458	1.65	1.87	0.246805[a]	2.1 [−4][a]
								0.2468[b]	2.27 [−4][b]
								0.246715[e]	
								0.246653[d]	
	6	0.23871	1.1 [−4]	5.50686	0.01649	1.49	2.18	0.238705[a]	1.1 [−4][a]
								0.238645[d]	
								0.238597[e]	
	7	0.23404	6.0 [−5]	6.50455	0.01182	1.39	1.83	0.234035[a]	6.6 [−5][a]
								0.233963[e]	
	8	0.23110	4.0 [−5]	7.50469	0.00878	1.34	1.50		
	9	0.22914	3.0 [−5]	8.50162	0.00692	1.26	1.33		
	10	0.22754	7.0 [−5]	9.69661	0.00532	1.30	0.42		
B	4	0.25826	1.7 [−4]	3.72483	0.03604			0.25826[a]	1.68 [−4][a]
								0.2583[b]	1.83 [−4][b]
								0.258275[c]	1.5 [−4][c]
								0.258205[d]	
								0.258199[e]	
	5	0.24438	1.2 [−4]	4.75031	0.02216	1.62	1.42	0.244385[a]	1.1 [−4][a]
								0.2444[b]	1.14 [−4][b]
								0.244345[d]	
								0.244341[e]	
	6	0.23730	7.0 [−5]	5.75859	0.01508	1.47	1.71	0.237295[a]	6.6 [−5][a]
								0.237265[d]	
								0.237255[e]	
	7	0.23315	4.0 [−5]	6.76424	0.01093	1.38	1.75	0.233155[a]	
								0.233113[e]	
	8	0.23051	3.0 [−5]	7.76723	0.00829	1.32	1.34		
	9	0.22885	1.7 [−4]	8.68562	0.00663	1.25	0.18		
C	5	0.24130	6.9 [−11]	5.11942	0.01908			0.2413[a]	
								0.2413[b]	1.61 [−11][b]
								0.24124[d]	
								0.241293[e]	

(Continues)

TABLE 5 (Continued)

Class	n	$-E_r$	Γ	n^*	$\in_k$	$R_\in$	R_Γ	Other works $-E_r$	Other works Γ
	6	0.23560	3.1 [−12]	6.11354	0.01338	1.43	22.26	0.2356[a]	
								0.235535[d]	
								0.235563[e]	
	7	0.23211	5.6 [−10]	7.11468	0.00988	1.35	0.01	0.2321[a]	
	8	0.22982	4.3 [−9]	8.11226	0.00759	1.31	0.13		
	9	0.22824	1.9 [−8]	9.14566	0.00598	1.27	0.23		

Note: Present results are compared with the available theoretical estimates. Classes A, B, and C represent the dominant configurations 3*dnd* [$n \geq 3$], 3*pnf* [$n \geq 4$], and 3*dng* [$n \geq 5$], respectively. The notation P[±Q] stands for $P \times 10^{\pm Q}$.
[a]Kar and Ho[8]; stabilization method.
[b]Bachau et al[61]; pseudo-potential Feshbach projection operator method.
[c]Ho and Callway[60]; complex rotation method.
[d]Callway[59]; hard wall strategy of stabilization method.
[e]Lipsky et al[58]; truncated diagonalization method.

TABLE 6 The expectation values of repulsive potential $\langle V_r \rangle$, attractive potential $\langle -V_a \rangle$ [their ratio $\eta = \frac{\langle V_r \rangle}{\langle -V_a \rangle}$], interelectronic angles $\langle \theta_{12} \rangle$ (in degree) and different one and two-particle moments for example, $\langle r_1 \rangle$, $\langle r_1^2 \rangle$, $\langle r_{12} \rangle$, $\langle r_{12}^2 \rangle$ for different $^3F^e$ resonances states of *He* below *He* + (3*p*) threshold

Class	*n*	$\langle V_r \rangle$	$\langle -V_a \rangle$	η	$\langle r_1 \rangle$	$\langle r_1^2 \rangle$	$\langle r_{12} \rangle$	$\langle r_{12}^2 \rangle$	$\langle \theta_{12} \rangle$
A	3	1.10 [−1]	7.54 [−1]	1.46 [−1]	6.84 [+0]	6.56 [+1]	1.08 [+1]	1.46 [+2]	97.776
	4	6.67 [−2]	5.98 [−1]	1.12 [−1]	1.07 [+1]	1.61 [+2]	1.83 [+1]	3.77 [+2]	103.335
	5	4.34 [−2]	5.39 [−1]	8.03 [−2]	1.65 [+1]	4.39 [+2]	2.94 [+1]	9.73 [+2]	104.469
	6	2.99 [−2]	5.09 [−1]	5.88 [−2]	2.39 [+1]	1.02 [+3]	4.42 [+1]	2.19 [+3]	105.469
	7	2.18 [−2]	4.91 [−1]	4.44 [−2]	3.28 [+1]	2.05 [+3]	6.21 [+1]	4.32 [+3]	105.932
	8	1.66 [−2]	4.79 [−1]	3.46 [−2]	4.33 [+1]	3.69 [+3]	8.30 [+1]	7.71 [+3]	106.243
	9	1.30 [−2]	4.72 [−1]	2.76 [−2]	5.54 [+1]	6.19 [+3]	1.07 [+2]	1.28 [+4]	106.413
	10	1.11 [−2]	4.68 [−1]	2.37 [−2]	6.97 [+1]	1.03 [+4]	1.34 [+2]	2.05 [+4]	89.384
B	4	6.50 [−2]	5.84 [−1]	1.11 [−1]	1.11 [+1]	1.71 [+2]	1.74 [+1]	3.34 [+2]	89.435
	5	4.12 [−2]	5.31 [−1]	7.76 [−2]	1.75 [+1]	5.05 [+2]	2.97 [+1]	9.93 [+2]	88.397
	6	2.85 [−2]	5.04 [−1]	5.66 [−2]	2.53 [+1]	1.17 [+3]	4.53 [+1]	2.31 [+3]	87.902
	7	2.09 [−2]	4.88 [−1]	4.28 [−2]	3.48 [+1]	2.33 [+3]	6.41 [+1]	4.61 [+3]	87.667
	8	1.59 [−2]	4.77 [−1]	3.34 [−2]	4.57 [+1]	4.16 [+3]	8.58 [+1]	8.27 [+3]	87.424
	9	1.63 [−2]	4.78 [−1]	3.41 [−2]	5.34 [+1]	6.16 [+3]	1.02 [+2]	1.23 [+4]	90.249
C	5	4.07 [−2]	5.24 [−1]	7.77 [−2]	1.67 [+1]	4.45 [+2]	2.73 [+1]	8.17 [+2]	79.635
	6	2.83 [−2]	4.99 [−1]	5.65 [−2]	2.51 [+1]	1.14 [+3]	4.37 [+1]	2.16 [+3]	78.277
	7	2.06 [−2]	4.85 [−1]	4.26 [−2]	3.52 [+1]	2.41 [+3]	6.37 [+1]	4.62 [+3]	77.478
	8	1.58 [−2]	4.75 [−1]	3.31 [−2]	4.68 [+1]	4.42 [+3]	8.68 [+1]	8.56 [+3]	77.139
	9	1.26 [−2]	4.69 [−1]	2.68 [−2]	5.99 [+1]	7.46 [+3]	1.13 [+2]	1.46 [+4]	76.877

Note: Classes A, B, and C represent the dominant configurations 3*dnd* [$n \geq 3$], 3*pnf* [$n \geq 4$], and 3*dng* [$n \geq 5$] respectively. The notation P[±Q] stands for $P \times 10^{\pm Q}$. All values are given in atomic units.

two-particle moments increase gradually for resonance states approaching *He* + (3*p*) threshold. It appears that the electrons are moving apart from each other as well as from the nucleus that establishes the diffused nature of the resonance states as they approach *He* + (3*p*) threshold. The last column of Table 6 shows that the expectation values of $\langle \theta_{12} \rangle$ increase for class A and decrease for classes B and C, as the resonance states come closer to *He* + (3*p*) threshold.

We have estimated the two particle probability density [$\rho(r_1, r_2)$] for a better understanding of the classification of states. The probability density $\rho(r_1, r_2)$ is being calculated by using the formula as,

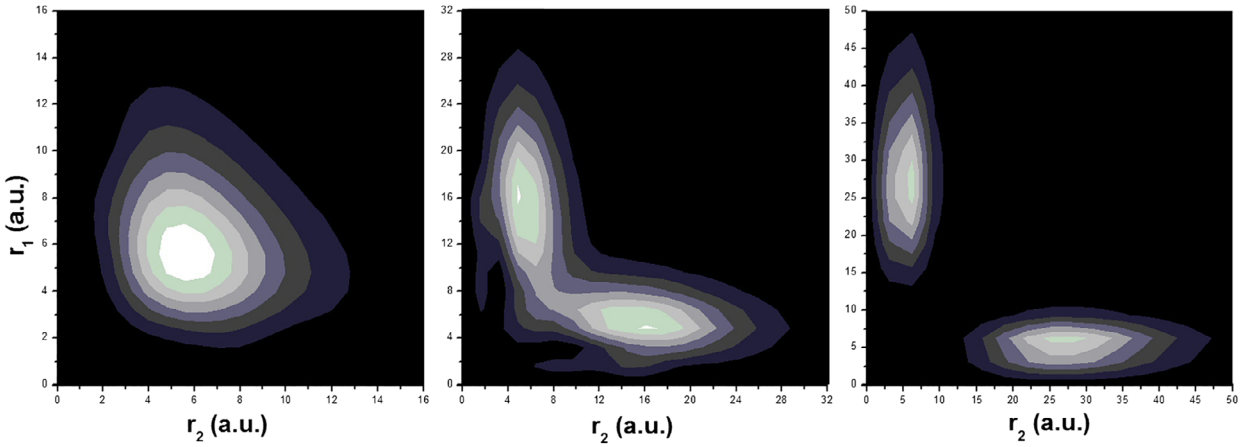

FIGURE 4 Two particle probability density $\rho(r_1, r_2)$ for the three $^3F^e$ resonance states of He atom [lying below $He^+(3p)$ threshold] having dominant $3d^2$ (left), $3p4f$ (middle), and $3d5g$ (right) configurations

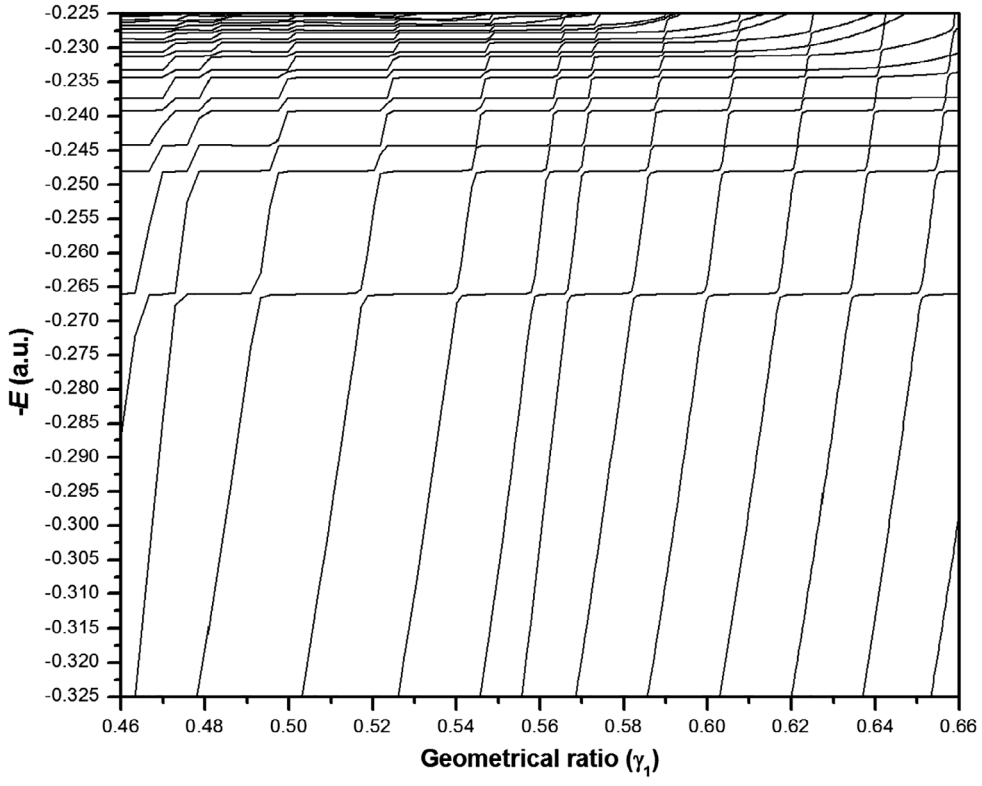

FIGURE 5 Stabilization plot for $^3F^e$ states of neutral He atom in the energy range −0.325 a.u. to −0.225 a.u. First 60 diagonalized energy eigenroots are plotted for N = 900 number of terms in the Hyllerass-type wavefunction comprises of only *pf* configuration

$$\rho(r_1, r_2) = \int_{\theta=0}^{\pi}\int_{\varphi=0}^{2\pi}\int_{\psi=0}^{2\pi}\int_{r_{12}=|r_1\sim r_2|}^{r_1+r_2} |\Psi|^2 d\tau \tag{10}$$

where, the volume element is $d\tau = sin\theta d\theta d\phi d\psi r_{12} dr_{12}$. Two particle radial probability density $\rho(r_1, r_2)$ for the $^3F^e$ resonance states of *He* having configurations $3d^2$ (class A), $3p4f$ (class B), and $3d5g$ (class C) lying below $He^+(3p)$ threshold are plotted in Figure 4. The density plot for $3d^2$ configuration exhibits similar behavior as that of the helium ground state, that is, the density plot shows a maximum along the symmetry line $r_1 = r_2$. In contrast, the maximum probability density appears at two different regions on the either sides of the symmetry line for both $3p4f$ and $3d5g$ configurations. The difference of the features of two particle radial probability density between the $3p4f$ and $3d5g$ configurations lies in the fact that there is a small probability density along $r_1 = r_2$ for the former state, while vanishes for the latter in Figure 4.

Figure 5 shows the stabilization diagram in the energy range −0.325 a.u. to −0.225 a.u. by using 900 terms in the nine exponent wavefunction where *dd* configuration is excluded. The necessity of the inclusion of the *dd* configuration in the wavefunction would be realized if we compare the

TABLE 7 Positions ($-E_r$ in a.u.), widths (Γ in a.u.), effective quantum number (n^*), the ratio between expectation values of repulsive potential $\langle V_r \rangle$, attractive potential $\langle -V_a \rangle$ [$\eta = \frac{\langle V_r \rangle}{\langle -V_a \rangle}$], interelectronic angles $\langle \theta_{12} \rangle$ (in degree) and different one and two-particle moments for example, $\langle r_1 \rangle$, $\langle r_1^2 \rangle$, $\langle r_{12} \rangle$, $\langle r_{12}^2 \rangle$ for different $^3F^e$ resonances states of *He* below *He* + (4*p*) threshold

States	$-E_r$	Γ	n^*	η	$\langle r_1 \rangle$	$\langle r_1^2 \rangle$	$\langle r_{12} \rangle$	$\langle r_{12}^2 \rangle$	$\langle \theta_{12} \rangle$
1	0.22207	1.8 [−4]	2.26956	3.28 [−2]	5.73 [+1]	7.72 [+3]	1.09 [+2]	1.54 [+4]	89.085
2	0.2187	2.1 [−4]	2.31001	4.02 [−2]	4.76 [+1]	5.47 [+3]	9.02 [+1]	1.09 [+4]	89.448
3	0.21389	3.1 [−4]	2.37169	4.76 [−2]	4.02 [+1]	3.98 [+3]	7.56 [+1]	7.96 [+3]	90.454
4	0.20705	3.7 [−4]	2.46857	5.50 [−2]	3.40 [+1]	2.91 [+3]	6.29 [+1]	5.79 [+3]	88.530
5	0.19788	5.3 [−4]	2.61927	6.33 [−2]	2.92 [+1]	2.19 [+3]	5.34 [+1]	4.38 [+3]	89.512
6	0.18903	5.4 [−4]	2.79443	1.04 [−1]	1.67 [+1]	7.45 [+2]	2.95 [+1]	1.58 [+3]	104.178
	0.18822[a]	2.78 [−3][a]							
7	0.18404	2.4 [−4]	2.91012	8.64 [−2]	2.21 [+1]	1.33 [+3]	3.96 [+1]	2.68 [+3]	94.377
8	0.17834	1.2 [−3]	3.06167	1.27 [−1]	1.49 [+1]	5.32 [+2]	2.39 [+1]	1.07 [+3]	91.943
	0.17892[a]	3.0 [−3][a]							
9	0.16668	9.2 [−4]	3.46354	9.77 [−2]	1.99 [+1]	1.06 [+3]	3.42 [+1]	2.11 [+3]	89.631
	0.16633[a]	1.33 [−3][a]							
10	0.15878	6.0 [−5]	3.84729	1.10 [−1]	1.82 [+1]	6.79 [+2]	3.06 [+1]	1.45 [+3]	100.183
	0.15879[a]	2.8 [−5][a]							
11	0.15778	2.6 [−4]	3.90553	1.07 [−1]	1.79 [+1]	5.09 [+2]	3.15 [+1]	1.23 [+3]	110.336
	0.15788[a]	1.28 [−3][a]							
12	0.15224	5.9 [−4]	4.28431	1.08 [−1]	2.04 [+1]	8.34 [+2]	3.34 [+1]	1.67 [+3]	90.229
	0.15224[a]	1.3 [−3][a]							
13	0.1476	3.0 [−4]	4.70360	1.24 [−1]	1.81 [+1]	4.57 [+2]	2.83 [+1]	9.18 [+2]	90.594
	0.14759[a]	3.3 [−4][a]							
14	0.14685	1.2 [−4]	4.78364	1.02 [−1]	2.21 [+1]	9.99 [+2]	3.76 [+1]	2.05 [+3]	93.799
15	0.1455	4.0 [−5]	4.93864	9.21 [−2]	2.24 [+1]	7.48 [+2]	3.88 [+1]	1.70 [+3]	103.584
16	0.14514	9.0 [−5]	4.98259	1.19 [−1]	1.93 [+1]	5.33 [+2]	2.93 [+1]	1.01 [+3]	85.276
17	0.1434	5.0 [−4]	5.21286	9.03 [−1]	2.19 [+1]	1.01 [+3]	3.82 [+1]	2.11 [+3]	95.959
18	0.14075	4.4 [−4]	5.63436	9.13 [−2]	2.55 [+1]	1.08 [+3]	4.30 [+1]	2.21 [+3]	92.365
19	0.13998	2.4 [−4]	5.77735	9.49 [−2]	2.58 [+1]	1.06 [+3]	4.26 [+1]	2.08 [+3]	88.699
20	0.13925	1.7 [−4]	5.92348	7.72 [−2]	2.97 [+1]	1.47 [+3]	5.40 [+1]	3.35 [+3]	109.571
21	0.13877	3.6 [−4]	6.02584	8.38 [−2]	2.80 [+1]	1.31 [+3]	4.88 [+1]	2.79 [+3]	97.637
22	0.13747	9.0 [−5]	6.33215	7.27 [−2]	3.48 [+1]	2.48 [+3]	6.18 [+1]	4.91 [+3]	88.794
23	0.13564	5.0 [−5]	6.85510	5.97 [−2]	3.97 [+1]	2.75 [+3]	7.47 [+1]	6.24 [+3]	115.556
25	0.13314	8.0 [−5]	7.83741	6.02 [−2]	4.52 [+1]	3.91 [+3]	8.15 [+1]	7.88 [+3]	92.945
26	0.13154	1.0 [−4]	8.74371	5.39 [−2]	5.54 [+1]	6.14 [+3]	1.01 [+2]	1.23 [+4]	89.327
27	0.13032	2.0 [−4]	9.69458	5.54 [−2]	6.19 [+1]	8.14 [+3]	1.14 [+2]	1.63 [+4]	88.458
28	0.12878	2.9 [−4]	11.50109	4.97 [−2]	7.26 [+1]	1.16 [+4]	1.35 [+2]	2.32 [+4]	89.766
29	0.12766	2.1 [−4]	13.71021	4.86 [−2]	7.24 [+1]	1.18 [+4]	1.35 [+2]	2.35 [+4]	88.858
30	0.12588	1.8 [−4]	23.83656	5.90 [−2]	5.76 [+1]	8.03 [+3]	1.07 [+2]	1.62 [+4]	96.553

Note: The notation $P[\pm Q]$ stands for $P \times 10^{\pm Q}$. All values are given in atomic units.

[a]Using the products of Slater-orbital type wave functions with expansion lengths up to 319 terms by complex coordinate method.[65]

stabilization diagrams for the same energy range as given in Figures 2 and 5. In Figure 2 the first appearance of the flat plateau above $He^+(2p)$ threshold is at −0.31075 a.u. corresponding to the $3d^2$ configuration while the same appears at −0.26607 a.u. in Figure 5. Hence, it is clear that the inclusion of the *dd* configuration in the wavefunction contributes 14% to the resonance energy value for the $3d^2$ configuration. We have found that the above contribution decreases as we move toward the $He^+(3p)$ threshold for example, it decreases to 3% for the sixth resonance state below the $He^+(3p)$ threshold. It is known that the higher configurations can be included in the wavefunction through the powers of r_{12}. Bhatia[52] opined that for D^o states arising from *pd* configuration, the inclusion of the *df* configuration will facilitate the convergence of the metastable bound energies.

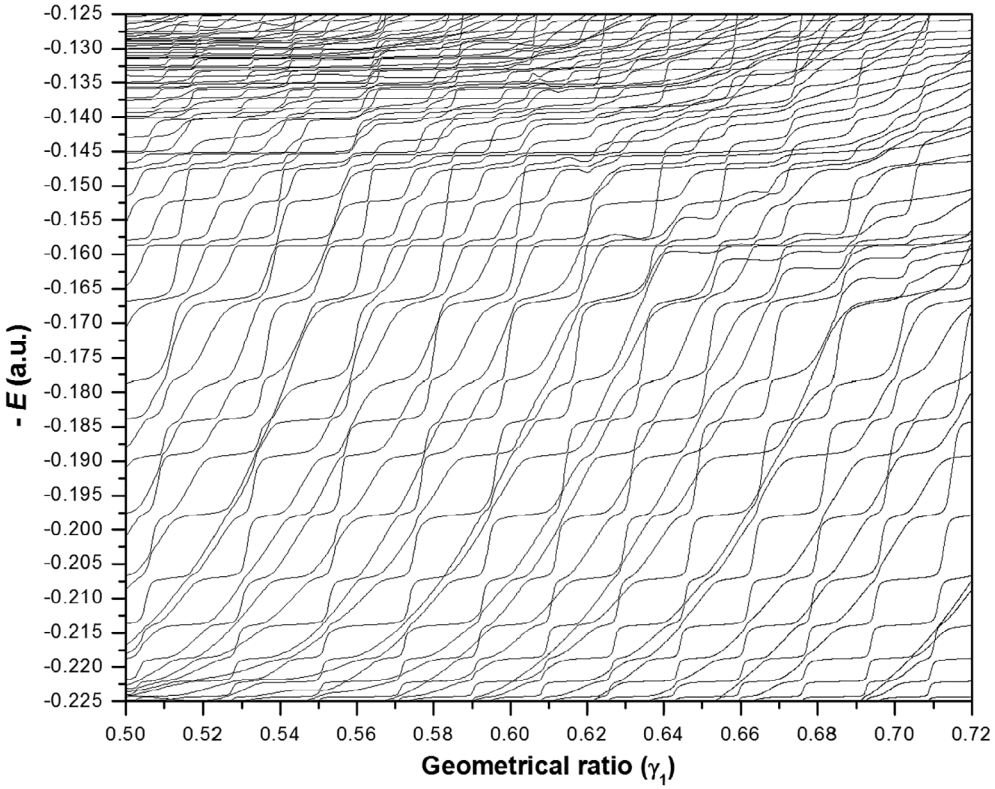

FIGURE 6 Stabilization plot for $^3F^e$ states of neutral He atom in the energy range −0.225 a.u. to −0.125 a.u. Twenty-fifth to 125th diagonalized energy eigenroots are plotted for N = 1530 number of terms in the symmetric nine exponent Hylleraas-type basis set

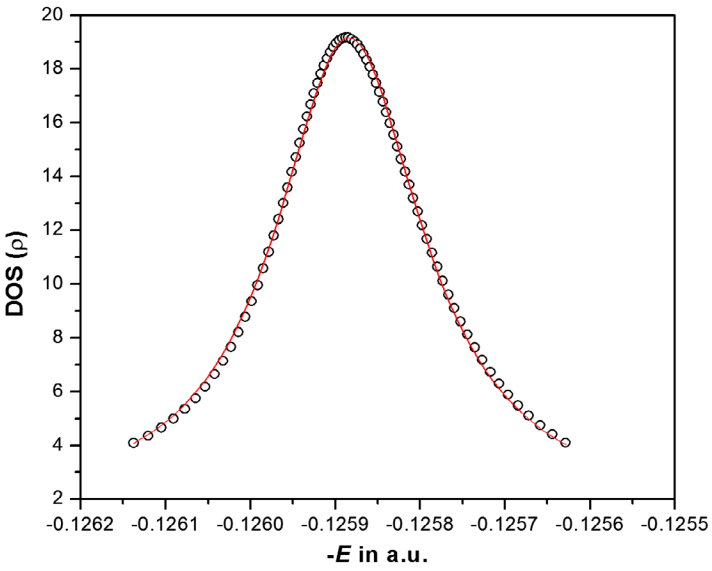

FIGURE 7 Calculated DOS (hollow circles) of 67th root and the fitted Lorentzian (red line) for the highest-lyng $^3F^e$ resonance state of He atom below $He^+(4p)$ threshold. The resonance parameters E_r = 0.12588 a.u. and Γ = 0.00018 a.u. are obtained with $\chi^2 = 2.8 \times 10^{-2}$

Such improvement of convergence is also observed in the present work, where the *dd* configuration contributes 0.001% to the energy of the metastable bound $2p4f$ state as mentioned in Section 3.1. The fact that the contribution of *dd* configuration rises to 14% while calculating resonance parameters of $3d^2$ state indicates the absolute necessity of the inclusion of *dd* configuration in the wavefunction. We are of the opinion that it is not possible to include *dd* configuration by just increasing the powers of r_{12} in the *pf* configuration, because the resonance position of $3d^2$ state is lower than that of $3p4f$ state. This insight will be useful while calculating the resonance parameters of such higher symmetry states in future.

Resonance energy (E_r) and width (Γ) of first 30 $^3F^e$ resonance states between *He* + (3*p*) and *He* + (4*p*) thresholds are summarized in Table 7. The $^3F^e$ resonances below *He* + (4*p*) threshold can arise from $4dnd$ [$n \geq 4$], $4pnf$ [$n \geq 4$], $4fnf$ [$n \geq 4$], $4fnh$ [$n \geq 6$], and $4dng$ [$n \geq 5$] dominant configurations. Different structural parameters, for example, n^*, $\langle V_r \rangle$, $\langle -V_a \rangle$, $\eta = \frac{\langle V_r \rangle}{\langle -V_a \rangle}$, $\langle \theta_{12} \rangle$, $\langle r_1 \rangle$, $\langle r_1^2 \rangle$, $\langle r_{12} \rangle$ and $\langle r_{12}^2 \rangle$ of the respective resonance states are also given in Table 7 with a view to classify them according to the dominant configurations. It is clear from Table 7 that in contrast to the resonances below *He* + (3*p*) threshold, any such systemic trend of the structural parameters can hardly be found for the classification of resonance states below *He*

TABLE 8 Positions ($-E_r$ in a.u.), widths (Γ in a.u.), effective quantum number (n^*) for different $^3F^e$ resonances states of *He* below *He* + (5*p*), *He* + (6*p*), and *He* + (7*p*) threshold

	Below *He* + (5*p*)			Below *He* + (6*p*)			Below *He* + (7*p*)		
States	$-E_r$	Γ	n^*	$-E_r$	Γ	n^*	$-E_r$	Γ	n^*
1	0.12385	6.2 [−5]	3.37676	0.07941	6.0 [−5]	4.57825	0.05346	2.5 [−4]	6.28851
	0.12408[a]	2.52 [−3][a]							
2	0.12187	1.5 [−5]	3.45568	0.07723	4.3 [−4]	4.80298	0.05297	2.6 [−4]	6.41403
3	0.12058	2.3 [−4]	3.51017	0.07604	3.8 [−4]	4.94052	0.05104	3.3 [−4]	6.99328
4	0.11920	3.8 [−4]	3.57142	0.07557	1.3 [−4]	4.99819	0.05082	3.8 [−4]	7.06976
	0.11944[a]	3.44 [−3][a]							
5	0.11898	2.5 [−4]	3.58149	0.07445	3.0 [−4]	5.14420	0.05024	1.0 [−4]	7.28408
6	0.11760	5.1 [−4]	3.64662	0.07292	2.8 [−4]	5.36604	0.05005	1.4 [−4]	7.35864
7	0.11656	6.5 [−4]	3.69812	0.07175	7.1 [−4]	5.55650	0.04859	1.2 [−4]	8.01995
	0.11537[a]	2.61 [−3][a]							
8	0.11427	6.7 [−5]	3.81968	0.06709	7.4 [−4]	6.58395	0.04686	1.5 [−4]	9.09566
9	0.11312	6.7 [−4]	3.88543	0.06686	3.0 [−4]	6.65059	0.04516	1.6 [−4]	10.72893
10	0.11224	3.5 [−4]	3.93810	0.06494	2.1 [−4]	7.29929	0.04290	1.7 [−4]	15.49066
11	0.11085	5.5 [−4]	4.02584	0.06438	2.9 [−4]	7.52733			
12	0.10926	7.0 [−4]	4.13378	0.06263	1.3 [−4]	8.40695			
	0.1094[a]	2.99 [−3][a]							
13	0.10822	1.3 [−4]	4.20926	0.06228	2.6 [−4]	8.62296			
14	0.10638	1.2 [−4]	4.35359	0.06139	8.0 [−5]	9.25731			
	0.10676[a]	0.92 [−4][a]							
15	0.10539	2.6 [−4]	4.43765	0.06007	5.2 [−4]	10.52404			
	0.10577[a]	1.48 [−3][a]							
16	0.10394	2.6 [−4]	4.57007	0.05819	7.0 [−4]	13.77655			
17	0.10227	2.0 [−4]	4.73832	0.05717	3.6 [−4]	17.59841			
	0.10252[a]	0.89 [−3][a]							
18	0.10191	2.2 [−4]	4.77709	0.05564	1.2 [−4]	76.94837			
19	0.10008	8.4 [−5]	4.99002						
20	0.09803	2.1 [−4]	5.26651						
21	0.09753	8.8 [−5]	5.34064						
22	0.09572	2.5 [−4]	5.63901						
23	0.09285	2.0 [−4]	6.23831						
24	0.09044	3.3 [−4]	6.91880						
25	0.08871	1.4 [−4]	7.57706						
26	0.08775	8.7 [−5]	8.03167						
27	0.08691	1.1 [−4]	8.50578						
28	0.085845	6.8 [−5]	9.24895						
29	0.085052	1.2 [−4]	9.94840						
30	0.084614	1.9 [−4]	10.40989						
31	0.083472	7.6 [−5]	12.00038						
32	0.082917	1.4 [−4]	13.09232						
33	0.08171	2.1 [−4]	17.09963						

Note: The notation $P[\pm Q]$ stands for $P \times 10^{\pm Q}$. All values are given in atomic units.

[a]Using the products of Slater-orbital type wave functions with expansion lengths up to 319 terms by complex coordinate method.[65]

+(4*p*) threshold. Hence, it can be concluded that as we move toward the continuum above $He^+(3p)$ threshold the contributions of different configurations become appreciable to an extent such that it is impossible to assign a dominant configuration to the resonance state. Figure 6 shows the stabilization diagram between $He^+(3p - 4p)$ threshold. The resonance parameters E_r = −0.12588 a.u. and Γ = 0.00018 a.u. obtained from 67th root is shown in Figure 7. Finally, the resonance parameters for resonance states lying between $He^+(4p\text{-}7p)$ threshold are given in the Table 8.

4 | CONCLUSIONS

In the present work, we have investigated the doubly excited $^3F^e$ metastable bound and resonance states of neutral helium atom using explicitly correlated Hylleraas type wavefunctions in the framework of the Ritz variational principle and stabilization method, respectively. The explicit inclusion of *dd* configuration results in better convergence of the energy values of metastable bound states. The effect of such inclusion in the wavefunction is remarkable in determining the parameters of the resonance states. A justification of the classification of the resonance states is given by estimating several structural properties. It can be concluded that the use of "soft wall" strategy of the stabilization method with a sufficient number of terms in the Hylleraas basis set may yield accurate resonance parameters as well as provide useful structural information for a wide range of resonance states of helium. The present method may be extended for other resonances of different symmetries where such kind of explicit configuration mixing is extremely necessary.

ACKNOWLEDGMENTS

J.K.S. acknowledges the partial financial support from the DHESTB, Govt. of West Bengal, India under grant number 249(Sanc.)/ST/P/S&T/16G-26/2017.

ORCID

Jayanta K. Saha https://orcid.org/0000-0002-1159-1905
Tapan K. Mukherjee https://orcid.org/0000-0001-7247-5337

REFERENCES

[1] G. Tanner, K. Richter, J. M. Rost, *Rev. Mod. Phys.* **2000**, *72*, 497 and references therein.
[2] M. Bylicki, C. Nicolaides, *Phys. Rev A* **2000**, *61*, 052508.
[3] M. Bylicki, C. Nicolaides, *Phys. Rev A* **2000**, *61*, 052509.
[4] M. Zitnik, K. Bucar, M. Stuhec, F. Penent, R. I. Hall, P. Lablanquie, *Phys. Rev. A* **2002**, *65*, 032520.
[5] T. K. Mukherjee, P. K. Mukherjee, *Phys. Rev. A* **2004**, *69*, 064501.
[6] S. Kar, Y. K. Ho, *J. Phys. B* **2007**, *40*, 1403.
[7] S. Bhattacharyya, T. K. Mukherjee, J. K. Saha, P. K. Mukherjee, *Phys. Rev. A* **2008**, *78*, 032505.
[8] S. Kar, Y. K. Ho, *Int. J. Quant. Chem.* **2008**, *108*, 1491.
[9] S. Kar, Y. K. Ho, *Phys. Rev. A* **2009**, *79*, 062508.
[10] J. K. Saha, T. K. Mukherjee, *Phys. Rev. A* **2009**, *80*, 022513.
[11] J. Eiglsperger, B. Piraux, J. Madronero, *Phys. Rev. A* **2010**, *81*, 042527.
[12] J. Eiglsperger, B. Piraux, J. Madronero, *Phys. Rev. A* **2010**, *81*, 042528.
[13] J. K. Saha, S. Bhattacharyya, T. K. Mukherjee, *J. Chem. Phys.* **2010**, *132*, 134107.
[14] J. K. Saha, S. Bhattacharyya, P. K. Mukherjee, T. K. Mukherjee, *Chem. Phys. Lett.* **2011**, *517*, 223.
[15] S. Kar, Z. Jiang, *At. Data Nu. Data Tab.* **2015**, *102*, 42.
[16] S. Kar, Y. Wang, W. Qi Li, X. D. Sun, *Few-Body Syst.* **2015**, *56*, 651.
[17] J. P. R. Cuartas, J. L. Sanz-Vicario, *Phys. Rev. A* **2015**, *91*, 052301.
[18] X. Q. Hu, Y. Wang, Z. Jiang, P. Jiang, S. Kar, *Phys. Plasmas* **2015**, *22*, 112107.
[19] A. Igarashi, *Eur. Phys. J. D* **2016**, *70*, 216.
[20] F. F. Goryaev, L. A. Vainshtein, A. M. Urnov, *At. Data Nucl. Data Tables* **2017**, *113*, 117.
[21] A. Ghoshal, Y. K. Ho, *Phys. Rev. A* **2017**, *95*, 052502.
[22] J. H. Ou, Y. K. Ho, *Chem. Phys. Lett.* **2017**, *689*, 116.
[23] V. I. Pupyshev, H. E. Montgomery, *Theor. Chem. Acc.* **2017**, *136*, 138.
[24] S. Dutta, A. N. Sil, J. K. Saha, T. K. Mukherjee, *Int. J. Quant. Chem.* **2017**, *118*, e25577.
[25] S. Kar, Y. K. Ho, *Phys. Lett. A* **2018**, *382*, 1787.
[26] S. Kar, Y. K. Ho, *Eur. Phys. J. D* **2018**, *72*, 193.
[27] A. K. Bhatia, A. Temkin, *Phys. Rev. A* **1975**, *11*, 2018.
[28] A. K. Bhatia, A. Temkin, *Phys. Rev. A* **1984**, *29*, 1895.
[29] A. K. Bhatia, *Atoms* **2016**, *4*, 27 and references therein.
[30] D. H. Oza, *Phys. Rev. A* **1986**, *33*, 824.

[31] A. S. Kadyrov, I. Bray, *J. Phys. B: At. Mol. Opt. Phys.* **2016**, *49*, 222002 and references therein.
[32] C. Froese-Fischer, M. Indrees, *J. Phys. B* **1990**, *23*, 679.
[33] T. Carette, J. M. Dahlström, L. Argenti, E. Lindroth, *Phys. Rev. A* **2013**, *87*, 023420 and references therein.
[34] J. Tang, S. Watanabe, M. Matsuzawa, *Phys. Rev. A* **1992**, *46*, 2437.
[35] A. Igarashi, N. Toshima, *Eur. Phys. J. D* **2008**, *46*, 425 and references therein.
[36] E. Lindroth, *Phys. Rev. A* **1994**, *49*, 4413.
[37] Y. K. Ho, *J. Phys. B* **1979**, *12*, 387.
[38] V. A. Mandelshtam, T. R. Ravuri, H. S. Taylor, *Phys. Rev. Lett.* **1993**, *70*, 1932.
[39] J. Muller, X. Yang, J. Burgdorfer, *Phys. Rev. A* **1994**, *49*, 2470.
[40] S. S. Tan, Y. K. Ho, *Chin. J. Phys.* **1997**, *35*, 701.
[41] G. W. F. Drake, A. Dalgarno, *Phys. Rev. A* **1970**, *1*, 1325.
[42] E. Holøien, *Nucl. Instrum. Methods* **1970**, *90*, 229.
[43] P. Feldman, R. Novick, *Phys. Rev. Lett.* **1963**, *11*, 278.
[44] T. W. Gorczyca, J. -E. Rubensson, C. Sathe, M. Strom, M. Agaker, D. Ding, S. Stranges, R. Richter, M. Alagia, *Phys. Rev. Lett.* **2000**, *85*, 1202.
[45] M. K. Odling-Smee, E. Sokell, P. Hammond, M. A. MacDonald, *Phys. Rev. Lett.* **2000**, *84*, 2598.
[46] J. G. Lambourne, F. Penent, P. Lablanquie, R. I. Hall, M. Ahmad, M. Zitnik, K. Bucar, M. K. Odling-Smee, J. R. Harries, P. Hammond, D. K. Waterhouse, S. Stranges, R. Richter, M. Alagia, M. Coreno, M. Ferianis, *Phys. Rev. Lett.* **2003**, *90*, 153004.
[47] S. Kasthurirangan, J. K. Saha, A. Agnihotri, S. Bhattacharyya, D. Misra, A. Kumar, P. K. Mukherjee, J. P. Santos, A. M. Costa, P. Indelicato, T. K. Mukherjee, L. C. Tribedi, *Phys. Rev. Lett.* **2013**, *111*, 243201.
[48] E. Holøien, *J. Chem. Phys.* **1958**, *29*, 676. *Phys. Norv.* **1961**, *1*, 53.
[49] A. K. Bhatia, *Phys. Rev. A* **1970**, *2*, 1667.
[50] Y. K. Ho, A. K. Bhatia, *Phys. Rev. A* **1993**, *47*, 2628.
[51] H. Doyle, M. Openheimer, G. W. F. Drake, *Phys. Rev. A* **1972**, *5*, 26.
[52] A. K. Bhatia, *Phys. Rev. A* **1972**, *6*, 2498. *Phys. Rev. A* **1972**, *6*, 120.
[53] A. K. Bhatia, *Phys. Rev. A* **1977**, *15*, 1315.
[54] S. R. Samanta, M. A. Ali, *J. Phys. B* **1977**, *10*, 2073.
[55] R. Bruch, G. Paul, J. Andra, L. Lipsky, *Phys. Rev. A* **1975**, *12*, 1808.
[56] H. W. van der Hart, J. E. Hansen, *J. Phys. B* **1993**, *26*, 641.
[57] D. R. Herrick, O. Sinanoglu, *Phys. Rev. A* **1975**, *11*, 97.
[58] L. Lipsky, R. Anania, *At. Data Nu. Data Tab.* **1977**, *20*, 127.
[59] J. Callaway, *Phys. Lett.* **1978**, *66A*, 201.
[60] Y. K. Ho, J. Callaway, *J. Phys. B* **1985**, *18*, 3481.
[61] H. Bachau, F. Martin, A. Riera, M. Yanez, *At. Data Nu. Data Tab.* **1991**, *48*, 167.
[62] A. K. Bhatia, A. Temkin, *Rev. Mod. Phys.* **1964**, *36*, 1050.
[63] T. K. Mukherjee, P. K. Mukherjee, *Phys. Rev. A* **1994**, *50*, 850.
[64] J. A. Nelder, R. Mead, *Comput. J.* **1965**, *7*, 308.
[65] Y. K. Ho, *Z. Phys. D* **1989**, *11*, 277.

How to cite this article: Dutta S, Sil AN, Saha JK, Mukherjee TK. Extensive investigations for metastable-bound and resonance $^3F^e$ states of He atom. *Int J Quantum Chem*. 2019;e25981. https://doi.org/10.1002/qua.25981

Commun. Theor. Phys. **71** (2019) 853–860 Vol. 71, No. 7, July 1, 2019

Doubly Excited $^{1,3}F^e$ States of Two-Electron Atoms under Weakly Coupled Plasma Environment*

S. Dutta,[1,2] J. K. Saha,[3,†] S. Bhattacharyya,[4] and T. K. Mukherjee[2]

[1]Belgharia Texmaco Estate School, Belgharia, Kolkata 700056, India

[2]Department of Physics, Narula Institute of Technology, Agarpara, Kolkata 700109, India

[3]Department of Physics, Aliah University, IIA/27, Newtown, Kolkata 700160, India

[4]Department of Physics, Acharya Prafulla Chandra College, New Barrackpore, Kolkata 700131, India

(Received December 31, 2018; revised manuscript received February 28, 2019)

Abstract *Precise energy eigenvalues of metastable bound doubly excited $^{1,3}F^e$ states originating from $2pnf$ ($n = 4$–6) configuration of helium-like ions ($Z = 2$–4) under weakly coupled plasma (WCP) environment have been estimated within the framework of Ritz variational method. The wavefunction is expanded in explicitly correlated Hylleraas type basis set. The screened Coulomb potential is consideredas mimic the WCP environment. The atomic systems tend towards gradual instability and the number of excited metastable bound states reduces with increasing plasma strength. The wavelengths corresponding to $2pnf$ ($^{1,3}F^e$) $\rightarrow$ $2pn'd$ ($^{1,3}D^o$) ($n = 4$–6; $n' = 3$–6) transitions occurring between doubly excited states of plasma embedded two-electron ions are also reported.*

DOI: 10.1088/0253-6102/71/7/853

Key words: two-electron atom, doubly excited states, variational method, weakly coupled plasma, Hylleraas co-ordinate

1 Introduction

Doubly excited states (DESs) of two-electron atom is a topic of active interest in recent times, both from theoretical and experimental aspects.[1−9] The abundance of such DESs is noted in various astrophysical observations as well as in high temperature laboratory plasma.[10−19] The DESs of two-electron atom having unnatural parity ($\pi = (-1)^{L+1}$, L is the total angular momentum quantum number) and lying below the second ionization threshold, are metastable bound. These states favorably can decay to a lower state via radiative process rather than decaying through non-radiative autoionization channel. Examples of such DESs of unnatural parity are $^{1,3}P^e$, $^{1,3}D^o$, $^{1,3}F^e$ states arising out of dominant pp, pd, pf configurations respectively.

Atomic systems under external environments have been studied by various researchers during the past several decades, as they provide useful information about the environment. A large number of investigations[20−30] are there in the literature on the modified properties of plasma embedded atomic systems. Extensive review articles[31−32] are available on this topic. Plasma coupling strength (Γ) is defined as the ratio between average inter-particle electrostatic energy to the average thermal kinetic energy. The high temperature and low density classical plasma are categorized as weakly coupled ($\Gamma < 1$). According to the Debye-Hückel theory[33] a short range Yukawa-type or screened Coulomb model potential is considered to mimic the modified inter-particle interaction under WCP environment. Due to its simplicity and effectiveness, such screened Coulomb potential has been used widely by researchers for the investigation of spectral and structural properties of atomic systems under WCP environment. In this model, plasma electron density (n_e) and temperature (T) are combinedly expressed through the plasma screening length (D).[33] As the screened Coulomb potential is more positive in nature than the "pure" Coulomb potential, in general, with the decrease of plasma screening length (D), the energy levels are pushed up and the gap between two successive energy level decreases.[20] This causes the transition energy to decrease and a red shift[21] may be observed. However, it is remarkable that for some specific transitions between two doubly excited energy levels, the wavelengths get blue shifted or show a pattern with both red and blue shift *w.r.t.* the plasma screening length (D).[21]

In the present work, we have estimated the non-relativistic energy eigenvalues of doubly excited metastable bound $2pnf$ ($n = 4$–6) ($^{1,3}F^e$) states of two-electron ions ($Z = 2$–4) as well as the $2s$ and $2p$ states of the respective one-electron ions under WCP environment. According to the Debye-Hückel theory,[33] in a two-electron Hamilto-

*Supported under Grant No. EMR/2017/000737 from DST-SERB, Govt. of India, Grant No. 23(Sanc.)/ST/P/S&T/16G-35/2017 from DHESTB, Govt. of West Bengal, India, and by the DHESTB, Govt. of West Bengal, India under Grant No. 249(Sanc.)/ST/P/S&T/16G-26/2017

†E-mail: jksaha.phys@aliah.ac.in

nian, the effect of plasma screening should be reflected in both the one-particle electron-nucleus attraction terms and the electron-electron repulsion term of the total potential. Although the effect of screening on the electron-nucleus attraction term predominates overthe electron-electron repulsion term in determining the properties of plasma embedded two electron atom, we have considered the effect of screening on both attractive electron-nucleus part and repulsive electron-electron part in the potential. Computationally, it is difficult to include the effect of screening in repulsive electron-electron part even for a partially correlated CI type basis constructed with Slater-type orbitals as the analytic solution of the corresponding basis integrals becomes extremely cumbersome.[34−35] However, we have been able to develop the methodology to estimate the basis integral for the trial wavefunction is expanded in multi-exponent Hylleraas type basis set in a way that the effect of screening in repulsive electron-electron part has been considered fully without any perturbative approximation. Ritz variational method is used to determine the energy eigenroots. The wavelengths for the dipole allowed transitions between doubly excited metastable bound states $2pnf$ [n = 4–6] (^{1,3}F^e) and $2pn'd$ (n' = 3–6) (^{1,3}D^o) are determined for different values of plasma screening length (D). The non-relativistic energy-eigenvalues of $2pnd$ (n = 3–6) (^{1,3}D^o) states are taken from an earlier work of Saha *et al.*[21] The details of the methodology are given in Sec. 2 followed by the discussion on the results in Sec. 3 and finally concluded in Sec. 4.

2 Method

The non-relativistic Hamiltonian (in a.u.) of a two-electron atom immersed in WCP environment may be written as

$$H = \sum_{i=1}^{2} \Big(-\frac{1}{2}\nabla_i^2 - Z\frac{\mathrm{e}^{-r_i/D}}{r_i}\Big) + \frac{\mathrm{e}^{-r_{12}/D}}{r_{12}}\,, \qquad (1)$$

where, in case of screening by both ions and electrons, the Debye screening length (D) reads as[33]

$$D = \Big(\frac{kT}{4\pi(1+Z_e)n_e}\Big)^{1/2}. \qquad (2)$$

For a fully ionized plasma comprising of a single nuclear species, the effective nuclear charge is $Z_e = Z$ whereas in case of screening by electrons only, $Z_e = 0$. After seperation of the centre of mass coordinates, the wave function of ^{1,3}F^e states due to dominant pf configuration of a two-electron atom can be written in terms of six co-ordinates $(r_1, r_2, \theta_{12}; \theta, \varphi, \psi)$ as,[36−37]

$$\Psi = f_3^0 D_3^0 + f_3^{2+} D_3^{2+} + f_3^{2-} D_3^{2-}\,, \qquad (3)$$

where, $D_L^{\kappa\pm}$ are the rotational harmonics and functions of three Eulerian angles (θ, φ, ψ) that define the orientation of the triangle formed by the two electrons and the nucleus in space; κ is the angular momentum quantum number about the body fixed axis of rotation.[36] The radial parts of the wavefunction are given by $f_3^0 = -F_1 \sin\theta_{12}$, $f_3^{2+} = (\sqrt{15}/6)F_1 \sin 2\theta_{12}$ and $f_3^{2-} = (\sqrt{15}/6)F_2(1-\cos 2\theta_{12})$; where, $F_1 = (f \mp \tilde{f})$, $F_2 = (f \pm \tilde{f})$ with the condition $\tilde{f} = f(r_2, r_1)$ and θ_{12} is the angle between $\vec{r}_1$ and $\vec{r}_2$. The upper sign corresponds to the singlet state and the lower sign to the triplet state. The trial radial wave function corresponding to pf configurations is expanded in Hylleraas basis set as

$$\begin{aligned} f(r_1, r_2, r_{12}) = &\sum_{i=1}^{A} r_1^{l_i+3}\; r_2^{m_i+1}\; r_{12}^{n_i} \\ &\times \Big[\sum_{k_1=1}^{p} C_{ik_1k_1}\eta_{k_1}(1)\eta_{k_1}(2) \\ &+ \sum_{k_1=1}^{p}\sum_{k_2=1}^{p} C_{ik_1k_2}\eta_{k_1}(1)\eta_{k_2}(2)\Big]\,, \end{aligned} \qquad (4)$$

with the features: (a) The powers of r_1, r_2 and r_{12} satisfies $(l_i, m_i, n_i) \geq (0,0,0)$; (b) A is the total number of (l_i, m_i, n_i) set considered in the calculation; (c) $\eta_i(j) = \mathrm{e}^{-\rho_i r_j}$ are the Slater-type orbitals where ρ's are the non-linear parameters; (d) p denotes the total number of non-linear parameters; (e) In the double sum of Eq. (4), $k_1 < k_2$; (f) $C_{ik_1k_2}$ are the linear variational parameters. The effect of the radial correlation is incorporated through different ρ's in the wave function whereas, the angular correlation effect is taken care of through different powers of r_{12}. The number of terms in the basis set expansions for the trial radial wave function f is therefore $N = [p(p+1)/2] \times A$. In the present case, we have considered a nine-exponent ($p = 9$) basis set where the non-linear parameters are taken in a geometrical sequence following $\rho_i = \rho_{i-1}\gamma$, γ is the geometrical ratio. After choosing the proper trial radial wave function, the energy eigenvalues are obtained by solving the generalized eigenvalue equation.[38] The details regarding the analytic evaluation of the correlated basis integrals are discussed in Dutta *et al.*[38]

The variational equation for the nl-state of the respective one-electron atoms under WCP environment can be written as

$$\delta \int \Big[\Big(\frac{\partial f}{\partial r}\Big)^2 + \frac{l(l+1)}{r^2} - E + Z\frac{\mathrm{e}^{-r/D}}{r}\Big]\mathrm{d}r = 0\,. \qquad (5)$$

The radial function $f(r)$ is expanded in terms of a pure exponential basis set as

$$f(r) = \sum_i C_i\, \mathrm{e}^{-\sigma_i r}\,. \qquad (6)$$

We have used 101 number of terms in the basis set and the exponents are taken in a geometrical sequence $\sigma_i = \sigma_{i-1}\beta$, β is the geometrical ratio. The energy eigenvalues E's and linear variational coefficients C_i's are determined by matrix diagonalization procedure. All calculations are carried out in quadruple precision. Such procedure is repeated for different plasma screening length (D) considered in the present case.

3 Results and Discussion

Table 1 shows the convergence behavior of the energy eigenvalues of $2pnf$ (n = 4–6) (^{1,3}F^e) states of He with respect to the total number of terms $N = 540$ and $N = 675$ in the 9-exponent basis set for three different Debye screening lengths $D = 100$, 50, and 20 (in a.u.). It can be seen from Table 1 that, all the energy eigenvalues converge at least up to sixth decimal place for $D = 100$ a.u. and $D = 50$ a.u. whereas, energies of $2p5f$ and $2p6f$ converge up to fourth and third decimal places respectively for $D = 20$ a.u. The energy values of $2pnf$ (n = 4–6) (^{1,3}F^e) states of two-electron ions (Z = 2–4) in the presence of WCP environment are given in Tables 2–4 respectively. Only the values obtained from the wave function of maximum basis size ($N = 675; A = 15$) are reported in Tables 2–4. It is observed that as the plasma screening length (D) decreases, the two-electron energy levels are pushed towards the continuum. Such behaviour is quite consistent with the fact that the screened Coulomb potential becomes more and more positive with respect to the decrease in plasma screening length (D). Moreover, Tables 2–4 show that for all the ions the singlet states are more bound than the triplet states from low to moderate plasma screening. At high screening (i.e. at low values of screening length D), we see that the singlet and triplet states become exactly or nearly degenerate. As the plasma screening increases, the two-electron energy levels become largely affected by the continuum embedded states through configuration interactions. At very high screening region, the energy values of two-electron states come very close to the one-electron continuum and tend to merge into the $2p$ threshold of the respective one-electron system.

Table 1 Energy eigenvalues ($-E$) for the $2pnf$ (n = 4–6) ^{1,3}F^e states of He for different number of terms N in the basis set with respect to different Debye screening length (D). All quantities are given in a.u.

		$-E$					
		^{1}F^e			^{3}F^e		
D	N	$2p4f$	$2p5f$	$2p6f$	$2p4f$	$2p5f$	$2p6f$
100	540	0.503 055	0.492 022	0.486 401	0.503 047	0.492 017	0.486 397
	675	0.503 055	0.492 022	0.486 401	0.503 047	0.492 017	0.486 397
50	540	0.476 090	0.466 543	0.462 494	0.476 083	0.466 539	0.462 493
	675	0.476 090	0.466 543	0.462 494	0.476 083	0.466 539	0.462 493
20	540	0.406 087	0.405 792	0.405 550	0.406 086	0.405 792	0.405 550
	675	0.406 087	0.405 856	0.405 709	0.406 086	0.405 856	0.405 709

Table 2 Variation of energy eigenvalues ($-E$) for the $2pnf$ (n = 4–6) ^{1,3}F^e states of He and $2s$, $2p$ states of He$^+$ w.r.t. the Debye screening length (D). All quantities are given in a.u.

	^{1}F^e			^{3}F^e				
D	$2p4f$	$2p5f$	$2p6f$	$2p4f$	$2p5f$	$2p6f$	He$^+(2s)$	He$^+(2p)$
100	0.503 055	0.492 022	0.486 401	0.503 047	0.492 017	0.486 397	0.480 296	0.480 247
	0.502 956[a]	0.491 928[a]	0.486 314 5[a]	0.502 952[a]	0.491 925 5[a]	0.486 313[a]		
	0.503 060 68[b]			0.503 052 113[b]				
90	0.499 965	0.489 058	0.483 572	0.499 957	0.489 052	0.483 569	0.478 143	0.478 083
80	0.496 136	0.485 400	0.480 100	0.496 128	0.485 394	0.480 097	0.475 462	0.475 386
70	0.491 267	0.480 775	0.475 736	0.491 259	0.480 770	0.475 733	0.472 031	0.471 932
	0.491 074[a]	0.480 599 5[a]	0.475 583 5[a]	0.491 070 5[a]	0.480 597[a]	0.475 580 5[a]		
60	0.484 869	0.474 742	0.470 087	0.484 862	0.474 737	0.470 085	0.467 484	0.467 350
50	0.476 090	0.466 543	0.462 494	0.476 083	0.466 539	0.462 493	0.461 173	0.460 981
	0.475 737 5[a]	0.466 241 5[a]	0.462 223 5[a]	0.475 733 5[a]	0.466 237[a]	0.462 197[a]		
	0.476 090 624[b]			0.476 087 092[b]				
40	0.463 300	0.454 773	0.451 782	0.463 293	0.454 770	0.451 781	0.451 823	0.451 525
	0.462 784[a]	0.454 351[a]		0.462 78[a]	0.454 334[a]			
30	0.442 973	0.436 545	0.435 913	0.442 968	0.436 543	0.435 913	0.436 545	0.436 025
	0.442 158 5[a]			0.442 148 5[a]				
20	0.406 087	0.405 856	0.405 709	0.406 086	0.405 856	0.405 709	0.407 104	0.405 970
	0.406 087 6[b]			0.406 087 1[b]				
10	0.322 848	0.322 699	0.321 485	0.322 848	0.322 699	0.321 485	0.327 085	0.322 761

[a]Ref. [34], [b]Ref. [35].

Table 3 Variation of energy eigenvalues ($-E$) for the $2pnf$ ($n = 4$–16) $^{1,3}\mathrm{F}^e$ states of Li^+ and $2s$, $2p$ states of Li^{2+} w.r.t. the Debye length (D). All quantities are given in a.u.

	$^1\mathrm{F}^e$			$^3\mathrm{F}^e$				
D	$2p4f$	$2p5f$	$2p6f$	$2p4f$	$2p5f$	$2p6f$	$Li^{2+}(2s)$	$Li^{2+}(2p)$
100	1.203 600	1.158 000	1.133 734	1.203 510	1.157 937	1.133 693	1.095 298	1.095 248
90	1.198 297	1.152 835	1.128 727	1.198 207	1.152 772	1.128 687	1.092 033	1.091 973
80	1.191 703	1.146 433	1.122 542	1.191 614	1.146 371	1.122 503	1.087 964	1.087 887
70	1.183 284	1.138 288	1.114 706	1.183 195	1.138 227	1.114 668	1.082 748	1.082 648
60	1.172 159	1.127 578	1.104 457	1.172 071	1.127 517	1.104 420	1.075 823	1.075 687
50	1.156 775	1.112 862	1.090 478	1.156 688	1.112 803	1.090 442	1.066 182	1.065 987
40	1.134 107	1.091 381	1.070 283	1.134 022	1.091 326	1.070 251	1.051 840	1051 537
30	1.097 393	1.057 098	1.038 579	1.097 312	1.057 048	1.038 553	1.028 251	1.027 719
20	1.027 813	0.993 914	0.982 019	1.027 745	0.993 879	0.982 008	0.982 227	0.981 057
10	0.848 931	0.846 906	0.844 900	0.848 912	0.845 428	0.841 774	0.852 947	0.848 554

Table 4 Variation of energy eigenvalues ($-E$) for the $2pnf$ ($n = 4$–6) $^{1,3}\mathrm{F}^e$ states of Be^{2+} and $2s$, $2p$ states of Be^{3+} w.r.t. the Debye screening length (D). All quantities are given in a.u.

	$^1\mathrm{F}^e$			$^3\mathrm{F}^e$				
D	$2p4f$	$2p5f$	$2p6f$	$2p4f$	$2p5f$	$2p6f$	$Be^{3+}(2s)$	$Be^{3+}(2p)$
100	2.216 939	2.114 095	2.058 854	2.216 686	2.113 923	2.058 745	1.960 298	1.960 249
90	2.216 938	2.114 095	2.051 646	2.209 165	2.106 546	2.051 536	1.955 923	1.955 862
80	2.200 052	2.097 554	2.042 712	2.199 800	2.097 382	2.042 603	1.950 465	1.950 388
70	2.188 072	2.085 861	2.031 351	2.187 821	2.085 691	2.031 243	1.943 464	1.943 364
60	2.172 202	2.070 428	2.016 417	2.171 952	2.070 259	2.016 311	1.934 159	1.934 022
50	2.150 179	2.049 114	1.995 905	2.150 086	2.048 951	1.995 806	1.921 186	1.920 990
40	2.117 577	2.017 784	1.965 994	2.117 332	2.017 621	1.965 895	1.901 848	1.901 543
30	2.064 350	1.967 188	1.918 278	2.064 110	1.967 033	1.918 192	1.869 937	1.869 400
20	1.961 936	1.871 780	1.830 341	1.961 713	1.871 646	1.830 273	1.807 292	1.806 102
10	1.685 196	1.628 246	1.623 064	1.685 048	1.628 199	1.619 216	1.628 414	1.623 879

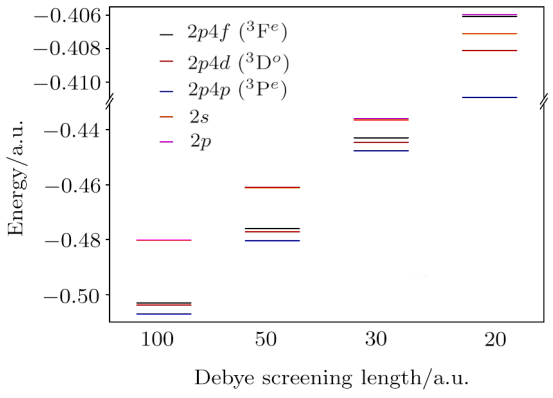

Fig. 1 Relative positions of $2p4f$ ($^3\mathrm{F}^e$), $2p4d$ ($^3\mathrm{D}^o$) and $2p4p$ ($^3\mathrm{P}^e$) energy levels of He and $2s$, $2p$ levels of He^+ in different plasma conditions.

The $2s$ and $2p$ threshold energies of respective one-electron atoms are also included in Tables 2–4 for a comprehensive analysis of the position of two-electron energy levels. The departure from Coulomb potential facilitates the removal of l-degeneracy in the one-electron atoms and it is evident that the $2s$ level remains more bound compared to the $2p$ level as D decreases. Figure 1 illustrates the comparative behavior of different doubly excited triplet $2p4p$ (P^e), $2p4d$ (D^o) and $2p4f$ (F^e) states below $He^+(2p)$ threshold. The energy values of $2p4p$ ($^3\mathrm{P}^e$) and $2p4d$ ($^3\mathrm{D}^o$) states of helium, immersed in WCP environment have been taken from Refs. [20] and [21] respectively. In Fig. 1, we have shown the position of triplet $2p4p$, $2p4d$, $2p4f$ energy levels of helium along with the $2s$ and $2p$ thresholds of He^+ at different plasma screening strength. We note that at low screening regions when the system is almost equivalent to a free system, the one-electron $2s$ and $2p$ levels are merged on each other due to their l-degeneracy. These levels are split when l-degeneracy is sufficiently lifted at a higher screening in presence of plasma environment which is evident from the diagram. It is seen from Fig. 1 that the $2p4p$ ($^3\mathrm{P}^e$) and $2p4d$ ($^3\mathrm{D}^o$) states always lie below both the $2s$ and $2p$ thresholds of He^+, but the $2p4f$ ($^3\mathrm{F}^e$) level crosses the $2s$ threshold of He^+ when the plasma screening length (D) is sufficiently small. Hence, at a low value of D, the $2p4f$ ($^3\mathrm{F}^e$) level of helium merges to the one-electron continuum.

Table 5 Absolute values of the $2pnf(^{1,3}\mathrm{F}^e) \rightarrow 2pn'd(^{1,3}\mathrm{D}^o)$ (n = 4–6; n' = 3–6) transition energies (in meV) of plasma embedded He below the $\mathrm{He}^+(2p)$ threshold under Debye screening.

	Debye screening length (D) in a.u.								
Transition	100	90	80	70	60	50	40	30	20
$^1\mathrm{F}^e \rightarrow {}^1\mathrm{D}^o$									
$2p4f \rightarrow 2p3d$	854.25	851.72	848.21	843.20	835.57	823.21	801.09	754.79	623.78
$\rightarrow 2p4d$	71.70	72.01	72.44	73.01	73.81	75.06	76.97	79.81	77.62
$\rightarrow 2p5d^*$	264.68	360.44	381.82	413.23					
$\rightarrow 2p6d^*$	433.29								
$2p5f \rightarrow 2p3d$	1154.46	1148.52	1140.35	1128.69	1111.15	1082.97	1033.10	929.71	630.08
$\rightarrow 2p4d$	371.91	368.81	364.58	358.50	349.40	334.82	308.98	254.73	83.92
$\rightarrow 2p5d^*$	35.53	63.63	89.69	127.74					
$\rightarrow 2p6d^*$	133.06								
$2p6f \rightarrow 2p3d$	1307.43	1297.78	1284.57	1265.82	1237.82	1193.17	1114.51	946.91	634.08
$\rightarrow 2p4d$	524.89	518.07	508.80	495.63	476.06	445.02	390.38	271.94	87.92
$\rightarrow 2p5d$	188.50	85.62	54.53	9.39					
$\rightarrow 2p6d$	19.89								
$^3\mathrm{F}^e \rightarrow {}^3\mathrm{D}^o$									
$2p4f \rightarrow 2p3d$	734.25	732.05	729.02	724.65	718.03	707.29	688.04	647.69	532.15
$\rightarrow 2p4d$	21.93	22.59	23.48	24.75	26.60	29.49	34.28	42.84	55.08
$\rightarrow 2p5d^*$	288.62	284.67	279.28	271.66					
$\rightarrow 2p6d^*$	445.89								
$2p5f \rightarrow 2p3d$	1034.40	1028.79	1021.08	1010.07	993.54	966.98	919.97	822.52	538.40
$\rightarrow 2p4d$	322.07	319.32	315.55	310.17	302.12	289.18	266.21	217.67	61.33
$\rightarrow 2p5d$	11.53	12.07	12.79	13.77					
$\rightarrow 2p6d^*$	145.74								
$2p6f \rightarrow 2p3d$	1187.31	1177.99	1165.24	1147.14	1120.14	1077.10	1001.31	839.68	542.41
$\rightarrow 2p4d$	474.99	468.52	459.71	447.24	428.72	399.29	347.55	234.83	65.34
$\rightarrow 2p5d$	164.44	161.26	156.95	150.84					
$\rightarrow 2p6d$	7.17								

$^*pf$ level lines energetically lower than the pd level.

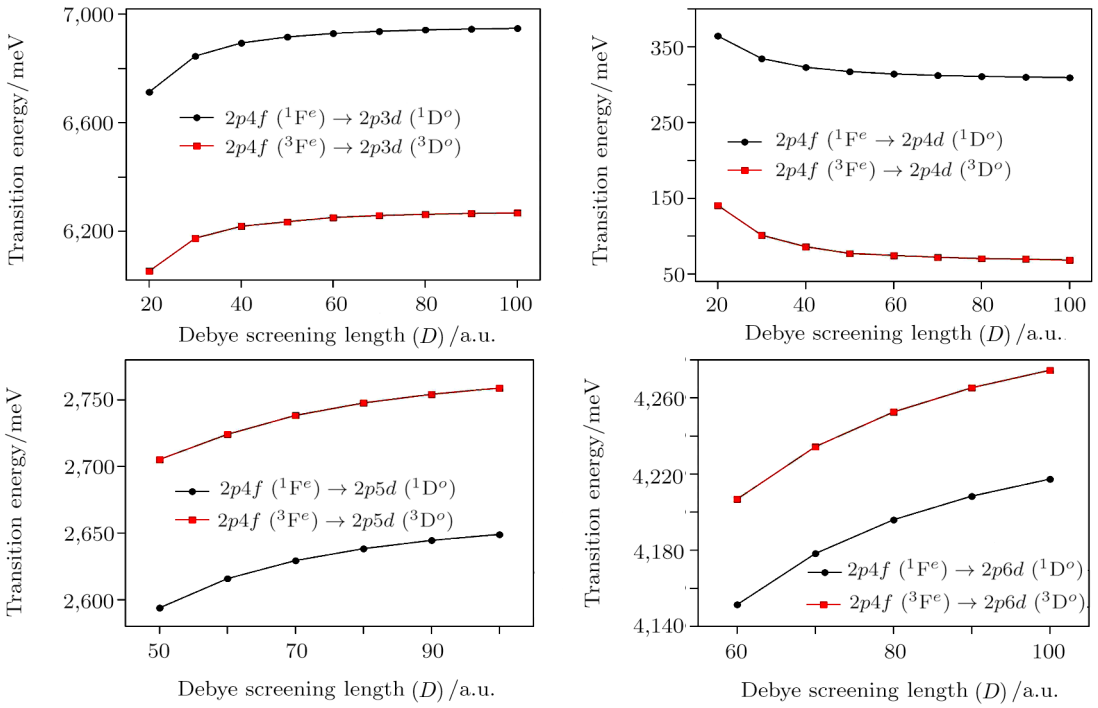

Fig. 2 Variation of transition energies (meV) for $2p4f\ (^{1,3}\mathrm{F}^e) \rightarrow 2pnd(^{1,3}\mathrm{D}^o)$ transitions (n = 3–6) of Be^{2+} in presence of weakly coupled plasma.

Table 6 Absolute values of the $2pnf(^{1,3}\mathrm{F}^e) \rightarrow 2pn'd(^{1,3}\mathrm{D}^o)$ (n = 4–6; n' = 3–6) transition energies (in meV) of plasma embedded Li^+ below the $Li^{2+}(2p)$ threshold under Debye screening.

	Debye screening length (D) in a.u.								
Transition	100	90	80	70	60	50	40	30	20
$^1\mathrm{F}^e \rightarrow {}^1\mathrm{D}^o$									
$2p4f \rightarrow 2p3d$	3229.53	3226.99	3223.50	3218.43	3210.71	3198.09	3175.37	3127.69	2997.69
$\rightarrow 2p4d$	190.39	190.91	191.65	192.69	194.25	196.75	201.14	209.82	230.55
$\rightarrow 2p5d^*$	1148.05	1143.86	1138.06	1129.78	1117.30	1097.24			
$\rightarrow 2p6d^*$	1848.71	1840.33	1828.78	1812.33	1787.67				
$2p5f \rightarrow 2p3d$	4470.37	4464.07	4455.36	4442.83	4423.82	4393.02	4338.01	4224.17	3920.13
$\rightarrow 2p4d$	1431.23	1427.99	1423.51	1417.09	1407.36	1391.68	1363.78	1306.30	1152.99
$\rightarrow 2p5d$	92.79	93.22	93.80	94.62	95.81	97.69			
$\rightarrow 2p6d^*$	607.87	603.24	596.92	587.93	574.56				
$2p6f \rightarrow 2p3d$	5130.68	5120.08	5105.47	5084.53	5052.98	5002.12	4912.11	4728.10	4243.81
$\rightarrow 2p4d$	2091.54	2084.00	2073.62	2058.79	2036.52	2000.78	1937.88	1810.23	1476.67
$\rightarrow 2p5d$	753.10	749.23	743.90	736.32	724.96	706.79			
$\rightarrow 2p6d$	52.44	52.77	53.18	53.77	54.59				
$^3\mathrm{F}^e \rightarrow {}^3\mathrm{D}^o$									
$2p4f \rightarrow 2p3d$	2839.04	2836.78	2833.64	2829.13	2822.23	2810.97	2790.70	2748.17	2632.07
$\rightarrow 2p4d$	44.19	44.97	46.07	47.64	49.99	53.78	60.47	73.87	107.00
$\rightarrow 2p5d^*$	1216.58	1212.10	1205.91	1197.05	1183.72	1162.29			
$\rightarrow 2p6d^*$	1885.17	1876.47	1864.50	1847.42	1821.85				
$2p5f \rightarrow 2p3d$	4079.14	4073.13	4064.77	4052.77	4034.61	4005.14	3952.52	3843.81	3553.62
$\rightarrow 2p4d$	1284.29	1281.32	1277.19	1271.28	1262.37	1247.95	1222.29	1169.51	1028.54
$\rightarrow 2p5d$	23.52	24.25	25.21	26.59	28.65	31.88			
$\rightarrow 2p6d^*$	645.07	640.12	633.38	623.78	609.48				
$2p6f \rightarrow 2p3d$	4738.85	4728.51	4714.25	4693.84	4663.11	4613.62	4526.00	4347.08	3876.64
$\rightarrow 2p4d$	1944.00	1936.71	1926.67	1912.35	1890.87	1856.42	1795.77	1672.79	1351.57
$\rightarrow 2p5d$	683.23	679.64	674.69	667.67	657.15	640.35			
$\rightarrow 2p6d^*$	14.64	15.27	16.10	17.29	19.02				

$^*pf$ level lines energetically lower than the pd level.

We have also estimated the energy (in meV) corresponding to the

$$2pnf\ (^{1,3}\mathrm{F}^e) \rightarrow 2pn'd\ (^{1,3}\mathrm{D}^o)$$

transitions (n = 4–6; n' = 3–6) for different two-electron atoms (Z = 2–4) embedded in WCP environment. The $2pn'd$ ($^{1,3}\mathrm{D}^o$) energy values are taken from Saha *et al.*[21] and the results are exhibited in Tables 5–7 for Z = 2–4 respectively. We mention that the absolute values of the difference between the position of the energy levels are given. The sequence for transition we maintain in the table is $2pnf \rightarrow 2pnd$ whereas in all the cases the $2pnf$ states are not high lying. For instance, in the case of triplet states of Li^+, $2p4f$ state lies energetically higher than $2p3d$ and $2p4d$ states but lower than the $2p5d$ and $2p6d$ states. We have used the conversion relation 1 a.u. of energy = 27.21138 eV.[39] It is worthwhile to mention that for $2pn'd$ ($^3\mathrm{D}^o$) $\rightarrow$ $2p3p$ ($^3\mathrm{P}^e$) transitions in WCP environment, an initial blue shift followed by a red shift with respect to decreasing plasma screening length was reported in Ref. [21] whereas in the present case no such behavior is seen for

$$2pnf\ (^3\mathrm{F}^e) \rightarrow 2pn'd\ (^3\mathrm{D}^o)$$

transitions. The transition energies, in a systematic manner, follow either a blue shift or a red shift for a particular transition scheme. For example, the $2p4f$ ($^3\mathrm{F}^e$) $\rightarrow$ $2p3d$ ($^3\mathrm{D}^o$) line for Z = 4 gets a gradual red shift with respect to decreasing plasma screening length (D) and a blue shift is observed for the $2p4f$ ($^3\mathrm{F}^e$) $\rightarrow$ $2p4d$ ($^3\mathrm{D}^o$) of the same ion under similar conditions. Such features are evident from Fig. 2 where the $2p4f(^{1,3}\mathrm{F}^e) \rightarrow 2pnd(^{1,3}\mathrm{D}^o)$ transition energies (n = 3–6) of Z = 4 are plotted as a function of Debye screening length (D).

Table 7 Absolute values of the $2pnf(^{1,3}\mathrm{F}^e) \rightarrow 2pn'd(^{1,3}\ \mathrm{D}^o)\,(n = 4\text{–}6;\ n' = 3\text{–}6)$ transition energies (in meV) of plasma embedded Be^{2+} below the $Be^{3+}(2p)$ threshold under Debye screening.

	Debye screening length (D) in a.u.								
Transition	100	90	80	70	60	50	40	30	20
$^1\mathrm{F}^e \rightarrow\ ^1\mathrm{D}^o$									
$2p4f \rightarrow 2p3d$	6948.14	6945.64	6942.18	6937.13	6929.45	6916.18	6894.02	6845.82	6713.53
$\rightarrow 2p4d$	309.27	309.91	310.81	312.08	314.03	317.18	322.84	334.38	364.21
$\rightarrow 2p5d^*$	2649.02	2644.54	2638.32	2629.38	2615.82	2593.85			
$\rightarrow 2p6d^*$	4217.37	4208.40	4196.01	4178.25	4151.41				
$2p5f \rightarrow 2p3d$	9746.64	9740.19	9731.29	9718.44	9698.86	9666.27	9609.52	9489.74	9166.80
$\rightarrow 2p4d$	3107.77	3104.46	3099.92	3093.38	3083.44	3067.28	3038.34	2978.29	2817.48
$\rightarrow 2p5d$	149.48	150.02	150.80	151.92	153.59	156.24			
$\rightarrow 2p6d^*$	1418.87	1413.85	1406.90	1396.94	1382.00				
$2p6f \rightarrow 2p3d$	11249.80	11238.81	11223.59	11201.73	11168.58	11114.14	11018.80	10820.54	10294.42
$\rightarrow 2p4d$	4610.93	4603.07	4592.22	4576.68	4553.16	4515.14	4447.62	4309.09	3945.09
$\rightarrow 2p5d$	1652.63	1648.63	1643.10	1635.21	1623.30	1604.11			
$\rightarrow 2p6d$	84.29	84.76	85.40	86.35	87.71				
$^3\mathrm{F}^e \rightarrow\ ^3\mathrm{D}^o$									
$2p4f \rightarrow 2p3d$	6267.78	6265.49	6262.34	6257.71	6250.67	6509.08	6218.23	6174.16	6053.13
$\rightarrow 2p4d$	68.33	69.63	70.35	72.00	74.54	77.13	86.03	101.20	140.68
$\rightarrow 2p5d^*$	2758.91	2754.21	2747.67	2738.34	2724.12	2705.26			
$\rightarrow 2p6d^*$	4274.57	4265.36	4252.62	4234.40	4206.86				
$2p5f \rightarrow 2p3d$	9064.10	9057.90	9049.27	9036.81	9017.88	8987.00	8931.50	8815.76	8503.97
$\rightarrow 2p4d$	2864.65	2862.04	2857.28	2851.10	2841.75	2829.15	2799.30	2742.80	2591.53
$\rightarrow 2p5d$	37.41	38.20	39.26	40.76	43.08	46.77			
$\rightarrow 2p6d^*$	1478.25	1472.95	1465.69	1455.30	1439.65				
$2p6f \rightarrow 2p3d$	10565.57	10554.80	10539.88	10518.41	10485.88	10433.15	10339.04	10144.79	9629.79
$\rightarrow 2p4d$	4366.12	4358.94	4347.90	4332.71	4309.75	4275.30	4206.84	4071.83	3717.34
$\rightarrow 2p5d$	1538.88	1535.10	1529.87	1522.37	1511.08	1492.91			
$\rightarrow 2p6d$	23.22	23.95	24.93	26.31	28.35				

$^*pf$ level lines energetically lower than the pd level.

4 Conclusion

We report the behaviour of doubly excited energy levels of helium-like ions in WCP environment considering screened Coulomb potential. The two-electron energy levels as well as the respective one-electron thresholds become more positive as the plasma screening length decreases. The position of different doubly excited states has been compared extensively. The transition wavelengths between doubly excited states are found to undergo a gradual blue shift or a red shift with respect to the variation in plasma screening length. Such features have implications in interpreting complex atomic spectra like those of laboratory plasma experiments or astrophysical observations.

References

[1] M. A. Albert, S. Laulan, and S. Barmaki, Can. J. Phys.**97** (2019) 317, https://doi.org/10.1139/cjp-2018-0222.

[2] D. Busto, L. Barreau, M. Isinger, *et al.*, J. Phys. B **51** 044002, (2018).

[3] F. F. Goryaev, L. A. Vainshtein, and A. M. Urnov, At. Data Nucl. Data Tables **113** (2017) 117.

[4] S. Kajita, K. Suzuki, H. Tanaka, and N. Ohno, Phys. Plasmas. **25** (2018) 063303.

[5] S. Kar, Y. Wang, W. Li, and X. Sun, Few-Body Sys. **56** (2015) 10.

[6] A. Müller, A. Borovik Jr., K. Huber, *et al.*, Phys. Rev. A **97** (2018) 022709.

[7] A. Müller, E. Lindroth, S. Bari, *et al.*, Phys. Rev. A **98** (2018) 033416.

[8] R. Si, S. Li, K. Wang, *et al.*, Astron. Astrophys. **600** (2017) A85.

[9] J. M. N. Djiokap and A. F. Starace, J. Optics **19** (2017) 09.

[10] S. Nakazaki, K. Sakimoto, and Y. Itikawa, Phys. Scr. **47** (1993) 359.

[11] W. Schwanda and K. Eidman, Phys. Rev. Lett. **69** (1992) 3507.

[12] St. Boddeker, S. Gunter, A. Konies, *et al.*, Phys. Rev. E **47** (1990) 2785.

[13] A. B. C. Walker Jr. and H. R. Rugge, Astrophys. J. **164** (1971) 181.

[14] G. A. Doschek, P. Meekins, R. W. Kerplin, *et al.*, Astrophys. J. **164** (1971) 165.

[15] J. L. Culhane, *et al.*, Sol. Phys. **136** (1991) 89.

[16] U. Feldman, Phys. Scr. **46** (1992) 202.

[17] RESIK & Diogeness NEWS, Week 42 (2002), website: http://www.cbk.pan.wroc.pl/resik_archive/resik_weekly_14_20_Oct/News.htm.

[18] J. Sylwester, B. Sylwester, and K. J. H. Phillips, Astrophys. J. **681** (2008) L117.

[19] C. Chang and W. Cui, Astrophys. J. **663** (2007) 1207.

[20] J. K. Saha, S. Bhattacharyya, T. K. Mukherjee, and P. K. Mukherjee, J. Phys. B **42** (2009) 245701.

[21] J. K. Saha, S. Bhattacharyya, T. K. Mukherjee, and P. K. Mukherjee, J. Quant. Spectrosc. Radiat. Transfer **111** (2010) 675.

[22] J. K. Saha, T. K. Mukherjee, P. K. Mukherjee, and B. Fricke, Eur. Phys. J. D **62** (2011) 205.

[23] J. K. Saha, T. K. Mukherjee, P. K. Mukherjee, and B. Fricke, Eur. Phys. J. D **66** (2012) 43.

[24] J. K. Saha, S. Bhattacharyya, and T. K. Mukherjee, Int. Rev. At. Mol. Phys. **3** (2012) 1.

[25] J. K. Saha, T. K. Mukherjee, P. K. Mukherjee, and B. Fricke, Phys. Plas. **20** (2013) 042703.

[26] S. Bhattacharyya, J. K. Saha, and T. K. Mukherjee, Phys. Rev. A **91** (2015) 042515.

[27] S. Dutta, J. K. Saha, S. Bhattacharyya, and T. K. Mukherjee, Int. Rev. At. Mol. Phys. **6** (2015) 73.

[28] S. Dutta, J. K. Saha, and T. K. Mukherjee, Phys. Plas. **22** (2015) 062103.

[29] S. Dutta, J. K. Saha, R. Chandra, and T. K. Mukherjee, Phys. Plas. **23** (2016) 042107.

[30] J. K. Saha, S. Bhattacharyya, and T. K. Mukherjee, Phys. Plas. **23** (2016) 092704.

[31] A. N. Sil, S. Canuto, and P. K. Mukherjee, Adv. Quantum Chem. **58** (2009) 115 and references therein for comprehensive list of works till (2009).

[32] S. Dutta, J. K. Saha, S. Bhattacharyya, and T. K. Mukherjee, Asian J. Phys. **25** (2016) 1331.

[33] A. I. Akhiezer, I. A. Akhiezer, R. A. Polovin, *et al.*, *Plasma Electrodynamics Linear Response Theory*, Pergamon, Oxford (1975) 1.

[34] S. Kar and Y. K. Ho, Int. J. Quantum Chem. **108** (2008) 1491.

[35] S. Kar and Y. K. Ho, Phys. Rev. A **79** (2009) 062508.

[36] A. K. Bhatia and A. Temkin, Rev. Mod. Phys. **36** (1964) 1050.

[37] T. K. Mukherjee and P. K. Mukherjee, Phys. Rev. A **50** (1994) 850.

[38] S. Dutta, A. N. Sil, J. K. Saha, and T. K. Mukherjee, Int. J. Quantum Chem. **118** (2017) e25577.

[39] NIST, Scientific and Technical Databases, Atomic and Molecular Physics.

Journal of Atomic, Molecular, Condensate & Nano Physics
Vol. 7, No. 1, pp. 51–60, 2020
ISSN 2349-2716 (online); 2349-6088 (print)
Published by RGN Publications

http://www.rgnpublications.com

DOI: 10.26713/jamcnp.v7i1.1389

Resonance States of Hadronic Three-Body Ions: Stabilization Method

Research Article

S. Dutta[1], J. K. Saha[*2], S. Bhattacharyya[3] and T. K. Mukherjee[4]

[1] *Belgharia Texmaco Estate School, Belgharia, Kolkata 700056, India*
[2] *Department of Physics, Aliah University, IIA/27, Newtown, Kolkata 700156, India*
[3] *Department of Physics, Acharya Prafulla Chandra College, New Barrackpore, Kolkata 700131, India*
[4] *Department of Physics, Narula Institute of Technology, Agarpara, Kolkata 700109, India*
[*] **Corresponding author:** jsaha84@gmail.com

Abstract. Bound and resonance states of symmetric three-body exotic pXX negative atomic ions ($X = \mu^-, \pi^-, K^-$) as well as exotic ppX positive molecular ions for total angular momentum $J = 0$, are studied in details under the framework of Stabilization method. The resonance states under consideration lie below $N = 2$ ionization threshold of the corresponding pX atom. The wave-function is expanded in correlated multi-exponent Hylleraas type basis set for explicit incorporation of p-p, μ-μ, π-π or K-K correlations. The methodology has been tested by estimating the parameters of the resonance states of $(p\mu\mu)^-$, $(pp\mu)^+$, $(p\pi\pi)^-$ and $(pp\pi)^+$ and comparing with the results existing in the literature. The interparticle interactions for all the systems under consideration are purely Coulombic.

Keywords. Three-body systems; Stabilization method; Hylleraas coordinate; Resonance state; Correlation

PACS. 31.15ac; 31.15ve; 36.10Gv

Received: April 4, 2020 **Accepted:** April 28, 2020

1. Introduction

The non-separability of the dynamical equation of motion of three body systems in both classical and quantum mechanics, draws a considerable attention by the researchers around the globe [9, 35]. From the very beginning of quantum mechanics various approximation methods had been used to study the structural properties of such systems. Being a quintessential quantum mechanical three body system, the non-relativistic upper bound energy eigenvalue of helium atom was estimated by Hylleraas [17] in the year 1929, using variational approach.

In this work [17] Hylleraas used a new coordinate system to expand the wavefunction in terms of inter-particle (electron-nucleus and electron-electron) distances. After this pioneering work of Hylleraas [17], different variants of this correlated variational framework has been evolved [12,13,16,17,20,21,27,29,32,33] which adequately account for the effect of inter-particle correlation in the basis set.

Quantum mechanical three body system with arbitrary comparable masses bounded via Coulomb interaction also drags considerable attention in recent years. In general, there are two class of energy levels for these systems: the bound states lying below the first ionization threshold ($N = 1$) and the resonant states embedded in the continuum. Thus the bound states are stable against autoionization, while the resonant states decays to an neutral atomic configuration by ejecting particle due to the autoionizing process and thus posses a finite lifetime. It has been observed that when massive negatively charged particles, such as antiprotons ($\bar{p}$), kaons (K), pions (π), and muons (μ), enters into matter, they slow down as they excite and ionize the atoms or molecules of the matter and at the end the particles being captured by the positive ions present in the medium, form the bound or resonance states of exotic atoms [2, 11, 30, 36]. Thus during the decay of these three-body ions, X-rays are emmited during bound-bound transition or one of the particle is ejected from it via Augey process [30]. Such investigations are going into full swing in case of muonic-, pionic- and kaonic-hydrogen atoms [1, 3, 15, 25, 26, 31].

Although the structural properties of bound states of these systems have extensively been studied by adopting various quantum chemical methods [5, 7, 8, 10, 14, 18, 22, 24], but the same for the resonance states are rather considerably less in number [18, 19]. In the present work, we have made an attempt to estimate the energy eigenvalues of ground states and the parameters (position and width) of first three resonant states of ppX positive molecular ions and first two resonant states of pXX negative atomic ions ($X = \mu^-, \pi^-, K^-$), below the $2s$ threshold of pX atom. For this purpose, we have expanded the basis set in the explicitly correlated multi-exponent Hylleraas type basis set and carried out calculations under the framework of Stabilization method [28, 34]. In order to check the consistency of the present methodology, we have compared the resonance parameters (position and width) with few existing theoretical data [18, 19].

2. Method

Here we use the designation of two identical particles (pp or XX) as particle 3 and the non-identical one (p or X) as particle 3. Due to translation symmetry of the Hamiltonian of three-body system, it is possible to describe the motion of the system with respect to their center of mass in six co-ordinates. If the distances of the particles 1 and 2 with respect to the 3rd particle are r_1 and r_2 and the distance between particles 1 and 2 is r_{12}, then r_1, r_2 and r_{12} form the sides of a triangle. Besides these three coordinates (r_1, r_2 and r_{12}), the remaining three coordinates are the Eulerian angles [4] defining the orientation of the triangle in space. For the spherically symmetric ground state ($^1S^e$), the three-body general variational equation [23] reduces to

$$\delta \int \left[\frac{1}{2} \left(\frac{1}{m} + \frac{1}{M} \right) \left\{ \left(\frac{\partial \Psi}{\partial r_1} \right)^2 + \left(\frac{\partial \Psi}{\partial r_2} \right)^2 \right\} + \frac{1}{m} \left(\frac{\partial \Psi}{\partial r_{12}} \right)^2 + \frac{1}{M} \cos(r_1, r_2) \frac{\partial \Psi}{\partial r_1} \cdot \frac{\partial \Psi}{\partial r_2} \right.$$

$$+\frac{1}{m}\left\{\cos(r_2,r_{12})\frac{\partial\Psi}{\partial r_2}\cdot\frac{\partial\Psi}{\partial r_{12}}+\cos(r_1,r_{12})\frac{\partial\Psi}{\partial r_1}\cdot\frac{\partial\Psi}{\partial r_{12}}\right\}+(V-E)\Psi^2\Bigg]d\tau=0 \tag{2.1}$$

where the volume element is $d\tau = r_1 r_2 r_{12} dr_1 dr_2 dr_{12}$ and the potential is given by

$$V=-\frac{1}{r_1}-\frac{1}{r_2}+\frac{1}{r_{12}} \tag{2.2}$$

and we have defined

$$\cos(r_i,r_j)=\frac{r_i^2+r_j^2-r_k^2}{2\,r_i\,r_j} \tag{2.3}$$

where, the indices $(i,j,k)\equiv(1,2,12)$ and the m and M are the masses of the identical and non-identical particles respectively. The masses (in a.u.) of p and X ($X=\mu^-,\pi^-,K^-$) particles are taken as $m_p = 1836.152\ 6675$, $m_\mu = 206.768\ 262$, $m_\pi = 273.132\ 426$ and $m_K = 966.101\ 6949$ respectively. The trial radial wave function $\Psi(r_1,r_2,r_{12})$ can be written as,

$$\Psi(r_1,r_2,r_{12})=\sum_{k=1}^{s} r_1^{l_k}\, r_2^{m_k}\, r_{12}^{n_k}\left[\sum_{i=1}^{p} C_{kii}\eta_i(1)\eta_i(2)+\sum_{i=1}^{p}\sum_{j=1}^{p} C_{kij}\eta_i(1)\eta_j(2)\right]. \tag{2.4}$$

In the second sum $i<j$ and $\eta_i(m)=e^{-\rho_i r_m}$, ρ being the non-linear parameter. p denotes the number of non-linear parameters which are taken in a geometrical sequence following $\rho_i=\rho_{i-1}\gamma$; γ being the geometrical sequence. The function $g(1,2)$ containing correlation terms, is expanded into Hylleraas basis set as follows, the effect of the radial correlation is incorporated through different ρ's in the wave function whereas, the angular correlation effect is taken care of through different powers of r_{12}. The dimension of the full multi-exponent basis (N) is $\left[\frac{p(p+1)}{2}\times s\right]$, where s is the number of terms involving r_{12} and p is the number of exponents. For a fixed number of basis, p and s should be chosen in such a manner that the effect of radial as well as angular correlation is properly incorporated in the wavefunction.

After choosing the proper trial radial wave function, the energy eigenvalues are obtained by solving the generalized eigenvalue equation involving the Hamiltonian and overlap matrices given by

$$\underline{\underline{H}}\;\underline{C}=E\underline{\underline{S}}\;\underline{C}, \tag{2.5}$$

where $\underline{\underline{H}}$ and $\underline{\underline{S}}$ are Hamiltonian and overlap matrices respectively. The necessary basis integrals of the form

$$A(m,n,l;a_1,a_2)=\int_{r_1=0}^{\infty}\int_{r_2=0}^{\infty}\int_{|r_1-r_2|}^{r_1+r_2} r_1^m r_2^n r_{12}^l e^{-a_1 r_1-a_2 r_2}dr_1 dr_2 dr_{12} \tag{2.6}$$

with the condition, $m\geq 0$, $n\geq 0$, $l\geq 0$ and $a_1,a_2>0$. This integral has been evaluated following Calais and Lowdin [6]. All calculations are carried out in quadruple precision in order to have a better numerical accuracy. Repeated diagonalization of the Hamiltonian matrix in the Hylleraas basis set of 675 parameters is done in the present work for 200 different values of γ. The plot of each energy eigenroot versus γ produces the stabilization diagram. The density of resonance states is then calculated from the stabilization diagram and by fitting with a Lorentzian profile we have estimated the parameters of a particular resonance state.

3. Results and Discussions

A portion of the stabilization diagram for $^1S^e$ states originating from two negatively charged kions (K) of exotic pKK ion is given in Figure 1. In this diagram we have plotted first 40

eigenroots of $^1S^e$ symmetry of exotic pKK ion for 200 different values of γ ranging from 0.63058 a.u. to 0.74954 a.u. From Figure 1, one can see that there exist two classes of states:

(1) There exists only one energy level below $N = 1$ ionization threshold of pK at -316.515 a.u., formed due to ground state $(1s^2)$ configuration remains invariant with the variation in γ. The energy eigenvalue of this level is -330.800637 which is consistent with the value obtained by Dutta et al. [10] using 990 terms in the multi-exponant Hylleraas type basis set.

(2) Roots lying above $N = 1$ but below $N = 2$ ionization threshold of pK at -79.129 a.u. are sensitive with the variation in γ and give rise to flat plateau in the vicinity of avoided crossings of the energy eigenroots for some particular energy value which is a clear signature of resonance states.

Similar classes of states are also observed for the other exotic systems like $p\mu\mu$, $pp\mu$, $p\pi\pi$, $pp\pi$ and ppK. The ground state energies of atomic $(pXX)^-$ ion and molecular $(ppX)^+$ ion $[X = \mu, \pi, K]$ are given in Table 1 and the present results are compared with the lowest energy eigenvalues available in literature [5, 10, 18].

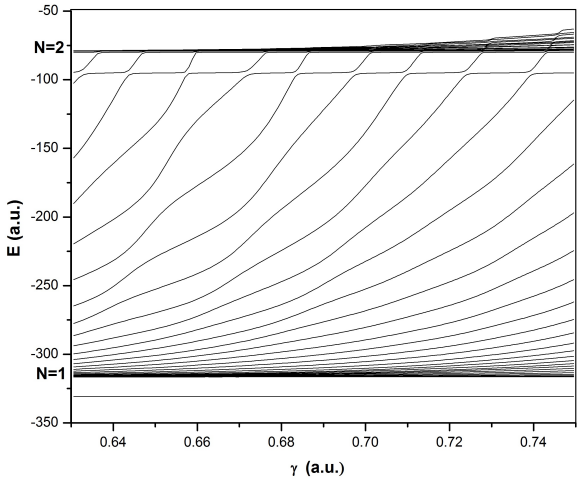

Figure 1. Stabilization diagram for $^1S^e$ states of exotic pKK ion

Table 1. Bound states energies ($-E$ in a.u.) of atomic $(pXX)^-$ ion and molecular $(ppX)^+$ ion below pX $(1s)$ threshold $E_{pX} = -\frac{\lambda}{2}$ a.u.; λ being the reduced mass of the exotic pX atom

$E_{p\mu} = -92.920\ 408$		$E_{p\pi} = -118.882\ 182$		$E_{pK} = -316.514\ 843$	
$p\mu\mu$	$pp\mu$	$p\pi\pi$	$pp\pi$	pKK	ppK
97.566 983	102.223 503	124.690 678	129.718 076	330.798 993	334.575 390
97.566 984 59[a]	102.223 503 6[b]	124.690 674[c]	129.718 073[c]	330.800 637[c]	334.575 377[c]

[a] [5]; [b] [18]; [c] [10]

Enlarged view of the stabilization diagram (Figure 1) for $^1S^e$ state of exotic pKK ion in the energy range -100 a.u. to -78.5 a.u. is given in Figure 2. From a closer look at Figure 2, one can see that for a short range of γ each eigenroot becomes almost flat in the vicinity of avoided crossings in the neighborhood of a particular resonance state. The density of states $\rho_n(E)$ is

calculated by evaluating the inverse of the slope at a number of points near the flat plateau of each energy eigenroot using the formula [28, 34] given by:

$$\rho_n(E) = \left| \frac{\gamma_{i+1} - \gamma_{i-1}}{E_n(\gamma_{i+1}) - E_n(\gamma_{i-1})} \right|_{E_n(\gamma_i)=E_i} . \tag{3.1}$$

The calculated density of resonance states $\rho_n(E)$ is then fitted to the following Lorentzian form [28, 34],

$$\rho_n(E) = y_0 + \frac{A}{\pi} \frac{\Gamma_r/2}{(E-E_r)^2 + (\Gamma_r/2)^2} , \tag{3.2}$$

where y_0 is the baseline background, A is the total area under the curve from the baseline, E_r gives the position of the centre of the peak of the curve and Γ_r represents the full width of the peak of the curve at half height. Among different fitting curves for each eigenroot corresponding to a particular resonance state, the fitting curve with least χ^2 and the square of correlation closer to unity leads to the desired resonance energy (E_r) and width (Γ) as mentioned in ref. [28]. For example, from the stabilization plot of Figure 2 for the first $^1S^e$ resonance state below $N = 2$ ionization threshold of pK, we have calculated the inverse of the slope by using (3.1) at different points near the flat plateau of 24th eigenvalues in the interval of $\gamma = 0.724 - 0.738$.

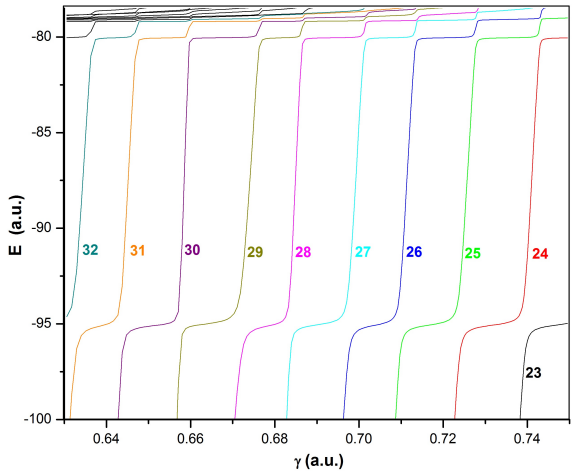

Figure 2. Enlarged view of the Stabilization diagram for $^1S^e$ states of exotic pKK ion below $N = 2$ ionization threshold of pK

The corresponding fitted curve is obtained by using (3.2) and is shown in Figure 3. The circles in Figure 3 are the calculated values of $\rho_n(E)$ while the solid line (red) corresponds to the fitted curve. Repeated calculations of $\rho_n(E)$ near the flat plateau of each of the eigenroot for first $^1S^e$ resonance state resulted Lorentzian fitted curve similar to that of Figure 3. Among all this fitting curve, we have found that 24th eigenroot corresponds to the best fit and from which $-E_r = 95.06738$(a.u.) and $\Gamma_r = 0.31004$(a.u.) are obtained. Similarly, the best fits for the second and third $^1S^e$ resonance states are shown in Figure 4 and 5, respectively.

Table 2 shows all the resonance energies (E_r in a.u.) and widths (Γ_r in a.u.) of $^1S^e$ states of exotic atomic $(pXX)^-$ ions and molecular $(ppX)^+$ ions [$X = \mu, \pi, K$] below $N = 2$ ionization threshold of pX atom. The results are being compared with those available in literature [18, 19] for $(pXX)^-$ and $(ppX)^+$ [$X = \mu, \pi$] ions. The comparison shows that resonance energies and widths are in very good agreement with the available results [18, 19]. To the best of our

knowledge the present calculated resonance energies and widths of $(pKK)^-$ and $(ppK)^+$ ions are given for the first time in the literature. Table 2 shows that the widths of the negative ions (pXX) are higher than the corresponding three body positive counterpart (ppX), which indicates that the resonance states of the molecular $(ppX)^+$ ions are more long lived than that of the atomic $(pXX)^-$ ions.

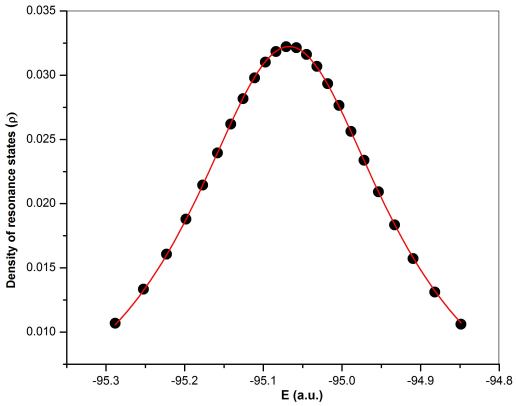

Figure 3. Calculated density (circles) and the fitted Lorentzian (solid line in red) for the ${}^1S^e$ resonance state [$-E_r = 95.06738$(a.u.) and $\Gamma_r = 0.31004$(a.u.)] of exotic pKK ion

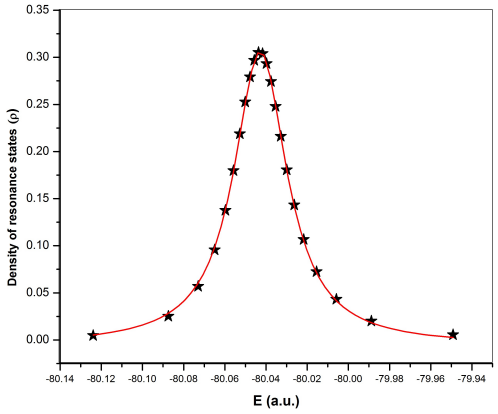

Figure 4. Calculated density (stars) and the fitted Lorentzian (solid line in red) for the ${}^1S^e$ resonance state [$-E_r = 80.0428$(a.u.) and $\Gamma_r = 0.03131$(a.u.)] of exotic pKK ion

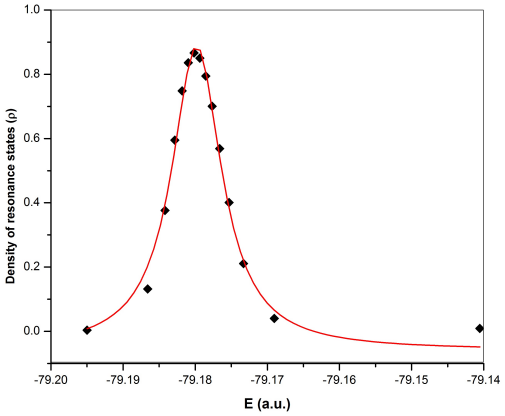

Figure 5. Calculated density (diamonds) and the fitted Lorentzian (solid line in red) for the ${}^1S^e$ resonance state [$-E_r = 79.1798$(a.u.) and $\Gamma_r = 0.0084$(a.u.)] of exotic pKK ion

Table 2. Resonance energies ($-E_r$ in a.u.) and widths (Γ_r in a.u.) of $L = 0$ states of atomic $(pXX)^-$ ion and corresponding ro-vibrational states of molecular $(ppX)^+$ ion below pX $(2s)$ threshold $E_{pX} = -\frac{\lambda}{8}$ a.u.; λ being the reduced mass of the exotic pX atom. Parameters are given for the best lorentzian fitting (*i.e.* for least χ^2) of the numerically estimated DOS of an energy eigen roots of the stabilization diagrams. The notation $P[\pm Q]$ stands for $P \times 10^{\pm Q}$

		$E_{p\mu} = -23.230\ 102$		$E_{p\pi} = -29.720\ 545$		$E_{pK} = -79.128\ 711$	
States	Parameters	$p\mu\mu$	$pp\mu$	$p\pi\pi$	$pp\pi$	pKK	ppK
1	$-E_r$	27.651 07	30.271 80	35.414 51	38.399 77	95.067 38	98.051 24
			30.271 841 23[a]		38.399 777 312 3[b]		
	Γ	27.608[-2]	5.963[-5]	30.258[-2]	9.220[-5]	31.004[-2]	8.68[-3]
			6.353[-5][a]		5.443[-5][b]		
2	$-E_r$	23.420 34	26.649 33	29.965 33	33.400 63	80.042 80	82.079 05
			26.649 428 350[a]		33.400 857 338[b]		
	Γ	1.902[-2]	1.030[-4]	2.788[-2]	3.274[-4]	3.131[-2]	4.35[-3]
			1.108[-4][a]		7.068[-5][b]		
3	$-E_r$		24.403 99		30.698 68	79.179 80	79.472 55
			24.404 608 394[a]		30.698 940 424 1[b]		
	Γ		2.065[-4]		2.153[-4]	8.40[-3]	6.486[-4]
			8.146[-5][a]		3.509[-5][b]		

[a] [18]
[b] [19]

4. Conclusion

In the present work we have adopted extended Hylleraas type basis set to estimate the ground state energy eigenvalues of exotic atomic $(pXX)^-$ ions and molecular $(ppX)^+$ ions $[X = \mu, \pi, K]$ below $N = 1$ ionization threshold of pX atom. Stabilization method is used to calculate the resonance energies and widths of the above mentioned exotic systems below $N = 2$ ionization threshold of pX atom. The present results consistent with those available in literature. The advantage of the present method lies in the fact that a single methodology enables us to predict reasonably accurate bound state energies and resonance parameters with much lesser number of terms in the basis set expansion thus minimizing the computational time. The resonance parameters for ppK and pKK ions are given for the first time in the literature. We hope the present results will be useful for the future references.

Acknowledgments

JKS acknowledges the partial financial support from the Department of Science and Technology, Govt. of West Bengal, India under grant number 249(Sanc.)/ST/P/ S& T/16G-26/2017. SB acknowledges the partial financial support from the Department of Science and Technology, Govt. of West Bengal, India under grant number 23(Sanc.)/ST/P/ S& T/16G-35/2017.

Competing Interests

The authors declare that they have no competing interests.

Authors' Contributions

All the authors contributed significantly in writing this article. The authors read and approved the final manuscript.

References

[1] D. F. Anagnostopoulos, S. Biri, G. Borchert, W. Breunlich, M. Cargnelli, J.-P. Egger, H. Fuhrmann, D. Gotta, M. Giersch, A. Gruber, M. Hennebach, P. Indelicato, T. S. Jensen, F. Kottmann, Y.-W. Liu, B. Manil, V. M. Markushin, J. Marton, N. Nelms, G. C. Oades, G. Rasche, P. A. Schmelzbach, L. M. Simons and J. Zmeskal, The pionic hydrogen experiment at PSI, *Hyperfine Interactions*, **138** (2001), 131, DOI: 10.1023/A:1020815220597.

[2] G. Backenstoss, in *Progress in Atomic Spectroscopy* (eds. W. Hanle and H. Kleinpoppen), 1385, Plenum, New York (1979).

[3] G. Beer, A. M. Bragadireanu, M. Cargnelli, C. Curceanu-Petrascu, J.-P. Egger, H. Fuhrmann, C. Guaraldo, M. Iliescu, T. Ishiwatari, K. Itahashi, M. Iwasaki, P. Kienle, T. Koike, B. Lauss, V. Lucherini, L. Ludhova, J. Marton, F. Mulhauser, T. Ponta, L. A. Schaller, R. Seki, D. L. Sirghi, F. Sirghi and J. Zmeskal, Measurement of the kaonic hydrogen X-ray spectrum, *Physical Review Letters* **94** (2005), 212302, DOI: 10.1103/PhysRevLett.94.212302.

[4] A. K. Bhatia and A. Temkin, Symmetric euler-angle decomposition of the two-electron fixed-nucleus problem, *Reviews of Modern Physics* **36** (1964), 1050, DOI: 10.1103/RevModPhys.36.1050.

[5] S. Bhattacharyya, J. K. Saha, P. K. Mukherjee and T. K. Mukherjee, Three-body negative ions under Coulomb interaction, *Physica Scripta* **85** (2012), 065305, DOI: 10.1088/0031-8949/85/06/065305.

[6] J. L. Calais and P. O. Löwdin, A simple method of treating atomic integrals containing functions of r_{12}, *Journal of Molecular Spectroscopy* **8** (1962), 203, DOI: 10.1016/0022-2852(62)90021-8.

[7] J. C. Cohen, *Review of Fundamental Processes and Applications of Atoms and Ions*, 61, World Scientific, Singapore (1993).

[8] C. Cohen-Tannoudji, B. Diu and F. E. Lalo, *Quantum Mechanics*, Vol. **1**, 811, Wiley, New York (2005).

[9] N. Daldosso and L. Pavesi, Nanosilicon, Chapter 1, (ed. V. Kumar), Elsevier, New York (2005).

[10] S. Dutta, J. K. Saha, S. Bhattacharyya, P. K. Mukherjee and T. K. Mukherjee, Exotic systems under screened Coulomb interactions: a study on Borromean windows, *Physica Scripta* **89** (2014), 015401, DOI: 10.1088/0031-8949/89/01/015401.

[11] E. Fermi and E. Teller, The capture of negative Mesotrons in matter, *Physical Review* **72** (1947), 399, DOI: 10.1103/PhysRev.72.399.

[12] K. Frankowski and C. L. Pekeris, Logarithmic terms in the wave functions of the ground state of two-electron atoms, *Physical Review* **146** (1966), 46, DOI: 10.1103/PhysRev.146.46.

[13] K. Frankowski, Logarithmic terms in the wave functions of the 2^1S and 2^3S states of two-electron atoms, *Physical Review* **160** (1967), 1, DOI: 10.1103/PhysRev.160.1.

[14] P. Froelich, Muon catalysed fusion Chemical confinement of nuclei within the muonic molecule dtμ, *Advances in Physics* **41** (1992), 405, DOI: 10.1080/00018739200101533.

[15] D. Gotta, F. D. Amaro, D. F. Anagnostopoulos, A. B̈uhler, D. S. Covitab, H. Gorke, A. Gruber, M. Hennebach, A. Hirtl, P. Indelicato, T. Ishiwatari, E.-O. Le Bigot, J. Marton, M. Nekipelov, J. M. F. dos Santos, S. Schlesser, Ph. Schmid, L. M. Simons, Th. Strauch, M. Trassinelli, J. F. C. A. Veloso, J. Zmeskal, Pionic hydrogen, *Physics Procedia* **17** (2011), 69, DOI: 10.1016/j.phpro.2011.06.019.

[16] E. A. Hylleraas and B. Undheim, Numerische Berechnung der 2S-Terme von Ortho- und Par-Helium, *Zeitschrift für Physik* **65** (1930), 759, DOI: 10.1007/BF01397263.

[17] E. A. Hylleraas, Neue Berechnung der Energie des Heliums im Grundzustande, sowie des tiefsten Terms von Ortho-Helium, *Zeitschrift für Physik* **54** (1929), 347, DOI: 10.1007/BF01375457.

[18] S. Kar and Y. K. Ho, Bound states and resonance states of the plasma-embedded $pp\mu$ molecular ion, *Physical Review A* **75** (2007), 062509, DOI: 10.1103/PhysRevA.75.062509.

[19] S. Kilic, J.-P. Karr and L. Hilico, Coulombic and radiative decay rates of the resonances of the exotic molecular ions $pp\mu$, $pp\pi$, $dd\mu$, $dd\pi$ and $dt\mu$, *Physical Review A* **70** (2004), 042506, DOI: 10.1103/PhysRevA.70.042506.

[20] W. Kolos, C. C. J. Roothaan and R. A. Sack, Ground state of systems of three particles with coulomb interaction, *Reviews of Modern Physics* **32** (1960), 178, DOI: 10.1103/RevModPhys.32.178.

[21] V. I. Korobov, Nonrelativistic ionization energy for the helium ground state, *Physical Review A* **66** (2002), 024501, DOI: 10.1103/PhysRevA.66.024501.

[22] J. Kulpa and S. Wycech, On the formation of Pionium, *Acta Physica Polonica B* **27** (1996), 941, URL: `https://www.actaphys.uj.edu.pl/R/27/4/941/pdf`.

[23] T. K. Mukherjee and P. K. Mukherjee, Variational equation of states of arbitrary angular momenta for three-particle systems, *Physical Review A* **51** (1995), 4276, DOI: 10.1103/PhysRevA.51.4276.

[24] M. Pawlak, M. Bylicki and P. K. Mukherjee, On the limit of existence of Borromean binding in three-particle systems with screened Coulomb interactions, *Journal of Physics B: Atomic, Molecular and Optical Physics* **47** (2014), 095701, DOI: 10.1088/0953-4075/47/9/095701.

[25] R. Pohl, H. Daniel, F. J. Hartmann, P. Hauser, F. Kottmann, V. E. Markushin, M. Mühlbauer, C. Petitjean, W. Schott, D. Taqqu and P. Wojciechowski-Grosshauser, Observation of long-lived Muonic hydrogen in the 2S state, *Physical Review Letters* **97** (2006), 193402, DOI: 10.1103/PhysRevLett.97.193402.

[26] W. W. Repko and D. A. Dicus, Muonic hydrogen and the proton size, *Physical Review D 98* (2018), 013002, DOI: 10.1103/PhysRevD.98.013002.

[27] M. B. Ruiz, J. T. Margraf and A. M. Frolov, Hylleraas-configuration-interaction analysis of the low-lying states in the three-electron Li atom and Be^+ ion, *Physical Review A* **88** (2013), 012505, DOI: 10.1103/PhysRevA.88.012505.

[28] J. K. Saha and T. K. Mukherjee, Doubly excited bound and resonance ($^3P^e$) states of helium, *Physical Review A* **80** (2009), 022513, DOI: 10.1103/PhysRevA.80.022513.

[29] C. Schwartz, Experiment and theory in computations of the he atom ground state, *International Journal of Modern Physics E* **15** (2006), 877, DOI: 10.1142/S0218301306004648.

[30] I. Shimamura, Moleculelike metastable states of antiprotonic and mesic helium, *Physical Review A* **46** (1992), 3776, DOI: 10.1103/PhysRevA.46.3776.

[31] SIDDHARTA Collaboration, M. Bazzi, G. Beer, L. Bombelli, A. M. Bragadireanua, M. Cargnelli, G. Corradi, C. Curceanu (Petrascu), A. d'Uffizi, C. Fiorini, T. Frizzi, F. Ghio, B. Girolami, C. Guaraldo, R. S. Hayano, M. Iliescua, T. Ishiwatari, M. Iwasaki, P. Kienlee, P. Levi Sandri, A. Longoni, V. Lucherini, J. Marton, S. Okada, D. Pietreanua, T. Ponta, A. Rizzo, A. Romero Vidal, A. Scordo, H. Shi, D. L. Sirghia, F. Sirghia, H. Tatsuno, A. Tudorache, V. Tudorache, O. Vazquez Doce, E. Widmann and J. Zmeskal, A new measurement of kaonic hydrogen X-rays, *Physics Letters B* **704** (2011), 113, DOI: 10.1016/j.physletb.2011.09.011.

[32] J. S. Sims and S. Hagstrom, Combined configuration-interaction-Hylleraas-type wave-function study of the ground state of the Beryllium atom, *Physical Review A* **4** (1971), 908, DOI: 10.1103/PhysRevA.4.908.

[33] K. Szalewicz, H. J. Monkhorst, W. Kolos and A. Scrinzi, Variational calculation of the energy levels for the tdμ ion, *Physical Review A* **36** (1987), 5494, DOI: 10.1103/PhysRevA.36.5494.

[34] S. S. Tan and Y. K. Ho, Determination of resonance energy and width by calculation of the density of resonance states using the stabilisation method, *Chinese Journal of Physics* **35** (1997), 701, `https://www.ps-taiwan.org/cjp/download.php?type=paper&vol=35&num=6-I&page=701`.

[35] G. Tanner, K. Richter and J. M. Rost, The theory of two-electron atoms: between ground state and complete fragmentation, *Reviews of Modern Physics* **72** (2000), 497, DOI: 10.1103/RevModPhys.72.497.

[36] A. S. Wightman, Moderation of negative mesons in hydrogen I: moderation from high energies to capture by an H_2 molecule, *Physical Review* **77** (1950), 521, DOI: 10.1103/PhysRev.77.521.

Atomic Data and Nuclear Data Tables 158 (2024) 101649

Contents lists available at ScienceDirect

Atomic Data and Nuclear Data Tables

journal homepage: www.elsevier.com/locate/adt

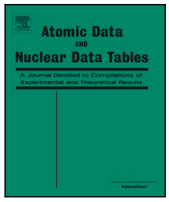

Precise structure calculations of $^{1,3}F^e$ states of helium atom under exponentially screened Coulomb potential

A.N. Sil [a], S. Dutta [b,c], D. Ghosh [d], J.K. Saha [e], S. Bhattacharyya [c], T.K. Mukhopadhyay [f,*]

[a] Department of Physics, Jogamaya Devi College, Kolkata 700026, India
[b] Belgharia Texmaco Estate School, Belgharia, Kolkata 700056, India
[c] Jadavpur University, Kolkata 700032, West Bengal, India
[d] Department of Physics, Bangabasi Evening College, Kolkata 700009, India
[e] Aliah University, ll-A/27, Action Area II, Newtown, Kolkata, West Bengal 700160, India
[f] Department of Physics, Narula Institute of Technology, Agarpara, Kolkata 700109, India

ARTICLE INFO

Keywords:
Classical weakly coupled plasma
Exponentially screened Coulomb potential
Helium atom
Doubly excited $^{1,3}F^e$ states
Explicitly correlated multi-exponent
Hylleraas-type wavefunction
Stabilization method

ABSTRACT

The structural properties of doubly excited $^{1,3}F^e$ metastable-bound and resonance states of neutral helium atom under exponentially screened Coulomb potential are studied using explicitly correlated multi-exponent Hylleraas type basis set. Precise energy eigenvalues of $2pnf(^{1,3}F^e)$ states $[n = 4 - 15]$ are estimated in the framework of Ritz variational principle. Stabilization method has been employed to calculate the resonance parameters (energy and width) of $^{1,3}F^e$ states below $He^+(3p)$ and $He^+(4p)$ thresholds for different screening conditions. The resonance parameters above $He^+(3p)$ threshold under screened Coulomb environment are reported for the first time in literature. Furthermore, pioneering calculations for the variation of structural properties such as one- and two-particle moments and inter-electronic angles are carried out for both metastable-bound and resonance $^{1,3}F^e$ states of He atom under screened Coulomb potential. The present results may serve as benchmark for future references.

* Corresponding author.
E-mail addresses: ansil05@gmail.com (A.N. Sil), sayantand.physics.rs@jadavpuruniversity.in (S. Dutta), deepanwita.ghosh@gmail.com (D. Ghosh), jksaha.phys@aliah.ac.in (J.K. Saha), sukhamoyb.physics@jadavpuruniversity.in (S. Bhattacharyya), tapan.mukherjee@nit.ac.in (T.K. Mukhopadhyay).

https://doi.org/10.1016/j.adt.2024.101649
Received 9 October 2023; Received in revised form 24 November 2023; Accepted 31 March 2024
Available online 21 April 2024
0092-640X/

Contents

1. Introduction

Atomic systems confined under various external environments like plasma [1–26], quantum dot [27,28], fullerene cages [29–31], zeolite sieves [32,33], helium droplets [34] etc., have become an attractive field of research over the years. Such investigations are significant because they offer an excellent testing ground for many quantum chemical approximation techniques, such as variation, perturbation, various numerical techniques, etc., and they provide a wealth of information about the confining environment. Among these different confinements plasma is being widely studied due to its abundance in both natural and laboratory scenario [35]. Depending on the Coulomb coupling parameter (Γ_C) defined by the ratio of average potential energy to average kinetic energy of the plasma particles, plasma can be classified into two category — weakly coupled plasma ($\Gamma_C < 1$) and strongly coupled plasma ($\Gamma_C \geq 1$). The Debye–Hückel potential or exponentially screened Coulomb potential (ESCP) [36], is mostly used to mimic the interactions between the particles within weakly coupled plasma environment while various other types of potentials are used in case of strongly coupled plasma [37]. Precise atomic data, particularly of H-like and He-like ions produced by using such model potentials serve as important tools for plasma diagnostics. Ionization potential depression, level shifting phenomena, line merging, vanishing of spectral lines etc. of He-like systems provide useful information [24,26,38–42] about different physical properties of plasma like density, temperature etc.

The study of doubly excited states (DES) of He-like systems have acquired a lot of attention because of their importance in the field of plasma physics, astrophysics, laser technology etc. [43–46]. Lot of investigations [21,47–57] for $S, P, D-$ symmetry states have been conducted to determine the structural properties of DES of He-like systems in plasma environments. Similar type of calculation for the next higher angular momentum F^e states are quite limited [9,25,58]. Using CI-type basis functions, Kar and Ho calculated energies of meta-stable bound $^{1,3}F^e$ states below $n = 2$ ionization threshold [9,58] and the resonance parameters (energy and width) of $^{1,3}F^e$ resonance states below $n = 3$ ionization threshold [9] of He-atom embedded in the weakly coupled plasma environment modelled by ESCP. Kar and Ho [9,58] approximated the screened electron–electron repulsion term by Taylor expansion for the sake of simplicity in their calculations. In our earlier investigation [25], we estimated the energy eigenvalues of meta-stable bound $^{1,3}F^e$ states and the transition wavelengths between $2pnf(^{1,3}F^e)$ and $2pn'd(^{1,3}D^o)$ states ($n = 4-6; n' = 3-6$) of two-electron systems like He, Li^+ and Be^{2+} under ESCP where the screening was considered in both electron–electron and electron-nucleus parts of the potential without any approximation. The wavefunction used in that work [25] consists of only pf configuration. In another work [59] we took the explicit effect of pf and dd configurations in the wavefunction while studying the meta-stable bound and resonance $^3F^e$ states of free He-atom. We showed that the mixing of pf and dd configurations in the wavefunction expedite the convergence rate of the meta-stable bound state energies. In comparison to the meta-stable bound states, it was demonstrated that the dd configuration significantly adds to the computations of the resonance parameters [59]. Thus it is necessary to investigate the structural properties of meta-stable bound and resonance $^{1,3}F^e$ states using a complete wavefunction containing both pf and dd configurations explicitly under the ESCP where the screening is to be considered in both the parts of the potential without any approximation.

In this communication, we have made an extensive investigation on the structural properties of $^{1,3}F^e$ states of He-atom under ESCP using wavefunction consisting of both pf and dd configurations expanded in multi-exponent Hylleraas-type basis set. Energies of the meta-stable bound $^{1,3}F^e$ states are calculated using Ritz variation principle for different screening conditions of the potential. "Soft wall" strategy [59–61] of the stabilization method [62] has been used to determine the resonance parameters of $^{1,3}F^e$ states of He atom lying below $He^+(3p)$ and $He^+(4p)$ thresholds for various screening of ESCP. The basis integral arising in the matrix elements for both the attractive and repulsive parts of ESCP are calculated analytically in a closed form without any approximation although the effective potential to describe the interaction is not being constructed from the first principle. The resonance parameters above $He^+(3p)$ threshold under screened Coulomb environment are reported for the first time in literature for $^{1,3}F^e$ states of He-atom. Other structural properties like one- and two-particle moments, expectation values of inter-electronic angles etc. under ESCP are also estimated to study how the overall structure of the atom alters as screening changes. Atomic units are used throughout unless otherwise specified.

2. Method

The general variational equation of a two-electron system can be written as

$$\delta \int [H - E]\Psi d\tau = 0 \tag{1}$$

where the volume element is $d\tau = r_1\, r_2\, r_{12}\, dr_1\, dr_2\, dr_{12}\, \sin\theta\, d\theta\, d\phi\, d\psi$; r_1 and r_2 being the respective distances of the electrons from the nucleus, r_{12} being the inter-electronic distance and (θ, ϕ, ψ) being the Eulerian angles [63] which specify the rotation of the triangle formed by r_1, r_2 and r_{12} in space. E is the energy eigenvalue of the atom considered. The Hamiltonian (H) of the two-electron system is given by,

$$H = -\frac{1}{2}\nabla_1^2 - \frac{1}{2}\nabla_2^2 + V_{eff} \tag{2}$$

where V_{eff} is the effective potential of the two-electron system which takes the following form under ESCP

$$V_{eff} = -\frac{Ze^{-r_1/\lambda_D}}{r_1} - \frac{Ze^{-r_2/\lambda_D}}{r_2} + \frac{e^{-r_{12}/\lambda_D}}{r_{12}} \tag{3}$$

where Z is the nuclear charge and λ_D is the plasma screening length [25].

The wavefunction of the $^{1,3}F^e$ state can be written as the sum of the products of the radial and the angular parts [59] as given below,

$$\Psi = f_3^0 D_3^0 + f_3^{2+} D_3^{2+} + f_3^{2-} D_3^{2-} \tag{4}$$

The angular parts $D_L^{\kappa\pm}$ (L being the angular momentum of the state) are the real symmetric Wigner functions [63] which are the eigenfunctions

of the two-electron angular momentum operator. The explicit forms of D_3^0, D_3^{2+} and D_3^{2-} as a function of the Eulerian angles (θ, ϕ, ψ) [63] are given by

$$\begin{aligned} D_3^0 &= \frac{5\cos^3\theta - 3\cos\theta}{2} \\ D_3^{2+} &= \frac{\sqrt{15}}{2}\cos 2\psi \sin^2\theta\cos\theta \\ D_3^{2-} &= \frac{\sqrt{15}}{2}\sin 2\psi \sin^2\theta\cos\theta \end{aligned} \tag{5}$$

The radial parts $f_L^{\kappa\pm}$ consist of two most dominant configurations *pf* and *dd*. The explicit forms of $f_L^{\kappa\pm}$ [59] are given by

$$\begin{aligned} f_3^0 &= -(f \mp \tilde{f})\sin\theta_{12} - \sqrt{\frac{10}{7}}(g \mp \tilde{g})\sin\theta_{12}\cos\theta_{12} \\ f_3^{2+} &= \frac{\sqrt{15}}{6}(f \mp \tilde{f})\sin 2\theta_{12} + \sqrt{\frac{50}{21}}(g \mp \tilde{g})\sin\theta_{12} \\ f_3^{2-} &= \frac{\sqrt{15}}{6}(f \pm \tilde{f})(1 - \cos 2\theta_{12}) \end{aligned} \tag{6}$$

Upper and lower signs in the parentheses correspond to singlet and triplet states respectively. Here θ_{12} is the angle between $\vec{r_1}$ and $\vec{r_2}$. In Eq. (6), $f(r_1, r_2, r_{12})$ and $g(r_1, r_2, r_{12})$ functions are associated with *pf* and *dd* configurations respectively where $\tilde{f} = f(r_2, r_1, r_{12})$ and $\tilde{g} = g(r_2, r_1, r_{12})$. The trial radial functions f and g are expanded in nine-exponent Hylleraas type basis set as given below

$$\begin{aligned} f(r_1, r_2, r_{12}) &= \sum_{i=1}^{i_{max}} r_1^{a_i}\, r_2^{b_i}\, r_{12}^{c_i} \left[\sum_{\alpha=1}^{9} C_{i\alpha\alpha} e^{-\rho_\alpha(r_1+r_2)} + \sum_{\alpha=1}^{9}\sum_{\beta=1}^{9} C_{i\alpha\beta} e^{-\rho_\alpha r_1 - \rho_\beta r_2}\right] \\ g(r_1, r_2, r_{12}) &= \sum_{i=1}^{i_{max}} r_1^{a'_i}\, r_2^{b'_i}\, r_{12}^{c'_i} \left[\sum_{\alpha=1}^{9} D_{i\alpha\alpha} e^{-\sigma_\alpha(r_1+r_2)} + \sum_{\alpha=1}^{9}\sum_{\beta=1}^{9} D_{i\alpha\beta} e^{-\sigma_\alpha r_1 - \sigma_\beta r_2}\right] \end{aligned} \tag{7}$$

In Eq. (7), the powers (a_i, b_i, c_i) and (a'_i, b'_i, c'_i) are positive integers and i_{max} is the maximum number of the set of powers of r_1, r_2 and r_{12}. In the above equation ρ_α and ρ_β are the non-linear parameters for electrons 1 and 2 respectively. The first summation for f in Eq. (7) corresponds to $\alpha = \beta$ and that of the second summation corresponds to $\alpha \neq \beta$. In the double sum of Eq. (7), $\alpha < \beta$ is being taken while $\tilde{f}$ takes care of the terms with $\alpha > \beta$. Similar notations are being used for g functions. $C_{i\alpha\beta}$ and $D_{i\alpha\beta}$ are the linear expansion coefficients of f and g respectively. The number of terms in the summation of α and β is $9(9+1)/2$ *i.e.* 45. Hence, combining f and g, the total number of terms in the basis set is $N = 90 \times i_{max}$. In the present calculation we have taken $N = 900$. The non-linear parameters of *pf* and *dd* configurations are produced in a geometrical progression using the relations $\rho_i = \rho_{i-1}\gamma$ and $\sigma_i = \sigma_{i-1}\gamma'$, where γ and γ' are geometrical progression ratios in f and g functions respectively. The energy eigenvalues (E) are derived by solving the generalized eigenvalue equation,

$$\underline{\underline{H}}\ \underline{C} = E\underline{\underline{S}}\ \underline{C} \tag{8}$$

where $\underline{\underline{H}}$ is the Hamiltonian matrix, $\underline{\underline{S}}$ is the overlap matrix and $\underline{C}$ is a column matrix made up of linear variational coefficients. To estimate the matrix elements of $\underline{\underline{H}}$ and $\underline{\underline{S}}$, one need to evaluate the basis integrals of the following form :

$$A(m, n, l; a_1, a_2) = \int_{r_1=0}^{\infty}\int_{r_2=0}^{\infty}\int_{|r_1-r_2|}^{r_1+r_2} r_1^m r_2^n r_{12}^l e^{-a_1 r_1 - a_2 r_2} dr_1 dr_2 dr_{12} \tag{9}$$

The analytic forms of $A(m, n, l; a_1, a_2)$ are given in our previous work [64]. The linear variational parameters as obtained from Eq. (8) are used to determine different one and two-particle moments such as $\langle r_1\rangle$, $\langle r_1^2\rangle$, $\langle r_{12}\rangle$, $\langle r_{12}^2\rangle$ and inter-electronic angles $\langle\theta_{12}\rangle$ by estimating $\langle\cos\theta_{12}\rangle$ and using the following relation [65]

$$\langle\theta_{12}\rangle \approx \frac{\pi}{2} - \frac{3\pi}{2}\langle\cos\theta_{12}\rangle \tag{10}$$

These expectation values altogether contribute to understand the geometry of the atom quite clearly.

To explore the behaviour of two-electron energy levels under ESCP, it is essential to calculate the respective one-electron threshold energy (E_{th}) under ESCP. The radial variational equation for $2p$ state of He^+ ion under the ESCP environment can be written as

$$\delta\int\left\{\left(\frac{\partial\chi}{\partial r}\right)^2 + \frac{2}{r^2}\chi^2 + \frac{2e^{-r/\lambda_D}}{r}\chi^2 - E_{th}\chi^2\right\} dr = 0 \tag{11}$$

The radial function $\chi(r)$ is expanded in the following type of basis set as

$$\chi(r) = \sum_i C_i\ r^{n_i}\ e^{-\xi_i r} \tag{12}$$

In the present work, the basis set in Eq. (12) contains 44 terms, and the exponents are taken in a geometrical sequence, $\xi_i = \xi_{i-1}\zeta$; ζ being the geometrical ratio. The matrix diagonalization approach using Eq. (8) determines the energy eigenvalues E_{th} and linear variational coefficients C_i's. In the current situation, this technique is repeated for each different screening length (λ_D). All computations are performed with quadruple precision.

3. Results and discussions

A typical stabilization diagram for $^3F^e$ state of He atom ($\lambda_D = 70$ a.u.) is given in Fig. 1. For a fixed value of γ' repeated diagonalization has been done for 432 different values of γ. The plot 1 up to $He^+(4p)$ threshold energy −0.098644 a.u. shows two classes of states:

(i) The energy eigenroots which are insensitive to the variation of γ lies below $He^+(2p)$ threshold energy −0.471931 a.u. are the metastable bound states (MBS) having dominant configurations $2pnf$ $[4 \le n \le 8]$.
(ii) Above the $He^+(2p)$ threshold energy, the variation of energy eigenroots with γ show avoided crossings and plateaus which indicates the presence of resonance states (RS).

The convergence of the energy eigenvalues of $2pnf$ $(n = 4-6)$ MBS $(^{1,3}F^e)$ for two different screening lengths $\lambda_D = 100$ a.u. and $\lambda_D = 40$ a.u. are shown in the table Table A. It is clear from Table A that the energy eigenvalues are converged at least up to 7th decimal place. For the free He atom, the convergence behaviour of the energy eigenvalues was shown in our earlier work [59]. In the succeeding tables we have given the energy eigenvalues up to 6th decimal place.

The optimized MBS $(^{1,3}F^e)$ energy eigenvalues of He atom for different λ_D are given in Tables B and C. With the decrease in λ_D, the MBSs gradually move towards the respective dressed threshold of $He^+(2p)$ under plasma. As a consequence the number of MBS decreases sharply. It is noticeable that below $\lambda_D = 20$ a.u., there exists no MBS of $^3F^e$ symmetry of He atom. The comparison of the present results with those of Kar and Ho [58,66] as shown in Tables B and C reveals that the present energy eigenvalues of metastable bound $2pnf$ $(n = 4-6)$ states for $\lambda_D = \infty$ are consistent up to sixth decimal place. In fact, we find that under the plasma scenario ($\lambda_D \le 100$ a.u.), our present calculated energy values for MBS are lowest yet obtained as evident from Tables B and C. The Ritz variational calculation provides an upper bound to the exact energy eigenvalues for bound states, and hence, the present results are more accurate in a sense that they are supposed to be closer to the exact values, as compared to other existing results. The reason behind this accuracy of the present method lies in the fact that Kar and Ho [58,66] used an approximated form of the screened inter-electronic repulsion by expanding it in a Taylor series truncated up to a finite limit as

$$\frac{e^{-r_{12}/\lambda_D}}{r_{12}} \approx \sum_{n=0}^{m}(-1)^n \frac{r_{12}^{n-1}}{\lambda_D^n n!}$$

In contrast we have used the exact analytic form of the screened inter-electronic repulsion and estimated the matrix element analytically. Tables D and E show different structural properties like repulsive

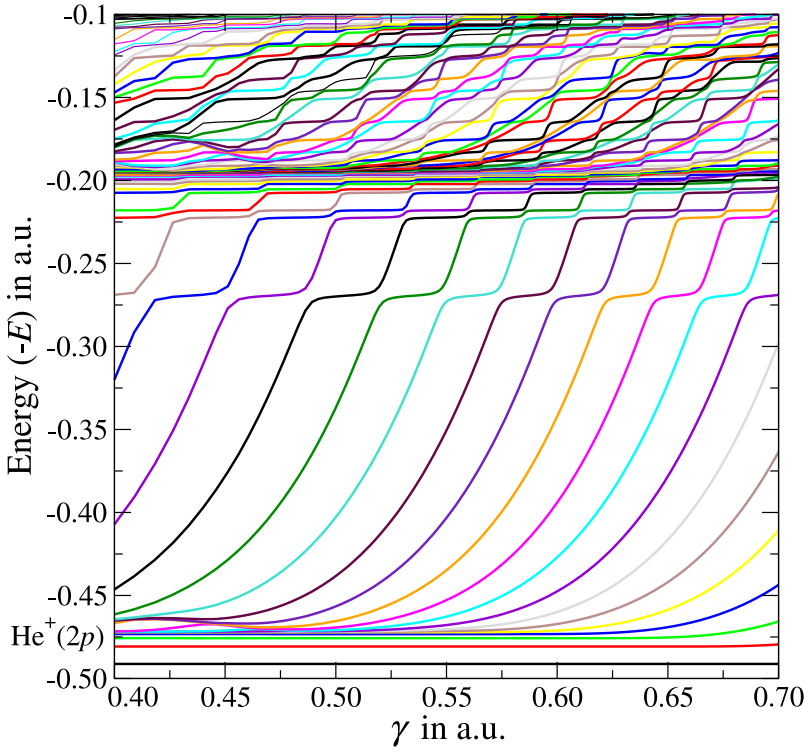

Fig. 1. Stabilization plot of first 250 diagonalized energy eigenroots using $N = 900$ terms in the basis set for $^3F^e$ state of He-atom in the energy range −0.5 a.u. to −0.098644 a.u. for $\lambda_D = 70$ a.u. showing existence of both metastable bound and resonance states.

Table A
Convergence table for the energy eigenvalues (E in a.u.) of $2pnf$ ($n = 4 - 6$) MBS ($^{1,3}F^e$) for screening lengths $\lambda_D = 100$ a.u. and $\lambda_D = 40$ a.u. and basis sizes $N = 720, 810$ and 900.

$\lambda_D = 100$						
	$^3F^e$			$^1F^e$		
N	$2p4f$	$2p5f$	$2p6f$	$2p4f$	$2p5f$	$2p6f$
720	−0.50305211	−0.49202045	−0.48639964	−0.50305606	−0.49202303	−0.48640116
810	−0.50305211	−0.49202045	−0.48639965	−0.50305606	−0.49202304	−0.48640117
900	−0.50305211	−0.49202047	−0.48639966	−0.50305606	−0.49202305	−0.48640117
$\lambda_D = 40$						
	$^3F^e$			$^1F^e$		
N	$2p4f$	$2p5f$	$2p6f$	$2p4f$	$2p5f$	$2p6f$
720	−0.46329714	−0.45477196	−0.45178121	−0.46330037	−0.45477358	−0.45178169
810	−0.46329714	−0.45477196	−0.45178123	−0.46330037	−0.45477358	−0.45178170
900	−0.46329714	−0.45477197	−0.45178124	−0.46330037	−0.45477359	−0.45178172

Table B
Energy eigenvalues (E in a.u.) of metastable bound $2pnf$ $^3F^e$ [$n \geq 4$] states of He below $He^+(2p)$ threshold and $2p$ state of He^+ ion for different screening length λ_D in a.u.

States	λ_D									
	∞	100	70	50	40	30	25	20	15	12
$He^+(2p)$	−0.5	−0.480247	−0.471931	−0.460980	−0.451525	−0.436025	−0.423853	−0.405969	−0.377135	−0.349478
$2p4f$	−0.531991	−0.503052	−0.491264	−0.476087	−0.463297	−0.442971	−0.427595	−0.406086		
	−0.5319915[a]	−0.502952[a]	−0.4910705[a]	−0.4757335[a]	−0.46278[a]	−0.442148[a]	−0.426497[a]			
	−0.531991326[b]	−0.503052113[b]		−0.476087092[b]				−0.4060871[b]		
$2p5f$	−0.520383	−0.492020	−0.480773	−0.466541	−0.454771	−0.436544				
	−0.520383[a]	−0.491925[a]	−0.480597[a]	−0.466237[a]	−0.454334[a]					
$2p6f$	−0.514111	−0.486399	−0.475734	−0.462493	−0.451781					
	−0.514111[a]	−0.486313[a]	−0.475580[a]	−0.462197[a]						
$2p7f$	−0.510344	−0.483338	−0.473276	−0.461041						
$2p8f$	−0.507906	−0.481645	−0.472187							
$2p9f$	−0.506238	−0.480744								
$2p10f$	−0.505044	−0.480330								
$2p11f$	−0.504144									
$2p12f$	−0.503410									
$2p13f$	−0.502832									

(*continued on next page*)

Table B (*continued*).

States	λ_D									
	∞	100	70	50	40	30	25	20	15	12
$2p14f$	−0.502296									
$2p15f$	−0.501224									

[a] [66].
[b] [58].

Table C
Energy eigenvalues (E in a.u.) of metastable bound $2pnf\ ^1F^e$ $[n \geq 4]$ states of He below $He^+(2p)$ threshold and $2p$ state of He^+ ion for different screening length λ_D in a.u.

States	λ_D									
	∞	100	70	50	40	30	25	20	15	12
$He^+(2p)$	−0.5	−0.480247	−0.471931	−0.460980	−0.451525	−0.436025	−0.423853	−0.405969	−0.377135	−0.349478
$2p4f$	−0.531995	−0.503056	−0.491268	−0.476090	−0.463300	−0.442973	−0.427597	−0.406087		
	−0.5319955[a]	−0.502956[a]	−0.491074[a]	−0.4757375[a]	−0.462784[a]	−0.4421585[a]	−0.426532[a]			
	−0.531995436[b]	−0.503056068[b]		−0.476090624[b]				−0.4060876[b]		
$2p5f$	−0.520385	−0.492023	−0.480775	−0.466543	−0.454773	−0.436545				
	−0.5203855[a]	−0.491928[a]	−0.4805995[a]	−0.4662415[a]	−0.454351[a]					
$2p6f$	−0.514113	−0.486401	−0.475736	−0.462494	−0.451781					
	−0.514113[a]	−0.4863145[a]	−0.4755835[a]	−0.4622235[a]						
$2p7f$	−0.510345	−0.483339	−0.473276	−0.461042						
$2p8f$	−0.507907	−0.481645	−0.472187							
$2p9f$	−0.506239	−0.480745								
$2p10f$	−0.505045	−0.480330								
$2p11f$	−0.504144									
$2p12f$	−0.503411									
$2p13f$	−0.502832									
$2p14f$	−0.502296									
$2p15f$	−0.501230									

[a] [66].
[b] [58].

Table D
Expectation values of repulsive potential $\langle V_r \rangle$, attractive potential $\langle V_a \rangle$, ratio of attractive to repulsive potential $\eta = \left|\frac{\langle V_a \rangle}{\langle V_r \rangle}\right|$, $\langle \cos\theta_{12} \rangle$, inter-electronic angles $\langle \theta_{12} \rangle$ (in degree) using (10), different one and two-particle moments of metastable bound $2pnf\ ^3F^e$ $[n = 4-15]$ states of He atom below $He^+(2p)$ threshold for different screening length λ_D. The notation $A[\pm B]$ stands for $A \times 10^{\pm B}$. All values are given in atomic units.

States	λ_D	$\langle V_r \rangle$	$\langle V_a \rangle$	η	$\langle r_1 \rangle$	$\langle r_1^2 \rangle$	$\langle r_{12} \rangle$	$\langle r_{12}^2 \rangle$	$\langle \cos\theta_{12} \rangle$	$\langle \theta_{12} \rangle$
$2p4f$	∞	6.38[−2]	−1.12[+0]	17.65	9.96[+0]	1.72[+2]	1.76[+1]	3.47[+2]	−1.32[−2]	93.59
	100	5.39[−2]	−1.08[+0]	20.17	1.00[+1]	1.78[+2]	1.79[+1]	3.57[+2]	−1.28[−2]	93.47
	70	4.97[−2]	−1.07[+0]	21.53	1.02[+1]	1.83[+2]	1.81[+1]	3.67[+2]	−1.24[−2]	93.36
	50	4.41[−2]	−1.04[+0]	23.74	1.04[+1]	1.93[+2]	1.86[+1]	3.88[+2]	−1.17[−2]	93.17
	40	3.93[−2]	−1.02[+0]	26.15	1.07[+1]	2.06[+2]	1.91[+1]	4.13[+2]	−1.09[−2]	92.95
	30	3.13[−2]	−9.96[−1]	31.78	1.14[+1]	2.39[+2]	2.05[+1]	4.79[+2]	−9.34[−3]	92.52
	25	2.48[−2]	−9.69[−1]	38.96	1.23[+1]	2.86[+2]	2.24[+1]	5.73[+2]	−7.76[−3]	92.09
	20	1.41[−2]	−9.28[−1]	65.49	1.59[+1]	5.32[+2]	2.94[+1]	1.06[+3]	−4.64[−3]	91.25
$2p5f$	∞	4.07[−2]	−1.08[+0]	26.56	1.66[+1]	5.41[+2]	3.09[+1]	1.08[+3]	−6.77[−3]	91.82
	100	3.08[−2]	−1.04[+0]	33.79	1.71[+1]	5.79[+2]	3.19[+1]	1.15[+3]	−6.27[−3]	91.69
	70	2.67[−2]	−1.02[+0]	38.36	1.77[+1]	6.19[+2]	3.30[+1]	1.23[+3]	−5.81[−3]	91.56
	50	2.13[−2]	−1.00[+0]	46.93	1.88[+1]	7.03[+2]	3.52[+1]	1.40[+3]	−5.02[−3]	91.35
	40	1.67[−2]	−9.83[−1]	58.64	2.02[+1]	8.27[+2]	3.81[+1]	1.65[+3]	−4.17[−3]	91.12
	30	8.98[−3]	−9.51[−1]	105.83	2.56[+1]	1.37[+3]	4.88[+1]	2.74[+3]	−2.41[−3]	90.65
$2p6f$	∞	2.81[−2]	−1.05[+0]	37.48	2.48[+1]	1.26[+3]	4.72[+1]	2.52[+3]	−3.90[−3]	91.05
	100	1.84[−2]	−1.01[+0]	55.18	2.64[+1]	1.43[+3]	5.04[+1]	2.87[+3]	−3.34[−3]	90.90
	70	1.44[−2]	−1.00[+0]	69.09	2.81[+1]	1.64[+3]	5.39[+1]	3.28[+3]	−2.86[−3]	90.77
	50	9.42[−3]	−9.78[−1]	103.87	3.22[+1]	2.17[+3]	6.21[+1]	4.34[+3]	−2.04[−3]	90.55
	40	5.01[−3]	−9.60[−1]	191.34	4.06[+1]	3.52[+3]	7.89[+1]	7.05[+3]	−1.15[−3]	90.31
$2p7f$	∞	2.06[−2]	−1.04[+0]	50.39	3.44[+1]	2.50[+3]	6.65[+1]	5.00[+3]	−2.45[−3]	90.66
	100	1.10[−2]	−1.00[+0]	90.45	3.86[+1]	3.14[+3]	7.48[+1]	6.28[+3]	−1.85[−3]	90.50
	70	7.34[−3]	−9.86[−1]	134.26	4.37[+1]	4.04[+3]	8.50[+1]	8.08[+3]	−1.35[−3]	90.36
	50	2.53[−3]	−9.65[−1]	381.10	6.40[+1]	8.91[+3]	1.25[+2]	1.78[+4]	−5.17[−4]	90.13
$2p8f$	∞	1.57[−2]	−1.03[+0]	65.32	4.56[+1]	4.45[+3]	8.89[+1]	8.90[+3]	−1.64[−3]	90.44
	100	6.43[−3]	−9.92[−1]	154.20	5.53[+1]	6.51[+3]	1.08[+2]	1.30[+4]	−1.01[−3]	90.27
	70	2.95[−3]	−9.77[−1]	331.09	7.15[+1]	1.09[+4]	1.40[+2]	2.18[+4]	−5.20[−4]	90.14
$2p9f$	∞	1.24[−2]	−1.02[+0]	82.20	5.83[+1]	7.33[+3]	1.14[+2]	1.46[+4]	−1.16[−3]	90.31
	100	3.38[−3]	−9.86[−1]	291.23	8.00[+1]	1.37[+4]	1.57[+2]	2.74[+4]	−5.12[−4]	90.13
$2p10f$	∞	9.99[−3]	−1.02[+0]	102.05	7.31[+1]	1.15[+4]	1.43[+2]	2.31[+4]	−8.09[−4]	90.21
	100	1.33[−3]	−9.82[−1]	733.41	1.25[+2]	3.38[+4]	2.48[+2]	6.76[+4]	−1.96[−4]	90.05
$2p11f$	∞	7.99[−3]	−1.01[+0]	127.19	9.15[+1]	1.81[+4]	1.80[+2]	3.63[+4]	−5.13[−4]	90.14
$2p12f$	∞	6.15[−3]	−1.01[+0]	164.69	1.17[+2]	3.00[+4]	2.33[+2]	6.00[+4]	−3.16[−4]	90.08
$2p13f$	∞	6.75[−3]	−1.01[+0]	149.84	1.33[+2]	4.07[+4]	2.64[+2]	8.15[+4]	−5.17[−4]	90.14
$2p14f$	∞	5.08[−3]	−1.00[+0]	198.36	1.83[+2]	7.49[+4]	3.63[+2]	1.49[+5]	−3.51[−4]	90.09
$2p15f$	∞	7.02[−3]	−1.00[+0]	142.97	2.12[+2]	1.11[+5]	4.22[+2]	2.23[+5]	−7.68[−4]	90.20

Table E

Expectation values of repulsive potential $\langle V_r \rangle$, attractive potential $\langle V_a \rangle$, ratio of attractive to repulsive potential $\eta = \left|\frac{\langle V_a \rangle}{\langle V_r \rangle}\right|$, $\langle \cos\theta_{12} \rangle$, inter-electronic angles $\langle \theta_{12} \rangle$ (in degree) using (10), different one and two-particle moments of metastable bound $2pnf\ ^1F^e$ $[n = 4-15]$ states of He atom below $He^+(2p)$ threshold for different screening length λ_D. The notation $A[\pm B]$ stands for $A \times 10^{\pm B}$. All values are given in atomic units.

States	λ_D	$\langle V_r \rangle$	$\langle V_a \rangle$	η	$\langle r_1 \rangle$	$\langle r_1^2 \rangle$	$\langle r_{12} \rangle$	$\langle r_{12}^2 \rangle$	$\langle \cos\theta_{12} \rangle$	$\langle \theta_{12} \rangle$
$2p4f$	∞	6.39[−2]	−1.12[+0]	17.64	9.96[+0]	1.72[+2]	1.76[+1]	3.46[+2]	−1.28[−2]	93.46
	100	5.39[−2]	−1.08[+0]	20.15	1.00[+1]	1.77[+2]	1.78[+1]	3.57[+2]	−1.24[−2]	93.36
	70	4.97[−2]	−1.07[+0]	21.52	1.02[+1]	1.83[+2]	1.81[+1]	3.67[+2]	−1.20[−2]	93.25
	50	4.41[−2]	−1.04[+0]	23.73	1.04[+1]	1.93[+2]	1.86[+1]	3.87[+2]	−1.13[−2]	93.07
	40	3.93[−2]	−1.02[+0]	26.14	1.07[+1]	2.06[+2]	1.91[+1]	4.13[+2]	−1.06[−2]	92.87
	30	3.13[−2]	−9.96[−1]	31.76	1.14[+1]	2.39[+2]	2.05[+1]	4.79[+2]	−9.11[−3]	92.45
	25	2.49[−2]	−9.69[−1]	38.93	1.23[+1]	2.86[+2]	2.24[+1]	5.73[+2]	−7.59[−3]	92.05
	20	1.41[−2]	−9.28[−1]	65.43	1.59[+1]	5.32[+2]	2.94[+1]	1.06[+3]	−4.57[−3]	91.23
$2p5f$	∞	4.07[−2]	−1.08[+0]	26.55	1.66[+1]	5.41[+2]	3.09[+1]	1.08[+3]	−6.43[−3]	91.73
	100	3.08[−2]	−1.04[+0]	33.76	1.71[+1]	5.79[+2]	3.19[+1]	1.15[+3]	−5.96[−3]	91.61
	70	2.67[−2]	−1.02[+0]	38.33	1.77[+1]	6.18[+2]	3.30[+1]	1.23[+3]	−5.53[−3]	91.49
	50	2.13[−2]	−1.00[+0]	46.90	1.88[+1]	7.03[+2]	3.52[+1]	1.40[+3]	−4.80[−3]	91.29
	40	1.67[−2]	−9.83[−1]	58.59	2.02[+1]	8.27[+2]	3.81[+1]	1.65[+3]	−4.00[−3]	91.08
	30	8.99[−3]	−9.51[−1]	105.71	2.56[+1]	1.37[+3]	4.88[+1]	2.74[+3]	−2.33[−3]	90.63
$2p6f$	∞	2.82[−2]	−1.05[+0]	37.46	2.48[+1]	1.26[+3]	4.72[+1]	2.52[+3]	−3.67[−3]	90.99
	100	1.84[−2]	−1.01[+0]	55.14	2.64[+1]	1.43[+3]	5.04[+1]	2.87[+3]	−3.15[−3]	90.85
	70	1.44[−2]	−1.00[+0]	69.04	2.81[+1]	1.64[+3]	5.39[+1]	3.28[+3]	−2.70[−3]	90.73
	50	9.43[−3]	−9.78[−1]	103.78	3.22[+1]	2.17[+3]	6.21[+1]	4.34[+3]	−1.94[−3]	90.52
	40	5.02[−3]	−9.60[−1]	191.11	4.06[+1]	3.52[+3]	7.88[+1]	7.05[+3]	−1.10[−3]	90.29
$2p7f$	∞	2.06[−2]	−1.04[+0]	50.37	3.44[+1]	2.50[+3]	6.65[+1]	5.00[+3]	−2.29[−3]	90.61
	100	1.10[−2]	−1.00[+0]	90.38	3.86[+1]	3.14[+3]	7.48[+1]	6.28[+3]	−1.74[−3]	90.46
	70	7.35[−3]	−9.86[−1]	134.16	4.37[+1]	4.04[+3]	8.50[+1]	8.08[+3]	−1.27[−3]	90.34
	50	2.53[−3]	−9.65[−1]	380.59	6.40[+1]	8.91[+3]	1.25[+2]	1.78[+4]	−4.91[−4]	90.13
$2p8f$	∞	1.57[−2]	−1.03[+0]	65.29	4.56[+1]	4.44[+3]	8.89[+1]	8.90[+3]	−1.53[−3]	90.41
	100	6.44[−3]	−9.92[−1]	154.09	5.52[+1]	6.51[+3]	1.08[+2]	1.30[+4]	−9.50[−4]	90.25
	70	2.95[−3]	−9.77[−1]	330.77	7.14[+1]	1.09[+4]	1.40[+2]	2.18[+4]	−4.89[−4]	90.13
$2p9f$	∞	1.24[−2]	−1.02[+0]	82.17	5.83[+1]	7.33[+3]	1.14[+2]	1.46[+4]	−1.07[−3]	90.29
	100	3.39[−3]	−9.86[−1]	291.01	8.00[+1]	1.37[+4]	1.57[+2]	2.74[+4]	−4.78[−4]	90.12
$2p10f$	∞	9.99[−3]	−1.02[+0]	102.02	7.31[+1]	1.15[+4]	1.43[+2]	2.31[+4]	−7.48[−4]	90.20
	100	1.34[−3]	−9.82[−1]	732.32	1.25[+2]	3.38[+4]	2.48[+2]	6.76[+4]	−1.83[−4]	90.04
$2p11f$	∞	7.99[−3]	−1.01[+0]	127.14	9.14[+1]	1.81[+4]	1.80[+2]	3.63[+4]	−4.70[−4]	90.12
$2p12f$	∞	6.15[−3]	−1.01[+0]	164.66	1.17[+2]	3.00[+4]	2.33[+2]	6.00[+4]	−2.85[−4]	90.07
$2p13f$	∞	6.74[−3]	−1.01[+0]	150.09	1.33[+2]	4.07[+4]	2.64[+2]	8.15[+4]	−4.67[−4]	90.13
$2p14f$	∞	5.07[−3]	−1.00[+0]	198.97	1.83[+2]	7.49[+4]	3.64[+2]	1.49[+5]	−3.09[−4]	90.08
$2p15f$	∞	6.76[−3]	−1.00[+0]	147.92	2.15[+2]	1.13[+5]	4.27[+2]	2.26[+5]	−6.59[−4]	90.17

potential $\langle V_r \rangle$, attractive potential $\langle V_a \rangle$, $\langle \cos\theta_{12} \rangle$, $\langle \theta_{12} \rangle$, $\langle r_1 \rangle$, $\langle r_1^2 \rangle$, $\langle r_{12} \rangle$ and $\langle r_{12}^2 \rangle$ of $^3F^e$ and $^1F^e$ MBSs for different λ_D values. It can be seen from Tables D and E that both the one and two-particle moments $\langle r_1 \rangle$ and $\langle r_{12} \rangle$ increase when λ_D decreases for $^{1,3}F^e$ states. This indicates that the size of the atom increases with the decrease of λ_D, *i.e.* expansion of the atom occurs.

We have used the "soft-wall" technique [59,60,67] of the well celebrated stabilization method [61,62] to estimate the energy (E_r) and width (Γ_r) of the RSs. Firstly we calculate the density of states (DOS) of a single RS as the inverse of the slope of the stabilization plot, taking points from the plateau region as given in the following formula,

$$\rho_k(E) = \left| \frac{\gamma_{i+1} - \gamma_{i-1}}{E_k(\gamma_{i+1}) - E_k(\gamma_{i-1})} \right| \tag{13}$$

Finally, the resonance parameters (E_r, Γ_r) are obtained by Lorentzian fitting of the DOS as

$$\rho_k(E) = y_0 + \frac{A}{\pi} \frac{\Gamma_r/2}{(E - E_r)^2 + (\Gamma_r/2)^2} \tag{14}$$

where y_0 is the baseline background, A is the total area under the curve from the baseline, E_r gives the position of the centre of the peak of the curve, and Γ_r represents the full width at half maximum. For example, Fig. 2 shows the plot of DOS of the 9-th root with respect to energy values (E) which is fitted by Lorentzian curve using Eq. (14). The fitting gives the resonance parameters as $E_r = -0.026947$ a.u. and $\Gamma_r = 0.00195$ a.u. All plotting and fitting operations are done using the QtiPlot software, and the plot with least χ^2 fitting is considered.

The values of E_r and Γ_r of resonance $^3F^e$ states below the $He^+(3p)$ threshold for various λ_D are provided in Tables F and G, respectively. The feature of the decrease of the number of RS with respect to the decrease in λ_D is similar to that of MBS. Estimated resonance parameters $(E_r,\ \Gamma_r)$ are compared with the only available values of Kar and Ho [66] below the $He^+(3p)$ threshold in the Tables F and G. We have obtained a greater number of RSs than reported by Kar and Ho [66] for each λ_D. The resonance $^3F^e$ state can originate from the electronic configurations $3dnd$ $[n \geq 3]$, $3pnf$ $[n \geq 4]$ and $3dng$ $[n \geq 5]$. The identification [59,66] of the configurations are given below:

(i) $^3F^e(1)$,$^3F^e(2)$,$^3F^e(4)$,$^3F^e(7)$,$^3F^e(10)$,$^3F^e(13)$,$^3F^e(16)$ and $^3F^e(19)$ states originate from the dominant $3dnd$ $[3 \leq n \leq 10]$ configurations.

(ii) $^3F^e(3)$,$^3F^e(5)$,$^3F^e(8)$,$^3F^e(11)$,$^3F^e(14)$,$^3F^e(17)$ and $^3F^e(20)$ states originate from the dominant $3pnf$ $[4 \leq n \leq 10]$ configurations.

(iii) $^3F^e(6)$,$^3F^e(9)$,$^3F^e(12)$,$^3F^e(15)$ and $^3F^e(18)$ states originate from the dominant $3dng$ $[5 \leq n \leq 9]$ configurations.

From Table G it can be seen that the width Γ_r of RS decreases with the decrease of λ_D for most of the states except the RSs having dominant configurations $3dng$ $[5 \leq n \leq 9]$. Fig. 3 depicts the variation of Γ_r with respect to $\frac{1}{\lambda_D}$ for the $^3F^e(1)$,$^3F^e(3)$ and $^3F^e(6)$ RS, corresponding to the dominant electronic configurations $3d^2, 3p4f$ and $3d5g$ respectively. A similar feature for the resonance widths of $^3P^e$ symmetry of two-electron systems are reported in literature [68,69].

We have estimated the changes of the structural properties with the change of screening length λ_D. The structural properties like $\langle V_r \rangle$, $\langle V_a \rangle$, $\eta \left(= \left|\frac{\langle V_a \rangle}{\langle V_r \rangle}\right|\right)$, $\langle \cos\theta_{12} \rangle$, $\langle \theta_{12} \rangle$ using (10), $\langle r_1 \rangle$, $\langle r_1^2 \rangle$, $\langle r_{12} \rangle$ and $\langle r_{12}^2 \rangle$ of resonance $^3F^e$ states of He atom below $He^+(3p)$ threshold are given in the Table H. Like the MBSs, $\langle V_a \rangle$ and $\langle V_r \rangle$ decrease while the ratio η increases with the decrease of λ_D. Table H shows that similar to MBS, $\langle r_1 \rangle$, $\langle r_1^2 \rangle$, $\langle r_{12} \rangle$ and $\langle r_{12}^2 \rangle$ increases as λ_D decreases. From the last column of Table H it can be seen that, $\langle \theta_{12} \rangle$ values of $3dnd$ and

Table F
Resonance energy E_r (a.u.) of $^3F^e$ states of He atom below $He^+(3p)$ threshold and energy of $3p$ state of He^+ ion for different screening length λ_D in a.u.

States	λ_D									
	∞	100	70	50	40	30	25	20	15	12
$He^+(3p)$	−0.222222	−0.202835	−0.194885	−0.184610	−0.175918	−0.162017	−0.151409	−0.136315	−0.113232	−0.092587
$^3F^e(1)$	−0.31072	−0.28159	−0.26947	−0.25385	−0.24059	−0.21926	−0.20291	−0.17953	−0.14352	−0.11113
	−0.31069[a]	−0.28135[a]	−0.269175[a]	−0.253315[a]	−0.23978[a]	−0.217945[a]	−0.2011[a]	−0.176905[a]	−0.139385[a]	−0.10523[a]
$^3F^e(2)$	−0.26283	−0.23404	−0.22239	−0.20750	−0.19505	−0.17546	−0.16080	−0.14047		
	−0.262825[a]	−0.23388[a]	−0.22211[a]	−0.206995[a]	−0.194305[a]	−0.17426[a]	−0.159195[a]	−0.138115[a]		
$^3F^e(3)$	−0.25826	−0.22956	−0.21801	−0.20327	−0.19098	−0.17171	−0.15734	−0.13759		
	−0.25826[a]	−0.229345[a]	−0.217605[a]	−0.202535[a]	−0.1899[a]	−0.16996[a]	−0.155015[a]			
$^3F^e(4)$	−0.24681	−0.21852	−0.20739	−0.19338	−0.18188	−0.16426				
	−0.246805[a]	−0.218385[a]	−0.20712[a]	−0.192915[a]	−0.18122[a]	−0.16309[a]				
$^3F^e(5)$	−0.24438	−0.21621	−0.20524	−0.19145	−0.18018	−0.16300				
	−0.244385[a]	−0.21604[a]	−0.20485[a]	−0.19077[a]	−0.179205[a]					
$^3F^e(6)$	−0.2412	−0.21318	−0.20213	−0.18840	−0.17724					
	−0.2413[a]	−0.2129[a]	−0.2017[a]	−0.1876[a]	−0.1762[a]					
$^3F^e(7)$	−0.23871	−0.21104	−0.20046	−0.18741	−0.17691					
	−0.238705[a]	−0.210905[a]	−0.20022[a]	−0.186985[a]						
$^3F^e(8)$	−0.23730	−0.20979	−0.19936	−0.18655	−0.17631					
	−0.237295[a]	−0.209605[a]	−0.199015[a]	−0.18593[a]						
$^3F^e(9)$	−0.23560	−0.20815	−0.19776	−0. 18513						
	−0.2356[a]	−0.2079[a]	−0.19735[a]							
$^3F^e(10)$	−0.23403	−0.20705	−0.19705	−0.18494						
	−0.234035[a]	−0.20693[a]	−0.196835[a]							
$^3F^e(11)$	−0.23314	−0.20636	−0.19650							
	−0.233155[a]	−0.206175[a]	−0.19618[a]							
$^3F^e(12)$	−0.23207	−0.20526	−0.19559							
	−0.2321[a]	−0.2052[a]	−0.19525[a]							
$^3F^e(13)$	−0.23108	−0.20483	−0.19543							
$^3F^e(14)$	−0.23071	−0.20443	−0.19518							
$^3F^e(15)$	−0.22975	−0.20340								
$^3F^e(16)$	−0.22906									
$^3F^e(17)$	−0.22882									
$^3F^e(18)$	−0.22743									
$^3F^e(19)$	−0.22624									
$^3F^e(20)$	−0.22401									

[a] [66].

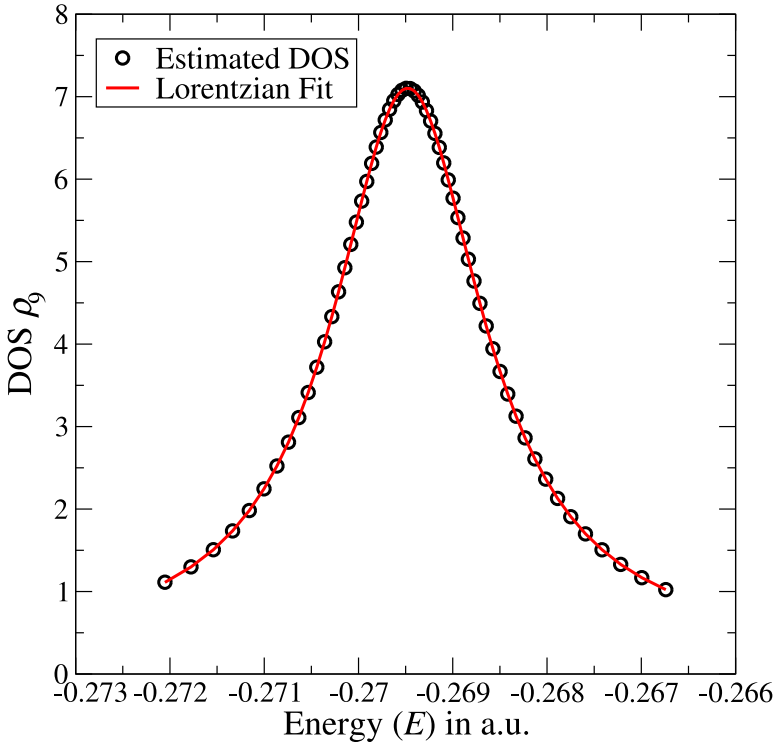

Fig. 2. Calculated DOS (hollow black circles) and the fitted Lorentzian (red line) for the first resonance $^3F^e$ state of He-atom below $He^+(3p)$ threshold for $\lambda_D = 70$ a.u. which gives the resonance energy and width $E_r = -0.026947$ a.u. and $\Gamma_r = 0.00195$ a.u. respectively.

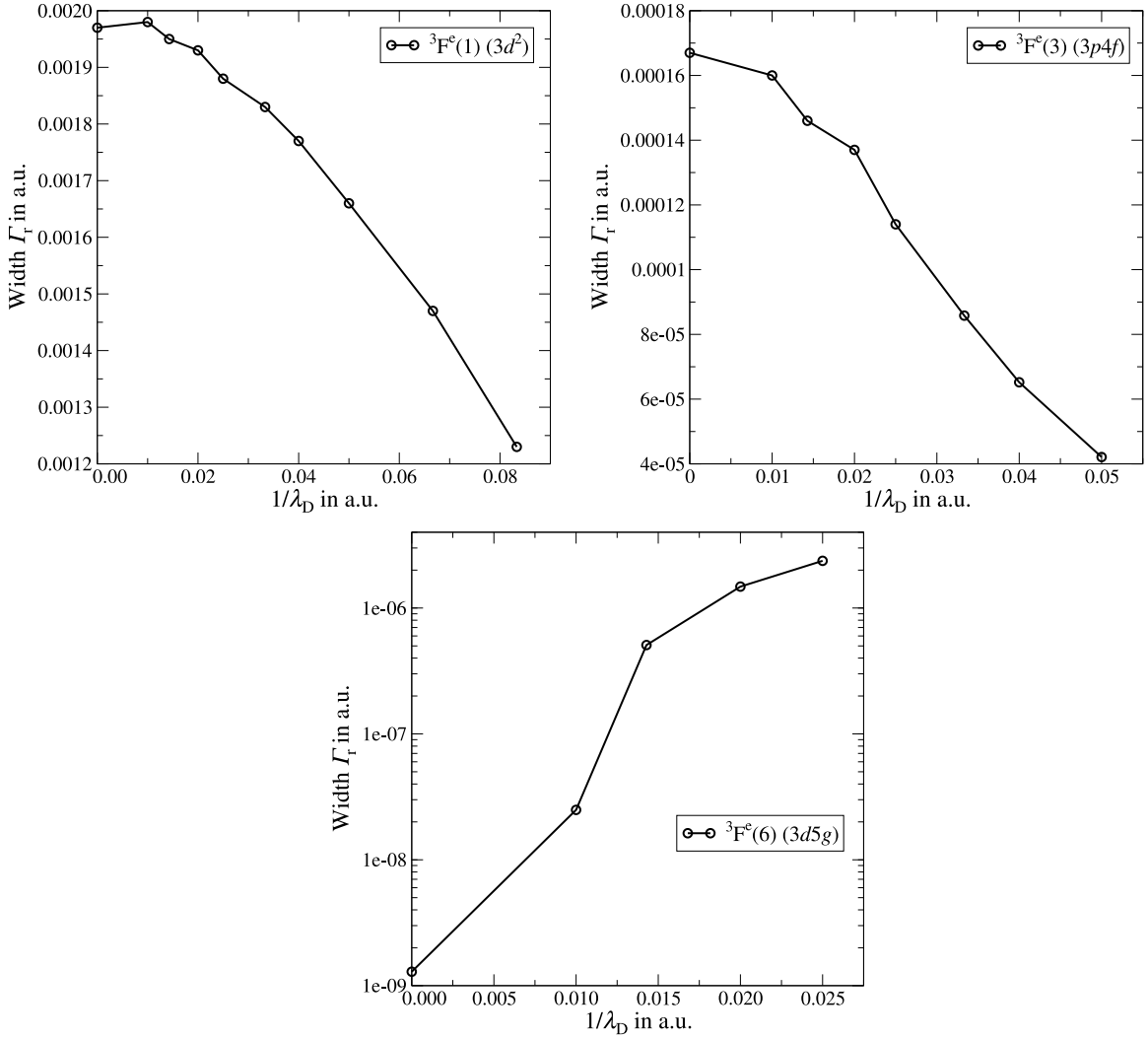

Fig. 3. The variation of resonance widths for the ${}^3F^e(1)$,${}^3F^e(3)$ and ${}^3F^e(6)$ states corresponding to the dominating configurations $3d^2, 3p4f$ and $3d5g$ respectively, with respect to the reciprocal of screening lengths $\left(\frac{1}{\lambda_D}\right)$.

Table G
Resonance width Γ_r (a.u.) of ${}^3F^e$ states of He below $He^+(3p)$ threshold for different screening length λ_D in a.u. The notation $A[\pm B]$ stands for $A \times 10^{\pm B}$.

States	λ_D									
	∞	100	70	50	40	30	25	20	15	12
${}^3F^e(1)$	1.97[−3]	1.98[−3]	1.95[−3]	1.93[−3]	1.88[−3]	1.83[−3]	1.77[−3]	1.66[−3]	1.47[−3]	1.23[−3]
	1.98[−3][a]	1.975[−3][a]	1.965[−3][a]	1.945[−3][a]	1.925[−3][a]	1.88[−3][a]	1.835[−3][a]	1.76[−3][a]	1.61[−3][a]	1.4[−3][a]
${}^3F^e(2)$	4.50[−4]	4.49[−4]	4.37[−4]	4.31[−4]	4.12[−4]	3.80[−4]	3.46[−3]	2.79[−4]		
	4.515[−4][a]	4.47[−4][a]	4.425[−4][a]	4.33[−4][a]	4.205[−4][a]	3.905[−4][a]	3.575[−4][a]	3.01[−4][a]		
${}^3F^e(3)$	1.67[−4]	1.60[−3]	1.46[−4]	1.37[−4]	1.14[−4]	8.58[−5]	6.52[−5]	4.21[−5]		
	1.68[−4][a]	1.57[−4][a]	1.465[−4][a]	1.29[−4][a]	1.115[−4][a]	8.25[−5][a]	0.615[−4][a]			
${}^3F^e(4)$	2.08[−4]	1.99[−4]	1.92[−4]	1.83[−4]	1.68[−4]	1.14[−4]				
	2.065[−4][a]	2.005[−4][a]	1.945[−4][a]	1.805[−4][a]	1.635[−4][a]	1.305[−4][a]				
${}^3F^e(5)$	1.12[−4]	1.04[−4]	8.10[−5]	6.63[−5]	5.04[−5]	4.09[−5]				
	1.06[−4][a]	9.25[−5][a]	8.1[−5][a]	6.4[−5][a]	5.05[−5][a]					
${}^3F^e(6)$	1.29[−9]	2.49[−8]	5.08[−7]	1.48[−6]	2.37[−6]					
${}^3F^e(7)$	1.09[−4]	9.55[−5]	9.26[−5]	7.43[−5]	4.48[−5]					
	1.105[−4][a]	1.035[−4][a]	9.45[−5][a]	7.75[−5][a]						
${}^3F^e(8)$	6.61[−5]	5.24[−5]	3.94[−5]	3.64[−5]	2.75[−5]					
	6.6[−5][a]	5.2[−5][a]	4.15[−5][a]	3.0[−5][a]						
${}^3F^e(9)$	1.18[−8]	1.73[−7]	1.22[−5]	1.73[−5]						
${}^3F^e(10)$	5.96[−5]	5.37[−5]	4.39[−5]	1.41[−5]						
	6.6[−5][a]	5.95[−5][a]								
${}^3F^e(11)$	5.37[−5]	2.71[−5]	1.07[−5]							
${}^3F^e(12)$	2.45[−7]	2.91[−6]	1.16[−5]							
${}^3F^e(13)$	1.84[−4]	1.11[−4]	4.36[−5]							

(*continued on next page*)

Table G (*continued*).

States	λ_D									
	∞	100	70	50	40	30	25	20	15	12
$^3F^e(14)$	1.61[−4]	3.05[−5]	1.16[−5]							
$^3F^e(15)$	4.06[−6]	9.0[−5]								
$^3F^e(16)$	6.53[−5]									
$^3F^e(17)$	1.06[−4]									
$^3F^e(18)$	7.46[−5]									
$^3F^e(19)$	1.60[−4]									
$^3F^e(20)$	1.83[−4]									

[a] [66].

Table H

Expectation values of repulsive potential $\langle V_r\rangle$, attractive potential $\langle V_a\rangle$, ratio of attractive to repulsive potential $\eta = \left|\frac{\langle V_a\rangle}{\langle V_r\rangle}\right|$, $\langle\cos\theta_{12}\rangle$, inter-electronic angles $\langle\theta_{12}\rangle$ (in degree) using (10), different one and two-particle moments of resonance $^3F^e$ states of He atom below $He^+(3p)$ threshold. The notation $A[\pm B]$ stands for $A\times10^{\pm B}$. All values are given in atomic units.

States	λ	$\langle V_r\rangle$	$\langle V_a\rangle$	η	$\langle r_1\rangle$	$\langle r_1^2\rangle$	$\langle r_{12}\rangle$	$\langle r_{12}^2\rangle$	$\langle\cos\theta_{12}\rangle$	$\langle\theta_{12}\rangle$
$^3F^e(1)$	∞	1.11[−1]	−7.49[−1]	6.75	6.70[+0]	5.70[+1]	1.04[+1]	1.28[+2]	−1.36[−1]	126.85
	100	1.01[−1]	−7.10[−1]	7.01	6.63[+0]	5.46[+1]	1.03[+1]	1.24[+2]	−1.37[−1]	127.06
	70	9.74[−2]	−6.93[−1]	7.12	6.62[+0]	5.42[+1]	1.03[+1]	1.23[+2]	−1.36[−1]	126.86
	50	9.23[−2]	−6.71[−1]	7.26	6.61[+0]	5.39[+1]	1.02[+1]	1.22[+2]	−1.35[−1]	126.69
	40	8.84[−2]	−6.49[−1]	7.35	6.59[+0]	5.27[+1]	1.02[+1]	1.20[+2]	−1.37[−1]	127.12
	30	8.13[−2]	−6.18[−1]	7.60	6.62[+0]	5.38[+1]	1.02[+1]	1.22[+2]	−1.35[−1]	126.68
	25	7.60[−2]	−5.93[−1]	7.79	6.64[+0]	5.42[+1]	1.03[+1]	1.23[+2]	−1.35[−1]	126.64
	20	6.86[−2]	−5.55[−1]	8.09	6.71[+0]	5.51[+1]	1.04[+1]	1.25[+2]	−1.36[−1]	126.77
	15	5.69[−2]	−4.94[−1]	8.68	6.88[+0]	5.83[+1]	1.07[+1]	1.32[+2]	−1.35[−1]	126.50
	12	4.63[−2]	−4.32[−1]	9.33	7.14[+0]	6.34[+1]	1.11[+1]	1.44[+2]	−1.35[−1]	126.52
$^3F^e(2)$	∞	6.67[−2]	−5.96[−1]	8.93	1.07[+1]	1.59[+2]	1.82[+1]	3.74[+2]	−2.31[−1]	152.41
	100	5.70[−2]	−5.57[−1]	9.76	1.08[+1]	1.62[+2]	1.83[+1]	3.80[+2]	−2.29[−1]	152.03
	70	5.30[−2]	−5.40[−1]	10.17	1.09[+1]	1.66[+2]	1.85[+1]	3.87[+2]	−2.28[−1]	151.71
	50	4.79[−2]	−5.17[−1]	10.80	1.10[+1]	1.71[+2]	1.88[+1]	3.99[+2]	−2.26[−1]	151.04
	40	4.35[−2]	−4.98[−1]	11.43	1.12[+1]	1.79[+2]	1.91[+1]	4.15[+2]	−2.24[−1]	150.50
	30	3.65[−2]	−4.66[−1]	12.77	1.16[+1]	1.95[+2]	1.99[+1]	4.47[+2]	−2.19[−1]	149.18
	25	3.11[−2]	−4.41[−1]	14.18	1.20[+1]	2.13[+2]	2.07[+1]	4.85[+2]	−2.15[−1]	148.05
	20	2.33[−2]	−4.03[−1]	17.30	1.30[+1]	2.56[+2]	2.25[+1]	5.75[+2]	−2.10[−1]	146.73
$^3F^e(3)$	∞	6.50[−2]	−5.83[−1]	8.96	1.10[+1]	1.70[+2]	1.73[+1]	3.34[+2]	9.91[−3]	87.32
	100	5.53[−2]	−5.43[−1]	9.81	1.11[+1]	1.73[+2]	1.74[+1]	3.39[+2]	1.11[−2]	86.99
	70	5.13[−2]	−5.26[−1]	10.24	1.12[+1]	1.76[+2]	1.76[+1]	3.45[+2]	1.17[−2]	86.83
	50	4.63[−2]	−5.04[−1]	10.89	1.13[+1]	1.82[+2]	1.79[+1]	3.56[+2]	1.39[−2]	86.22
	40	4.19[−2]	−4.84[−1]	11.56	1.15[+1]	1.89[+2]	1.82[+1]	3.71[+2]	1.53[−2]	85.84
	30	3.48[−2]	−4.53[−1]	12.99	1.20[+1]	2.08[+2]	1.90[+1]	4.05[+2]	2.05[−2]	84.46
	25	2.93[−2]	−4.27[−1]	14.57	1.25[+1]	2.31[+2]	1.99[+1]	4.50[+2]	2.70[−2]	82.68
	20	2.08[−2]	−3.89[−1]	18.69	1.39[+1]	3.01[+2]	2.25[+1]	5.81[+2]	4.78[−2]	77.07
$^3F^e(4)$	∞	4.32[−2]	−5.38[−1]	12.46	1.65[+1]	4.41[+2]	2.95[+1]	9.81[+2]	−2.54[−1]	158.78
	100	3.37[−2]	−4.99[−1]	14.79	1.67[+1]	4.58[+2]	3.00[+1]	1.01[+3]	−2.44[−1]	155.89
	70	2.97[−2]	−4.82[−1]	16.24	1.72[+1]	4.86[+2]	3.09[+1]	1.07[+3]	−2.48[−1]	156.97
	50	2.47[−2]	−4.60[−1]	18.61	1.78[+1]	5.29[+2]	3.21[+1]	1.16[+3]	−2.41[−1]	155.25
	40	2.05[−2]	−4.41[−1]	21.45	1.86[+1]	5.85[+2]	3.37[+1]	1.27[+3]	−2.35[−1]	153.64
	30	1.38[−2]	−4.10[−1]	29.54	2.09[+1]	7.57[+2]	3.80[+1]	1.62[+3]	−2.28[−1]	151.75
$^3F^e(5)$	∞	4.12[−2]	−5.30[−1]	12.88	1.74[+1]	5.05[+2]	2.97[+1]	9.95[+2]	2.79[−2]	82.44
	100	3.19[−2]	−4.92[−1]	15.40	1.77[+1]	5.23[+2]	3.01[+1]	1.02[+3]	4.34[−2]	78.25
	70	2.76[−2]	−4.74[−1]	17.17	1.83[+1]	5.61[+2]	3.13[+1]	1.10[+3]	3.78[−2]	79.77
	50	2.26[−2]	−4.52[−1]	20.01	1.91[+1]	6.20[+2]	3.28[+1]	1.21[+3]	4.89[−2]	76.79
	40	1.83[−2]	−4.33[−1]	23.58	2.02[+1]	7.01[+2]	3.48[+1]	1.36[+3]	6.31[−2]	72.94
	30	1.14[−2]	−4.02[−1]	35.09	2.34[+1]	9.83[+2]	4.09[+1]	1.90[+3]	1.00[−1]	62.83
$^3F^e(6)$	∞	4.04[−2]	−5.23[−1]	12.93	1.68[+1]	4.55[+2]	2.75[+1]	8.35[+2]	1.81[−1]	40.86
	100	3.04[−2]	−4.83[−1]	15.89	1.73[+1]	4.85[+2]	2.85[+1]	8.96[+2]	1.77[−1]	42.11
	70	2.59[−2]	−4.65[−1]	17.98	1.79[+1]	5.31[+2]	2.98[+1]	9.85[+2]	1.72[−1]	43.44
	50	2.00[−2]	−4.43[−1]	22.13	1.92[+1]	6.26[+2]	3.24[+1]	1.17[+3]	1.63[−1]	45.81
	40	1.40[−2]	−4.21[−1]	30.12	2.25[+1]	9.20[+2]	3.89[+1]	1.75[+3]	1.35[−1]	53.29
$^3F^e(7)$	∞	2.98[−2]	−5.08[−1]	17.01	2.39[+1]	1.02[+3]	4.42[+1]	2.20[+3]	−2.65[−1]	161.74
	100	2.04[−2]	−4.69[−1]	22.95	2.49[+1]	1.12[+3]	4.62[+1]	2.40[+3]	−2.56[−1]	159.20
	70	1.66[−2]	−4.52[−1]	27.17	2.61[+1]	1.23[+3]	4.86[+1]	2.64[+3]	−2.56[−1]	159.15
	50	1.20[−2]	−4.31[−1]	35.91	2.84[+1]	1.49[+3]	5.31[+1]	3.16[+3]	−2.49[−1]	157.30
	40	8.87[−3]	−4.13[−1]	46.62	3.08[+1]	1.81[+3]	5.78[+1]	3.81[+3]	−2.22[−1]	150.06
$^3F^e(8)$	∞	2.85[−2]	−5.03[−1]	17.67	2.53[+1]	1.17[+3]	4.53[+1]	2.31[+3]	3.58[−2]	80.32
	100	1.90[−2]	−4.64[−1]	24.32	2.65[+1]	1.29[+3]	4.75[+1]	2.54[+3]	5.54[−2]	75.03
	70	1.51[−2]	−4.47[−1]	29.51	2.81[+1]	1.46[+3]	5.05[+1]	2.87[+3]	5.94[−2]	73.93
	50	1.14[−2]	−4.29[−1]	37.65	3.01[+1]	1.72[+3]	5.52[+1]	3.44[+3]	1.09[−3]	89.70
	40	6.73[−3]	−4.08[−1]	60.73	3.57[+1]	2.44[+3]	6.53[+1]	4.78[+3]	1.15[−1]	58.94
$^3F^e(9)$	∞	2.80[−2]	−4.99[−1]	17.76	2.52[+1]	1.16[+3]	4.40[+1]	2.20[+3]	2.04[−1]	34.77
	100	1.79[−2]	−4.59[−1]	25.59	2.71[+1]	1.36[+3]	4.78[+1]	2.58[+3]	1.91[−1]	38.17
	70	1.37[−2]	−4.42[−1]	32.17	2.92[+1]	1.60[+3]	5.20[+1]	3.06[+3]	1.81[−1]	40.89

(*continued on next page*)

Table H (*continued*).

States	λ	$\langle V_r \rangle$	$\langle V_a \rangle$	η	$\langle r_1 \rangle$	$\langle r_1^2 \rangle$	$\langle r_{12} \rangle$	$\langle r_{12}^2 \rangle$	$\langle \cos\theta_{12} \rangle$	$\langle \theta_{12} \rangle$
	50	6.80[−3]	−4.18[−1]	61.46	3.96[+1]	3.12[+3]	7.32[+1]	6.15[+3]	7.65[−2]	69.33
$^3F^e(10)$	∞	2.17[−2]	−4.90[−1]	22.52	3.29[+1]	2.05[+3]	6.21[+1]	4.33[+3]	2.71[−1]	163.34
	100	1.25[−2]	−4.51[−1]	35.86	3.55[+1]	2.41[+3]	6.73[+1]	5.06[+3]	−2.56[−1]	159.16
	70	8.99[−3]	−4.35[−1]	48.40	3.89[+1]	2.93[+3]	7.41[+1]	6.12[+3]	−2.57[−1]	159.57
	50	4.71[−3]	−4.14[−1]	88.03	4.91[+1]	4.87[+3]	9.33[+1]	9.76[+3]	−2.41[−2]	96.51
$^3F^e(11)$	∞	2.09[−2]	−4.87[−1]	23.27	3.47[+1]	2.32[+3]	6.39[+1]	4.60[+3]	5.16[−2]	76.04
	100	1.14[−2]	−4.48[−1]	38.99	3.82[+1]	2.84[+3]	7.08[+1]	5.61[+3]	6.04[−2]	73.67
	70	7.94[−3]	−4.32[−1]	54.41	4.24[+1]	3.52[+3]	7.88[+1]	6.94[+3]	8.98[−2]	65.72
$^3F^e(12)$	∞	2.08[−2]	−4.84[−1]	23.20	3.48[+1]	2.36[+3]	6.30[+1]	4.52[+3]	2.21[−1]	30.16
	100	1.11[−2]	−4.45[−1]	39.99	3.96[+1]	3.12[+3]	7.28[+1]	6.04[+3]	1.93[−1]	37.76
	70	6.24[−3]	−4.28[−1]	68.58	4.97[+1]	5.04[+3]	9.30[+1]	9.84[+3]	1.63[−1]	45.72
$^3F^e(13)$	∞	1.64[−2]	−4.78[−1]	29.07	4.36[+1]	3.76[+3]	8.36[+1]	7.82[+3]	−2.69[−1]	162.69
	100	7.54[−3]	−4.40[−1]	58.37	5.00[+1]	4.97[+3]	9.62[+1]	1.02[+4]	−2.62[−1]	160.82
	70	4.50[−3]	−4.25[−1]	94.44	5.81[+1]	6.81[+3]	1.12[+2]	1.40[+4]	−2.52[−1]	158.04
$^3F^e(14)$	∞	1.59[−2]	−4.77[−1]	29.87	4.57[+1]	4.16[+3]	8.56[+1]	8.24[+3]	6.26[−2]	73.07
	100	7.80[−3]	−4.41[−1]	56.58	5.18[+1]	5.46[+3]	9.87[+1]	1.09[+4]	−1.20[−2]	93.25
	70	3.70[−3]	−4.23[−1]	114.22	6.48[+1]	8.56[+3]	1.23[+2]	1.69[+4]	1.19[−1]	57.61
$^3F^e(15)$	∞	1.54[−2]	−4.75[−1]	30.69	4.77[+1]	4.60[+3]	8.87[+1]	8.93[+3]	2.20[−1]	30.34
	100	4.92[−3]	−4.35[−1]	88.43	6.93[+1]	9.94[+3]	1.33[+2]	1.98[+4]	4.56[−3]	88.76
$^3F^e(16)$	∞	1.36[−2]	−4.72[−1]	34.67	5.47[+1]	6.13[+3]	1.05[+2]	1.25[+4]	−1.98[−1]	143.56
$^3F^e(17)$	∞	1.32[−2]	−4.72[−1]	35.67	5.67[+1]	6.63[+3]	1.08[+2]	1.32[+4]	8.88[−3]	87.60
$^3F^e(18)$	∞	1.06[−2]	−4.66[−1]	43.76	6.99[+1]	1.01[+4]	1.34[+2]	2.03[+4]	3.25[−3]	89.12
$^3F^e(19)$	∞	1.46[−2]	−4.78[−1]	32.76	6.41[+1]	9.26[+3]	1.23[+2]	1.85[+4]	−8.82[−4]	90.23
$^3F^e(20)$	∞	1.72[−2]	−4.82[−1]	28.01	5.17[+1]	6.17[+3]	9.84[+1]	1.23[+4]	−4.61[−3]	91.24

Table I
Resonance energy E_r (a.u.) of $^3F^e$ states of He atom below $He^+(4p)$ threshold and energy of $4p$ state of He^+ ion for different screening length λ_D in a.u.

States	λ_D									
	∞	100	70	50	40	30	25	20	15	12
$He^+(4p)$	−0.125	−0.106103	−0.098644	−0.089253	−0.081531	−0.069631	−0.060935	−0.049177	−0.032750	−0.019932
$^3F^e(1)$	−0.22202	−0.20241	−0.19440	−0.18395	−0.17523	−0.16051	−0.15062	−0.13401	−0.11073	−0.09137
$^3F^e(2)$	−0.21320	−0.20061	−0.19321	−0.18309	−0.17463	−0.15971	−0.14973	−0.13371	−0.10951	−0.09064
$^3F^e(3)$	−0.20705	−0.19778	−0.19119	−0.18161	−0.17354	−0.15838	−0.14921	−0.13304	−0.10896	−0.08733
$^3F^e(4)$	−0.20295	−0.19311	−0.18794	−0.17923	−0.17182	−0.15638	−0.14827	−0.13195	−0.10809	−0.08686
$^3F^e(5)$	−0.19788	−0.18588	−0.18301	−0.17563	−0.16924	−0.15354	−0.14684	−0.12799	−0.10680	−0.08622
$^3F^e(6)$	−0.17866	−0.17531	−0.17557	−0.17021	−0.16541	−0.14928	−0.14468	−0.12466	−0.10497	−0.08538
$^3F^e(7)$	−0.16622	−0.16197	−0.16471	−0.16264	−0.15979	−0.14329	−0.14158	−0.11989	−0.10239	−0.08401
$^3F^e(8)$	−0.16420	−0.15717	−0.15082	−0.15122	−0.15167	−0.13470	−0.13712	−0.11320	−0.09869	−0.08201
$^3F^e(9)$	−0.15838	−0.15052	−0.14595	−0.13672	−0.14008	−0.12263	−0.13082	−0.10385	−0.09353	−0.07923
$^3F^e(10)$	−0.15714	−0.14977	−0.13851	−0.13171	−0.12506	−0.10678	−0.12189	−0.09086	−0.08634	−0.07530
$^3F^e(11)$	−0.15085	−0.13829	−0.12623	−0.12417	−0.11987	−0.10134	−0.10927	−0.07409	−0.06270	−0.05173
$^3F^e(12)$	−0.14718	−0.13555	−0.11925	−0.11592	−0.11225	−0.09445	−0.09317	−0.06865	−0.04578	−0.03751
$^3F^e(13)$	−0.14593	−0.13052	−0.11803	−0.11107	−0.10816	−0.08210	−0.08758	−0.06165	−0.04131	−0.02294
$^3F^e(14)$	−0.14483	−0.12912	−0.11197	−0.10546	−0.10009	−0.08083	−0.08012	−0.05080		
$^3F^e(15)$	−0.14376	−0.12357	−0.10877	−0.10442	−0.09423	−0.07734	−0.06868	−0.05080		
$^3F^e(16)$	−0.13969	−0.11937	−0.10799	−0.09849	−0.09310	−0.07613	−0.06503			
$^3F^e(17)$	−0.13922	−0.11806	−0.10675	−0.09486	−0.08839	−0.07179	−0.06391			
$^3F^e(18)$	−0.13823	−0.11733	−0.10265	−0.09394	−0.08451	−0.06995				
$^3F^e(19)$	−0.13570	−0.11667	−0.10208	−0.09293	−0.08377					
$^3F^e(20)$	−0.13314	−0.11257	−0.10017	−0.09096	−0.08273					
$^3F^e(21)$	−0.13115	−0.11222								
$^3F^e(22)$	−0.12967	−0.11161								
$^3F^e(23)$	−0.12827	−0.10936								
$^3F^e(24)$	−0.12705	−0.10748								
$^3F^e(25)$	−0.12638									

$3pnf$ states decrease with the decrease of λ_D. The clear difference in the variation of $\langle \theta_{12} \rangle$ between $3dnd$ and $3pnf$ states lies in the fact that $\langle \theta_{12} \rangle$ is obtuse in case of $3dnd$ states whereas $\langle \theta_{12} \rangle$ assumes acute values in case of $3pnf$ states. The nature of variation of $\langle \theta_{12} \rangle$ for $3dng$ states is completely different from those of $3dnd$ and $3pnf$ states. In free case, $\langle \theta_{12} \rangle$ of $3dng$ states are smaller than that of $3pnf$ states. $\langle \theta_{12} \rangle$ of $3dng$ states increase as λ_D decreases. Thus it is evident that the variation of width Γ_r with respect to λ_D has a clear correlation with the changes in the inter-electronic angle $\langle \theta_{12} \rangle$. Small acute inter-electronic angles correspond to small widths *i.e.* higher autoionizing lifetime. Hence $3dng$ states are very much stable against autoionization in free case and become autoionizing prone as λ_D decreases. Resonance energy and width of $^3F^e$ states of He below $He^+(4p)$ threshold are given in Tables I and J respectively for different screening length λ_D. Unlike the variation of width for RSs below $He^+(3p)$ threshold, the variation of resonance widths (Γ_r) of some RSs below $He^+(4p)$ threshold does not always follow a fixed pattern. The resonance parameters of $^1F^e$ states below $He^+(3p)$ and $He^+(4p)$ thresholds are given in Tables K, L, M and N. These tables reveal similar features as discussed in case of $^3F^e$ states. Several structural properties like $\langle V_r \rangle$, $\langle V_a \rangle$, $\langle \cos\theta_{12} \rangle$, $\langle \theta_{12} \rangle$, $\langle r_1 \rangle$, $\langle r_1^2 \rangle$, $\langle r_{12} \rangle$ and $\langle r_{12}^2 \rangle$ of resonance $^1F^e$ states below $He^+(3p)$ threshold are given in Table O.

4. Conclusions

In the present investigation, we have estimated the structural properties of meta-stable bound and resonance $^{1,3}F^e$ states of He-atom where the electron-nucleus and electron–electron interactions are modelled by exponentially screened Coulomb potential. The trial radial wavefunction is expanded in explicitly correlated multi-exponent

Table J
Resonance width Γ_r (a.u.) of $^3F^e$ states of He atom below $He^+(4p)$ threshold for different screening length λ_D in a.u. The notation $A[\pm B]$ stands for $A \times 10^{\pm B}$.

States	λ_D									
	∞	100	70	50	40	30	25	20	15	12
$^3F^e(1)$	4.32[−4]	9.00[−5]	6.74[−5]	4.29[−5]	2.67[−5]	3.12[−5]	1.00[−4]	2.23[−5]	4.01[−4]	8.83[−5]
$^3F^e(2)$	4.53[−4]	3.00[−4]	9.27[−5]	7.68[−5]	3.80[−5]	5.51[−5]	1.36[−5]	6.17[−5]	1.52[−5]	3.88[−5]
$^3F^e(3)$	7.05[−4]	2.80[−4]	1.40[−4]	1.50[−4]	1.16[−4]	7.37[−5]	4.16[−5]	6.91[−5]	5.01[−5]	6.04[−7]
$^3F^e(4)$	6.08[−4]	4.61[−4]	2.87[−4]	1.98[−4]	1.38[−4]	1.51[−4]	6.02[−5]	9.51[−5]	6.09[−5]	2.09[−5]
$^3F^e(5)$	6.15[−4]	6.90[−4]	3.10[−4]	2.19[−4]	1.73[−4]	1.98[−4]	1.14[−4]	1.46[−4]	8.03[−5]	5.46[−5]
$^3F^e(6)$	1.05[−3]	5.65[−4]	4.86[−4]	4.28[−4]	2.29[−4]	2.70[−4]	1.48[−4]	1.65[−4]	1.32[−4]	9.38[−5]
$^3F^e(7)$	1.07[−3]	6.19[−4]	5.76[−4]	6.08[−4]	3.41[−4]	3.23[−4]	1.98[−4]	2.31[−4]	1.28[−4]	1.24[−4]
$^3F^e(8)$	8.00[−4]	6.36[−4]	6.37[−4]	5.79[−4]	4.92[−4]	4.70[−4]	2.61[−4]	3.05[−4]	1.47[−4]	1.01[−4]
$^3F^e(9)$	2.73[−4]	1.83[−3]	6.39[−4]	6.49[−4]	5.82[−4]	5.97[−4]	3.14[−4]	4.54[−4]	2.08[−4]	1.06[−4]
$^3F^e(10)$	4.98[−4]	1.18[−3]	1.24[−3]	6.09[−4]	6.58[−4]	6.47[−4]	4.69[−4]	5.90[−4]	2.65[−4]	1.41[−4]
$^3F^e(11)$	3.20[−4]	1.27[−3]	1.03[−3]	1.18[−3]	6.27[−4]	6.06[−4]	4.88[−4]	6.59[−4]	5.82[−4]	3.72[−4]
$^3F^e(12)$	4.99[−4]	7.67[−5]	4.91[−5]	4.31[−5]	1.03[−3]	2.36[−3]	6.77[−4]	5.86[−4]	5.36[−4]	5.68[−4]
$^3F^e(13)$	3.79[−4]	6.02[−5]	1.90[−4]	1.24[−3]	2.39[−5]	7.44[−4]	5.86[−4]	7.41[−4]	5.38[−4]	2.74[−4]
$^3F^e(14)$	5.93[−5]	2.96[−4]	2.37[−4]	4.58[−5]	9.39[−4]	7.31[−4]	8.24[−5]	2.85[−4]		
$^3F^e(15)$	2.26[−4]	6.27[−4]	2.67[−4]	2.21[−4]	4.56[−5]	2.51[−5]	6.56[−4]	2.85[−4]		
$^3F^e(16)$	9.67[−5]	4.30[−4]	1.31[−4]	1.80[−4]	1.76[−4]	9.53[−5]	1.44[−4]			
$^3F^e(17)$	2.25[−5]	2.01[−4]	7.53[−5]	1.06[−4]	2.33[−4]	2.63[−4]	4.07[−4]			
$^3F^e(18)$	2.28[−4]	5.96[−5]	4.71[−5]	7.98[−5]	2.48[−4]	1.42[−4]				
$^3F^e(19)$	1.71[−4]	9.57[−4]	2.73[−5]	8.27[−5]	8.36[−5]					
$^3F^e(20)$	2.50[−4]	1.91[−4]	2.88[−5]	4.15[−5]	1.54[−4]					
$^3F^e(21)$	1.90[−4]	1.80[−5]								
$^3F^e(22)$	3.23[−5]	6.29[−5]								
$^3F^e(23)$	9.07[−5]	3.47[−5]								
$^3F^e(24)$	2.36[−4]	6.07[−5]								
$^3F^e(25)$	3.30[−4]									

Table K
Resonance energy E_r (a.u.) of $^1F^e$ states of He atom below $He^+(3p)$ threshold and energy of $3p$ state of He^+ ion for different screening length λ_D in a.u.

States	λ_D									
	∞	100	70	50	40	30	25	20	15	12
$He^+(3p)$	−0.22222	−0.202835	−0.194885	−0.18461	−0.1759181	−0.162017	−0.151409	−0.136315	−0.113232	−0.092587
$^1F^e(1)$	−0.26853	−0.23968	−0.22798	−0.21299	−0.20040	−0.18051	−0.16554	−0.14459		
	−0.268535[a]	−0.23953[a]	−0.22769[a]	−0.21245[a]	−0.19961[a]	−0.179235[a]	−0.16384[a]	−0.14222[a]		
$^1F^e(2)$	−0.26096	−0.23215	−0.22050	−0.20559	−0.19312	−0.17350	−0.15885	−0.13862		
	−0.26096[a]	−0.231955[a]	−0.220125[a]	−0.204905[a]	−0.192105[a]	−0.17185[a]	−0.156635[a]			
$^1F^e(3)$	−0.24883	−0.22050	−0.20931	−0.19519	−0.18356	−0.16558	−0.15244			
	−0.248835[a]	−0.22035[a]	−0.209025[a]	−0.194695[a]	−0.182855[a]	−0.16451[a]				
$^1F^e(4)$	−0.24571	−0.21747	−0.20636	−0.19242	−0.18101	−0.16356				
	−0.24571[a]	−0.21727[a]	−0.20599[a]	−0.191765[a]	−0.18007[a]					
$^1F^e(5)$	−0.24130	−0.21317	−0.20214	−0.18842	−0.17749					
	−0.24131[a]	−0.21293[a]	−0.20173[a]	−0.18765[a]	−0.17685[a]					
$^1F^e(6)$	−0.23967	−0.21194	−0.20129	−0.18811	−0.17722					
	−0.239665[a]	−0.21180[a]	−0.20104[a]							
$^1F^e(7)$	−0.23802	−0.21041	−0.19990	−0.18696	−0.17660					
	−0.23803[a]	−0.210235[a]	−0.19961[a]	−0.18625[a]	−0.17615[a]					
$^1F^e(8)$	−0.23560	−0.20813	−0.19777	−0.18526						
	−0.23560[a]	−0.20792[a]	−0.197365[a]	−0.18475[a]						
$^1F^e(9)$	−0.23457	−0.20751	−0.19727	−0.18508						
	−0.23458[a]									
$^1F^e(10)$	−0.23358	−0.20667	−0.19675	−0.18481						
	−0.233595[a]	−0.20650[a]	−0.1963[a]							
$^1F^e(11)$	−0.23201	−0.20508	−0.19563							
	−0.2321[a]	−0.2052[a]	−0.1948[a]							
$^1F^e(12)$	−0.23106	−0.20456								
	−0.2314[a]	−0.2045[a]								
$^1F^e(13)$	−0.23078	−0.20350								
		−0.2035[a]								
$^1F^e(14)$	−0.22925									
$^1F^e(15)$	−0.22778									
$^1F^e(16)$	−0.22670									
$^1F^e(17)$	−0.22518									

[a] [66].

Hylleraas-type basis set having total 900 terms in the basis expansion. Instead of using truncated electron–electron screening terms, we have developed analytic closed versions of the electron–electron screening term for the structural determination of meta-stable bound and resonance $^{1,3}F^e$ states of He atom. The variation method is used to obtain energy eigenvalues of the meta-stable bound $^{1,3}F^e$ states and the results are in reasonable agreement with those available in the literature and many of them are the lowest yet obtained. It is found that, if λ_D decreases, the energies of the meta-stable bound states increases towards the destabilization limit and as a result the number of bound states decreases. The resonance parameters *i.e.* energy and widths of the resonance $^{1,3}F^e$ states of He atom are estimated for different λ_D using the stabilization method between $He^+(2p)$ to $He^+(4p)$ thresholds. For each λ_D, most of the resonance parameters below $He^+(3p)$ threshold

Table L
Resonance width Γ_r (a.u.) of $^1F^e$ states of He atom below $He^+(3p)$ threshold for different screening length λ_D in a.u. The notation $A[\pm B]$ stands for $A \times 10^{\pm B}$.

States	λ_D							
	∞	100	70	50	40	30	25	20
$^1F^e(1)$	1.99[−7]	1.95[−7]	1.91[−7]	1.84[−7]	1.68[−7]	1.32[−7]	1.04[−7]	5.76[−8]
	3.9[−7][a]	3.80[−7][a]	3.66[−7][a]	3.39[−7][a]	2.92[−7][a]			
$^1F^e(2)$	4.75[−5]	4.68[−5]	4.52[−5]	4.24[−5]	3.94[−5]	3.31[−5]	2.76[−5]	1.83[−5]
	9.68[−5][a]	9.39[−5][a]	9.10[−5][a]	8.58[−5][a]	8.00[−5][a]			
$^1F^e(3)$	6.20[−8]	4.26[−8]	2.47[−8]	6.20[−9]	5.92[−9]	2.71[−10]	2.38[−12]	
$^1F^e(4)$	2.92[−5]	2.72[−5]	2.36[−5]	1.93[−5]	1.73[−5]	1.52[−5]		
	5.41[−5][a]	5.04[−5][a]	4.69[−5][a]	4.07[−5][a]	3.42[−5][a]			
$^1F^e(5)$	1.23[−7]	2.03[−7]	8.10[−7]	1.30[−6]	7.97[−6]			
$^1F^e(6)$	5.49[−4]	1.38[−4]	3.38[−6]	2.15[−6]	9.69[−7]			
$^1F^e(7)$	1.35[−5]	1.29[−5]	1.14[−5]	1.13[−5]	4.88[−6]			
$^1F^e(8)$	1.87[−11]	1.01[−10]	1.63[−6]	6.86[−5]				
$^1F^e(9)$	4.37[−5]	2.48[−5]	2.26[−5]	1.74[−5]				
$^1F^e(10)$	3.62[−5]	2.04[−5]	1.24[−5]	3.83[−6]				
$^1F^e(11)$	1.09[−10]	2.99[−7]	9.69[−6]					
$^1F^e(12)$	5.84[−5]	4.83[−7]						
$^1F^e(13)$	3.96[−4]	2.66[−5]						
$^1F^e(14)$	3.59[−5]							
$^1F^e(15)$	1.57[−5]							
$^1F^e(16)$	1.37[−5]							
$^1F^e(17)$	9.44[−5]							

[a] [66].

Table M
Resonance energy E_r (a.u.) of $^1F^e$ states of He atom below $He^+(4p)$ threshold and energy of $4p$ state of He^+ ion for different screening length λ_D in a.u.

States	λ_D							
	∞	100	70	50	40	30	25	20
$He^+(4p)$	−0.12500	−0.10610	−0.09864	−0.08925	−0.08153	−0.06963	−0.06093	−0.0492
$^1F^e(1)$	−0.21747	−0.20156	−0.19378	−0.18414	−0.17543	−0.16117	−0.15112	
$^1F^e(2)$	−0.20937	−0.19942	−0.19225	−0.18349	−0.17489	−0.16071	−0.14982	
$^1F^e(3)$	−0.19736	−0.19589	−0.18978	−0.18236	−0.17408	−0.16008	−0.14945	
$^1F^e(4)$	−0.18227	−0.19057	−0.18603	−0.18050	−0.17275	−0.15906	−0.14876	
$^1F^e(5)$	−0.17932	−0.18204	−0.18029	−0.17775	−0.17070	−0.15753	−0.14760	
$^1F^e(6)$	−0.16237	−0.16982	−0.17172	−0.17361	−0.16772	−0.15522	−0.14583	
$^1F^e(7)$	−0.15679	−0.15428	−0.15901	−0.16751	−0.16332	−0.15190	−0.14344	
$^1F^e(8)$	−0.15455	−0.15149	−0.14244	−0.15860	−0.15694	−0.14716	−0.13988	
$^1F^e(9)$	−0.15289	−0.13365	−0.14049	−0.14556	−0.14772	−0.14037	−0.13496	
$^1F^e(10)$	−0.15006	−0.12862	−0.12297	−0.12799	−0.13438	−0.13067	−0.12787	
$^1F^e(11)$	−0.14773	−0.12649	−0.11729	−0.12662	−0.11595	−0.11680	−0.11786	
$^1F^e(12)$	−0.14559	−0.12472	−0.11480	−0.10910	−0.11514	−0.09711	−0.10367	
$^1F^e(13)$	−0.14433	−0.12205	−0.11355	−0.10354	−0.09772	−0.08014	−0.08358	
$^1F^e(14)$	−0.14170	−0.12002	−0.11182	−0.10158	−0.09235	−0.07565	−0.06799	
$^1F^e(15)$	−0.14041	−0.11774	−0.10944	−0.09958	−0.09057	−0.07402	−0.06335	
$^1F^e(16)$	−0.13913	−0.11669	−0.10706	−0.09830	−0.08787	−0.07110	−0.06207	
$^1F^e(17)$	−0.13841	−0.11433	−0.10627	−0.09646	−0.08732	−0.07054		
$^1F^e(18)$	−0.13640	−0.11327	−0.10394	−0.09397	−0.08604			
$^1F^e(19)$	−0.13609	−0.11191	−0.10329	−0.09346	−0.08384			
$^1F^e(20)$	−0.13592	−0.11175	−0.10214	−0.09177	−0.08310			
$^1F^e(21)$	−0.13530	−0.11014	−0.10174	−0.09124	−0.08219			
$^1F^e(22)$	−0.13354	−0.10973	−0.10064	−0.09031	−0.08172			
$^1F^e(23)$	−0.13337	−0.10890	−0.10025	−0.08988				
$^1F^e(24)$	−0.13110	−0.10692	−0.09969	−0.08943				
$^1F^e(25)$	−0.12979	−0.10632	−0.09906					
$^1F^e(26)$	−0.12832							
$^1F^e(27)$	−0.12592							

agree reasonably well with those available in literature and a few resonance states are reported for the first time below $He^+(3p)$ threshold. It is found that the resonance energies increase as well as the number of such states decrease with the decrease of λ_D. Widths of the resonance states having dominant configurations $3dnd$ $[3 \le n \le 10]$ and $3pnf$ $[4 \le n \le 10]$ decreases with the decrease of λ_D. The resonance states having dominant configuration $3dng$ $[5 \le n \le 9]$ have very small widths ($\sim 10^{-8} - 10^{-12}$ a.u.) in free environment and the widths increase with respect to the decrease of λ_D. In this context, we have shown that if the inter-electronic angle increases with decrease in λ_D, the width of the states will decrease. These theoretical predictions call for studies to be conducted to determine the widths of resonance $^{1,3}F^e$ states of both free atoms and atoms embedded in plasma. The resonance parameters of $^{1,3}F^e$ states of He atom between the $He^+(3p)$ to $He^+(4p)$ thresholds are given for the first time in the literature. The variations of other structural properties like ratio of attractive to repulsive potential,

Table N
Resonance width Γ_r (a.u.) of $^1F^e$ states of He atom below $He^+(4p)$ threshold for different screening length λ_D in a.u. The notation $A[\pm B]$ stands for $A\times10^{\pm B}$.

States	λ_D						
	∞	100	70	50	40	30	25
$^1F^e(1)$	1.06[−4]	2.66[−5]	5.07[−5]	3.67[−5]	3.47[−5]	5.51[−5]	3.28[−5]
$^1F^e(2)$	3.72[−4]	3.31[−5]	4.55[−5]	2.09[−5]	1.31[−5]	1.60[−5]	2.06[−6]
$^1F^e(3)$	8.25[−5]	2.65[−4]	5.48[−5]	3.43[−5]	1.69[−5]	2.84[−5]	7.91[−5]
$^1F^e(4)$	5.83[−4]	9.78[−5]	7.59[−5]	8.47[−5]	6.58[−5]	4.35[−5]	7.28[−5]
$^1F^e(5)$	7.33[−5]	3.41[−4]	1.49[−4]	6.47[−5]	7.87[−5]	9.35[−5]	9.33[−5]
$^1F^e(6)$	2.11[−5]	6.84[−5]	1.19[−4]	8.01[−5]	8.77[−5]	1.47[−4]	8.87[−5]
$^1F^e(7)$	1.14[−5]	2.69[−3]	7.31[−5]	9.56[−5]	8.17[−5]	1.49[−4]	1.30[−4]
$^1F^e(8)$	2.56[−4]	6.81[−5]	5.34[−4]	7.66[−5]	9.48[−5]	1.57[−4]	1.19[−4]
$^1F^e(9)$	9.00[−5]	2.55[−4]	5.29[−5]	6.03[−5]	1.15[−4]	1.04[−4]	8.55[−5]
$^1F^e(10)$	4.66[−4]	1.10[−5]	1.41[−5]	5.23[−4]	5.82[−5]	1.04[−4]	1.05[−4]
$^1F^e(11)$	1.67[−5]	2.60[−4]	9.61[−5]	6.15[−5]	5.60[−4]	4.49[−5]	7.45[−5]
$^1F^e(12)$	2.97[−5]	9.17[−5]	3.73[−5]	5.45[−5]	5.63[−5]	4.64[−5]	4.89[−5]
$^1F^e(13)$	1.37[−4]	4.29[−4]	2.84[−5]	8.86[−5]	1.21[−5]	7.07[−3]	4.40[−5]
$^1F^e(14)$	1.04[−5]	8.39[−6]	1.93[−5]	1.88[−4]	8.71[−5]	1.17[−4]	6.75[−5]
$^1F^e(15)$	8.66[−6]	1.66[−5]	8.88[−6]	5.24[−5]	2.13[−4]	3.85[−4]	9.70[−5]
$^1F^e(16)$	4.88[−4]	1.65[−4]	2.25[−5]	2.82[−6]	6.28[−5]	2.41[−5]	4.04[−4]
$^1F^e(17)$	8.81[−6]	2.10[−4]	1.45[−4]	1.03[−5]	2.87[−6]	2.82[−6]	
$^1F^e(18)$	2.57[−6]	2.86[−5]	3.16[−5]	3.48[−5]	8.99[−6]		
$^1F^e(19)$	1.16[−5]	2.94[−4]	3.63[−5]	9.04[−5]	5.74[−5]		
$^1F^e(20)$	1.66[−4]	1.35[−4]	6.97[−5]	2.81[−5]	3.51[−5]		
$^1F^e(21)$	2.49[−4]	4.48[−6]	1.34[−4]	1.90[−6]	3.11[−6]		
$^1F^e(22)$	9.06[−6]	1.49[−5]	1.22[−5]	3.08[−5]	1.48[−5]		
$^1F^e(23)$	3.33[−5]	9.83[−6]	1.27[−5]	1.72[−5]			
$^1F^e(24)$	2.51[−4]	4.33[−6]	2.09[−5]	4.81[−6]			
$^1F^e(25)$	1.75[−4]	4.94[−6]	3.46[−5]				
$^1F^e(26)$	1.75[−4]						
$^1F^e(27)$	1.86[−4]						

Table O
Expectation values of repulsive potential $\langle V_r\rangle$, attractive potential $\langle V_a\rangle$, ratio of attractive to repulsive potential $\eta=\left|\frac{\langle V_a\rangle}{\langle V_r\rangle}\right|$, $\langle\cos\theta_{12}\rangle$, inter-electronic angles $\langle\theta_{12}\rangle$ (in degree) using (10), different one and two-particle moments of resonance $^1F^e$ states of He–atom below $He^+(3p)$ threshold. The notation $A[\pm B]$ stands for $A\times10^{\pm B}$. All values are given in atomic units.

States	λ_D	$\langle V_r\rangle$	$\langle V_a\rangle$	η	$\langle r_1\rangle$	$\langle r_1^2\rangle$	$\langle r_{12}\rangle$	$\langle r_{12}^2\rangle$	$\langle\cos\theta_{12}\rangle$	$\langle\theta_{12}\rangle$
$^1F^e(1)$	∞	6.55[−2]	−6.02[−1]	9.18	1.01[+1]	1.37[+2]	1.68[+1]	3.07[+2]	−1.67[−1]	135.10
	100	5.60[−2]	−5.63[−1]	10.04	1.01[+1]	1.38[+2]	1.68[+1]	3.10[+2]	−1.66[−1]	134.91
	70	5.22[−2]	−5.46[−1]	10.45	1.01[+1]	1.40[+2]	1.69[+1]	3.14[+2]	−1.65[−1]	134.74
	50	4.74[−2]	−5.24[−1]	11.05	1.02[+1]	1.43[+2]	1.71[+1]	3.20[+2]	−1.64[−1]	134.47
	40	4.34[−2]	−5.05[−1]	11.64	1.03[+1]	1.46[+2]	1.73[+1]	3.27[+2]	−1.63[−1]	134.21
	30	3.71[−2]	−4.75[−1]	12.78	1.06[+1]	1.54[+2]	1.77[+1]	3.43[+2]	−1.62[−1]	133.78
	25	3.24[−2]	−4.50[−1]	13.88	1.08[+1]	1.62[+2]	1.81[+1]	3.61[+2]	−1.61[−1]	133.49
	20	2.59[−2]	−4.15[−1]	16.03	1.13[+1]	1.81[+2]	1.90[+1]	3.99[+2]	−1.60[−1]	133.32
$^1F^e(2)$	∞	7.01[−2]	−5.92[−1]	8.44	1.00[+1]	1.32[+2]	1.58[+1]	2.76[+2]	−6.98[−2]	108.87
	100	6.04[−2]	−5.52[−1]	9.14	1.01[+1]	1.34[+2]	1.59[+1]	2.81[+2]	−6.84[−2]	108.47
	70	5.64[−2]	−5.36[−1]	9.49	1.02[+1]	1.37[+2]	1.60[+1]	2.85[+2]	−6.65[−2]	107.96
	50	5.12[−2]	−5.13[−1]	10.02	1.03[+1]	1.42[+2]	1.63[+1]	2.94[+2]	−6.39[−2]	107.26
	40	4.68[−2]	−4.94[−1]	10.55	1.05[+1]	1.47[+2]	1.65[+1]	3.04[+2]	−5.98[−2]	106.16
	30	3.96[−2]	−4.62[−1]	11.67	1.09[+1]	1.62[+2]	1.72[+1]	3.32[+2]	−5.22[−2]	104.11
	25	3.38[−2]	−4.37[−1]	12.89	1.14[+1]	1.80[+2]	1.80[+1]	3.67[+2]	−4.29[−2]	101.59
	20	2.49[−2]	−3.97[−1]	15.97	1.26[+1]	2.37[+2]	2.03[+1]	4.77[+2]	−2.08[−2]	95.63
$^1F^e(3)$	∞	4.19[−2]	−5.39[−1]	12.86	1.58[+1]	4.03[+2]	2.81[+1]	8.75[+2]	−1.86[−1]	140.41
	100	3.25[−2]	−5.00[−1]	15.37	1.61[+1]	4.18[+2]	2.86[+1]	9.05[+2]	−1.84[−1]	139.72
	70	2.88[−2]	−4.83[−1]	16.76	1.63[+1]	4.33[+2]	2.90[+1]	9.36[+2]	−1.82[−1]	139.14
	50	2.42[−2]	−4.62[−1]	19.05	1.68[+1]	4.62[+2]	2.99[+1]	9.95[+2]	−1.78[−1]	138.28
	40	2.05[−2]	−4.44[−1]	21.66	1.74[+1]	4.99[+2]	3.10[+1]	1.06[+3]	−1.76[−1]	137.66
	30	1.47[−2]	−4.14[−1]	28.17	1.88[+1]	5.95[+2]	3.38[+1]	1.26[+3]	−1.76[−1]	137.76
	25	1.03[−2]	−3.90[−1]	37.80	2.07[+1]	7.47[+2]	3.76[+1]	1.58[+3]	−1.87[−1]	140.57
$^1F^e(4)$	∞	4.32[−2]	−5.34[−1]	12.36	1.62[+1]	4.22[+2]	2.77[+1]	8.60[+2]	−5.00[−2]	103.51
	100	3.36[−2]	−4.95[−1]	14.72	1.66[+1]	4.44[+2]	2.83[+1]	9.01[+2]	−4.47[−2]	102.08
	70	2.97[−2]	−4.78[−1]	16.09	1.69[+1]	4.66[+2]	2.90[+1]	9.41[+2]	−3.80[−2]	100.27
	50	2.47[−2]	−4.56[−1]	18.47	1.76[+1]	5.11[+2]	3.02[+1]	1.02[+3]	−2.50[−2]	96.76
	40	2.04[−2]	−4.37[−1]	21.44	1.86[+1]	5.78[+2]	3.20[+1]	1.15[+3]	−1.05[−2]	92.85
	30	1.36[−2]	−4.07[−1]	29.82	2.10[+1]	7.59[+2]	3.64[+1]	1.49[+3]	3.71[−2]	79.96
$^1F^e(5)$	∞	4.04[−2]	−5.23[−1]	12.93	1.68[+1]	4.56[+2]	2.75[+1]	8.35[+2]	1.86[−1]	39.67
	100	3.03[−2]	−4.83[−1]	15.93	1.74[+1]	4.91[+2]	2.86[+1]	9.04[+2]	1.82[−1]	40.59
	70	2.57[−2]	−4.65[−1]	18.07	1.80[+1]	5.38[+2]	3.00[+1]	9.97[+2]	1.78[−1]	41.81
	50	1.98[−2]	−4.42[−1]	22.28	1.94[+1]	6.40[+2]	3.27[+1]	1.19[+3]	1.68[−1]	44.57
	40	8.91[−3]	−4.15[−1]	46.58	2.88[+1]	1.53[+3]	5.34[+1]	3.18[+3]	−1.61[−1]	133.47
$^1F^e(6)$	∞	2.90[−2]	−5.08[−1]	17.52	2.32[+1]	9.53[+2]	4.26[+1]	2.01[+3]	−1.98[−1]	143.51
	100	1.97[−2]	−4.69[−1]	23.73	2.40[+1]	1.03[+3]	4.43[+1]	2.18[+3]	−1.92[−1]	141.86

(*continued on next page*)

Table O (*continued*).

States	λ_D	$\langle V_r \rangle$	$\langle V_a \rangle$	η	$\langle r_1 \rangle$	$\langle r_1^2 \rangle$	$\langle r_{12} \rangle$	$\langle r_{12}^2 \rangle$	$\langle \cos\theta_{12} \rangle$	$\langle \theta_{12} \rangle$
	70	1.62[−2]	−4.53[−1]	27.86	2.49[+1]	1.11[+3]	4.60[+1]	2.35[+3]	−1.88[−1]	140.92
	50	1.21[−2]	−4.32[−1]	35.59	2.65[+1]	1.28[+3]	4.92[+1]	2.69[+3]	−1.80[−1]	138.82
	40	1.41[−2]	−4.22[−1]	29.74	2.21[+1]	8.79[+2]	3.82[+1]	1.67[+3]	1.43[−1]	51.32
$^1F^e(7)$	∞	2.95[−2]	−5.05[−1]	17.12	2.39[+1]	1.02[+3]	4.29[+1]	2.07[+3]	−4.05[−2]	100.93
	100	1.98[−2]	−4.66[−1]	23.46	2.53[+1]	1.16[+3]	4.54[+1]	2.33[+3]	−2.09[−2]	95.65
	70	1.62[−2]	−4.50[−1]	27.71	2.63[+1]	1.26[+3]	4.74[+1]	2.53[+3]	−2.17[−2]	95.86
	50	1.15[−2]	−4.28[−1]	37.22	2.90[+1]	1.55[+3]	5.25[+1]	3.10[+3]	4.51[−3]	88.78
	40	7.69[−3]	−4.10[−1]	53.33	3.32[+1]	2.11[+3]	6.08[+1]	4.20[+3]	3.18[−2]	81.39
$^1F^e(8)$	∞	2.80[−2]	−4.99[−1]	17.77	2.52[+1]	1.16[+3]	4.40[+1]	2.19[+3]	2.12[−1]	32.73
	100	1.80[−2]	−4.59[−1]	25.48	2.71[+1]	1.37[+3]	4.78[+1]	2.59[+3]	2.03[−1]	35.04
	70	1.38[−2]	−4.42[−1]	32.02	2.91[+1]	1.59[+3]	5.18[+1]	3.04[+3]	1.93[−1]	37.80
	50	5.38[−3]	−4.16[−1]	77.29	4.25[+1]	3.54[+3]	8.05[+1]	7.23[+3]	−1.23[−1]	123.43
$^1F^e(9)$	∞	2.12[−2]	−4.90[−1]	23.09	3.20[+1]	1.93[+3]	6.01[+1]	4.03[+3]	−2.03[−1]	145.03
	100	1.21[−2]	−4.51[−1]	37.05	3.44[+1]	2.25[+3]	6.49[+1]	4.67[+3]	−1.95[−1]	142.75
	70	8.96[−3]	−4.36[−1]	48.62	3.69[+1]	2.61[+3]	6.88[+1]	5.41[+3]	−1.88[−1]	140.87
	50	7.31[−3]	−4.19[−1]	57.28	3.74[+1]	2.77[+3]	6.98[+1]	5.42[+3]	1.24[−1]	56.30
$^1F^e(10)$	∞	2.15[−2]	−4.88[−1]	22.70	3.32[+1]	2.09[+3]	6.11[+1]	4.20[+3]	−3.09[−2]	98.36
	100	1.21[−2]	−4.49[−1]	36.97	3.63[+1]	2.53[+3]	6.72[+1]	5.07[+3]	−1.23[−2]	93.32
	70	8.61[−3]	−4.33[−1]	50.36	3.99[+1]	3.08[+3]	7.42[+1]	6.16[+3]	8.76[−3]	87.63
	50	4.51[−3]	−4.13[−1]	91.55	4.95[+1]	4.95[+3]	9.33[+1]	9.89[+3]	2.59[−2]	82.99
$^1F^e(11)$	∞	2.12[−2]	−4.85[−1]	22.80	3.50[+1]	2.40[+3]	6.33[+1]	4.61[+3]	2.19[−1]	30.81
	100	7.51[−3]	−4.40[−1]	58.68	4.79[+1]	4.55[+3]	9.17[+1]	9.34[+3]	−1.81[−1]	138.97
	70	5.00[−3]	−4.26[−1]	85.22	5.31[+1]	5.65[+3]	1.01[+2]	1.14[+4]	−9.96[−2]	116.89
$^1F^e(12)$	∞	1.63[−2]	−4.77[−1]	29.20	4.39[+1]	3.81[+3]	8.24[+1]	7.64[+3]	−1.77[−2]	94.78
	100	7.21[−3]	−4.39[−1]	60.89	5.20[+1]	5.40[+3]	9.79[+1]	1.07[+4]	5.12[−2]	76.15
$^1F^e(13)$	∞	1.62[−2]	−4.77[−1]	29.47	4.42[+1]	3.87[+3]	8.31[+1]	7.76[+3]	−2.45[−2]	96.62
	100	3.96[−3]	−4.32[−1]	109.24	7.34[+1]	1.10[+4]	1.39[+2]	2.17[+4]	1.89[−1]	38.90
$^1F^e(14)$	∞	1.32[−2]	−4.72[−1]	35.70	5.39[+1]	5.94[+3]	1.02[+2]	1.19[+4]	−2.21[−2]	95.96
$^1F^e(15)$	∞	1.06[−2]	−4.66[−1]	44.05	6.76[+1]	9.49[+3]	1.30[+2]	1.90[+4]	−5.83[−3]	91.57
$^1F^e(16)$	∞	9.74[−3]	−4.65[−1]	47.74	7.58[+1]	1.21[+4]	1.46[+2]	2.43[+4]	−5.52[−3]	91.49
$^1F^e(17)$	∞	1.59[−2]	−4.79[−1]	30.11	5.82[+1]	7.98[+3]	1.11[+2]	1.59[+4]	−1.15[−3]	90.31

different one and two-particle moments etc. with respect to different λ_D values are also studied for the first time for both metastable bound and resonance $^{1,3}F^e$ states of He-atom.

CRediT authorship contribution statement

A.N. Sil: Data curation, Methodology, Software, Writing – original draft. **S. Dutta:** Data curation, Methodology, Writing – review & editing. **D. Ghosh:** Data curation, Software. **J.K. Saha:** Formal analysis, Writing – review & editing. **S. Bhattacharyya:** Formal analysis, Writing – review & editing. **T.K. Mukhopadhyay:** Conceptualization, Supervision, Writing – review & editing.

Declaration of competing interest

The authors declare the following financial interests/personal relationships which may be considered as potential competing interests: Tapan Kumar Mukhopadhyay reports financial support was provided by Board of Research in Nuclear Sciences. Tapan Kumar Mukhopadhyay reports financial support was provided by Science and Engineering Research Board. Jayanta K. Saha reports financial support was provided by Science and Engineering Research Board.

Data availability

All relevant data are given in the manuscript and also available on request.

Acknowledgements

Tapan Kumar Mukhopadhyay acknowledges the partial financial support from the Department of Atomic Energy, Board of Research in Nuclear Sciences (DAE-BRNS), Govt. of India under grant number 58/14/10/2021-BRNS and Science and Engineering Research Board (SERB), Govt. of India under grant number CRG/2022/004280. Jayanta K. Saha acknowledges partial financial support from Science and Engineering Research Board (SERB), Govt. of India under file number CRG/2022/003547.

References

[1] H. Margenau, M. Lewis, Rev. Modern Phys. 31 (1959) 569.
[2] F. Rogers, H. Graboske, D. Harwood, Phys. Rev. A 1 (1970) 1577.
[3] J. Doyle, F. Keenan, Astron Astrophys. 157 (1986) 116–118.
[4] J. Seidel, S. Arndt, W. Kraeft, Phys. Rev. E 52 (1995) 5387.
[5] D. Ray, Phys. Rev. E 62 (2000) 4126.
[6] B. Saha, P. Mukherjee, G. Diercksen, Astron. Astrophys. 396 (2002) 337.
[7] B. Saha, P. Mukherjee, D. Bielinska-Waz, J. Karwowski, J. Quant. Spectrosc. Radiat. Transfer 78 (1) (2003) 131–137.
[8] A. Sil, P. Mukherjee, Int. J. Quantum Chem. 102 (2005) 1061–1068.
[9] S. Kar, Y. Ho, Int. J. Quantum Chem. 108 (2008) 1491–1504.
[10] L. Xie, J. Wang, R. Janev, Y. Qu, C. Dong, Eur. Phys. J. D 66 (2012) 125.
[11] Y.-C. Lin, C.-Y. Lin, Y.K. Ho, Phys. Rev. A 85 (2012) 042516.
[12] P. Serra, S. Kais, J. Phys. B: At. Mol. Opt. Phys. 45 (23) (2012) 235003.
[13] L. Jiao, Y. Ho, Phys. Plasmas 20 (2013) 083303.
[14] M. Belkhiri, C.J. Fontes, M. Poirier, Phys. Rev. A 92 (2015) 032501.
[15] M. Belkhiri, C.J. Fontes, J. Phys. B: At. Mol. Opt. Phys. 49 (2016) 175002.
[16] X.-F. Li, G. Jiang, H.-B. Wang, M. Wu, Q. Sun, Phys. Scr. 92 (2017) 075401.
[17] Z.-B. Chen, J. Quant. Spectrosc. Radiat. Transfer 237 (2019) 106615.
[18] X. Li, F. Rosmej, Phys. Lett. A 384 (2020) 126478.
[19] A. Singh, D. Dawra, M. Dimri, A.K. Jha, R.K. Pandey, M. Mohan, Phys. Lett. A 384 (2020) 126369.
[20] M.-A. Martínez-Sánchez, C. Martínez-Flores, R. Vargas, J. Garza, R. Cabrera-Trujillo, K. Sen, Phys. Rev. E 103 (2021) 043202.
[21] J.K. Saha, S. Bhattacharyya, T. Mukherjee, P. Mukherjee, J. Quant. Spectrosc. Radiat. Transfer 111 (2010) 675–688.
[22] J.K. Saha, T. Mukherjee, P. Mukherjee, B. Fricke, Phys. Plasmas 20 (2013) 042703.
[23] S. Dutta, J.K. Saha, S. Bhattacharyya, P.K. Mukherjee, T.K. Mukherjee, Phys. Scr. 89 (2013) 015401.
[24] S. Bhattacharyya, J. Saha, T. Mukherjee, Phys. Rev. A 91 (2015) 042515.
[25] S. Dutta, J.K. Saha, S. Bhattacharyya, T.K. Mukherjee, Commun. Theor. Phys. 71 (2019) 853.
[26] R. Chandra, S. Bhattacharyya, J. Saha, X. Li, T. Mukherjee, J. Quant. Spectrosc. Radiat. Transfer 272 (2021) 107830.
[27] N.F. Johnson, J. Phys.: Condens. Matter 7 (1995) 965.

[28] R. Ashoori, Nature 379 (1996) 413.
[29] J. Connerade, V. Dolmatov, S. Manson, J. Phys. B: At. Mol. Opt. Phys. 32 (1999) L395.
[30] V. Dolmatov, Adv. Quant. Chem. 58 (2009) 13.
[31] J. Ludlow, T.-G. Lee, M. Pindzola, J. Phys. B: At. Mol. Opt. Phys. 43 (2010) 235202.
[32] T. Nakano, Y. Nozue, Adv. Phys. X 2 (2017) 254.
[33] S.-M. Wu, X.-Y. Yang, C. Janiak, Angew. Chem. 131 (2019) 12468.
[34] A.S. Chatterley, B. Shepperson, H. Stapelfeldt, Phys. Rev. Lett. 119 (2017) 073202.
[35] J.A. Bittencourt, Fundamentals of plasma physics, Springer Science & Business Media, 2004.
[36] P. Debye, E. Huckel, Phys. Zeitschrift 24 (9) (1923) 185–206.
[37] S. Dutta, J.K. Saha, S. Bhattacharyya, T.K. Mukherjee, Asian J. Phys. 25 (2016) 1339.
[38] M. Dharma-Wardana, F. Perrot, Phys. Rev. A 45 (1992) 5883.
[39] M. Nantel, G. Ma, S. Gu, C. Cote, J. Itatani, D. Umstadter, Phys. Rev. Lett. 80 (1998) 4442.
[40] D.J. Hoarty, P. Allan, S.F. James, C.R.D. Brown, L.M.R. Hobbs, M.P. Hill, J.W.O. Harris, J. Morton, M.G. Brookes, R. Shepherd, J. Dunn, H. Chen, E. Von Marley, P. Beiersdorfer, H.K. Chung, R.W. Lee, G. Brown, J. Emig, Phys. Rev. Lett. 110 (2013) 265003.
[41] C. Stillman, P. Nilson, S. Ivancic, I. Golovkin, C. Mileham, I. Begishev, D. Froula, Phys. Rev. E 95 (2017) 063204.
[42] P. Beiersdorfer, G. Brown, A. McKelvey, R. Shepherd, D. Hoarty, C. Brown, M. Hill, L. Hobbs, S. James, J. Morton, et al., Phys. Rev. A 100 (2019) 012511.
[43] A. Doschek, F. Meeking, W. Kreplin, A. Chubb, H. Friedman, Astrophys. J. 164 (1971) 165.
[44] A.B. Walker Jr., H.R. Rugge, Astrophys. J. 164 (1971) 181.
[45] S.M. Kahn, Phys. Scr. 1999 (1999) 23.
[46] J.S. Parker, B.J. Doherty, K.T. Taylor, K.D. Schultz, C.I. Blaga, L.F. DiMauro, Phys. Rev. Lett. 96 (2006) 133001.
[47] Z. Wang, P. Winkler, Int. J. Quantum Chem. 36 (1989) 89–94.
[48] S. Kar, Y. Ho, Chem. Phys. Lett. 402 (2005) 544–548.
[49] S. Kar, Y.K. Ho, Phys. Rev. A 72 (2005) 010703.
[50] S. Kar, Y. Ho, Eur. Phys. J. D 44 (2007) 1–8.
[51] S. Kar, Y. Ho, J. Phys. B: At. Mol. Opt. Phys. 42 (2009) 055001.
[52] J.K. Saha, S. Bhattacharyya, T.K. Mukherjee, P.K. Mukherjee, J. Phys. B: At. Mol. Opt. Phys. 42 (2009) 245701.
[53] S. Kar, Y. Ho, Phys. Rev. A 83 (2011) 042506.
[54] L.G. Jiao, Y.K. Ho, Int. J. Quantum Chem. 113 (2013) 2569–2579.
[55] S. Kar, Y. Wang, Z. Jiang, S. Li, K. Ratnavelu, Phys. Plasmas 21 (2014) 012105.
[56] L. Jiao, Y. Ho, J. Quant. Spectrosc. Radiat. Transfer 144 (2014) 27–35.
[57] C. Zhou, Y. Yu, S. Yang, H. Qiao, Chin. Phys. B 31 (2021) 030301.
[58] S. Kar, Y.K. Ho, Phys. Rev. A 79 (2009) 062508.
[59] S. Dutta, A.N. Sil, J.K. Saha, T.K. Mukherjee, Int. J. Quantum Chem. 119 (2019) e25981.
[60] S. Tan, Y. Ho, Chinese J. Phys. 35 (1997) 701.
[61] J. Muller, X. Yang, B. Burgdorfer, Phys. Rev. A 49 (1994) 2470.
[62] V. Mandelshtam, T. Ravuri, H. Taylor, Phys. Rev. Lett. 70 (1993) 1932.
[63] A. Bhatia, A. Temkin, Rev. Modern Phys. 36 (1964) 1050.
[64] S. Dutta, A.N. Sil, J.K. Saha, T.K. Mukherjee, Int. J. Quantum Chem. 118 (2018) e25577.
[65] T. Koga, H. Matsuyama, A.J. Thakkar, Chem. Phys. Lett. 512 (2011) 287–289.
[66] S. Kar, Y.K. Ho, Int. J. Quantum Chem. 108 (2008) 1491–1504.
[67] J.K. Saha, T.K. Mukherjee, Phys. Rev. A 80 (2009) 022513.
[68] S. Kar, Y. Ho, J. Phys. B: At. Mol. Opt. Phys. 40 (2007) 1403.
[69] J. Saha, S. Bhattacharyya, T. Mukherjee, Int. Rev. Atomic Molecular Phys. 3 (2012) 1–15.

IISER KOLKATA

Certificate of Participation

पऊवि DAE

This is to certify that SAYANTAN DUTTA *of*

NARULA INSTITUTE OF TECHNOLOGY ; AGARPARA , W.B

has ~~delivered a talk~~ / ~~presented a poster~~/ participated in

3rd DAE-BRNS Symposium on Atomic, Molecular and Optical Physics held at Indian Institute of Science Education and Research, Kolkata from December 14 – 17, 2012.

INSTITUTE OF SCIENCE EDUCATION & RESEARCH ★ INDIAN IISER Kolkata

ISAMP Conference 2012
Convenor

P. K. Panigrahi

Prasanta K. Panigrahi

DST-SERC School on Physics of Highly Charged Ions

TIFR, Mumbai, 2013

Certificate

This is to certify that Tapantan Dutta *of* B.I.E.S School *participated in the DST-SERC School on Physics of Highly Charged Ions held at HBCSE Campus, TIFR, Mumbai during February 10– March 3, 2013*

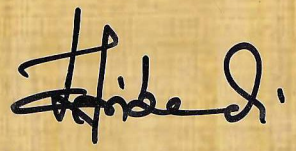

(Prof. Lokesh Tribedi)
Course Director, DST-SERC School

Mumbai, March 3, 2013

Topical Conference on Atomic Processes in Plasmas
ISAMP-TC-2013

Certificate of Participation

This is to certify that Mr./Ms./Dr. Sayantan Dutta affiliated to Belgaaria Texmaco estate school; Kolkata has attended the Topical Conference on Atomic Processes in Plasmas ISAMP-TC-2013 organized by Institute for Plasma Research, Gandhinagar, Gujarat during **18th to 20th November 2013.**

Ajai Kumar

Ajai Kumar,
Convener, ISAMP-TC-2013

ICDSMB 2014

International Conference on Dynamical Systems and Mathematical Biology

November 17 - 19, 2014

Certificate of Participation

This is to certify that Prof./Dr./Mr./Ms. Sayantan Dutta of Assistant Teacher in Belgharia Texmaco Estate School has participated in the International Conference on Dynamical Systems and Mathematical Biology (ICDSMB 2014) at Department of Mathematics, Jadavpur University during 17-19 November 2014 and presented a keynote/invited talk/plenary speech/contributory talk entitled Meijer's G Function and it's Identities to Evaluate Integrals in Different Physical Problems.

Dr. Nandadulal Bairagi
Secretary, Biomathematical Society of India

Prof. Prakash Chandra Mali
Head of the Department, Dept. of Mathematics, JU

Dr. Priti Kumar Roy
Organizing Secretary, ICDSMB -2014

JOGAMAYA DEVI COLLEGE
आत्मदीपो भव

UGC SPONSORED NATIONAL SEMINAR ON

FRONTIERS IN MODERN PHYSICS

राष्ट्रीय उच्चतर शिक्षा अभियान
NATIONAL HIGHER EDUCATION MISSION

21 & 22 November, 2016

Organised by

DEPARTMENT OF PHYSICS JOGAMAYA DEVI COLLEGE

92, Shyamaprasad Mukherjee Road, Kolkata-700 026

In Collaboration with

Centre for Interdisciplinary Research and Education

404B, Jodhpur Park, Kolkata-700 068

Certified that SRI. SAYANTAN DUTTA of

BELGHORIA TEXMACO ESTATE SCHOOL

has participated / presented a paper the seminar.

Ruma Basu 22/11/16

BALLARI CHAKRABARTI / RUMA BASU
Convenors

Suchismita Roy 22 16.11.16

Principal / Teacher-in-charge

International Conference on Science, Technology & Communication Skills (TCSCON-2024)

Organized by Department of Basic Science and Humanities, Narula Institute of Technology, Kolkata

Certificate

of Presentation

This certificate is awarded to

Sayantan Dutta of Belgharia Texmaco Estate School

for presenting a paper in the International Conference on Science, Technology & Communication Skills (TCSCON-2024) held on 22-24 February, 2024.

Paper Title: *"Transition properties of moving H-atom in plasma environment"*

Dr. Sarbani Ganguly
Convenor
HOD, BS&HU, Narula Institute of Technology

Dr. Soumen Banerjee
Conference Chair
Principal, Narula Institute of Technology